

Copyright

by

José Manuel Gallardo Méndez

2014

**The Dissertation Committee for José Manuel Gallardo Méndez  
certifies that this is the approved version of the following dissertation:**

**Model of Strain-Related Prestress Losses in Pretensioned Simply  
Supported Bridge Girders**

**Committee:**

---

Oguzhan Bayrak, Supervisor

---

James O. Jirsa

---

Sharon L. Wood

---

Harovel G. Wheat

---

Maria G. Juenger

**Model of Strain-Related Prestress Losses in Pretensioned Simply  
Supported Bridge Girders**

**by**

**José Manuel Gallardo Méndez, B.C.E.; M.S.E.**

**Dissertation**

Presented to the Faculty of the Graduate School of  
The University of Texas at Austin  
in Partial Fulfillment  
of the Requirements  
for the Degree of

**Doctor of Philosophy**

**The University of Texas at Austin**

**May 2014**

## **Dedication**

*Para: Ailenne Isabel*

*Con cariño por todo tu amor, tus cuidados y consejos*

*(From the bottom of my heart, thanks for your love, your care and advises)*



## Acknowledgements

Thanks god for the things you gave to me, including those things that I did not noticed. Gracias mamá y papá, por su amor, su ejemplo y por todo el tiempo que me dedicaron al crecer (i.e. por criarme y educarme). Gracias Ailenne por acompañarme en esta difícil tarea todos estos años, sacrificio que nunca podré pagar, y sin el cual no hubiera podido mantenerme cuerdo para terminar. Thanks Greisy, Marce, Adam, Ricardo, Yumiko, Gloriana, Vasilis, Jaime, Lalo, Samy, Perla, Dani, Juan Diego, Dave Dunkman, Steven, Eliud, Bitia and all those friends who made company to me and Ailenne during these four years<sup>i</sup>. Thanks to Sep, Andy, Kostas, Kerry, Batts, Nick and Trey, Hemal, Ali Morovat, Drit, Chris, Josh and to all others who shared with me part of their time, food, knowledge, happiness, hobbies and/or other sources of support and inspiration.

Thanks to my advisor, Oguzhan Bayrak, for introducing me to such a fascinating research topic and for the opportunity of working with a wonderful group of professionals. Thanks Dr. James O. Jirsa, Dr. Sharon L. Wood, Dr. Harovel G. Wheat and Dr. Maria G. Juenger for your comments through which you shared with me your knowledge. I want to acknowledge the support of TxDOT in the development of this project.

I want to thank and acknowledge my friends David Benjamin Garber, and Dean Joseph Deschenes, their thoughts and hard work made possible the completion of this document. Thanks to my friends Ali E. Abu Yousef, Hossein Yousefpour, and Guillermo David Huaco Cárdenas for their key help in such busy days. Thanks to Andrew Valentine, Blake Stassney and Dennis Phillip for their help in the lab floor and valuable input regarding testing set-up. Thanks to Barbara Howard, Jessica Hanten, Anise Langley, and Michelle Damvar for all their hard and efficient work with the administration; their support was of key importance to the development of this research.

---

<sup>i</sup>The names of some of those great friends can be found in various paragraphs in this page

# **Model of Strain-Related Prestress Losses in Pretensioned Simply Supported Bridge Girders**

José Manuel Gallardo Méndez, Ph.D.

The University of Texas at Austin, 2013

Supervisor: Oguzhan Bayrak

Prestressed concrete construction relies on the application of compressive stresses to concrete elements. The prestressing force is typically applied through the tensioning of strands that react against the concrete and induce compression in the concrete. Loss of prestress is the decrease of this pre-applied stress. The conservative estimation of the prestress losses is imperative to prevent undesired cracking of the prestressed element under service loads.

A large fraction of the prestress losses is a consequence of concrete deformations. This fraction of the losses can be identified as strain-related losses, and these occur due to instantaneous elastic shortening, and time-dependent creep and shrinkage. Creep and shrinkage of concrete depend on many factors that are extremely variable within concrete structures. The time-dependent behavior of concrete is not well-understood, but recent findings in the topics of concrete creep and shrinkage provide a better understanding of the underlying mechanisms affecting the nature of these two phenomena. However, current design practices and prestress loss estimation methods do not reflect the state-of-the-art knowledge regarding creep and shrinkage.

The main objective of this dissertation was the study and estimation of strain-related prestress losses in simply supported pretensioned bridge girders. Simply supported pretensioned girders are widely designed, produced and frequently used in bridge construction. Due to this common use, pretensioned concrete bridge girders has become fairly standardized elements, which results in a reduced variability in the behavior of pretensioned bridge girders, as compare to that of less standardized concrete structures. Hence, a simplified method was calibrated to estimate prestress losses within pretensioned girders to an adequate level of accuracy. To achieve an acceptable accuracy experimental data from the monitoring of pretensioned simply supported girders was used for the calibration of the method. The accuracy of this simplified method is comparable to that achievable using more elaborate methods developed for generic concrete structures.

## Table of Contents

<b>CHAPTER 1 Introduction .....</b>	<b>1</b>
1.1 Overview.....	1
1.2 Motivation.....	2
1.3 Objective and tasks .....	3
1.4 Organization.....	4
<b>CHAPTER 2 Background.....</b>	<b>6</b>
2.1 Overview.....	6
2.2 Brief Historical Review .....	7
2.3 Concrete Shrinkage.....	9
2.3.1 Hygral Shrinkage .....	12
2.3.2 Main Factors that affect Shrinkage .....	14
2.4 Concrete Creep.....	17
2.4.1 Short-Term Creep .....	18
2.4.2 Long-Term Creep.....	19
2.4.3 Creep-Shrinkage Interaction .....	24
2.4.4 Practical Factors that affect Creep .....	25
2.5 Prestress Losses in Pretensioned Bridge Girders.....	27
2.5.1 Considerations Regarding the Development of Prestress Losses .....	27
2.5.2 Main Factors Affecting Prestress Loss .....	28
2.6 Basic Models for Shrinkage, Creep, and Prestress Loss Estimation .....	30
2.6.1 Basic Modeling of Shrinkage.....	30
2.6.2 Basic Modeling of Creep .....	32
2.6.3 Basic Modeling of Prestress Losses.....	34
2.7 Experimental Results From Previous Research .....	37
2.7.1 Shrinkage Database.....	37
2.7.2 Creep Database .....	42
2.7.3 Prestress Losses Database (UTPS-Loss) .....	45

2.8	Summary .....	55
<b>CHAPTER 3 Experimental Program .....</b>		<b>56</b>
3.1	Overview .....	56
3.2	Development of Beam Specimens .....	57
3.2.1	Design .....	57
3.2.2	Fabrication .....	62
3.3	Conditioning of Beam Specimens .....	66
3.4	Assessment of Prestress Loss via Internal Strain Monitoring .....	70
3.4.1	Vibrating Wire Gage Installation .....	70
3.4.2	Periodic Monitoring .....	72
3.4.3	Consideration of Strand Relaxation Effects .....	73
3.4.4	Consideration of Temperature Effects .....	74
3.4.5	Prestress Loss Calculation / Analysis .....	75
3.5	Summary .....	77
<b>CHAPTER 4 Experimental Results .....</b>		<b>79</b>
4.1	Overview .....	79
4.2	Summary of Experimental Results .....	80
4.2.1	Concrete Properties .....	80
4.2.2	Final Strain-Related Prestress Losses .....	82
4.3	Analysis of Experimental Results .....	83
4.3.1	Time Dependency of Losses .....	83
4.3.2	Influence of Concrete Properties .....	86
4.3.3	Influence of Climate Conditions .....	91
4.3.4	Influence of Cross-Sectional Geometry .....	92
4.4	Summary .....	94
<b>CHAPTER 5 Development of a Prestress Loss Model Using Materials Test Data ...</b>		<b>96</b>
5.1	Introduction .....	96
5.2	Basic Approach to Model Concrete Behavior .....	96
5.3	Basic Model of Creep Behavior .....	98

5.3.1	Calibration of Creep Model Coefficients.....	102
5.3.2	Proposed Creep Model.....	106
5.4	Basic Model of Shrinkage Behavior.....	107
5.4.1	Time Dependent Development of Shrinkage Strains.....	108
5.4.2	Calibration of Shrinkage Model Coefficients.....	113
5.4.3	Proposed Shrinkage Model.....	115
5.5	Materials-Based Prestress Losses Estimation Method.....	115
5.5.1	Effect of Deck Shrinkage.....	116
5.5.2	Effect of Ongoing Prestress Losses.....	117
5.5.3	Proposed Method to Estimate Prestress Losses.....	119
5.6	Summary.....	122
<b>CHAPTER 6 Development of a Prestress Loss Model Using Girder Test Data.....</b>		<b>123</b>
6.1	Introduction.....	123
6.2	Motivation for the Development of a Prestress Loss Model Using Girder Test Data.....	124
6.3	Assessment of Sectional Creep and Shrinkage through Girder Strain Monitoring.....	127
6.3.1	Sectional Creep and Shrinkage Coefficients.....	127
6.3.2	Simplification of Sectional Creep and Shrinkage Expressions.....	131
6.3.3	Measurement of Sectional Creep and Shrinkage.....	133
6.4	Calibration of Time-Dependent Prestress Loss Model on Basis of Girder Data.....	137
6.4.1	Time-Dependent Sectional Creep Model.....	138
6.4.2	Sectional Shrinkage Model.....	143
6.5	Ultimate Prestress Loss Model Developed on Basis of Girder Data.....	144
6.6	Girder-Based Prestress Losses Estimation Method.....	147
6.6.1	Evaluation of the Performance of the Girder-Based Methods.....	149
6.7	Summary.....	153
<b>CHAPTER 7 Summary, Conclusions, Recommendations and Further Work.....</b>		<b>154</b>
7.1	Summary.....	154
7.2	Conclusion.....	156

7.2.1 Prestress losses estimation method .....	159
7.3 Recommendations.....	160
7.4 Further Research.....	162
7.4.1 Effect of the environmental relative humidity on the long-term creep.....	163
7.4.2 Applicability of cylinder behavior to estimate creep and shrinkage of concrete girders.....	165
<b>APPENDIX A Vibrating Wire Gage Data.....</b>	<b>168</b>
<b>APPENDIX B Vibrating Wire Gage Data.....</b>	<b>230</b>
<b>APPENDIX C Alternative Procedures to Develop Simplified Expressions to Estimate Prestress Losses.....</b>	<b>242</b>
C.1 Estimation Based on the Measured Prestress Losses versus Elastic Shortening .....	242
C.2 Estimation Based on Simplification of Existing Methods.....	245
C.3 Recommended approximate method to estimate prestress losses.....	251
<b>APPENDIX D Database Specimen Information.....</b>	<b>256</b>
D.1 Overview.....	256
D.2 Collection Database References .....	256
D.3 Evaluation Database.....	259
<b>APPENDIX E Sectional Creep and Shrinkage Coefficients.....</b>	<b>269</b>
<b>References.....</b>	<b>300</b>
<b>Vita.....</b>	<b>304</b>

## List of Tables

Table 2-1:	Changes in parameters that increase shrinkage induced by capillary pressure .....	16
Table 2-2:	Practical factors affecting shrinkage.....	17
Table 2-3:	Main factors influencing shrinkage and creep behavior (adapted from Mindess, Young and Darwin (2003)) .....	26
Table 2-4:	Filtering Criteria for Shrinkage Evaluation Database.....	38
Table 2-5:	Criteria for filtering specimens according to monitoring period (see Section 5.3.1) .....	39
Table 2-6:	Criteria considered for Creep Database filtering .....	43
Table 2-7:	Filtering Criteria to Develop UTPS-Loss Strain Evaluation Database .....	47
Table 2-8:	Properties investigated to determine accuracy of prestress loss estimate reported by each study .....	47
Table 3-1:	Experimental Program Matrix .....	56
Table 3-2:	Design parameters for specimens of each series .....	59
Table 3-3:	Fabricator information .....	63
Table 3-4:	Typical concrete mixture proportions.....	63
Table 3-5:	Timeline of beam conditioning.....	69
Table 3-6:	Variation of specimen characteristics with respect to influential parameters .....	78
Table 4-1:	Summary of concrete properties.....	80
Table 4-2:	Summary of prestress loss assessments .....	84
Table 4-3:	Average K1 correction factor for each series .....	90
Table 4-4:	Summary of relevant cross-sectional geometry properties.....	93



Table 5-1:	Calculation of Long-Term Creep Strain .....	101
Table 5-2:	Derivation of CST based on measured creep coefficients.....	105
Table 5-3:	Derivation of CLT coefficient using average trend of measured creep .....	106
Table 5-4:	Characteristics of database specimens used to calibrate shrinkage model	113
Table 5-5:	Development of shrinkage model .....	114
Table 5-6:	Expressions proposed to estimate prestress losses .....	120
Table 6-1	Parameters with limited variability in pretensioned bridge girders.....	126
Table 6-2	Difference in conditions between pretensioned bridge girders and concrete material samples .....	126
Table 6-3	Expressions resulting from Assumption Set 1 .....	132
Table 6-4	Expressions resulting from Assumption Set 2.....	133
Table 6-5	Sectional Coefficients Before Deck Casting on the Basis of Measured Girder Strains.....	136
Table 6-6	Derivation of $1/C'_{LT}$ from girder data for Specimen I-1 .....	140
Table 6-7	Derivation of $1/C'_{ST}$ from girder data for Specimen I-1 .....	140
Table 6-8	Inverse of coefficients $C'_{LT}$ and $C'_{ST}$ derived from girder data .....	142
Table 6-9	Sectional shrinkage model expressions .....	144
Table 6-10	Coefficient for combined creep spring, CST+LT .....	146
Table 6-11	Deck weight effect on short-term creep (i.e. creep recovery) .....	147
Table 6-12	Simplified Design Method to Estimate Ultimate Losses ( $t_f=75$ years)....	147
Table 6-13	Simplified Time-Dependent Prestress Losses Estimation.....	149
Table 6-14	Statistics for the ratio of estimated to measured strain related losses; estimated values for AASHTO 2012 Approximate and for the Girder-Based method .....	151
Table 7-1	Simplified Time-Dependent Prestress Losses Estimation Method .....	161

Table C-1	Set of values and categories used on prestress losses equation simplifications.....	246
Table C-2	Additional Nomenclature used on prestress losses equations for each method .....	247
Table C-3	Simplified creep induced losses for TxDOT 0-6374.....	248
Table C-4	Simplified shrinkage induced losses for TxDOT 0-6374 .....	248
Table C-5	Conservative creep coefficient (ACI), $\phi_{ACI}$ .....	249
Table C-6	Conservative shrinkage strain (ACI), $\epsilon_{SH} - ACI$ .....	249
Table C-7	Simplified creep-related losses for ACI-209 .....	249
Table C-8	Simplified shrinkage-related losses for ACI-209 .....	250
Table C-9	Simplified creep induced loss for PCI Design Handbook .....	250
Table C-10	Simplified shrinkage induced loss for PCI Design Handbook .....	251
Table C-11	Summary of equations for simplified method to estimate losses .....	252
Table C-12	Statistics for the ratio of estimated to measured strain related losses for the proposed Simplified method.....	255
Table D-1	Evaluation Database .....	260

## List of Figures

Figure 2-1	Scheme of shrinkage classification. Adapted from Wittmann (1982), and Tazawa et al. (2000).....	11
Figure 2-2:	Development of creep with logarithm of time (Brooks 2005).....	20
Figure 2-3:	Compliance development with time for various loading ages (Ulm, Maou and Boulay 2000).....	21
Figure 2-4:	Creep rate for (a) a normal strength concrete, $w/c=0.5$ , and (b) a high strength concrete, $w/c = 0.33$ (Vandamme and Ulm 2009).....	22
Figure 2-5:	Scheme of the proposed shrinkage model.....	32
Figure 2-6:	Burger Model .....	33
Figure 2-7:	Volume-to-Surface ratio for shrinkage specimens.....	40
Figure 2-8:	Conditioning Relative Humidity for Shrinkage Specimens.....	41
Figure 2-9:	Concrete Strength for Shrinkage Specimens .....	41
Figure 2-10:	Stress-to-Strength Ratio at Loading of Creep Specimens.....	44
Figure 2-11:	Concrete Strength of Creep Specimens .....	44
Figure 2-12:	Method used for measuring loss .....	49
Figure 2-13:	Location where specimens were fabricated/conditioned .....	50
Figure 2-14:	Average reported relative humidity for location where specimens were conditioned.....	51
Figure 2-15:	(a) Girder length and (b) girder height of specimens.....	52
Figure 2-16:	(a) Gross area and (b) volume-to-surface area ratio of specimens .....	52
Figure 2-17:	(a) Type of concrete mixture and (b) type of aggregate used to construct specimens.....	53

Figure 2-18: Release strength and ultimate strength of concrete used to construct specimens.....	54
Figure 2-19: Prestressing ratio of specimens .....	55
Figure 3-1: Comparison of specimens and scale of Tx girders .....	58
Figure 3-2: Longitudinal elevation of specimens .....	60
Figure 3-3: Prestressing strand layout (dimensions are offsets from bottom of girder and measured in inches) .....	61
Figure 3-4: Fabrication and storage locations .....	62
Figure 3-5: Fabrication of a typical specimen: (a) harping of strands, (b) tensioning of strands, (c) placement of mild reinforcement, (d) installation of side forms, (e) concrete placement, (f) internal vibration, (g) external vibration .....	65
Figure 3-6: Fabrication of a typical specimen: (a) form removal, (b) counter-weight location, (c) torch-cutting of strands, (d) temporary storage in precast plant .....	66
Figure 3-7: Austin storage site (Series I, II, III and IV) .....	67
Figure 3-8: Lubbock conditioning site (Series I, II and III) .....	68
Figure 3-9: Record of relative humidity and temperature at (a) Austin, and (b) Lubbock (NOAA 2012) .....	69
Figure 3-10: Vibrating wire gage installation: (a) cable routing, (b) gage supported by auxiliary reinforcement, (c) gage supported by a strand, (d) midspan distribution of gages.....	71
Figure 3-11: VWG embedment locations (at midspan section).....	72
Figure 3-12: Remote DAQ system: (a) General view and (b) electronic components.....	73
Figure 3-13: Determination of strain in prestressing strands centroid.....	76
Figure 4-1: Concrete modulus of elasticity for all series at release and at testing date ..	82

Figure 4-2: Prestress loss ( $\Delta f_p(t)$ ) normalized by loss occurring one year after placement ( $\Delta f_p(1 \text{ year})$ ) .....	85
Figure 4-3: Short- and long-term prestress losses in Series III specimens.....	86
Figure 4-4: Average measured modulus of elasticity ( $E_c$ ) for each series.....	87
Figure 4-5: Total prestress loss for each series divided into elastic shortening ( $\Delta f_{pES}$ ) and long-term loss components ( $\Delta f_{pLT}$ ) .....	88
Figure 4-6: Average losses vs. time for (a) Series I and II and (b) Series III and IV.....	89
Figure 4-7: Average prestress loss vs. time for Series III specimens.....	92
Figure 4-8: Total prestress loss for each series separated into elastic shortening ( $\Delta f_{pES}$ ) and long-term loss components ( $\Delta f_{pLT}$ ), comparing geometry .....	94
Figure 5-1: Burgers model with proposed stiffness and viscosities .....	98
Figure 5-2: Creep coefficient for cylinder specimens .....	103
Figure 5-3: Creep coefficient for cylinder specimens loaded at 1 day of age .....	103
Figure 5-4: Creep coefficient for cylinder specimens loaded at 3 days of age.....	104
Figure 5-5: Proposed creep model for concrete loaded at 1-3 days .....	107
Figure 5-6: Proposed shrinkage model.....	108
Figure 5-7: Determination of shrinkage halftime.....	109
Figure 5-8: Shrinkage halftime vs. volume-to-surface ratio.....	110
Figure 5-9: Time-dependent development of shrinkage.....	112
Figure 5-10: Variation of ultimate shrinkage strain with $-\ln(RH)/E_c$ .....	114
Figure 5-11: Proposed shrinkage model .....	115
Figure 5-12: Proposed prestress loss model (stress condition before deck).....	118
Figure 5-13: Proposed prestress loss model (stress condition after deck).....	118
Figure 5-14: Material-based estimation vs. measured prestress losses.....	121

Figure 6-1: Examples of determination of sectional coefficients for specimen UTPS-Loss#62; experimental data from (Gamble 1970).	135
Figure 6-2: Proposed Creep Model	138
Figure 6-3: Time-development of effective creep coefficient for Specimen I-1	139
Figure 6-4: Variation of ultimate shrinkage strain with $-\ln(RH)/E_c$	143
Figure 6-5: Model to estimate ultimate strains due to initial stress and shrinkage	145
Figure 6-6: Performance evaluation of the girder-based time-dependent loss estimation.	150
Figure 6-7: Estimated vs Measured Ultimate Prestress losses	152
Figure A-1: VWG embedment locations (at midspan section)	169
Figure A-2: Strain data for girder I-1, top gage ( y = 36 in.)	170
Figure A-3: Temperature data for girder I-1, top gage ( y = 36 in.)	170
Figure A-4: Strain data for girder I-1, web gage ( y = 18 in.)	171
Figure A-5: Temperature data for girder I-1, web gage ( y = 18 in.)	171
Figure A-6: Strain data for girder I-1, bottom gage 1 ( y = 6 in.)	172
Figure A-7: Temperature data for girder I-1, bottom gage 1 ( y = 6 in.)	172
Figure A-8: Strain data for girder I-1, bottom gage 2 ( y = 6 in.)	173
Figure A-9: Temperature data for girder I-1, bottom gage 2 ( y = 6 in.)	173
Figure A-10: Strain data for girder I-5, top gage ( y = 36 in.)	174
Figure A-11: Temperature data for girder I-5, top gage ( y = 36 in.)	174
Figure A-12: Strain data for girder I-5, web gage ( y = 18 in.)	175
Figure A-13: Temperature data for girder I-5, web gage ( y = 18 in.)	175
Figure A-14: Strain data for girder I-5, bottom gage 1 ( y = 6 in.)	176
Figure A-15: Temperature data for girder I-5, bottom gage 1 ( y = 6 in.)	176
Figure A-16: Strain data for girder I-5, bottom gage 2 ( y = 6 in.)	177

Figure A-17: Temperature data for girder I-5, bottom gage 2 ( y = 6 in.).....	177
Figure A-18: Strain data for girder I-3, top gage ( y = 36 in.).....	178
Figure A-19: Temperature data for girder I-3, top gage ( y = 36 in.).....	178
Figure A-20: Strain data for girder I-3, web gage ( y = 18 in.) .....	179
Figure A-21: Temperature data for girder I-3, web gage ( y = 18 in.) .....	179
Figure A-22: Strain data for girder I-3, bottom gage 1 ( y = 6 in.).....	180
Figure A-23: Temperature data for girder I-3, bottom gage 1 ( y = 6 in.).....	180
Figure A-24: Strain data for girder I-3, bottom gage 2 ( y = 6 in.).....	181
Figure A-25: Temperature data for girder I-3, bottom gage 2 ( y = 6 in.).....	181
Figure A-26: Strain data for girder I-7, top gage ( y = 36 in.).....	182
Figure A-27: Temperature data for girder I-7, top gage ( y = 36 in.).....	182
Figure A-28: Strain data for girder I-7, web gage ( y = 18 in.) .....	183
Figure A-29: Temperature data for girder I-7, web gage ( y = 18 in.) .....	183
Figure A-30: Strain data for girder I-7, bottom gage 1 ( y = 6 in.).....	184
Figure A-31: Temperature data for girder I-7, bottom gage 1 ( y = 6 in.).....	184
Figure A-32: Strain data for girder I-7, bottom gage 2 ( y = 6 in.).....	185
Figure A-33: Temperature data for girder I-7, bottom gage 2 ( y = 6 in.).....	185
Figure A-34: Strain data for girder II-1, top gage ( y = 36 in.).....	186
Figure A-35: Temperature data for girder II-1, top gage ( y = 36 in.).....	186
Figure A-36: Strain data for girder II-1, web gage ( y = 18 in.).....	187
Figure A-37: Temperature data for girder II-1, web gage ( y = 18 in.) .....	187
Figure A-38: Strain data for girder II-1, bottom gage 1 ( y = 6 in.) .....	188
Figure A-39: Temperature data for girder II-1, bottom gage 1 ( y = 6 in.).....	188
Figure A-40: Strain data for girder II-1, bottom gage 2 ( y = 6 in.) .....	189
Figure A-41: Temperature data for girder II-1, bottom gage 2 ( y = 6 in.).....	189

Figure A-42: Strain data for girder II-6, top gage ( y = 36 in.).....	190
Figure A-43: Temperature data for girder II-6, top gage ( y = 36 in.).....	190
Figure A-44: Strain data for girder II-6, web gage ( y = 18 in.).....	191
Figure A-45: Temperature data for girder II-6, web gage ( y = 18 in.) .....	191
Figure A-46: Strain data for girder II-6, bottom gage 1 ( y = 6 in.) .....	192
Figure A-47: Temperature data for girder II-6, bottom gage 1 ( y = 6 in.).....	192
Figure A-48: Strain data for girder II-6, bottom gage 2 ( y = 6 in.) .....	193
Figure A-49: Temperature data for girder II-6, bottom gage 2 ( y = 6 in.).....	193
Figure A-50: Strain data for girder II-3, top gage ( y = 36 in.).....	194
Figure A-51: Temperature data for girder II-3, top gage ( y = 36 in.).....	194
Figure A-52: Strain data for girder II-3, web gage ( y = 18 in.).....	195
Figure A-53: Temperature data for girder II-3, web gage ( y = 18 in.) .....	195
Figure A-54: Strain data for girder II-3, bottom gage 1 ( y = 6 in.) .....	196
Figure A-55: Temperature data for girder II-3, bottom gage 1 ( y = 6 in.).....	196
Figure A-56: Strain data for girder II-3, bottom gage 2 ( y = 6 in.) .....	197
Figure A-57: Temperature data for girder II-3, bottom gage 2 ( y = 6 in.).....	197
Figure A-58: Strain data for girder II-8, top gage ( y = 36 in.).....	198
Figure A-59: Temperature data for girder II-8, top gage ( y = 36 in.).....	198
Figure A-60: Strain data for girder II-8, web gage ( y = 18 in.).....	199
Figure A-61: Temperature data for girder II-8, web gage ( y = 18 in.) .....	199
Figure A-62: Strain data for girder II-8, bottom gage 1 ( y = 6 in.) .....	200
Figure A-63: Temperature data for girder II-8, bottom gage 1 ( y = 6 in.).....	200
Figure A-64: Strain data for girder II-8, bottom gage 2 ( y = 6 in.) .....	201
Figure A-65: Temperature data for girder II-8, bottom gage 2 ( y = 6 in.).....	201
Figure A-66: Strain data for girder III-1, top gage ( y = 43.5 in.) .....	202



Figure A-67: Temperature data for girder III-1, top gage ( y = 43.5 in.) .....	202
Figure A-68: Strain data for girder III-1, web gage ( y = 16.5 in.).....	203
Figure A-69: Temperature data for girder III-1, web gage ( y = 16.5 in.).....	203
Figure A-70: Strain data for girder III-1, bottom gage ( y = 7.5 in.) .....	204
Figure A-71: Temperature data for girder III-1, bottom gage ( y = 7.5 in.).....	204
Figure A-72: Strain data for girder III-5, top gage ( y = 43.5 in.) .....	205
Figure A-73: Temperature data for girder III-5, top gage ( y = 43.5 in.) .....	205
Figure A-74: Strain data for girder III-5, web gage ( y = 16.5 in.).....	206
Figure A-75: Temperature data for girder III-5, web gage ( y = 16.5 in.).....	206
Figure A-76: Strain data for girder III-5, bottom gage ( y = 7.5 in.) .....	207
Figure A-77: Temperature data for girder III-5, bottom gage ( y = 7.5 in.).....	207
Figure A-78: Strain data for girder III-3, top gage ( y = 43.5 in.) .....	208
Figure A-79: Temperature data for girder III-3, top gage ( y = 43.5 in.) .....	208
Figure A-80: Strain data for girder III-3, web gage ( y = 16.5 in.).....	209
Figure A-81: Temperature data for girder III-3, web gage ( y = 16.5 in.).....	209
Figure A-82: Strain data for girder III-3, gage ( y = 7.5 in.) .....	210
Figure A-83: Temperature data for girder III-3, gage ( y = 7.5 in.).....	210
Figure A-84: Strain data for girder III-7, top gage ( y = 43.5 in.) .....	211
Figure A-85: Temperature data for girder III-7, top gage ( y = 43.5 in.) .....	211
Figure A-86: Strain data for girder III-7, web gage ( y = 16.5 in.).....	212
Figure A-87: Temperature data for girder III-7, web gage ( y = 16.5 in.).....	212
Figure A-88: Strain data for girder III-7, bottom gage ( y = 7.5 in.) .....	213
Figure A-89: Temperature data for girder III-7, bottom gage ( y = 7.5 in.).....	213
Figure A-90: Strain data for girder IV-SCC-1, top gage ( y = 43 in.) .....	214
Figure A-91: Temperature data for girder IV-SCC-1, top gage ( y = 43 in.) .....	214

Figure A-92: Strain data for girder IV-SCC-1, web gage ( y = 18 in.).....	215
Figure A-93: Temperature data for girder IV-SCC-1, web gage ( y = 18 in.).....	215
Figure A-94: Strain data for girder IV-SCC-1, bottom gage ( y = 5.2 in.).....	216
Figure A-95: Temperature data for girder IV-SCC-1, bottom gage ( y = 5.2 in.) .....	216
Figure A-96: Strain data for girder IV-SCC-2, top gage ( y = 43 in.) .....	217
Figure A-97: Temperature data for girder IV-SCC-2, top gage ( y = 43 in.) .....	217
Figure A-98: Strain data for girder IV-SCC-2, web gage ( y = 18 in.).....	218
Figure A-99: Temperature data for girder IV-SCC-2, web gage ( y = 18 in.).....	218
Figure A-100: Strain data for girder IV-SCC-2, bottom gage ( y = 5.2 in.).....	219
Figure A-101: Temperature data for girder IV-SCC-2, bottom gage (y= 5.2 in.) .....	219
Figure A-102: Strain data for girder IV-SCC-3, top gage ( y = 43 in.) .....	220
Figure A-103: Temperature data for girder IV-SCC-3, top gage ( y = 43 in.) .....	220
Figure A-104: Strain data for girder IV-SCC-3, bottom gage ( y = 5.2 in.).....	221
Figure A-105: Temperature data for girder IV-SCC-3, bottom gage (y= 5.2 in.) .....	221
Figure A-106: Temperature data for girder IV-CC-1, top gage ( y = 43 in.) .....	222
Figure A-107: Strain data for girder IV-CC-1, bottom gage ( y = 5.2 in.) .....	223
Figure A-108: Temperature data for girder IV-CC-1, bottom gage ( y = 5.2 in.) .....	223
Figure A-109: Strain data for girder IV-CC-2, top gage ( y = 43 in.) .....	224
Figure A-110: Temperature data for girder IV-CC-2, top gage ( y = 43 in.) .....	224
Figure A-111: Strain data for girder IV-CC-2, web gage ( y = 18 in.).....	225
Figure A-112: Temperature data for girder IV-CC-2, web gage ( y = 18 in.).....	225
Figure A-113: Strain data for girder IV-CC-2, bottom gage ( y = 5.2 in.) .....	226
Figure A-114: Temperature data for girder IV-CC-2, bottom gage ( y = 5.2 in.) .....	226
Figure A-115: Strain data for girder IV-SCC-3, top gage ( y = 43 in.) .....	227
Figure A-116: Temperature data for girder IV-SCC-3, top gage ( y = 43 in.) .....	227

Figure A-117: Strain data for girder IV-CC-3, web gage ( y = 18 in.).....	228
Figure A-118: Temperature data for girder IV-CC-3, web gage ( y = 18 in.).....	228
Figure A-119: Strain data for girder IV-CC-3, bottom gage ( y = 5.2 in.).....	229
Figure A-120: Temperature data for girder IV-CC-3, bottom gage ( y = 5.2 in.) .....	229
Figure B-1: Effective creep coefficient in terms of time for Girder UTPS#4 (2B) .....	232
Figure B-2: Effective creep coefficient in terms of time for Girder UTPS#59 (B-SCC1) .....	232
Figure B-3: Effective creep coefficient in terms of time for Girder UTPS#60 (B-SCC2) .....	233
Figure B-4: Effective creep coefficient in terms of time for Girder UTPS#61 (B-CM) ...	233
Figure B-5: Effective creep coefficient in terms of time for Girder UTPS#62 (BX-1)...	234
Figure B-6: Effective creep coefficient in terms of time for Girder UTPS#222 (I-1) ..	234
Figure B-7: Effective creep coefficient in terms of time for Girder UTPS#228 (I-7) ..	235
Figure B-8: Effective creep coefficient in terms of time for Girder UTPS#230 (II-1).	235
Figure B-9: Effective creep coefficient in terms of time for Girder UTPS#235 (II-6)...	236
Figure B-10: Effective creep coefficient in terms of time for Girder UTPS#232 (II-3).	236
Figure B-11: Effective creep coefficient in terms of time for Girder UTPS#237 (II-8).	237
Figure B-12: Effective creep coefficient in terms of time for Girder UTPS#238 (III-1)..	237
Figure B-13: Effective creep coefficient in terms of time for Girder UTPS#242 (III-5)..	238
Figure B-14: Effective creep coefficient in terms of time for Girder UTPS#240 (III-3)..	238
Figure B-15: Effective creep coefficient in terms of time for Girder UTPS#244 (III-7)..	239
Figure B-16: Effective creep coefficient in terms of time for Girder UTPS#246 (SCC-1)	239
Figure B-17: Effective creep coefficient in terms of time for Girder UTPS#247 (SCC-2).	240
Figure B-18: Effective creep coefficient in terms of time for Girder UTPS#248 (SCC-3).	240
Figure B-19: Effective creep coefficient in terms of time for Girder UTPS#250 (CC-2)...	241

Figure B-20: Effective creep coefficient in terms of time for Girder UTPS#251 (CC-3)...	241
Figure C-1: Calibration of equation based on experimental prestress losses and elastic shortening.....	245
Figure C-2: Ratio of Creep Losses to Elastic Shortening for Proposed Simplistic Methods .....	252
Figure C-3: Shrinkage losses for Proposed Simplistic Methods.....	253
Figure C-4: Estimated vs. Measured Total Prestress losses (deck weight effect not included). Estimation using proposed simplified equation & measured elastic shortening. ....	254
Figure C-5: Estimated vs Measured Total Prestress losses (deck weight effect not included). The estimations are based on measured concrete strength and modulus of elasticity when reported.....	255
Figure E-1: Sectional CR&SH Coefficients Set 1: Girder UTPS#4 (2B).....	269
Figure E-2: Sectional CR&SH Coefficients Set 1: Girder UTPS#56 (A-SCC1) .....	270
Figure E-3: Sectional CR&SH Coefficients Set 1: Girder UTPS#57 (A-SCC2) .....	270
Figure E-4: Sectional CR&SH Coefficients Set 1: Girder UTPS#58 (A-CM).....	271
Figure E-5: Sectional CR&SH Coefficients Set 1: Girder UTPS#59 (B-SCC1).....	271
Figure E-6: Sectional CR&SH Coefficients Set 1: Girder UTPS#60 (B-SCC2).....	272
Figure E-7: Sectional CR&SH Coefficients Set 1: Girder UTPS#61 (B-CM).....	272
Figure E-8: Sectional CR&SH Coefficients Set 1: Girder UTPS#62 (BX-1) .....	273
Figure E-9: Sectional CR&SH Coefficients Set 1: Girder UTPS#105 (BX-3) .....	273
Figure E-10: Sectional CR&SH Coefficients Set 1: Girder UTPS#106 (BX-4) .....	274
Figure E-11: Sectional CR&SH Coefficients Set 1: Girder UTPS#119 (FT#1).....	274
Figure E-12: Sectional CR&SH Coefficients Set 1: Girder UTPS#120 (FT#2).....	275
Figure E-13: Sectional CR&SH Coefficients Set 1: Girder UTPS#222 (A1) .....	275

Figure E-14: Sectional CR&SH Coefficients Set 1: Girder UTPS#224 (A3) .....	276
Figure E-15: Sectional CR&SH Coefficients Set 1: Girder UTPS#226 (A5) .....	276
Figure E-16: Sectional CR&SH Coefficients Set 1: Girder UTPS#228 (A7) .....	277
Figure E-17: Sectional CR&SH Coefficients Set 1: Girder UTPS#230 (E1).....	277
Figure E-18: Sectional CR&SH Coefficients Set 1: Girder UTPS#232 (E3).....	278
Figure E-19: Sectional CR&SH Coefficients Set 1: Girder UTPS#235 (E6).....	278
Figure E-20: Sectional CR&SH Coefficients Set 1: Girder UTPS#237 (E8).....	279
Figure E-21: Sectional CR&SH Coefficients Set 1: Girder UTPS#238 (Q1) .....	279
Figure E-22: Sectional CR&SH Coefficients Set 1: Girder UTPS#240 (Q3) .....	280
Figure E-23: Sectional CR&SH Coefficients Set 1: Girder UTPS#242 (Q5) .....	280
Figure E-24: Sectional CR&SH Coefficients Set 1: Girder UTPS#244 (Q7) .....	281
Figure E-25: Sectional CR&SH Coefficients Set 1: Girder UTPS#246 (SCC-1) .....	281
Figure E-26: Sectional CR&SH Coefficients Set 1: Girder UTPS#247 (SCC-2) .....	282
Figure E-27: Sectional CR&SH Coefficients Set 1: Girder UTPS#248 (SCC-3) .....	282
Figure E-28: Sectional CR&SH Coefficients Set 1: Girder UTPS#250 (CC-2) .....	283
Figure E-29: Sectional CR&SH Coefficients Set 1: Girder UTPS#251 (CC-3) .....	283
Figure E-30: Sectional CR&SH Coefficients Set 1: Girder UTPS#262-624 (average of girders A, B & C).....	284
Figure E-31: Sectional CR&SH Coefficients Set 2: Girder UTPS#4 (2B) .....	284
Figure E-32: Sectional CR&SH Coefficients Set 2: Girder UTPS#56 (A-SCC1) .....	285
Figure E-33: Sectional CR&SH Coefficients Set 2: Girder UTPS#57 (A-SCC2) .....	285
Figure E-34: Sectional CR&SH Coefficients Set 2: Girder UTPS#58 (A-CM).....	286
Figure E-35: Sectional CR&SH Coefficients Set 2: Girder UTPS#59 (B-SCC1).....	286
Figure E-36: Sectional CR&SH Coefficients Set 2: Girder UTPS#60 (B-SCC2).....	287
Figure E-37: Sectional CR&SH Coefficients Set 2: Girder UTPS#61 (B-CM).....	287

Figure E-38: Sectional CR&SH Coefficients Set 2: Girder UTPS#62 (BX-1) .....	288
Figure E-39: Sectional CR&SH Coefficients Set 2: Girder UTPS#105 (BX-3) .....	288
Figure E-40: Sectional CR&SH Coefficients Set 2: Girder UTPS#106 (BX-4) .....	289
Figure E-41: Sectional CR&SH Coefficients Set 2: Girder UTPS#119 (FT#1) .....	289
Figure E-42: Sectional CR&SH Coefficients Set 2: Girder UTPS#120 (FT#2) .....	290
Figure E-43: Sectional CR&SH Coefficients Set 2: Girder UTPS#222 (A1) .....	290
Figure E-44: Sectional CR&SH Coefficients Set 2: Girder UTPS#224 (A3) .....	291
Figure E-45: Sectional CR&SH Coefficients Set 2: Girder UTPS#226 (A5) .....	291
Figure E-46: Sectional CR&SH Coefficients Set 2: Girder UTPS#228 (A7) .....	292
Figure E-47: Sectional CR&SH Coefficients Set 2: Girder UTPS#230 (E1).....	292
Figure E-48: Sectional CR&SH Coefficients Set 2: Girder UTPS#232 (E3).....	293
Figure E-49: Sectional CR&SH Coefficients Set 2: Girder UTPS#235 (E6).....	293
Figure E-50: Sectional CR&SH Coefficients Set 2: Girder UTPS#237 (E8).....	294
Figure E-51: Sectional CR&SH Coefficients Set 2: Girder UTPS#238 (Q1) .....	294
Figure E-52: Sectional CR&SH Coefficients Set 2: Girder UTPS#240 (Q3) .....	295
Figure E-53: Sectional CR&SH Coefficients Set 2: Girder UTPS#242 (Q5) .....	295
Figure E-54: Sectional CR&SH Coefficients Set 2: Girder UTPS#244 (Q7) .....	296
Figure E-55: Sectional CR&SH Coefficients Set 2: Girder UTPS#246 (SCC-1) .....	296
Figure E-56: Sectional CR&SH Coefficients Set 2: Girder UTPS#247 (SCC-2) .....	297
Figure E-57: Sectional CR&SH Coefficients Set 2: Girder UTPS#248 (SCC-3) .....	297
Figure E-58: Sectional CR&SH Coefficients Set 2: Girder UTPS#250 (CC-2) .....	298
Figure E-59: Sectional CR&SH Coefficients Set 2: Girder UTPS#251 (CC-3) .....	298
Figure E-60: Sectional CR&SH Coefficients Set 2: Girder UTPS#262-624 (average of girders A, B & C).....	299

# CHAPTER 1

## Introduction

### 1.1 OVERVIEW

Prestressed concrete construction relies on the application of compressive stresses to concrete elements. The primary objective of prestressing is to reduce the maximum tensile stresses in the element during service. The prestressing force is typically applied through the tensioning of strands that react against the concrete and induce compression in the concrete. Loss of prestress is the decrease of this pre-applied stress. The conservative estimation of the prestress losses is important to prevent undesired cracking of the prestressed element under service loads.

A large fraction of the prestress losses is a consequence of concrete deformations. This fraction of the losses can be identified as strain-related losses, and these occur due to *instantaneous* elastic shortening, and *time-dependent* creep and shrinkage. Creep and shrinkage of concrete depend on many factors that are extremely variable within concrete structures. The time-dependent behavior of concrete is not well-understood, but recent findings in the topics of concrete creep and shrinkage provide a better understanding of the underlying mechanisms affecting the nature of these two phenomena. However, current design practices and prestress loss estimation methods do not reflect the state-of-the-art knowledge regarding creep and shrinkage.

Simply supported pretensioned girders are frequently used in bridge construction. Due to this common use, pretensioned concrete bridge girders have become standardized elements, which results in a reduced variability in the behavior of pretensioned bridge girders (standardization leads to alike structures, which can be expected to behave alike),

as compared to that of less standardized concrete structures (such as cast in place bridge abutments). Hence, simplified methods can be calibrated to estimate prestress losses within pretensioned girders to an adequate level of accuracy. The accuracy of simplified methods calibrated for standardized structural elements can be expected to be comparable to that achievable using more elaborate methods developed for generic concrete structures. To achieve an acceptable accuracy using simplified methods, the availability of relevant experimental data that can be used for the calibration of such methods is of paramount importance.

This study originated as part of Project 0-6374 funded by the Texas Department of Transportation (TxDOT). The aforementioned project involves an experimental evaluation and an engineering assessment of the validity of the new prestress loss estimates currently outlined in AASHTO LRFD 2012. More details of Project 0-6374 can be found in Garber et al. (2013).

## **1.2 MOTIVATION**

Further research is still needed in several aspects of prestress losses to enable a better understanding of the problem and prevent unexpected cracking of girders in service. There has been little research conducted to monitor full-scale bridge girders in a manner that isolates the most relevant parameters for prestress losses. Results obtained from long-term monitoring can support a better assessment of the dependency of prestress losses on such relevant parameters (e.g. level of prestress, concrete stiffness, volume-to-surface ratio) under realistic conditions. For example, the simultaneous fabrication and conditioning of two sets of girders using different mix designs but otherwise identical girders, would allow the isolated study of the mix design effect on the



development of prestress losses; without the interference of other parameters such as geometry, environmental conditions, and age at release.

Compilation of the experimental results from prestress loss studies reported in the literature is critically needed to support current and future examinations of prestress losses. The resulting database of experimental results can also enable statistical evaluation of the adequacy of current prestress loss estimation methods in terms of variability, precision and conservativeness of the estimated-to-measured ratio of prestress losses.

A considerable number of recent findings regarding the creep and shrinkage of concrete are not utilized in the currently available methods for estimating prestress losses. Consideration of the contributions from these studies will result in a better understanding and improved estimation of prestress losses. The integration of this knowledge in a detailed estimation method is a valuable means to support the transfer of knowledge from researchers to bridge designers who need to consider the various mechanisms involved in prestress losses. The desired outcome of the utilization of the research findings is the identification of the basic mechanisms involved in prestress losses. On the other hand, an accurate simplified method to estimate prestress losses, which is based on a large set of experimental results, is desirable for the design of common bridges.

### **1.3 OBJECTIVE AND TASKS**

The general objective of this study is to further the transfer and application of knowledge in the area of strain-related prestress losses. This study is primarily focused on prestress losses in simply supported pretensioned bridge girders. The specific objectives are:

- to provide a compilation of available experimental data that supports the verification or calibration of current and future estimation methods,

- to provide experimental support to study the development of prestress losses through the generation of data from strain monitoring of a comprehensive set of specimens, that allows the study of the most relevant parameters affecting the development of prestress losses,
- to promote the transfer of knowledge in the topic of creep and shrinkage from research to practical estimation of prestress losses,
- to provide a simple tool to conduct preliminary estimations of prestress losses.

The main tasks related to these objectives were completed as part of or in support of the TxDOT Project 0-6374 (Garber, et al. 2013), as follows:

- a database containing experimental results from 32 studies on prestress losses
- a comprehensive experimental program that includes the monitoring of 30 full-size girders
- a method to estimate prestress losses in simply supported girders that illustrates the basic nature of the mechanisms involved in these phenomena, and
- a simplified method to estimate prestress losses calibrated on the basis of full-scale girder behavior.

#### **1.4 ORGANIZATION**

An introduction to this study is provided in this chapter. The topic of prestress losses and the main mechanisms involved are briefly introduced. Then, the motivation for this study, is presented. Later, the objectives of the study are enumerated followed by the tasks developed in order to achieve such objectives.

A literature review is presented in Chapter 2 to describe the current state-of-knowledge on creep, shrinkage and prestress losses in pretensioned girders. Chapter 2

presents the key conclusions of the main papers that lead to commonly accepted theories. Also, three collection databases that compile experimentally measured shrinkage strain (expanded from Bažant and Li (2008)), creep strain (Bažant and Li 2008), and prestress losses (UTPS-Loss Database expanded from TxDOT Project 0-6374 (Garber, et al. 2013)) are analyzed.

The experimental program developed as a mean to provide experimental support to study the development of prestress losses is presented in Chapter 3. A summary of the material test results and measured losses from this experimental program are presented and briefly discussed in Chapter 4. Such comprehensive experimental study was originally conducted as part of the TxDOT Project 0-6374 (Garber, et al. 2013).

A novel prestress loss model, developed on the basis of basic concrete models for elastic deformations, creep and shrinkage is presented as the “Materials-Based Model” in Chapter 5. Then, this model is simplified in Chapter 6, and the “Girder-Based Model” is developed. The Girder-Based model is calibrated using experimental data from pretensioned girders. Finally, an approximate method to estimate ultimate losses is developed. All the models and estimation methods presented are aimed at pretensioned simply-supported concrete girders.

Chapter 7 includes the conclusions and recommendations of this study. Appendix A contains graphs with the strains and temperatures from the monitoring of the girder specimens obtained during the development of the experimental program. Appendix B includes the plots used to determine the “sectional shrinkage” and “sectional creep coefficients” that were used to calibrate the “Element-Based Model”. Appendix C includes a discussion on alternative approaches for the simplification of estimation methods. Appendix D contains the relevant data of the specimens included in the UTPS-Loss Evaluation Databases.

## CHAPTER 2

### Background

#### 2.1 OVERVIEW

Concrete consists primarily of cement, aggregates, water and air, although other components might be present. Once the primary components are mixed, the cement reacts with the water forming various hydration products, which gradually form a solid porous material (hardened cement paste) holding together the aggregates. The pores formed in the cement paste during hydration hold water and air, with the air containing a percentage of dissolved water. The origins of the main types of strains experienced by concrete are related to the hydration process, hydration products, hardened concrete matrix structure, temperature, environmental relative humidity and externally applied stresses.

The amount of water contained in the pores changes with time because: (1) the water-cement chemical reaction continues consuming free-water available in the pores during several months or years, and (2) there is migration of water from the pores to the environment, and vice versa, towards equilibrium of the internal (pore) and external (environmental) relative humidity. The change in the amount of water contained in the pores is interlinked with a change in the pore water pressure; this is a pressure internally applied to the cement paste. This internal pressure (acting in the cement paste) causes changes in the concrete element strains. This phenomenon can be considered as the origin of shrinkage.

The joining capacity of the cement paste is mainly dependent on the action of the C-S-H particles, the “glue” in the cement paste. The stress on the C-S-H links can be very large, and are randomly distributed. Changing stress conditioning in the cement paste

(due to external or internally applied stresses) can cause breakage of the links, formation of new links, and repositioning of the C-S-H particles. These phenomena can be considered as the origin of creep.

In practice, strains occurring in concrete may be classified as: (a) creep (the global-stress-induced long-term strains) and (b) shrinkage (the non-thermal, global-stress-independent strains), and also as (c) elastic (instantaneous strains related only to global stresses). These three classifications are simple and pragmatic in and of themselves, however, they are not independent of each other, and their interdependency is complex. Treating them separately allows for them to be simply accounted for while introducing a relatively low amount of inaccuracy.

When these strains occur in a prestressed pretensioned concrete element the elastic strain of the strands is changed, resulting in changes in the strand stress (i.e. resulting in prestress losses). A theoretical background related to the occurrence of creep, shrinkage and prestress losses is presented in this chapter.

## **2.2 BRIEF HISTORICAL REVIEW**

Various aspects of the time-dependent behavior of cementitious materials have been of interest for engineers since long ago. As early as 15 BC, Vitruvius provided practical advice to prevent deleterious effects of mortar drying, probably based on visual assessment and empirical experience of his era. However, the relevance of time-dependent deformation on the behavior of structures was not specifically recognized until Hatt (1907) and White (1911) reported on the topics of creep and shrinkage respectively.

While creep and shrinkage have a large impact on many aspects of concrete design, the time-dependent effects on prestressing force (i.e. prestress loss) in pretensioned members is one of the most significant. Losses caused by creep and

shrinkage were the reasons that initially hindered the use of prestress concrete. In 1928, Eugene Freyssinet overcame this barrier with the use of high-strength steel strands to apply prestressing. Large initial strains applied to the strands exceeded the potential strains due to creep and shrinkage (Lin 1955). Later, the estimation of prestress losses became one of the incentives to develop research in the topic of long-term concrete deformation.

With the use of prestress becoming more prevalent, methods to estimate prestress losses were needed. Due to the intricate interrelation of many factors that affect creep and shrinkage and the lack of technology that allowed the deep investigation of the topic, early prestress loss estimation methods were developed from field experience and limited experimentation. This was reflected in the initial methods (lump-sum methods) used to estimate time-dependent prestress losses, which commonly allowed the estimation of losses as a constant value, around 35 ksi. In more detailed methods, the creep and shrinkage were estimated separately. Commonly the creep was (and still is) estimated as a product of elastic strains times a factor (creep coefficient). In such methods, strain and the creep coefficient were chosen by the designer from a range of recommended values according to the environmental conditions (ACI-ASCE Committee 323 1958). Later more elaborate methods commonly included equations or graphs for the estimation of both creep coefficients and shrinkage strains based on experimental results. The most common parameters considered in such equations and graphs were the relative humidity, volume-to-surface ratio, concrete strength and age at loading.

For many decades, the complexity of long-term concrete behavior has prevented a complete understanding of the mechanisms involved in time-dependent deformations. Recent advances in technology have allowed the development of several studies that have contributed to the partial deciphering of creep and shrinkage mechanisms. For example,

nanindentation, a load bearing test of the nano particles of the cement paste, allows the characterization of long-term creep in a matter of minutes instead of the years previously required (Vandamme, et al. 2013). While these technological advances have allowed for a more complete understanding of these complex phenomena, difficulty lies in the practical implementation of such findings.

Current methods to estimate prestress losses do not yet reflect the most accepted mechanisms of creep and shrinkage. The formulation of a method on the basis of modern creep and shrinkage theories would promote the transfer of knowledge from research to design. Moreover, the current “Approximate” method in AASHTO LRFD 2012 is unconservative when compared to experimental loss results. Such an “Approximate” method has the advantage of simplicity, and is likely to be applied during the routine design of simply supported bridge girders. A more precise simplified method for the estimation of prestress losses is desirable. Given the current state of creep, shrinkage and prestress loss knowledge, a more precise method to estimate losses on the basis of the most relevant parameters is considered viable.

### **2.3 CONCRETE SHRINKAGE**

Shrinkage can be defined as the reduction in volume observed in unloaded, unrestrained, concrete specimens. The magnitude of shrinkage strain is commonly defined in term of volume-to-surface ratio, compressive strength and relative humidity. Empirical evidence has shown that these parameters affect the measured shrinkage strains. However, the current definition of the effect of these parameters does not reflect the nature of the basic mechanisms at the origin of shrinkage. In-depth understanding of shrinkage mechanisms will aid the development of loss estimation methods, because such understanding allows the identification of the most relevant parameters, and the

formulation of a robust model based on the basic mechanisms. The convenience of models based on such mechanisms, is also that it allows room for improvement without the modification of the concept, i.e. other parameters considered to be relevant can be included in the method without major modifications to the mechanism-based model. Conventionally, concrete shrinkage is classified according to the conditions under which it is observed. This classification usually includes four types of shrinkage:

- *Thermal shrinkage* is generated by the cooling of concrete mainly during the first hours after set
- *Drying shrinkage* is due to migration of water from the concrete to the environment
- *Carbonation shrinkage* is initiated by chemical changes that take place when carbon dioxide (from the environment) reacts with the calcium in the cement paste
- *Autogenous shrinkage* is defined as the shortening (mainly caused by water consumption during hydration) observed in concrete with no transfer of moisture to or from the environment.

Autogenous shrinkage includes the inherent decrease in volume resulting from cement hydration, as the products of cement hydration occupy less volume than that originally used by the cement and water. The autogenous shrinkage also includes shrinkage due to self-desiccation, crystallization, conversion and dehydration.

Alternatively, shrinkage can be divided in hygral shrinkage (due to change in internal water pressure) and non-hygral (unrelated to water loss). Non-hygral shrinkage is known as chemical shrinkage (Bažant and Wittmann 1982), but this name was not used because some authors refer to autogenous shrinkage as chemical shrinkage ). This classification allow for the shrinkage due to drying shrinkage and self-desiccation



shrinkage (the two larger fractions of shrinkage) to be lumped into one type of shrinkage. Such classification is illustrated in Figure 2-1.

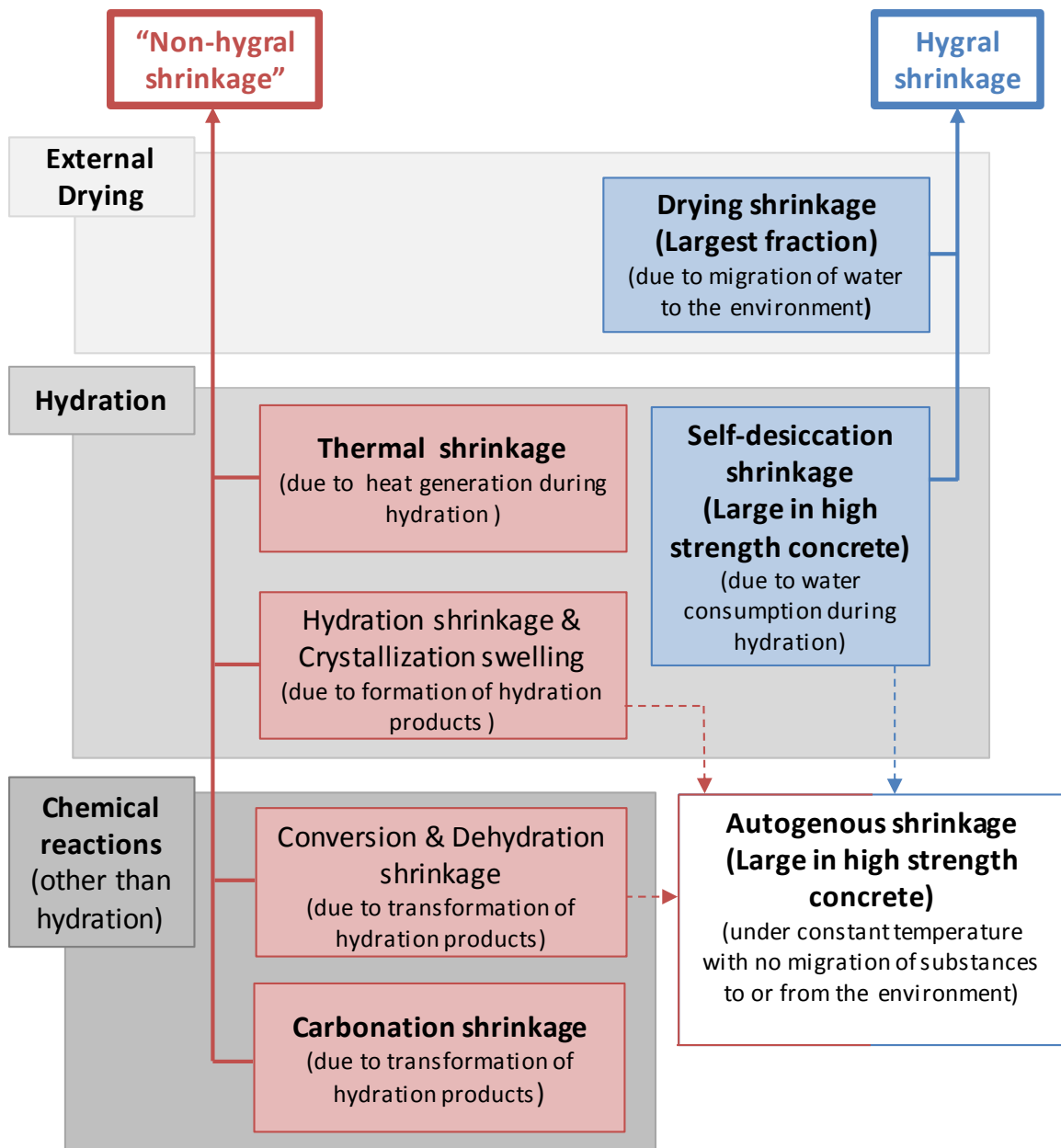


**Figure 2-1 Scheme of shrinkage classification. Adapted from Wittmann (1982), and Tazawa et al. (2000).**

Drying and the autogenous shrinkage make up the largest fraction of total shrinkage. Drying shrinkage is especially relevant in structures with relatively low volume-to-surface area ratios (typically 3 inches or less) made using concrete with a high permeability, high water-to-cement ratios, or those exposed to low ambient relative humidity environments. In the opposite case (e.g. high volume-to-surface ratio, low water-to-cement ratio), autogenous shrinkage makes up the largest fraction of total shrinkage. In short, the loss of water from the concrete system (into the atmosphere or through further cement hydration) is the main cause of concrete shrinkage.

### **2.3.1 Hygral Shrinkage**

T.C. Powers (1968) suggested that the shrinkage was due to the “change in the balance of forces and counterforces” occurring during drying within the concrete specimen. In fact, it is widely agreed upon that the main phenomenon related to shrinkage is the change in pore water pressure. This change in pressure is due to the decrease in the relative humidity within the pores, resulting from the consumption of water during hydration and migration of water from the concrete to a drying environment.

The shrinkage due to changes in the water pressure (chemical potential) is related to three main phenomena (Mindess, Young and Darwin 2003):

- *Capillary pressure*: In capillary pores, the reduction in the amount of water results in the formation of menisci in the water. The menisci in the water generate a capillary stress that is dependent to the radii of the void (among other parameters). The capillary pressure is a negative pressure

(suction) that “pulls” the walls of the capillary pores, therefore compressing (and shortening) the cement paste and the concrete matrix. The capillary water pressure is proportional to the logarithm of the relative humidity (Equation (2-1)).

- *Disjoining pressure*: The uniform orientation of layers of water particles adsorbed by C-S-H generates a disjoining pressure that holds the C-S-H particles apart from each other. During drying there is a migration of adsorbed water out of the adsorbed layers. With water migration the disjoining pressure is reduced, and the C-S-H particles tend to get closer, leading to volume reduction, i.e. shrinkage.
- *Surface free energy*: Similarly to liquids, the solid particles are subjected to a type of surface tension due to the free energy in its surface. When all adsorbed water is removed from the surface of the C-S-H particles, the free energy of the surface acts as a tensile stress surrounding the C-S-H particle (as metal bands act on a wooden barrel). This effect of surface energy would occur only below about 45% relative humidity, and therefore is not expected to occur in common bridge applications.

$$\sigma_{cap} = \frac{R \cdot T}{V_m} \ln(RH) \quad (2-1)$$

where:

$\sigma_{cap}$  = capillary pressure

$R$  = the gas constant

$T$  = temperature in Kelvin

$V_m$  = molar volume of water

The effect of the internal water pressures can be represented by the use of an “equivalent uniaxial pressure.” Values on the order of 0.3 to 1.9 ksi (2 to 13 MPa) have been found for such equivalent pressure after self-desiccation for autogenous shrinkage conditions. For these conditions, the larger pressures correspond to lower w/c ratios. It is considered that this pressure also induces matrix creep (Ulm, Maou and Boulay 2000)

In general, shrinkage is not fully reversible with rewetting after drying. This is linked to the fact that some of the pores that are emptied will not be filled again when relative humidity is regained. The extent of the reversibility of the shrinkage experienced has been shown to be dependent on the volume and size distribution of pores present in the cement paste (Juenger and Jennings 2002).

### **2.3.2 Main Factors that affect Shrinkage**

One of the causes of shrinkage has been identified as the increase in capillary pressure in concrete (among other causes initiated by the migration of water). Capillary pressure is the simplest of the most accepted causes of shrinkage, and, for the range of humidity of interest for concrete structures, its trends are in general similar to those generated by more complex internal pressures occurring at the origin of shrinkage. For the reason that the reason, the effects of various parameters will be assessed by considering a model that describes the strains in a porous material subjected to capillary pressure. The strains due to such pressure can be expressed by Equations (2-2) through (2-4), in which the strain and pressure are functions of the cement past stiffness ( $K$ ), stiffness of the solid phase of the hardened cement paste ( $K_s$ ), saturation ( $S$ ), temperature ( $T$ ), pore relative humidity ( $RH$ ), and “pore water” properties ( $R$  and  $V_m$ ). The porosity effect is included by considering the relationship of the bulk modulus of the solid with the bulk modulus of the porous cement paste. Equation (2-6) is equivalent to Equation (2-2), but instead of

using the pore relative humidity and temperature to predict capillary pressure, the capillary pore ratio ( $r$ ) and the water surface tension( $\gamma$ ) are used. The effect of some of these parameters on shrinkage is shown in Table 2-1, and can be linked to Equations (2-4) and (2-6).

$$\varepsilon_{SH-CAP} = -\frac{\sigma_{water} \cdot S \left( \frac{K_s - K}{K_s} \right)}{3K} \quad (2-2)$$

$$\sigma_{water} = R/V_m \ln(RH) T \quad (2-3)$$

$$\varepsilon_{SH-CAP} = \frac{R/V_m \ln(RH) T \cdot S \left( \frac{K_s - K}{K_s} \right)}{3K} \quad (2-4)$$

$$\sigma_{water} = 2\gamma/r \quad (2-5)$$

$$\varepsilon_{SH-CAP} = -\frac{2\gamma/r \cdot S \left( \frac{K_s - K}{K_s} \right)}{3K} \quad (2-6)$$

The radius of the voids that are being emptied depends on the geometry of the voids in the paste, the available water in the pores, and the degree of hydration of the cement paste. All of these factors are heavily dependent on the concrete strength, due to the fact that the gain in strength in a given concrete is related to the degree of hydration. Stronger and stiffer concrete will experience smaller magnitudes of shrinkage and typically have smaller pore sizes, due to less water typically being used. In addition to size, the pervasiveness of the pores will also affect the pore tension on the gross mass. From all the concrete properties, the stiffness is the most relevant parameter that directly affects shrinkage strains and can be measured in common material test laboratories.

**Table 2-1: Changes in parameters that increase shrinkage induced by capillary pressure**

	Parameter	Reason of increase of shrinkage	Example
$\epsilon_{SH-cap} \uparrow$	Internal moisture: $RH_{pore} \downarrow$	The capillary stress increases	Small specimens conditioned under low $RH_{ext}$ ( $RH_{pores}$ comes in equilibrium with $RH_{ext}$ ). Large specimens with low w/c ratio consume the water in the small pores.
	Matrix Stiffness: $K \downarrow$ or $E/(1-2\nu) \downarrow$	Less stiff concrete matrix will experience larger strains under same stress	Concrete with less stiff aggregate.
	Porosity related coefficient: $(1-K/K_s) \uparrow$	The area that can be affected by capillary stress is related to the porosity, the higher the porosity the higher the shrinkage.	A concrete with high volume of small pores
	Radius of the pores: $r_{pore} \downarrow$	Capillary pressure generated due to consumption of water from smaller pores is larger than that for larger pores	Sealed concrete with higher volume of small pores (high strength concrete)

From a more practical point of view, shrinkage is influenced by the factors outlined in Table 2-2. Shrinkage is mainly affected by the paste content of the concrete; higher paste content will result in a larger magnitude of shrinkage. Because the paste content is the most influential factor, anything that decreases paste content (e.g. greater quantity of aggregate, larger maximum aggregate size, less water, etc.) while other parameters are kept constant will result in lower shrinkage. An aggregate with a high modulus of elasticity will also result in less shrinkage, as the aggregate stiffness will resist shrinkage-induced stresses. It has been shown in several concrete material studies that concrete shrinkage will be greater in specimens conditioned in lower humidity climates and in specimens with smaller volume-to-surface area ratios.

**Table 2-2: Practical factors affecting shrinkage**

Mixture Effects	<ul style="list-style-type: none"> <li>- Size/grading of aggregate</li> <li>- Water-to-cement ratio</li> <li>- Aggregate properties</li> <li>- Cement characteristics</li> <li>- Admixtures</li> </ul>
Environment Effects	<ul style="list-style-type: none"> <li>- Relative humidity</li> <li>- Temperature</li> </ul>
Design and Construction Effects	<ul style="list-style-type: none"> <li>- Period of curing</li> <li>- Type of curing</li> <li>- Specimen size and shape</li> </ul>

## 2.4 CONCRETE CREEP

The application of stress to concrete causes deformation; with an immediate deformation occurring at the time of stress application (elastic deformation). The deformation caused by the stress continues increasing with time; this increase in

deformation is called creep. Creep is a complex phenomenon resulting from two mechanisms: short-term creep and long-term creep. The short-term creep is developed during the first days after loading, and is related to creep recovery. The long-term creep grows indefinitely at an always decreasing rate, and is irrecoverable. Due to the complexity of the phenomena, creep estimation is typically empirical in nature.

#### **2.4.1 Short-Term Creep**

During short-term loading, the cement paste behaves as a viscoelastic material (Hansen, Radjy and Sellevold 1973). The viscoelastic material responds in such a way that a portion of the elastic deformation due to loading requires some time (typically relatively short) to be developed. The time needed for the development of this phenomenon depends on the age of the concrete at the time of loading. If the concrete is loaded at early ages, the development of short-term creep can take several days; if loaded several weeks after casting, development can take several months.

Short-term creep involves the movement of pore water away from high internal pressure locations (Ulm, Maou and Boulay 2000). The time the water diffusion takes dictates the time short term creep takes to develop. In this sense, short-term creep and shrinkage are the result of pore water movement, as suggested by Powers (1968). Furthermore, when concrete is dry the creep strains are small (Hansen, Radjy and Sellevold 1973). One interesting aspect of short-term creep is that it is “not directly accessible to indentation testing”, meaning that testing at a macroscale (involving testing periods of few days to few months) is required for the characterization of short-term creep. (Vandamme, et al. 2013)

Creep recovery is a consequence of the viscoelastic behavior of concrete. When the concrete is unloaded, the pore water has the potential to reenter the spaces that were



emptied by the stress-induced movement of water. The short-term creep is not fully recoverable, however, because of changes to the pore structure that can occur with the development of short-term creep. Such pore structure changes are similar to those that cause non-recoverable shrinkage. Short-term creep and creep recovery have similar characteristic times because both are a reflection of the same mechanism. For this reason, creep recovery is fully developed in several weeks, or less if the unloading occurs when the concrete is young.

#### **2.4.2 Long-Term Creep**

The long-term creep grows indefinitely (for the range of ages of interest) at an always decreasing rate; it has been observed to develop linearly with the logarithm of time. The longest period of creep monitoring reported in the literature lasted 30 years (Brooks 2005); a sampling of results from this study are shown in Figure 2-2. The logarithmic relationship of creep over time can be observed in this figure.

The origin of long-term creep is related to the breakage of overstressed bonds that join the C-S-H particles (the “glue” of the concrete). The bonds are overstressed by repulsive forces applied by the adsorbed water on the micropore walls (Ulm, Maou and Boulay 2000). The breakage of bonds allows the slip of C-S-H particles and formation of new bonds. The rearrangement of C-S-H particles leads to a more stable configuration with an increased packing density. This process produces an always decreasing rate of creep (Vandamme and Ulm 2009).

The aging effect on creep occurs with or without external loading. However, when external load is applied to concrete, the C-S-H slip is more likely to occur in favor of strains in the loading direction. Hence, the creep due to loading is the consequence of

the accumulation of slips that favor straining in the direction of the load. Further study of the long-term creep rate is included in Section 2.4.2.1

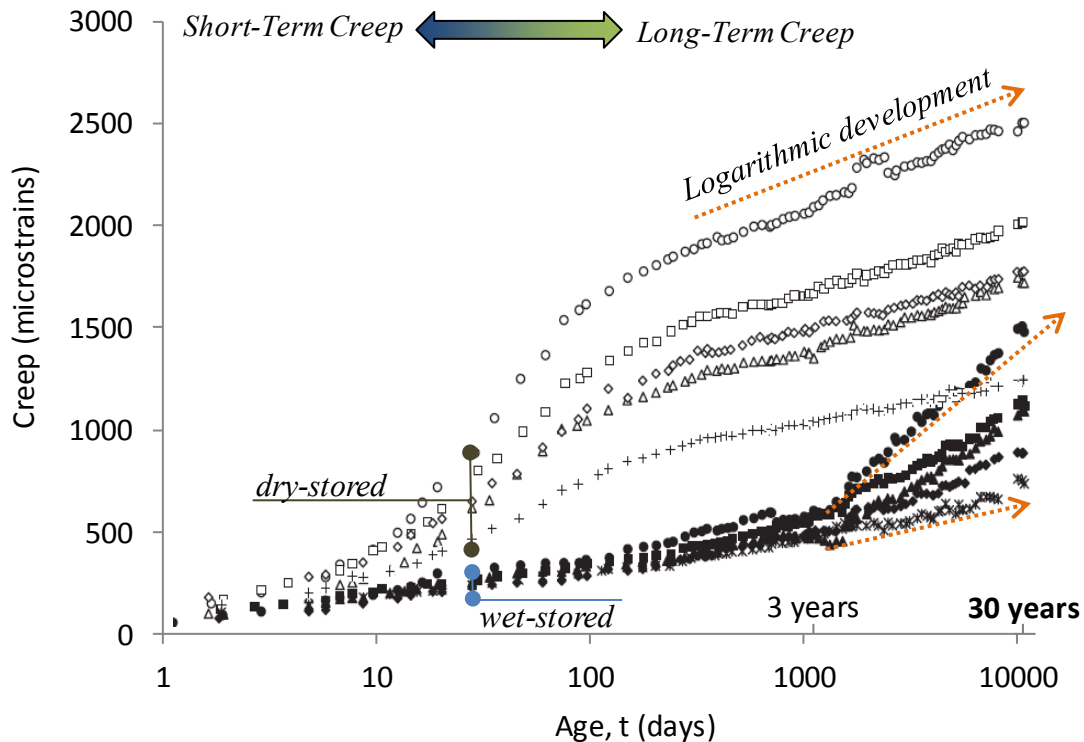


**Figure 2-2: Development of creep with logarithm of time (Brooks 2005)**

#### **2.4.2.1 Rate of Development of Long-Term Creep**

The development of creep in specimens loaded at various ages is presented in Figure 2-3 (Vandamme and Ulm 2009); normal strength concrete and high performance concrete specimens are included. In this figure the creep is presented in terms of the creep compliance ( $J$ ), which is defined as the creep strain per unit stress ( $J = \epsilon_{CR}/\sigma$ ). The creep compliance-versus-age plots are almost parallel for all specimens within each type of concrete. This similarity in the slopes indicates that the specimens show the same long-term creep development rate; albeit different creep magnitude depending on the age

at loading. Within each of the two groups of specimens, the long-term creep develops at the same rate regardless of the loading age: the specimen loaded at 20 hours shows the same long-term creep rate as the specimen loaded at 28 days. The previous loading or creep history has no relevant effect on the later long-term creep rate. This might indicate that the number of “weak” links remaining “available” for creep development is comparable for all specimens independent of the load history.

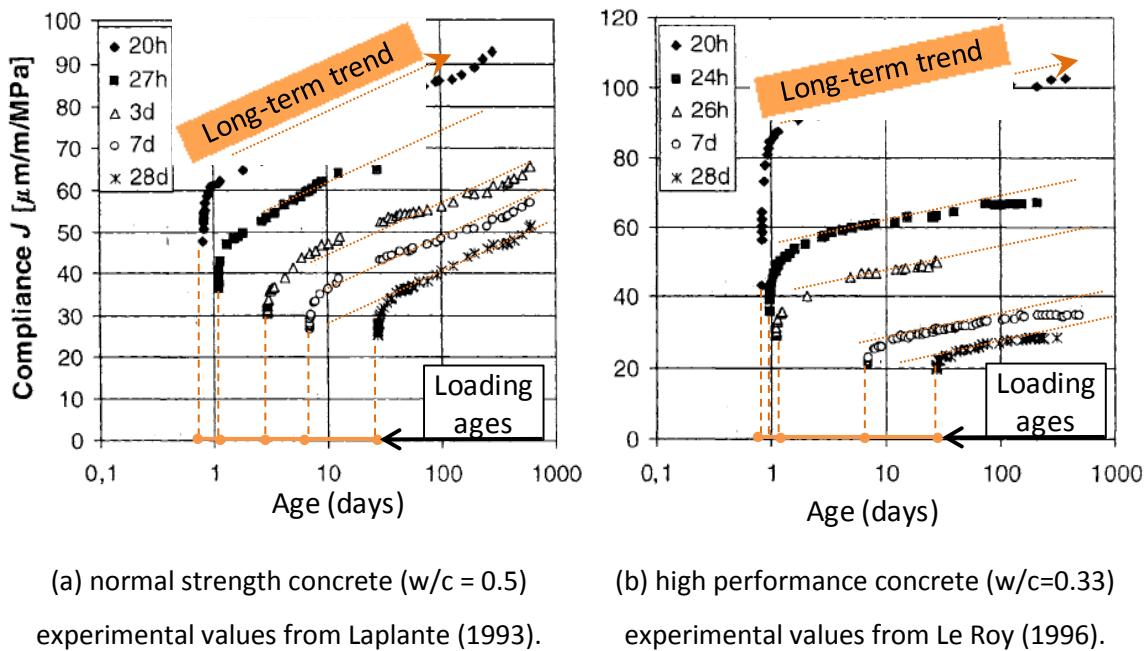


**Figure 2-3: Compliance development with time for various loading ages (Ulm, Maou and Boulay 2000)**

The data presented in Figure 2-3 (Ulm, Maou and Boulay 2000) is alternatively shown in terms of the creep compliance rate in Figure 2-4 (Vandamme and Ulm 2009). The creep compliance rate ( $dJ/dt$ ), shown in Figure 2-4, is a normalized form of the creep rate. A clear trend is observed for the long-term data shown in Figure 2-4; the long-term creep rate converges to a function proportional to the inverse of concrete age,

represented by the straight line in the plots. The trend suggests that the long-term creep develops at a rate that is approximately proportional to the inverse of concrete age (i.e.  $d\varepsilon_{CR}/dt \propto t^{-1}$ ) and independent of age of loading.

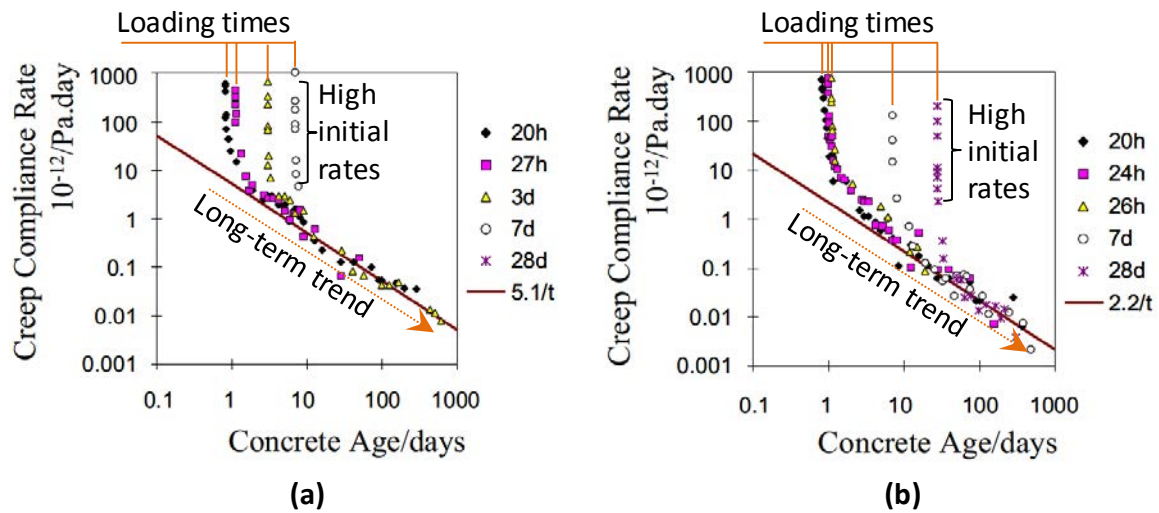


**Figure 2-4: Creep rate for (a) a normal strength concrete,  $w/c=0.5$ , and (b) a high strength concrete,  $w/c = 0.33$  (Vandamme and Ulm 2009)**

High initial rates are observed in Figure 2-4 for short periods after loading, because short-term creep is developed at high-rate during few days after loading time. The high-rate development of short-term creep begins immediately after loading and continues for several days or weeks, after such periods the data of all specimens follow a single long-term trend.

Two theories are considered illustrative of the general behavior of creep and creep rate development: (1) the slipping and bond-breakage theory suggested by Feldman (1972), Wittmann (1982), and others and (2) the packing density theory suggested by Vandamme and Ulm (2009). Feldman (1972) considered that the “slipping, microcracking, bond breaking and reforming” processes may determine the rate of creep.

Wittmann (1982) suggested that the creep rate is governed by the continuous depletion of weak links. He also suggested that the aging (i.e. the decrease in the long-term creep rate with respect to time) is due to the continuous increase in the stability of links achieved with the age of concrete (Bažant and Wittmann 1982). Provided that the rate of long-term creep is related to the frequency of bond breaks, the decreased creep rate (with respect to time) is thought to be related to a decreased amount of “overstressed” C-S-H links (“creep sites”) available at later ages.

Vandamme and Ulm (2009) suggested that the creep rate magnitude depends on the packing density of clusters of particles. The trend in the long-term creep rate can then be explained “due to the rearrangement of nanoscale particles around limit packing densities”. In this model, the decrease in the creep rate is interpreted as a consequence of the decrease in the “free” spaces where the C-S-H particles will relocate after breakage. The condition of less free space results in a lower probability of space being vacant for a C-S-H particle to occupy. This lower probability results in a decreased rate of packing density and a lower creep rate at later ages (Vandamme and Ulm 2009). This theory satisfies the observed proportionality of creep rate to the inverse of age, and consequently, the linearity of creep development with respect to the logarithm of time.

If the rate of development of creep depends only on the rate of change in packing density, then the asymptotic limit for packing density would imply the existence of an asymptotic limit for creep. However, this consideration might lack practical significance as the change in packing density in a conventional structure is almost negligible, compared to the packing density limit. For this reason, the asymptotic behavior is not noticeable during the service life of such structures. It is also likely that more than one mechanism can drive long-term creep, and that some of them do not depend on an increase in packing density.

#### ***2.4.2.2 Stress-Independent Aging of Long-Term Creep***

The stress-independent aging can be explained by the idea that the breakage of overstressed links occurs similarly in unloaded and loaded specimen due to random processes. This is in agreement with the generally accepted microprestress-solidification theory, which implies that bond breaks occur at overstressed sites (“creep sites”) resulting from large internal stresses “essentially independent of the applied macroscopic stress” (Bažant, Hauggaard, et al. 1997). In summary, it can be theorized that the occurrence of bond breaks would be almost independent of the applied stress due to these large internal stresses.

Therefore, being said, the applied external stresses might act in favor of the accumulation of strain in the direction of the stress. While in unstressed specimens the breaks occur randomly in all directions, an externally applied stress may cause the alignment of breaks and increase the developed strain. Additionally, the consideration of internal stresses due to drying (shrinkage) leads to the conclusion that the strain in unloaded specimens under drying is partially a reflection of creep occurring under internal stress. In this sense, Ulm, Maou and Boulay (2000) suggest that the capillary pressure is related to the development of “long term autogenous shrinkage due to matrix creep”.

#### **2.4.3 Creep-Shrinkage Interaction**

It is widely known that “creep and shrinkage are not independent” (Hansen, Radjy and Sellevold 1973). This interaction is known as the Picket effect, and is many times interpreted as drying creep, or load-induced shrinkage. Jennings (2004) suggest that this interaction could be a consequence of the possibility that C-S-H bonds could be more easily broken when the combination of load and drying act together. Moreover, the

interaction of creep and shrinkage is further complicated by the simultaneous occurrence of other phenomena:

- *Water Movement*: the movement of water generates changes in the stresses (due to internal pressure) and therefore generates elastic strains and C-S-H link breakage
- *External Load Induced Link Breakage*: the occurrence of link breakage due to external loading causes small changes in the pore volume, therefore causing some movement of the pore water
- *Temperature Changes*: changes in the temperature causes changes in the pore water pressure, the water migration rates, and internal stress conditions
- *Cracking*: the elastic stresses can cause cracking which will cause important changes in the water migration, in the internal stress distributions, and in the link breakage

In summary, the water migration, link breakage, temperature change, and global stress are interrelated and can lead to changes in the: elastic strains, internal pressure, creep, and concrete cracking. Models or equations to capture this type of interaction have been considered by various researchers, such as Bažant, Hauggaard, et al. (1997), Jennings (2004) Lee, et al. (2006). However, these are elaborate models, and no generic and simple approaches to consider these interactions were found in the literature.

#### **2.4.4 Practical Factors that affect Creep**

The definition of well-defined independent parameters affecting creep is difficult due to the complex interdependency of the parameters involved in the behavior of concrete. From a pragmatic point of view, the identification of practical factors that have a consistent effect on creep is feasible. Such factors serve as a guide to the structural and

concrete mix designers when concerns exist about creep. Factors commonly found in the literature are summarized in Table 2-3.

**Table 2-3: Main factors influencing shrinkage and creep behavior (adapted from Mindess, Young and Darwin (2003))**

Category	Main practical factors	Conditions to decrease creep
Concrete Properties	-Quantity and properties of Aggregate -Water-to-cement ratio -Cement composition* -Admixtures*	-Large amount of stiff aggregate -Low water-to-cement ratio -see note below* -see note below*
Environment	-Temperature -Relative humidity*	- Low temperature -see note below*
Design and Construction	-Stress -Loading age -Curing duration -Curing conditions -Specimen volume-to-surface ratio	-Lower stress -Later age at loading -Longer curing -High temperature curing -Larger volume-to-surface ratio

\*the effect of these parameters cannot be generalized, case by case consideration is necessary.

Similar to elastic shortening and shrinkage, creep is largely dependent on the stiffness of the concrete, and is thereby largely influenced by the aggregate quantity and stiffness. The magnitude of the load placed on the concrete is also important; the larger the magnitude of load placed on the concrete, the larger the creep. The most relevant environmental conditions are the humidity and temperature history. Shrinkage increases with low relative humidity. For normal conditions, the creep increases with temperature (Hansen, Radjy and Sellevold 1973). On the other side, the dependency of creep on environmental humidity is more complex. A constant low internal relative humidity leads



to a decrease in the creep; however, the change in humidity from saturation (at casting) to low humidity (when exposed to the environment) causes an increase in the creep. These two effects counteract each other, therefore the effect of environmental relative humidity on creep is not definite.

## **2.5 PRESTRESS LOSSES IN PRETENSIONED BRIDGE GIRDERS**

The loss of prestress can be defined as the strain-related decrease in the strand stress (permanent or temporary), which is mainly caused by creep, shrinkage and elastic strains. Creep and shrinkage were examined in Sections 2.3 and 2.4, respectively. The study of prestress losses requires consideration of these aforementioned phenomena constrained to the sectional behavior of a girder element, which will be the primary focus of this section. This investigation will be centered on pretensioned concrete elements, but many of the theories are applicable to more general concrete elements. Thermal effects and losses due to strand relaxation are not included in this study.

### **2.5.1 Considerations Regarding the Development of Prestress Losses**

The behavior of a pretensioned girder can be reasonably approximated assuming a linear distribution of stresses and uniformity of creep and shrinkage properties. This simplification is commonly used because it is the basis of methods used to estimate prestress losses on prestress girders (e.g. AASHTO (2012), ACI committee 209 (2005), and PCI (2004)). The global stresses, calculated using such a sectional approach, are unlikely to accurately represent the state of stress occurring locally in the region experiencing cracking. For example, cracking can occur in an unloaded, externally unrestrained element due to differential shrinkage, while the global analysis indicates that the stress is zero. In such a case, the cracking is caused by tensile stresses present in the outermost fibers of the element, because its local shrinkage is restrained by the internal

fibers that are drying at a lower rate. This does not induce a large error if the “right” method of assessing the global tensile strength of concrete is used (direct tension, splitting cylinder, or modulus of rupture test). In practice, the design method is calibrated to result in the right prediction of the global behavior, without need to determine the local strength and stress conditions.

Strains occurring in pretensioned concrete result in a change in the elastic strain of the strands, which in turn changes the strand stress (i.e. causes prestress loss). The development of prestress loss then changes the global stresses in the section. There are infinite possibilities regarding the relative magnitude (i.e. long-term losses can reduce the concrete stress by 5% or 50%) and development rate (i.e. slow or fast rate) of this stress change. The variability in girder and strand stress, compared to the constant state of global stress within a creep test specimen (i.e. concrete cylinders), creates complications when attempting to apply knowledge gained from creep tests to girder sections. Therefore, aging factors accounting for the effect of the change in stress with time (calibrated on the basis of cylinder data) might not be truly representative of conditions occurring in the girder. Complete information on the modeling of prestress girders including variable stress history can be found in Neville, Dilger and Brooks (1983) and Equations (2-10) and (2-11) which will be discussed in Section 2.6.3.

### **2.5.2 Main Factors Affecting Prestress Loss**

As the prestress losses are dependent on elastic strain, creep and shrinkage, the main factors affecting such phenomena should be included as relevant factors for the study of prestress losses. The factors affecting creep and shrinkage were previously outlined in Sections 2.3.2 and 2.4.4 respectively. A brief review of these factors and their application to pretensioned girders will be presented in this section.

Prestress loss due to creep is primarily dependent on the stiffness of the concrete, which varies with concrete strength and aggregate type, and on the magnitude of the stress sustained on the concrete. Prestress loss due to shrinkage is heavily dependent on the material properties of the concrete (i.e. concrete stiffness, concrete strength, aggregate type and quantity, paste content, etc.). The influential variables for both mechanisms are generally agreed upon by researchers; this agreement is reflected in different specifications generally considering the same variables.

Regarding the properties of the girder, the volume-to-surface area ratio, the cross-sectional shape, the amount of prestress reinforcement, and prestress force applied to the section influence the occurrence of prestress losses. The global behavior is affected by local properties, and the local properties are affected by the global behavior. For example, considering the early shrinkage strains in an unreinforced section with a large (bulky) bottom flange and slender web and top flange, the girder will curl (bending that is a global behavior induced by local behavior). Another example is a long girder with double symmetry, with similar large flanges at both top and bottom, the girder will shorten uniformly regardless of the largest local shrinkage in the web and smaller local shrinkage in the flanges (an uniform shrinkage everywhere, which is a local behavior forced by the global behavior). In both the first and second cases, either the deformations or the stress distributions would have been wrongly estimated if the interaction between global and local behavior was not considered.

As previously mentioned, the local behavior is difficult to quantify, and unnecessary if the design method has been calibrated to estimate the global behavior based on global properties. Estimation of the behavior of complex structures (different than the structures used to calibrate the method) could result in unexpected inaccuracy.

An example of such complex structures might be fix support arches, which are indeterminate and have a stress profile different than girders.

The load history is also a relevant factor that should be taken into account. The level of stress at the centroid of the strands is much larger before deck placement than after deck placement. Considering that larger creep will develop with larger stress, the time of deck placement affects the magnitude of final creep. The magnitude of the deck shrinkage-induced stress is relevant, because the larger these shrinkage stresses, the larger the reduction in prestress loss. It is important to mention that this reduction of losses is commonly called “gain of prestress” because it represents an increase in the strand stress. However, this nomenclature might mislead the designer because the total effect of the deck shrinkage in the concrete is an increase in tensile stress (which is detrimental); alternatively, this effect can be called “gain of stress”. In any case, the designer should consider the complete effect of deck shrinkage during design; including the increase in strand stress and the increase in the concrete stress.

## **2.6 BASIC MODELS FOR SHRINKAGE, CREEP, AND PRESTRESS LOSS ESTIMATION**

Information from the literature regarding the use of basic models to estimate creep and shrinkage is presented and discussed. In this section, the review is limited to the simplest model that can simulate (and illustrate) the basic mechanisms of creep and shrinkage.

### **2.6.1 Basic Modeling of Shrinkage**

As previously discussed, the mechanisms that are the primary causes of shrinkage in concrete can be divided in hygral shrinkage and non-hygral shrinkage. The first is due to the change in pore water pressure that cause volumetric deformations of the cement paste skeleton (hygral shrinkage). The second mechanism is due mainly (but not

exclusively) to particle volume changes occurring as a result of chemical reactions and particle migration (referred to as non-hygral shrinkage).

Non-hygral shrinkage represents only a small fraction of the total strains occurring during prestress losses development. It is important to mention that because we refer to chemical shrinkage as only dependent on chemical reactions and not related to pore water pressure (capillary pressure, disjoining pressure), non-hygral shrinkage here is not equivalent to autogenous shrinkage. No basic model was found in the literature for the non-hygral shrinkage. This is mainly due to the dependency of this phenomenon on many parameters that have intricate interactions. Considering the limited relevance of this type of shrinkage, and that only complex models were found in the literature, no model is studied here for the estimation of non-hygral shrinkage.

The hygral shrinkage occurs due to pore water reduction, which causes an increase in the internal water pressure. This increase in internal water pressure “pulls” together the walls of the cement paste pores and causes a reduction in surface forces that “repels” the cement paste particles. Equation (2-7), based on work by Bishop (1959), is a basic equation that has been commonly used to support models for the estimation of shrinkage (Jennings, Thomas and Vlahinic. 2009). This type of equation was previously presented in Section 2.3.2. The calculation of shrinkage using this equation involves the use of parameters that are difficult to estimate in an existing structure, and that are impractical to be specified in a design.

More simplistically, hygral shrinkage can be modeled as the deformation of the concrete caused by the pore water pressure change ( $\sigma_{water}$ ), resisted by the stiffness of the specimen “multiplied by an area factor” ( $C \cdot E_c$ ), as suggested by Powers (1968). Equation (2-7) is based on this model, by assuming that the coefficient  $C$  is defined as

shown in Equation (2-8). The scheme of the described hygral shrinkage model is shown in Figure 2-5. The hygral strains from this model can be calculated using Equation (2-9).

$$\frac{-}{(\text{---})} \quad (2-7)$$

$$\frac{-}{(\text{---})/E} \quad (2-8)$$

$$\text{---} \quad (2-9)$$

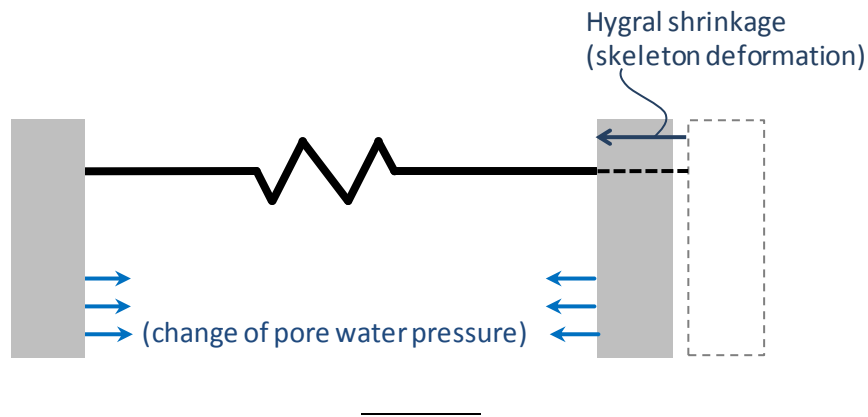


**Figure 2-5: Scheme of the proposed shrinkage model**

### 2.6.2 Basic Modeling of Creep

The modeling of creep should include: short-term and long-term creep. These mechanisms can be modeled using a Kelvin-Voigt Element in series with a Maxwell Element, which form a Burger Model as shown in Figure 2-6. Kelvin-Voigt chains have been previously used by Hilaire (2013) and De Schutter (1999) to model concrete

behavior, because they adequately model the three main characteristics of short-term creep:

- *Time dependency*: It is time-dependent as it involves the migration of pore water under stress to stress free zones.
- *Delayed elastic deformation*: It considers the delayed elastic deformation of the cement paste skeleton. This deformation can be defined by the applied stress, the overall concrete stiffness, and the contribution of the cement paste to the overall stiffness.
- *Creep recovery*: In the event of loading reversal, short-term creep strain may be recovered.

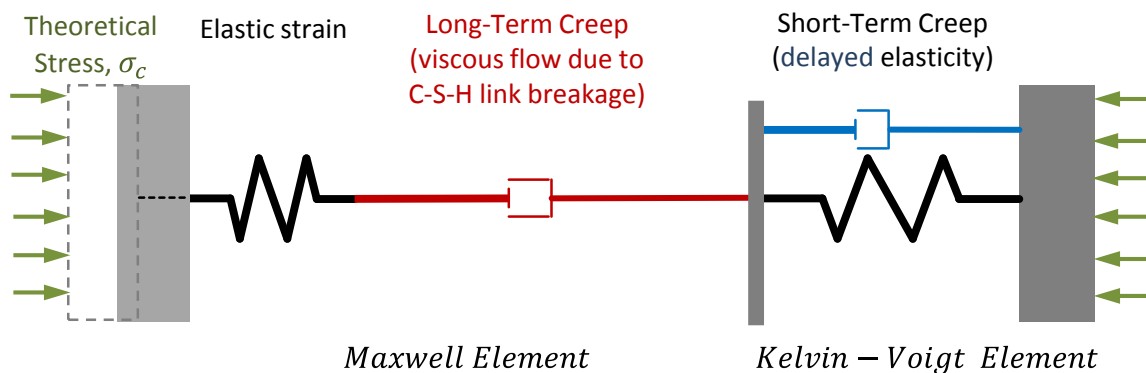


**Figure 2-6: Burger Model**

As mentioned previously, the long-term creep is considered to be a consequence of C-S-H link breakages, and can be modeled using a viscous element with viscosity proportional to the concrete age (Hilaire 2013). The viscous element adequately reflects the main characteristic of long-term creep under a sustained compressive stress:

- *Irreversibility*: Long-term creep involves breakage and reformation of C-S-H links, and therefore generates permanent deformations.
- *Unbounded magnitude*: According to current theories, the long-term creep continues indefinitely with time.
- *Logarithmic development*: The creep rate is thought to be inversely proportional to the age of the concrete. This behavior can be defined as a logarithmic development of creep strains.

Another relevant deformation that needs to be modeled is the elastic strain, which can be represented as a spring. When connected in series with the long-term dashpot, a Maxwell model is formed. The Kelvin-Voigt and the Maxwell models may be combined in series to fully model the creep mechanism (Figure 2-6). This set of springs and dashpots (Burgers Model) is considered to be a basic built-up model of creep behavior (Neville, Dilger and Brooks 1983). While the use of the Kelvin and Maxwell models independently with constant spring stiffness can be a simpler approach, the combination of the two models is essential because the Kelvin model cannot capture elastic strains or unbounded creep, while the Maxwell cannot model creep recovery.

### **2.6.3 Basic Modeling of Prestress Losses**

The modeling of prestress losses involves the use of creep and shrinkage models of some form. In the simplest form, creep and shrinkage are modeled using a fixed creep coefficient and shrinkage strain for the entire concrete element over its complete lifetime. More detailed loss models can be established allowing for interaction between the prestressing strand and surrounding concrete to be accounted for and providing an opportunity to use detailed creep and shrinkage models.



A detailed model to estimate prestress loss was developed by Neville, Dilger and Brooks (1983), as shown in Equation (2-10) through Equation (2-13), for concrete members with one layer of steel. Due to the assumption that there is no slip between the prestressing steel and the surrounding concrete, the steel will provide some restraint against concrete shrinkage and creep; this resistance is included within Equation (2-10). The creep and shrinkage strains required for loss estimation may be obtained using any concrete creep and shrinkage models, such as those presented above.

$$\Delta\varepsilon_p = \frac{\varepsilon_{cr}(t, t_0) + \varepsilon_{sh}(t, t_0)}{1 + \rho n_0 \left(1 + \frac{y_1^2}{r^2}\right) \left[1 + \chi \frac{\varepsilon_{cr}(t, t_0)}{\varepsilon_{el}}\right]} \quad (2-10)$$

Adapted from  
Neville (1983)

- $\varepsilon_{cr}(t, t_0)$  = creep strain experienced at time  $t$  for concrete loaded at time  $t_0$
- $\varepsilon_{sh}(t, t_0)$  = free shrinkage developed between times  $t_0$  and  $t$
- $\varepsilon_{el}$  = elastic strain occurring at time of loading
- $\rho$  = prestressing ratio,  $A_p/A_c$
- $n_0$  = modular ratio ( $E_p/E_{ci}$ )
- $E_p$  = modulus of elasticity of prestressing strands
- $E_{ci}$  = modulus of elasticity of concrete at time of release
- $y_1$  = distance from the centroidal axis to the outer layer of reinforcement
- $r^2$  =  $I_c/A_c$
- $\chi$  = concrete aging coefficient
- $A_p$  = total area of prestressing steel
- $I_c$  = second moment of area of the net concrete section
- $A_c$  = cross-sectional area of the net concrete section

By multiplying Equation (2-10) by the modulus of elasticity of the prestressing steel ( $E_p$ ), redefining several terms and adding in a term to account for strand-relaxation-

induced stress loss ( $\Delta f_{pRE\infty}$ ), the prestress losses at an arbitrarily large concrete age ( $\Delta f_{p\infty}$ ) can be obtained, as shown in Equation (2-11)

$$\Delta f_{p\infty} = \frac{n_0 \sigma_{c0} \psi_{\infty} + \varepsilon_{SH\infty} E_p + \Delta f_{pRE\infty}}{1 + \rho n_o (1 + y_1^2 / r^2) (1 + \chi \psi_{\infty})} \quad (2-11)$$

Adapted from  
Neville (1983)

$\sigma_{c0}$  = initial stress in concrete at level of the prestressing tendon at time  $t_0$  due to the initial prestressing force  $P_0$ , calculated with the net area of concrete

$\psi_{\infty}$  = creep coefficient at an arbitrarily large age for concrete loaded at time  $t_0$

$\varepsilon_{SH\infty}$  = free shrinkage developed between times  $t_0$  and an arbitrarily large final age

$\Delta f_{pRE\infty}$  = intrinsic relaxation of steel accumulated up to an arbitrarily large final age

Equation (2-11) can be further modified to account for the final stress in the concrete at the level of the prestressing tendon ( $\sigma_{c\infty}$ ). The residual prestress force ( $P_{\infty}$ ) after all losses have taken place may be used in this modified expression, providing flexibility to the designer.

$$\Delta f_{p\infty} = - \frac{n_0 \sigma_{c\infty} \psi_{\infty} + \varepsilon_{SH\infty} E_p + \Delta f_{pRE\infty}}{1 + \rho n_o (1 + y_1^2 / r^2) [1 - (1 - \chi) \psi_{\infty}]} \quad (2-12)$$

Adapted from  
Neville (1983)

Making several further simplifications leads to a very simple design equation, as shown in Equation (2-13), which is obtained for creep coefficients  $\psi_{\infty} \sim 2$  to 3 and aging coefficient  $\chi \sim 0.8$ .

$$\Delta f_{p\infty} = -(n_0 \sigma_{c\infty} \psi_{\infty} + \varepsilon_{SH\infty} E_p + \Delta f_{pRE\infty}) \quad (2-13)$$

Adapted from  
Neville (1983)

The ability to develop detailed loss models offering theoretically accurate solutions for prestress loss estimation was shown in Equations (2-10) through (2-13). These equations can be used together with a creep model based on the Burgers Model presented above, but coefficients need to be carefully calibrated at the times of interest to use such models properly. These expressions provided guidance for the materials-based loss expression derived in Chapter 5 and the simplified model in Chapter 6.

## **2.7 EXPERIMENTAL RESULTS FROM PREVIOUS RESEARCH**

The outcomes from relevant research were collected during the course of a thorough literature review. Experimental data from concrete shrinkage, creep, and prestress loss research studies, was assembled into three databases, presented in Sections 2.7.1 to 2.7.3. The databases enabled calibration and evaluation of the models introduced in Section 2.6 and further developed in Chapter 5. For each database, a filtering process was conducted to ensure that models would only be evaluated on the basis of relevant data. These databases will serve as a useful tool for the evaluation of creep, shrinkage, and prestress loss estimation (for pretensioned members) methods in this study and in future research efforts.

### **2.7.1 Shrinkage Database (expanded from Bažant and Li (2008))**

An existing database (Bažant and Li 2008) containing 490 shrinkage test results was used as the basis for calibration of the shrinkage model proposed in Chapter 5 of this study. The shrinkage data was expanded with 154 specimens found in more recent

literature, bringing the total collection database for the study of shrinkage to 644 specimens.

An evaluation database was generated with the objectives of this study in mind; specimens complying with the criteria shown in Table 2-4 were included. The filtering criteria used in this study were selected to eliminate the *specimens for which critical data could not be discovered*. The data necessary to calibrate the shrinkage model described previously includes: ultimate shrinkage strains, relative humidity, and modulus of elasticity. Furthermore, the filtering process provided assurance that the experimental data was representative of the conditions expected in pretensioned bridge girders.

**Table 2-4: Filtering Criteria for Shrinkage Evaluation Database**

Shrinkage Collection Database		644 tests
Filtering	Information to interpolate Modulus of Elasticity at 28 days not provided	-338
	Relative humidity above 95%	-68
	Monitoring time less than the time at which final shrinkage is estimated to occur (Table 2-5)	-177
Evaluation Database		61

The modulus of elasticity was considered at a standard age of 28 days. A linear interpolation with respect to the logarithm of the age was used for studies in which the modulus of elasticity was provided at ages less than and greater than 28 days, and these specimens were still included. Specimens conditioned in high relative humidity (greater than 95 percent) were filtered out.

Specimens conditioned and monitored for an insufficient amount of time were eliminated through the final filtering criteria. The criteria for which the final conditions were considered representative of ultimate are summarized with respect to the volume-to-surface area ratio ( $v/s$ ) in Table 2-5; this criterion is a product of the time-development factor calibration in Section 5.4.1. As can be observed in Figure 2-7, the evaluation database only contains specimens with volume-to-surface ratios of up to 1.5 inches. Specimens with larger volume-to-surface ratios are not included in the evaluation database, because the studies available in large specimens do not provide data during long conditioning periods, of seven years or more, required for ultimate conditions in larger specimens. Some of the considered studies included long monitoring periods (more than seven years), but only in specimens with volume-to-surface ratio smaller than 2 in.

**Table 2-5: Criteria for filtering specimens according to monitoring period (see Section 5.3.1)**

volume-to-surface ratio ( $v/s$ )	Filtering criteria for final time ( $t_f \geq$ )
0.75 in.	1 year
1.0 in.	2 year
1.5 in.	4 year
2.0 in.	7 year
2.5 in.	10 year
3.0 in.	15 year
4.0 in	30 year
5.0 in	40 year
6.0 in	60 year

The Shrinkage Evaluation Database contains the specimens meeting the qualifications outlined above. The main parameters of the specimens included are

presented in Figure 2-7, Figure 2-8, and Figure 2-9, including relative humidity, concrete strength, and volume-to-surface ratio. The majority of the specimens were conditioned in an ambient relative humidity of between 60 and 70 percent. While the majority of the specimens had a concrete strength between 4 and 8 ksi, there are several high strength concretes (greater than 8 ksi) represented in the database.

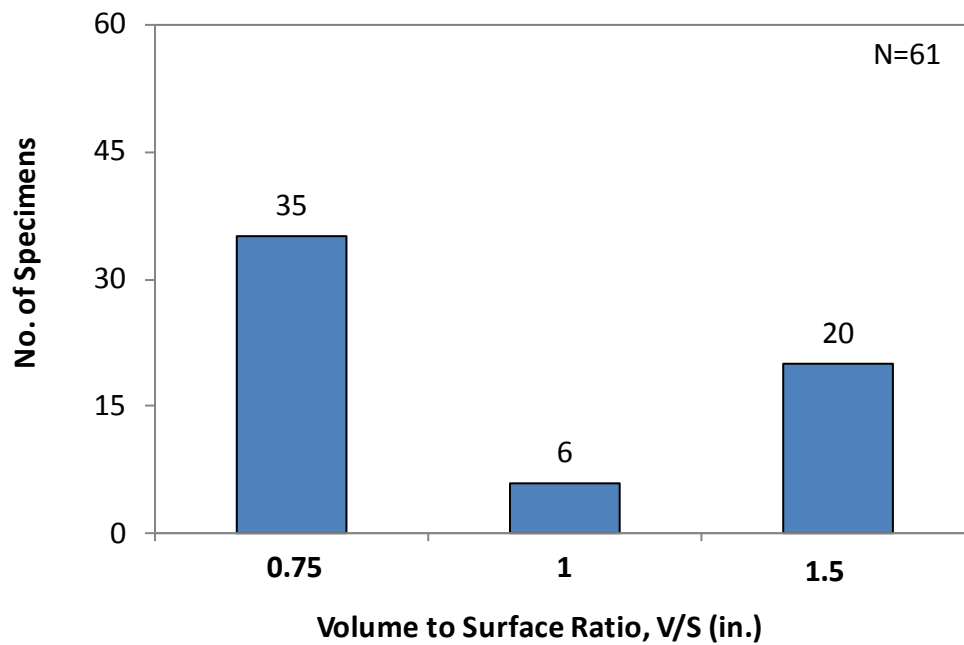


**Figure 2-7: Volume-to-Surface ratio for shrinkage specimens**

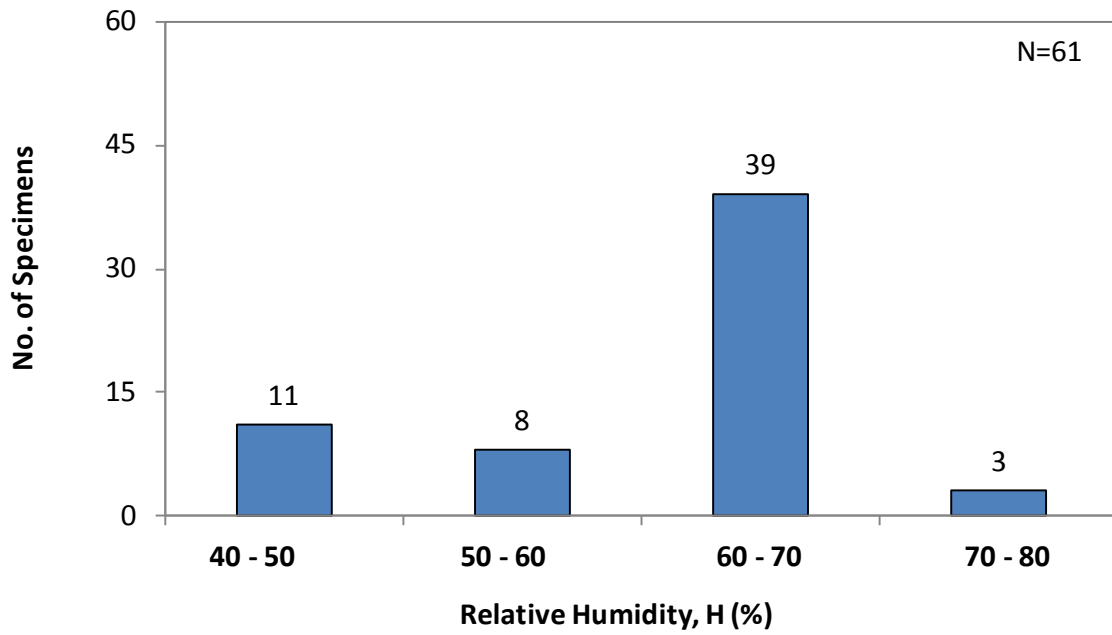


**Figure 2-8: Conditioning Relative Humidity for Shrinkage Specimens**

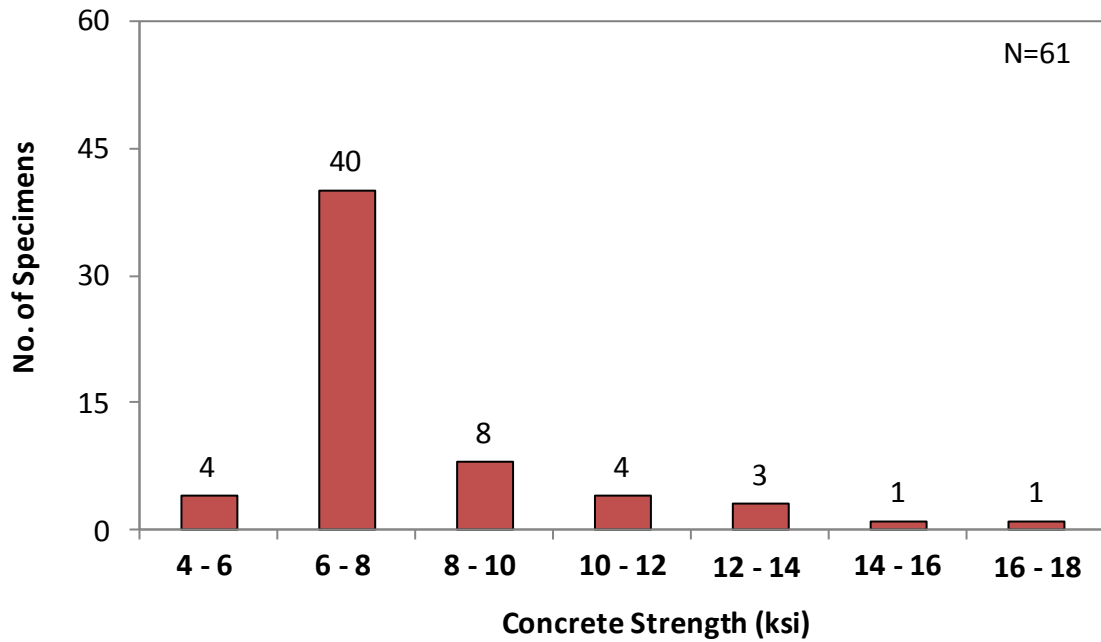


**Figure 2-9: Concrete Strength for Shrinkage Specimens**

### 2.7.2 Creep Database (Bažant and Li 2008)

An existing database (Bažant and Li 2008) of 621 creep test results was used to calibrate the creep model proposed in Chapter 5 of this study. The main objective of the filtering process was to provide assurance that the evaluated specimens were representative of the conditions expected in pretensioned bridge girders. In this sense, the main condition that separates a pretensioned girder from other types of structures is the age at loading, typically between 1 and 3 days for pretensioned girders. The age at loading is especially relevant in concrete loaded at ages when cement hydration is still occurring at a high rate, because the short-term creep is highly dependent on the degree of hydration. In addition to filtering according to loading age, specimens stored in high relative humidity (larger than 95%) climates were also filtered out.

Similar to other databases in this study, specimens were filtered to eliminate those *in which critical data was missing*. This critical data included: the loading age and strain at loading, and the history of compliance versus age. As expected, the history of compliance is contained for all the specimens, but the compliance at loading is missing for some specimens, and is reported as zero for other specimens, which needed to be filtered out. Further study could develop a method to calibrate the creep model without requiring the use of compliance at loading, but it is out of the scope of this dissertation. Filtering of the creep collection database is presented in Table 2-6.



**Table 2-6: Criteria considered for Creep Database filtering**

Creep Collection Database		621 tests
Filtering	Specimens loaded at age of more than 3 days	-590 tests
	RH>95%	-4 tests
	Strain at loading not discovered	-13 tests
Evaluation Database		14 tests

The Creep Evaluation Database contains the specimens that met the qualifications outlined above. This Creep Evaluation Database is not statistically significant; therefore future research is needed to achieve a statistically significant number of tests with which the models can be recalibrated. The concrete strength and the stress-to-strength ratio at loading for such specimens are presented in Figure 2-10 and Figure 2-11. The majority of the specimens were loaded with a stress to strength ratio of between 0.3 and 0.4, as shown in Figure 2-10. While this ratio is lower than typical pretensioned applications, specimens under these lower stress ranges will still adequately represent the general creep behavior. All of the concrete strengths of the specimens fell between 4 and 10 ksi, as shown in Figure 2-11, which represents well the general range of concrete strengths in pretensioned members.

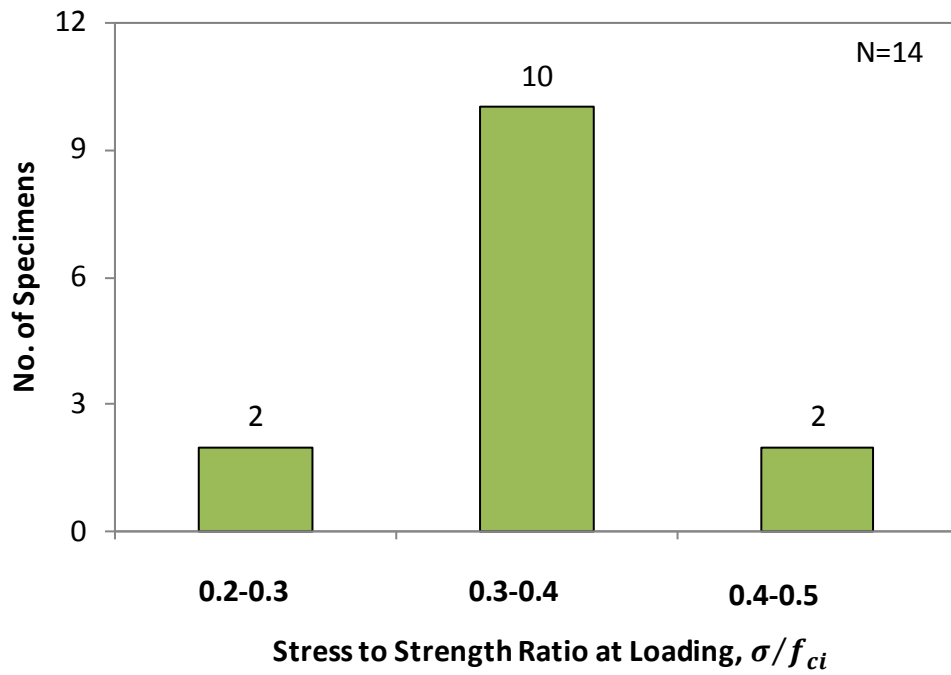


**Figure 2-10: Stress-to-Strength Ratio at Loading of Creep Specimens**

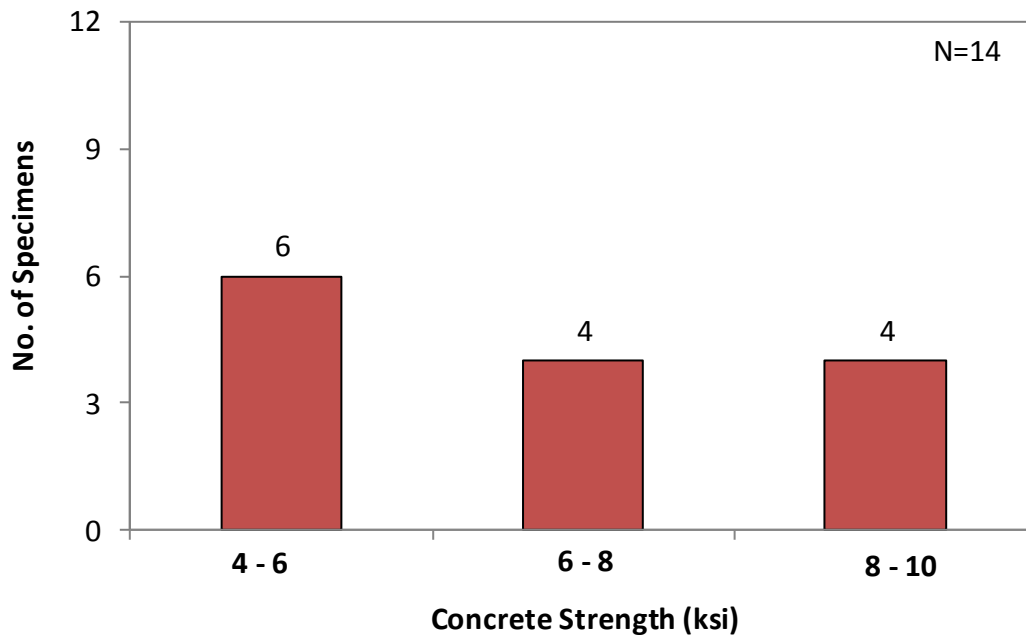


**Figure 2-11: Concrete Strength of Creep Specimens**

### **2.7.3 Prestress Losses Database (on the basis of Garber, et al. (2013))**

A database containing prestress loss studies of pretensioned girders was developed and expanded on the basis of the UTPS-Loss Database compiled during TxDOT Project 0-6374 (Garber, et al. 2013). The UTPS-Loss Collection Database includes 32 studies published between 1970 and 2013, and prestress loss data for 280 specimens investigated in these studies (including 30 specimens reported by Garber, et al. (2013)). The prestress loss was primarily measured through the use of either service load testing or internal strain measurements. The specimens and the corresponding prestress losses represented a broad range of materials (including high strength concrete) and girder geometries. All of the specimens contained in this database are pretensioned girders.

In some of the studies, prestress losses occurring in the specimens were explicitly reported; these results being verified through the use of other data reported in the study. In other studies, losses were calculated based on other necessary data. These prestress losses were assembled within the collection database.

#### ***2.7.3.1 UTPS-Loss Strain Evaluation Database Filtering Process***

Several specimens were eliminated from the Collection Database to generate the UTPS-Loss Strain Evaluation Database, as shown in Table 2-7. During the filtering process, specimens were eliminated in which strain related losses were not reported. Additionally, specimens not representative of field conditions were eliminated.

The filtering process ensured that the database specimens serve as an accurate representation of the strain-related losses in pretensioned girders used in modern bridge applications. The accuracy of the prestress loss calculated from or reported within the data of the studies was further evaluated using the evaluation criteria found in Table 2-8.

All of the losses for specimens remaining after the first two filtering criteria were deemed accurate through this final evaluation.

As mentioned, the purpose of the filtering process was to eliminate specimens with inaccurate or incomplete reported prestress losses, and to ensure that the specimens within the UTPS-Loss Strain Evaluation Database possessed scale and detailing representative of pretensioned simply supported bridge girders. Each of the specimens in the UTPS-Loss Strain Evaluation Database is accompanied by sufficient detail to accurately estimate the prestress loss and compare it to a reported/calculated value. Two parameters (refer to Table 2-7) were examined to make this determination:

- *Specimen Height (h)*: The smallest section commonly used by TxDOT is limited to a height of 20 inches. All specimens under 20 inches in depth were therefore eliminated from Evaluation Database.
- *Support Conditions*: The Evaluation Database was for simply-supported girders, therefore all continuous spans and specimens with fixed end conditions were eliminated.

The Evaluation Database contains the specimens from the Collection Database that met the height and support condition qualifications outlined above. The origin of the reference, geometry of the specimens, concrete materials used, and amount of prestressing in the specimens included in the Evaluation Database will be briefly discussed in the following sections.

**Table 2-7: Filtering Criteria to Develop UTPS-Loss Strain Evaluation Database**

UTPS-Loss Collection Database (TxDOT Project 6374)		280 tests
Filtering	Strain monitoring not reported	- 120 tests
	Girder not representative of this study +Height less than 20 inches	- 58 tests
	Support conditions are not representative of this study +indeterminate support conditions +continuous span	-7 test
	+Critical information not reported	-0 test
UTPS-Loss Strain Evaluation Database		95 tests

**Table 2-8: Properties investigated to determine accuracy of prestress loss estimate reported by each study**

Property		Factor (relative relevance of the parameters)
$w_c$	Unit weight of concrete assumed	1
$w_{c,d}$	Unit weight of deck concrete assumed	1
$E_p$	Strand modulus assumed to be 28,500-ksi	1
$f'_{cd}$	Compressive strength of deck concrete assumed to be 4-ksi	2
$t_i$	Time of release assumed to be 0.75-days	1
$t_d$	Time of deck placement assumed to be 120-days	1
$E_{ci}$	Concrete modulus at release calculated using measured or specified $f'_c$	3
$f_{pi}$	Strand stress prior to transfer assumed to be 202.5-ksi	1

### 2.7.3.2 UTPS-Loss Strain Evaluation Database Characteristics

The UTPS-Loss Strain Evaluation Database was used heavily in evaluation of the past, present and future prestress loss provisions reviewed and proposed in this report. The methods used to measure the prestress loss in the specimens contained in the Evaluation Database are shown in Figure 2-12. The measurement of strains in the studies was conducted through the use of vibrating wire gages, mechanical gages, or fiber-optic gages.

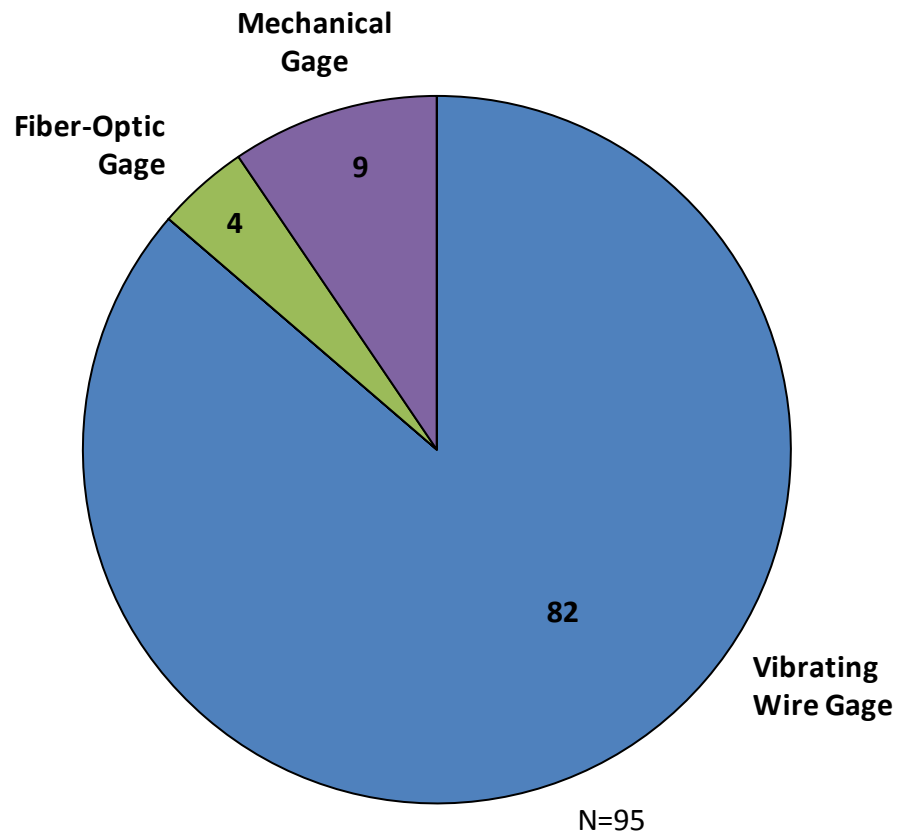
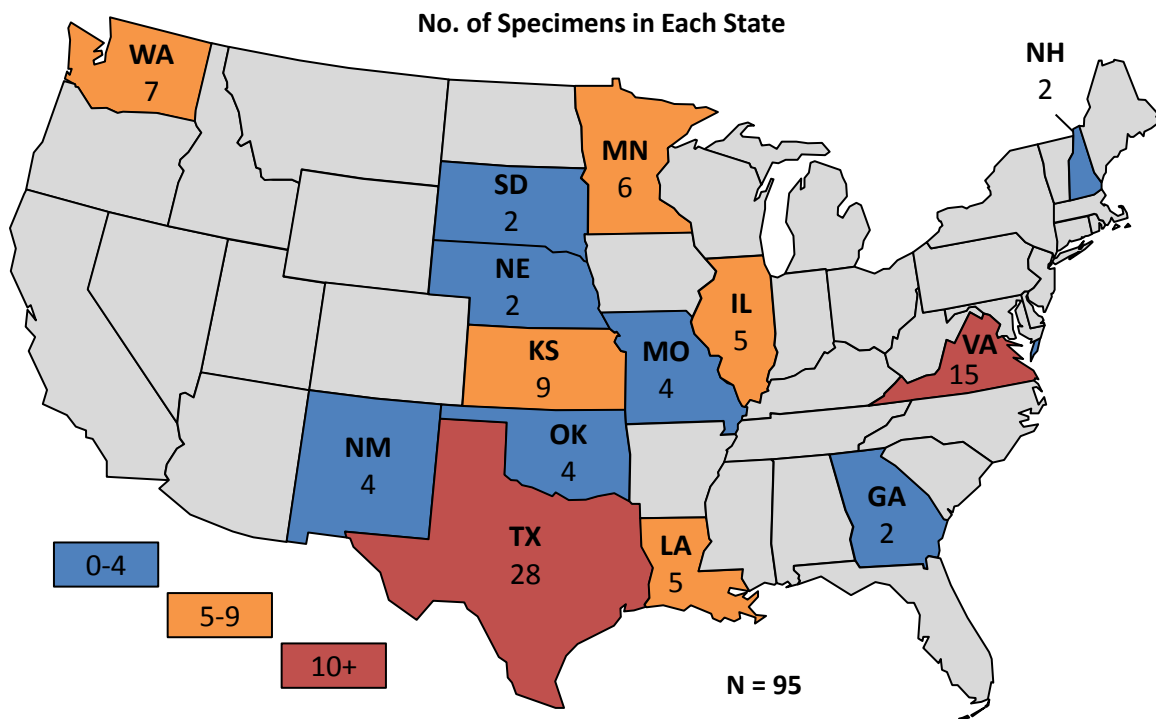
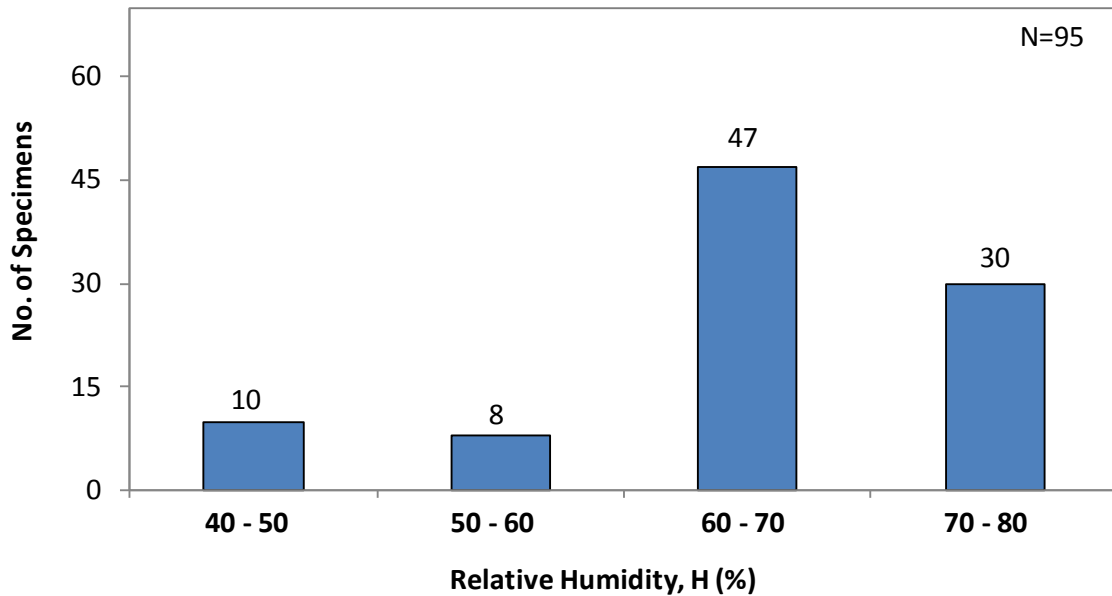


Figure 2-12: Method used for measuring loss

The fabrication and conditioning locations of the specimens are presented in Figure 2-13. Although the majority of the specimens are from Texas and Virginia, many other states are also represented, ensuring that various climates are captured by the database. The average relative humidity reported for the conditioning location is shown in Figure 2-14. It should be noted that most of Texas, and the entire country for that matter, has an average ambient relative humidity between 60 and 75 percent (Figure 5.4.2.3.3-1 - AASHTO 2012). The climatic exposure of a majority of the specimens within the Evaluation Database is consistent with that generalization.



**Figure 2-13: Location where specimens were fabricated/conditioned**



**Figure 2-14: Average reported relative humidity for location where specimens were conditioned**

A variety of different specimen geometries are captured by the specimens included in the Evaluation Database. Variation of the specimen length and height are presented in Figure 2-15. The majority of the specimens are 25 to 100 feet in length and 20 to 60 inches in height, although longer spans and deeper cross-sections are also present.

The gross cross-sectional area and the volume-to-surface area ratio of the specimens are presented in Figure 2-16. It should be noted that the majority of the specimens have a volume-to-surface area ratio of between three and four; nearly all typical cross-sections have a volume-to-surface ratio within this range.



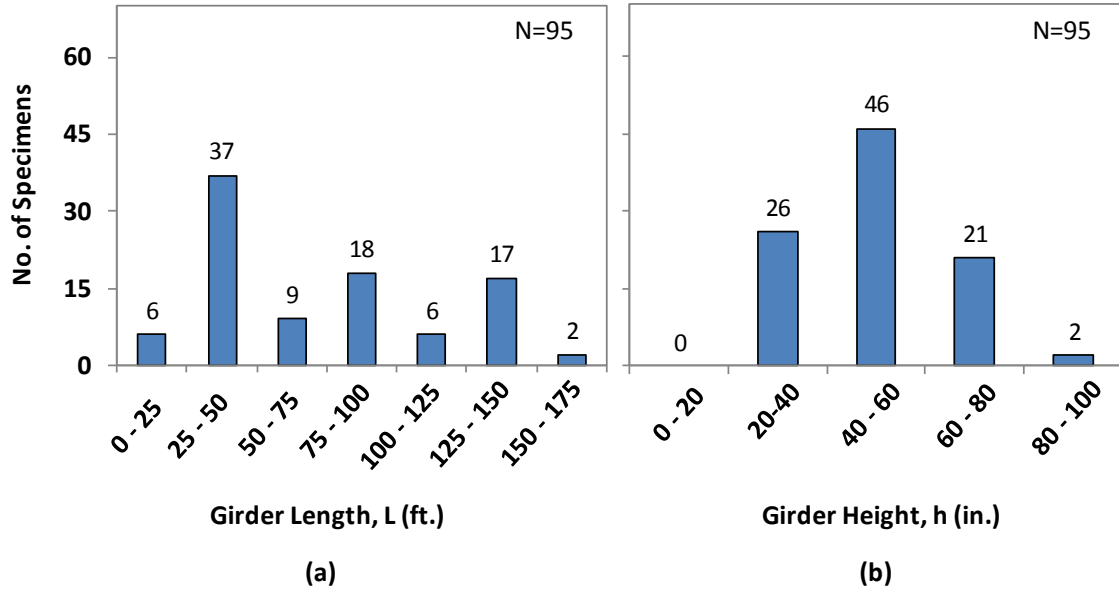


Figure 2-15: (a) Girder length and (b) girder height of specimens

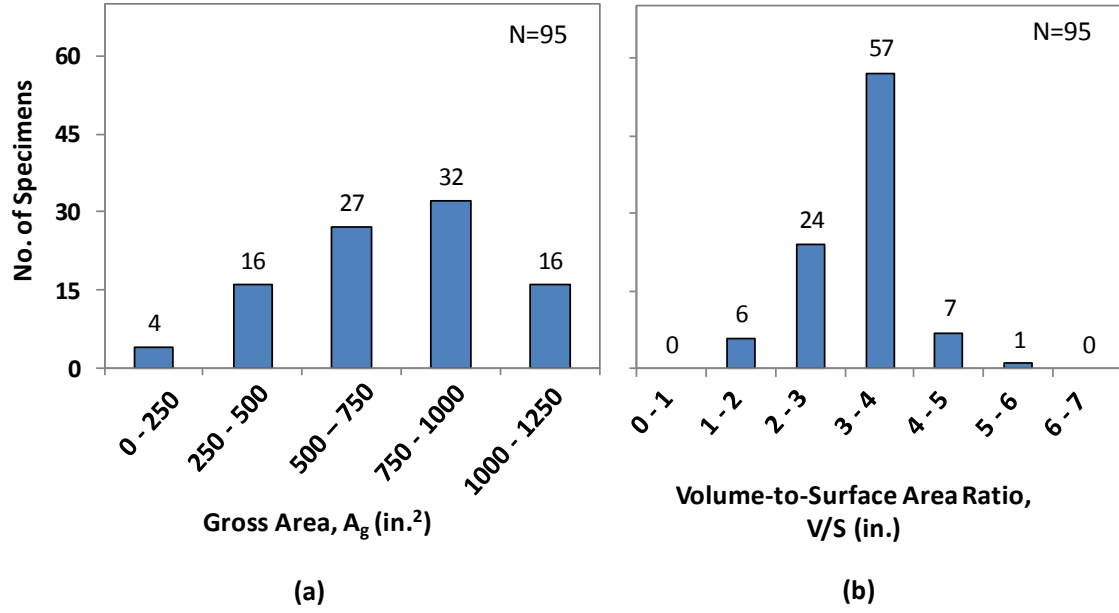
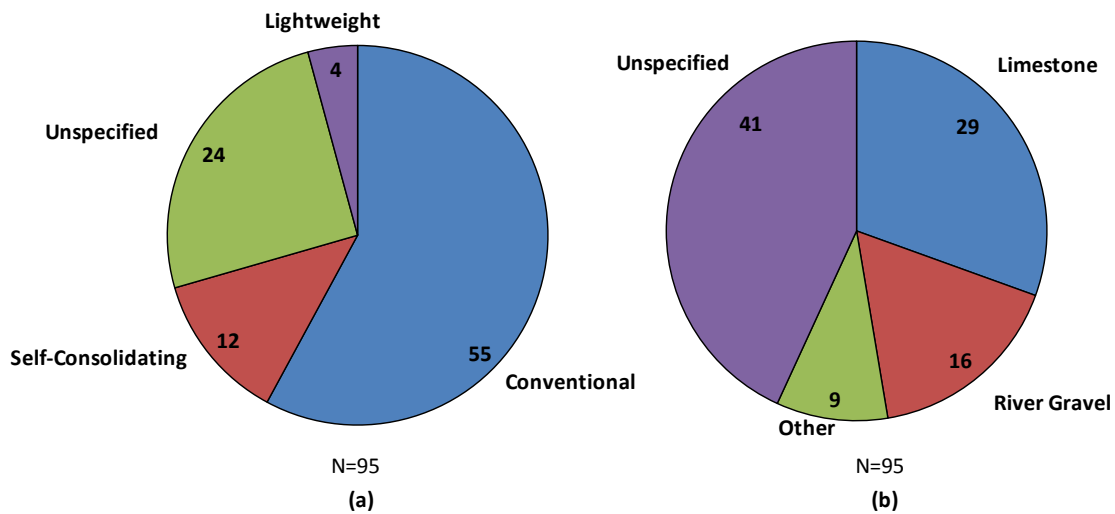


Figure 2-16: (a) Gross area and (b) volume-to-surface area ratio of specimens

A variety of concrete mixtures with different types of aggregates are included in the Evaluation Database, as shown in Figure 2-17. The majority of the specimens were fabricated using conventional concrete, although some specimens were fabricated using self-consolidating concrete. The two main types of coarse aggregate used in common practice, river gravel and limestone; make up the majority of the specimens in the database.

The Evaluation Database contains a wide variety of concrete strengths, as shown in Figure 2-18. This wide variety for both release and ultimate strengths helps to ensure that the loss equations are properly calibrated for all commonly used concrete strengths. The concrete design is typically chosen so that the concrete will reach the desired release strength less than a day after casting. This release strength is typically around 6 ksi and results in a concrete mix with a 28 day strength of between 10 and 12 ksi. These typical values make up a large portion of the specimens contained in the database.



**Figure 2-17: (a) Type of concrete mixture and (b) type of aggregate used to construct specimens**

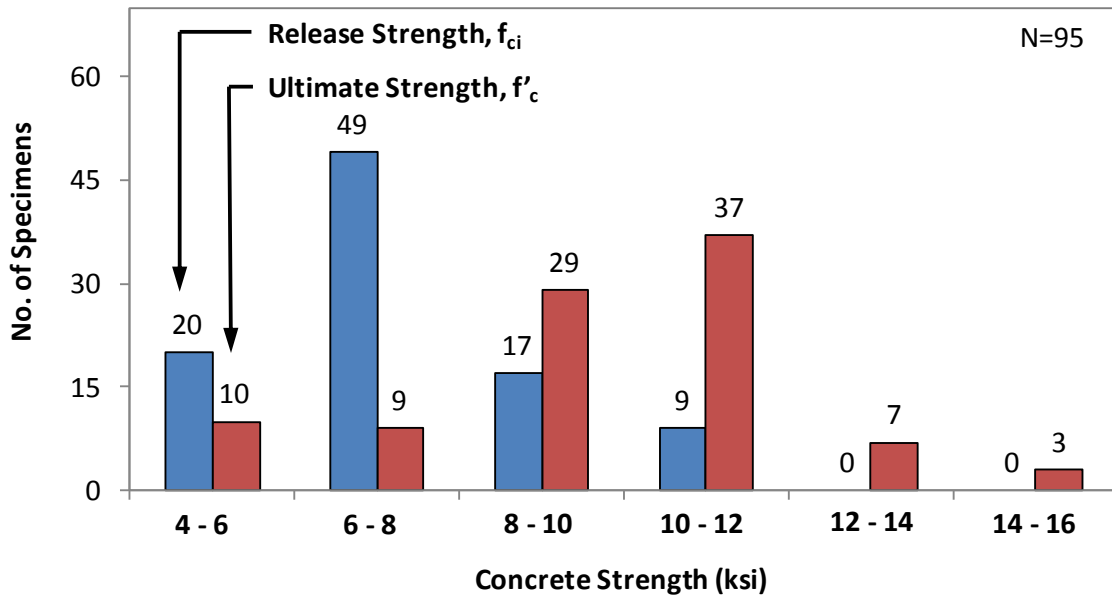


**Figure 2-18: Release strength and ultimate strength of concrete used to construct specimens**

The prestressed reinforcement ratios for the specimens contained in the Evaluation Database are shown in Figure 2-19. It is not practical to have a prestress ratio higher than 1.5 percent, as these higher ratios lead to compressive stress concerns. This practical limit is reflected in the specimens contained in the Evaluation Database.

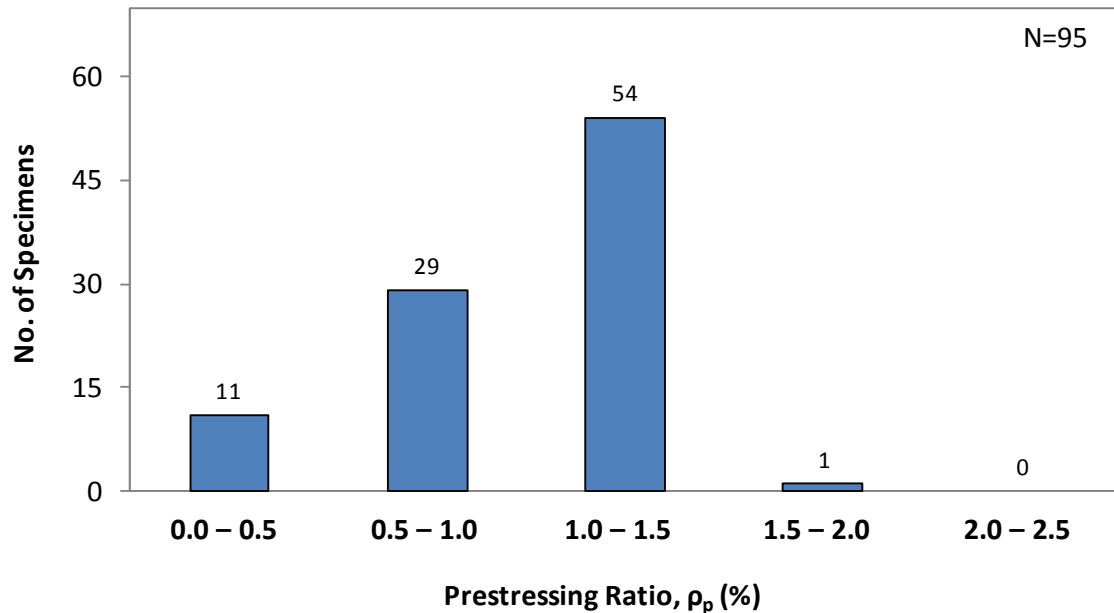


**Figure 2-19: Prestressing ratio of specimens**

## 2.8 SUMMARY

A literature review has been presented in this chapter to describe the current state-of-knowledge on creep, shrinkage and prestress losses in pretensioned girders and the key conclusions of the main papers that lead to commonly accepted theories are presented. The main mechanisms involved in the development of prestress losses were presented, including the effect of the pore water pressure on the development of shrinkage, the migration of water from high pressure regions to free pores during short-term creep, and the breakage of C-S-H links as a main reason for the long-term creep.

Finally, three collection databases that are a compilation of experimentally measured shrinkage strain, creep strain, and prestress losses were also presented. The specimens from the collection databases were filtered in order to obtain evaluation

databases, which included specimens that are representative of the conditions expected in pretensioned bridge girders.

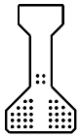
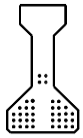
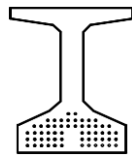
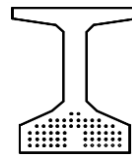
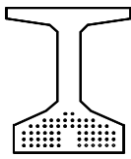
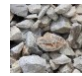




# CHAPTER 3

## Experimental Program

### 3.1 OVERVIEW

Eighteen full-scale prestressed concrete beams, were fabricated, instrumented and conditioned to enable comprehensive assessment of strain-related prestress losses. These eighteen beams are a subset of the beams investigated during TxDOT Project 0-6374 (Garber, et al. 2013). The scope of the experimental program is summarized in Table 3-1. The details of this experimental program are presented in this chapter, including the development of specimens, conditioning of specimens, and the assessment of prestress losses via internal strain monitoring. The results of this experimental program are presented in Chapter 4 and are used to calibrate the prestress loss estimation method proposed in Chapter 6.

**Table 3-1: Experimental Program Matrix**

	Series I	Series II	Series III	Series IV-CC	Series IV-SCC
Cross-section & # of ½” strands	Type C  38 strands	Type C  38 strands	Tx46  58 strands	Tx46  56 strands	Tx46  56 strands
Conc. Type	CC	CC	CC	CC	SCC
Coarse Aggregate Type	Limestone 	River Gravel 	Limestone 	River Gravel 	River Gravel 
Storage Location	Austin (2) Lubbock (2)	Austin (2) Lubbock (2)	Austin (2) Lubbock (2)	Austin(3)	Austin (3)
Final Age (Conditioning)	960 days	940 days	690 days	250 days	250 days

The specimens were representative of a fairly broad range of factors that most affect prestress losses, including (1) type of concrete (conventional or self-consolidating), (2) type of coarse aggregate (limestone or river gravel), (3) specimen geometry (Type C or Tx46 beams), and (4) climate (relative humidity of 51% or 62%). The specimens were conditioned for periods ranging from 230 to 980 days (an average of 660 days) at two storage locations in Texas (Austin and Lubbock). The long-term loss of prestress in each specimen was assessed through the use of internal strain monitoring.

### **3.2 DEVELOPMENT OF BEAM SPECIMENS**

The specimens were designed, fabricated and conditioned to be representative of typical construction practices and field conditions in Texas. Two different mid-size cross-section types commonly used in Texas (40 in. to 46 in. depth) were selected. The prestressing steel was designed in order to generate high initial compressive stresses, on the order of  $0.65 f'_{ci,design}$ , to maximize the potential for prestress losses.

Specimens were fabricated at multiple precast plants to assess the influence of plant-specific concrete mix designs and constituents. Overall, the main differences in the concrete mix between plants were the coarse aggregate type (river gravel versus limestone) and the type of concrete mix (conventional versus self-consolidating). The conditioning of the specimens was conducted in Austin (average relative humidity of 62 percent and temperature of 71°F) and Lubbock (average relative humidity of 51 percent and average temperature of 62°F).

#### **3.2.1 Design**

Type C and Tx46 cross-sections were selected for the experimental program. Both cross-sections are broadly used, and can be referred to as mid-size when considering other TxDOT sections, as shown in Figure 3-1. The specimen length (45.5 ft.) was selected through consideration of the test objectives and the practicalities of girder transportation and handling. It is important to avoid regions with disturbed stress fields (e.g. within the strand transfer length) to ensure that plane sections will remain plane and that the concrete and strand strains will indeed be compatible. The specimen length (45.5

ft.) was at least an order of magnitude longer than the strand transfer length in this study, ensuring that the gages (located at midspan) were not placed in a region with a disturbed stress field. While the use of long beams was necessary to ensure representative specimens, the use of even larger beams (more than 50 ft. long or 50 kip weight) was avoided because it would have complicated the operations considerably.

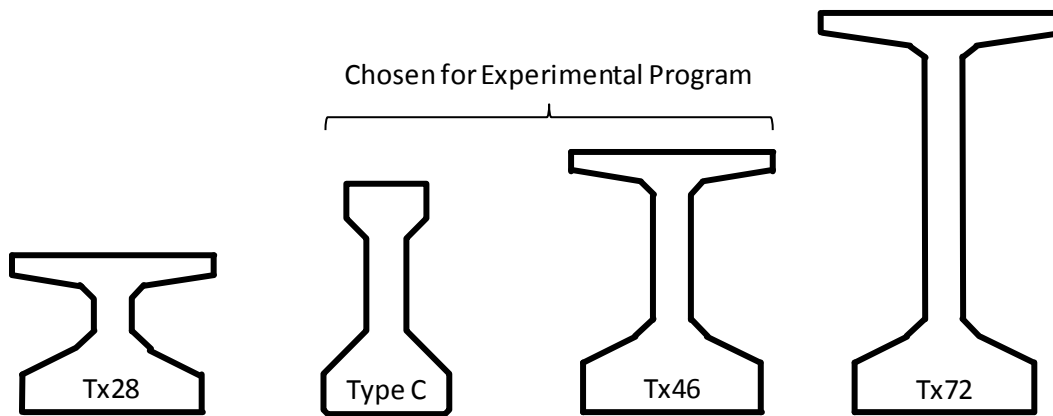


**Figure 3-1: Comparison of specimens and scale of Tx girders**

The main design parameters for each of the series of specimens are summarized in Table 3-2. An initial stress in the strands of 202.5 ksi ( $0.75f_{pu}$ ) is typical in the prestressing industry, and it was also used during the design of the specimens. The prestressed reinforcement for specimens within all series was proportioned and configured to obtain a uniform stress of approximately  $0.65f'_{ci,design}$  along the bottom flange. The Tx46 section is slightly larger than the Type C section – as indicated by the larger gross cross-sectional area ( $A_g$ ) and moment of inertia ( $I_g$ ) – therefore, a larger amount of prestressing steel was required in the Tx46 specimens to maintain a consistent bottom-fiber compressive stress across all series.

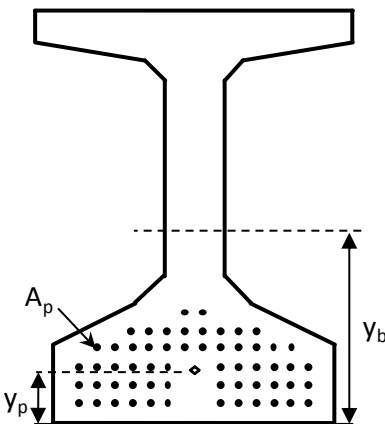
An approximately uniform stress condition was maintained along the length of each specimen through the use of harping, as shown in Figure 3-2 and Figure 3-3. A minor amount (2 bars of 0.5 in. diameter, i.e. 2-#4) of mild reinforcement was placed within the top flange to control cracking due to unanticipated tensile stress demands.



**Table 3-2: Design parameters for specimens of each series**

Series (# of Specimens)	$f'_{ci-design}$	$A_p$ ( $in^2$ )	$y_p$ ( $in$ )	Beam Type	$y_b$ ( $in.$ )	$A_g$ ( $in^2$ )	$I_g$ ( $in^4$ )	V/S ( $in.$ )
I (4)	6.30 ksi	5.81	6.63	C	17.1	495	82600	3.96
II (4)	6.30 ksi	5.81	6.63					
III (4)	6.30 ksi	8.87	6.43	Tx46	20.1	761	198100	3.86
IV-SCC (3)	6.05 ksi	8.57	6.64					
IV-CC (3)	6.05 ksi	8.57	6.64					



$A_p$ : Total area of strands

$y_p$ : Centroid of strands at midspan section

$y_b$ : Height of the centroid of gross section

$A_g$ : Gross area

$I_g$ : Moment of inertia of gross area

V/S: Ratio of volume to surface

$d_p$ : Strand diameter (0.5 in.)

$f_{p,i}$ : Initial strand stress (202.5 ksi)

1

<sup>1</sup> For clarity non-prestressed reinforcement is not shown

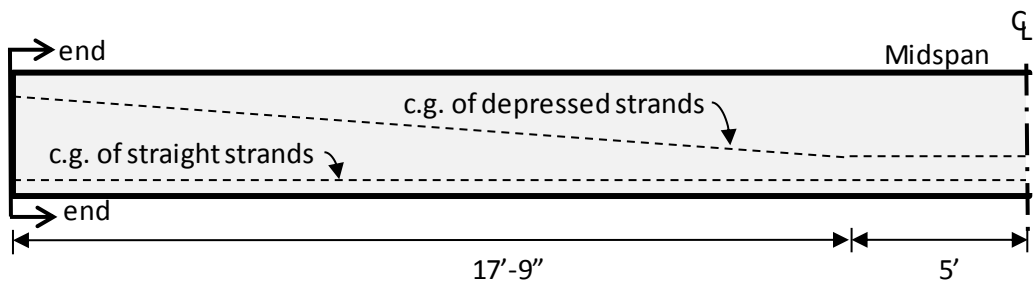


**Figure 3-2: Longitudinal elevation of specimens**

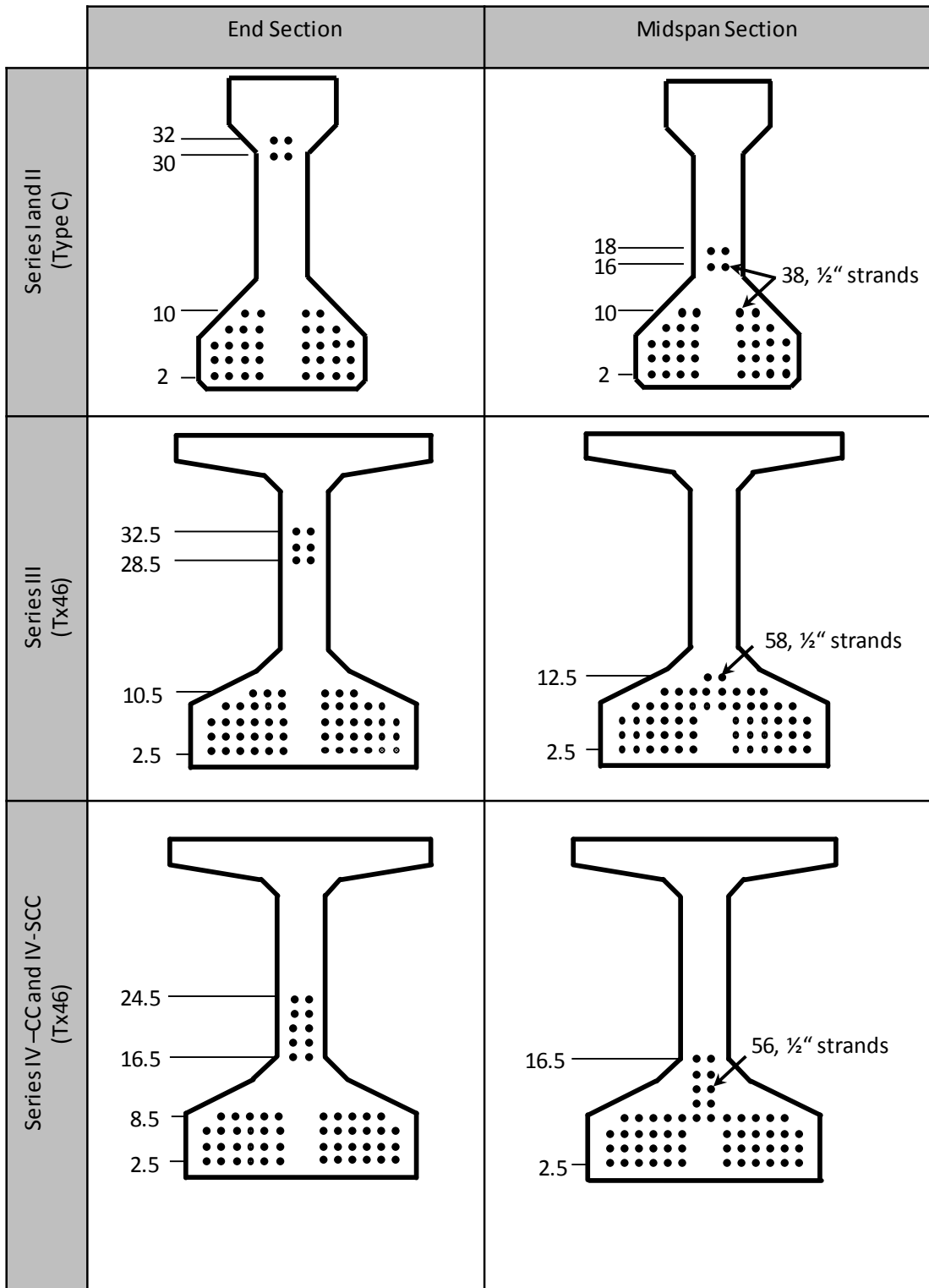


**Figure 3-3: Prestressing strand layout (dimensions are offsets from bottom of girder and measured in inches)**

### 3.2.2 Fabrication

Specimens were obtained from multiple fabrication plants to assess the influence of plant-specific materials and techniques on the development of prestress loss. The geographic location of each fabricator is shown in Figure 3-4. The most relevant details of each fabricator, including coarse aggregate type and average local humidity, are presented in Table 3.3. The concrete mixtures utilized by the fabricator for each of the series are presented in Table 3-4.

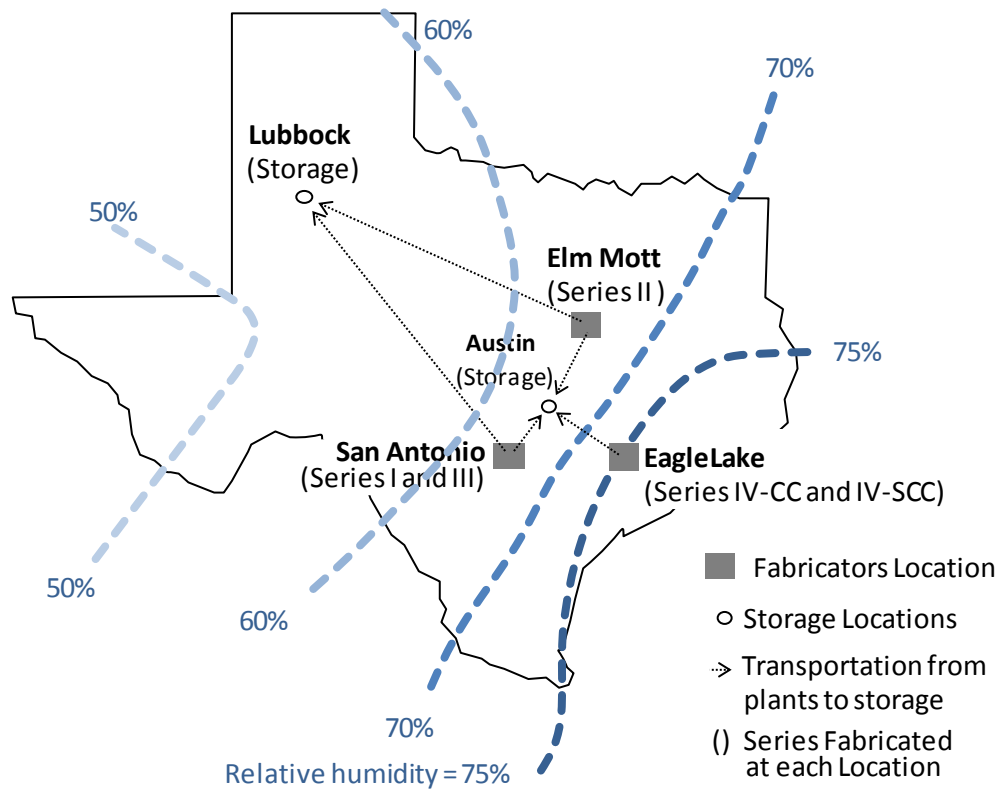


**Figure 3-4: Fabrication and storage locations**

**Table 3-3: Fabricator information**

Fabricator	Series	Location	Coarse Aggregate	Concrete Type	Average Humidity at Plant Location*
<i>A</i>	I and III	San Antonio	Limestone	Conventional	65%
<i>B</i>	II	Elm Mott	River Gravel	Conventional	65%
<i>C</i>	I V	Eagle Lake	River Gravel	Conventional and SCC	75%

\*Based on Humidity map in AASHTO 2012

**Table 3-4: Typical concrete mixture proportions**

Material	Units	Quantity per Series					
		I	II	III	IV-CC	IV-SCC	
Type III Portland Cement	lb/cy	540	530	660	600	700	
Fly Ash	lb/cy	170	170	220	200	230	
Coarse Aggregate	lb/cy	1850	1970	1850	1780	1540	
Coarse Aggregate Type	-	¾" Crushed Limestone	¾" Natural Gravel	¾" Crushed Limestone	½" Natural Gravel	½" Natural Gravel	
Fine Aggregate: Sand	lb/cy	1220	1310	1030	1220	1240	
Water	lb/cy	180	115	180	220	270	
Water/Cement Ratio	-	0.34	0.22	0.27	0.37	0.39	
Admixture	HRWR	oz/cy	33	50	18	36	37
	Set Retardant	oz/cy	31	14	44	12	9
	CNI	oz/cy	-	-	-	144	115
	Viscosity-Modifying	oz/cy	-	-	-	-	15

The fabrication of each specimen was consistent with the practices used on a routine basis at local precast plants. The researchers of TxDOT Project 0-6374 did not intervene during, or impose special requirements on, the fabrication process to ensure that the prestress loss assessments would be representative of typical girders. Relevant aspects of the fabrication process are summarized in Figure 3.5 and 3.6.

After the prestressing strands were loosely located along the length of the pretensioning bed, the hardware required to achieve the harped strand profile was installed, and then the tensioning procedures started. Each fabricator tensioned the prestressing strands to an initial stress of 202.5 ksi on an individual basis as shown in Figure 3.5(b). The reinforcement cages for each specimen were assembled around the fully stressed strands and the internal instrumentation (refer to Section 3.4 for more detail) was installed thereafter. All of the concrete was batched at the precast plant; mix proportions can be found in Table 3-4. Both external and internal vibrators were used during placement of the conventional concrete mixtures to ensure proper consolidation; while only limited internal vibration (and no external vibration) was used for SCC.

The beams were moist cured until the specified release strength ( $f'_{ci}$ ) was attained. At that time, the formwork was removed and the prestressing force was transferred from the pretensioning heads to the specimens. Torch-cutting of the strands at the beam ends and release of the hold-down devices completed transfer of the prestressing force. A counterweight, shown in Figure 3-6 (b), was utilized as necessary to minimize the potential for cracking during prestress transfer (the transfer of forces can occur in sudden increments, then the dynamic effect can crack the top flange of the girders; the counterweight statically reduces the tensile stresses in the top flange, and also its mass helps reducing the dynamic effect of sudden steps in during release). The beams were placed in the precast storage yard until a shipment could be arranged.



**Figure 3-5: Fabrication of a typical specimen: (a) harping of strands, (b) tensioning of strands, (c) placement of mild reinforcement, (d) installation of side forms, (e) concrete placement, (f) internal vibration, (g) external vibration**

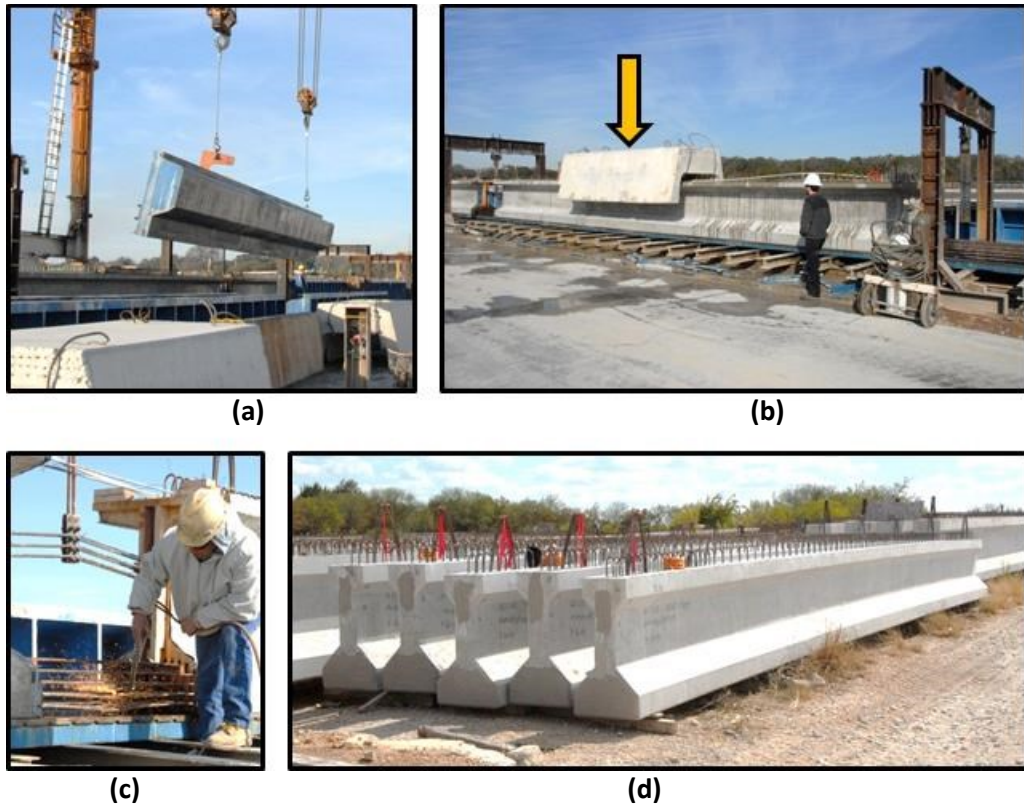


**Figure 3-6: Fabrication of a typical specimen: (a) form removal, (b) counter-weight location, (c) torch-cutting of strands, (d) temporary storage in precast plant**

### 3.3 CONDITIONING OF BEAM SPECIMENS

Previous research (ACI 209R 2008) has indicated that humidity and temperature have a notable effect on the shrinkage and creep of concrete. The study of long-term prestress loss (as driven by creep and shrinkage) in different climatic conditions was therefore an essential consideration for the current effort.

The fabrication of each series was generally completed in less than three days and the specimens were shipped to their conditioning locations within two to three weeks of initial prestress transfer. The two conditioning locations are characterized below. Meteorological data was obtained from the National Climatic Data Center (NOAA 2012).



*Lubbock:* The climate of Lubbock is classified as mild, semiarid. The annual average relative humidity is 71 percent in the morning and 53 percent in the afternoon. Approximately 19 inches of precipitation falls each year, including 10 inches of sleet and snow. Lubbock experiences approximately 160 clear days and 102 partly cloudy days each year under an average wind speed of 12 miles per hour. In comparison to Austin, the semiarid, windy climate of Lubbock was expected to have greater influence on development of the prestress losses.

*Austin:* The climate of Austin is classified as humid subtropical. The annual average relative humidity is 81 percent in the morning and 64 percent in the afternoon. Approximately 34 inches of precipitation falls each year over approximately 136 cloudy days and 114 partly cloudy days. The average annual wind speed in Austin is 8 miles per hour.

Four specimens within Series I through III were evenly split between the two primary storage locations of Austin and Lubbock, shown in Figure 3-7 and Figure 3-8. All of the Series IV-CC and IV-SCC beams were stored in Austin. The locations of conditioning sites are shown in Figure 3-4.



**Figure 3-7: Austin storage site (Series I, II, III and IV)**



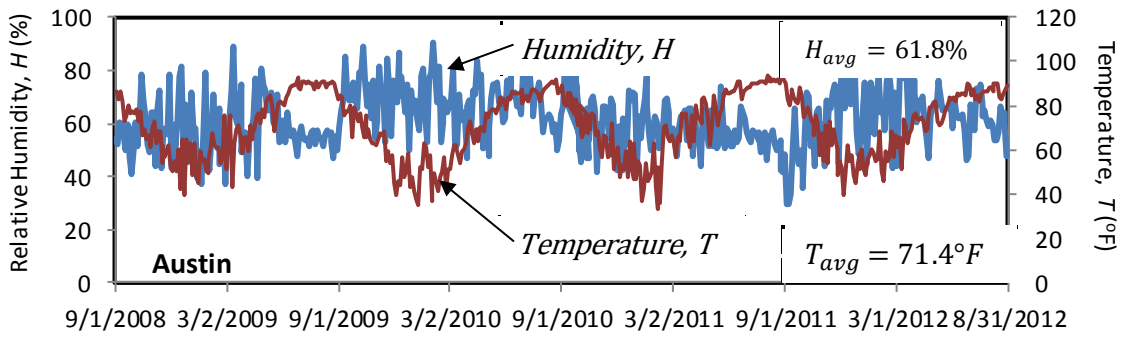
**Figure 3-8: Lubbock conditioning site (Series I, II and III)**

The timeline of the fabrication-conditioning-end of monitoring process for each series is detailed in Table 3-5. During storage, each specimen was supported on both ends, creating a span length of approximately 44 feet. The specimens remained uncovered (fully exposed to the site climate) during the conditioning time and were periodically monitored for changes in strain (as indicative of prestress losses).

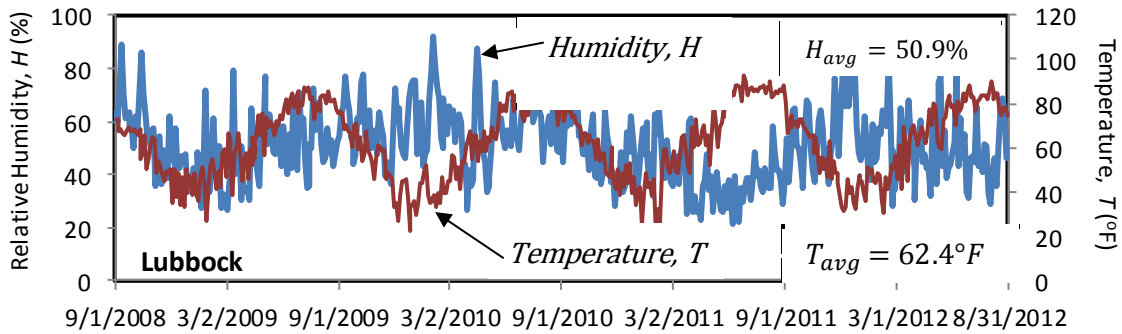
The variation of relative humidity and temperature at each of the storage locations is summarized in Figure 3-9. Despite significant variation of the climatic conditions during the course of TxDOT Project 0-6374 (i.e. Central Texas drought), the average temperature and humidity at each of the conditioning sites was relatively consistent with the historical data referenced above. Specimens stored in Lubbock were exposed to an average relative humidity of approximately 51 percent, while those stored in Austin were exposed to an average relative humidity of approximately 62 percent. The data reported here was taken from the nearest weather stations as reported by the National Climate Data Center.

**Table 3-5: Timeline of beam conditioning**

Series	08	2009	2010	2011	2012
I	Fabrication →				
II					
III					
IV-CC					
IV-SCC					← End of monitoring



(a)



(b)

**Figure 3-9: Record of relative humidity and temperature at (a) Austin, and (b) Lubbock (NOAA 2012)**

### **3.4 ASSESSMENT OF PRESTRESS LOSS VIA INTERNAL STRAIN MONITORING**

The development of prestress loss in the 18 specimens included in this study was monitored through the use of internal strain instrumentation. Concrete strains and temperatures were measured at several points through the depth of each instrumented cross-section and used to calculate the change of strain at the centroid of the prestressing strands. Due to compatibility between the prestressing strands and the surrounding concrete, it was possible to further calculate the loss in prestressing force on the basis of the prestressing strand modulus and area.

The concrete strain and temperature were measured periodically throughout the conditioning of each specimen. Internal concrete strains were monitored through the use of vibrating wire gages (VWGs), which were well suited for the long-term measurements completed during the course of TxDOT Project 0-6374. Gage installation, periodic monitoring and assessment of the prestress losses are examined in the following sections.

#### **3.4.1 Vibrating Wire Gage Installation**

A vibrating wire gage consists of a length of steel wire stretched between two end blocks; the wire is enclosed and free to deform with the movement of the end blocks. When embedded in concrete, the vibrating wire gage can be used to measure concrete strain: the wire in the gage is plucked electromagnetically and the change in the resonant frequency of its response indicates the change in strain of the wire, which is the same as the average strain in the surrounding concrete.

Vibrating wire gages (as opposed to foil strain gages) were chosen because of the long-term stability of their readings and their durability in the highly alkaline environment of hardened concrete. Confidence in the latter of these benefits was provided by a past TxDOT project (Gross and Burns, 2000) involving the measurement of prestress losses; the functionality of vibrating wire gage over the course of a five year period far exceeded that of foil strain gages.

Typical installation of the vibrating wire gages within the TxDOT Project 0-6374 specimens is illustrated in Figure 3-10. Installation of the vibrating wire gages was

completed immediately after the mild reinforcement was fully tied. Three to four gages were installed at three distinct heights within the midspan cross-section and oriented to measure strains along the longitudinal axis of the specimen.

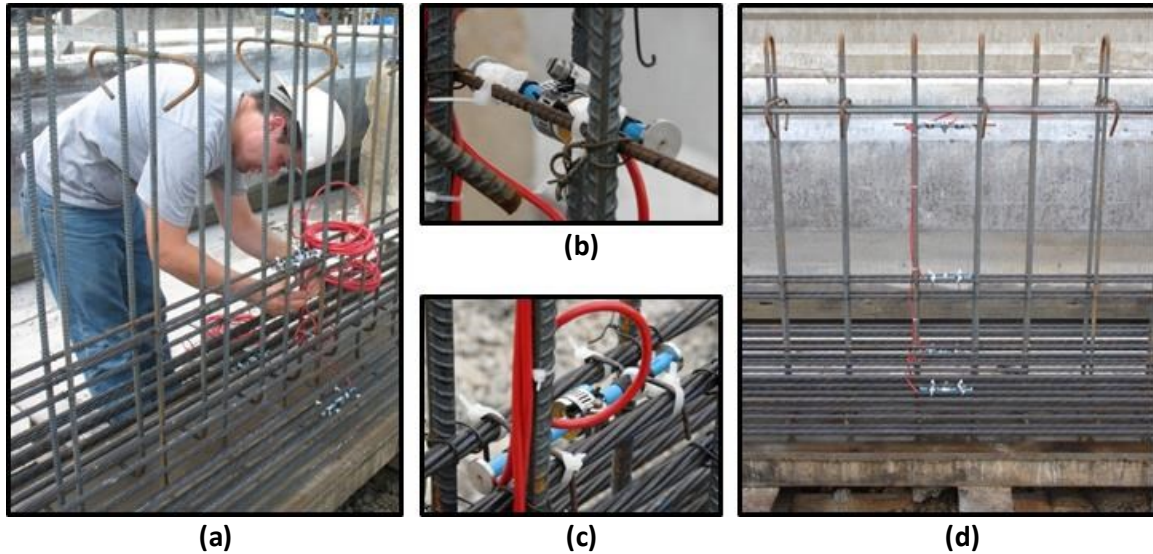


**Figure 3-10: Vibrating wire gage installation: (a) cable routing, (b) gage supported by auxiliary reinforcement, (c) gage supported by a strand, (d) midspan distribution of gages**

The VWG embedment locations for each series of specimens are illustrated in Figure 3-11. All of the gages in each specimen were installed at the midspan cross-section. The midspan section was chosen because it is the most relevant section to estimate prestress losses when conducting stress checks for long term conditions of single supported beams.

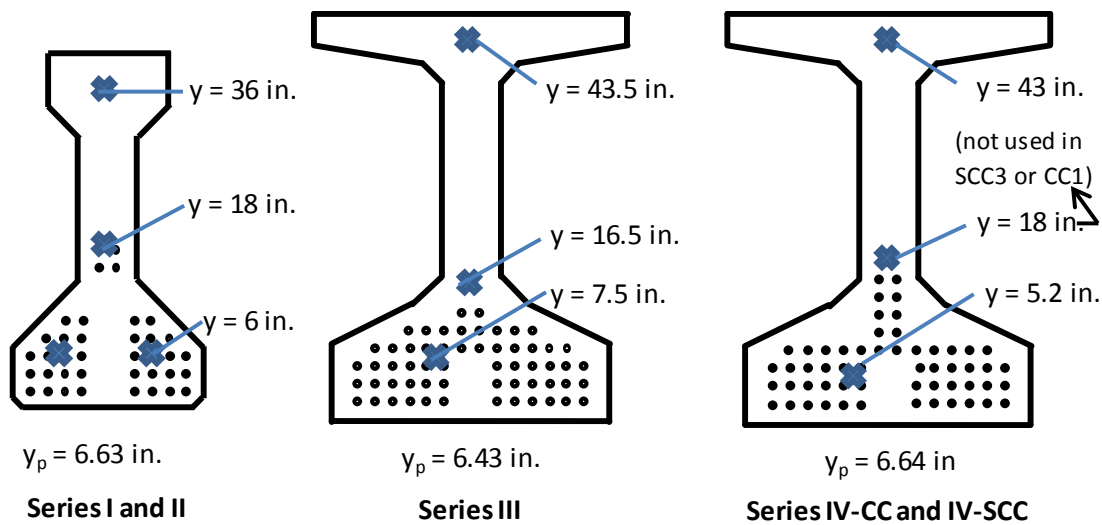


**Figure 3-11: VWG embedment locations (at midspan section)**

### 3.4.2 Periodic Monitoring

The concrete strains were measured before and after prestress transfer (to assess the prestress loss due to elastic shortening) and periodically throughout the conditioning process (to assess long-term prestress losses due to creep and shrinkage). It should be noted that by monitoring the beams in this manner, the total long-term prestress losses, not the individual components of creep and shrinkage, were directly assessed. However, a method to weigh the effect of each of these components (creep and shrinkage) based on the measurements is presented in Chapter 6.

The vibrating wire gage measurements were taken through the use of a handheld reader and/or a remote Data Acquisition System (DAQ). The remote DAQ, fabricated at FSEL, and deployed in Lubbock is shown in Figure 3-12. It consisted of a datalogger, cellular modem and solar power supply. The DAQ was programmed to periodically interrogate the VWGs (approximately once per hour) and store the concrete strains in memory. All of the data recorded by the DAQ was accessible from FSEL via cellular modem.

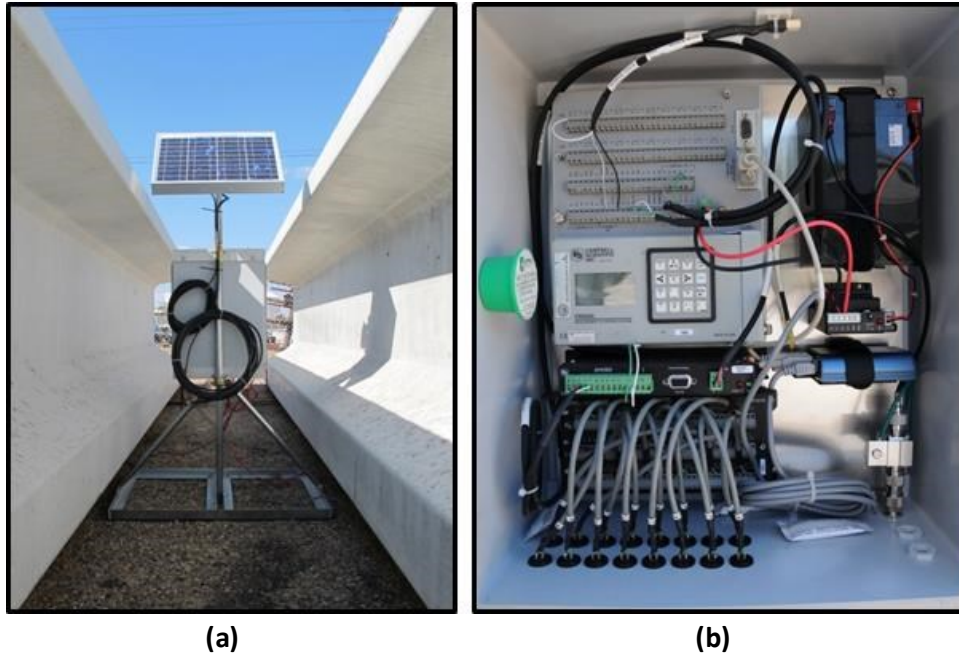


**Figure 3-12: Remote DAQ system: (a) General view and (b) electronic components**

### 3.4.3 Consideration of Strand Relaxation Effects

The strain monitoring technique is incapable of directly capturing the prestress losses due to strand relaxation as the phenomenon leads to a loss of stress without a corresponding proportional change in strain. However, the relaxation causes a decrease in the compressive stress and therefore in the strain; these relaxation-related strains are not directly differentiated from measured creep and shrinkage strains. This limitation was overcome by using Equation (3-1) to estimate the well-known phenomenon of strand relaxation loss ( $\Delta f_{p\_RE}$ ), which accounts for less than 5 percent of total final losses in most cases.

$$\Delta f_{p\_RE} = 2 \cdot \frac{f_{pt}}{30} \left( \frac{f_{pt}}{243 \text{ ksi}} - 0.55 \right) \quad (3-1)$$

*Modified from AASHTO 12 (5.9.5.4.2c-1)*

where:

$f_{pt}$  = stress in the strands after transfer (ksi)

This mentioned relaxation causes a tensile change in the strain at the strand centroid level; this strain change is opposite to strains caused by creep and shrinkage. Therefore, the occurrence of relaxation leads to smaller total strains than those that would have occur if no relaxation would have occur. The estimated relaxation loss is used to correct the measured strains so that the strains (and losses) induced by creep and shrinkage can be identified.

#### **3.4.4 Consideration of Temperature Effects**

There was a dependence observed between temperature and the losses assessed using the strain monitoring approach. These fluctuations reflect a real change in stress that occurs in the strands. When the temperature drops, the concrete and the strands would shorten individually according to their coefficients of thermal expansion. As these two materials are bonded, the concrete restricts the strand from shortening and a stress in the strand develops. This stress is proportional to the difference in coefficients of thermal expansion of the steel as compared to that for the beam. The change in stress is temporary, and for ages at which the losses are, in general, stable the losses appear to be reduced during some months and increased during others. A correction to eliminate this fluctuation (outlined below) was conducted as it was beneficial to assess the losses that permanently affected the stress in the strands.

Correction for the temperature effects consisted of subtracting the thermally induced stress from the calculated stress, as shown in Equations (3-2) through (3-4), using a datum temperature of 95°F (35°C). The normalized strain and strain related loss stress ( $\Delta\varepsilon_{p\_isothermal}$  and  $\Delta f_{p\_ \Delta\varepsilon}$ , respectively) are estimations of the strain and stress that would have been measured at the datum temperature, assuming the thermal expansion of the beam to be approximately equal to the coefficient of thermal expansion of the concrete. Coefficients of thermal expansion of the concrete based on measurements conducted on Series I through III were used for this correction (see Section 4.2.1).



$$\Delta\varepsilon_{p\_total} = \Delta\varepsilon_{p\_VWG} + \Delta T \cdot \alpha_{steel} \quad (3-2)$$

$$\Delta\varepsilon_{p\_isothermal} = \Delta\varepsilon_{p\_total} - \Delta T \cdot \alpha_{beam} \quad (3-3)$$

$$\Delta f_{p\_}\Delta\varepsilon = \Delta\varepsilon_{p\_isothermal} \cdot E_p \quad (3-4)$$

where:

- $\Delta f_{p\_}\Delta\varepsilon$  = Temperature corrected, strain related prestress losses (ksi)
- $\Delta\varepsilon_{p\_VWG}$  = Apparent strain change from VWG strain readings
- $\Delta\varepsilon_{p\_total}$  = Total strain estimated based on VWG strain and temperature readings
- $\Delta\varepsilon_{p\_isothermal}$  = Estimated strain change normalized to the datum temperature
- $E_p$  = Modulus of elasticity of the strand (ksi)
- $\Delta T$  = Temperature change respective to datum temperature (°C)
- $\alpha_{steel}$  = Coefficient of thermal expansion of strand and VWG (12  $\mu\varepsilon/^\circ\text{C}$ )
- $\alpha_{beam}$  = Coefficient of thermal expansion of the beam, approximately equal to that of the concrete ( $\mu\varepsilon/^\circ\text{C}$ ) (Section 4.2.1)

In order to make these corrections, the strains due to change in temperature are assumed to be proportional to the coefficient of thermal expansion of the material and to the change in temperature. These assumptions are not accurate if the temperature profile is nonlinear. In such a case, the strains at each point will depend not only on the change of temperature at that point, but also on the change in temperatures across the section. This being said, the strand stress can be completely defined based on the change of total strains ( $\Delta\varepsilon_{p\_total}$ ), the change in temperature ( $\Delta T$ ) and the relaxation ( $\Delta f_{p\_RE}$ ) of the strand.

### 3.4.5 Prestress Loss Calculation / Analysis

Measurement of the change in concrete strain from the time of prestress transfer to the time of interest provided a means of assessing the total prestress loss in each specimen. The relationship between strain related prestress loss, strand strain and concrete strain (equal to  $\Delta\varepsilon_{p\_VWG}$ ) is summarized in Equations (3-2) to (3-4).

Determination of the strain in the prestressing strands ( $\Delta$  ) is illustrated in Figure 3-13.

With the VWGs distributed through the depth of the midspan cross-section, a linear strain profile could be developed and the longitudinal strain at the location of interest (i.e. the centroid of the prestressing force) could be determined by linear interpolation or extrapolation. Using linear methods to find the strain at the location of interest was appropriate as plane sections remained plane on the mid-span section in the specimens; measured strains were in agreement with this tenet of beam theory. Moreover, the linearity of the strain distribution can be considered as a verification of the consistency of measured strains (Gamble 1970). The strain-related prestress loss was then calculated as the product of the concrete strain at the centroid of the prestressing strand times the modulus of elasticity of the prestressing strand; as done in Equation (3-4). The change in the measured concrete strains was determined by comparing the measured strain at the time of interest to the measurement taken just before prestress transfer.

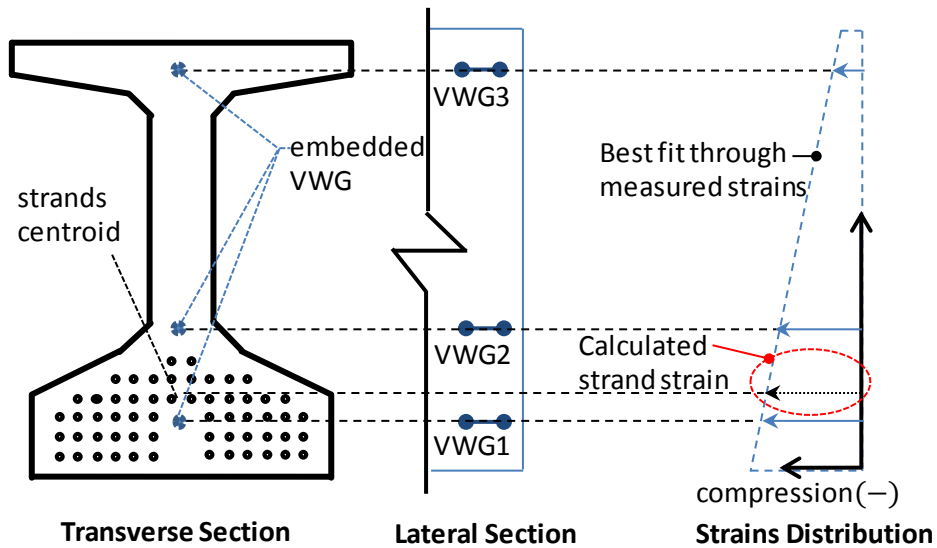


**Figure 3-13: Determination of strain in prestressing strands centroid.**

### 3.5 SUMMARY

The experimental program for this study included the assessment of prestress losses in 18 full-size standard bridge girders. The specimens were designed, fabricated and conditioned considering influential variables that may affect prestress losses in structures fabricated within the State of Texas, including type of concrete, specimen geometry, and climate.

The cross-section types selected were Type C and Tx46. The main differences in the concrete mix between series were the coarse aggregate type (river gravel versus limestone) and the type of concrete mix (conventional versus self-consolidating). The conditioning of the specimens was conducted in Austin and Lubbock in order to observe the effect of different climate conditions (relative humidity ranging from 51 to 62 percent). The final variation of the parameters within the experimental program is summarized in Table 3-6.

The development of prestress loss was monitored through internal strain instrumentation using vibrating wire gages. Concrete strains and temperatures were measured at several points through the depth of each cross-section and used to calculate the change of strain at the centroid of the prestressing strands. Due to compatibility between the prestressing strands and the surrounding concrete, it was possible to further calculate the loss in prestressing force on the basis of the prestressing strand modulus and area.

The results obtained from the internal strain monitoring, in combination with information compiled in the database (Chapter 2), are used to calibrate the prestress loss estimation method proposed within Chapter 6.

**Table 3-6: Variation of specimen characteristics with respect to influential parameters**

	Influential Parameter	Range
Conditioning	Final Age of Beam	230-980 days
	Storage Humidity	51% - 62%
Concrete	Concrete type	Conventional and SCC
	Coarse aggregate type	River Rock and Limestone
	Release Strength (f'ci)	5.8 – 7 ksi
	Standard Strength (f'c)	9.6 – 12 ksi
Concrete Stress	Max. stress/strength at midspan	0.57 – 0.62
Beam Geometry and Reinforcement	Length	45.5 ft
	Sectional Area	495-761 in <sup>2</sup>
	V/S	3.86 – 3.96 in.
	Prestress Reinforcement	1.13%-1.17%

# **CHAPTER 4**

## **Experimental Results**

### **4.1 OVERVIEW**

Eighteen full-scale prestressed concrete beams, were fabricated, conditioned and monitored to enable comprehensive assessment of strain-related prestress losses. These eighteen beams are a subset of the beams investigated during TxDOT Project 0-6374 (Garber, et al. 2013). At the time of final prestress loss assessment, the four series (4 to 6 specimens each) were representative of prestress bridge girders encountered in the State of Texas. Assessment of the specimens through long-term monitoring provided the data necessary to evaluate the impact of time, concrete properties, climate conditions and cross-sectional shape on the development of prestress losses in the State of Texas.

Limestone or river gravel was utilized as coarse aggregate in conventional and self-consolidating concrete mixtures. Type C and Tx46 girder cross-sections were fabricated at three different precast plants and transported to arid (Lubbock) and humid (Austin) locations for the long-term development of prestress losses. Further details of the experimental program are provided in Chapter 3.

A summary of the material test results and measured losses from the experimental program are presented and briefly discussed in this chapter. The experimental database was expanded with the addition of data collected during the experimental program. This data and associated insights provided a more thorough understanding of the behavior that guided the development of a simplified approximate method to estimate prestress losses in Chapter 6.

## 4.2 SUMMARY OF EXPERIMENTAL RESULTS

A review of the concrete material properties is first undertaken in order to later appreciate their influence on the measured prestress losses. The experimental results (i.e. results of the internal strain monitoring) will then be summarized.

### 4.2.1 Concrete Properties

The compressive strength and the modulus of elasticity (MOE) of the concrete mixtures used for each series were determined through extensive testing of companion 4-inch by 8-inch cylinders; these tests were completed by researchers at Ferguson Structural Engineering Laboratory (FSEL). The relevant concrete materials properties measured at release and 28 days are shown in Table 4-1. The compressive strength ( $f'_{ci}$ ) and modulus of elasticity ( $E_{ci}$ ) of each mixture were determined approximately one hour after release (“At Release” in Table 4-1), as these concrete properties are influential in the estimation and real magnitude of prestress loss. The compressive strength ( $f'_c$ ) was also measured at 28 days as this is a standard reference that allows comparisons with a myriad of reference documents.

**Table 4-1: Summary of concrete properties**

Series	At Release					28 days		
	Age (days)	$f'_{ci,design}$ (ksi)	$f'_{ci,measured}$ (ksi)	$E_{ci,design}$ (ksi)	$E_{ci,measured}$ (ksi)	$f'_{c,design}$ (ksi)	$f'_{c,measured}$ (ksi)	$E_{c,measured}$ (ksi)
I	1.08	6.2	7.0	4800	4490	8.5	10.7	4990
II	0.98	6.2	6.6	4800	6140	8.5	11.6	7180
III	1.77	6.5	6.6	4900	3990	8.5	9.6	4700
IV-SCC	0.74	6.0	6.3	4716	4810	12.0	11.5	5460
IV-CC			6.9		5440		12.0	6110
SCC = self-consolidating concrete; CC = conventional concrete								

In addition to the materials tests conducted at FSEL, the coefficients of thermal expansion were also measured by a subcontractor for Series I through III. The coefficients of thermal expansion were found to be  $6 \times 10^{-6}/^{\circ}\text{C}$  for the limestone concretes (Series I and III) and  $10 \times 10^{-6}/^{\circ}\text{C}$  for river gravel concrete (Series II).

The stiffness of the concrete at time of release ( $E_{ci}$ ) strongly influences the estimation of prestress losses. For design purposes, this stiffness is calculated on the basis of the prescribed strength of the concrete at time of release ( $f'_{ci}$ ) and may be estimated using Equation (4-1). If the concrete unit weight is 0.145 kips per cubic foot then Equation (4-2) is equivalent. This estimation is commonly used during the design because aggregate source and concrete weight is unknown during such stages. This estimation can be adjusted using the  $K_I$  parameter, which depends primarily on the coarse aggregate used.

The concrete stiffness was measured at time of release and at 28 days; results are plotted in Figure 4-1. The AASHTO LRFD 2012 expression for the concrete modulus of elasticity as commonly used during design – adjusted by the  $K_I$  value and unit weight of 0.145 kips – is also plotted in Figure 4-1. Conventional concrete made using river gravel coarse aggregate is generally stiffer than the modulus of elasticity estimated as described here. On the other hand, conventional concrete made using limestone coarse aggregate is less stiff than estimated. For self-consolidating concrete (SCC), the measured modulus of elasticity fell both above and below the estimated modulus.

As will be shown when investigating the prestress losses, the concrete stiffness significantly impacts the total loss. Beams made with stiffer concrete, as was seen in the concrete with river gravel aggregate, will experience smaller prestress loss than beams made with softer concrete, as seen with limestone aggregate.

$$E_c = 33,000K_1w_c^{1.5}\sqrt{f'_c}$$

(4-1)

AASHTO 12 (5.4.2.4-1)

$$E_c = 1820\sqrt{f'_c}$$

(4-2)

(derived for 0.145 kcf and  $K_1=1.0$ )

where:

- $E_c$  = modulus of elasticity of concrete (ksi)
- $K_1$  = correction factor for source of aggregate
- $w_c$  = unit weight of concrete (kcf)

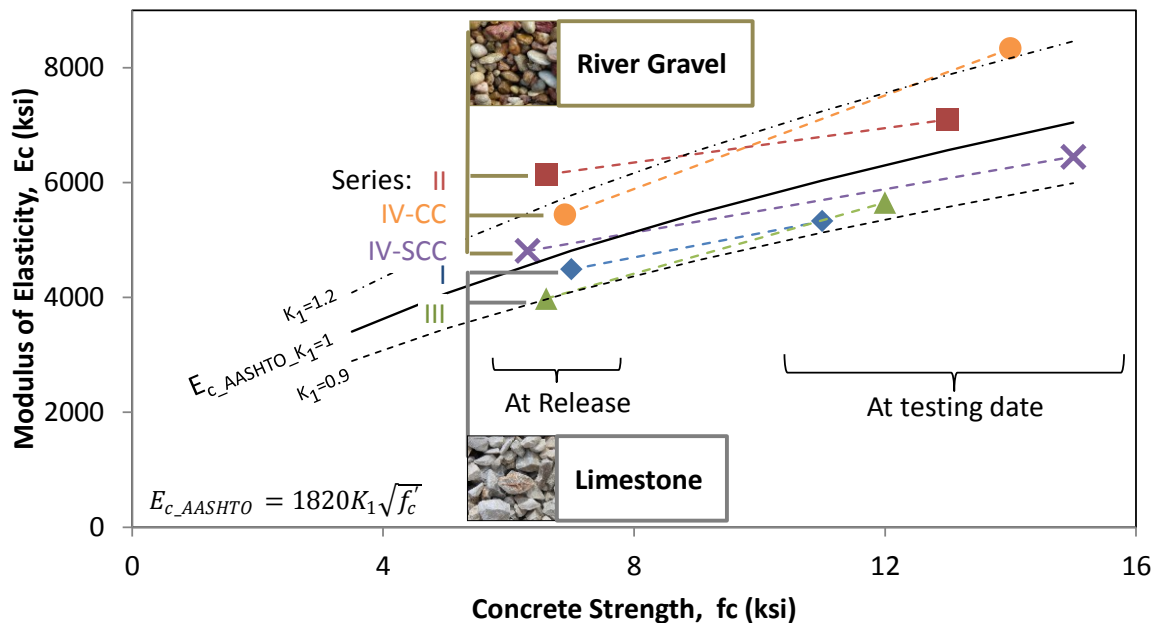


Figure 4-1: Concrete modulus of elasticity for all series at release and at testing date

#### 4.2.2 Final Strain-Related Prestress Losses

Vibrating wire gages (VWGs) were installed in the 18 specimens included in this study of the experimental program to allow for the development of prestress loss to be monitored over time. Final prestress losses obtained from internal strain measurement are reported in Table 4-2. This table contains the material properties for each series, relevant



information for each specimen, elastic shortening losses, and the final prestress loss assessed via internal strain monitoring (VWGs).

### **4.3 ANALYSIS OF EXPERIMENTAL RESULTS**

The influence of several parameters on the development and final magnitude of the measured prestress losses is examined in this section. The time dependency of prestress loss is investigated through review of the internal strain monitoring results. The effects of the concrete properties, climate conditions, and cross-sectional geometries included in the experimental program are also identified. This is accomplished through analysis of the final prestress losses reported in Table 4-2. This effort enabled identification of the key parameter for the prestress loss estimation developed in Chapter 5.

#### **4.3.1 Time Dependency of Losses**

The time-dependent development of the strain related prestress losses within all of the specimens that were conditioned for one year or longer is plotted in Figure 4-2. The prestress loss in a given specimen at a given point in time is normalized by the prestress loss measured at one year. The prestress loss measured at one year was selected as it is a fair representation of the full-term losses measured during the course of TxDOT Project 0-6374; prestress losses increased by less than 10 percent after the first year. Approximately 95 percent of the measured one-year loss occurs within the first four months, emphasizing the fact that the majority of prestress losses occur early in the specimen's life.

**Table 4-2: Summary of prestress loss assessments**

Series Properties		Storage Location (RH)	Beam ID	Final Age (days)	Shortening (ksi)		Final Prestress Loss (ksi)		
					Measured	Avg.	Measured	Avg.	
Section: Coarse agg.:	Type-C Limestone	SERIES I	Lubbock	I-1	980	26	27	46	49
A <sub>p</sub> :	5.81 in <sup>2</sup>		(52%)	I-5	975	27		51	
f <sub>ci</sub> :	7.0 ksi		Austin	I-3	948	26	27	46	48
E <sub>ci</sub> :	4490 ksi		(63%)	I-7	946	27		49	
Section: Coarse agg.:	Type-C River Gravel	SERIES II	Lubbock	II-1	955	16	17	32	34
A <sub>p</sub> :	5.81 in <sup>2</sup>		(51%)	II-6	949	17		36	
f <sub>ci</sub> :	6.6 ksi		Austin	II-3	932	17	17	34	34
E <sub>ci</sub> :	6140 ksi		(63%)	II-8	923	16		33	
Section: Coarse agg.:	TX-46 River Gravel	SERIES III	Lubbock	III-1	695	29	29	58	58
A <sub>p</sub> :	8.87 in <sup>2</sup>		(49%)	III-5	703	29		58	
f <sub>ci</sub> :	6.6 ksi		Austin	III-3	677	29	29	54	54
E <sub>ci</sub> :	3990 ksi		(61%)	III-7	681	29		53	
Section: Coarse agg.:	TX-46 River Gravel	SERIES IV		IV-SCC1	249	22	22	43	43
A <sub>p</sub> :	8.57 in <sup>2</sup>			IV-SCC2	259	22		42	
f <sub>ci</sub> :	SCC: 6.3 ksi		Austin	IV-SCC3	230	22		43	
	CC: 6.9 ksi		(57%)	IV-CC1	237	21	21	39	39
E <sub>ci</sub> :	SCC: 4810 ksi			IV-CC2	257	20		38	
	CC: 5440 ksi			IV-CC3	251	22		40	

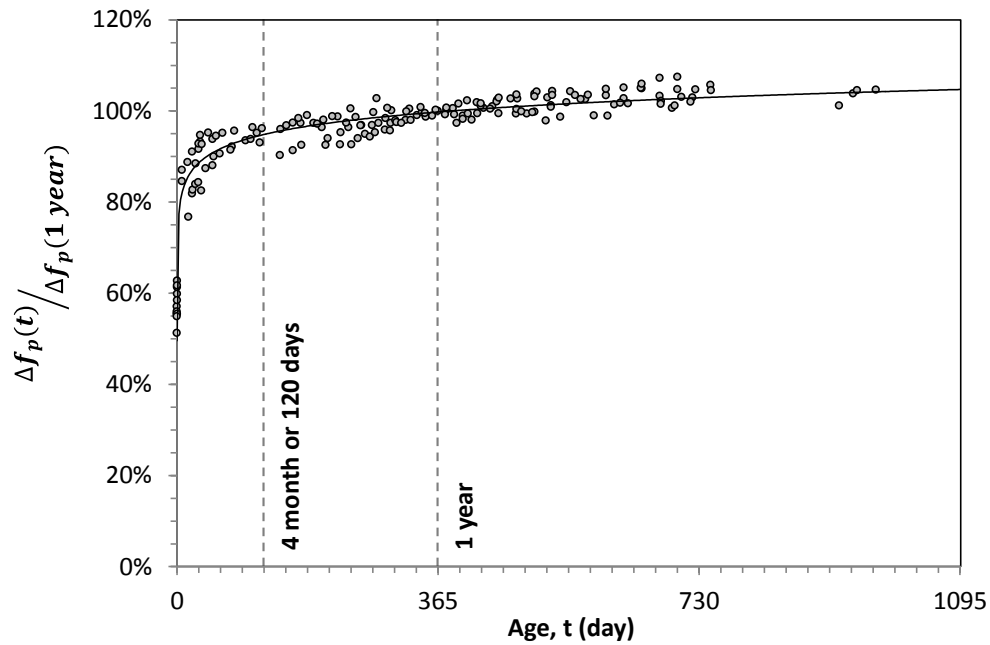


**Figure 4-2: Prestress loss ( $\Delta f_p(t)$ ) normalized by loss occurring one year after placement ( $\Delta f_p(1 \text{ year})$ )**

Prior to examining the next parameter, one additional aspect of the time-dependent loss measurements should be noted. The vibrating wire gages enabled independent assessment of the prestress losses resulting from elastic shortening and long-term creep and shrinkage. The instantaneous and long-term development of prestress loss within the Series III specimens stored in Austin is depicted in Figure 4-3. Elastic shortening losses determined from these plots are presented above in Table 4-2. The development of long-term losses was used to determine appropriate creep and shrinkage estimation in Chapter 6.

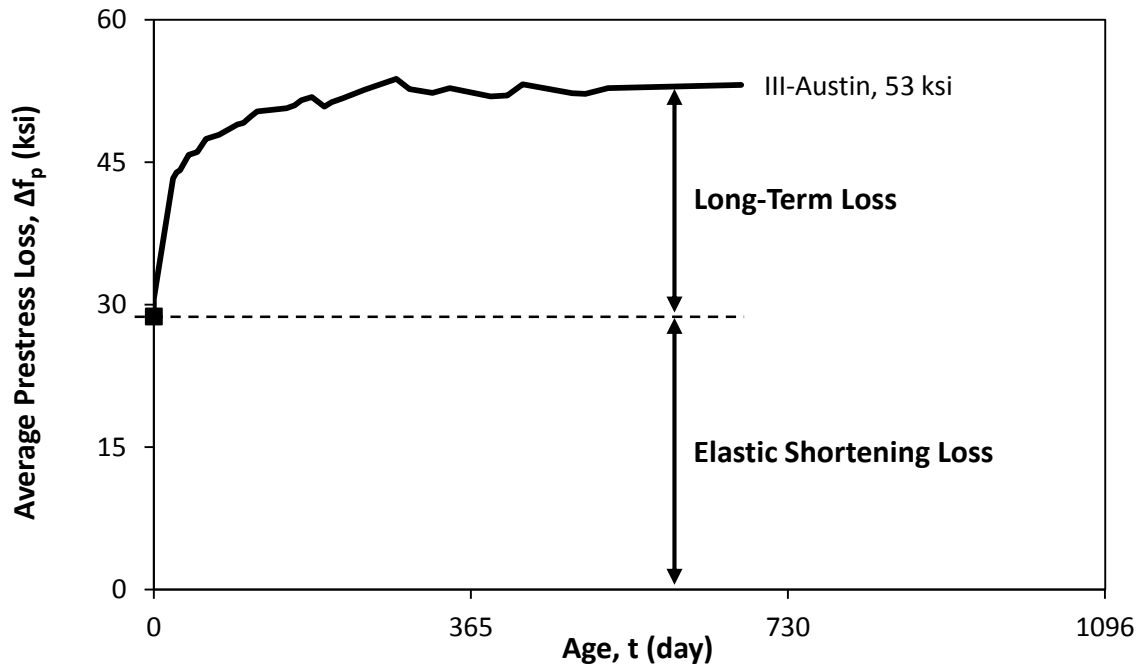


**Figure 4-3: Short- and long-term prestress losses in Series III specimens**

#### **4.3.2 Influence of Concrete Properties**

The concrete modulus of elasticity associated with each series of specimens was strongly influenced by the type, quality and quantity of the coarse aggregate. The specimens of Series I and III were constructed using concrete containing crushed limestone coarse aggregate; those in Series II and IV were constructed with river gravel coarse aggregate. The effect of the different coarse aggregate types can be seen in Figure 4-4, where the average modulus of elasticity is shown for each series. The concrete with the river gravel coarse aggregate was significantly stiffer than the concrete with crushed limestone; by as much as 50 percent.

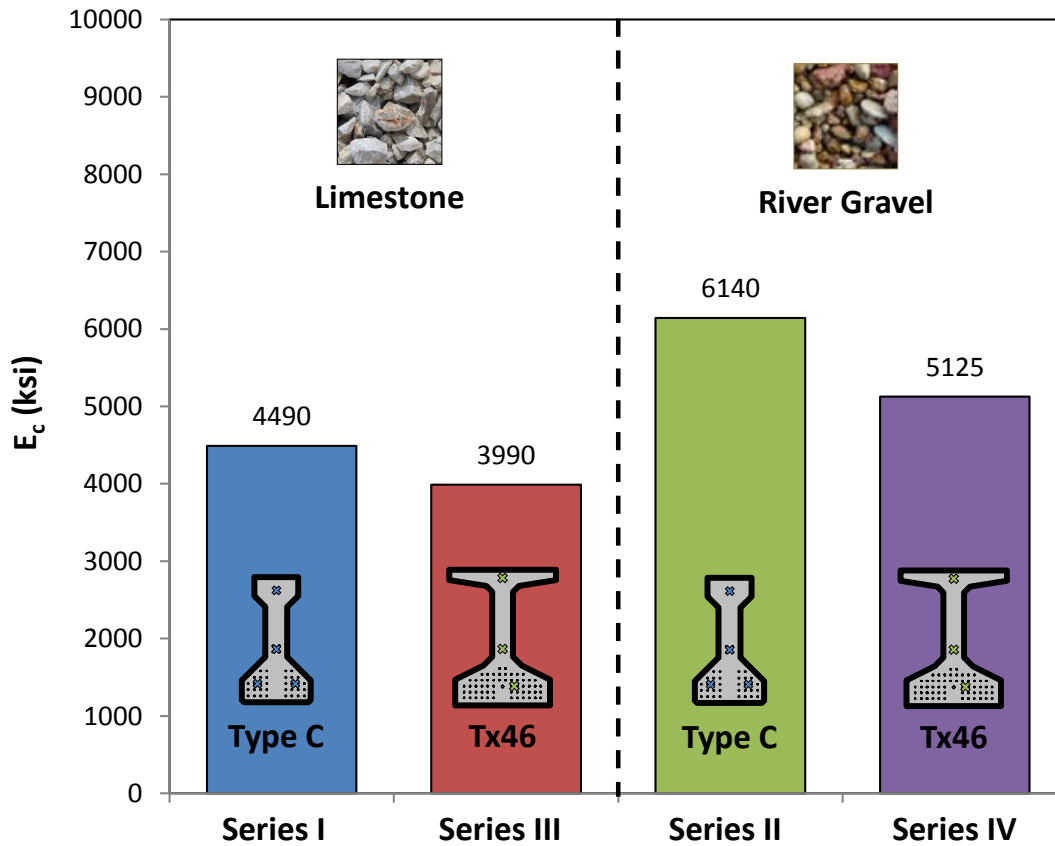


**Figure 4-4: Average measured modulus of elasticity ( $E_c$ ) for each series**

The total prestress losses were in turn greatly influenced by the stiffness of the concrete. The average final prestress loss for all the series is shown in Figure 4-5. The total loss is broken into elastic shortening ( $\Delta f_{pES}$ ) and long-term ( $\Delta f_{pLT}$ ) loss components to help illustrate the effect of the stiffness on each. The series of specimens constructed with stiffer, river gravel concrete experienced significantly smaller total prestress loss: Series I and III experienced total losses of 47 ksi and 54 ksi, respectively, while Series II and IV only experienced total losses of 31 ksi and 39 ksi, respectively.

The concrete stiffness also influenced long-term losses. This can be seen through comparison of the loss components of Series I and III as well as comparison of Series II and IV. The elastic shortening loss decreased from 27 ksi (Series I) to 19 ksi (Series III)

when a stiffer concrete was used, a decrease of 30 percent; the long-term loss decreased from 20 ksi to 12 ksi (40 percent) in the same specimens. The same trend was observed when comparing the specimens in Series II with the specimens in Series IV: elastic shortening loss decreased from 29 ksi to 23 ksi (20 percent) and the long-term loss from 25 ksi to 16 ksi (36 percent). These observations are consistent with common assertions that creep and shrinkage are heavily influenced by the coarse aggregate properties (ACI 209R, 2008).

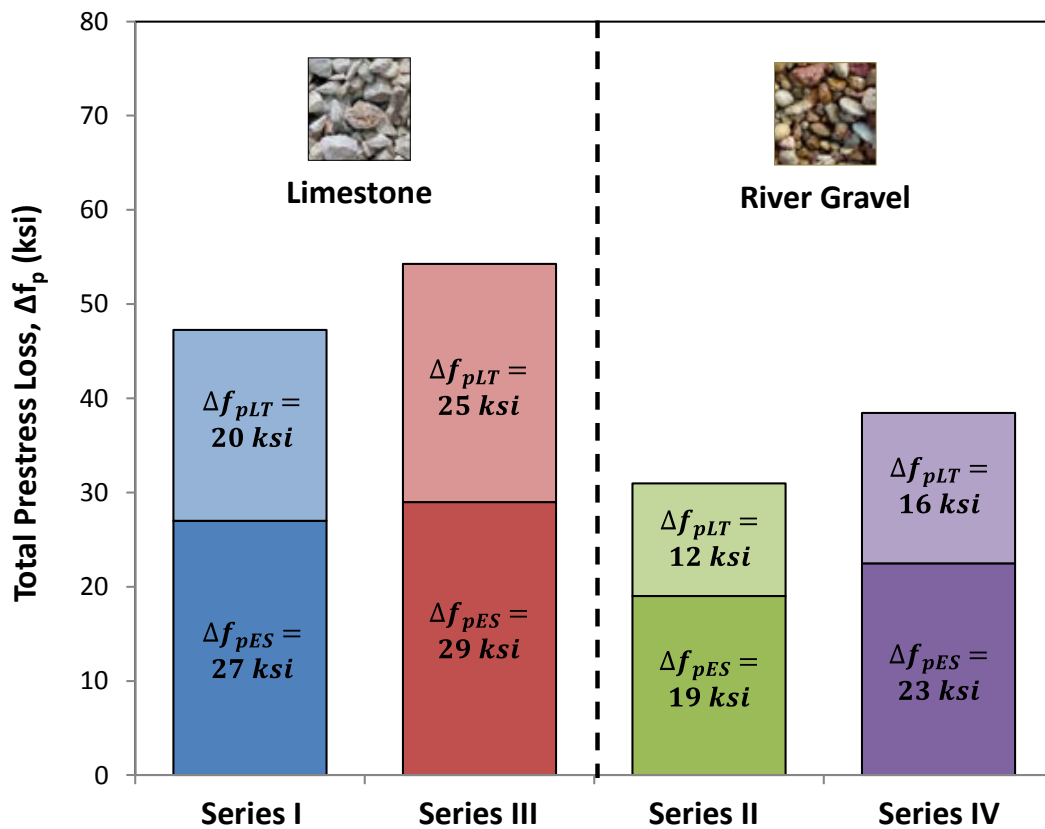


**Figure 4-5: Total prestress loss for each series divided into elastic shortening ( $\Delta f_{pES}$ ) and long-term loss components ( $\Delta f_{pLT}$ )**

The time-dependent variation of prestress losses for all internally instrumented specimens is shown in Figure 4-6. As noted above, the specimens with river gravel coarse

aggregate (Series II and IV) consistently exhibited lower prestress losses than those with limestone coarse aggregate (Series I and III).

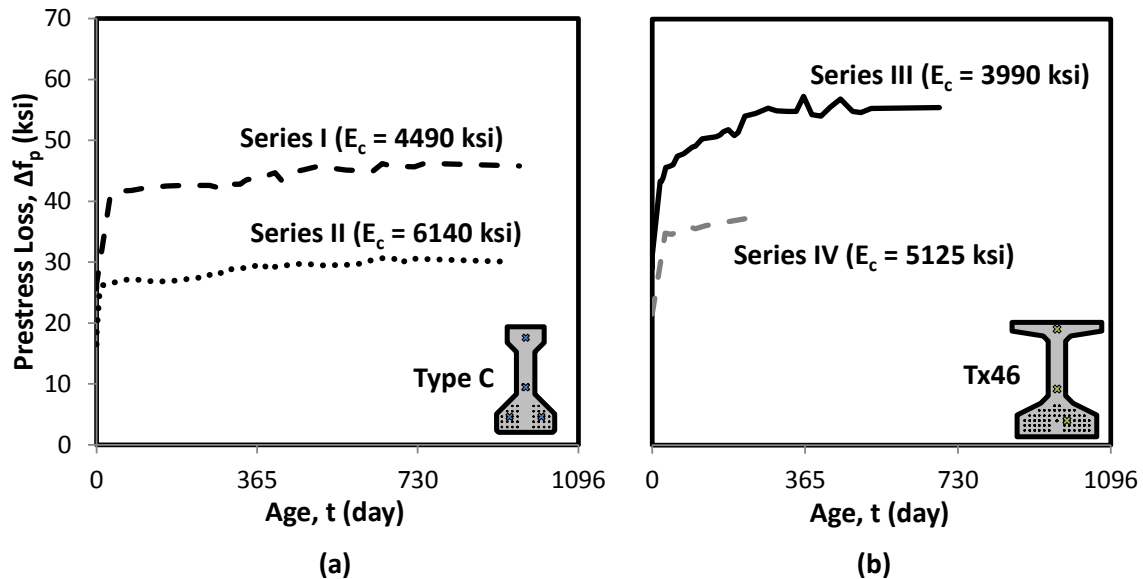


**Figure 4-6: Average losses vs. time for (a) Series I and II and (b) Series III and IV**

The effect of the proportion of coarse aggregate in the concrete mixture was also investigated. In Series IV, three of the six beams were fabricated using self-consolidating concrete (SCC), which in this case had a lower concentration of coarse aggregate than conventional concrete (CC) mixes; the other three beams were fabricated with conventional concrete. It was found that the conventional concrete was slightly stiffer than the self-consolidating concrete, with stiffness of 5,540 and 4,810 ksi respectively. The stiffer concrete translated to slightly smaller loss in the CC specimens versus the SCC specimens, 38.0 and 41.1 ksi respectively. This shows that the concentration of coarse aggregate may affect the concrete stiffness and total prestress loss, but not as significantly as the coarse aggregate properties.

During implementation of the AASHTO LRFD 2012 prestress loss provisions, the variation of concrete stiffness (as a result of constituent properties and/or mixture proportions) may be accounted for through use of the  $K_I$  factor, as introduced in Section 4.2.1, Equation (4-1) above. Given measurements of the concrete modulus and compressive strength,  $K_I$  may be calculated as the ratio of the measured concrete modulus and the concrete modulus estimated on the basis of the measured compressive strength; as done in Table 4-3. The  $K_I$  factor for each of the concrete mixtures used in the current project varied between 1.15 and 1.20 for conventional mixtures with river gravel coarse aggregate and between 0.87 and 0.91 for mixtures with limestone coarse aggregate.

**Table 4-3: Average  $K_I$  correction factor for each series**

Series	Aggregate Type	$E_{ci,estimated}$ (ksi)	$E_{ci,measured}$ (ksi)	Average $K_I$ (at release)
I	Limestone	4934	4490	0.91
II	River Gravel	5117	6140	1.20
III	Limestone	3897	3390	0.87
IV-SCC	River Gravel	4810	4810	1.00
IV-CC	River Gravel	4730	5440	1.15

The current language in AASHTO LRFD 2012 allows for  $K_I$  to be taken as 1.0 if material testing is not conducted. A bridge designer generally does not know which fabricator or what aggregates will be used for a given structure until the design is complete and the bridge has been let for construction. They will likely default to use of the default  $K_I$  value of 1.0. Moreover, it is likely – given the Chapter 2 assessments of AASHTO LRFD 2012 and the results discussed above – that such an approach will result



in unconservative estimates of prestress loss, especially for pretensioned girders fabricated with limestone coarse aggregate.

### **4.3.3 Influence of Climate Conditions**

Within each series, a portion of the specimens were conditioned in Lubbock, with an average annual ambient relative humidity of around 50 percent, and a portion in Austin, with a relative humidity of around 60 percent. This was done in order to investigate the influence of various climate conditions on the development of prestress losses.

The time dependent variation of prestress loss in Series III specimens conditioned in Lubbock and Austin are shown in Figure 4-7. It can be seen that the elastic shortening loss in both sets of specimens is identical, as was expected. The long-term loss was slightly larger in the specimens conditioned in Lubbock versus those conditioned in Austin, 29 and 24 ksi respectively. The prestress loss increase attained through conditioning in a lower humidity environment is consistent with the concrete creep and shrinkage models presented in ACI 209R and included in Article 5.4.2.3 of AASHTO LRFD 2012. It should be noted that comparison of the identical specimens within Series I and II did not reveal any significant effect of the conditioning environment.

The fact that the climate conditions had a noticeable effect in Series III, while not noticed in Series I and II, is related to the permeability and age of the concrete at the time of shipping to the conditioning sites. The largest fraction of the losses occurs in the first few weeks after casting. For this reason, the storage conditions during this period have a larger effect on prestress losses than the storage conditions at later ages. Series I and II were stored at the fabricator for longer times (51 and 22 days respectively) than Series III

(18 days), contributing to specimens in Series III being more sensitive to climate differences between Austin and Lubbock.

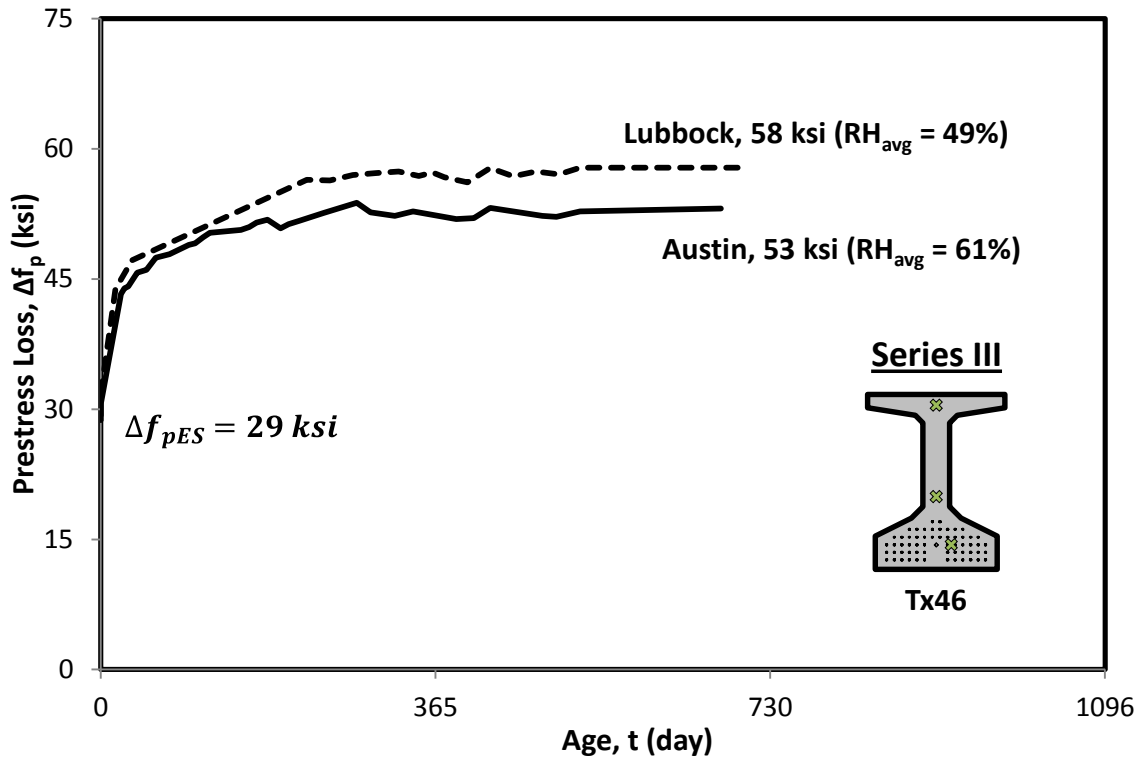


Figure 4-7: Average prestress loss vs. time for Series III specimens

The observations made here, substantiate the decision to consider ambient relative humidity as an influential parameter during development of prestress loss estimation method in Chapter 5, specifically for the estimation of shrinkage.

#### 4.3.4 Influence of Cross-Sectional Geometry

Historically, the cross-sectional geometry has been thought to affect the creep and shrinkage of the concrete. A larger volume-to-surface area ratio ( $V/S$ ) is thought to allow greater water transfer from the concrete to the atmosphere. Volume-to-surface area does not typically play a significant role in prestress concrete girder design, as most of the

commonly used cross-section types have volume-to-surface area ratios of around 4.0 inches.

Through the course of the experimental research, two different cross-section types (Type C and Tx46) were investigated. The relevant cross-sectional geometric properties are shown in Table 4-4. It can be seen that both of the sections have similar volume-to-surface area and prestress ratios ( $\rho_p$ ). The two sections do, however, have slightly different bottom flange volume-to-surface ratios, which is the ratio considering the bottom flange separate from the rest of the section.

**Table 4-4: Summary of relevant cross-sectional geometry properties**

Series	Section Type	$E_{ci,measured}$ (ksi)	Prestress Ratio ( $\rho_p$ )	Gross Area ( $in^2$ )	Volume-to-Surface Area Ratio ( $V/S$ ) (in)	Bottom Flange $V/S$ (in)
I	Type C	4490	0.012	494.9	4.0	4.1
II	Type C	6140	0.012	494.9	4.0	4.1
III	Tx46	3390	0.012	752.1	3.9	4.6
IV	Tx46	5125	0.012	752.1	3.9	4.6

The total final prestress loss for each series is shown in Figure 4-8 in order to show the effects of cross-section type on prestress loss. It can be seen that in both the specimens with limestone and river gravel coarse aggregate there was a slight increase in measured long-term losses when going from the Type C to Tx46 cross-section. This increase is likely due to the Tx46 specimens having less stiff concrete than the Type C girders. There is no definitive cross-sectional geometry effect between Type C and Tx46 cross-section types.

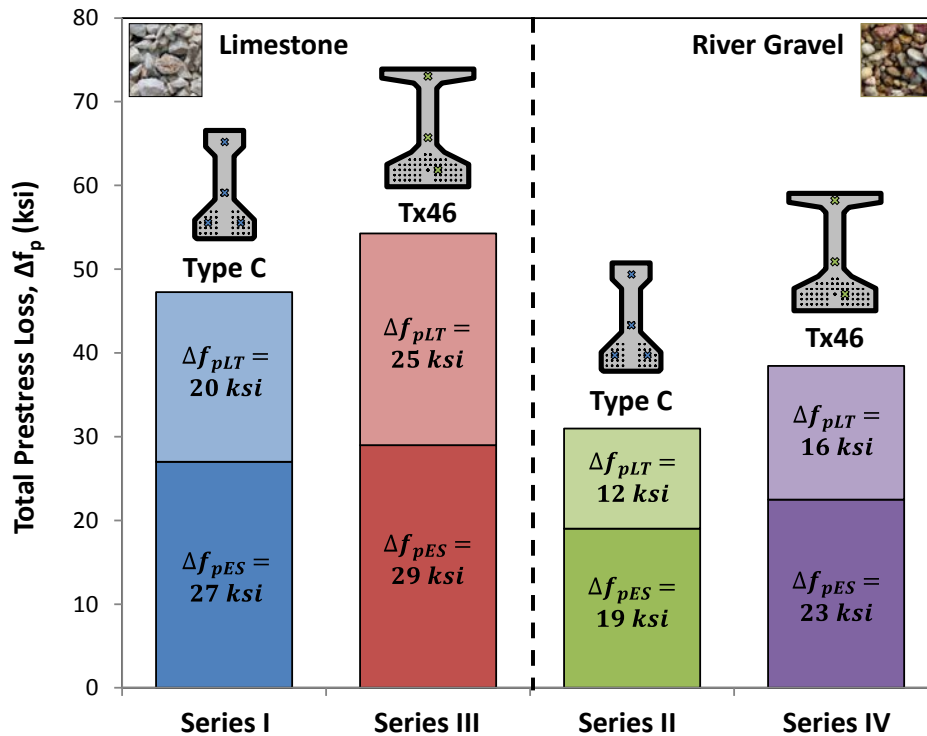


Figure 4-8: Total prestress loss for each series separated into elastic shortening ( $\Delta f_{pES}$ ) and long-term loss components ( $\Delta f_{pLT}$ ), comparing geometry

#### 4.4 SUMMARY

Results of the experimental program were presented in this chapter. Because prestress loss is strongly dependent on the concrete material properties, both material properties and prestress losses were investigated.

Concrete strength ranged from 5.8 to 7.0 ksi at release, and the elastic modulus from 4700 to 7200 ksi at the same age, both typical of current field practice. It was observed that the concrete made with river gravel concrete was stiffer than the concrete made with limestone. The final measured prestress losses ranged from 24 ksi to 61 ksi.

A clear influence of the coarse aggregate type on the losses was observed. Concrete made from limestone coarse aggregate resulted in a lower modulus than concrete made with river gravel coarse aggregate. A higher loss was observed in the

specimens made with limestone aggregate concrete versus those with river gravel aggregate.

The losses measured in Series III beams stored in dryer conditions are larger than those stored in more humid environments (a 10 percent decrease in the relative humidity resulted in an increase of almost 9 percent in the long-term loss within otherwise identical specimens). Series I and II did not show considerable difference within beams stored at different humidity. The main factors leading to this difference in the effect of the relative humidity are related to the age and permeability of the concrete in the beams when first exposed to the storage conditions. The effect of different humidity was noticeable in the younger and most permeable beams (i.e. those from Series III). Also, there was no definitive cross-sectional geometric effect on prestress loss.

## **CHAPTER 5**

### **Development of a Prestress Loss Model Using Materials Test Data**

#### **5.1 INTRODUCTION**

A novel prestress loss model was developed using basic concrete models for elastic deformation, creep and shrinkage. The model development was supported by commonly accepted creep and shrinkage theories published by Vandamme & Ulm (2009), Bažant, Hauggaard, Baweja, & Ulm (1997), and Powers (1968), and reviewed in Chapter 2. Existing databases of creep and shrinkage results (Bazant & Li, 2008) were expanded and filtered for use in calibration of the model expressions.

The proposed prestress loss model only includes the parameters necessary to represent the short- and long-term behavior of a pretensioned concrete member. This method is intended to be a tool for the designer who is interested in performing a more detailed study of these phenomena. In addition to providing numerical estimates to the prestress losses, this model is intended to illustrate the main mechanisms involved in the development of prestress loss. Also, the format of the material-based method can be used as a guide to develop future techniques to estimate prestress losses in more complex structural systems.

#### **5.2 BASIC APPROACH TO MODEL CONCRETE BEHAVIOR**

The deformation of concrete can be idealized as the summation of elastic and viscous deformations. Springs and dashpots are the theoretical elements used to model these deformations. Such elements have been used in multiple configurations in an effort to simulate time-dependent deformation of concrete (Neville A. M., 1983).

In this section the most basic model that can capture the elastic, creep and shrinkage deformations is used. As presented in Chapter 2, such basic models are: (1) a spring that is deformed by the action of pore water pressure used to model shrinkage, and (2) a Burgers model used to model creep. The stiffness of the springs, the viscosities of the dashpots and the magnitude of the internal water pressure used in this study are defined as functions of relevant parameters, as will be described in the following sections. The formats of these functions are based on the main mechanisms at the origin of elastic deformations and creep and shrinkage.

The definition of the model includes also proportionality coefficients that allow for empirical calibration. The calibration of the coefficients can be conducted using results from cylinder testing or alternatively it can be based on results from the monitoring of girders. The alternative of calibration of the model based on girder data is attractive because the girder data captures the effects of physical phenomena taking place within a girder section during loss of prestress forces; effects that are not accurately captured with cylinder testing (e.g. irregular sectional geometry and variable stress history). The development of an element-based model, calibrated using girder data is developed in Chapter 6.

On the other hand, the calibration of models based on cylinder testing data has its own advantages. The experimental evidence of cylinder behavior available is abundant and allows for an all-embracing calibration of models based on cylinder behavior. Such abundance of experimental results makes the use of cylinder data attractive, because it allows the characterization of phenomena that are difficult to characterize using girder instrumentation.

The model presented in this chapter (i.e. the materials-based model) is calibrated based on results from cylinder testing. With this in mind, the study of the behavior of

prestress girders, is based on models of creep of concrete under constant stress and of shrinkage under symmetric drying. Then, material models are used to formulate a method to estimate prestress losses in girders.

### 5.3 BASIC MODEL OF CREEP BEHAVIOR

A general model for the estimation of concrete creep is developed in this section. The basic nature of creep can be summarized by two time-related mechanisms: short-term creep and long-term creep. As discussed in Chapter 2, previous studies have used the Burgers model (Figure 5-1) to model creep strains. The Burgers model is considered to be an adequate representation of the basic nature of creep. Within this model, the Kelvin-Voigt element (a dashpot and a spring in parallel configuration) is used to capture the short-term creep, while the Maxwell element (a dashpot and a spring in series configuration) captures the long-term creep and the elastic deformation.

The use of the Burgers model requires the definition of the properties of four elements. The properties that need to be defined are: the stiffness of the spring modeling the elastic strain ( $K_{EL}$ ), the viscosity of the long-term creep dashpot ( $v_{LT}$ ), the stiffness of the spring to capture short-term creep ( $K_{ST}$ ), and the viscosity of the dashpot for the short-term creep ( $v_{ST}$ ).

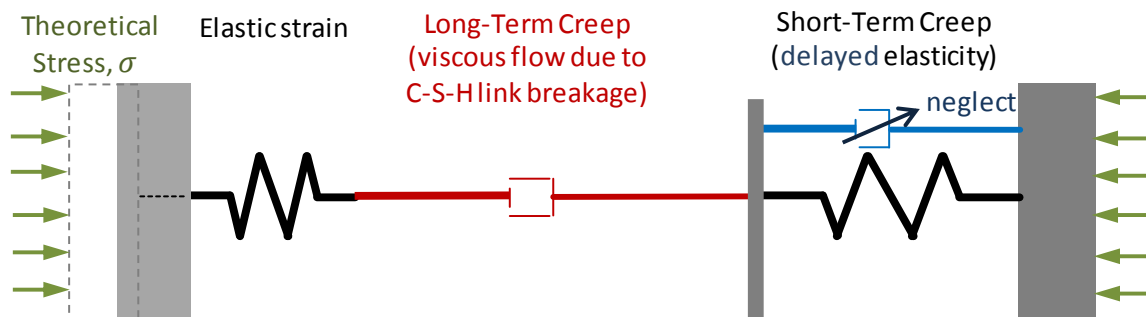


**Figure 5-1: Burgers model with proposed stiffness and viscosities**



The numerical values of the stiffnesses and viscosities within the model are set as dependent variables that are controlled by the concrete stiffness ( $E_{ci}$  or  $E_c$ ). This is due to the strong correlation between the long-term deformation and the concrete stiffness. The use of concrete stiffness is also convenient because it is the only property that: (1) is obtained through the measurement of concrete deformation, and (2) can be easily measured in most concrete testing laboratories or even in the field.

In this sense, the stiffness of the elastic strain spring is simply defined as the initial concrete stiffness, i.e.  $K_{EL} = E_{ci}$ . Also, since the short-term creep is considered a “delayed elasticity”, it is convenient and intuitive to make the stiffness of the short-term creep proportional to the concrete stiffness, i.e.  $K_{ST} \propto E_{ci}$ . The initial concrete stiffness is used because the short-term creep develops in few days after loading, and the concrete properties at loading are the most representative of the properties related to short-term creep.

Considering that the short-term creep usually is fully developed in few days (Ulm, Maou, & Boulay (2000) and Neville A. M. (1983)), then, for ages larger than few days the stress in the short-term-creep dashpot has been dissipated, and all the stress is transmitted through the short-term-creep spring. For the ages of interest for this study (larger than few days) the dashpot can be considered as having zero force, and then it can be excluded with no detriment to the model. Therefore, the short-term-creep viscosity is not included in the proposed model.

As previously mentioned the parameters are defined in terms of the concrete stiffness. Then, the viscosity for the long-term creep was assumed to be proportional to the concrete stiffness (i.e.  $v_{LT} \propto E_c$ ); an increase in the concrete stiffness will result in a reduction of creep and viceversa. In the parameter is set to be proportional to the standard concrete stiffness ( $E_c$ ), instead of the initial stiffness ( $E_{ci}$ ), because the long-term creep

rate (which depends on  $v_{LT}$ ) does not depend on age at loading –and the use of the initial stiffness would give that impression. The viscosity was furthermore made proportional to concrete age (i.e.  $v_{LT} \propto t$ ) to capture the always-increasing resistance of concrete to creep, which is explained as the consequence of a continuous depletion of creep potential by Bažant, Hauggaard, Baweja, & Ulm (1997) and Vandamme & Ulm (2009). Finally, the viscosity for the long-term dashpot is proportional to both the concrete stiffness and the age (i.e.  $v_{LT} \propto E_c \cdot t$ ).

Two constants,  $C_{ST}$  and  $C_{LT}$ , are used as proportionality constants to define the stiffness of the spring for short-term creep and the viscosity for long-term creep respectively. Then the function defining the stiffness of the short-term spring is  $K_{ST} = C_{ST}E_{ci}$  and the function defining the long-term creep viscosity is  $v_{LT} = C_{LT}E_c \cdot t$ .

The long-term creep strain can be determined on the basis of the theory underlying viscous element behavior, as that used in series in the Burgers model (see Figure 5-1). The deformation of a standard viscous element is defined by its rate ( $\dot{\epsilon}$ ), which is proportional to the applied stress ( $\sigma_c$ ) and inversely proportional to its viscosity (e.g.  $\dot{\epsilon}_{vLT} = \sigma_c/v_{LT}$ ). The creep rate is widely accepted to be inversely proportional to the age of concrete (Vandamme & Ulm, 2009). Such behavior is adequately modeled using a viscous element with viscosity proportional to the concrete age ( $t$ ) as part of the Burgers model (Figure 5-1). The derivation of the equation defining the long-term creep strain in accordance with the proposed model is shown in Table 5-1.

**Table 5-1: Calculation of Long-Term Creep Strain**

Definition of the deformation of general viscous elements	$\dot{\epsilon}_{vLT} = \frac{\sigma_c}{v_{LT}}$	(5-1)
	$\dot{\epsilon}_{vLT} = \frac{d\epsilon_{vLT}}{dt}$	(5-2)
	$\epsilon_{vLT} = \int_{t=t_0}^t \frac{\sigma_c}{v_{LT}} dt$	(5-3)
Proportionalities based on commonly accepted trends	$\dot{\epsilon}_{CR LT} \propto \frac{1}{t}$	(5-4)
	$\dot{\epsilon}_{CR LT} \propto \frac{1}{E_c}$	(5-5)
Modeling long-term creep as the strain in the “LT” dashpot (see $v_{LT}$ Figure 5-1)	$\dot{\epsilon}_{vLT} = \dot{\epsilon}_{CR LT}$	(5-6)
Plug (5-2), (5-4) and (5-5) into (5-6)	$\frac{\sigma_c}{v_{LT}} \propto \frac{1}{E_c} \frac{1}{t}$	(5-7)
Definition of the viscosity ( $v_{LT}$ ) using (5-7)	$v_{LT} = C_{LT} E_c \cdot t$	(5-8)
Plug (5-8) and (5-6) in (5-3)	$\epsilon_{CR LT} = \int_{t=t_0}^t \frac{\sigma_c}{C_{LT} E_c \cdot t} dt$	(5-9)
Solving (5-9)	$\epsilon_{CR LT} = \frac{\sigma_c}{C_{ST} E_c} [\ln(t) - \ln(t_0)]$	(5-10)
<p>Where:</p> <p><math>\sigma_c</math> = stress in the concrete</p> <p><math>E_c</math> = stiffness of concrete at 28 days</p> <p><math>t, t_0</math> = concrete age at which the strains are calculated, and age at loading</p> <p><math>\epsilon_{CR LT}</math> = long-term creep strain</p> <p><math>\dot{\epsilon}_{vLT}</math> = rate of strain in the long-term viscous element</p> <p><math>v_{LT}</math> = viscosity of the long-term viscous element</p> <p><math>C_{LT}</math> = proportionality constant to be calibrated for the long-term creep</p> <p><math>C_{ST}</math> = proportionality constant to be calibrated for the short-term creep</p>		

### 5.3.1 Calibration of Creep Model Coefficients

Calibration of the creep coefficients proposed in Burgers model in Figure 5-1 was a two-stage process. The proportionality coefficients for the short-term and long-term creep ( $C_{ST}$  and  $C_{LT}$ ) were calibrated using specimens in the creep database that were loaded at an early age. The evaluation subset of the creep Database used to calibrate the coefficients for the creep model is plotted in Figure 5-2. The data from those specimens can be found in Appendix D. Specimens used for the calibration of  $C_{ST}$  were either loaded at about 1 day or loaded at 3 days (Figure 5-4). This separation was found necessary because short-term creep occurs rapidly after loading. The specimens loaded at around 1 day would have developed an important fraction of short-term creep before the 3-day time mark at which the other specimens were loaded. Thus, evaluating both sets of data together would not give a good representation of the short-term creep.

A best-fit expression of the total creep coefficient was developed using the average values for the 1 and 3-day specimens separately. With these expressions, a coefficient  $C_{ST} = 3.1$  was obtained as outlined in Table 5-2. Some variability was observed in the short-term creep coefficient, the value chosen is the average obtained from the distinct loading ages.

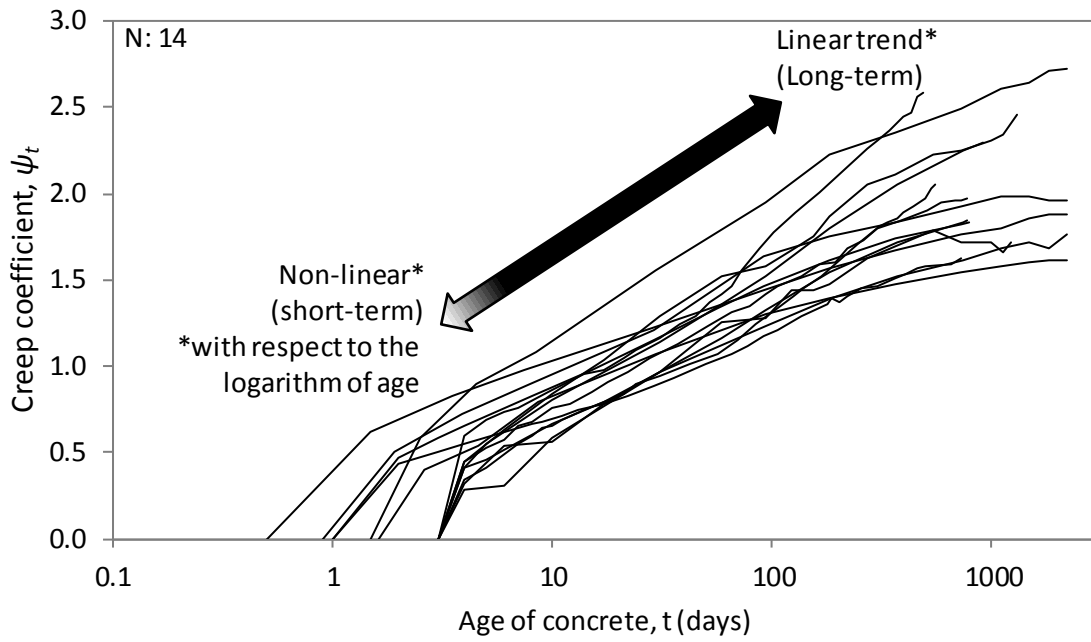


**Figure 5-2: Creep coefficient for cylinder specimens**

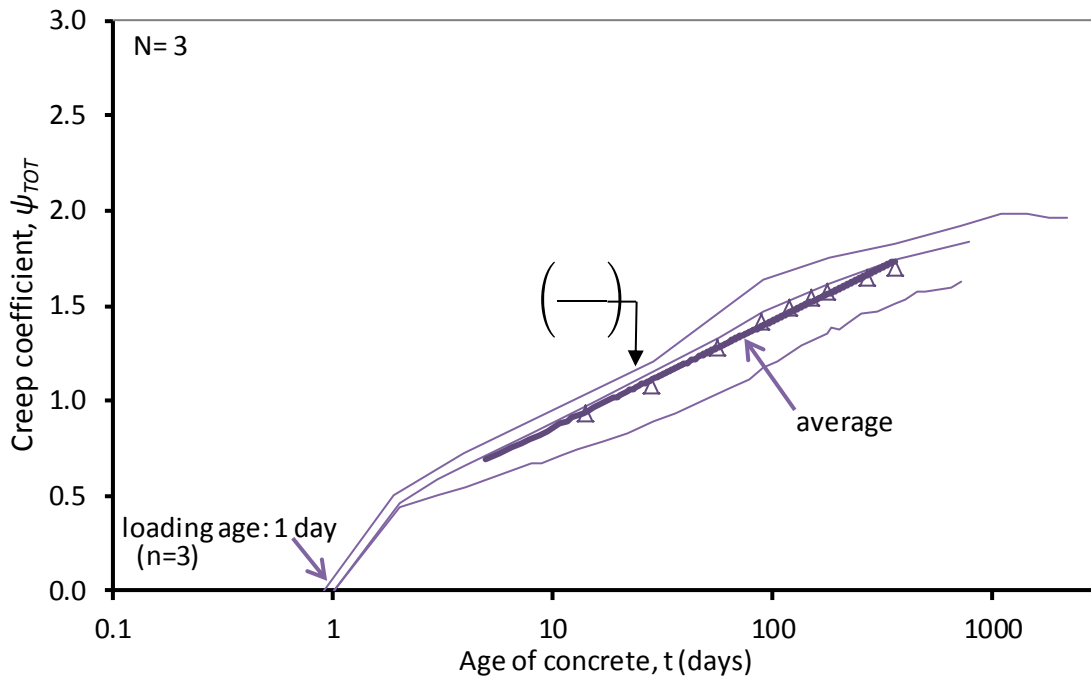


**Figure 5-3: Creep coefficient for cylinder specimens loaded at 1 day of age**

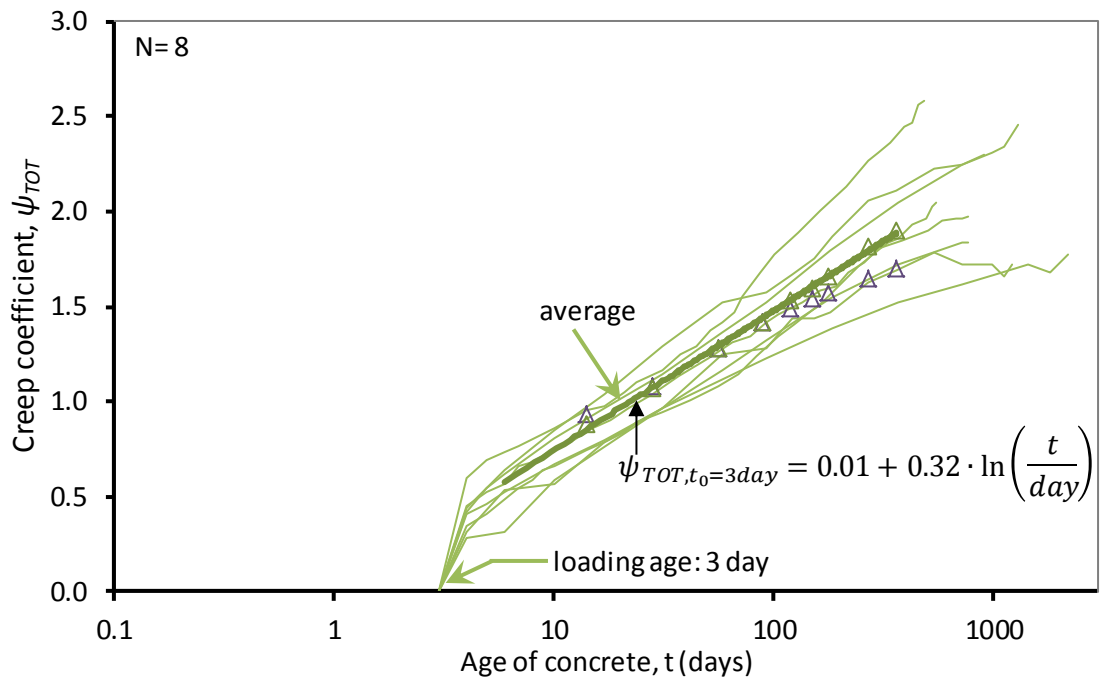


**Figure 5-4: Creep coefficient for cylinder specimens loaded at 3 days of age**

**Table 5-2: Derivation of  $C_{ST}$  based on measured creep coefficients**

By definition	$\psi_{ST} = \psi_{TOT} - \psi_{LT}$		(5-11)
	$\varepsilon_{CR ST} = \psi_{ST}\varepsilon_{ELAS}$		(5-12)
From Figure 5-4	For $t_0 \sim 1$ day	$t_0 = 3$ days	-
	$\psi_{TOT} = 0.29 + 0.24 \cdot \ln(t)$	$\psi_{TOT} = 0.01 + 0.32 \cdot \ln(t)$	(5-13)
	$\psi_{LT} = 0.24 \cdot [\ln(t) - \ln(1)]$	$\psi_{LT} = 0.32 \cdot [\ln(t) - \ln(3)]$	(5-14)
Plug (5-13) & (5-14) in (5-11)	$\psi_{ST,t_0 \sim 1} = 0.29 + 0.24 \cdot \ln(t) - 0.24 \cdot [\ln(t) - \ln(1)]$	$\psi_{ST,t_0 \sim 3} = 0.01 + 0.32 \cdot \ln(t) - 0.32 \cdot [\ln(t) - \ln(3)]$	(5-15)
Simplify and cancel (5-15)	$\psi_{ST,t_0 \sim 1} = 0.29$	$\psi_{ST,t_0 \sim 3} \cong 0.36$	(5-16)
Average	$\psi_{ST} \cong 0.32$		(5-17)
From Figure 5-1	$\varepsilon_{CR ST} = \frac{\sigma_c}{C_{ST}E_{ci}}$		(5-18)
	$\varepsilon_{ELAS} = \frac{\sigma_c}{E_{ci}}$		(5-19)
Plug (5-17), (5-18) & (5-19) in(5-12)	$\frac{\sigma_c}{C_{ST}E_{ci}} = 0.32 \frac{\sigma_c}{E_{ci}}$		(5-20)
Solving (5-20)	$C_{ST} \cong 3.1$		(5-21)

The long-term creep coefficient ( $C_{LT}$ ) was calibrated using the same set of specimens introduced in Figure 5-4 and Figure 5-4. After approximately 7 days of loading, the creep coefficient is assumed to vary linearly with the logarithm of age (indicating long-term creep). The average long-term calibration coefficient obtained from the creep evaluation database was  $C_{LT} = 3.3$  (Table 5-3). The complete creep model is presented in Section 5.3.2.

**Table 5-3: Derivation of  $C_{LT}$  coefficient using average trend of measured creep**

By definition	$\varepsilon_{CR LT} = \varepsilon_{ELAS} \cdot \psi_{LT}$		(5-22)
then	$\Delta\varepsilon_{CR LT}/\Delta \ln(t) = \varepsilon_{ELAS} \cdot \Delta\psi_{LT}/\Delta \ln(t)$		(5-23)
By definition	$\varepsilon_{ELAS} = \frac{\sigma_c}{E_{ci}}$		(5-24)
From Table 5-5	$\varepsilon_{CR LT} = \frac{\sigma_c}{C_{LT}E_c} [\ln(t) - \ln(t_0)]$		Re (5-10)
then	$\frac{\Delta\varepsilon_{CR LT}}{\Delta \ln(t)} = \frac{\sigma_c}{C_{LT}E_c}$		(5-25)
-	For $t_0 \sim 1$ day	$t_0 = 3$ days	-
From Figure 5-4	$\psi_{TOT} = 0.29 + 0.24 \cdot \ln(t)$	$\psi_{TOT} = 0.01 + 0.32 \cdot \ln(t)$	(5-26)
Then, for long term (late ages)	$\frac{\Delta\psi_{LT}}{\Delta \ln(t)} = 0.24$	$\frac{\Delta\psi_{LT}}{\Delta \ln(t)} = 0.32$	(5-27)
Plug (5-25), (5-24) & (5-27) in (5-23)	$\frac{\sigma_c}{C_{LT}E_c} = \frac{\sigma_c}{E_{ci}} 0.24$	$\frac{\sigma_c}{C_{LT}E_c} = \frac{\sigma_c}{E_{ci}} 0.32$	(5-28)
Assume $E_{ci}/E_c = 0.9$	$\frac{\sigma_c}{C_{LT}} = \frac{\sigma_c}{0.9} 0.24$	$\frac{\sigma_c}{C_{LT}} = \frac{\sigma_c}{0.9} 0.32$	(5-29)
Solving	$C_{LT} = 3.8$	$C_{LT} = 2.8$	(5-30)
Average	$C_{LT} = 3.3$		(5-31)

### 5.3.2 Proposed Creep Model

The final creep model is shown schematically in Figure 5-5. The model includes the calibrated short-term and long-term creep coefficients determined in the previous section. The application of this model is limited to concrete loaded at early ages (1 to 3 days); this limitation made formulation of the model feasible.



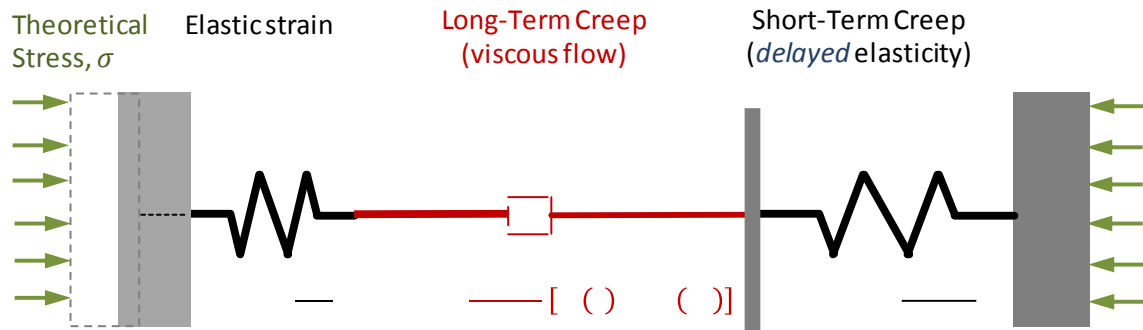


**Figure 5-5: Proposed creep model for concrete loaded at 1-3 days<sup>2</sup>**

#### 5.4 BASIC MODEL OF SHRINKAGE BEHAVIOR

As discussed in Chapter 2, the mechanisms causing shrinkage in concrete can be divided into hygral shrinkage and non-hygral shrinkage. The non-hygral shrinkage is considered here to be independent of the pore water pressure.

Hygral shrinkage can be modeled simplistically as the deformation of the concrete caused by an effective internal pressure proportional to the pore water pressure change ( $\sigma_{cSH}$ ) and resisted by an effective stiffness proportional to the concrete stiffness ( $\propto E_c$ ). The scheme of this proposed shrinkage model is shown in Figure 5-6. This model is congruent with basic definitions found in the literature (Powers, 1968).

The equivalent stress ( $\sigma_{cSH}$ ), presented in Figure 5-6, is assumed to be proportional to the natural logarithm of the internal relative humidity, i.e.  $\sigma$

( ). As presented in Chapter 2, this parameter ( $\ln(RH_{INTERNAL})$ ) is directly related to the change in pore water pressure (when other variables are held constant). The calibration of this model will be conducted using measured ultimate

---

<sup>2</sup> The coefficient of the modulus of elasticity in the long-term creep and short-term creep terms (i.e. 3.3 and 3.1) are not unified to a single coefficient (e.g. 3.2), because the use of different coefficients helps to keep in mind that the short-term and long-term creep are considered two different phenomena.

shrinkage strains ( $\epsilon_{SH,u}$ ), so that the reported external relative humidity can be considered as representative of the internal relative humidity ( $RH$ ). Using this assumption, the shrinkage can be expressed in the form of Equation (5-32).

$$\text{-----} \quad (5-32)$$

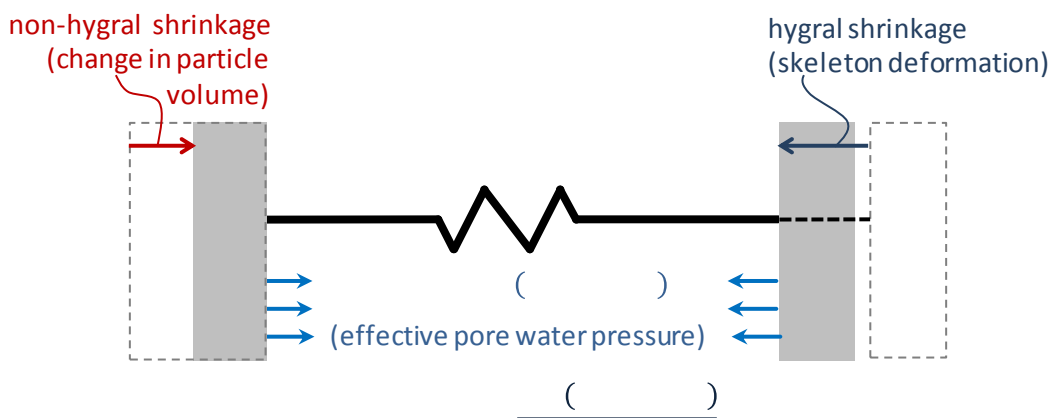


**Figure 5-6: Proposed shrinkage model**

#### 5.4.1 Time Dependent Development of Shrinkage Strains

In order to use strain data truly representative of ultimate shrinkage strains, the time dependent development of shrinkage needs to be investigated and understood. Using the specimens contained in the Shrinkage Evaluation Database, the average shrinkage strains for several small specimens (volume-to-surface area ratios of up to 1.5 in.) are plotted against the square root of time in Figure 5-7. The use of small specimens is most practical for this exercise as the ultimate shrinkage develops in a reasonably short period of time. Strains measured at ages of 4 years or greater were considered to be representative of ultimate shrinkage. The plateau observed in Figure 5-7 for the larger

times indicates that in fact the shrinkage in these specimens can be considered as fully developed at 4 years. This plot can be used to assess shrinkage development by determining the shrinkage halftime ( $\tau_{SH}$ ); defined as the time at which half of the ultimate shrinkage has developed.

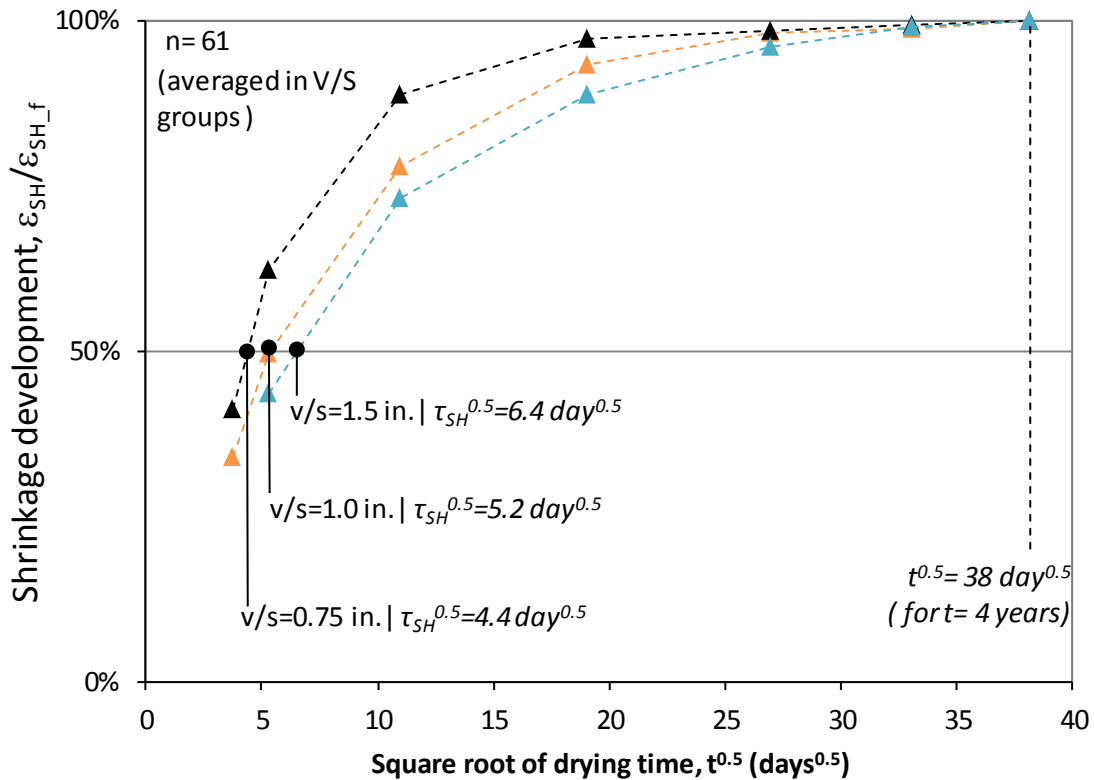


**Figure 5-7: Determination of shrinkage halftime.**

It is conventional to assume that the halftime of shrinkage is proportional to the square of the distance the water has to travel to arrive at the surface,  $\sqrt{\tau_{SH}} \propto D$  (Bažant & Kim, 1991). This distance is commonly considered to be equivalent to the volume-to-surface area ratio ( $v/s$ ), leading to the relationship:  $\sqrt{\tau_{SH}} \propto v/s$ . In Figure 5-8, the square root of the halftime is plotted versus the volume-to-surface ratio. A relation of  $\sqrt{\tau_{SH}} = 5 v/s$  (or  $\tau_{SH} = 25(v/s)^2$ ) was found to be an adequate approximation of the

halftime value. This time factor was derived to characterize the development of the hygral and not the non-hygral shrinkage. However for simplicity it is assumed that both shrinkage types are developed at the same rate.

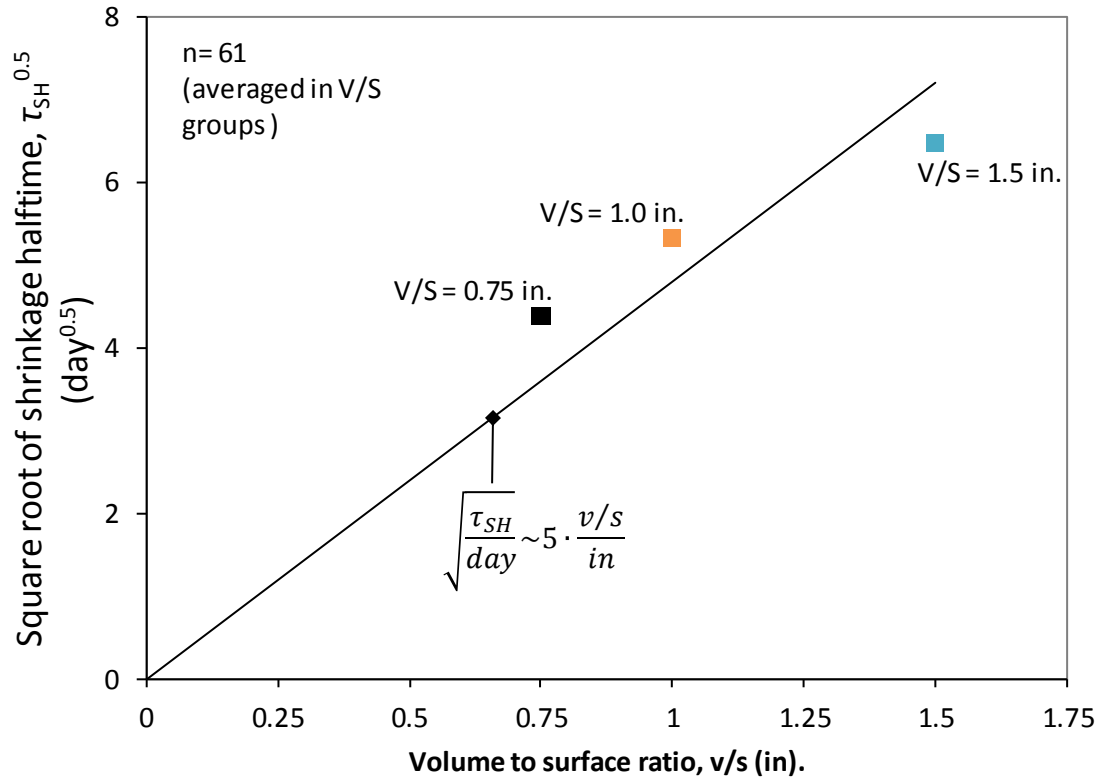


**Figure 5-8: Shrinkage halftime vs. volume-to-surface ratio.**

The development of shrinkage strains normalized by the shrinkage at halftime (obtained from Figure 5-8) versus the time factor ( $\sqrt{t/\tau_{SH}}$ ) is shown in Figure 5-9. It has been proposed that the development of drying shrinkage can be modeled to be proportional to the hyperbolic tangent of this time factor, i.e.  $\epsilon_{SH,t} \propto \epsilon_{SH,u} \tanh \sqrt{t/\tau_{SH}}$  (Bažant, 2000). The proposed relationship may be expressed in terms of the halftime shrinkage as shown in Equation (5-33).

$$\varepsilon_{SH,t}/2\varepsilon_{\tau_{SH}} = \tanh \sqrt{0.3 t/\tau_{SH}} \quad (5-33)$$

where

$t$  = time at which shrinkage is calculated

$\tau_{SH}$  = shrinkage halftime

$\varepsilon_{SH,t}$  = shrinkage strain at time  $t$

$\varepsilon_{\tau_{SH}}$  = shrinkage at halftime, i.e. at  $t = \tau_{SH}$

This adaptation serves the purpose of normalizing shrinkage strains in terms of the halftime shrinkage, which is commonly available for large specimens. The 0.3 coefficient was used to obtain a value of  $\varepsilon_{SH@t}/2\varepsilon_{\tau_{SH}} = 0.5$  when the time is equal to the halftime, to be consistent with the definition of the halftime. As shown in Figure 5-9, the proposed expression does an adequate job of modeling the time-dependent development of shrinkage. However, it is important to note that using this expression results in overestimation of shrinkage strains for large specimens ( $V/S > 1in.$ ). This may be the result of other effects related to the size that are not considered here. Generally, the size is not considered to affect the ultimate magnitude of shrinkage; however, this assumption is considered an open topic (Torrenti & Benboudjema, 2013).

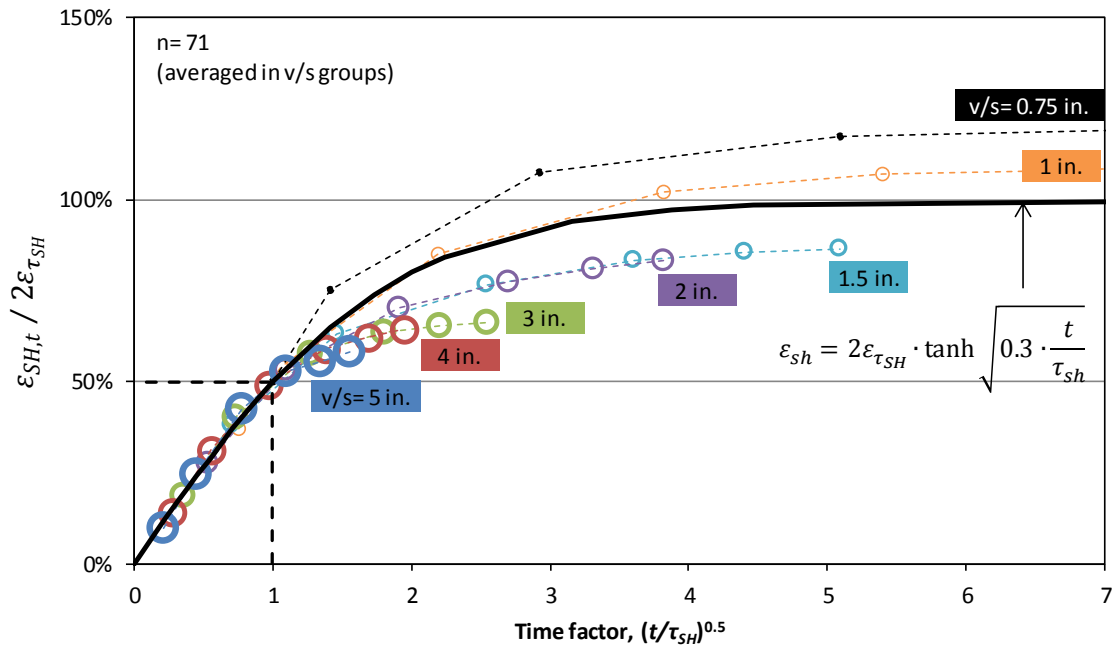


**Figure 5-9: Time-dependent development of shrinkage**

It is shown in Figure 5-9 that the shrinkage does not increase significantly after the time factor of about  $\sqrt{t/\tau_{SH}} = 5$ . Shrinkage strains thereby measured in specimens aged longer than  $t_u = 5^2\tau_{SH} = 625\text{day} \cdot (V/S)^2$  are considered representative of ultimate shrinkage. Given this relationship, shrinkage in specimens with a  $V/S$  ratio equal to 1.5 in. and 3 in. (typical of bridge girders) may be expected to plateau at 4 years and 15 years respectively. These ranges are based on the average observed trends; variability due to environmental conditions and concrete permeability is not captured. Experimental data for long periods of time were only available for small specimens in the database ( $V/S = 0.7$  in. to 1.5 in.). Considering the above, shrinkage for strains measured at final time,  $t_f \geq 625\text{day}/\text{in}^2 \cdot (v/s)^2$  were used to calibrate the shrinkage model. Larger specimens ( $V/S > 1.5$  in.) were therefore not used in the calibration.

### 5.4.2 Calibration of Shrinkage Model Coefficients

Calibration of the shrinkage model was completed using the Shrinkage Evaluation Database (introduced in Chapter 2). The calibration consisted of determining the values of  $C_{nonH}$  and  $C_{HYG}$  to establish the best fit of the theoretical relationship (5-31) with experimental data, as shown in Figure 5-10. For consistency with the creep recommendation, the concrete stiffness at loading ( $E_{ci}$ ) was used to define the shrinkage model as well. The model equations and parameters, including the equivalent stress ( $\sigma_{SH,u}$ ) acting in the short-term spring element ( $C_{ST}E_{ci}$ ), are shown in Table 5-5. The time factor is also presented in Table 5-5. It is important to note that Equation (5-36) of Table 5-5 was multiplied by  $\frac{ST}{t}$  to facilitate integration of Equation (5-37) with the creep model.

**Table 5-4: Characteristics of database specimens used to calibrate shrinkage model**

Volume-to-surface ratio (v/s)	Shrinkage halftime	Filtering criteria	num. of relevant specimens in the database (n)
0.75 in.	14 days	$\geq 1$ year	35
1.0 in.	25 days	$\geq 2$ year	6
1.5 in.	56 days	$\geq 4$ year	20
total			61

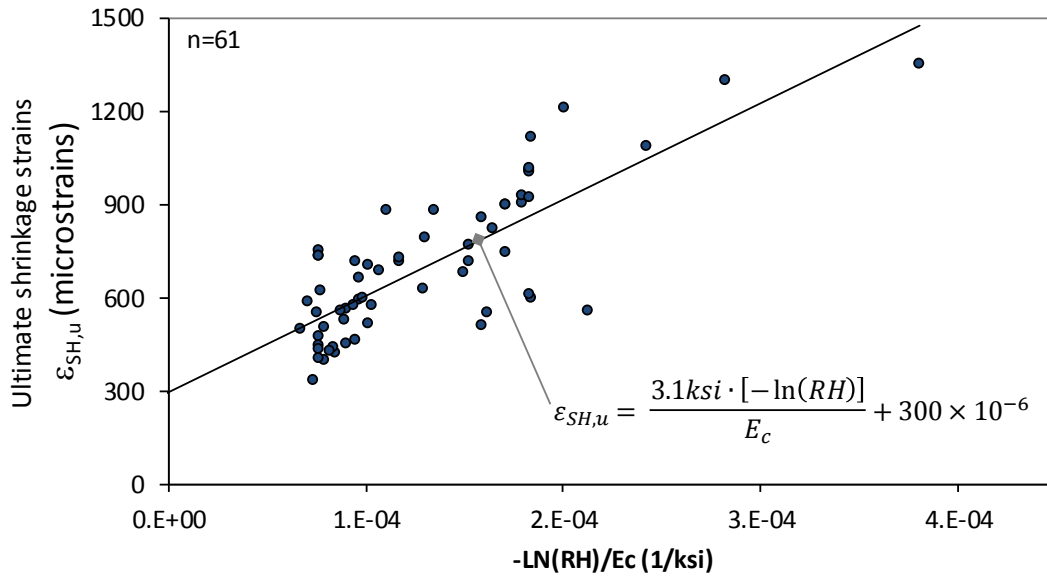


**Figure 5-10: Variation of ultimate shrinkage strain with  $-\ln(RH)/E_c$**

**Table 5-5: Development of shrinkage model**

From calibration using database (Figure 5-10)	$\epsilon_{SH,u} = 3.1ksi \frac{[-\ln(RH)]}{E_c} + 300 \times 10^{-6}$	(5-34)
Assumed relation of $E_c$ vs $E_{ci}$	$E_c = 1.25E_{ci}$	(5-35)
Plug (5-35) in (5-34)	$\epsilon_{SH,u} = 3.1ksi \frac{[-\ln(RH)]}{1.25E_{ci}} + 300 \times 10^{-6}$	(5-36)
Multiply by $1 = \frac{C_{ST}}{C_{ST}}$	$\epsilon_{SH,u} = C_{ST} \cdot 3.1ksi \frac{[-\ln(RH)]}{C_{ST} \cdot 1.25E_{ci}} + 300 \times 10^{-6}$	(5-37)
used nomenclature	$\epsilon_{nonH,u} = 300 \times 10^{-6}$	(5-38)
	$\sigma_{SH,u} = 7.7[-\ln(RH)]$	
Ultimate strain	$\epsilon_{SH,u} = \frac{\sigma_{SH,u}}{3.1E_{ci}} + \epsilon_{nonH,u}$	(5-39)
Halftime	$\tau_{SH} = 25(v/s)^2$	(5-40)
Strain at time $t_{drying}$	$\epsilon_{SH} = \epsilon_{SH,u} \cdot \tanh \sqrt{0.3 \frac{t_{drying}}{\tau_{SH}}}$	(5-41)



### 5.4.3 Proposed Shrinkage Model

Provided that shrinkage is the consequence of a stress (due to pore water pressure change), concrete should creep under this additional stress. Thus, to complete the model, the stress due to shrinkage will be imposed on the same spring that is used to capture deformations due to short-term creep (Figure 5-11); the irreversible fraction of the shrinkage will be neglected by the model. This arrangement was selected because it prevents the estimation of an unbounded shrinkage. Moreover, the relationship between the breakage of C-S-H links (represented by the long-term viscous element) with irreversible shrinkage is not well defined.



**Figure 5-11: Proposed shrinkage model**

## 5.5 MATERIALS-BASED PRESTRESS LOSSES ESTIMATION METHOD

A method for the estimation of prestress losses is presented in this section. The estimation method was developed using the creep and shrinkage models proposed in Sections 5.3 and 5.4, respectively. Development of a reliable method to estimate prestress losses on the basis of material models required careful consideration of the unique demands placed on a simply-supported pretensioned girder. Consideration of the deck shrinkage force and the effects of ongoing prestress losses is discussed prior to presentation of the estimation method.

### 5.5.1 Effect of Deck Shrinkage

Cast-in-place concrete decks are typically placed much later than the pretensioned girders (decks are usually cast within 4 months to 1 year after the fabrication of the girder); shrinkage of the deck occurs well after development of the girder shrinkage. Strain compatibility between the deck and girder results in tensile stress within the deck, compressive stress in the top of the girder, and tensile stress at the centroid of strands. The interaction of the deck and girder is extremely complex, for a number of reasons:

- Post-cracking behavior is involved, as the final shrinkage strains of the deck can be one order of magnitude larger than the elastic strain at cracking
- For later ages, creep tends to reduce the stress in the deck, while the remaining shrinkage tends to increase the stress.
- The use of different deck formwork or precast panels may partially restrain the effect of deck shrinkage and modify exposure of the deck to environmental conditions.

Additionally, the tensile strength of the deck concrete limits the force in the deck from zero to the tensile strength of the deck, which imposes a very small effect on the prestress losses. Using these bounds, the stress in the deck can be assumed to be:

- Equal to the tensile strength of concrete for initial ages, at which the shrinkage-induced stresses are developing faster than the creep-induced relaxation of stress.
- Zero when the age of the deck tends to infinity, due to the asymptotic behavior of shrinkage and the unbound behavior of creep that will continue to relax stresses after the shrinkage in the deck is fully developed.

Considering the above, the deck force is assumed to be limited by the tensile stress for the ages of interest, as shown in Equation (5-42). If precast concrete panels are

used, and the panel cross-sectional area is comparable to the cast-in place cross-sectional area, the deck force should be neglected. The aged deck panel will restrict shrinkage caused by the cast-in-place deck. Considering all the above it can be concluded that the effect of the cast-in-place deck is expected to be negligible when panels are present.

$$P_{deck} \cong f_{ctdeck} \cdot A_{d,CIP} \quad (5-42)$$

### 5.5.2 Effect of Ongoing Prestress Losses

The stress in the concrete at the centroid of the strands varies through time due to prestress losses, especially during the first months after release. For an accurate prediction, it is necessary to either integrate the creep rate considering the stress as a function of time or apply an aging coefficient to consider the variable nature of the stress. These aforementioned approaches result in estimation methods that are more elaborate and complex than desired here. Aiming for simplicity, the stress is assumed to remain constant within each of two stages: before and after deck placement. The stress before deck is determined using the model shown in Figure 5-12 and Equation 5-43. In this form, the representative stress includes the effect of the short-term creep and a fraction of the strand relaxation. The stress after deck is determined based on Figure 5-13 and Equation 5-44.

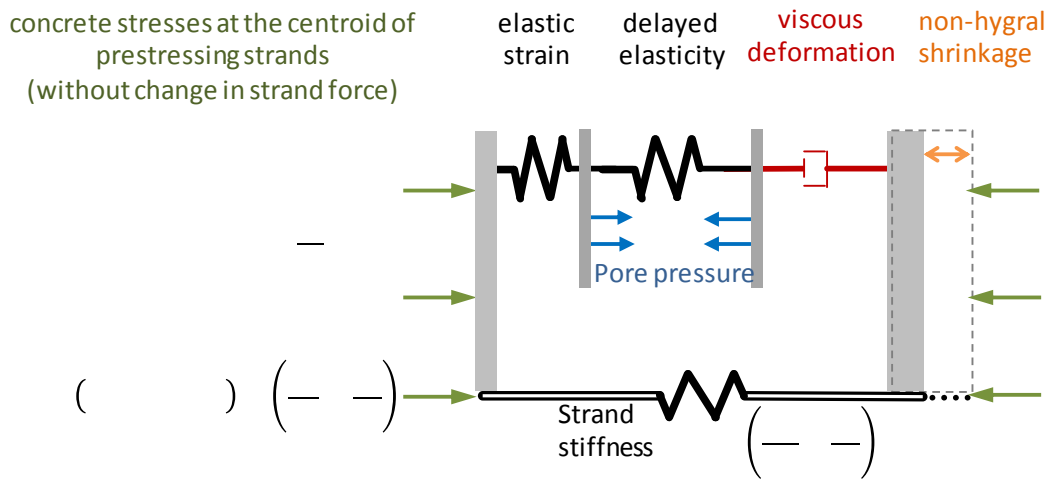


**Figure 5-12: Proposed prestress loss model (stress condition before deck)**

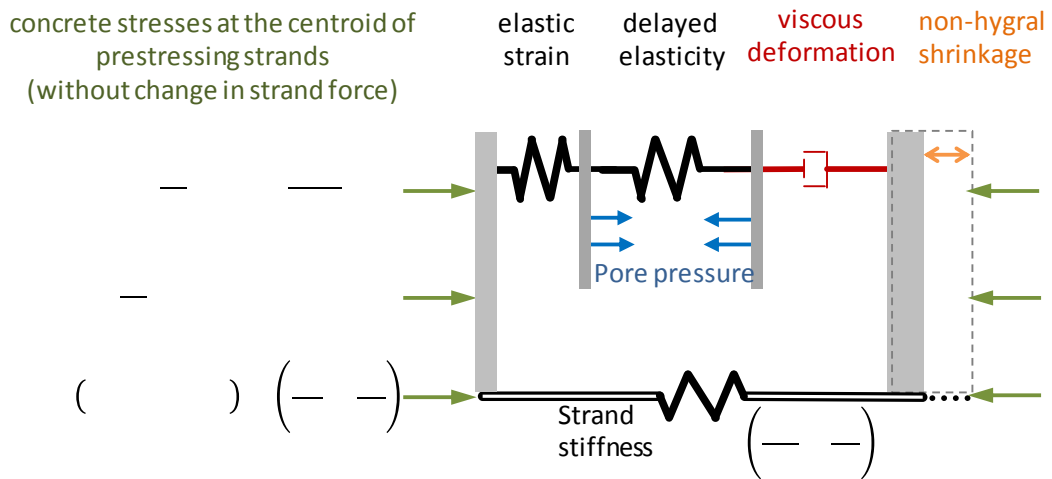


**Figure 5-13: Proposed prestress loss model (stress condition after deck)**

$$\sigma_{ci} = \frac{(f_{p0} - \Delta f_{pREeq})A_p \left( \frac{1}{A_g} + \frac{e_p^2}{I_g} \right) + (-M_{SW}) \frac{e_p}{I_g}}{1 + \frac{A_p E_p}{0.7 E_{ci}} \left( \frac{1}{A_g} + \frac{e_p^2}{I_g} \right)} \quad (5-43)$$

$$\sigma_{c@d} = (f_{p0} - \Delta f_{pRE1} - \varepsilon_{c@d} E_p) A_p \left( \frac{1}{A_g} + \frac{e_p^2}{I_g} \right) + (M_{SW} + M_{deck}) \frac{e_p}{I_g} + P_{deck} \frac{y_t e_p}{I_g} \quad (5-44)$$

where:

- $\sigma_{ci}$  = stress in the concrete shortly after release (short-term creep developed)
- $\sigma_{c@d}$  = stress in the concrete shortly after time of deck casting
- $\varepsilon_{c@d}$  = strain in concrete shortly after time of deck casting
- $f_{p0}$  = initial prestress applied to concrete
- $\Delta f_{pREeq}$  = equivalent relaxation effective shortly after release
- $E_p$  = modulus of elasticity of strands
- $E_{ci}$  = concrete stiffness at release
- $A_p, e_p$  = area and eccentricity of prestressing strands
  
- $A_g, I_g$  = gross area and gross inertia of concrete section
- $y_t$  = distance from top fiber of concrete section to the centroid of the section
- $P_{deck}$  = compressive force applied by the deck to the girder due to deck shrinkage
- $M_{SW}$  = moment due to girder self-weight
- $M_{deck}$  = moment due to deck weight

### 5.5.3 Proposed Method to Estimate Prestress Losses

Based on the model for concrete strains, a model to estimate prestress losses is presented in Figure 5-12 and Figure 5-13 and Using the coefficients and equations presented in Sections 5.3.2 and 5.4.3, combined with the considerations for pretensioned bridge girders discussed above, the concrete behavior model can be applied to the estimation of losses through the use of the equations presented in Table 5-6.

**Table 5-6: Expressions proposed to estimate prestress losses**

	$\frac{P}{A} \left( 1 - \frac{e^2}{r^2} \right)$	(5-45)
	$\left( \frac{P}{A} - \frac{e^2}{r^2} \right)$	(5-46)
General equations		(5-47)
	$\frac{i \left[ \frac{P}{A} - \frac{e^2}{r^2} \right]}{1 - \frac{e^2}{r^2}}$	(5-48)
	$\alpha y \left( \frac{v/s}{1 - \frac{e^2}{r^2}} \right)$	(5-49)
Shortly after release (short-term creep included)	$\frac{P}{A} \left( 1 - \frac{e^2}{r^2} \right)$	(5-50)
At deck placement time	$\frac{P}{A} \left[ \ln \left( \frac{P}{A} \right) \right]$	(5-51)
	$\sqrt{\frac{P}{A} / \dots}$	(5-52)
		(5-53)
	$\frac{P}{A} \left( \frac{P}{A} - \frac{e^2}{r^2} \right)$	(5-54)
	$\frac{P}{A} \left( \frac{P}{A} - \frac{e^2}{r^2} \right)$	(5-55)
	$\frac{P}{A} \left( \frac{P}{A} - \frac{e^2}{r^2} \right)$	(5-56)
Final time	$\frac{P}{A} \left[ \ln(t_f) \right]$	(5-57)
	$\sqrt{\frac{P}{A} / \dots}$	(5-58)
		(5-59)
	$\frac{P}{A} \left( \frac{P}{A} - \frac{e^2}{r^2} \right)$	(5-60)

The performance of the method is assessed by comparing the estimation versus measured values from the UTPC-Loss Strain Evaluation Database presented in Chapter 2. The performance of the method is found to be adequate and conservative. The coefficient of variation is 21%, which is comparable to that of methods to estimate creep and shrinkage Keitel & Dimmig-Osburg (2010) and Bažant & Baweja (2000). The estimation of prestress losses involves elastic behavior, which can be estimated more accurately and therefore reduce the variation in the estimation of total losses. This is counteracted by the larger variability in conditioning, which increases the variation in the estimation of total losses. With these factors in mind, a coefficient of variation for the estimation of prestress losses comparable to that for creep and shrinkage estimations is considered satisfactory.

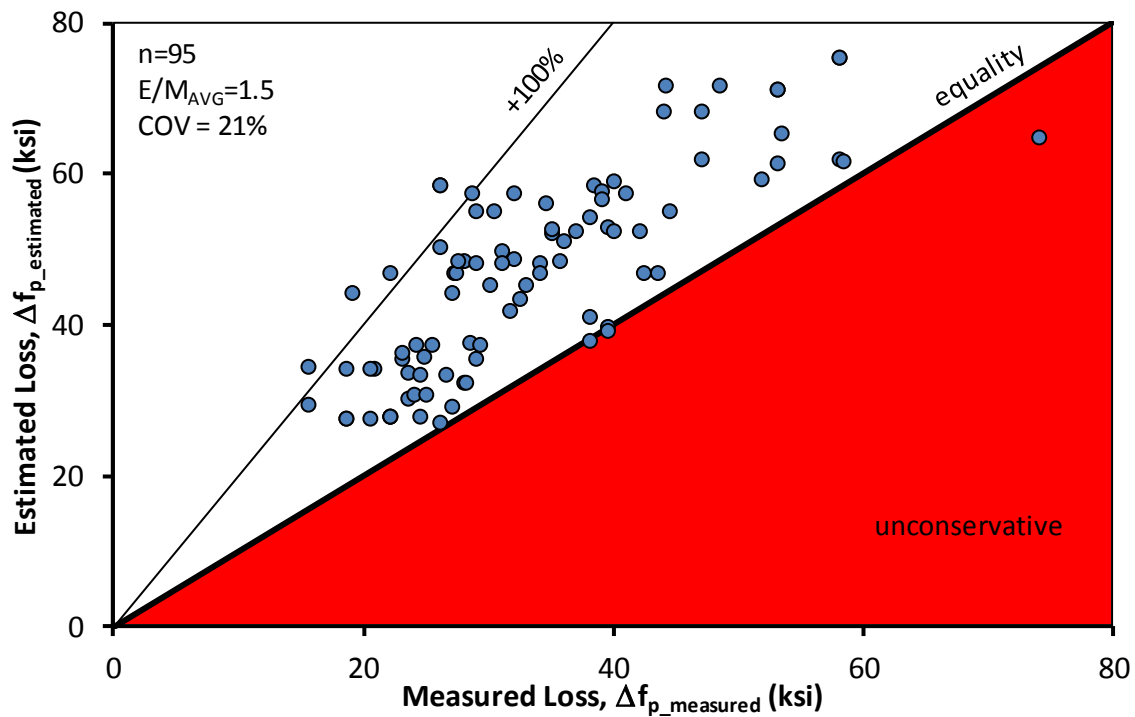


**Figure 5-14: Material-based estimation vs. measured prestress losses.**

## 5.6 SUMMARY

A novel prestress loss estimation method was developed on the basis of fundamental concrete behavior including elastic deformation, creep, and shrinkage. Widely accepted theories of creep and shrinkage mechanisms were incorporated into the method; which only reflects the most relevant parameters. The resulting expressions were calibrated using an existing database of experimental results from creep and shrinkage studies, slightly expanded with some specimens found in the literature. The materials-based model was further tailored to be representative of the conditions associated with the construction and behavior of a typical simply-supported bridge girder.



## CHAPTER 6

### Development of a Prestress Loss Model Using Girder Test Data

#### 6.1 INTRODUCTION

A theoretically accurate prestress loss estimation procedure for pretensioned determinate girders was developed in Chapter 5 on the basis of behavioral models for concrete creep and shrinkage. These models included several factors that have been shown to have an effect on the development of creep and shrinkage. While the development of these type of models may be necessary for complex structures, simplified models can and should be used for the estimation of losses in standardized elements that are well understood and feature little variation. Simplistic creep and shrinkage methods for the estimation of prestress losses in *prestressed pretensioned simply-supported bridge girders* are desirable and feasible.

In the following sections a simple prestress loss model using structural test data is developed. The development of such a model can be conducted as follows:

- Establish a conceptual *long-term concrete behavior model* on the basis of the main mechanisms at the origin of creep, shrinkage and elastic strains. Such a model should contain proportionality coefficients to allow for calibration (This type of model was developed in Chapter 5)
- Assess the creep and shrinkage behavior of structural elements on the basis of structural test data (the element behavior is here characterized using *sectional creep and shrinkage* coefficients, as shown in Section 6.3).
- Calibrate the creep and shrinkage *time-dependent model* proportionality coefficients using the time-dependent sectional creep and shrinkage

coefficients (Section 6.4). This type of model is especially useful for the verification of camber at various times during construction.

- Develop a simplified and conservative expression to estimate *ultimate conditions* by simplifying the model including common conservative design assumptions for the parameter used in the developed model (Section 6.5). This type of model is especially useful for stress-checks at ultimate time.
- Establish a *girder-based method* to implement the creep and shrinkage models in the estimation of prestress losses considering the conditions to which the element is subjected through its service live (Section 6.6)
- *Evaluate the performance* of the method using a comprehensive (statistically representative) data from testing of pretensioned girders, such as that available in the UTPS-Loss database (Section 6.7).

In summary, a simplified model of prestress loss developed on the basis of girder behavior is developed in this chapter. This model is similar to that developed in Chapter 5, but it is calibrated on the basis of girder behavior through the inclusion of girder-based sectional creep and shrinkage coefficients.

## **6.2 MOTIVATION FOR THE DEVELOPMENT OF A PRESTRESS LOSS MODEL USING GIRDER TEST DATA**

The complexity of the method used to estimate the prestress losses in standardized bridges should be in balance with the achievable (and expected) accuracy. The accuracy of complex methods is compromised when it requires the assumption of values for relevant parameters that are unknown during design (e.g. coarse aggregate type). During the construction of standardized bridges many of these assumptions are not verified, thus eliminating the advantage of a complex method (and its associated accuracy benefits)

over a simplistic one. In addition to such unverified assumptions, questions also arise about the use of parameters that have little or no impact on the design. If neglecting these parameters is conservative, especially if their use might lead to errors due to misinterpretation (e.g. deck shrinkage), they should likely be excluded from the model. Parameters with limited variability (see Table 6-1) can be generally considered as constant without affecting the method's accuracy in a meaningful way. A simplistic method developed with these points in mind may have the advantage of being clear, easy to use, and less prone to error.

When calibrating empirical equations it is beneficial to use the data that is most relevant to the given problem. The use of generalized creep and shrinkage models for the estimation of losses in pretensioned girders has several disadvantages. General methods are exclusively calibrated using cylinder or prism testing results, which have several marked difference from girder specimens (Table 6-2). Additionally, general methods are aimed at a broad range of cases, and are required to capture the effect of broad variations in various parameters. It is intuitive that less complexity is necessary in a method aimed to a singular type of structure: pretensioned girders. Through the use of data from a specific type of structure, the range of values to be considered is narrowed to that relevant for the type of structure in the study.

In summary, for the estimation of losses in pretensioned simply-supported bridge girders, a model based on girder testing data would be more representative than those based on generalized creep and shrinkage models.

**Table 6-1 Parameters with limited variability in pretensioned bridge girders**

Parameter		Typical range of values:		Main method used to consider the parameter.
Description	Variable	Pretensioned girders <sup>3</sup>	Concrete testing	
Age at first loading, or Age at release	$t_i$	0.5 to 3 days	> 7 days	Empirical correction factors (testing in the range of concern is scarce)
Volume to Surface Ratio	$v/s$	3 to 5 in.	1 in.	
Change in stress <sup>4</sup>	$\frac{\Delta\sigma_c}{\sigma_{ci}}$	-5% to - 50%	0	Superposition of strains and aging coefficient
Time of deck location	$t_d$	>4 months	--	
Prestressing Ratio	$\rho$	0.5% to 1.5%	0	Mechanics of materials

**Table 6-2 Difference in conditions between pretensioned bridge girders and concrete material samples**

Parameter or Conditions	Common Range of values for:		Main method used to consider the difference in condition.
	Pretensioned girders	Concrete testing	
Shape of specimen	Irregular (bulkier bottom flanges)	Circular or square	None (only v/s is considered)
Stress level	Variable with time	constant	Aging coefficient
Theoretical Stress profile	Linear through the section	uniform	None (Shrinkage and creep coefficient assumed constant through the section)
Environmental Relative Humidity	Irregular (with respect to time)	Constant	
Specimen Temperature (after hydration)	Irregular (respect to time and location)	Constant	

<sup>3</sup> approximately 90% of the specimens in the evaluation database fall in this ranges.

<sup>4</sup> i.e. changes after release, e.g. stress caused by deck weight, change of stress due to losses.

### 6.3 ASSESSMENT OF SECTIONAL CREEP AND SHRINKAGE THROUGH GIRDER STRAIN MONITORING

As discussed above, prestress loss models are typically empirical and based on measurements of creep and shrinkage in cylindrical samples. A prestress loss model based on measurements of pretensioned girder strains will be presented in this section. The analysis focuses on the deformation of the girder concrete, which is subjected to stresses due to self-weight, strand force, and externally applied forces. This approach results in determination of the *sectional creep coefficient* and *sectional shrinkage coefficient* which are useful to characterize the long-term deformation of the girder. It is shown that this model is simple and conservative for structures that fall within the ranges included in calibration of the model.

#### 6.3.1 Sectional Creep and Shrinkage Coefficients

When concrete deforms under constant stress, it is common to define the total strain as the addition of elastic ( $\epsilon_{ELA}$ ), creep ( $\epsilon_{CR}$ ), and shrinkage ( $\epsilon_{SH}$ ) strains as shown in Equation (6-1). It is also common to define creep strains in terms of the elastic strain and the creep coefficient<sup>5</sup> ( $\psi$ ) as shown in Equation (6-2).

$$\epsilon_c = \epsilon_{SH} + \epsilon_{ELA} + \epsilon_{CR} \quad (6-1)$$

$$\epsilon_{CR} = \psi \cdot \epsilon_{ELA} \quad (6-2)$$

In order to make these general strains specific to those occurring in girders ( $\epsilon'$ ), the Equation (6-1) can be rewritten as Equation (6-3) using *sectional shrinkage* ( $\epsilon'_{SH}$ ) and *sectional creep* ( $\epsilon'_{CR}$ ) strains. These sectional strains are used with the intent to capture the global behavior of the girder.

---

<sup>5</sup> the definition of creep in terms of the compliance is preferred by some researchers.

$$\varepsilon' = \varepsilon'_{SH} + \varepsilon_{ELA} + \varepsilon'_{CR} \quad (6-3)$$

$$\varepsilon_{ELA} = \frac{\sigma_c}{E_c} \quad (6-4)$$

$$\varepsilon'_{CR} = \psi' \cdot \varepsilon_{ELA} \quad (6-5)$$

where

$\sigma_c$  = sectional stress (calculated here based on loads and prestressing)

$E_c$  = concrete stiffness

The special nomenclature used for the girder strains was implemented to represent the global behavior of the girder, which in general is not representative of the local behavior of the concrete within the girder. This difference, which motivates the use of the sectional strain nomenclature, can be outlined using the example of an *unstressed-unloaded girder*, as follows:

- from a *sectional* behavior point of view the stress is zero ( $\sigma_c = 0$ ), then:
  - the creep and elastic strain are zero ( $\varepsilon'_{CR} = 0$  and  $\varepsilon_{ELA} = 0$ )
  - all the strain is regarded as shrinkage strain ( $\varepsilon' = \varepsilon'_{SH}$ )
- from a *local* perspective the shrinkage generates stress ( $\sigma_{c,LOCAL} \neq 0$ )<sup>6</sup>, then:
  - the concrete within the girder experiences elastic and creep strains
  - the local concrete strains ( $\varepsilon_c$ ) within the girder are the reflection of elastic, creep and shrinkage strains ( $\varepsilon_c = \varepsilon_{SH} + \varepsilon_{ELA} + \varepsilon_{CR}$ )

As presented above, the elastic strain ( $\varepsilon_{ELA}$ ) and the stress ( $\sigma_c$ ) as traditionally calculated are also sectional characteristics. However, these sectional parameters are broadly used and the calculation is simple in externally determinate structures. Therefore, for simplicity the “sectional” nomenclature will not be used to rename the sectional elastic strain and the sectional stress.

---

<sup>6</sup> the shortening of outermost regions that dry faster is restrained by the rest of the girder

Further break down of the terms in Equation (6-3) corresponding to elastic strains and creep are presented in Equations(6-6) and (6-7), respectively. Joining these equations leads to Equation (6-8), which is considered here as the simplest equation that includes all shrinkage, elastic, and creep strains in the girder. These equations consider the three main forces (acting in the concrete) that cause elastic strains in the concrete: (1) self-weight, (2) strand force, and (3) external loading.

$$\varepsilon_{ELA} = \varepsilon_{ES} + \varepsilon_{DL} + \varepsilon_{dSH} + \int_{t_i}^{t_f} d\varepsilon_{\Delta f_{LT}} \quad (6-6)$$

$$\varepsilon'_{CR} = \psi'_i \cdot \varepsilon_{ES} + \psi'_d \cdot \varepsilon_{DL} + \chi_{dsh} \psi'_d \varepsilon_{dSH} + \int_{t_i}^{t_f} \psi'_t d\varepsilon_{\Delta f_{LT}} \quad (6-7)$$

$\varepsilon' = \varepsilon'_{SH} + \varepsilon_{ES}(1 + \psi'_i) + \varepsilon_{DL}(1 + \psi'_d) + \varepsilon_{dSH}(1 + \chi_{dSH} \psi'_d) + \int_{t_i}^{t_f} (1 + \psi'_t) d\varepsilon_{\Delta f_{LT}} \quad (6-8)$
--

where

- $\varepsilon'$  = girder strain
- $\varepsilon'_{SH}$  = sectional shrinkage strain in the girder
- $\varepsilon'_{CR}$  = sectional creep strain in the girder
- $\varepsilon_{ELA}$  = sectional elastic strain in the girder
- $\varepsilon_{ES}$  = elastic shortening strain at release
- $\varepsilon_{DL}$  = strain due to dead load, mainly deck and barrier weight
- $\varepsilon_{dSH}$  = strain due to deck shrinkage
- $\varepsilon_{\Delta f_{LT}}$  = strain due to changes in strand force due to creep and shrinkage.
- $\psi'_i$  = final sectional creep coefficient related to elastic shortening (at time  $t_i$ )
- $\psi'_d$  = final sectional creep coefficient related to loads at time of deck casting ( $t_d$ )
- $\psi'_t$  = final sectional creep coefficient related to loads applied at time  $t$
- $t_f$  = time at which strains are to be determined

In Equation (6-6) the elastic shortening, dead load, and deck shrinkage strain are the result of the combined effect of two simultaneous occurrences: (1) forces acting on the concrete and (2) change in the strand force (restraining or stiffening effect on the reinforcement). The only other relevant elastic strain in the concrete is that due to change in the strand stress due to creep and shrinkage of the girder. The integral operator is used to allow the inclusion of time-dependent elastic strains. For simplicity, in Equation (6-8) the shrinkage strain is kept as a single coefficient ( $\epsilon'_{SH}$ ), this implies that the effects of complex phenomena, such as differential shrinkage and creep-shrinkage interaction, are neglected.

There is a notable difference between standard coefficients and sectional coefficients, when comparing the coefficients determined based on cylinder tests and those from girder data. The difference in magnitude between these coefficients can be attributed mainly to the different distribution of stress, shrinkage, and creep through the section. Small areas of the section are subjected to *local* shrinkage and creep; due to compatibility, the strains in such areas are governed by sectional behavior (plane sections remain plane) rather than by local behavior. As mentioned above, the *sectional* shrinkage and creep coefficients are aimed to be representative of the girder behavior, and should not be interpreted as representative of local or cylinder behavior.

The main assumption made in this formulation (and in current design methods) is that shrinkage and creep coefficients are constant through the section. While this assumption is necessary to avoid complexity, it requires calibration of the coefficient to be representative of the type of structure under study.

The variability of the *sectional* coefficients within pretensioned, simply-supported girders is expected to be much less than the variability observed within the complete



spectrum of plain concrete or concrete structures. This expectation is based on the fact that pretensioned girders usually share many characteristics, as presented in Section 6.1.

### **6.3.2 Simplification of Sectional Creep and Shrinkage Expressions**

Although the sectional behavior is complex and the non-uniformity of local stresses, creep, and shrinkage cannot be measured using currently available technology<sup>7</sup>, the sectional creep and shrinkage can still be measured. The approach presented here to obtain sectional creep and shrinkage based on sectional strain measurements implies assumptions commonly used in sectional design: (1) constant creep and shrinkage through the section (as mentioned in Section 6.4.1), (2) linear distribution of stress, and (3) superposition of creep.

While Equation (6-8) can be applied to any point measured in the beam to estimate strains, the large number of coefficients makes the equation impractical for empirical calibration purposes. Two sets of assumptions can be used to bound Equation (6-3) between two expressions for the sectional creep coefficients. For both approaches the characterization of the sectional behavior will be conducted for the period before deck casting. This is adopted to prevent the introduction of large uncertainty due to the complex interaction within girder and deck.

#### ***6.3.2.1 Assumption Set 1***

By assuming the elastic shortening is the only non-zero elastic strain, Equation (6-6) can be simplified to (6-9) and Equation (6-7) to (6-10). Implementing these simplified expressions into Equation (6-8) leads to (6-11). The use of these assumptions

---

<sup>7</sup> the local creep can be measured during nano-indentation, but the local creep occurring in a girder due to self-weight, prestressing and external loading cannot be measured.

together with an accurate sectional creep coefficient results in conservative estimations. The calibration of the sectional creep coefficient using this first set of assumptions together with experimental results leads to a lower bound sectional creep coefficient ( $\psi'_1$ ). The sectional shrinkage strain obtained from this approach will be called  $\varepsilon'_{SH1}$ .

**Table 6-3 Expressions resulting from Assumption Set 1**

Assumption	Expression
The only sources of elastic strain and creep is the elastic shortening	$\varepsilon_{ELA} = \varepsilon_{ES}$ (6-9)
	$\varepsilon'_{CR} = \varepsilon_{ES}\psi'_1$ (6-10)
Plug 6-28 and 6-29 into 6-24	$\varepsilon' = \varepsilon'_{SH1} + \varepsilon_{ES}(1 + \psi'_1)$ (6-11)

### 6.3.2.2 Assumption Set 2

By assuming the elastic strain is composed of strain caused by elastic shortening and that by the change in strand stress, Equation (6-6) can be simplified to Equation (6-12). The effect of strand stress on the elastic strain ( $\varepsilon_{\Delta f_{pLT}}$ ) is calculated assuming the stress change is proportional to the change in strand stress caused during elastic shortening; this implicitly is equivalent to assuming a constant modulus of elasticity. By assuming the final creep coefficient is constant and not dependent on the loading time, Equation (6-7) simplifies to (6-13). Implementing these simplifications into Equation (6-8) leads to (6-14). The use of these assumptions in the calibration procedure results in an upper bound sectional creep coefficient ( $\psi'_2$ ) and a reasonable estimate of shrinkage strain ( $\varepsilon'_{SH2}$ ).

**Table 6-4 Expressions resulting from Assumption Set 2**

Assumption	Expression
The sources of elastic strains are the elastic shortening and change in strand stress due to prestress losses	$\varepsilon_{ELA} = \varepsilon_{ES} + \varepsilon_{\Delta f_{LT}}$ (6-12)
The creep strain is proportional to the elastic strains defined in equation (6-12), and the proportionality can be defined with a single equivalent creep coefficient ( $\psi'_2$ )	$\varepsilon'_{CR} = (\varepsilon_{ES} + \varepsilon_{\Delta f_{LT}})\psi'_2$ (6-13)
Plug 6-31 and 6-32 into 6-24	$\varepsilon' = \varepsilon'_{SH,2} + (\varepsilon_{ES} + \varepsilon_{\Delta f_{LT}})(1 + \psi'_2)$ (6-14)

where:

$\varepsilon_{\Delta f_{LT}}$  = elastic strain due to the long-term change in prestressing force (due to creep and shrinkage). The assessment of this value requires the calculation of the strain due to self-weight load ( $\varepsilon_{SW}$ ), as shown below.

$$\varepsilon_{\Delta f_{LT}} = -\frac{(\Delta f_p - \Delta f_{pES})}{f_{p0} - \Delta f_{pES}} (\varepsilon_{ES} - \varepsilon_{SW}) \quad (6-15)$$

$\Delta f_p$  = total prestress losses

$\Delta f_{pES}$  = prestress losses due to elastic shortening

$f_{p0}$  = stress in the strand before release

### 6.3.3 Measurement of Sectional Creep and Shrinkage

In an instrumented section of a girder, the elastic shortening strain ( $\varepsilon_{ES}$ ) and the final measured strain ( $\varepsilon'$ ) are measured. The elastic strain due to long-term changes in the prestressing force ( $\varepsilon_{\Delta f_{LT}}$ ) can be estimated using (6-15).

A linear strain profile through the height of the cross-section can be established using the data from two or more gauges, as shown in Figure 6-1(a). The linearity of the measured strain across the cross-section could be verified using this data; the linearity for the specimens studied was at least  $R^2=0.95$ . The data from two or more gages can be input into Equation (6-16) to solve for  $\psi'_1$  and  $\varepsilon_{SH1}$ , and into (6-17) to solve for  $\psi'_2$  and

$\varepsilon_{SH2}$ . A linear regression is used here to find the solution for these coefficients, as shown in Figure 6-1 (b) and (c). The slope of the regression line represent the value of  $1 + \psi'$  and the intersect represents  $\varepsilon'_{SH}$ . The upper and lower bound coefficients simplistically capture the range within which the actual measured sectional creep coefficient and shrinkage strains should fall.

$$\varepsilon' = \varepsilon_{ES}(1 + \psi'_1) + \varepsilon'_{SH1} \quad (6-16)$$

$$\varepsilon' = (\varepsilon_{ES} + \varepsilon_{\Delta f_{LT}})(1 + \psi'_2) + \varepsilon'_{SH2} \quad (6-17)$$

The plots provided in Appendix E were used to determine the coefficients for 32 girders from the database (including 12 from project TxDOT Project 0-6374). The resulting final coefficients are summarized in Table 6-5. For the generation of this table, the coefficients were assessed *before the deck was cast*, or at the end of the monitoring period if a deck was not cast. This approach is only preliminary, and sets expectations with respect to the magnitude of values that are representative of ultimate conditions, and the associated variability (for different girders with different conditioning times). However, the proposed model includes time-dependent development of creep.

Both sets of assumptions give reasonable average values relative to each other and compared with calibrated cylinder coefficients. However, negative shrinkage strains were obtained with the method for some specific specimens. These negative strains are believed to be a consequence of differential shrinkage occurring within the section; however, verification of this behavior is out of the scope of this study. The values in Table 6-5 are not suggested as representative of the shrinkage strains and the creep coefficient for material properties in general, but will be used as a comparison point for development of the coefficients for the method in Section 6.6.

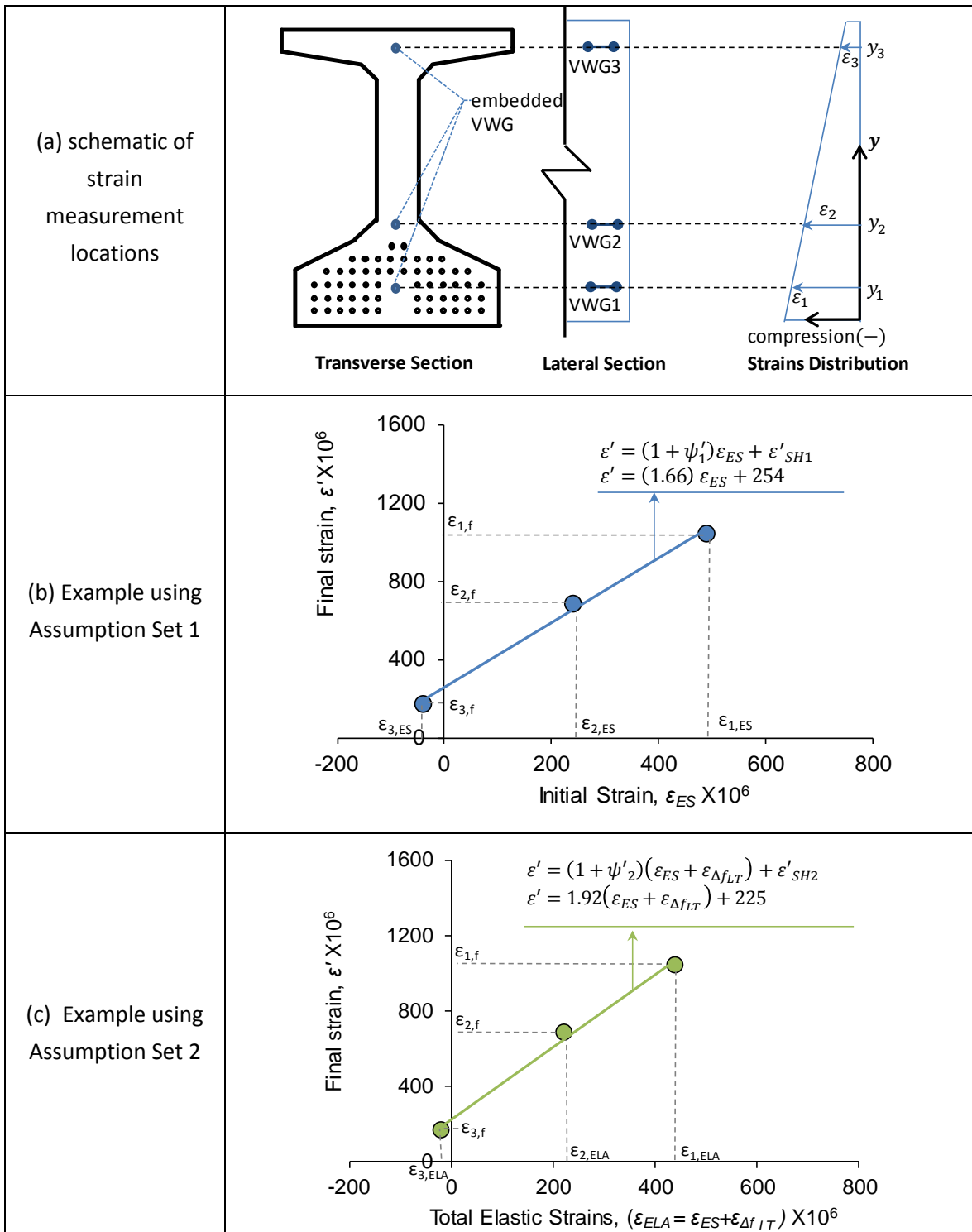


**Figure 6-1 Examples of determination of sectional coefficients for specimen UTPS-Loss#62; experimental data from (Gamble 1970).**

**Table 6-5 (a) Sectional Coefficients Before Deck Casting on the Basis of Measured Girder Strains**

UTPS-Loss Specimen No.	Source	Age	Sectional Creep		Sectional Shrinkage	
			$\psi'_1$	$\psi'_2$	$\epsilon_{SH1}$	$\epsilon_{SH2}$
4	Barr et al. (2000)	197	0.54	0.83	58	7
56	Erkmen et al. (2007)	600	0.77	1.00	103	91
57		580	0.92	1.24	86	70
58		600	0.52	0.63	128	123
59		475	0.70	0.88	115	108
60		460	0.79	0.99	99	92
61		475	0.70	0.86	78	71
62	Gamble (1970)	230	0.66	0.99	254	218
105	Houdeshell et al. (1972)	220	0.30	0.76	633	568
106		220	0.26	0.61	497	441
119	Larson (2006)	515	1.11	1.40	227	222
120		515	1.21	1.51	134	129
222	Garber et al. (2013)	978	0.71	0.90	21	7
224		948	0.52	0.69	136	124
226		976	0.13	0.27	620	610
228		946	0.60	0.79	99	85
230		701	0.73	0.85	56	49
232		932	0.68	0.81	81	75
235		951	0.77	0.92	49	42
237		923	0.63	0.75	87	81
238		693	0.97	1.31	16	-8
240		676	0.86	1.12	-23	-42
242		702	1.00	1.35	-27	-51
244		680	0.90	1.17	-37	-56
246		249	0.68	0.85	166	157

**Table 6-5(b) Final Sectional Coefficients Before Deck Casting on the Basis of Measured Girder Strains**

UTPS-Loss Specimen No.	Source	Age	Sectional Creep		Sectional Shrinkage	
			$\psi'_1$	$\psi'_2$	$\epsilon_{SH1}$	$\epsilon_{SH2}$
247	Garber et al. (2013)	258	0.67	0.82	124	116
248		220	0.51	0.65	190	183
250		256	0.50	0.62	138	133
251		250	0.49	0.61	167	161
262-264	Waldron (2004) (average of 3 specimens)	240	0.62	0.75	3	-9
Average			0.68	0.90	140	130
COV			35%	31%	120%	130%
Average + 2 COV			1.2	1.4	470	450

#### **6.4 CALIBRATION OF TIME-DEPENDENT PRESTRESS LOSS MODEL ON BASIS OF GIRDER DATA**

A time-dependent model to estimate the development of creep and shrinkage is presented in this section. The model is comparable to the model developed in Chapter 5, but is calibrated on the basis of girder behavior as opposed to cylinder behavior. Girder behavior was characterized in the experimental program presented in Chapter 3 and Chapter 4. The interest of estimating the time-development of losses could be the estimation of camber at various age. Considering that the camber estimation is expected to be accurate, instead of conservative, this model is aimed to accuracy. Thus, some values will be underestimated with this time-dependent model. In Section 6.5, a simplified conservative model of creep and shrinkage is presented; such model should be used to verify tensile stress in the concrete at ultimate age. In other words, creep and shrinkage models will be simplified and calibrated for two purposes: (1) accurate estimation of the time-dependent losses which is especially useful for the calculation of camber at time of deck placement, and (2) conservative estimation of ultimate loss, which

is adequate for serviceability stress checks. In Section 6.6 both models are integrated into a method to estimate prestress losses.

### 6.4.1 Time-Dependent Sectional Creep Model

In Chapter 5, the creep coefficients proposed in the Burgers model of Figure 5-1 were calibrated on the basis of materials test data. In this section, a similar procedure will be applied to calibrate the creep coefficients and will use data from experimental program of Chapter 3, Chapter 4 and from the UTPS-Loss Database. The model for which the coefficients will be calibrated is shown in Figure 6-2. The model includes the initial stress at release ( $\sigma_{ci}$ ), whose variation in time will be accomplished through the use of coefficients. The model is intended to capture the girder (including concrete and strands) creep under the action of an initial stress  $\sigma_{ci}$ . Under these conditions the Assumption Set 1 is more appropriate to define the sectional coefficients, because it assumes that the elastic strains and the stress are constant and equal to the initial conditions.

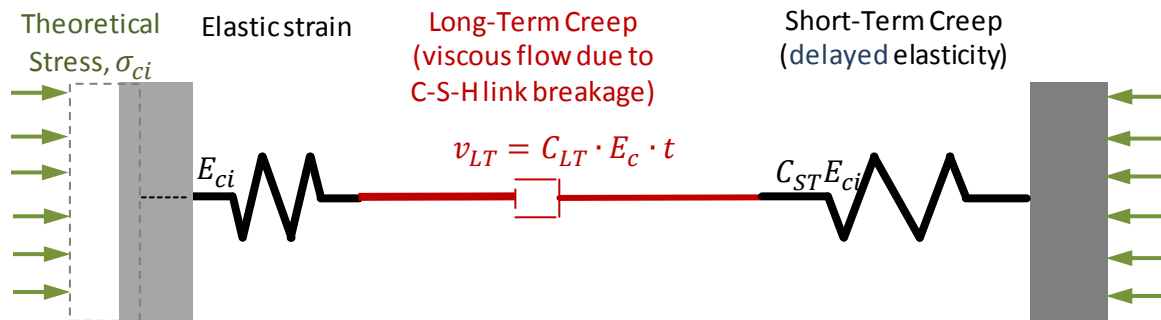


**Figure 6-2 Proposed Creep Model**

To calibrate the model coefficients  $C_{ST}$  and  $C_{LT}$ , sectional creep coefficients are obtained for various ages, and a time-dependent expression for the creep coefficient is formulated. Development of the time-dependent expression for sectional creep coefficients of the specimen I-1 (TxDOT Project 0-6374) is shown in Figure 6-3. An expression of the



total sectional creep coefficient ( $\psi'_1$ ) was obtained separately for each specimen by using a linear regression, as shown in the Figure 6-3 for Specimen I-1. With the expression for the creep coefficient, the inverse of the calibration coefficients<sup>8</sup> can be determined, as shown for Specimen I-1 in Table 6-6 and Table 6-7. Such expressions were developed in Appendix B for all the specimens within UTPS-Loss for which the strain profile history was discovered. The results for the studied specimens are presented in groups of similar specimens, fabricated simultaneously in the same prestressing plant, and stored in the same location. The coefficients of expressions resulting for such similar specimens are averaged into coefficients representative of the group, as shown in Table 6-8. It is important to note that not all of the specimens for which a final sectional behavior was defined could be used for the calibration of coefficients. This is mainly because for some of the specimen a reliable complete time-history of strain profiles was not discovered.

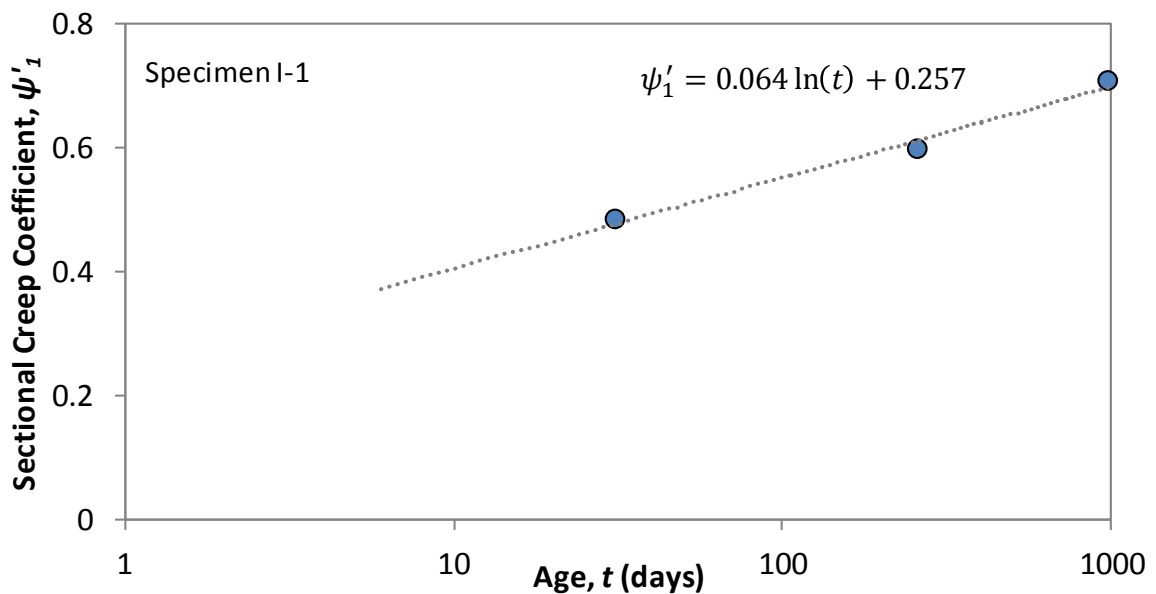


**Figure 6-3 Time-development of effective creep coefficient for Specimen I-1**

<sup>8</sup>it was intended to average the behavior of the specimens in terms of a parameter directly related to the measured magnitude (strains), such as the inverse of the calibration coefficients.

**Table 6-6 Derivation of  $1/C$  from girder data for Specimen I-1**

By definition		(6-18)
By definition	—	(6-19)
From table 5-1	$\frac{1}{n} [\ln(t) - \ln(t_i)]$	(6-20) Re (5-10)
From Figure 6-3	$\ln(t)$	(6-21)
Then, for long term	$0.64 [\ln(t) - \ln(t_i)]$	(6-22)
From Table 4-1		(6-23)
		(6-24)
Plug (6-19), (6-20) & (6-22) in (6-18)	$\frac{1}{n} [\ln(t) - \ln(t_i)] - 0.64 [\ln(t) - \ln(t_i)]$	(6-25)
Simplifying (6-25)	—	(6-26)

**Table 6-7 Derivation of  $1/C$  from girder data for Specimen I-1**

By definition		(6-27)
From Table 4-1		(6-28)
Plug (6-21) and (6-22) in (6-27)	$[0 - n(t) - 257] [\ln(t) - \ln(t_i)]$	(6-29)
solving		(6-30)
By definition		(6-31)
From figure 5.1	—	(6-32)
	—	(6-33)
Plug (6-32) & (6-33) in (6-31)	— —	(6-34)
Simplifying (6-34)	—	(6-35)

The behavior of the specimens results in average coefficients  $C'_{LT} = 12$  and  $C'_{ST} = 3.7$  as shown in Table 6-8. The sectional short-term coefficient is similar to that obtained from cylinder measurements (3.7 and 3.1 respectively). On the other hand, the sectional long-term coefficient is almost four times larger than the materials-based long-term coefficient (12 and 3.6 respectively). The reason behind this difference is unclear, all of the differences listed in the Table 6-2 might contribute, in different proportions to this difference. Further research is necessary to determine the main factors involved on the origin of this high coefficient related to viscosity that defines the long-term behavior of the girders.

Conservative coefficients can be obtained from the data in Table 6-8, by using the average plus twice the coefficient of variation, in this way the conservative coefficients  $C'_{ST\_CON} = 1.9$  and  $C'_{LT\_CON} = 6.0$  are obtained.

**Table 6-8 Inverse of coefficients  $C'_{LT}$  and  $C'_{ST}$  derived from girder data**

Groups of similar girders under same conditioning		Specimen n UTPS- Loss No.	Expression defining effective creep coefficient ( $\psi'_1$ )	Calibration Coefficients	
Source	↓			$1/C'_{LT}$	$1/C'_{ST}$
Barr et al. (2000)	2B	4	$0.056 \ln(t) + 0.199$	0.061	0.204
Erkmen et al. (2007)	B-SCC1	59	$0.108 \ln(t) + 0.008$	0.129	0.083
	B-SCC2	60	$0.131 \ln(t) - 0.024$	0.151	0.067
	B-CM	61	$0.105 \ln(t) + 0.037$	0.122	0.110
Gamble (1970)	BX-1	62	$0.090 \ln(t) + 0.205$	0.103	0.257
Garber et al. (2013)	I-1	222	$0.064 \ln(t) + 0.257$	0.071	0.260
	I-7	228	$0.042 \ln(t) + 0.304$	0.047	0.305
	II-1 & II-6	230	$0.044 \ln(t) + 0.413$	0.055	0.405
		235	$0.050 \ln(t) + 0.404$		
	II-3 & II-8	232	$0.034 \ln(t) + 0.429$	0.039	0.400
		237	$0.034 \ln(t) + 0.376$		
	III-1 & III-5	238	$0.103 \ln(t) + 0.293$	0.132	0.312
		242	$0.120 \ln(t) + 0.219$		
	III-3 & III-7	240	$0.071 \ln(t) + 0.418$	0.099	0.390
		244	$0.098 \ln(t) + 0.265$		
	IV-SCC-1, 2 and 3	246	$0.040 \ln(t) + 0.465$	0.040	0.418
		247	$0.048 \ln(t) + 0.412$		
		248	$0.019 \ln(t) + 0.413$		
	IV-CC-2 and 3	250	$0.012 \ln(t) + 0.442$	0.030	0.345
		251	$0.041 \ln(t) + 0.267$		
Average constants (used to define $C_{LT}$ and $C_{ST}$ )				$0.083 = \frac{1}{12}$	$0.273 = \frac{1}{3.7}$
COV				50%	46%
Conservative constants (average + 2 COV, used to define $C_{LT\_CON}$ and $C_{ST\_CON}$ )				$0.166 = \frac{1}{6}$	$0.522 = \frac{1}{1.9}$

### 6.4.2 Sectional Shrinkage Model

The definition of the sectional shrinkage model on the basis of girder data is conducted on this section. In contrast to cylinder shrinkage, no relationship was found in the shrinkage strain and the term used to define the ultimate shrinkage (i.e.  $-\ln(RH)/E_c$ ). The lack of a relationship is shown in Figure 6-4. This can be partially due to the lack of data from girders with monitoring periods long enough to allow the equilibrium of the internal relative humidity with the external relative humidity ( $RH$ ), but mainly due to the non-uniform shrinkage strains occurring through the section. It can be hypothesized that the effect of shrinkage on the girder behavior is of such a complex nature that its dependence on the main parameters driving local shrinkage cannot directly be detected. This main parameters are considered to be relative humidity and concrete stiffness. The detection of the relationship of this parameter with the sectional shrinkage requires the consideration of the complete profile of localized shrinkage and additional parameters such as creep-shrinkage interaction.

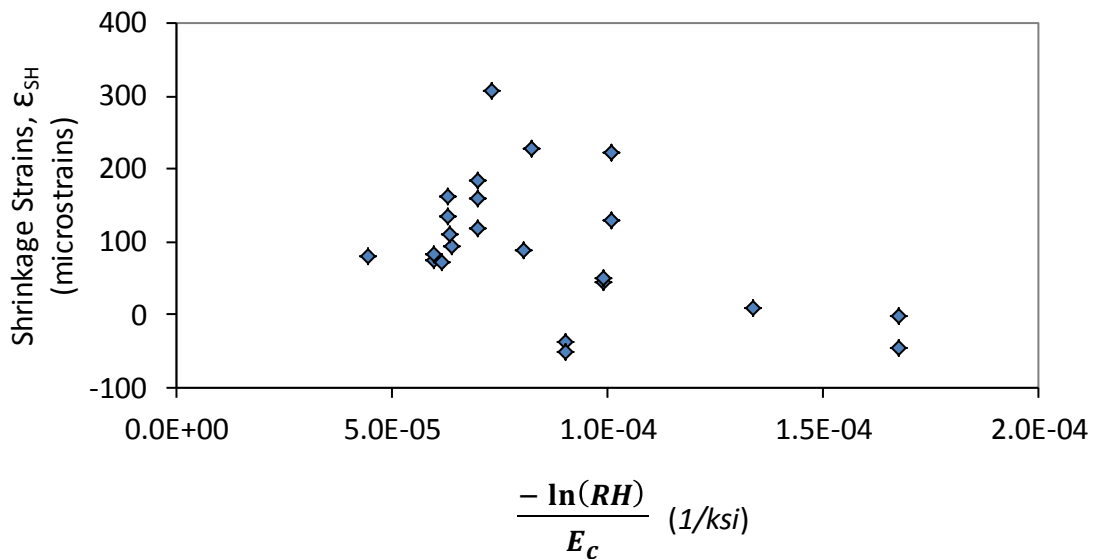


Figure 6-4 Variation of ultimate shrinkage strain with  $\frac{-\ln(RH)}{E_c}$

Based on the difficulty found in the attempt to model shrinkage on the basis of the simplest parameters, the use of a constant value for the ultimate shrinkage is proposed. The average value of the final sectional shrinkage (for assumption set 1) defined in Table 6-5 is propose to be used for the time-dependent estimation of losses (i.e.  $\epsilon'_{SHf} = 140 \times 10^{-6}$ ). A simplified version of the time-development factor for shrinkage from the materials-based model (Section 5.4.1) is proposed to be used for the sectional shrinkage. The simplification consists in not using the hyperbolic tangent function (proposed in chapter 5) but instead using only the argument of the hyperbolic tangent function, as shown in Equation (6-37). This simplification has no impact on the initial development of shrinkage (up to half-time), and is conservative for long-term shrinkage. This approach is simplistic and further research that could lead to more accurate estimations is recommended.

**Table 6-9 Sectional shrinkage model expressions**

Halftime	$\tau_{SH} = 1\text{day} \left( \frac{v/s}{0.2 \text{ in.}} \right)^2$	(6-36)
Simplified time factor	$F_{SH} = \sqrt{0.3 \frac{t_{drying}}{\tau_{SH}}} \leq 1$	(6-37)
Strain at time $t_{drying}$	$\epsilon'_{SH} = 140 \times 10^{-6} \cdot F_{SH}$	(6-38)

## 6.5 ULTIMATE PRESTRESS LOSS MODEL DEVELOPED ON BASIS OF GIRDER DATA

One of the main concerns of the designer, especially during initial stages of the design is the ultimate losses and resulting service stresses. In this section, a simplified conservative model to estimate ultimate losses (at the end of service live) is developed on the basis of the time-dependent model through the use of a few key assumptions. Conservative creep and shrinkage coefficients will be used for this approach.

A simpler creep model can be developed through the use of a single spring that represents the total creep (short-term plus long-term), as shown in Figure 6-5. This is not a possibility within a time-dependent model, but if the losses are to be calculated at a given age (e.g. design life), then the estimation age (i.e.  $t_f = 75 \text{ years}$ ) can be placed in the model to obtain an equivalent total creep spring stiffness ( $C_{ST+LT} \cdot E_{ci}$ ) as shown in Table 6-10. The results for the coefficient of this spring ( $C_{ST+LT}$ ) are shown in Table 6-10.

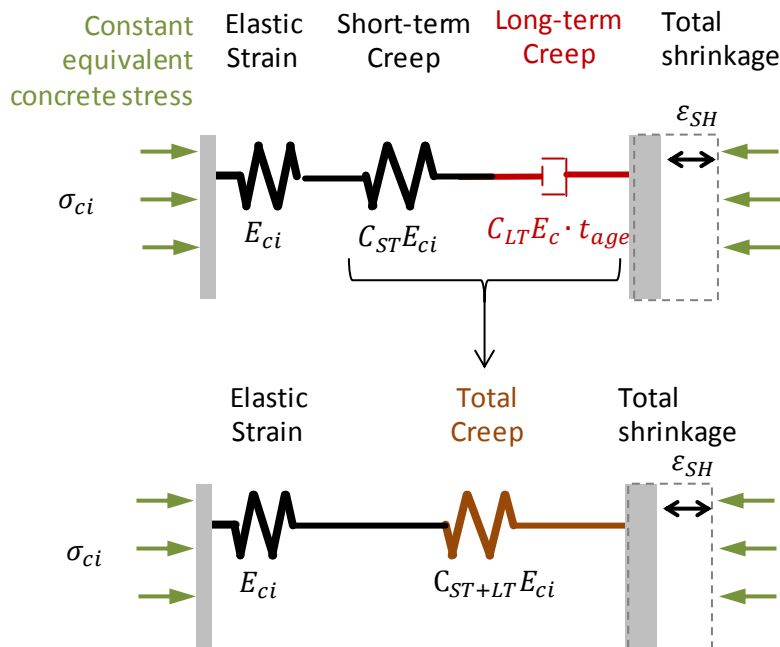


**Figure 6-5 Model to estimate ultimate strains due to initial stress and shrinkage**

In addition to the combined creep considered for the initial stress, the effect of the deck in the short-term creep (i.e. the creep recovery due to deck weight) is considered as shown in Table 6-11. The shrinkage will be assumed to be constant and similar to that used in Section 6.4.2 ( $\epsilon'_{SH_u} = 140 \times 10^{-6}$ ). The time dependency is not considered, because it is expected the shrinkage to be fully developed at the end of the service live of the bridge. This approach is very rudimentary, and the variability of the sectional

shrinkage coefficient is large, but further research is needed to determine the method that can be used to develop a more accurate model. Using these expressions, the general behavior of the model from can be calculated with the equations shown in Table 6-12

**Table 6-10 Coefficient for combined creep spring,  $C_{ST+LT}$**

Equation (5-18)	$\frac{1}{E} \left[ \frac{1}{1 + \frac{1}{2} \left( \frac{t}{t_i} \right)^{-n} + \frac{1}{2} \left( \frac{t}{t_i} \right)^{-2n}} \right]$	(6-39)
Equation (5-10)	$\frac{1}{E} \left[ \ln(t) - \ln(t_i) \right]$	(6-40)
by definition	$\frac{1}{E} \left[ \ln(t) - \ln(t_i) \right]$	(6-41)
Assume release time	$\frac{1}{E} \left[ \ln(t) - \ln(t_i) \right]$	(6-42)
Plug (6-39), (6-40) & (6-42) into (6-41)	$\frac{1}{E} \left[ \frac{1}{1 + \frac{1}{2} \left( \frac{t}{t_i} \right)^{-n} + \frac{1}{2} \left( \frac{t}{t_i} \right)^{-2n}} \right] \left[ \ln(t) - \ln(t_i) \right]$	(6-43)
By definition of stiffness, and from Figure 6-5	$\frac{1}{E} \left[ \ln(t) - \ln(t_i) \right]$	(6-44)
Equivalent stiffness for creep	$\frac{1}{E} \left[ \frac{1}{1 + \frac{1}{2} \left( \frac{t}{t_i} \right)^{-n} + \frac{1}{2} \left( \frac{t}{t_i} \right)^{-2n}} \right] \left[ \ln(t) - \ln(t_i) \right]$	(6-45)
Coefficient for total creep	$\frac{1}{E} \left[ \frac{1}{1 + \frac{1}{2} \left( \frac{t}{t_i} \right)^{-n} + \frac{1}{2} \left( \frac{t}{t_i} \right)^{-2n}} \right] \left[ \ln(t) - \ln(t_i) \right]$	(6-46)
Replacing $\frac{1}{E}$ , $\ln(t)$ , and assuming $\ln(t) - \ln(t_i) = 1$ then	$\frac{1}{E} \left[ \frac{1}{1 + \frac{1}{2} \left( \frac{t}{t_i} \right)^{-n} + \frac{1}{2} \left( \frac{t}{t_i} \right)^{-2n}} \right]$	(6-47)
Solving (6-47)	$= 0.48$	(6-48)
from Figure 6-5	$\frac{1}{E} \left[ \ln(t) - \ln(t_i) \right]$	(6-49)



**Table 6-11 Deck weight effect on short-term creep (i.e. creep recovery)**

From Table 5-5 Equation (5-18)	$\varepsilon_{CR ST} = \frac{\sigma_c}{C_{ST}E_{ci}} \quad (6-50)$
Stress due to deck weight	$\sigma_c = \Delta\sigma_{cDECK} \quad (6-51)$
From Table 6-13	$C_{ST} = 1.9 \quad (6-52)$
Plug (6-51) & (6-52) into (6-50)	$\varepsilon_{CR ST,DECK} = \frac{\Delta\sigma_{cDECK}}{1.9E_{ci}} \quad (6-53)$
Rearranging	$\varepsilon_{CR ST,DECK} \sim 0.53 \frac{\Delta\sigma_{cDECK}}{E_{ci}} \quad (6-54)$

**Table 6-12 Simplified Design Method to Estimate Ultimate Losses ( $t_f=75$  years)**

Initial Stress	$\sigma_{ci} = 0.9f_{pi}A_p \left( \frac{1}{A_g} + \frac{e_p^2}{I_g} \right) - M_{SW} \frac{e_p}{I_g} \quad (6-55)$
Stress due to deck weight	$\Delta\sigma_{cDECK} = -M_{DECK} \frac{e_p}{I_g} \quad (6-56)$
Ultimate strain	$\varepsilon'_u = \frac{\sigma_{ci}}{E_{ci}} + 2.1 \frac{\sigma_{ci}}{E_{ci}} + 1.53 \frac{\sigma_{cDECK}}{E_{ci}} + 480 \times 10^{-6} \quad (6-57)$

## 6.6 GIRDER-BASED PRESTRESS LOSSES ESTIMATION METHOD

Based on the time-dependent loss model developed in Section 6.4 and the ultimate loss model developed in Section 6.5, a method to estimate creep can be proposed. The proposed method is shown in Table 6-13. The determination of the prestress losses consists of determining the total strain in the girder, and multiplying it by the modulus of elasticity of the strand. The time-dependent strains considered for the estimation of losses are:

- short-term and long-term creep due to initial stress  $\sigma_{ci}$ , using the model from Section 6.4.1
- short-term creep due to deck-induced stress  $\Delta\sigma_{cDECK}$ , based on the model from Section 6.4.1
- shrinkage strain based on the model from Section 6.4.2

Additionally the complete strain due to elastic effects, creep and shrinkage for the estimation of ultimate losses is adopted from Section 6.5, which at the same time is a conservative simplification of Section 6.4. This method is limited to pretensioned girders, because the calibration of the creep and shrinkage models was conducted using such type of element. The calculation of the elastic shortening is adapted from the method described in TxDOT Project 0-6374 (Garber, et al. 2013).

**Table 6-13 Simplified Time-Dependent Prestress Losses Estimation**

Calibrated Coefficients		
Stress conditions	$\left( \frac{f_c}{f_{ps}} \right) -$	(6-58)
	$—$	(6-59)
Elasticity	$—$	(6-60)
Shrinkage at time t	$1 \text{ day} \left( \frac{v/s}{—} \right)$	(6-61)
	$\sqrt{0 —}$	(6-62)
Short-term Creep (delayed elasticity)	$—$	(6-63)
Long-term Creep (irrecoverable)	$— \ln \left( \frac{—}{—} \right)$	(6-64)
Total Losses at time t	$(\epsilon —)$	(6-65)
<b>Conservative</b> Ultimate Losses (for t ars)	$— — —$	(6-66)
		(6-67)

**6.6.1 Evaluation of the Performance of the Girder-Based Methods**

The performance of the time-dependent method presented above is evaluated using the UTPSC-Loss Strain Evaluation Database. The method shows good accuracy (COV = 21%), and precision  $((E/M)_{average} = 1.0)$ . Almost half of the measured loss values are underestimated; the method was calibrated for average behavior to give a good

estimate of the expected losses. While this is useful for the verification of camber, the use of this method for the verification of stresses should be carefully conducted. It is instead recommended that the conservative expressions of ultimate losses should be used for estimation of ultimate losses incorporated into concrete stress estimates.

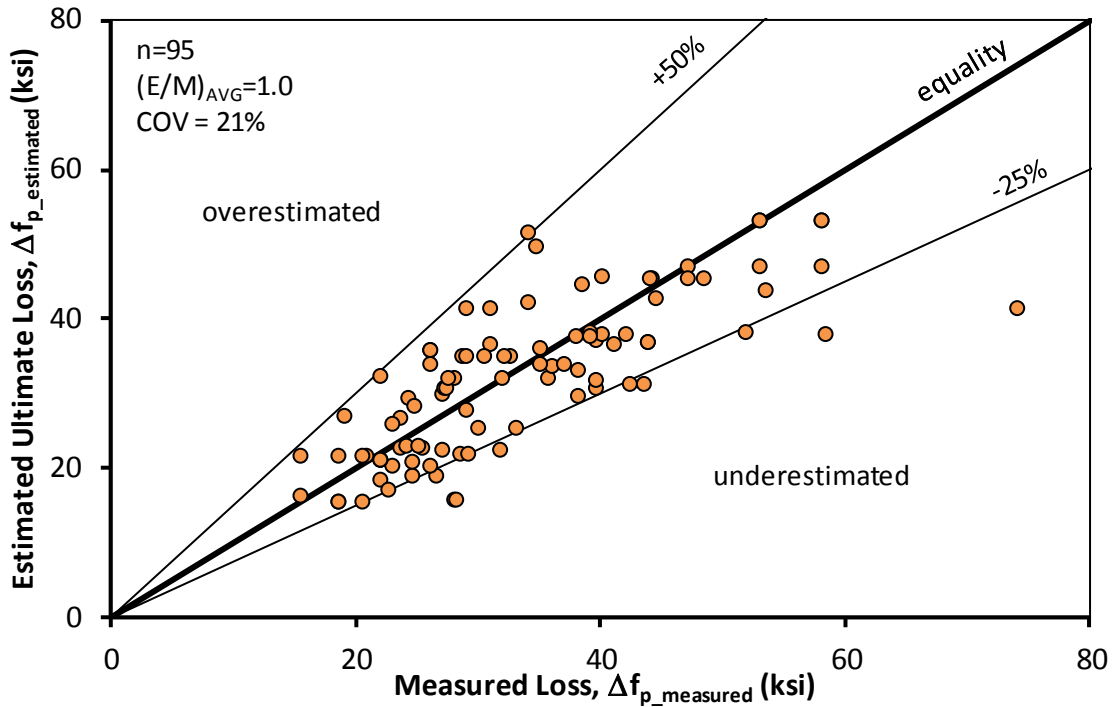


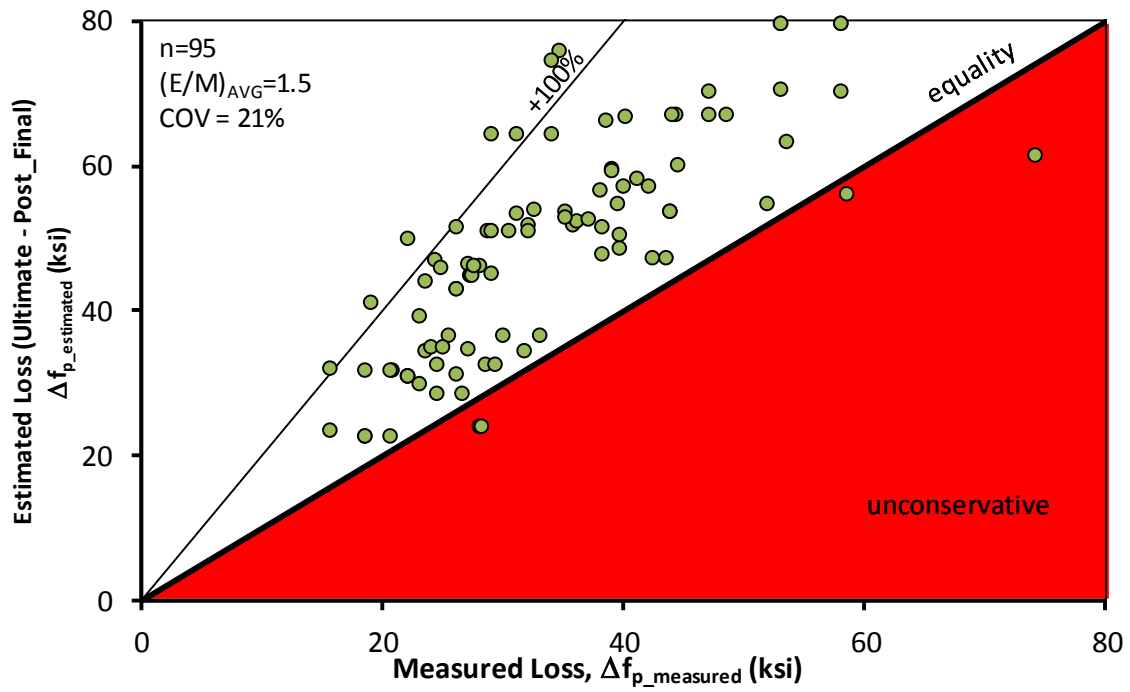
**Figure 6-6 Performance evaluation of the girder-based time-dependent loss estimation.**

The results of these estimations are presented in Figure 6-7 together with estimations based on AASHTO 2012 Approximate method. For this comparison the “post-final” losses were subtracted from the ultimate losses estimated with the approximate methods considered. This was necessary because it is considered that the losses in the specimens will experience “post-final” increase in the loss (from the final monitoring time until the end of the service life, i.e. 75 years). This small increase in losses was estimated through the use of the time-dependent model and subtracted from

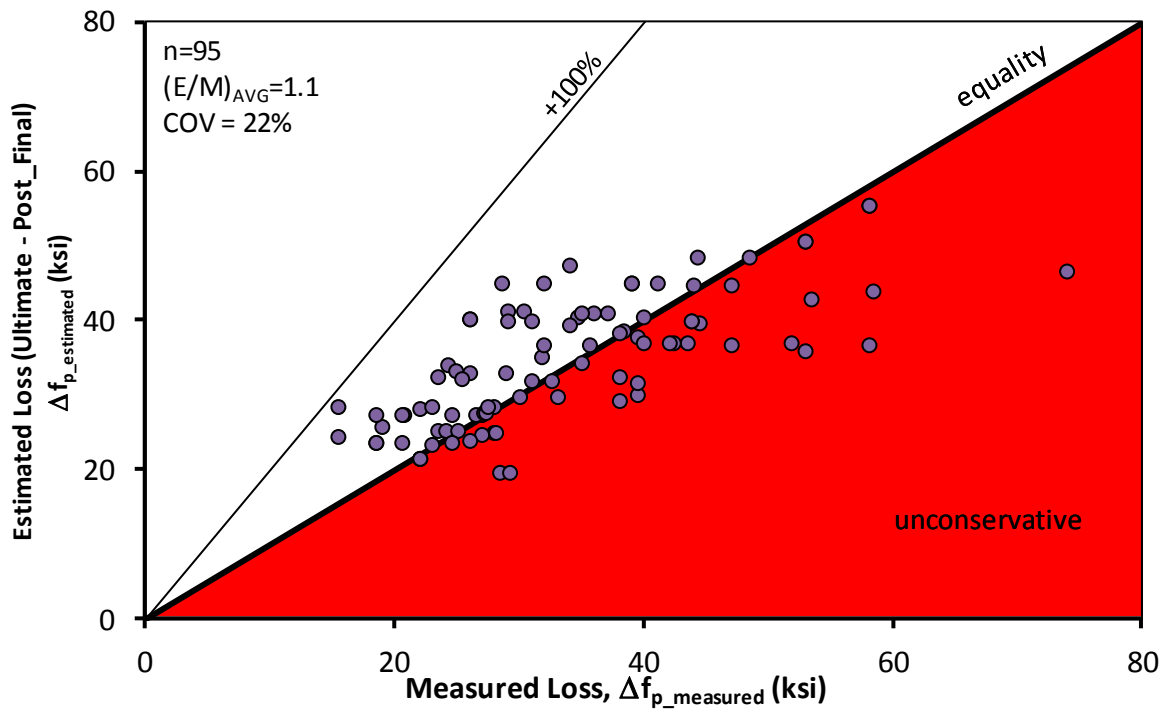
the ultimate losses estimated with the approximate methods. In Table 6-14, more statistics related to the performance of the method are presented. Based on the statistics of the results, it is considered that the method can satisfactorily estimate prestress losses of pretensioned, simply-supported girders with precision comparable to currently used methods.

**Table 6-14 Statistics for the ratio of estimated to measured strain related losses; estimated values for AASHTO 2012 Approximate and for the Girder-Based method**

Estimated/Measured Ratio	Proposed Girder-Based (ultimate losses expression)	AASHTO 2012 Approximate
Max	2.3	1.8
Average	1.5	1.1
Min	0.8	0.6
unconservative cases	4%	41%
COV	21%	22%



(a) Estimation using proposed Simplified method



(b) Estimation based on AASHTO 2012 Approximate method

**Figure 6-7 Estimated vs Measured Ultimate Prestress losses**

## **6.7 SUMMARY**

A prestress loss estimation method developed on basis of girder data was presented in this chapter. The method allows for the accurate estimation of time-dependent losses and includes an expression for the conservative estimations of ultimate losses. It is recommended to use the conservative expression to estimate ultimate losses when stress check are being performed. The precision of this method was found to be acceptable for the estimation of both the time-dependent losses and the ultimate losses.

## CHAPTER 7

### Summary, Conclusions, Recommendations and Further Work

#### 7.1 SUMMARY

This dissertation is oriented to the study and estimation of strain-related prestress losses in simply supported pretensioned bridge girders. The formulation of a simple and accurate prestress loss estimation method was achieved through:

- an extensive literature review,
- the compilation of the experimental results from previous research,
- the integration of basic long-term deformation mechanisms of concrete into a Materials-based model that is calibrated using cylinder test results, and
- the formulation of a Girder-based model to estimate prestress losses calibrated using results of simple supported girders strain monitoring.

The literature review (Chapter 2) included a summary of the current state-of-knowledge on creep, shrinkage and prestress losses in pretensioned girders; key conclusions of relevant papers on creep and shrinkage theory were presented. The main mechanisms involved in the development of prestress losses were presented, including the effect of the pore water pressure on the development of shrinkage, the migration of water from high pressure regions to lower pressure pores during short-term creep, and the breakage of C-S-H links as a main reason for the long-term creep. Databases that compile experimentally measured shrinkage strain (expanded from Bažant and Li (2008)) and creep strain (Bažant and Li 2008) are analyzed in Chapter 2. An experimental database compiled during TxDOT Project 0-6374 (Garber, et al. 2013) that included measured



prestress losses from 32 studies describing 280 specimens (including 30 specimens from Garber, et al. (2013)) was also presented as part of the literature review.

The study of prestress losses within 18 field-representative bridge girders was presented in Chapter 3. The girders were a subset of 30 girders studied during the course of TxDOT Project 0-6374 (Garber, et al. 2013). The girders were 45.5 feet in length and featured Type C (conventional TxDOT girder) and Tx46 (bulb- T) cross-sections. The amount of prestressing steel was approximately one percent of the gross cross-sectional area. This large amount of prestressing steel, for this short span, was used in order to generate high initial compressive stresses ( $0.65f'ci$ ), hence, maximizing the potential for prestress losses. The girders were fabricated at three different precast plants, and stored at two locations: Austin (RH $\approx$  62%), and Lubbock (RH $\approx$  51%). The girders were aged for 230 to 980 days under natural climatic conditions. During this period of time, the development of prestress losses was monitored via internal instrumentation.

The results of the experimental program were presented in Chapter 4. These results allowed the investigation of the effects of coarse aggregate type, concrete type, and climate on short- and long-term prestress losses. It was observed that the total prestress losses showed a strong correlation with the concrete stiffness. Consistently, a clear influence of the coarse aggregate type on the losses was observed. The losses measured in Series III beams stored in dryer conditions are larger than those stored in more humid environments (a 10 percent decrease in the relative humidity resulted in an increase of almost 9 percent in the long-term loss within otherwise identical specimens). The prestress loss increase attained through conditioning in a lower humidity environment is consistent with the larger time-dependent deformations expected in concrete under drying conditions, especially due to drying shrinkage. There was no definitive indication that the cross-sectional shape has any effect on prestress loss.

In Chapter 5, the materials-based model (a novel prestress loss estimation method) was developed on the basis of fundamental concrete behavior including elastic deformation, creep, and shrinkage. Widely accepted theories of creep and shrinkage mechanisms were incorporated into the method; which only reflects the most relevant parameters. The resulting expressions were calibrated using an existing database of experimental results from creep and shrinkage studies, slightly expanded with some specimens found in the literature. The materials-based model was further tailored to be representative of the conditions associated with the construction and behavior of a typical simply supported bridge girder.

In Chapter 6, the Element-Based model (a simple, conservative method for the estimation of strain-related prestress losses) was developed. The approach considered for the development of a simplified model, included an experimental determination of a sectional creep coefficient and a shrinkage coefficient that was based on the measurement of girder strains. Such a technique condenses all the phenomena occurring in the girder into equivalent creep and shrinkage coefficients. Based on the statistical evaluation of the results, the developed method satisfactorily estimates prestress losses in pretensioned simply supported girders, with precision comparable to that of the methods currently used.

## 7.2 CONCLUSION

The main conclusion of this study is:

- The long-term strains of simple supported bridge girders can be characterized by the use of *effective creep and shrinkage coefficients* that defines the sectional behavior of the girder. Such coefficients can

be calibrated on the basis of results from long-term strain monitoring of simple supported bridge girders.

Other conclusions of this study are:

- The *effective creep and shrinkage coefficients* can be used to accurately estimate the strains occurring in any point of a given cross section of a girder as a function of the elastic strain profile occurring in such section. This approach is empirical, and its use should be considered independently for each type of structure.
- The formulation of estimation methods calibrated using the results from *cylinder testing* does not capture the complete behavior of the girder. Nowadays, such a complex behavior can only be accurately experimentally captured (or verified) by the instrumentation of full scale girders. This is in part related to the irregular geometry of the girders and the complex interaction of various phenomena occurring within the section of the girder.
- The formulation of a prestress losses estimation method calibrated using results from *full scale girder instrumentations* is feasible, and results in a simple and accurate method applicable to structures similar to those used for the calibration.
- The effect of the shrinkage of the deck in the prestress losses is small.

The results of this study reaffirmed existing knowledge, such as:

- The unbounded logarithmic creep does not translate into unbounded prestress losses, because creep will only occur as long as stress is applied on the concrete. Therefore, the prestress losses approach a final value asymptotically, which can be simplistically approximated as that for which

the stress in the concrete at the centroid of the strands is zero. A similar conclusion can be stated based on Tadros et al. (2003), where it is mentioned that the stress, at the bottom fibers of bridge girders, due to the loads applied (including effective prestress effect) “add up to zero at time infinity”.

- A large fraction of the shrinkage can be interpreted as the deformation of the cement paste caused by the application of internal stresses (such as the disjoining pressure, as mentioned by Powers (1968)). Such stresses are caused by changes in the internal pore water pressure
- For ages later than one week, the short-term creep is fully developed (Ulm, Maou, & Boulay (2000) and Neville A. M. (1983)), and can be modeled similarly to an elastic deformation.
- Long-term creep is unbounded (Neville A. M. (1983)) and non-recoverable or irreversible (Acker and Ulm 2001). The long-term creep development occurs at a rate that can be assumed as inversely proportional to the age of concrete (Ulm, Maou and Boulay 2000); hence, it follows a logarithmic development.
- The long-term behavior of concrete is complex (Vandamme and Ulm 2009). However, the similitudes found within a specific type of structures limits the complexity of the problem.
- The rate of prestress loss decreases considerably after placement of the deck for two reasons: (1) the creep rate diminishes with age (Ulm, Maou and Boulay 2000) and is relatively small at deck casting, and (2) based on mechanics of materials and statics, the deck weight and prestress losses cause a reduction of bottom flange stress (stress at and after deck cast are

smaller than before deck cast), thereby reducing the creep rate after deck placement.

- The modulus of elasticity of concrete has a strong correlation with the long-term deformation of concrete. The previous and current use of creep coefficients is a direct application of this correlation in the estimation of creep strains. This correlation is reaffirmed by the results of this study: specimens fabricated with stiffer concrete experienced significantly smaller long term deformations (and smaller total prestress loss).

### **7.2.1 Prestress losses estimation method**

Two methods to estimate prestress losses were developed during the course of this study for simply supported pretensioned concrete girders. The first method (the materials-based method) was developed to transfer knowledge from research to practice. The second method (the element-based method) is a simplified technique developed for everyday use in the design of typical pretensioned bridge girders. Conclusions regarding these methods are:

- The materials-based method presented in Chapter 5 is an accurate method that includes each of the factors commonly considered to influence prestress losses. The use of this complex method in common bridges is not necessary, but the availability of this method in the literature will be useful for the designer who is interested in performing a more detailed study of the strain-related phenomena of creep and shrinkage. In addition, the format of the materials-based method can be used as a guide to develop future techniques to estimate prestress losses in more complex structural systems.

- The simplified method presented in Chapter 6 of this study offers a simple, conservative way to estimate prestress losses in simply supported bridge girders. This method is empirical, and is based on the concept that similar structures behave similarly. The method was deemed accurate when compared to the prestress losses database and existing methods.

### 7.3 RECOMMENDATIONS

Based on results from this study, the following recommendations are made:

- It is strongly recommended to the bridge designer to specify in the drawings the modulus elasticity of concrete (at least at release, i.e.  $E_{ci}$ ) that was used for the design of the girders, and to require that the fabricator must provide a concrete that satisfies or exceeds (being stiffer) such property of the concrete.
- For researchers interested in the study of strain-related prestress losses, it is recommended to use the Material-Based model presented in Chapter 5.
- It is recommended for bridge designers to use the “simplified time-dependent prestress losses estimation method” for the estimation of camber and deflections, and the “conservative ultimate losses” equation for the verification of stress levels in simple supported girders. It is important to note that the applicability of such method is limited to the type of bridge elements used for the calibration of the method (i.e. simply supported girders with standard sections, such as rectangular, bulb-T, or I girders). The recommended method is presented following in Table 7-1.

**Table 7-1 Simplified Time-Dependent Prestress Losses Estimation Method**

<i>Calibrated Coefficients</i>	<i>microstrains</i> <i>in</i>	
<i>Stress conditions</i>	$93f \left( \frac{—}{—} \right) —$	(7-1)
	$—$	(7-2)
<i>Elasticity</i>	$— —$	(7-3)
<i>Shrinkage at time t</i>	$ay \left( \frac{v/s}{—} \right)$	(7-4)
	$\sqrt{0 —}$	(7-5)
<i>Short-term Creep (delayed elasticity)</i>	$—$	(7-6)
<i>Long-term Creep (irrecoverable)</i>	$— \ln \left( \frac{—}{—} \right)$	(7-7)
<b>Total Losses at time t</b>	$\Delta f \left( \varepsilon \right)$	(7-8)
<b>Conservative Ultimate Losses (for <math>t_u</math> days)</b>	$— — —$	(7-9)
	$\Delta f$	(7-10)

- It is recommended to use the UTPS-Loss database, presented in Chapter 2, to verify the performance of prestress loss estimation methods during future research.

## 7.4 FURTHER RESEARCH

There are many areas in the topic of long term behavior of concrete that requires further work. In this section will be described some ideas to develop research in areas that require verification or further experimental. The description of two studies that are recommended for further research is included as subsections in the following pages. Brief general descriptions of research areas recommended for further research are presented following:

- The indeterminacy of continuous (multi-span) bridge girders can have a significant effect on the occurrence of prestress losses. However, very few experimental studies of continuous girders can be found in the literature. Therefore, strain monitoring of indeterminate (multi-span, continuous) girders is recommended.
- The implications of the use of strains measured in a single girder to assess the effective creep and shrinkage coefficients need further verification. These implications can be identified by assessing the creep and shrinkage strains independently. To identify the portion of losses caused by creep or shrinkage separately it is recommended to monitor strains in two similar girders, one prestressed and the other non-prestressed. Such approach has been use in previous studies, for example by Gamble (1970), but availability of results from this type of experiments is scarce in the literature.
- Develop an experimental program that allows a clear identification of shrinkage strains, early creep, and pure elastic strains that occur prior to the full release of the strands. To date, these strains are difficult to discern because they are developed in the girder simultaneously during release.



#### 7.4.1 Effect of the environmental relative humidity on the long-term creep

The origin of long-term creep is related to the breakage of overstressed bonds that join the C-S-H particles (the “glue” of the concrete). The bonds are overstressed by repulsive forces applied by the adsorbed water on the micropore walls (Ulm, Maou and Boulay 2000). Considering the above, it can be assumed that an increase in the amount of water (within the hardened cement paste) would cause an increase in the repulsive forces; then, it can be concluded that a higher environmental relative humidity would result in a higher rate of bond breakage, and therefore a higher long-term creep rate. However, results from previous research, as those by Brooks (2005), indicate that lower creep is observed in specimens with higher relative humidity. It is interesting to note that for some specimens with 30 years of conditioning, the final *creep rate* for “wet-stored” specimens is larger than the final creep rate of “dry-stored” specimens.

It would seem that the experimental results contradict the trend expected from the theoretical origin of long-term creep. However it is believed that the apparent contradiction is solved when clarifying the time-scale under consideration; an example of a possible explanation:

- when internal humidity is in equilibrium with the environment at early ages (e.g. in the order of one year), **lower external relative humidity** can result in low final creep rates and **low final creep** magnitude at large ages (e.g. in the order of 50 years)
- when internal humidity is in equilibrium with the environment at late ages (e.g. in the order of 10 years), **lower external relative humidity** can result in higher moisture movement rates during drying, inducing high creep rate and **high final creep** magnitude.

Further work is necessary to:

- determine under which conditions a **higher** external relative humidity generates a **higher** creep magnitude, and
- develop a method to capture the full range of scenarios regarding the effect of the external relative humidity on the creep magnitude.

For the development of such work, it is recommended to conduct long-term monitoring of the creep and shrinkage occurring on series of concrete prisms considering the following parameters:

- *conditioning period*: conduct conditioning during periods of more than the time  $t_f$  calculated as recommended in Section 5.4.1 (i.e.  $t_f = 625 \text{ day/in}^2 \cdot (v/s)^2$ ); this infers conditioning time of more than 7 years for specimens with a volume-to-surface ratio of 2 in.
- *conditioning relative humidity*: include a broad range of humidity (e.g. 45%, 70%, and submerged specimens)
- *volume-to-surface ratio*: include small volume-to-surface ratios and large volume-to-surface ratios. To prevent the need of extremely long monitoring period, it is recommended to limit the volume-to-surface ratios to at most 4 in.; values of 0.25, 0.5, 1, 2 and 4 inch are recommended.
- *Concrete permeability*: include at least one very permeable concrete and one concrete with very low permeability.
- *Temperature*: if possible, include two different temperatures for each relative humidity (e.g. average of 20 and 30 Celsius).
- *Age at loading*: Due to the complex dependency of creep rate on concrete age and humidity, it is necessary to consider different loading ages (e.g. on

the order of magnitudes of 1 day, 1 month and the ages at which the moisture migration is considered to be 50% and 95% developed)

- *Stress level*: A single level of stress is recommended (e.g.  $0.4 f'_{ci}$ )

#### **7.4.2 Applicability of cylinder behavior to estimate creep and shrinkage of concrete girders.**

The complex interaction of non-linear stress and moisture profiles, and the non-homogeneity of concrete, results in a complex long-term behavior of the concrete elements. Due to this complexity it is important to verify the applicability of the results of cylinder testing to estimate the behavior of structural elements. Some testing has been conducted simultaneously on girders and cylinder, however such testing have focused on the estimation of the long-term deformations on a discrete location within the girder's section (e.g the centroid of prestressing reinforcement).

The complete control of different stress and humidity conditions is practically impossible in medium and large scale concrete elements; however the fabrication of specimens conditioned under varied boundary conditions can be used to detect trends in the behavior. In this sense, results from a complete study of the behavior of concrete girders, segments of girders and cylinders under various stress conditions can serve as experimental support to decipher the aforementioned interaction. Furthermore, finite element analysis can be used as complement to the experimental results, especially in order to verify the applicability of material-based models to the element-level behavior.

A comprehensive experimental study is needed to contribute in the deciphering of the complex interaction of phenomena within the girder. Such study should support robust conclusions that can serve as basis to describe the nature of the interactions of stress, humidity and strain profile that take place within the element section; such description can be developed in a simple, qualitative and element-oriented way.

The experiments for the study described in this sub-section should include:

- monitoring of strains, temperature and relative humidity in all specimens as necessary to define the strain, temperature and moisture profiles .
- testing of concrete strength and modulus of elasticity and coefficient of thermal expansion at prestress transfer, 28 days, 56 days and one year. Curing of all the specimens for concrete properties testing should be aimed to achieve the best match of the properties in the monitored specimens as possible.

It is suggested that such experimental program include variations in the following parameters:

- *Specimen shapes*: the program should include standard I Girder, Box-beam, specimens with shape of segments of the girder and beam (the recommended segments are top flange, web, and bottom flange), and a prism (square section) or cylinder. Within the flange specimens and web specimens, the boundary conditions regarding water migration and thermal profiles should be aimed to mimic the conditions of the same segment of the girder section.
- *Externally applied stress conditions*: unstressed, uniformly stressed and linearly variable stress conditions are recommended. In the girders the unstressed condition can be study in a short girder of a length comparable to 5 times the largest sectional dimension of the girder (care should be exercised to eliminate restrains from the supports). In the girders the stress profiles can be applied using prestressing.
- *Restrain of reinforcement*: unreinforced and reinforced elements should be monitored for the unstressed girders, and for all the prisms and cylinders.

- *Stress history*: constant stress and time-dependent stress. It is difficult to apply constant stress (with respect to time) to the full size girder; therefore the option of constant stress might be only applied to the prisms. However the time dependent stress is applicable to both types of section using prestressing.
- *Environmental conditions*: Conduct all of the tests under dry conditions (e.g. 45% relative humidity) and medium conditions (around 70% relative humidity). If possible is preferable to choose two places with similar temperature histories.

A detailed analysis of the experimental results should be conducted to study the difference in the behavior of cylinders as compared to the behavior of girders, and of segments of the section of the girder (isolated from the rest of the section) as compared to the complete behavior of the section. An important conclusion of this analysis would be to determine if the change in stress conditions due to compatibility of deformations within the section generates a strain profile that:

- can be estimated using principles of mechanics of materials together with creep and shrinkage models based on the measured behavior of each flange and the web, or
- if the complexity of the interactions within the section hinders the efficacy of simple analysis and requires the use of finite element models with high resolution together with material-level creep, shrinkage and moisture migration models.

Also, the applicability of different models or estimation methods can be verified against the broad range of conditions studied in the experimental program; in this way the the performance of various models can be assessed and recommendations made.

## APPENDIX A

### Vibrating Wire Gage Data

In this appendix the data recorded from the VWG readings is shown for each gage in the Girders from the TxDOT Project 0-6374 (Garber, et al. 2013). The Location of the gages is shown (per each series) in Figure A-1. For each and all of the gages used the data is shown in this appendix. The only gage from which no strain data was obtained was IV-CC-1. The data is shown here without normalization, i.e. as readed strains and temperatures. The readed strains are those calculated as detailed for “apparent strains” in the VWG manual (Geokon, Inc. 2012).

The strains obtained directly from the VWG (i.e. apparent strains) are related to the stress in the wire because are obtained from the vibration frequency of the wire inside of the vibrating wire gage. The frequency of vibration of the wire under no strain is proportional to the stress in the wire. The total strain can be calculated from the VWG reading (strain and temperature as reported herein) using Equation (A-1), while the total non-thermal strains can be calculated using the equation (A-2).

$$\Delta\varepsilon_{total} = \Delta\varepsilon_{VWG} + \Delta T \cdot \alpha_{wire} \quad (\text{A-1})$$

$$\Delta\varepsilon_{isothermal} = \Delta\varepsilon_{total} - \Delta T \cdot \alpha_{Girder} \quad (\text{A-2})$$

where:

- $\Delta\varepsilon_{VWG}$  = Apparent strain change from VWG strain readings
- $\Delta\varepsilon_{total}$  = Total strain estimated based on VWG strain and temperature
- $\Delta\varepsilon_{isothermal}$  = Girder strain change normalized to a datum temperature

$\Delta T$  = Temperature change respective to a datum temperature ( $^{\circ}\text{C}$ )

$\alpha_{wire}$  = Coefficient of thermal expansion of strand and VWG ( $12 \mu\epsilon/^{\circ}\text{C}$ )

$\alpha_{Girder}$  = Coefficient of thermal expansion of the Girder.

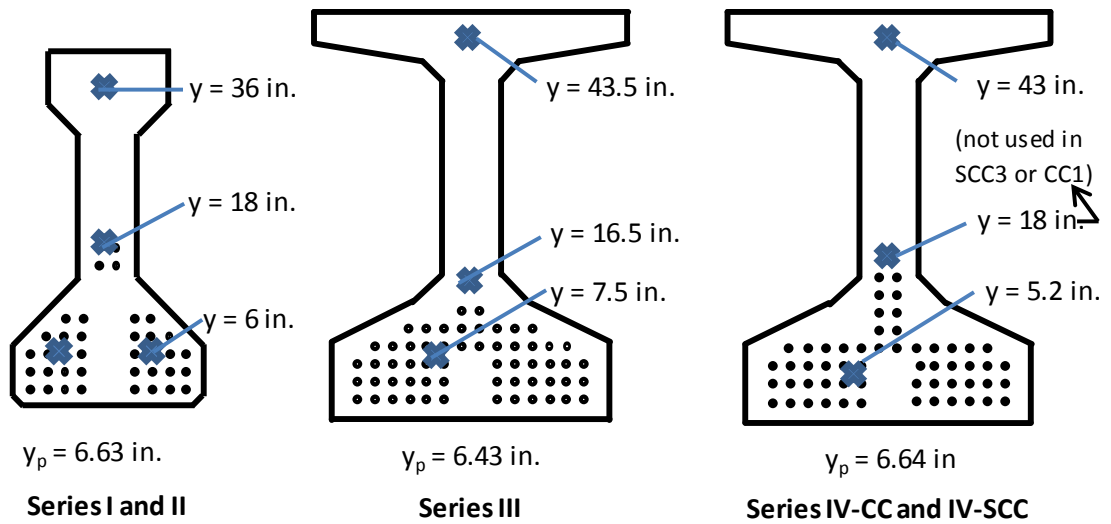


**Figure A-1 VWG embedment locations (at midspan section)**

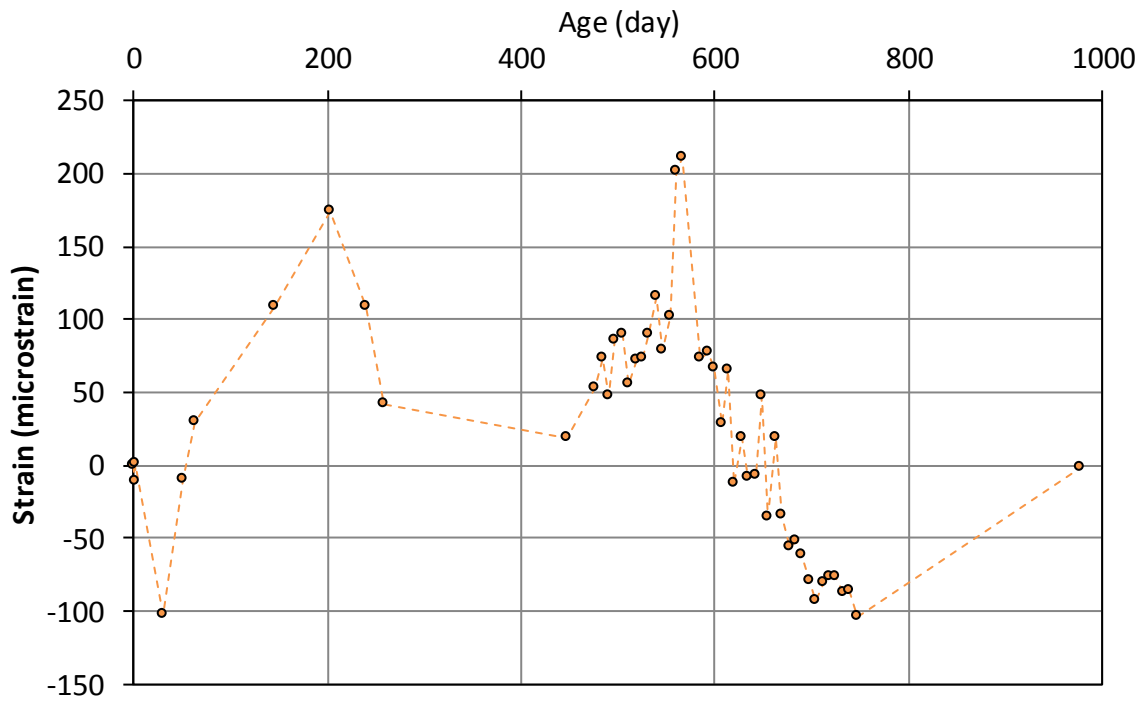


**Figure A-2 Strain data for girder I-1, top gage ( $y = 36$  in.)**

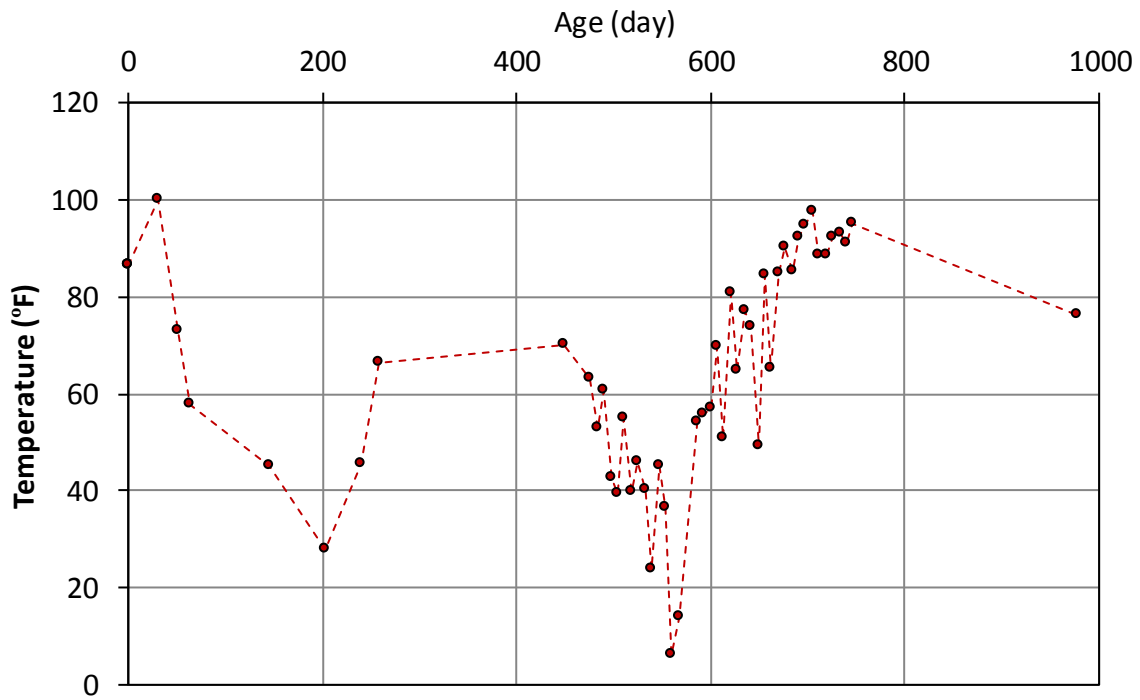


**Figure A-3 Temperature data for girder I-1, top gage ( $y = 36$  in.)**



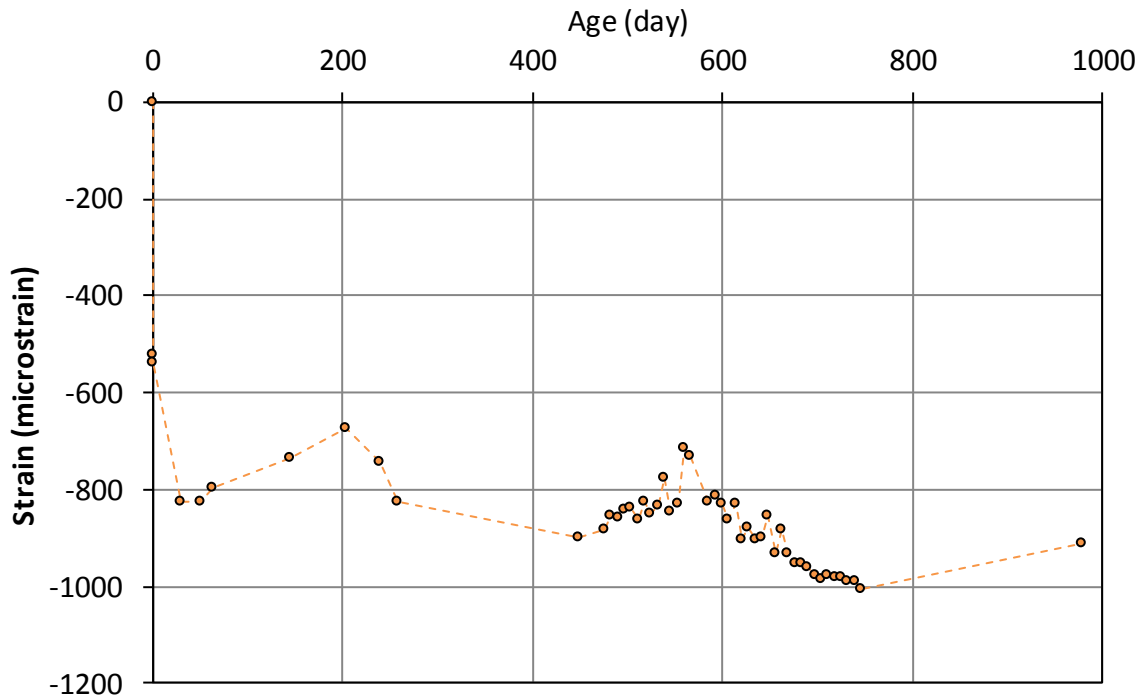


Figure A-4 Strain data for girder I-1, web gage ( $y = 18$  in.)

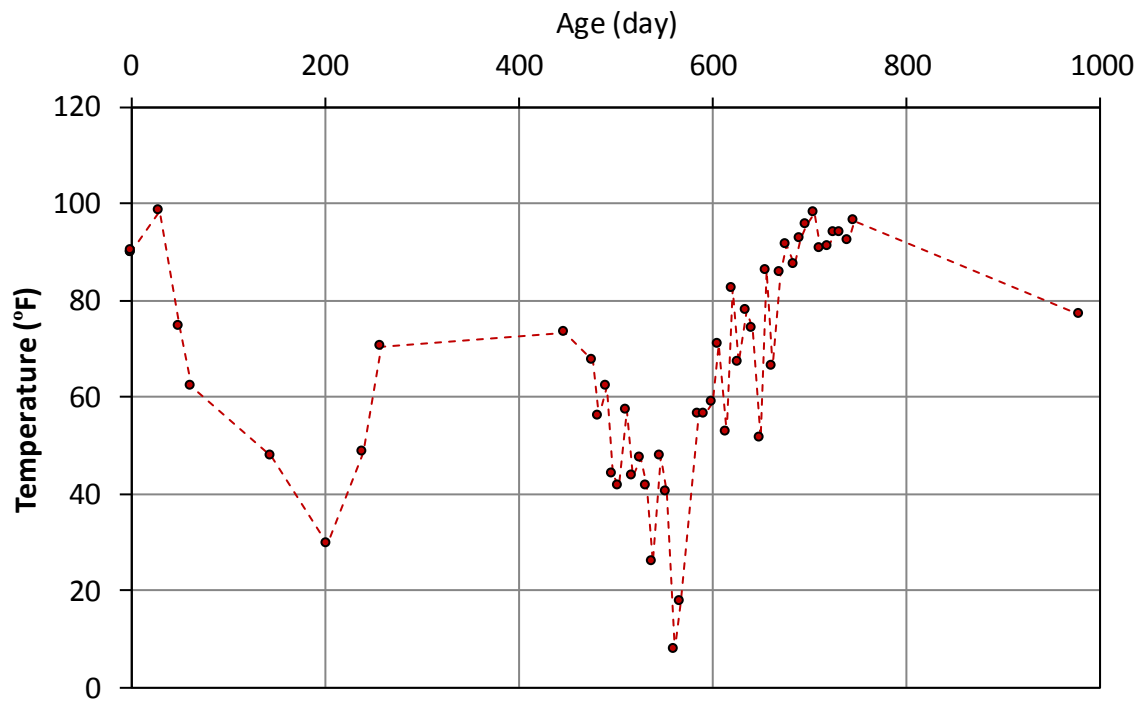
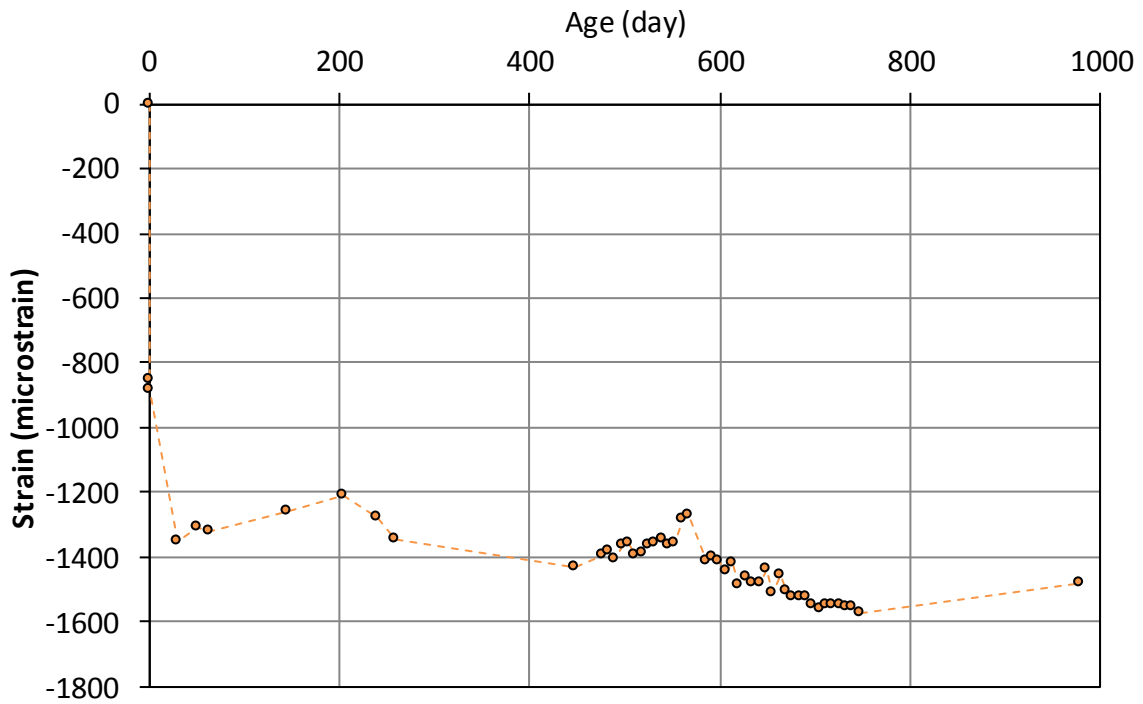
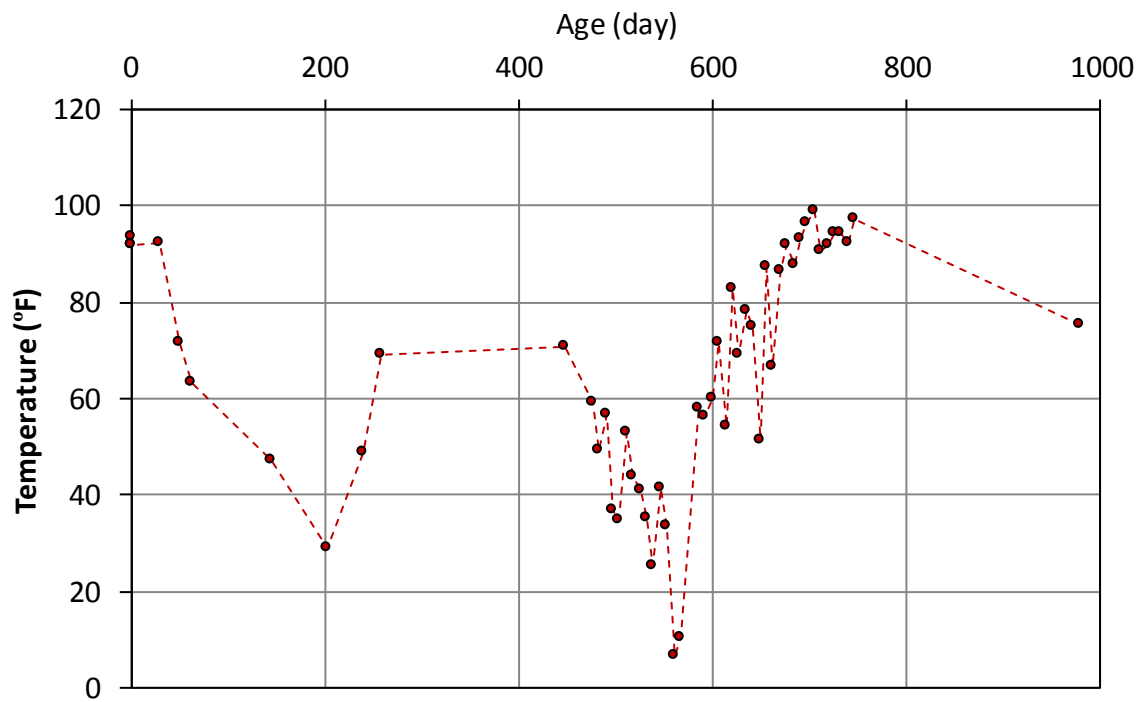


Figure A-5 Temperature data for girder I-1, web gage ( $y = 18$  in.)



**Figure A-6 Strain data for girder I-1, bottom gage 1 ( $y = 6$  in.)**



**Figure A-7 Temperature data for girder I-1, bottom gage 1 ( $y = 6$  in.)**

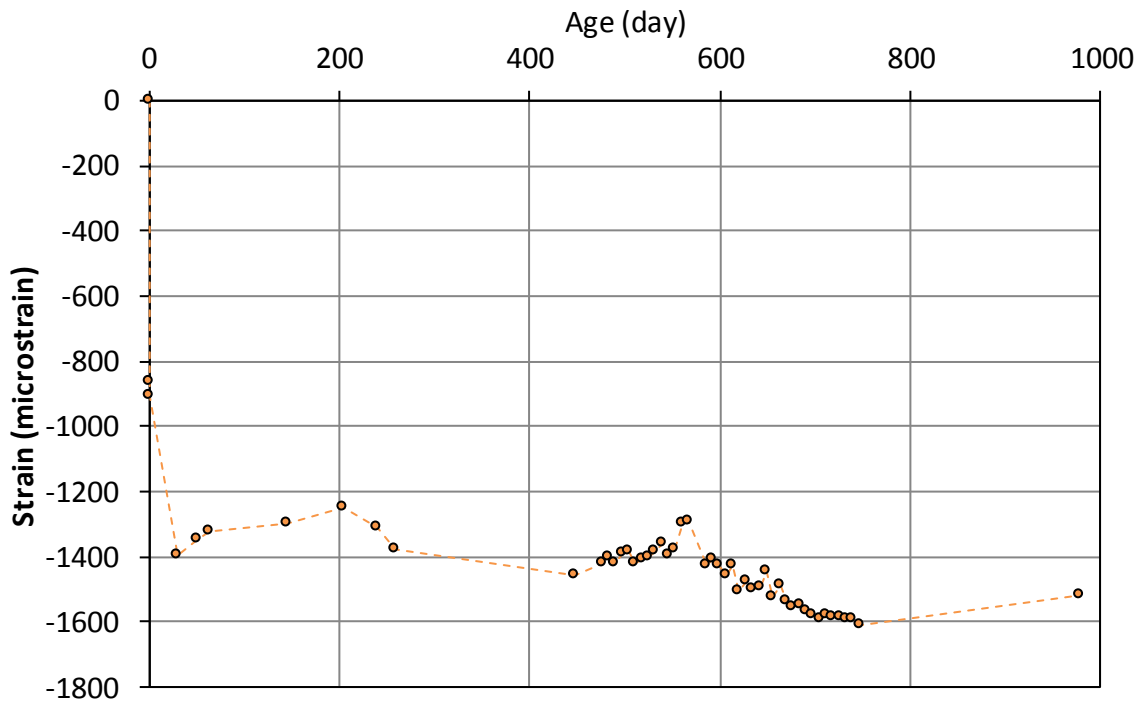


**Figure A-8 Strain data for girder I-1, bottom gage 2 ( $y = 6$  in.)**

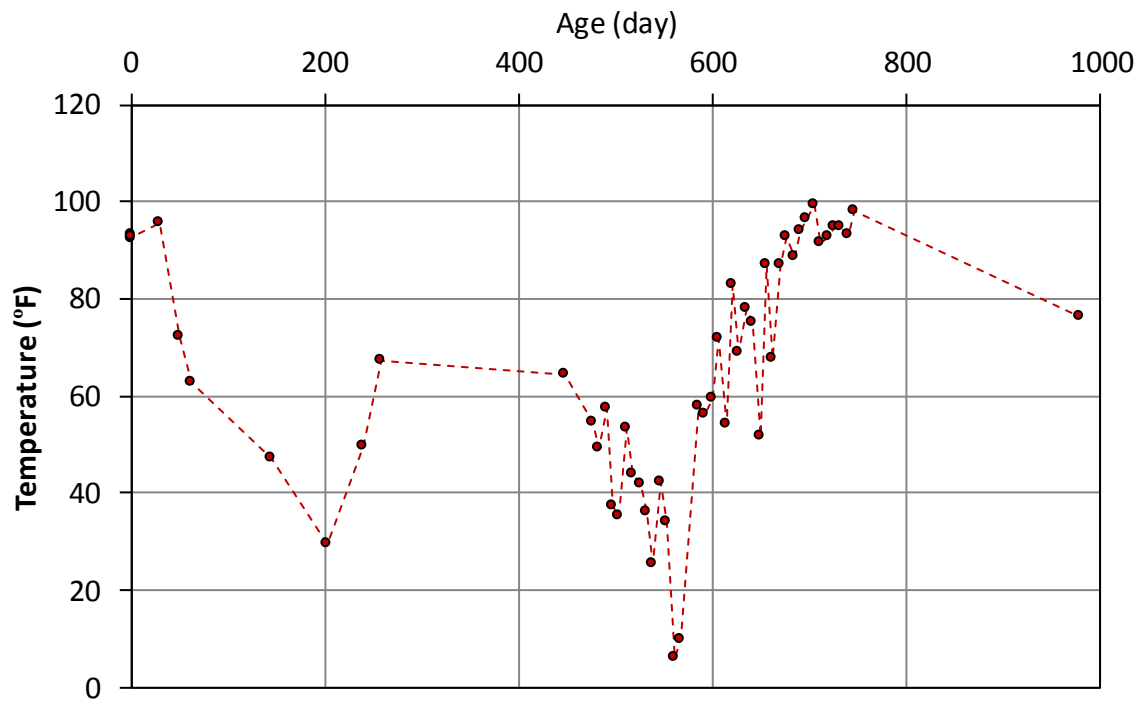


**Figure A-9 Temperature data for girder I-1, bottom gage 2 ( $y = 6$  in.)**

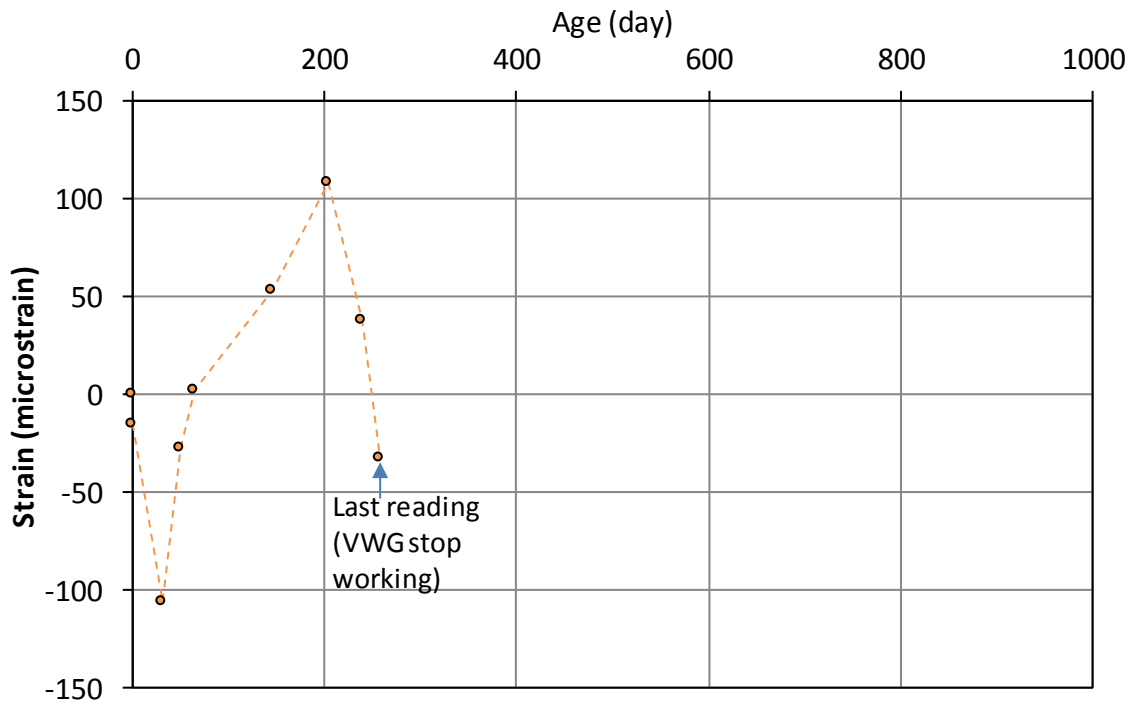


Figure A-10 Strain data for girder I-5, top gage (y = 36 in.)

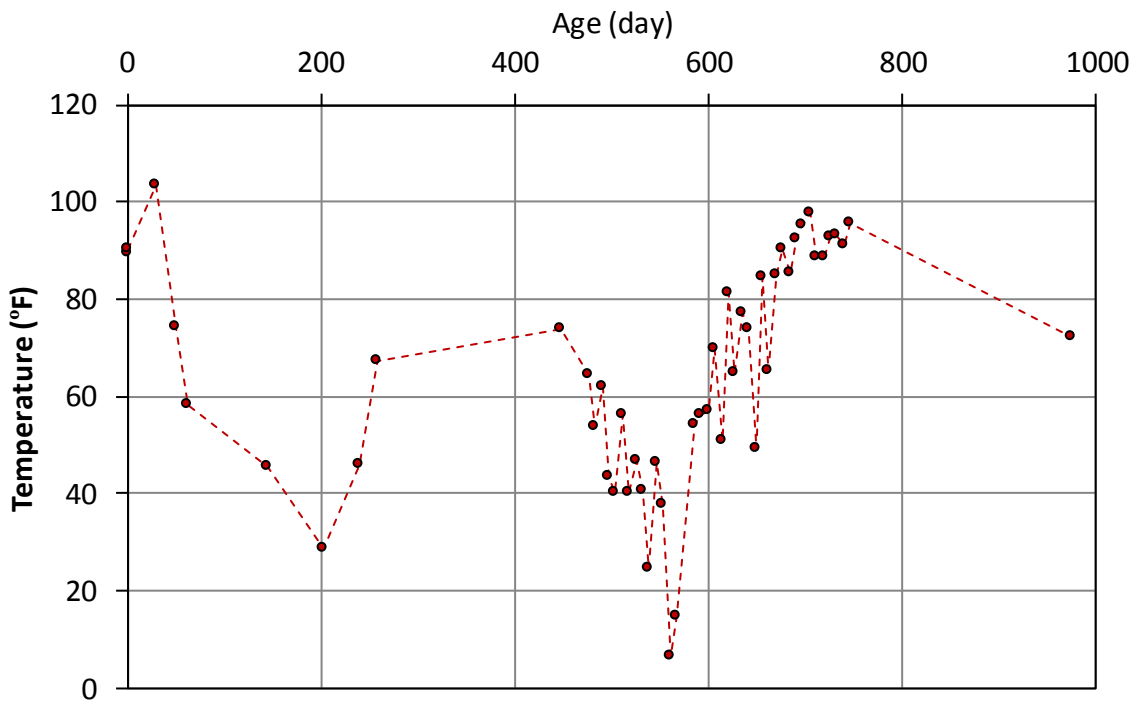


Figure A-11 Temperature data for girder I-5, top gage (y = 36 in.)

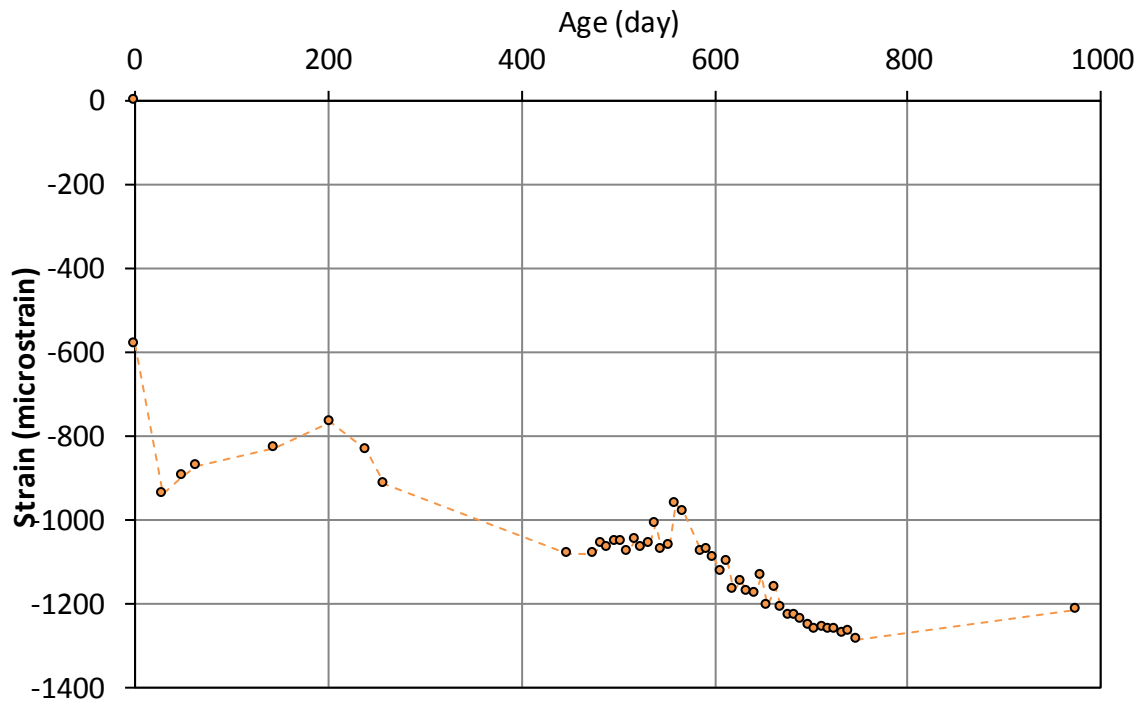


Figure A-12 Strain data for girder I-5, web gage ( $y = 18$  in.)

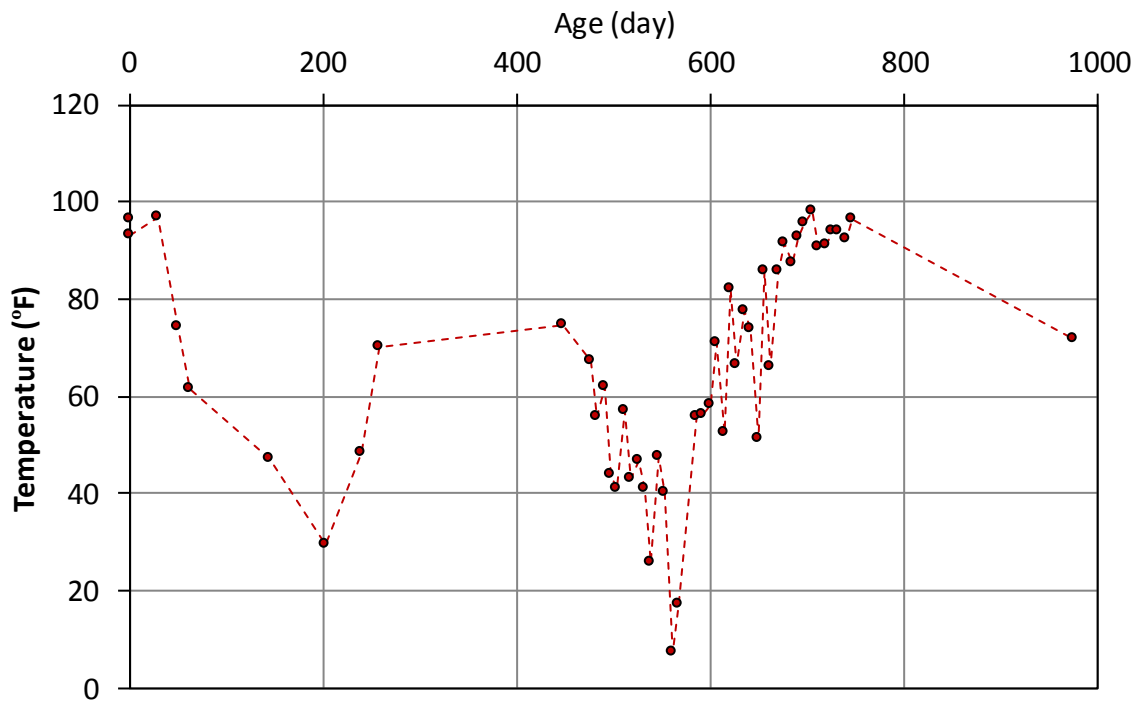
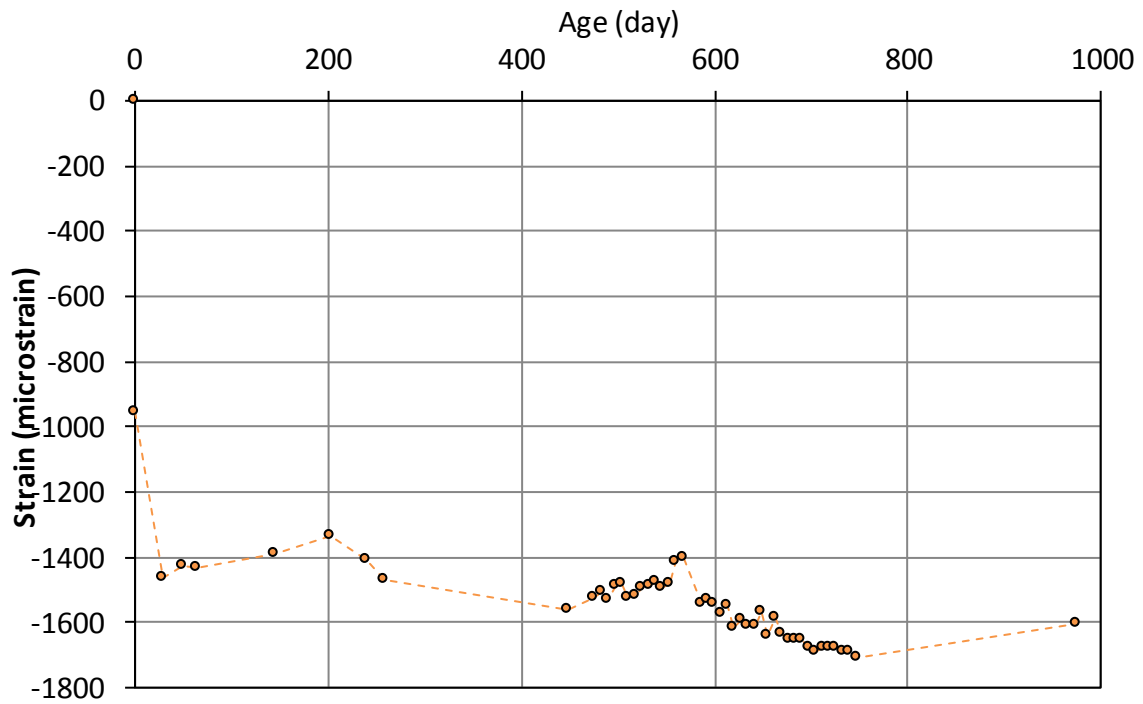
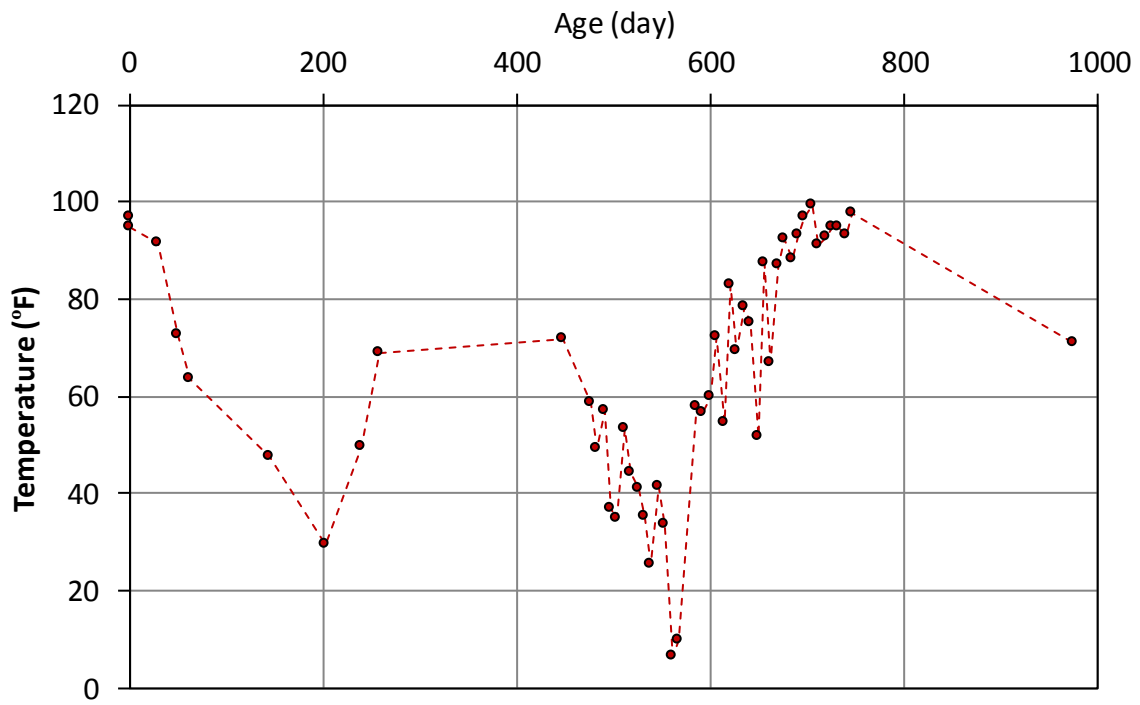


Figure A-13 Temperature data for girder I-5, web gage ( $y = 18$  in.)



**Figure A-14 Strain data for girder I-5, bottom gage 1 ( $y = 6$  in.)**



**Figure A-15 Temperature data for girder I-5, bottom gage 1 ( $y = 6$  in.)**

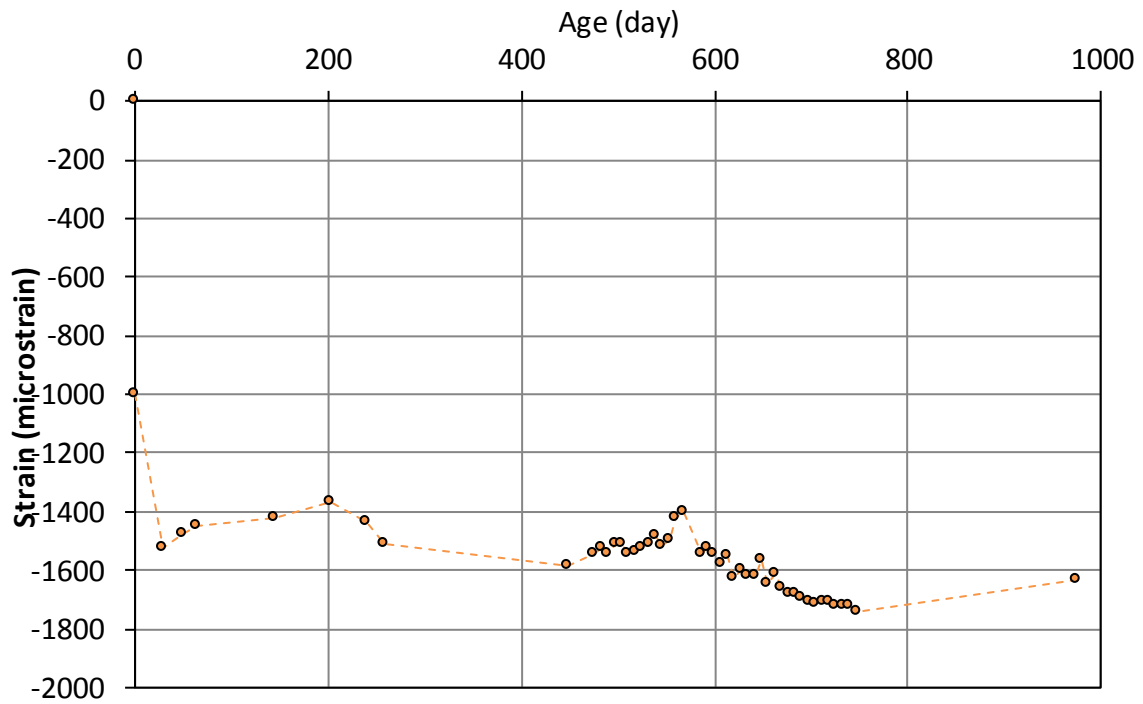


Figure A-16 Strain data for girder I-5, bottom gage 2 ( $y = 6$  in.)

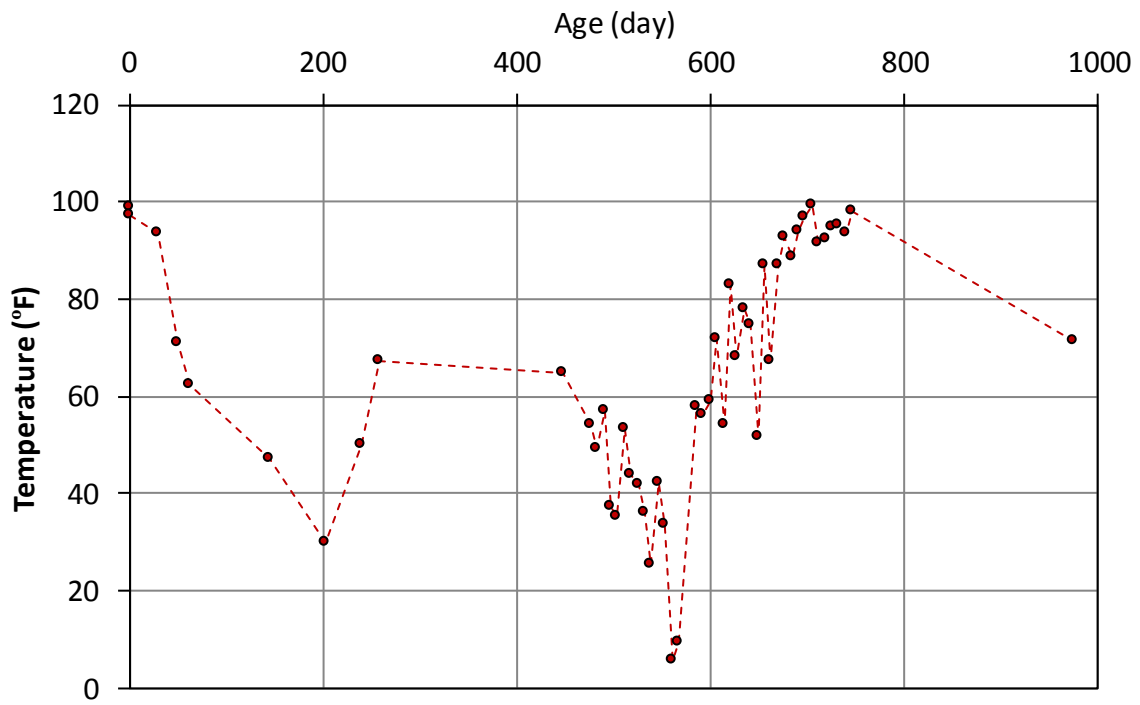


Figure A-17 Temperature data for girder I-5, bottom gage 2 ( $y = 6$  in.)

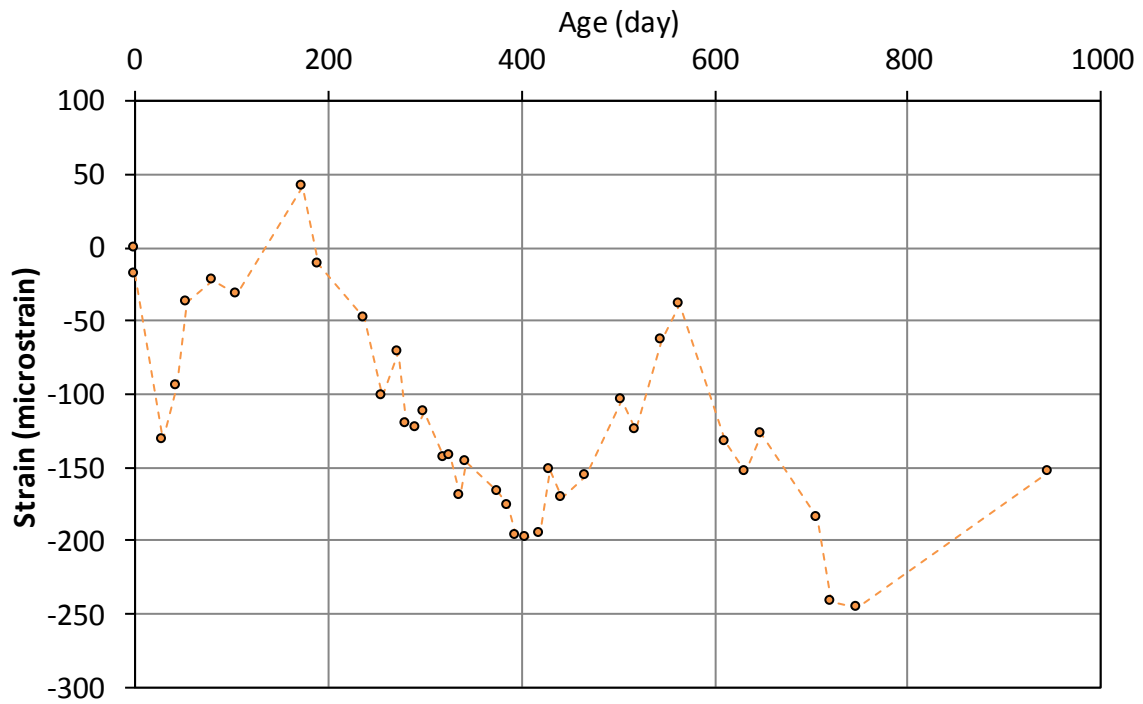


Figure A-18 Strain data for girder I-3, top gage ( $y = 36$  in.)

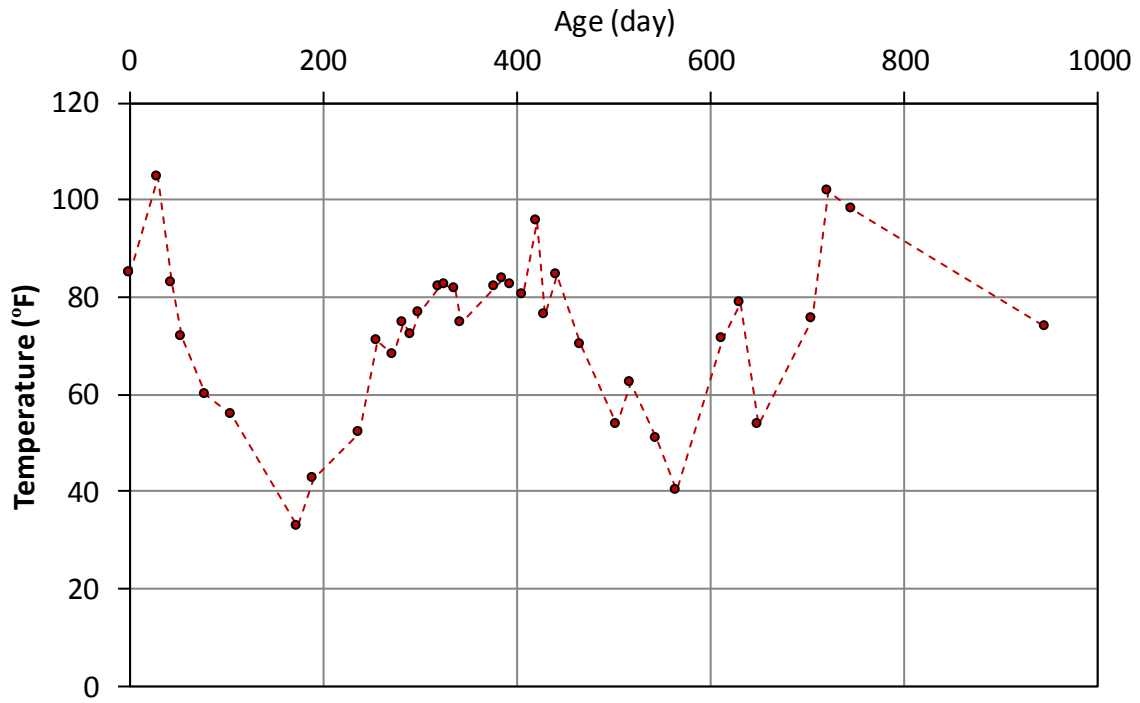
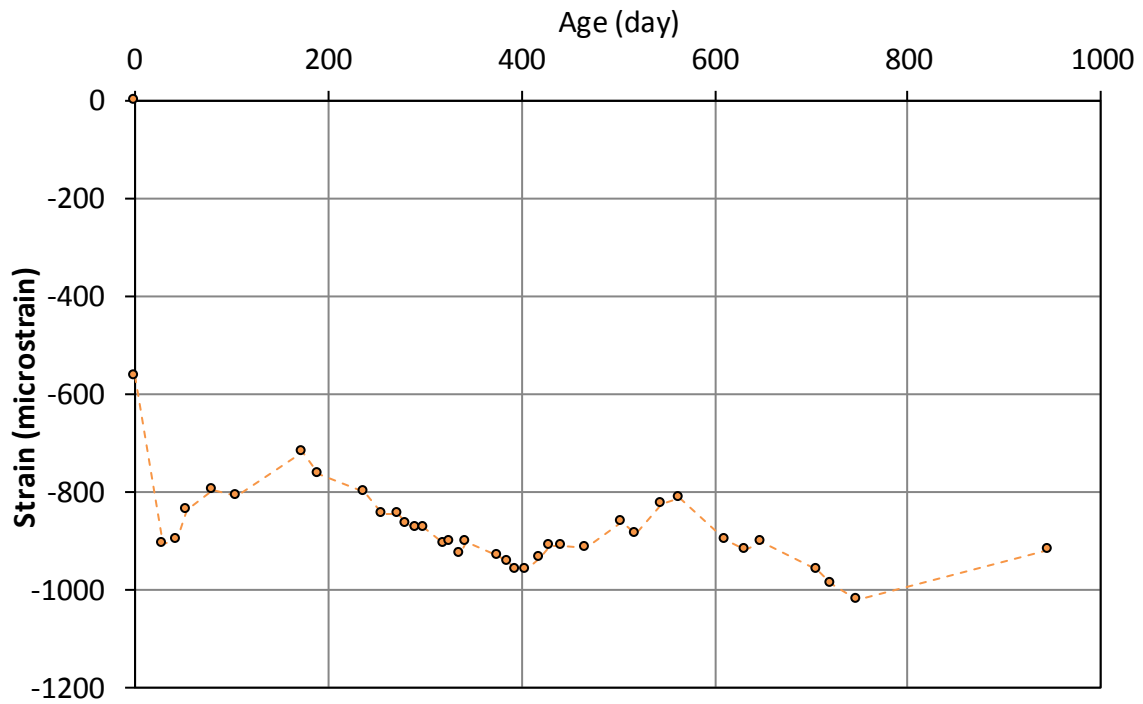
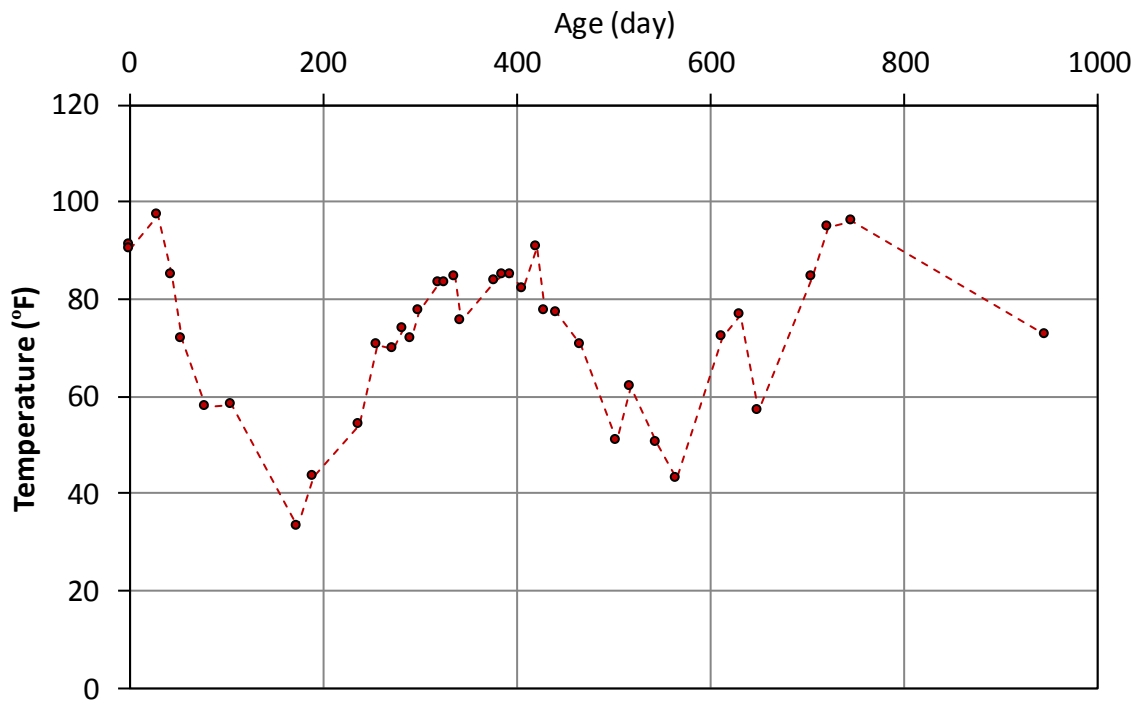


Figure A-19 Temperature data for girder I-3, top gage ( $y = 36$  in.)





**Figure A-20 Strain data for girder I-3, web gage ( $y = 18$  in.)**



**Figure A-21 Temperature data for girder I-3, web gage ( $y = 18$  in.)**

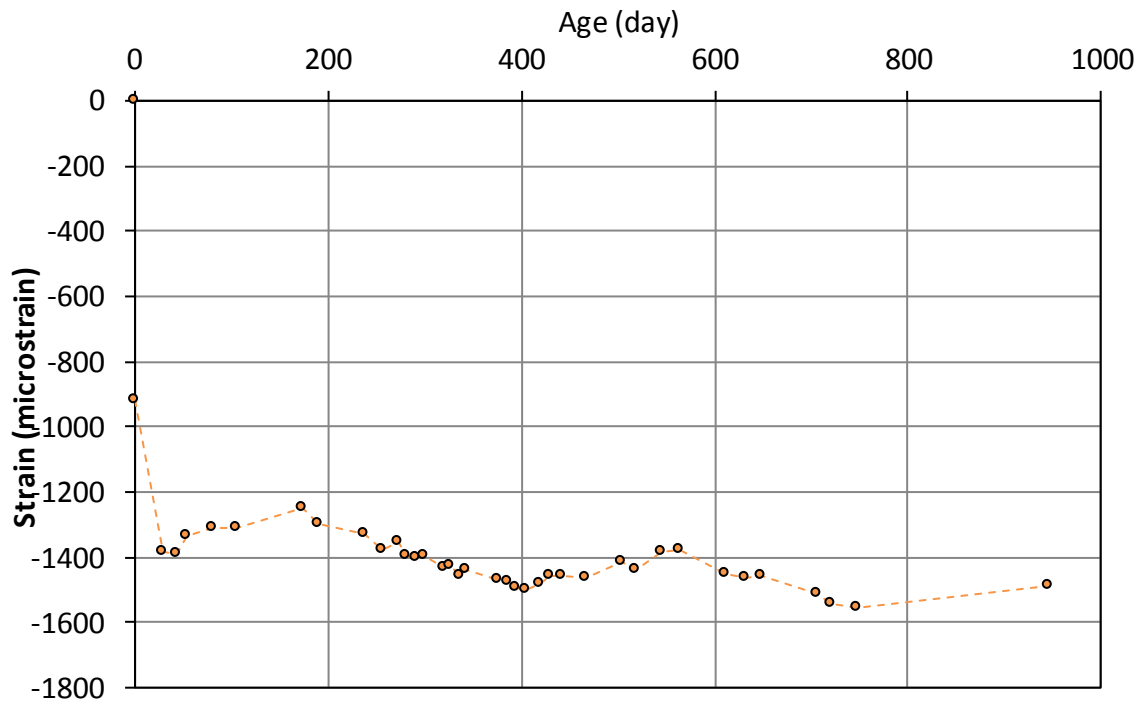


Figure A-22 Strain data for girder I-3, bottom gage 1 (y = 6 in.)

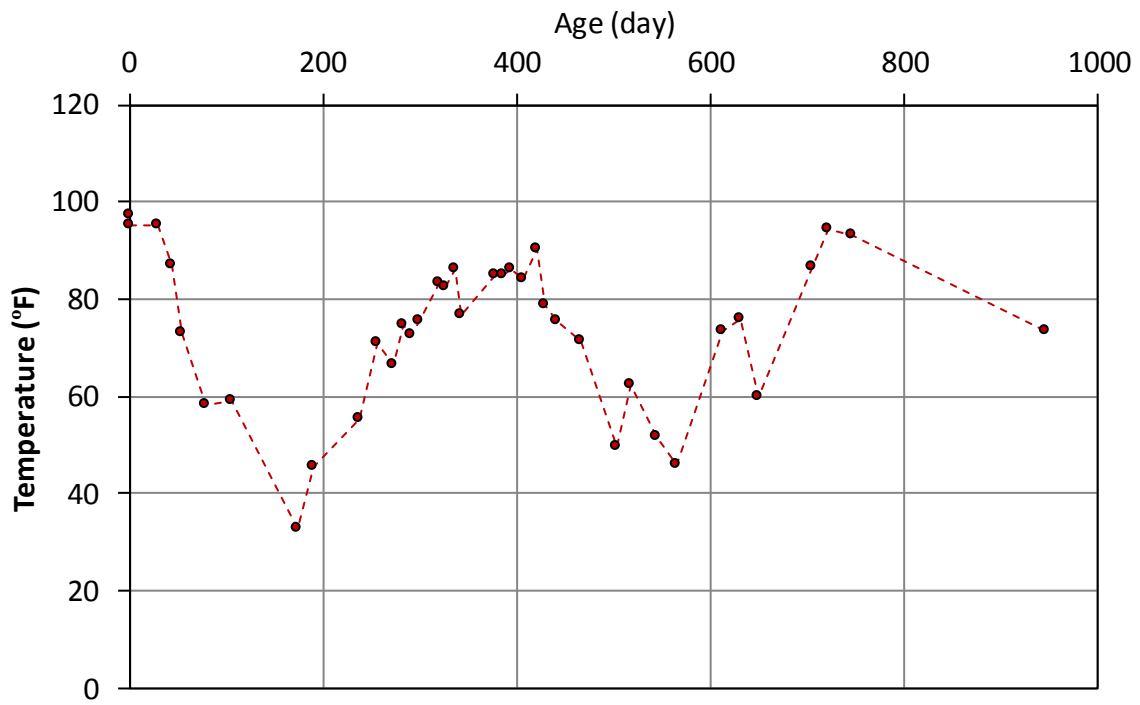


Figure A-23 Temperature data for girder I-3, bottom gage 1 (y = 6 in.)

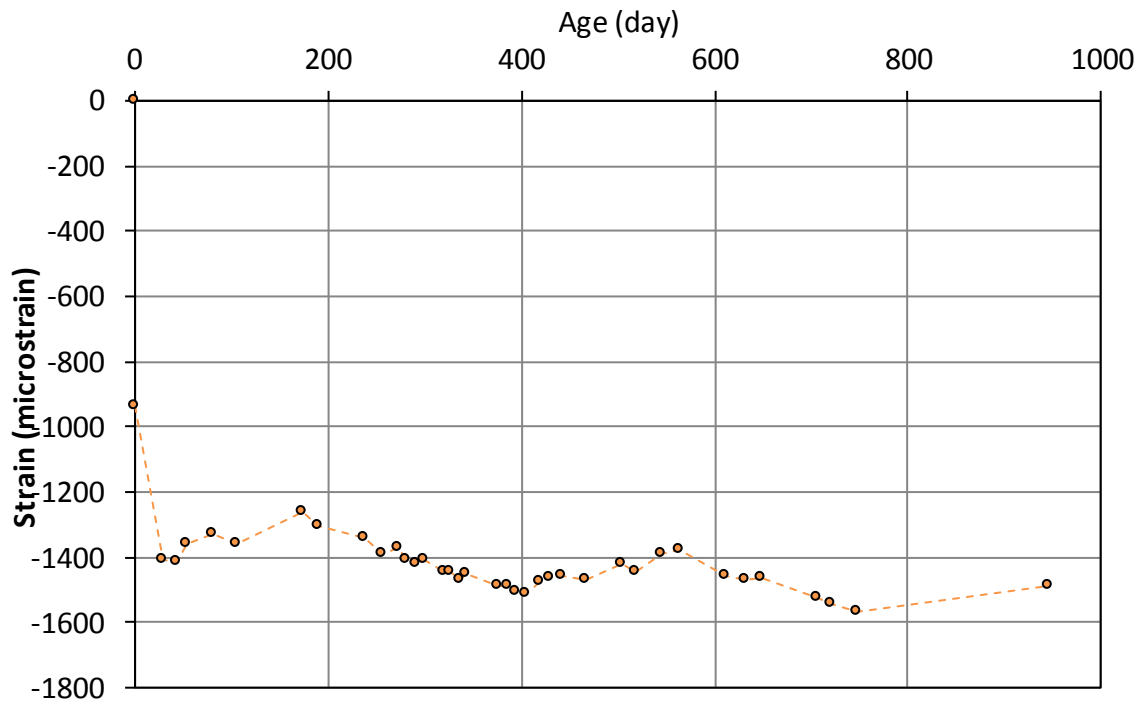


Figure A-24 Strain data for girder I-3, bottom gage 2 ( $y = 6$  in.)

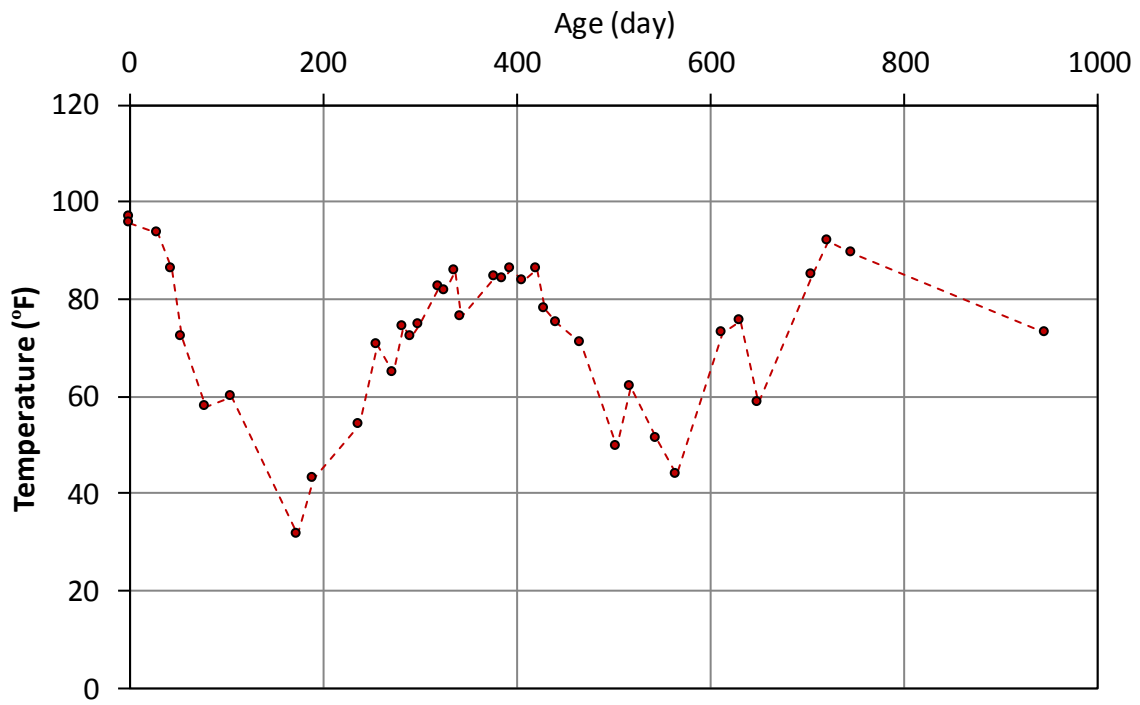


Figure A-25 Temperature data for girder I-3, bottom gage 2 ( $y = 6$  in.)

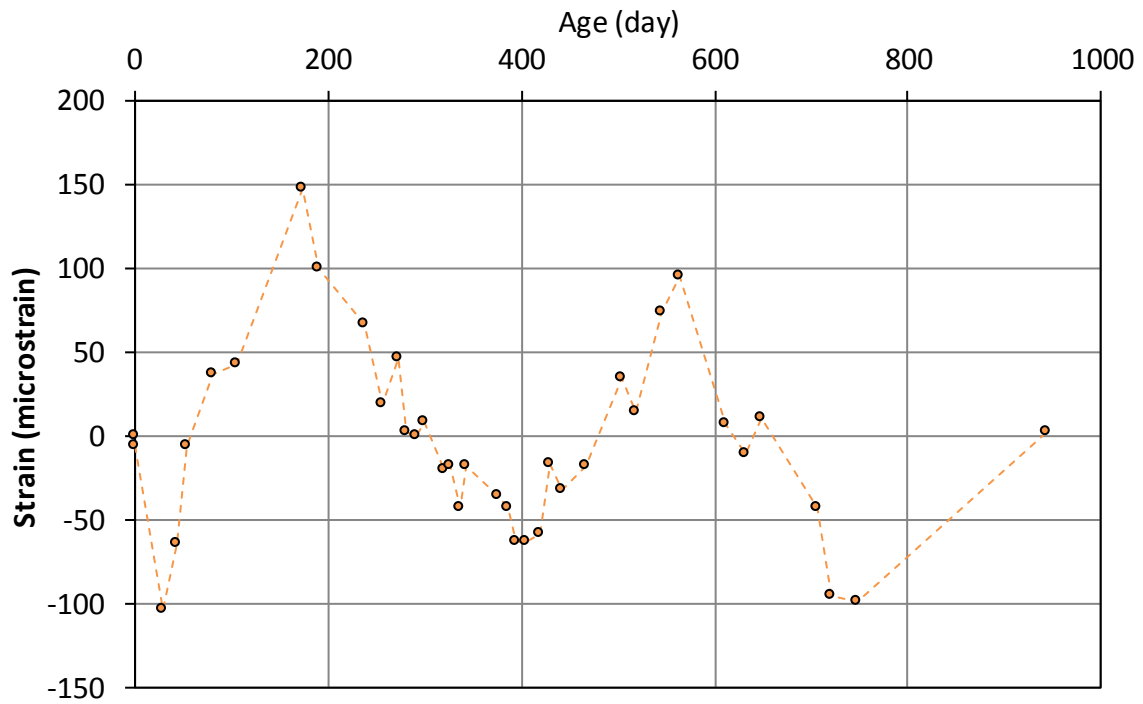


Figure A-26 Strain data for girder I-7, top gage ( $y = 36$  in.)

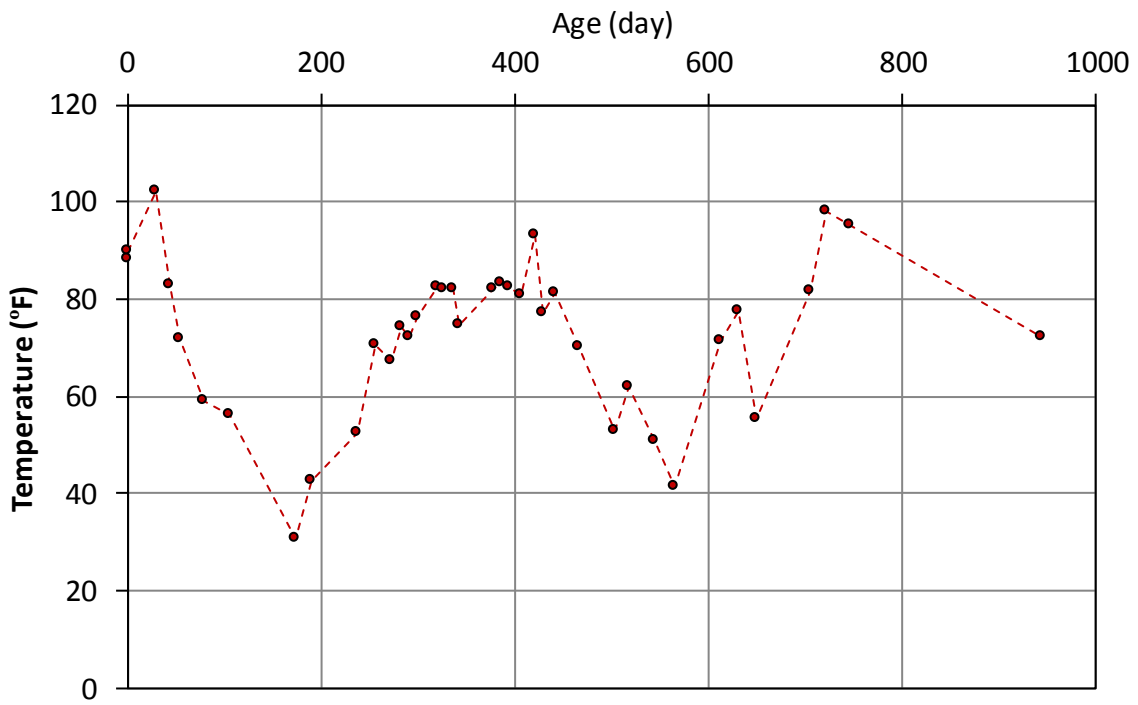


Figure A-27 Temperature data for girder I-7, top gage ( $y = 36$  in.)

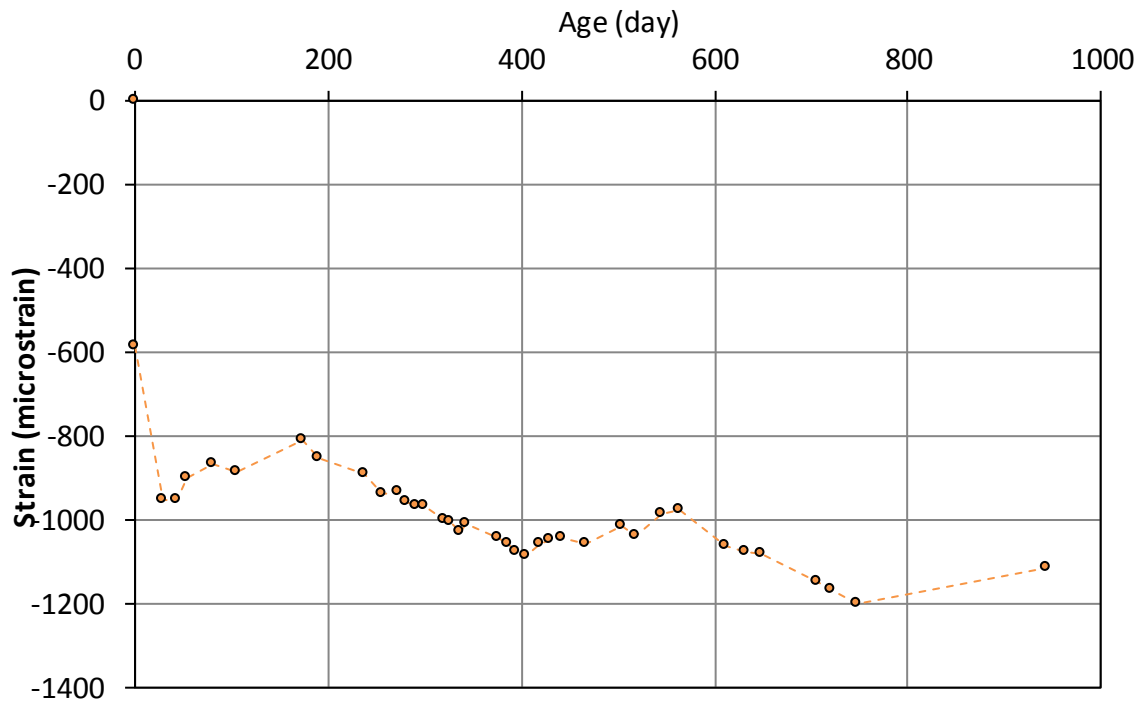


Figure A-28 Strain data for girder I-7, web gage ( $y = 18$  in.)

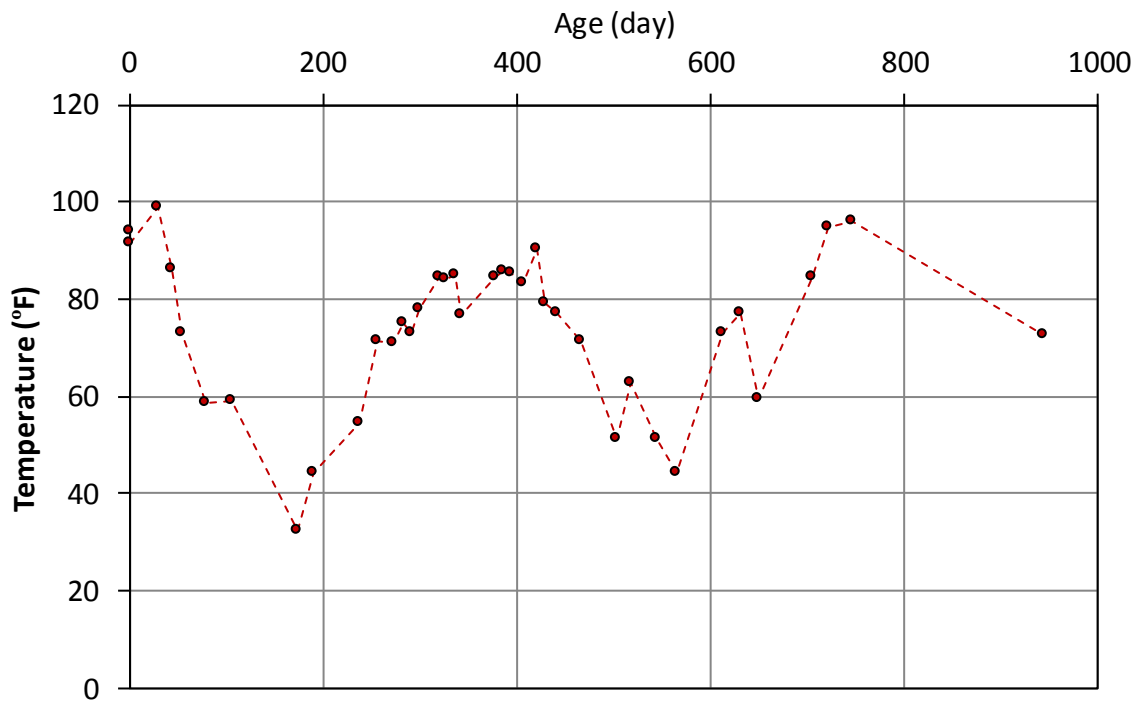


Figure A-29 Temperature data for girder I-7, web gage ( $y = 18$  in.)

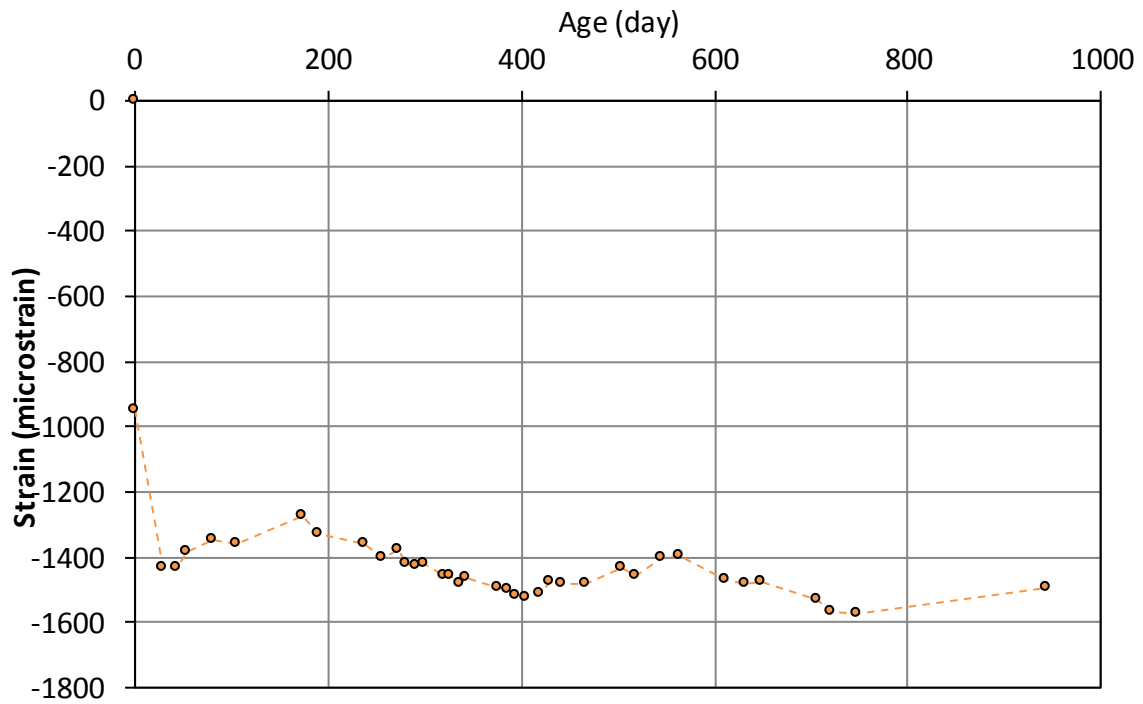


Figure A-30 Strain data for girder I-7, bottom gage 1 ( $y = 6$  in.)

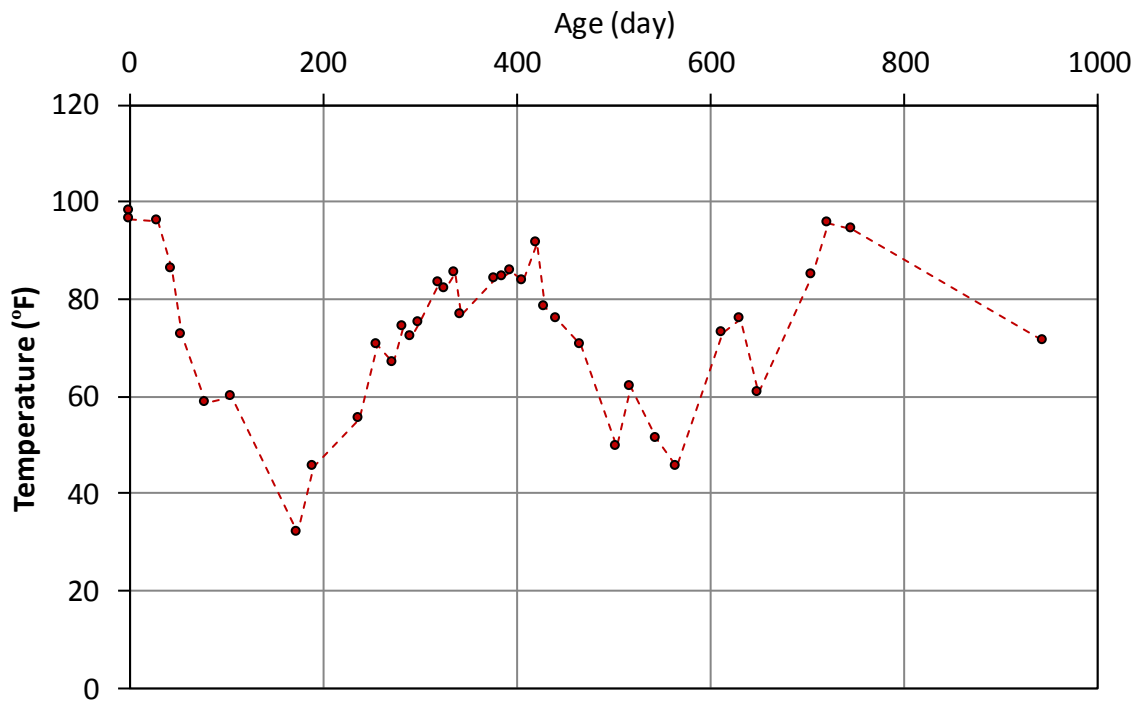


Figure A-31 Temperature data for girder I-7, bottom gage 1 ( $y = 6$  in.)

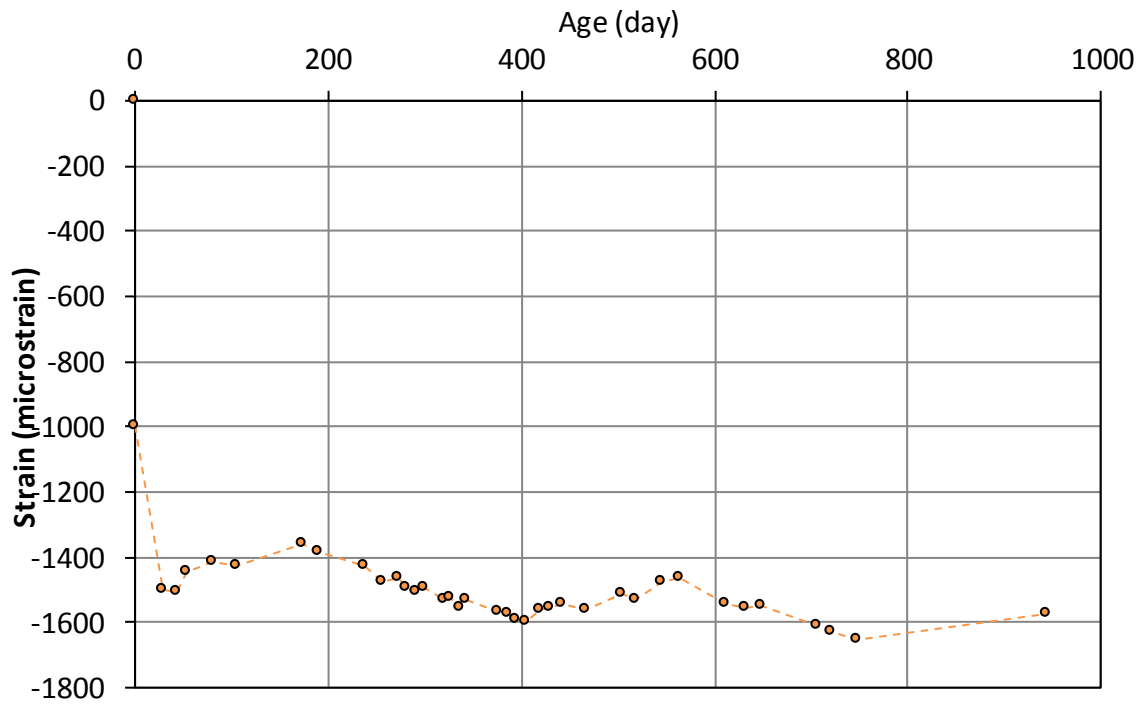


Figure A-32 Strain data for girder I-7, bottom gage 2 ( $y = 6$  in.)

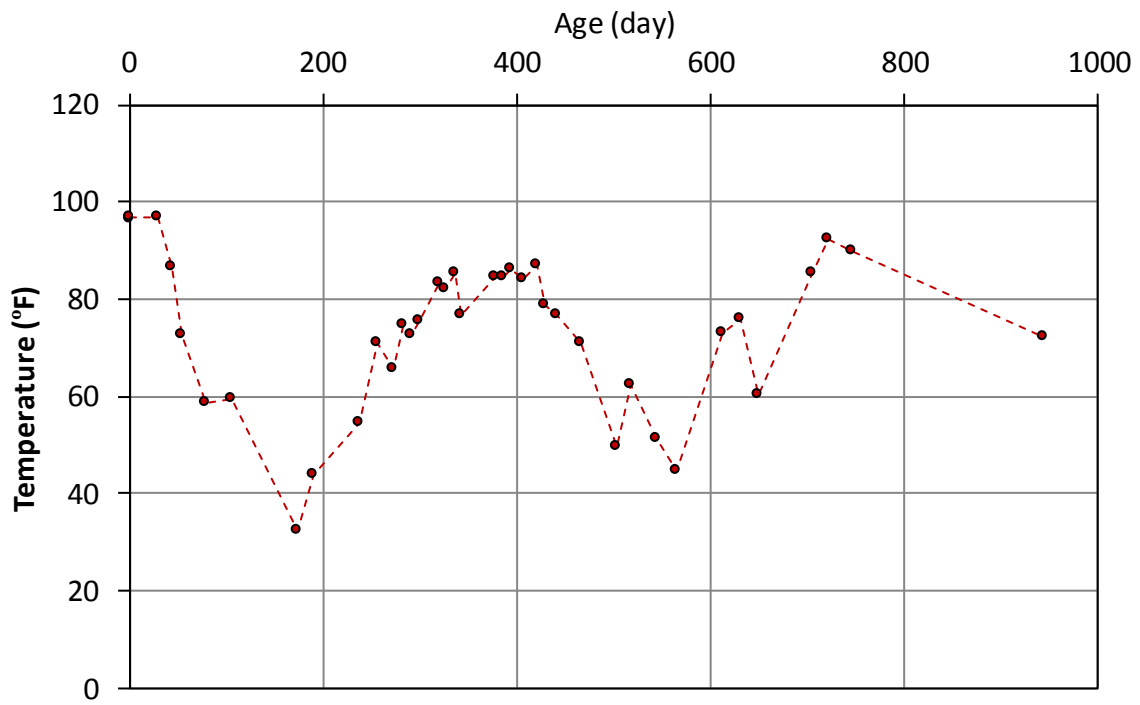


Figure A-33 Temperature data for girder I-7, bottom gage 2 ( $y = 6$  in.)

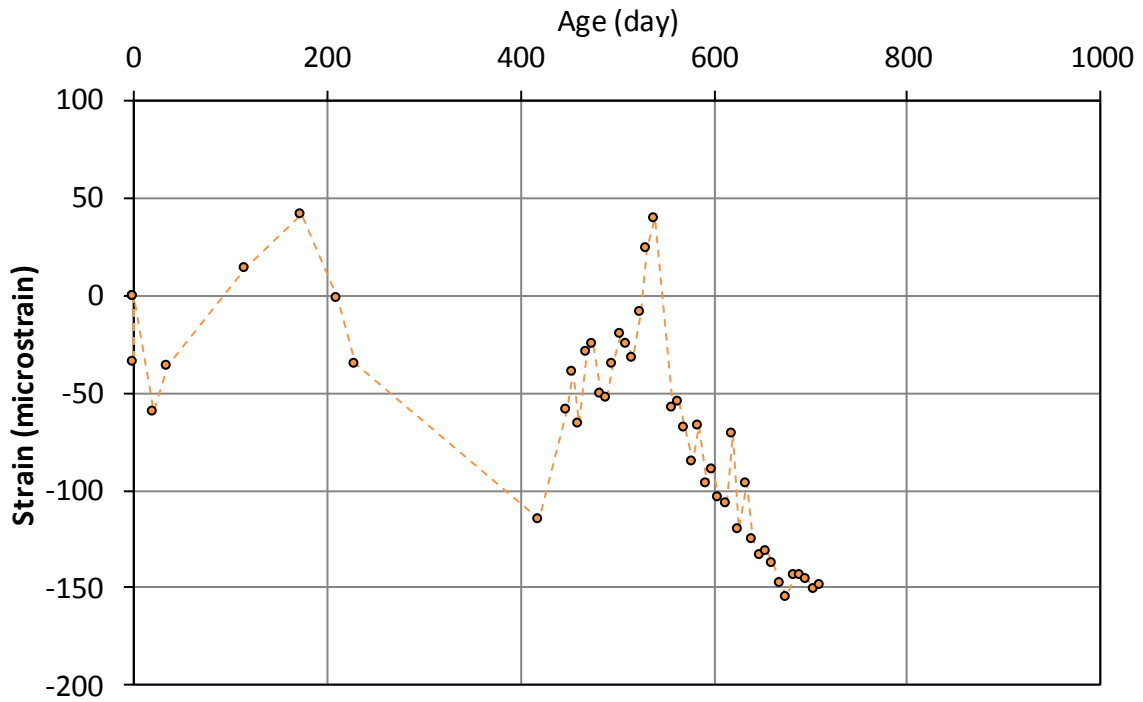


Figure A-34 Strain data for girder II-1, top gage ( $y = 36$  in.)

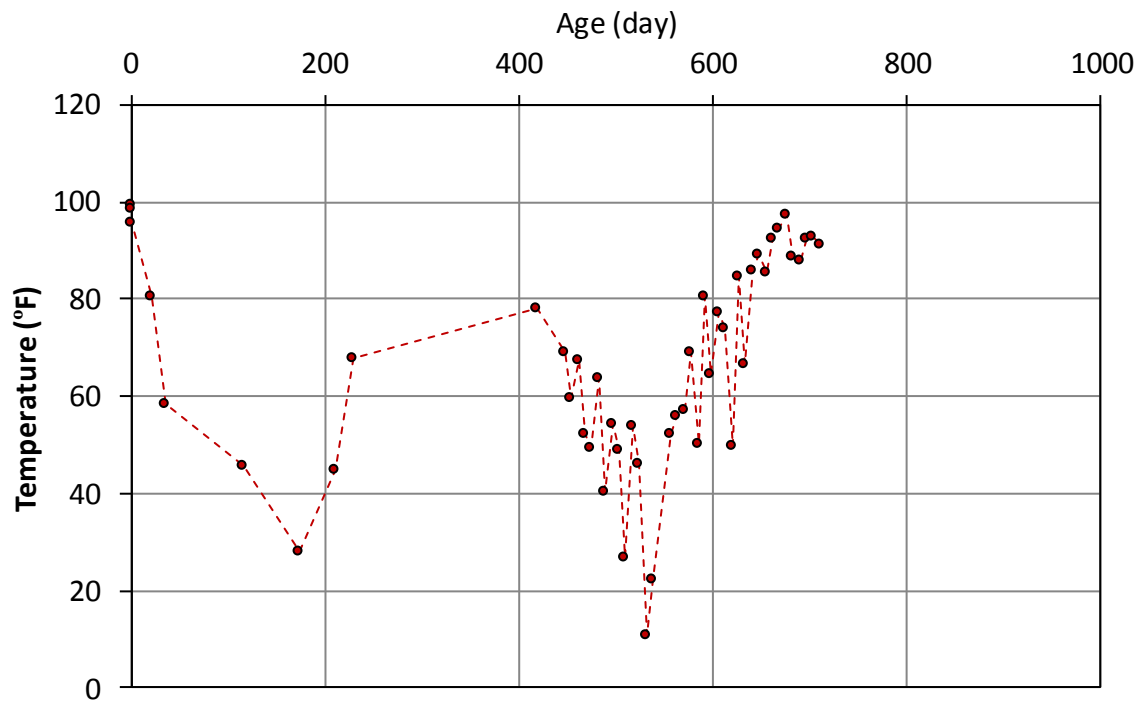


Figure A-35 Temperature data for girder II-1, top gage ( $y = 36$  in.)



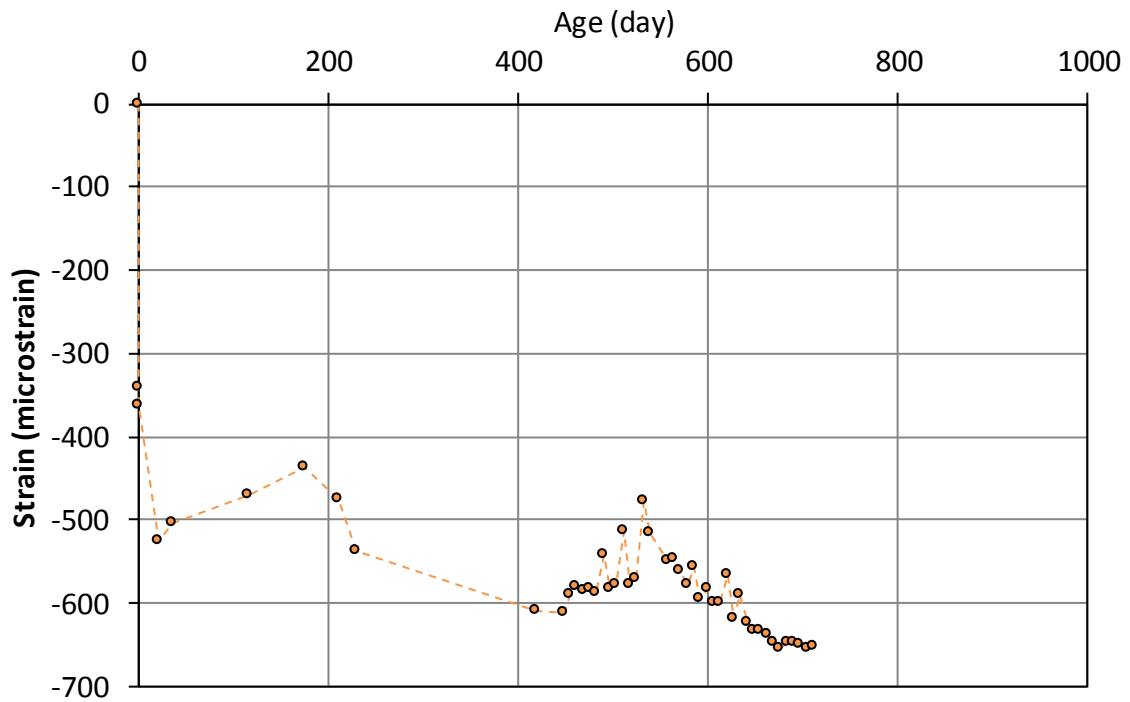


Figure A-36 Strain data for girder II-1, web gage ( $y = 18$  in.)

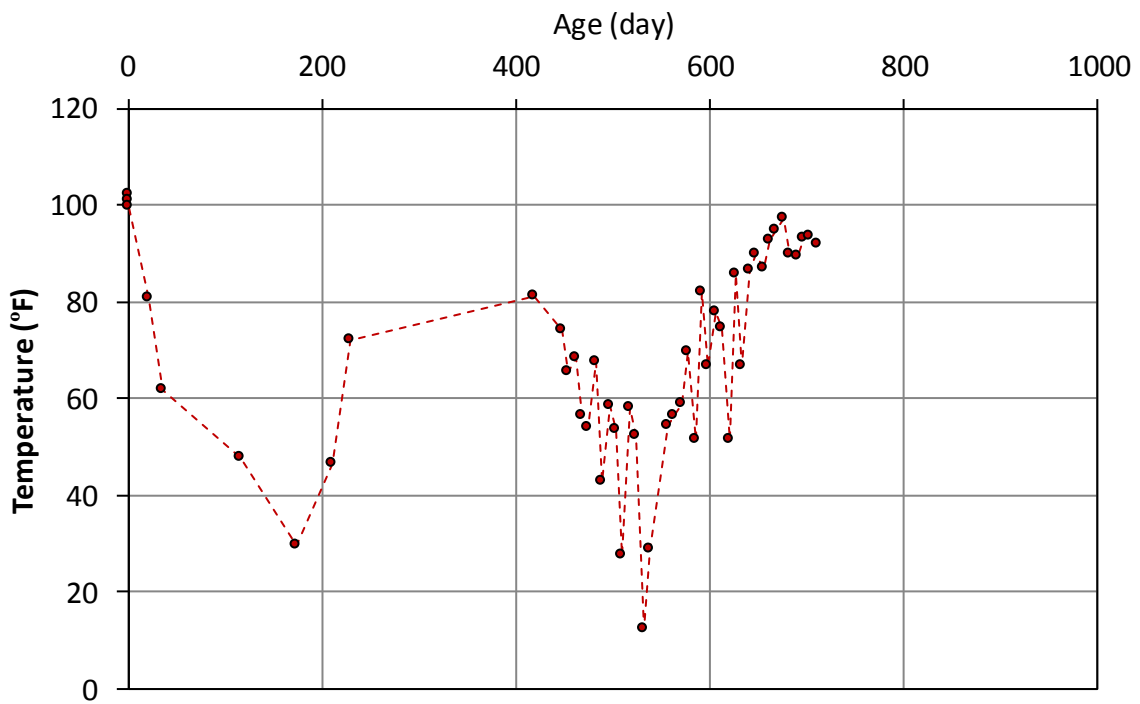


Figure A-37 Temperature data for girder II-1, web gage ( $y = 18$  in.)

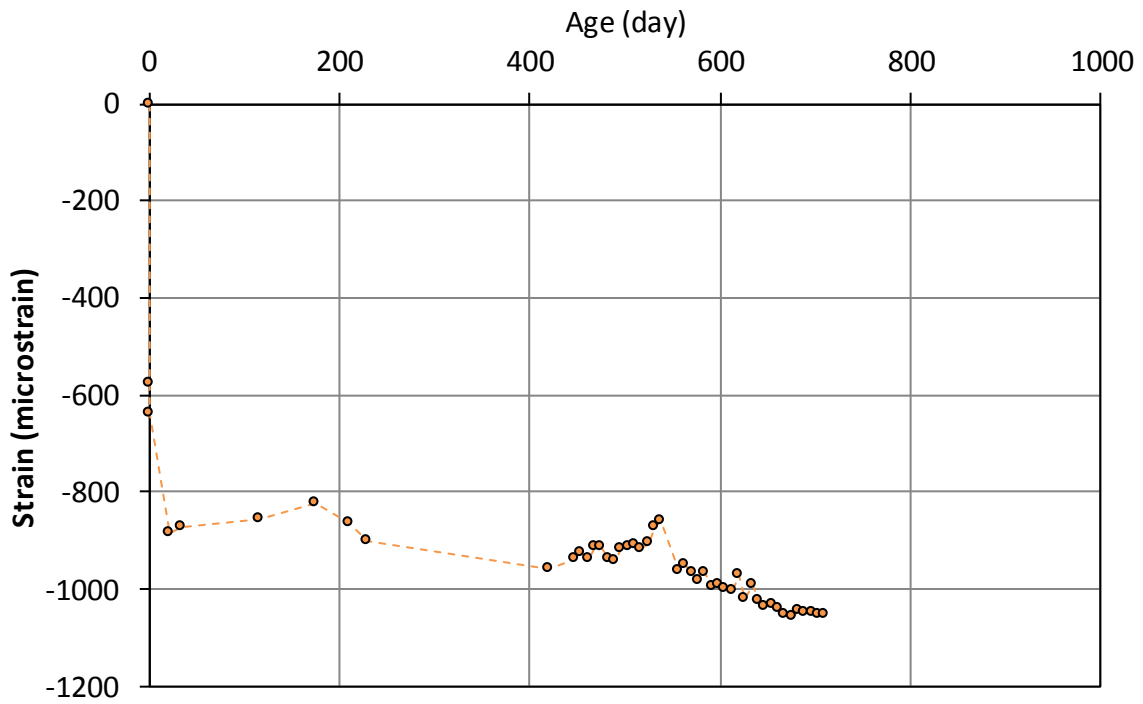


Figure A-38 Strain data for girder II-1, bottom gage 1 ( $y = 6$  in.)

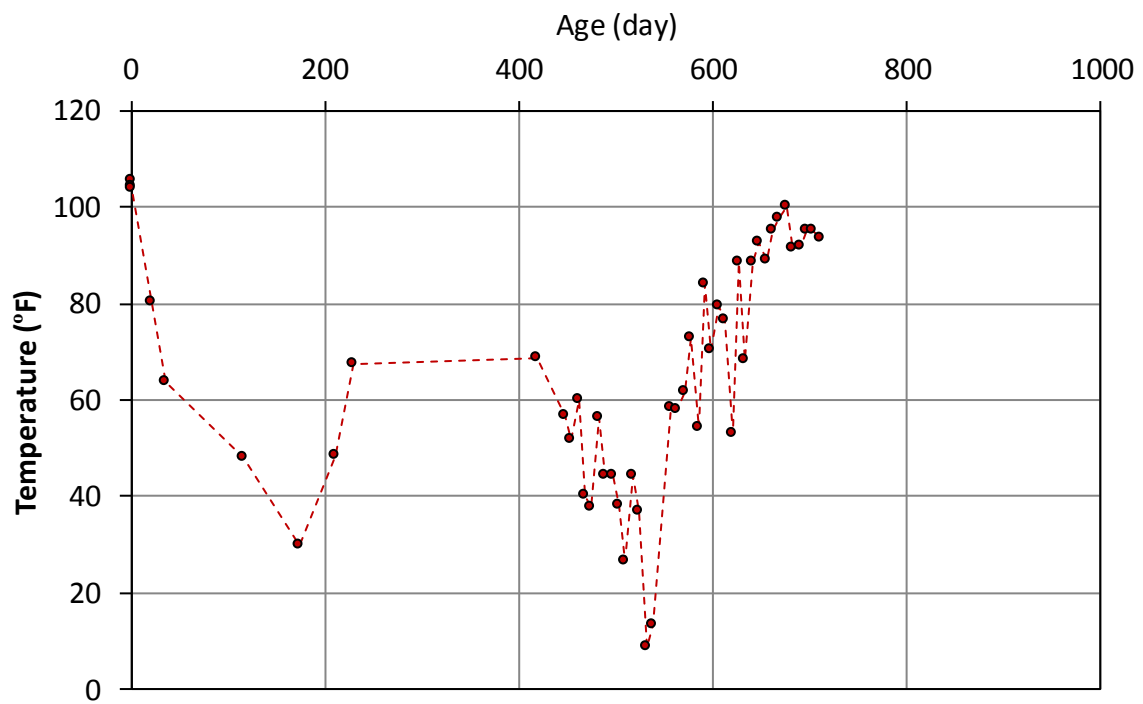


Figure A-39 Temperature data for girder II-1, bottom gage 1 ( $y = 6$  in.)

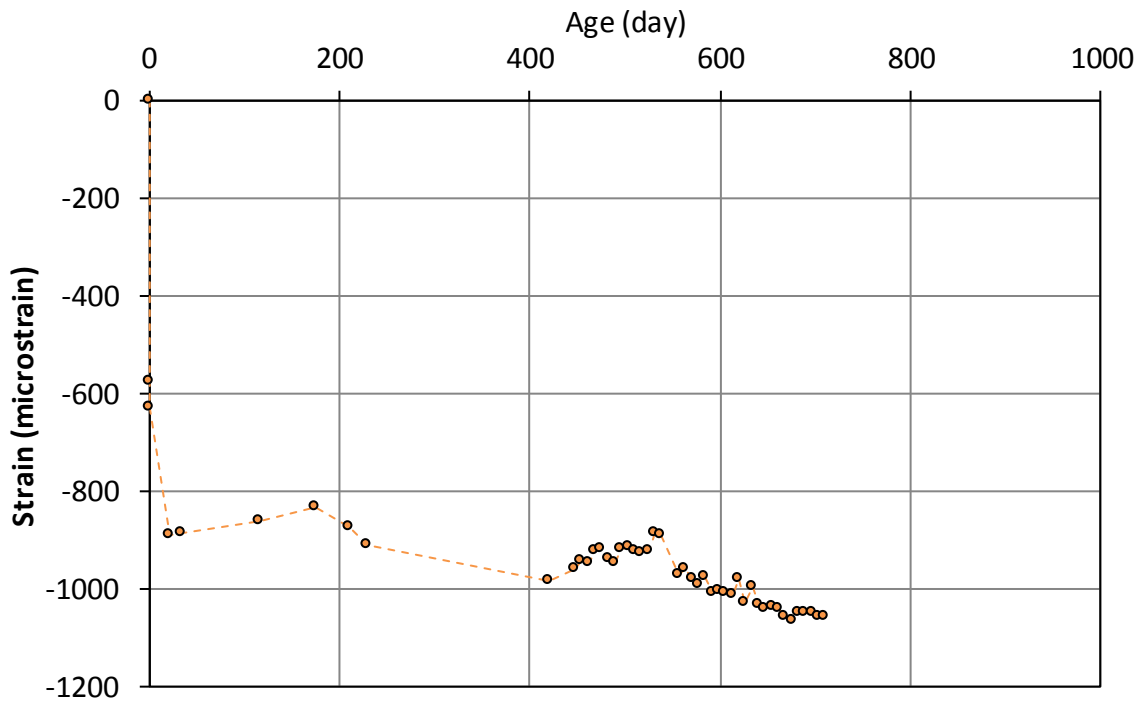


Figure A-40 Strain data for girder II-1, bottom gage 2 ( $y = 6$  in.)

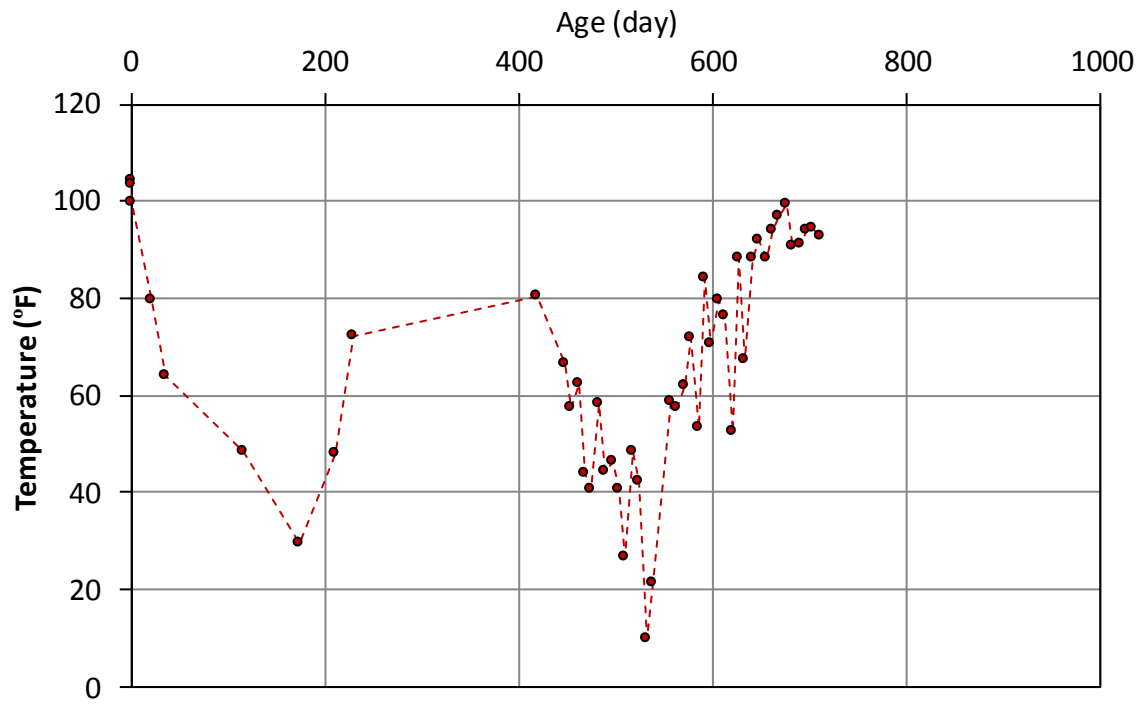
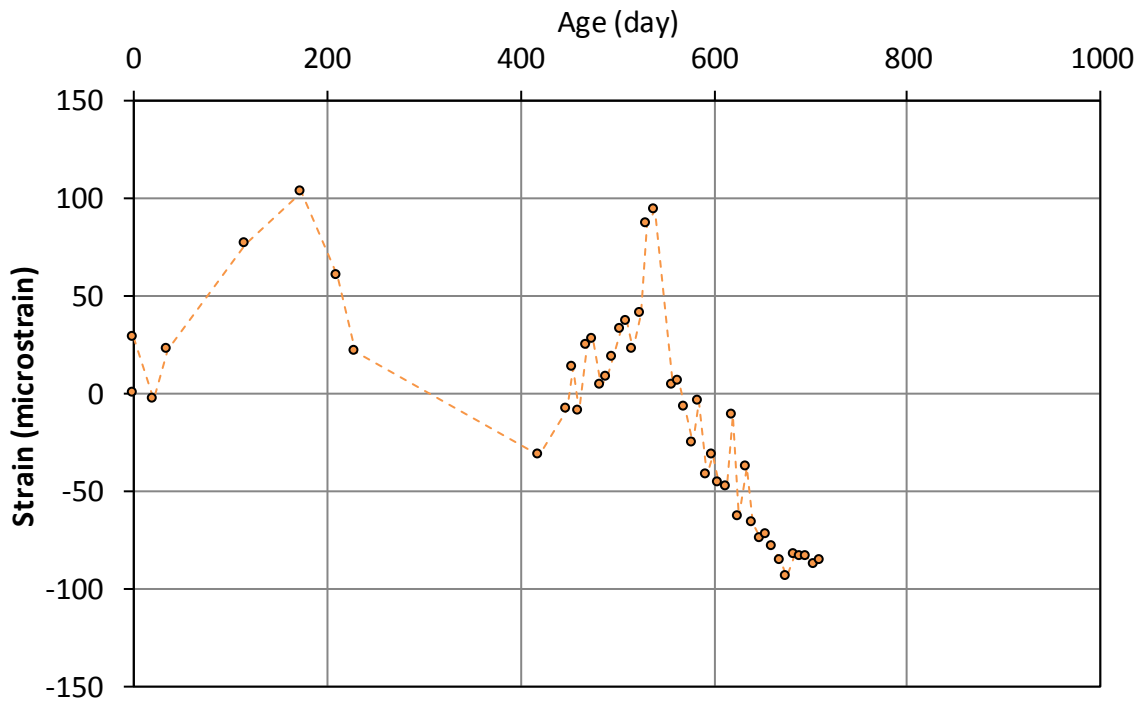
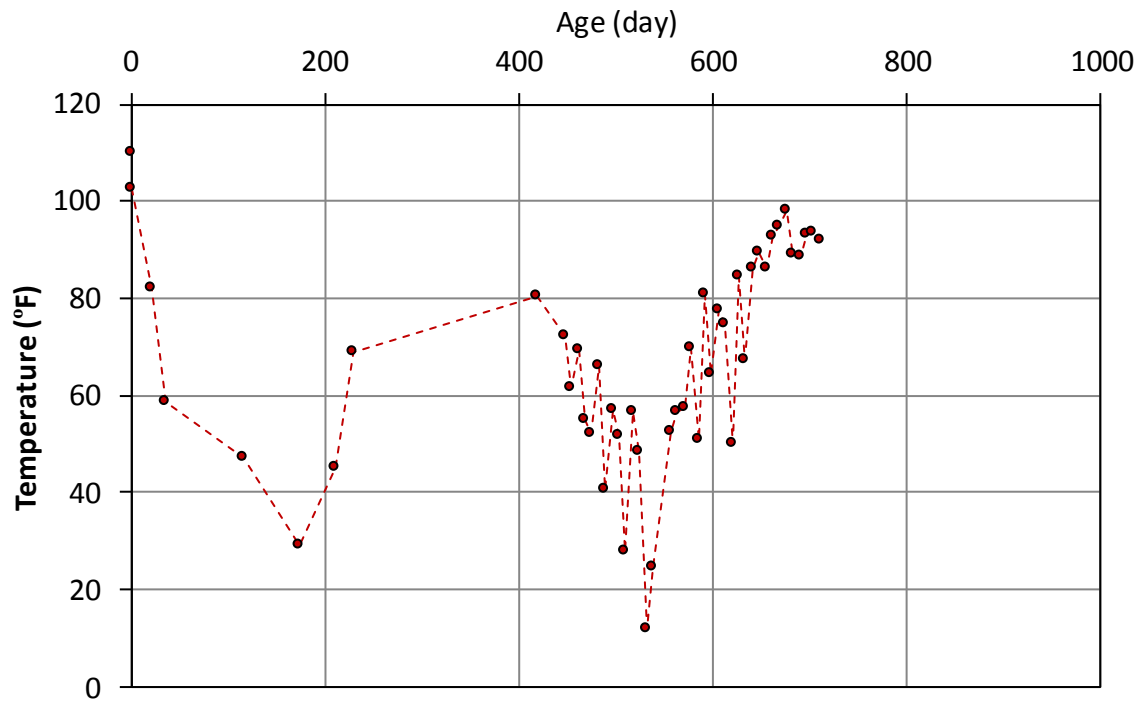


Figure A-41 Temperature data for girder II-1, bottom gage 2 ( $y = 6$  in.)



**Figure A-42 Strain data for girder II-6, top gage ( $y = 36$  in.)**



**Figure A-43 Temperature data for girder II-6, top gage ( $y = 36$  in.)**

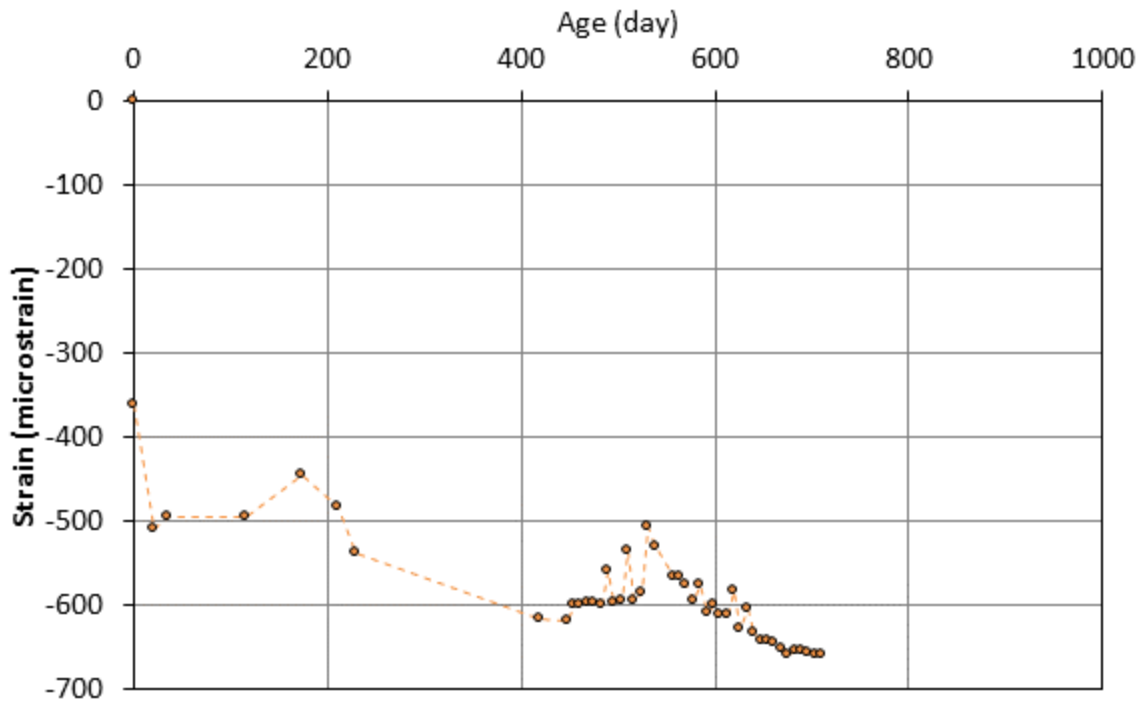


Figure A-44 Strain data for girder II-6, web gage ( $y = 18$  in.)

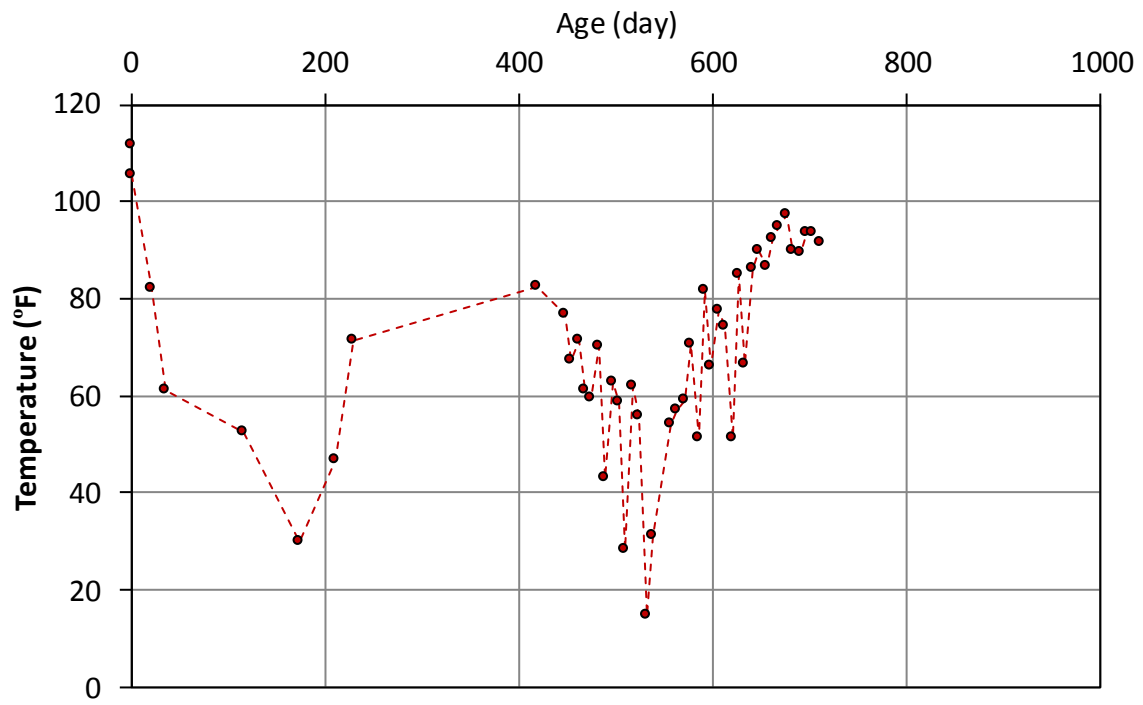


Figure A-45 Temperature data for girder II-6, web gage ( $y = 18$  in.)

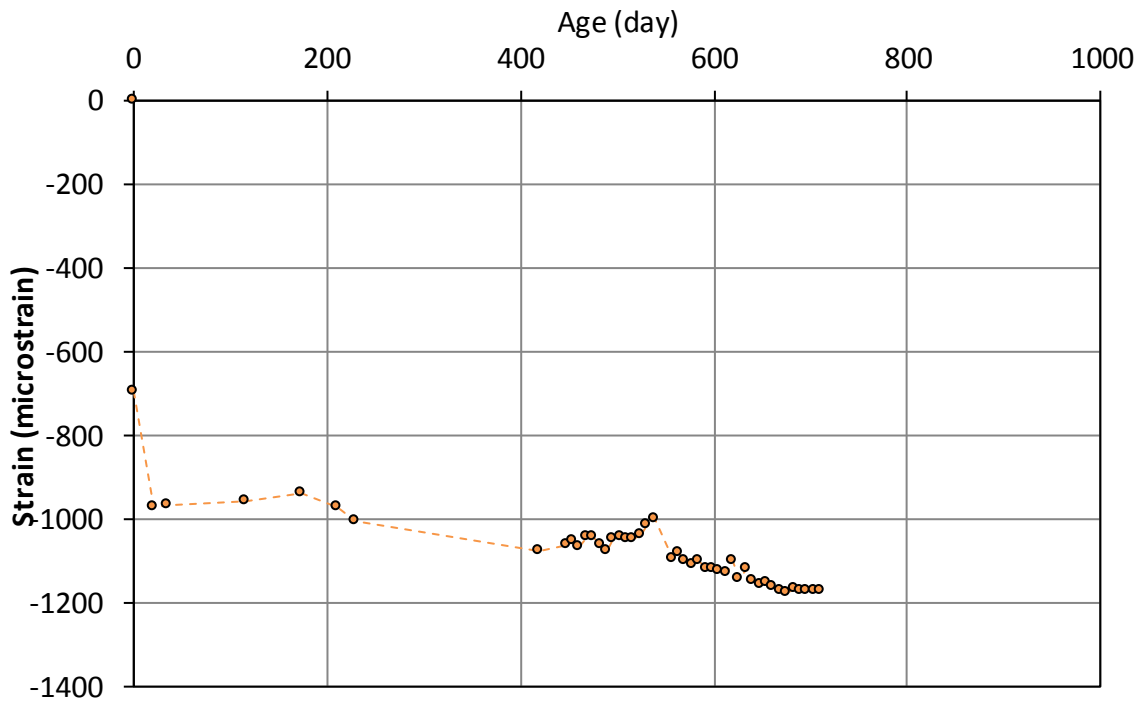


Figure A-46 Strain data for girder II-6, bottom gage 1 ( $y = 6$  in.)

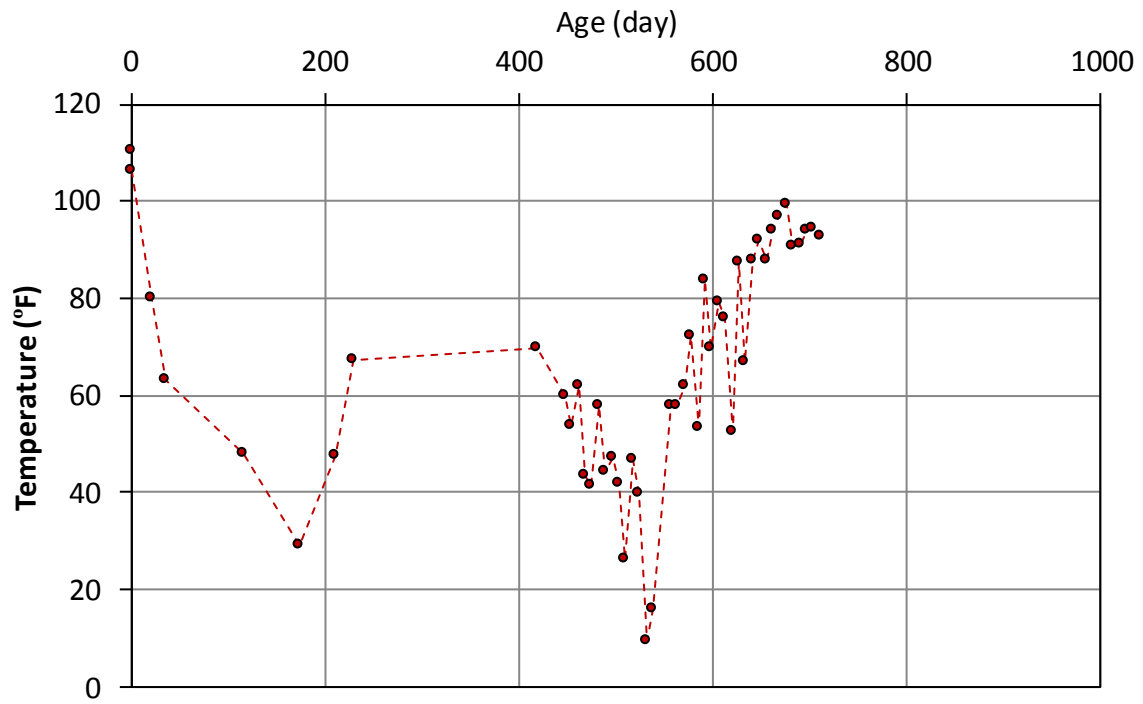
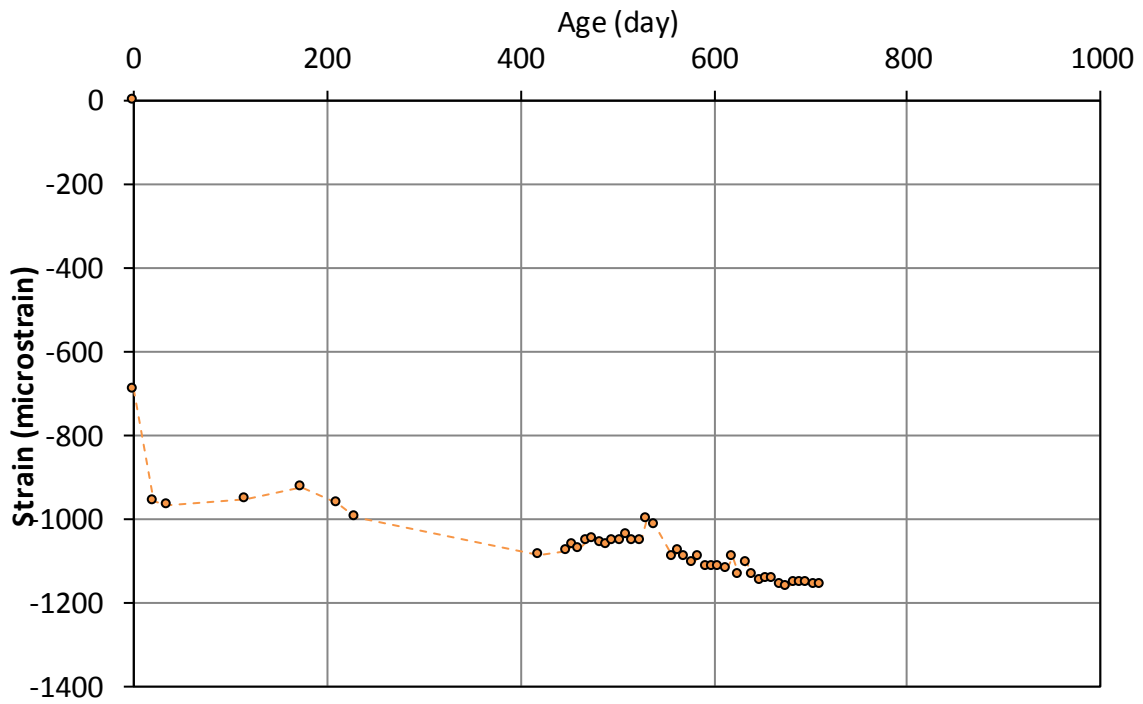
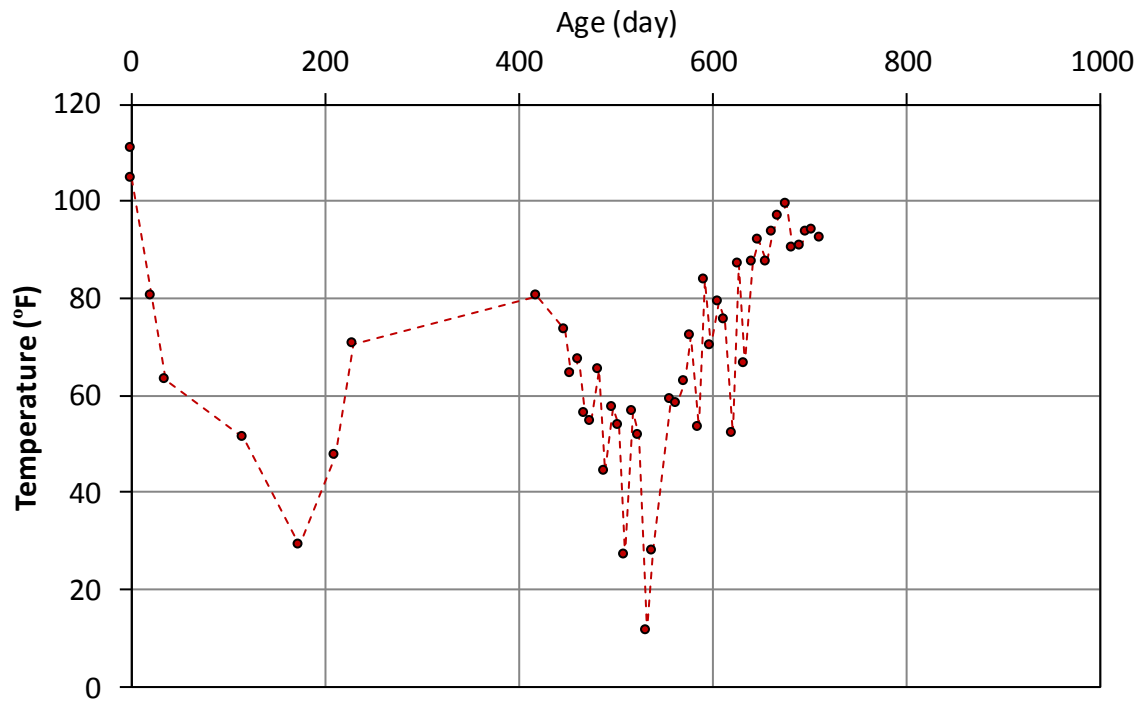


Figure A-47 Temperature data for girder II-6, bottom gage 1 ( $y = 6$  in.)



**Figure A-48 Strain data for girder II-6, bottom gage 2 ( $y = 6$  in.)**



**Figure A-49 Temperature data for girder II-6, bottom gage 2 ( $y = 6$  in.)**

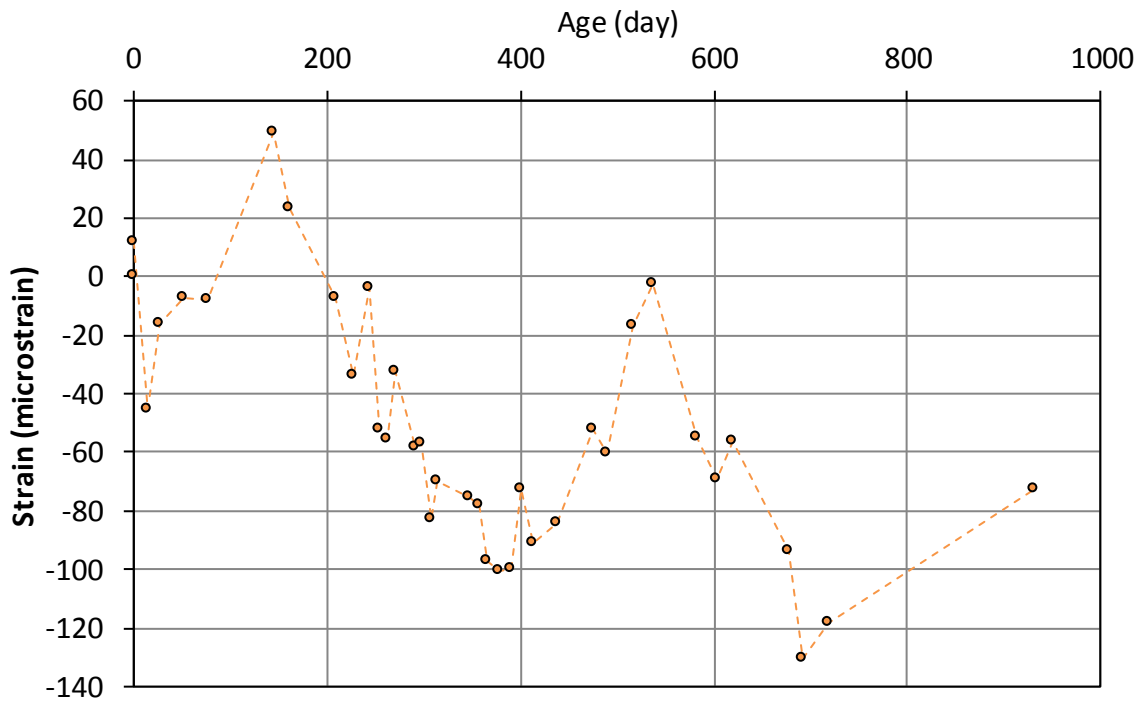


Figure A-50 Strain data for girder II-3, top gage ( $y = 36$  in.)

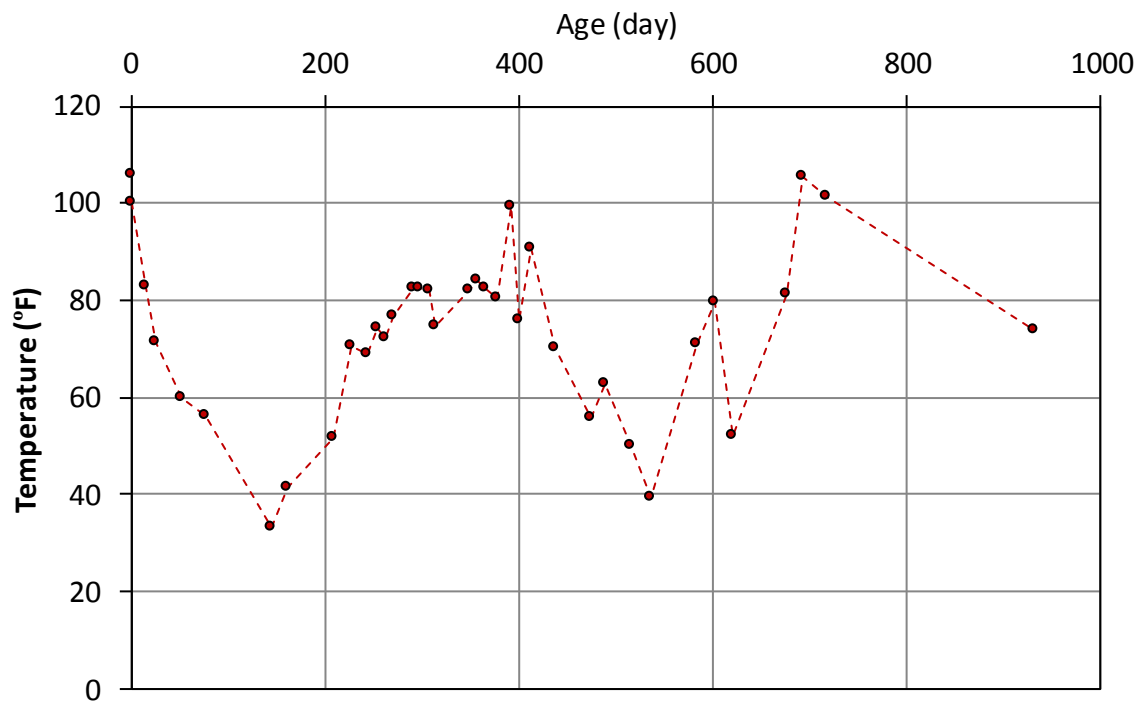


Figure A-51 Temperature data for girder II-3, top gage ( $y = 36$  in.)



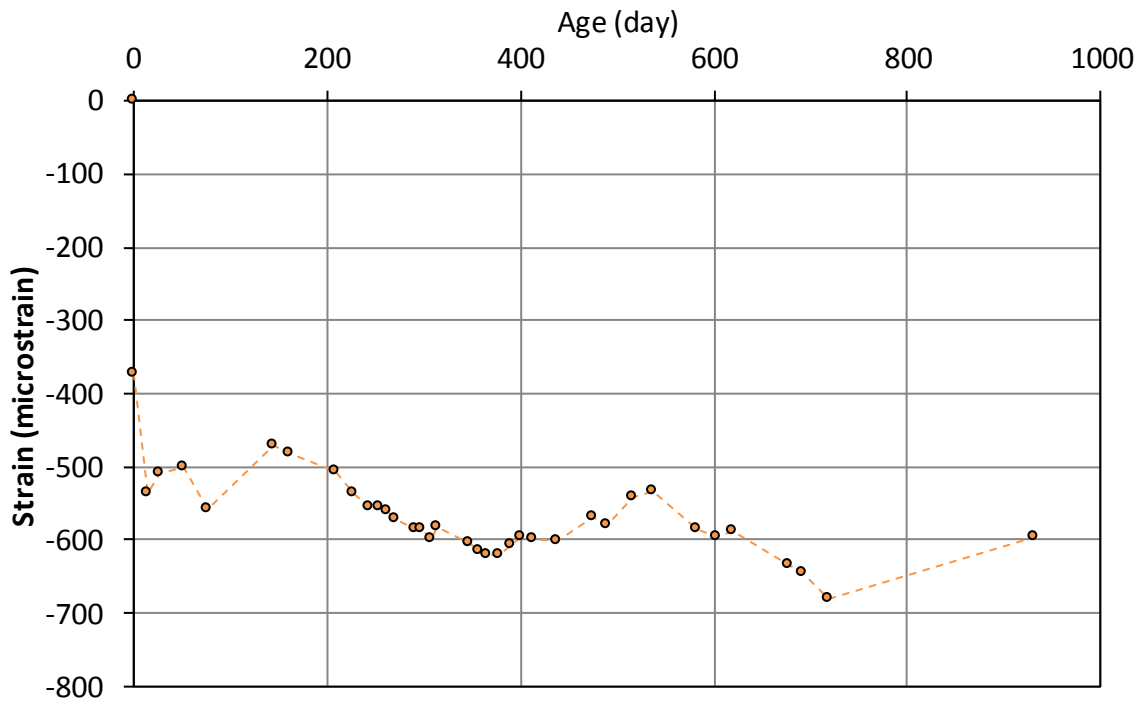


Figure A-52 Strain data for girder II-3, web gage ( $y = 18$  in.)

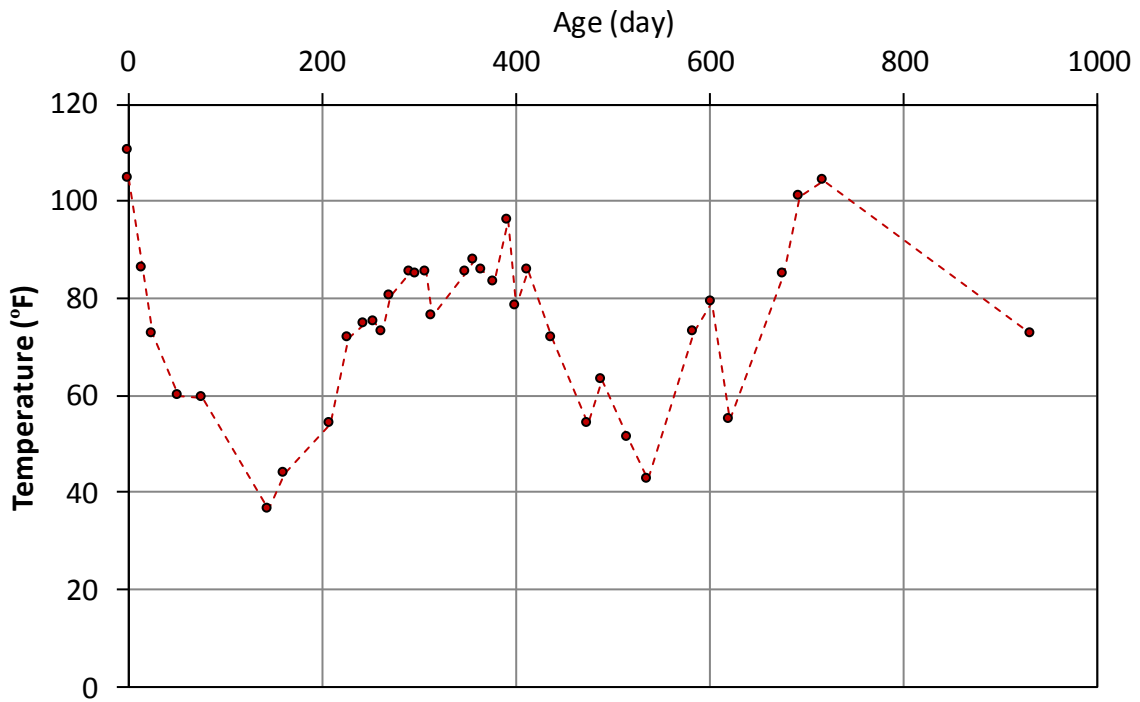


Figure A-53 Temperature data for girder II-3, web gage ( $y = 18$  in.)

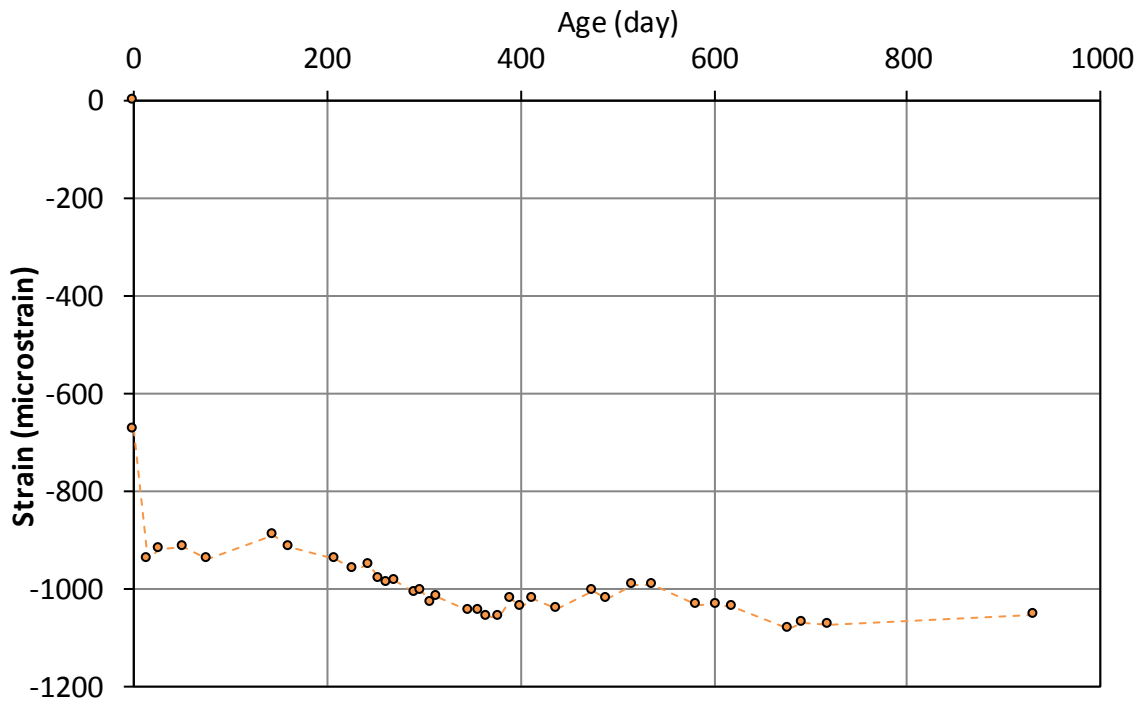


Figure A-54 Strain data for girder II-3, bottom gage 1 ( $y = 6$  in.)

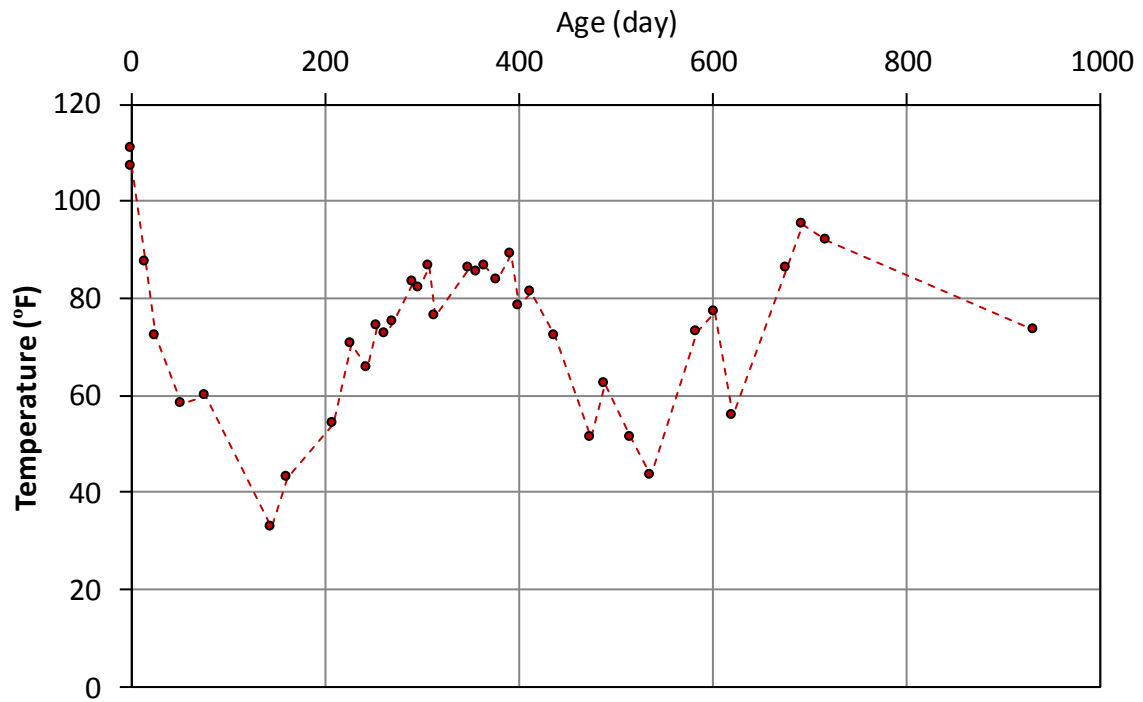


Figure A-55 Temperature data for girder II-3, bottom gage 1 ( $y = 6$  in.)

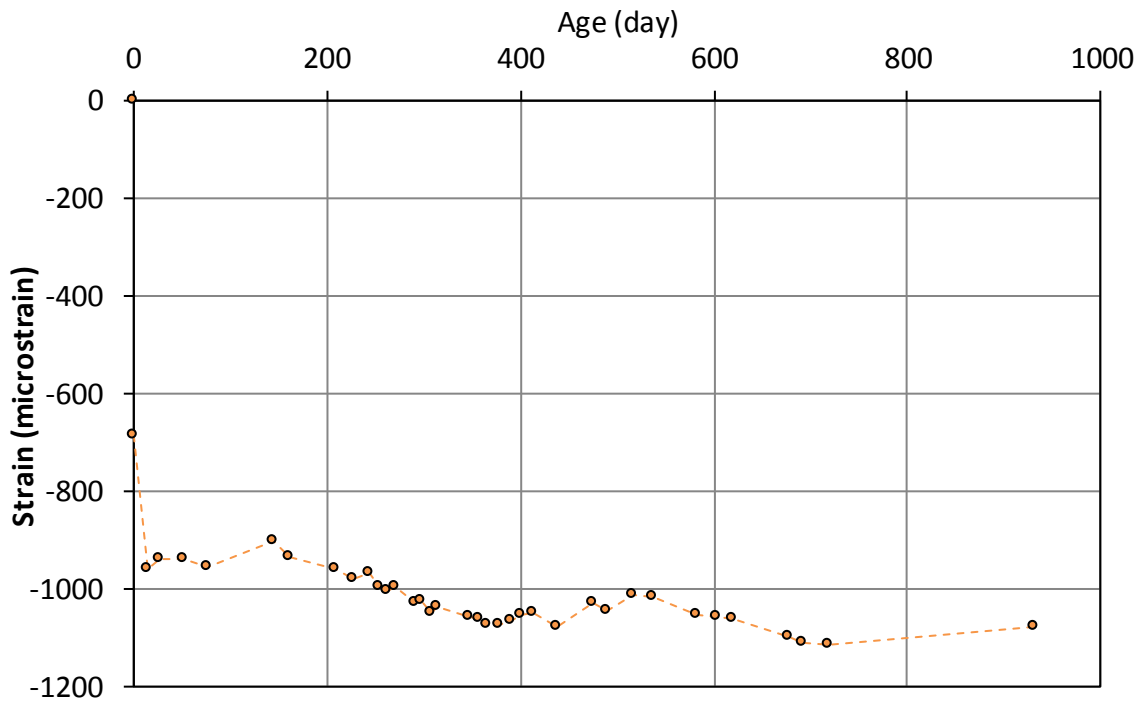


Figure A-56 Strain data for girder II-3, bottom gage 2 ( $y = 6$  in.)

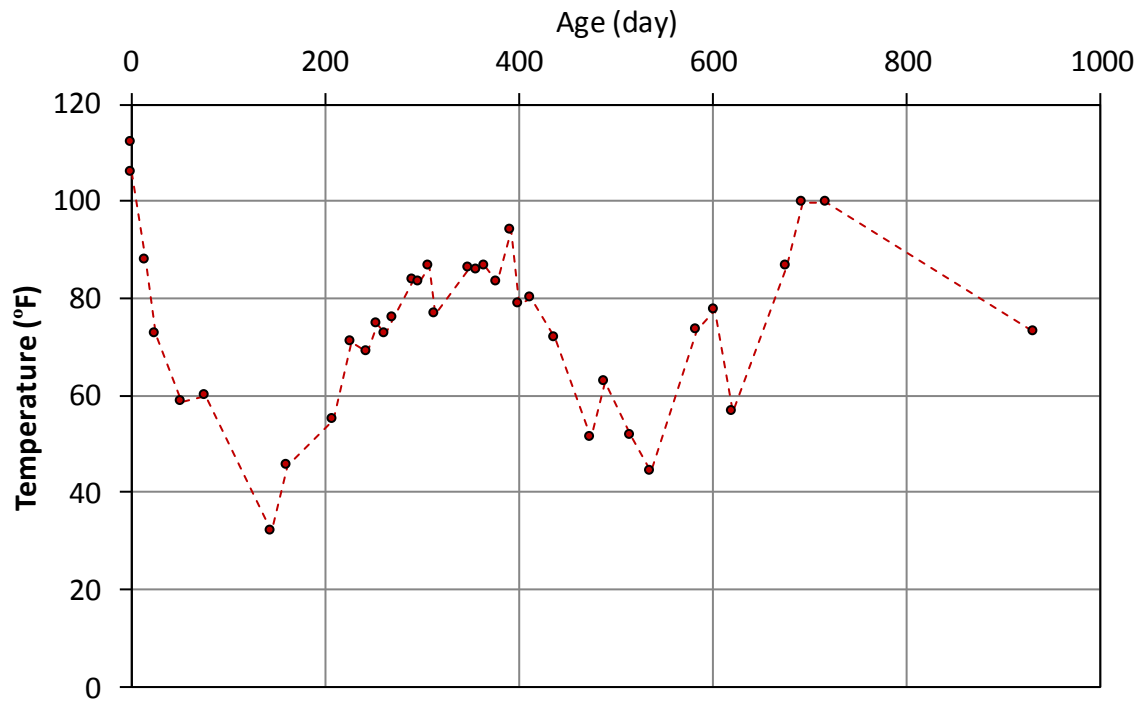


Figure A-57 Temperature data for girder II-3, bottom gage 2 ( $y = 6$  in.)

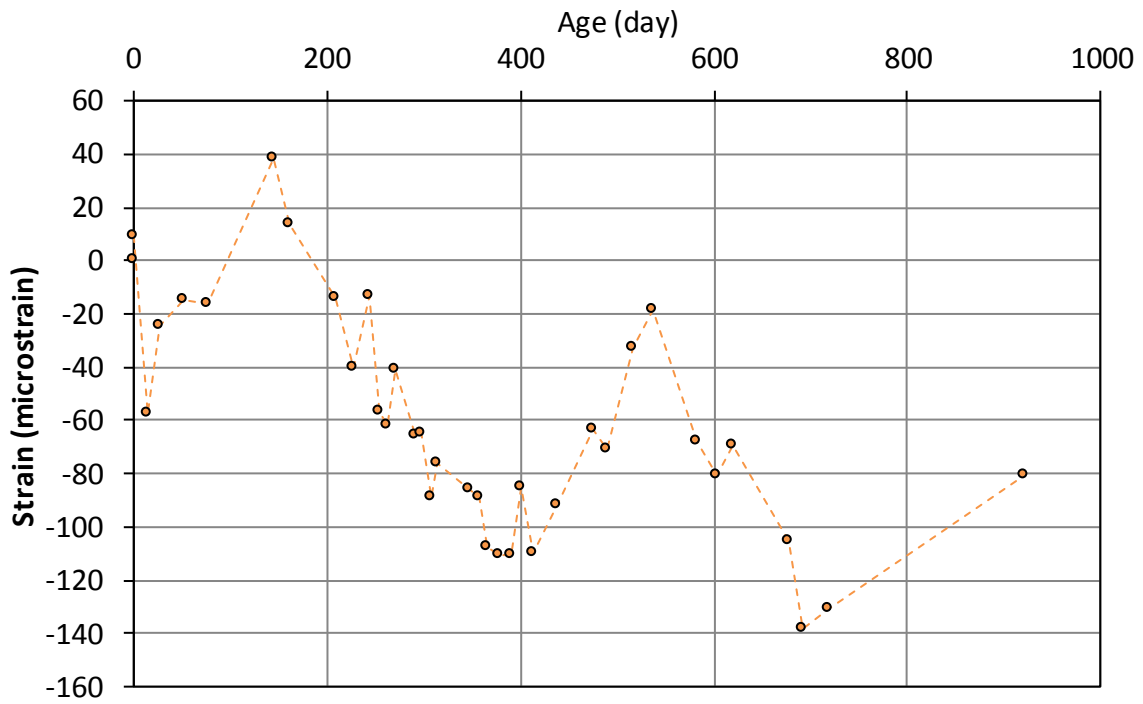


Figure A-58 Strain data for girder II-8, top gage ( $y = 36$  in.)

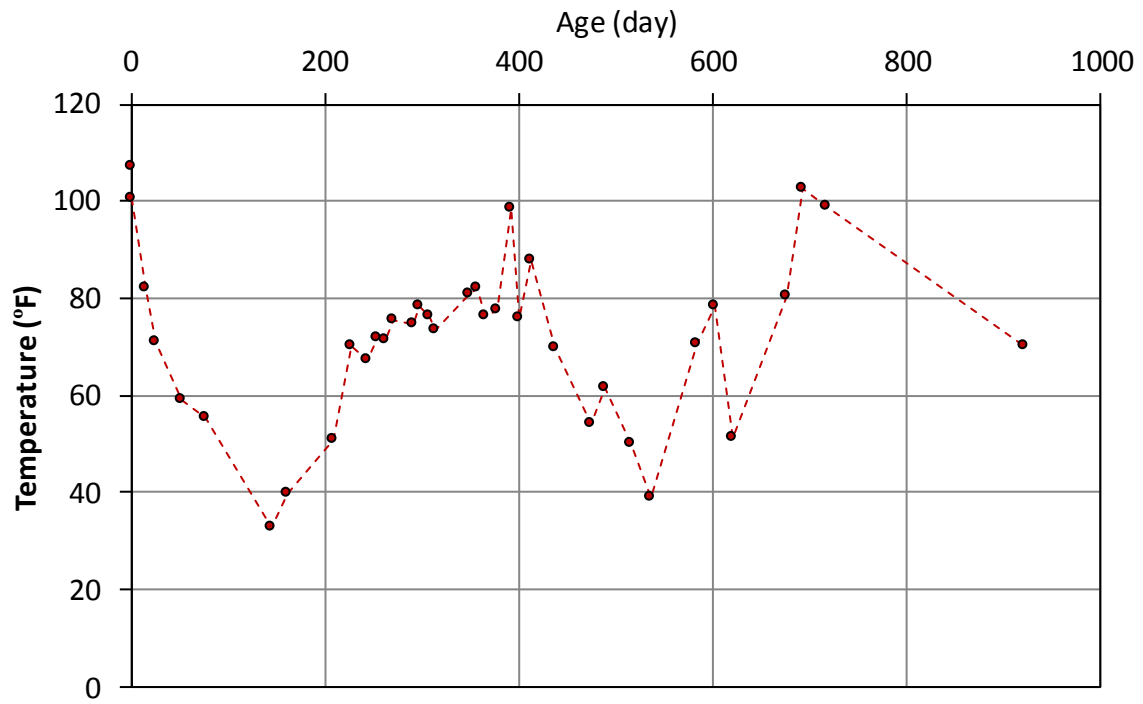


Figure A-59 Temperature data for girder II-8, top gage ( $y = 36$  in.)

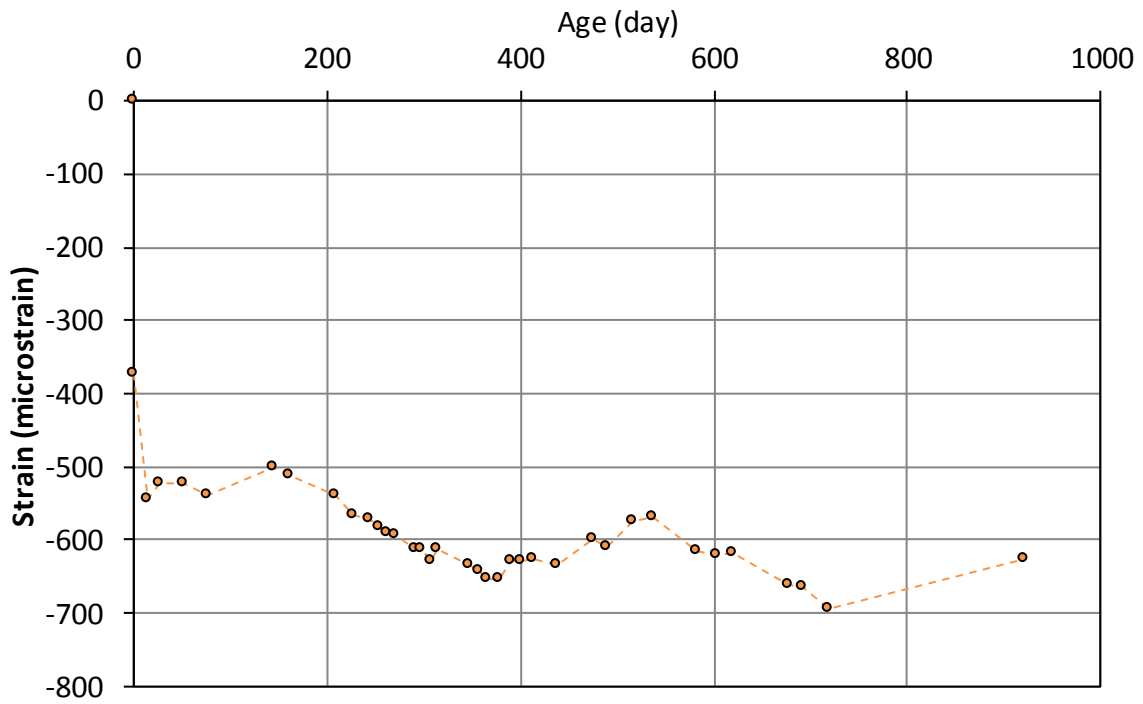


Figure A-60 Strain data for girder II-8, web gage ( $y = 18$  in.)

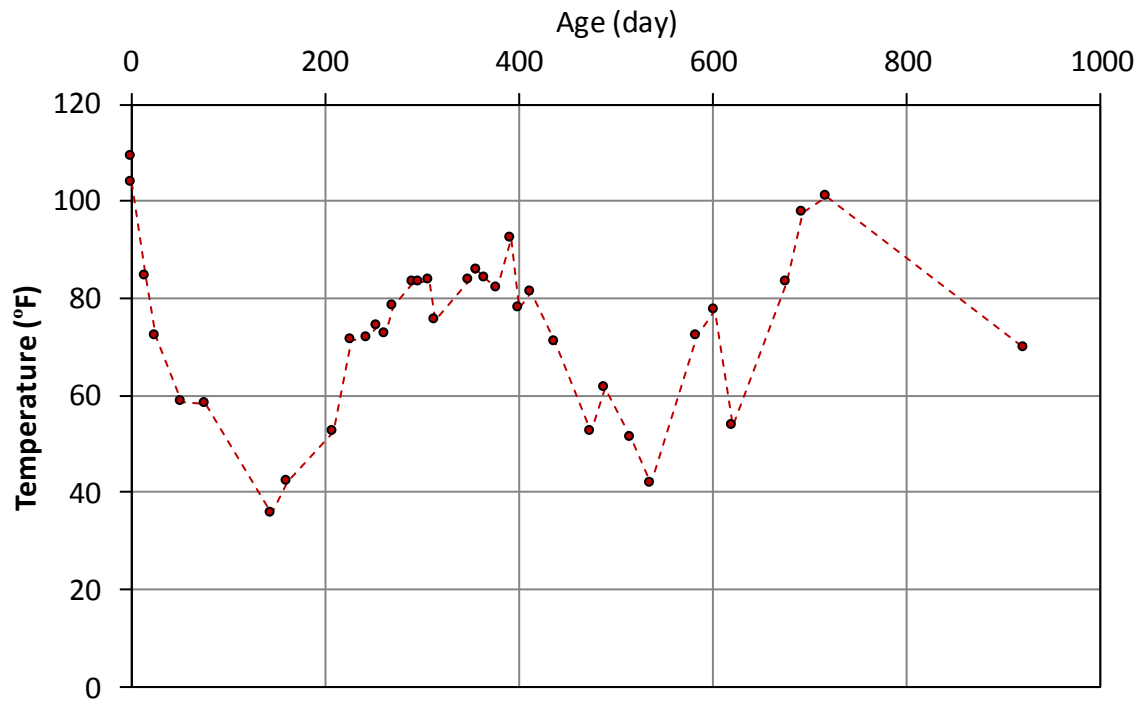


Figure A-61 Temperature data for girder II-8, web gage ( $y = 18$  in.)

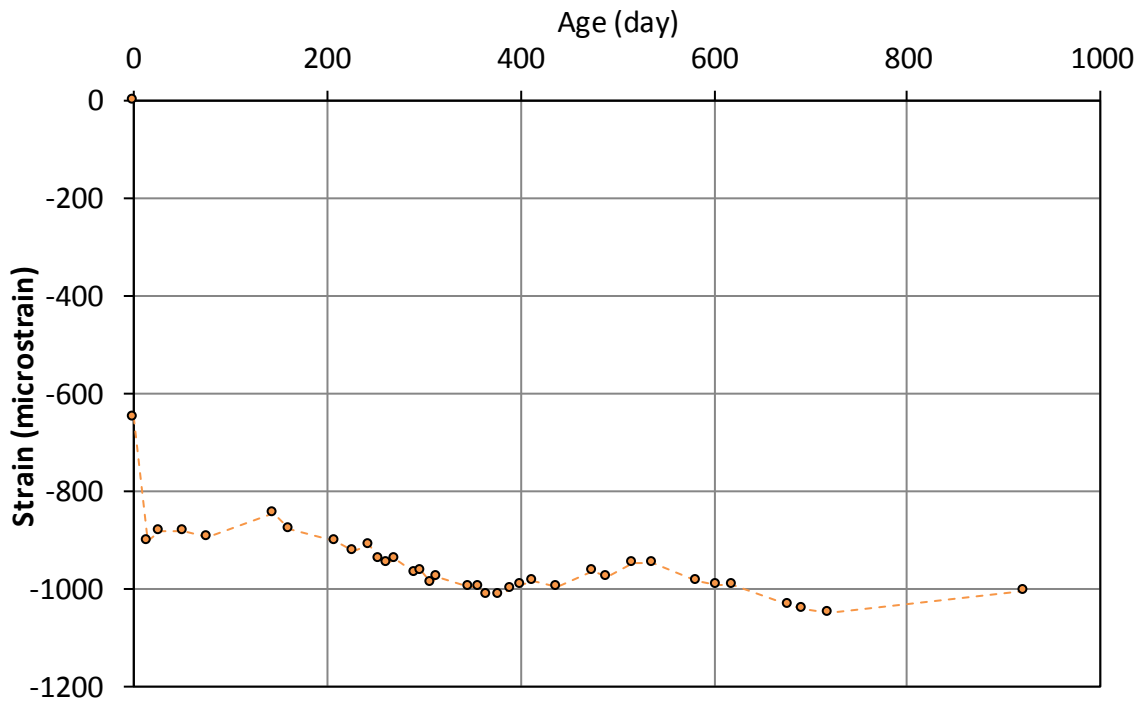


Figure A-62 Strain data for girder II-8, bottom gage 1 ( $y = 6$  in.)

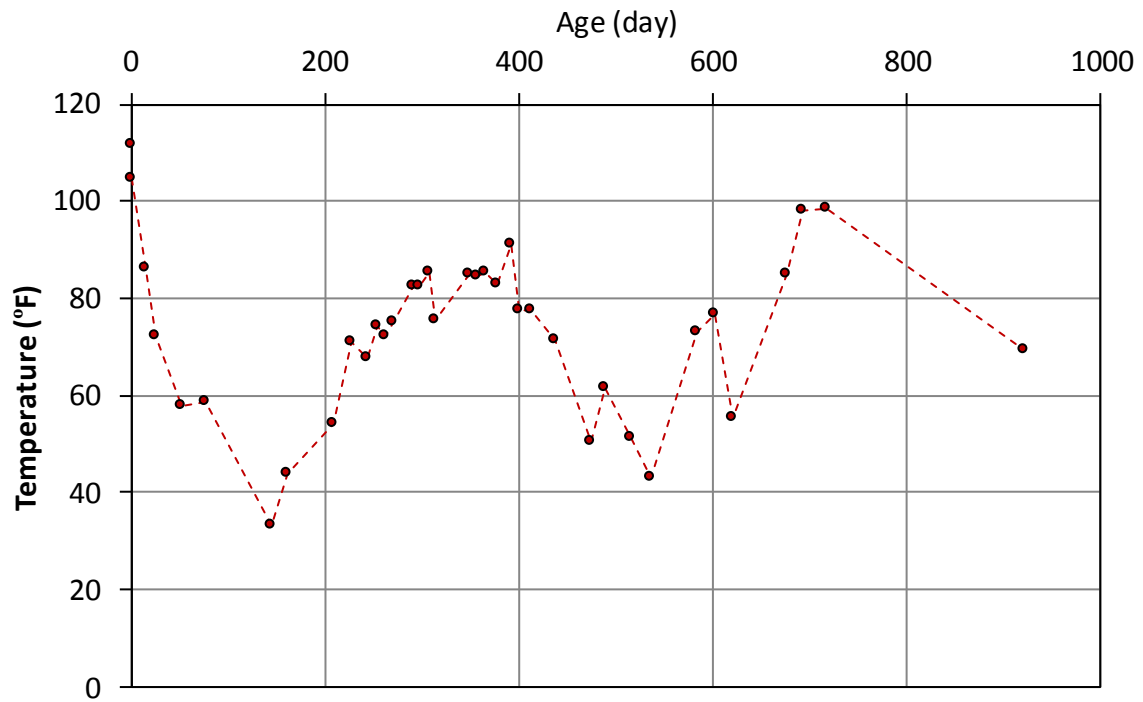


Figure A-63 Temperature data for girder II-8, bottom gage 1 ( $y = 6$  in.)

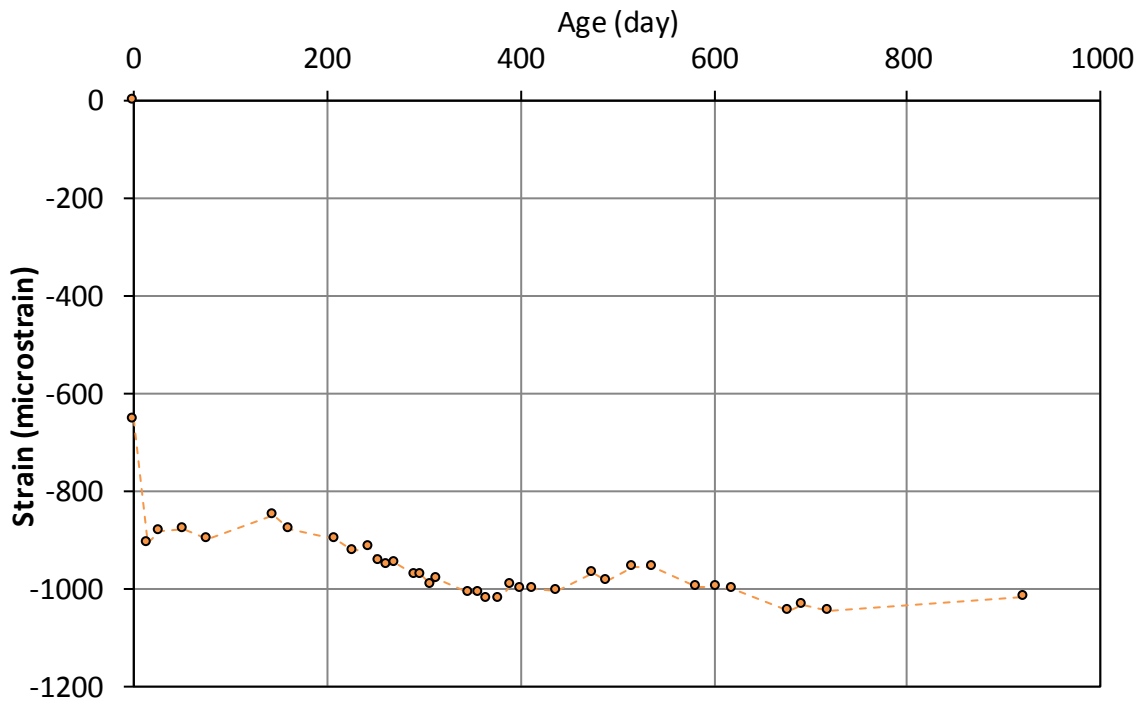


Figure A-64 Strain data for girder II-8, bottom gage 2 ( $y = 6$  in.)

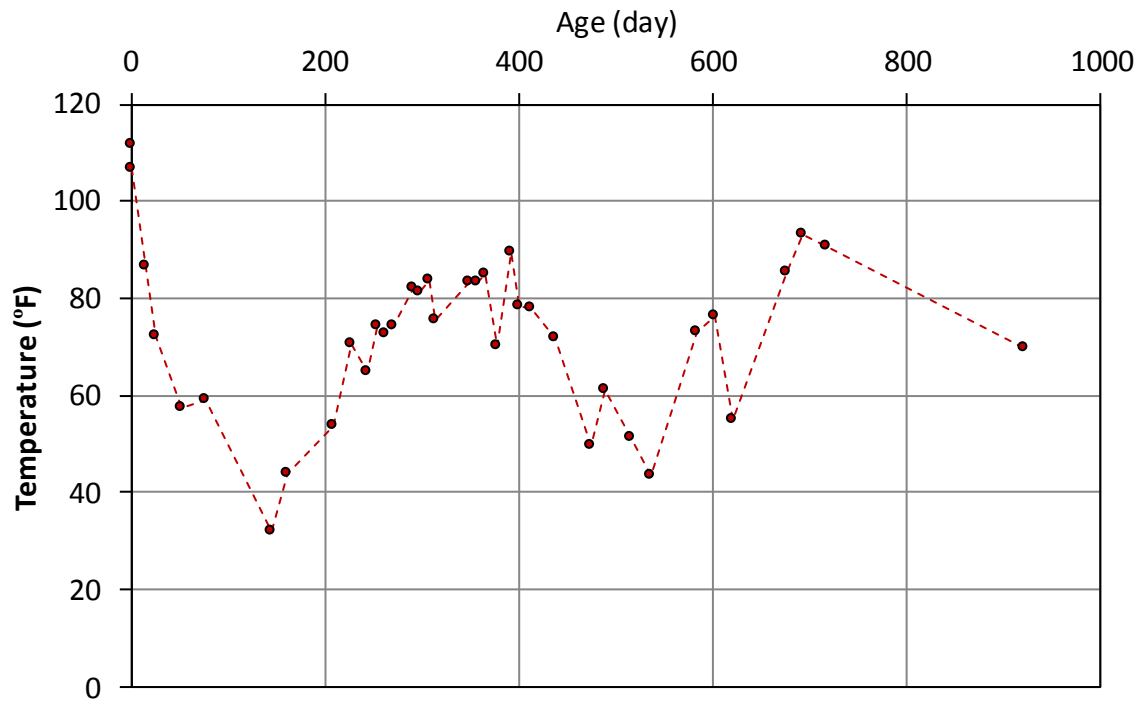
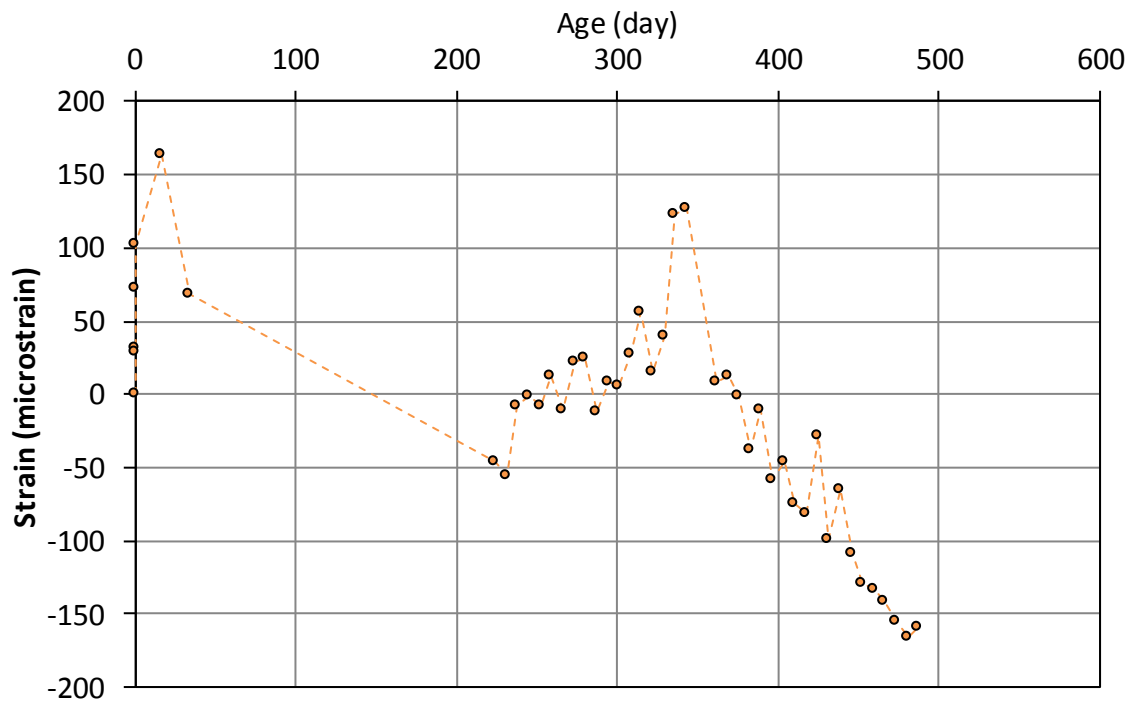
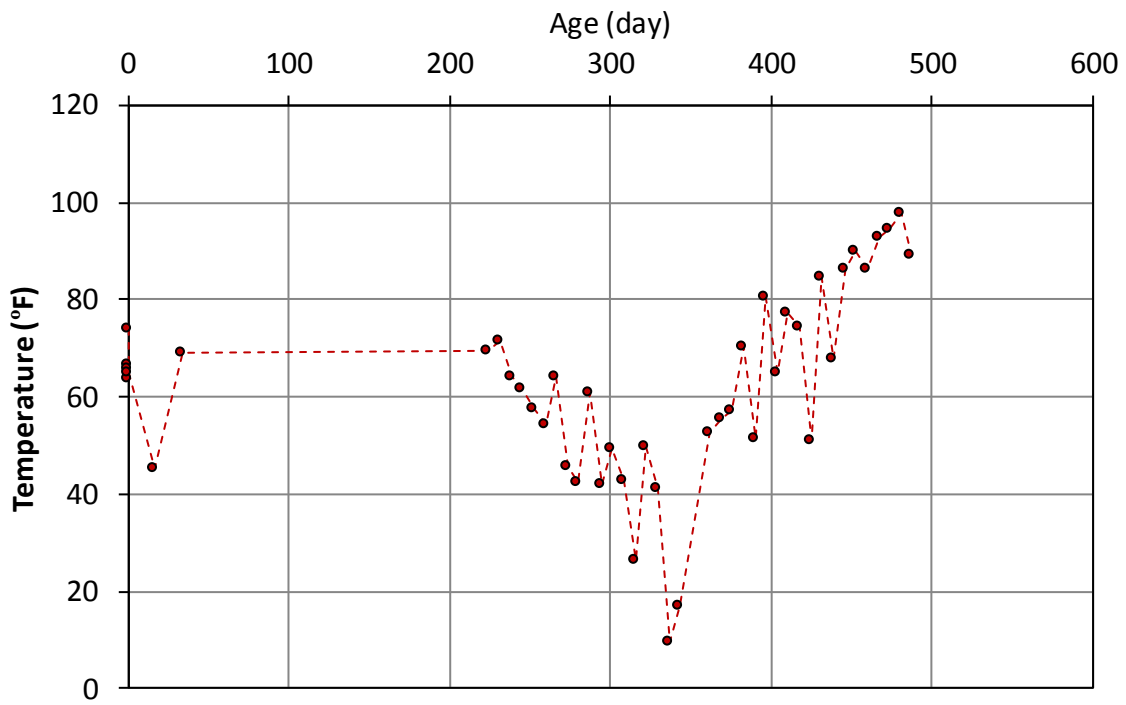


Figure A-65 Temperature data for girder II-8, bottom gage 2 ( $y = 6$  in.)



**Figure A-66 Strain data for girder III-1, top gage (y = 43.5 in.)**



**Figure A-67 Temperature data for girder III-1, top gage (y = 43.5 in.)**



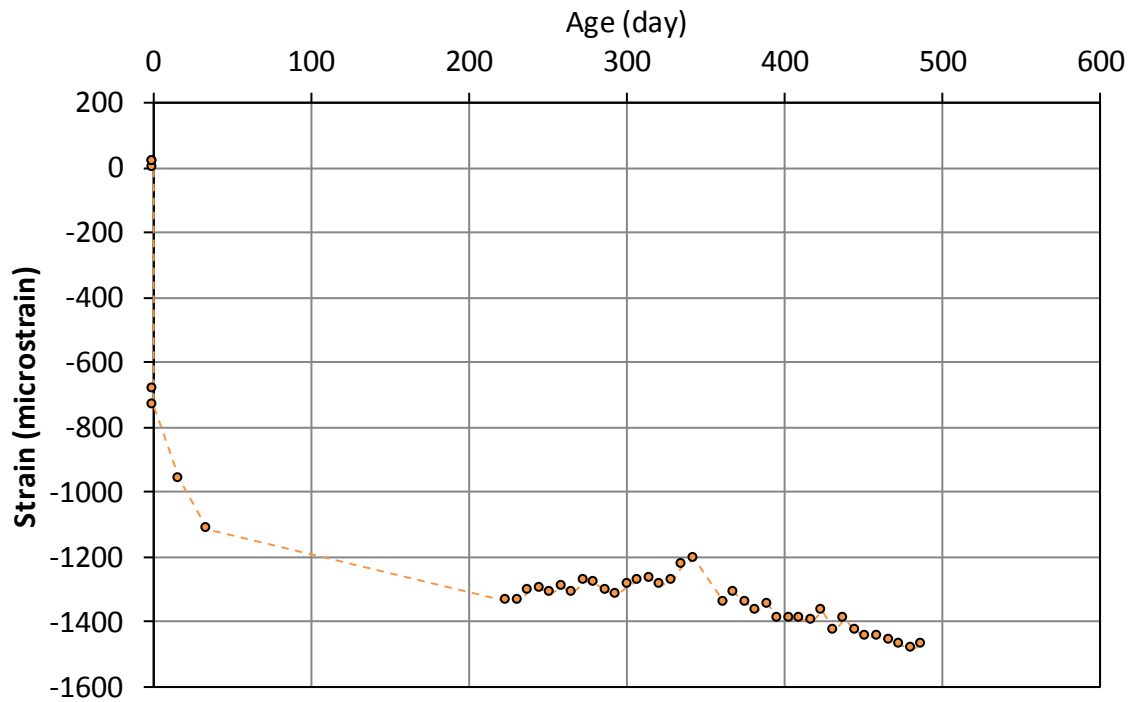


Figure A-68 Strain data for girder III-1, web gage ( $y = 16.5$  in.)

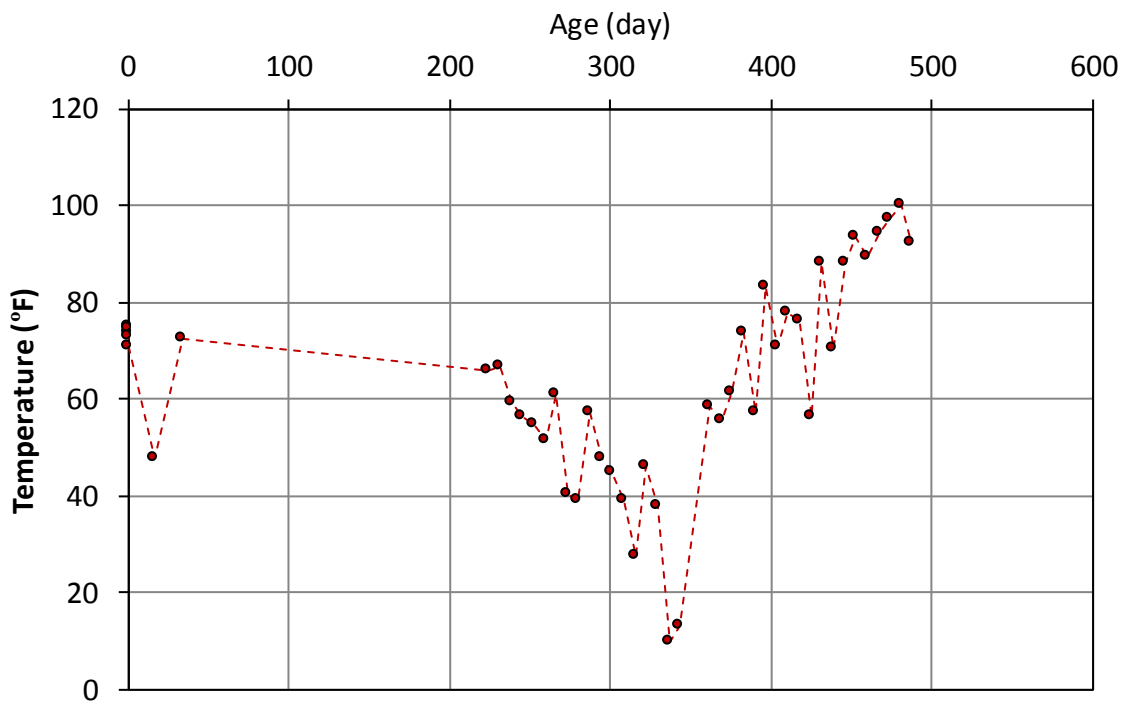
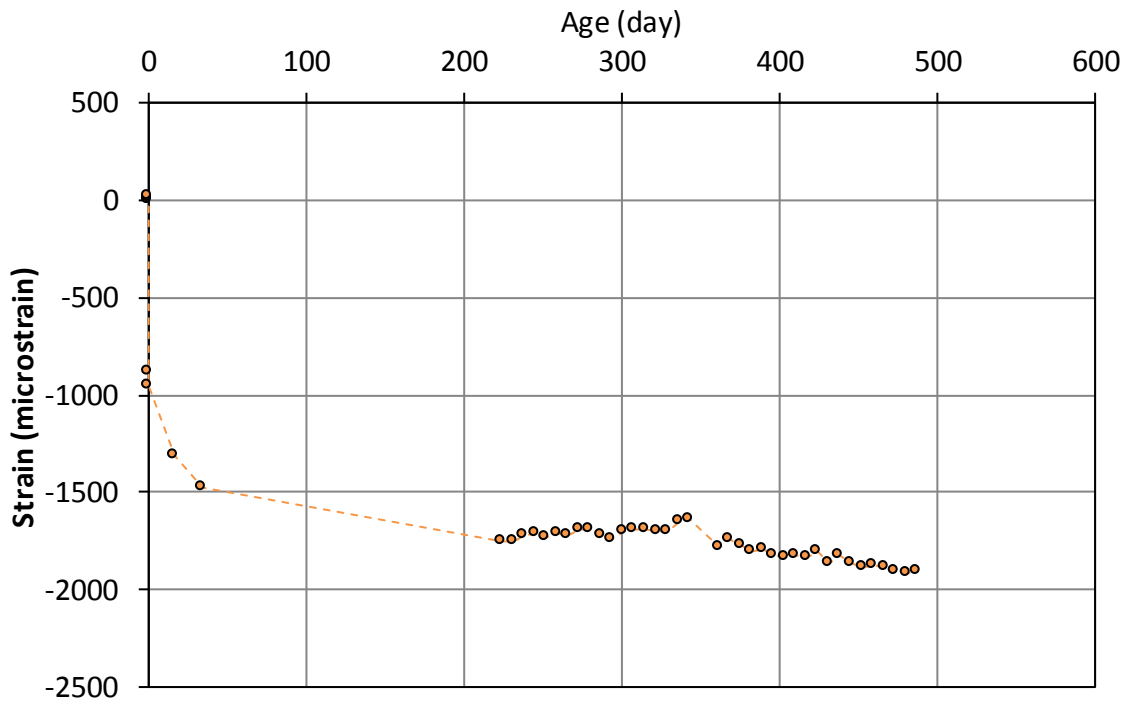
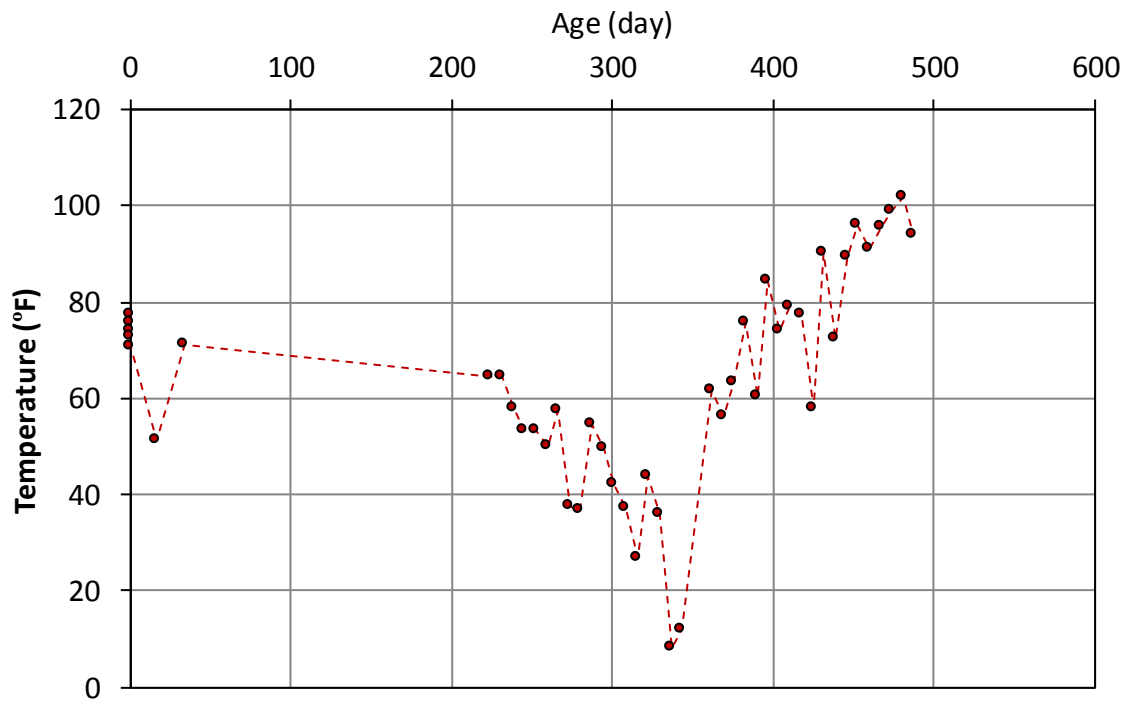


Figure A-69 Temperature data for girder III-1, web gage ( $y = 16.5$  in.)



**Figure A-70 Strain data for girder III-1, bottom gage ( $y = 7.5$  in.)**



**Figure A-71 Temperature data for girder III-1, bottom gage ( $y = 7.5$  in.)**

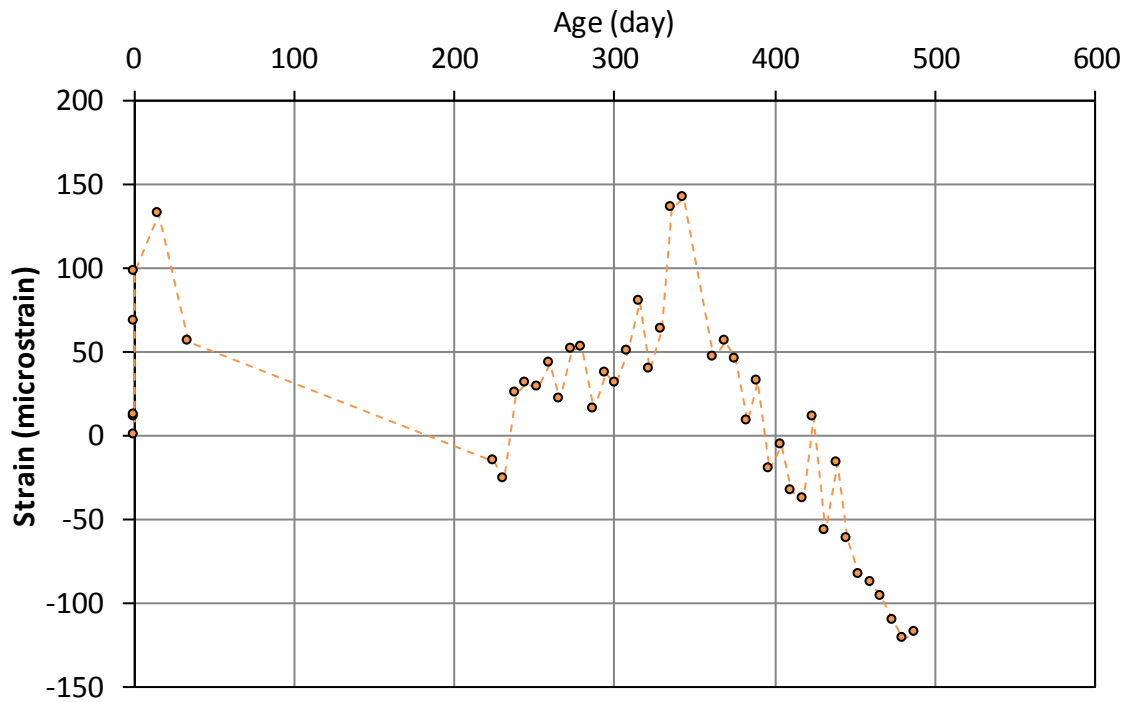


**Figure A-72 Strain data for girder III-5, top gage (y = 43.5 in.)**

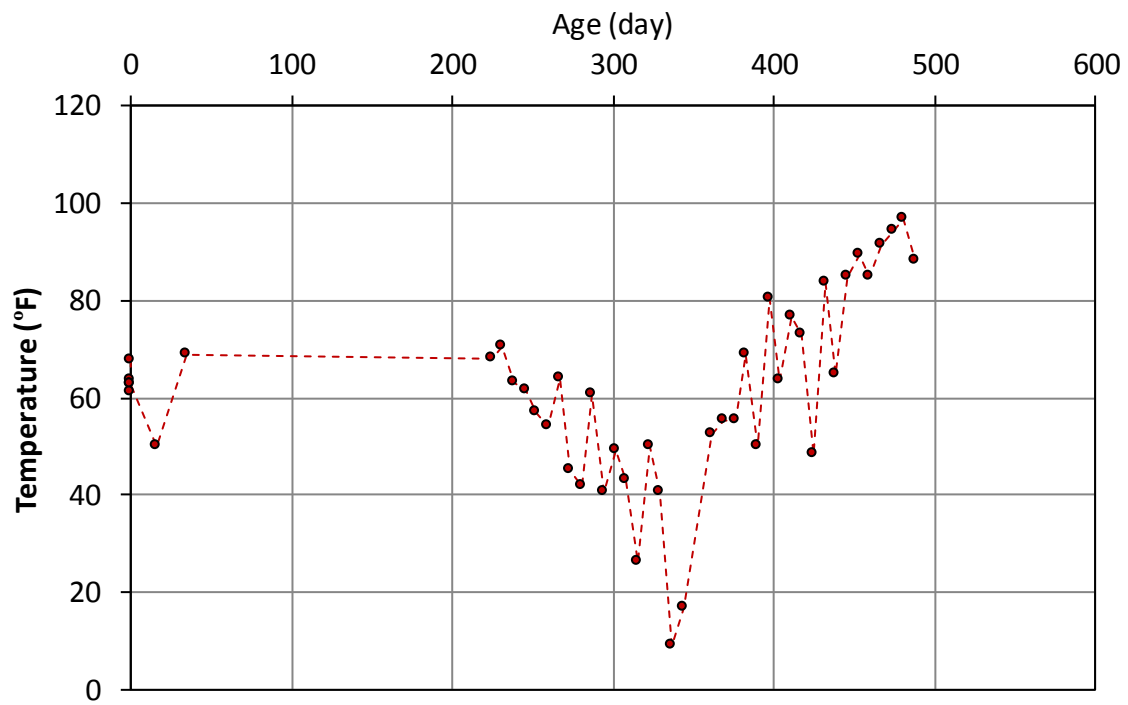


**Figure A-73 Temperature data for girder III-5, top gage (y = 43.5 in.)**

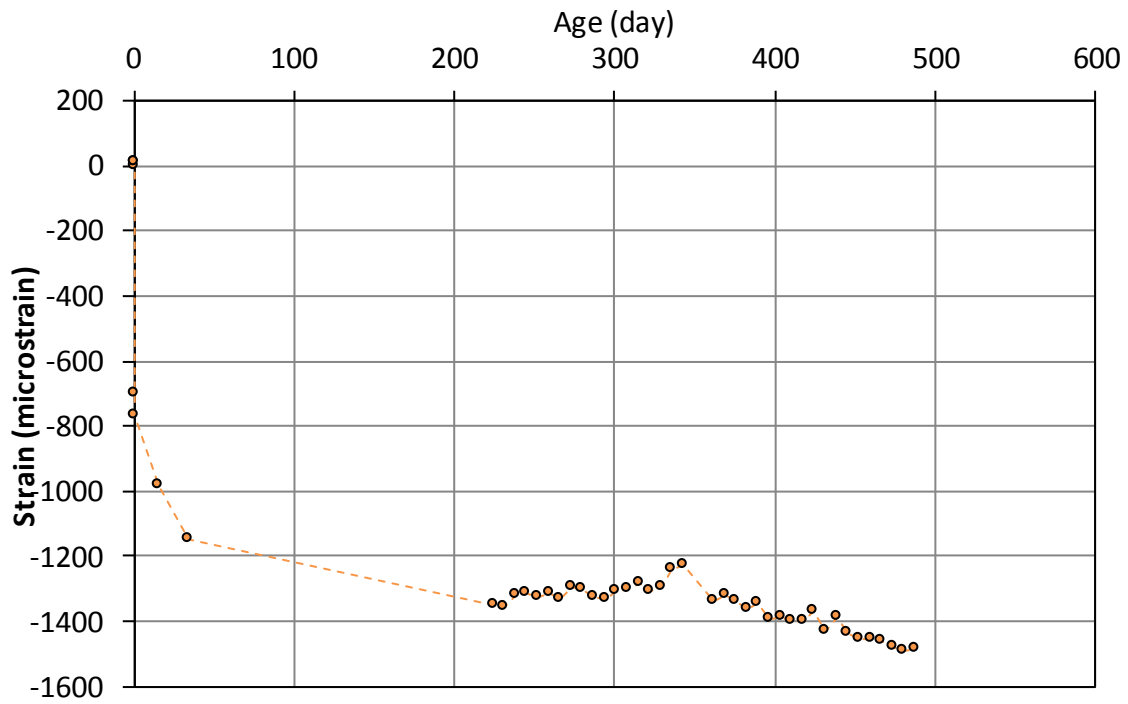


Figure A-74 Strain data for girder III-5, web gage ( $y = 16.5$  in.)

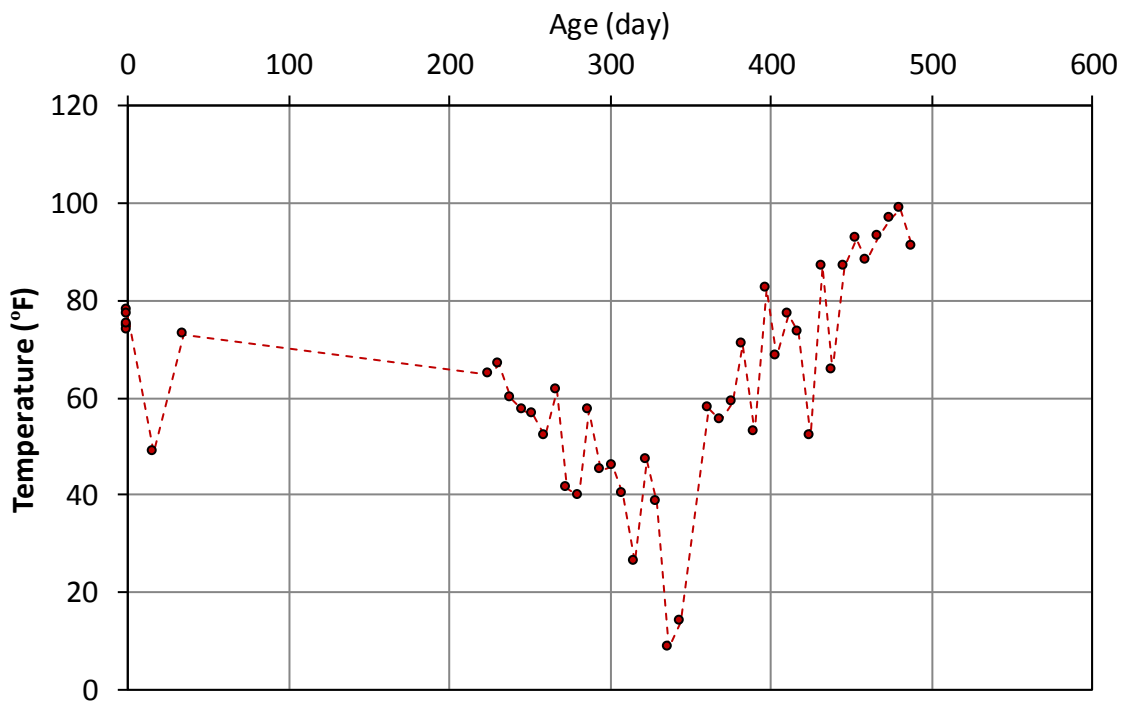
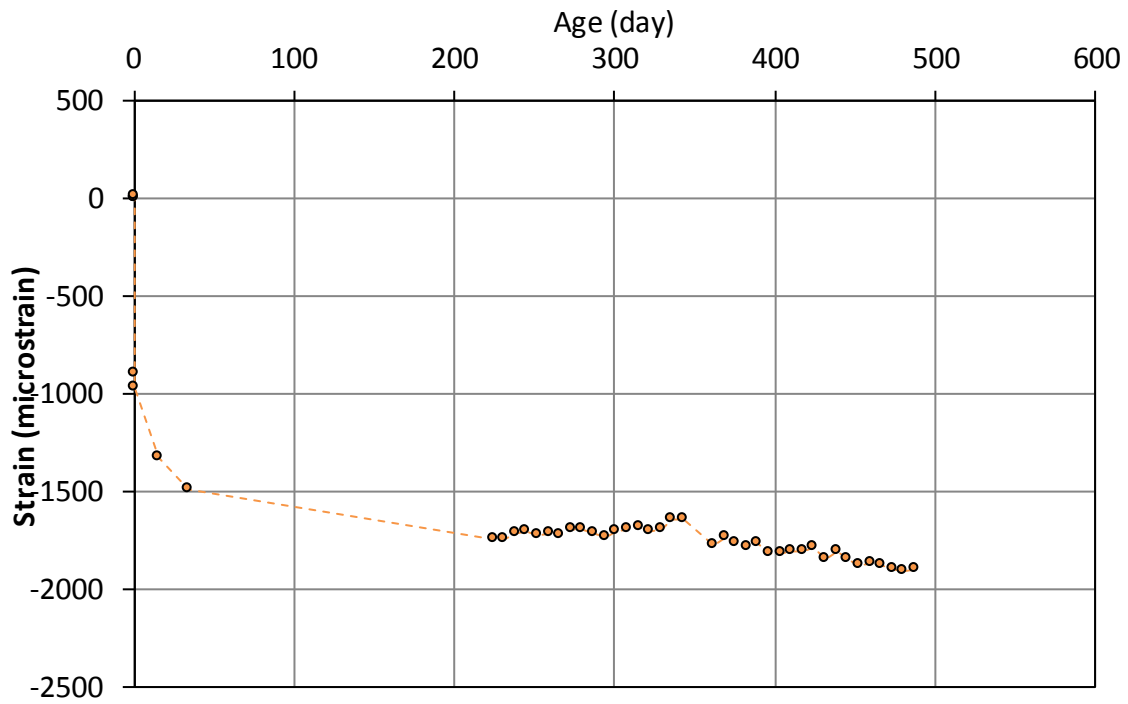
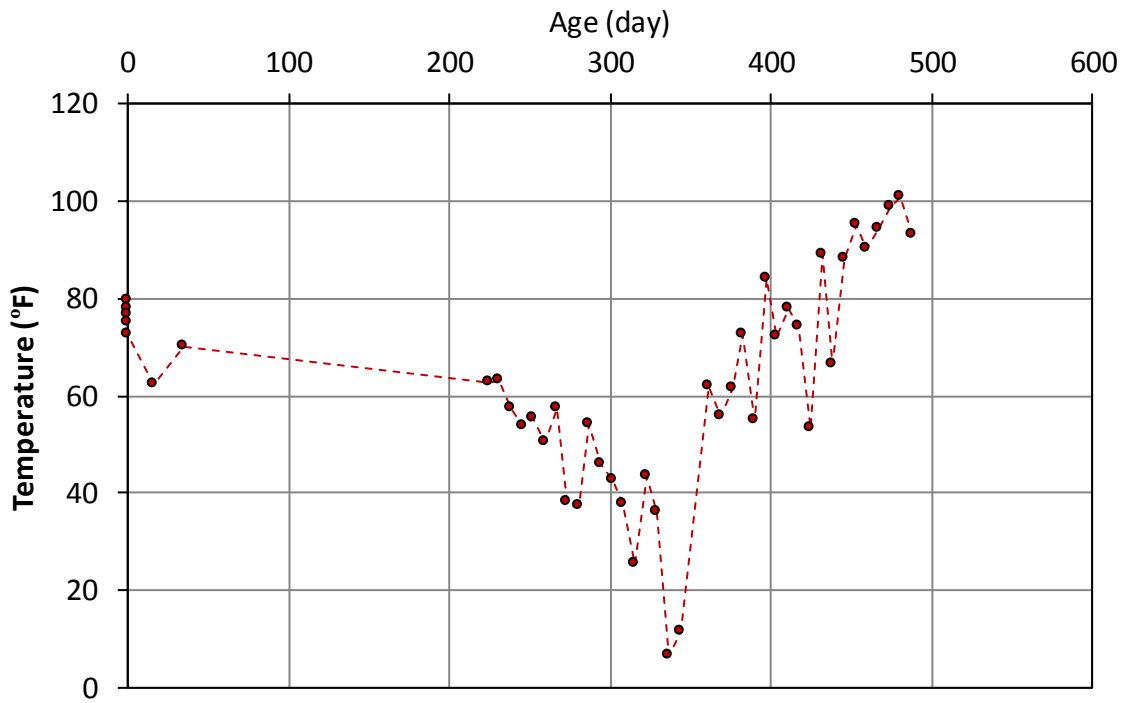


Figure A-75 Temperature data for girder III-5, web gage ( $y = 16.5$  in.)



**Figure A-76 Strain data for girder III-5, bottom gage ( $y = 7.5$  in.)**



**Figure A-77 Temperature data for girder III-5, bottom gage ( $y = 7.5$  in.)**

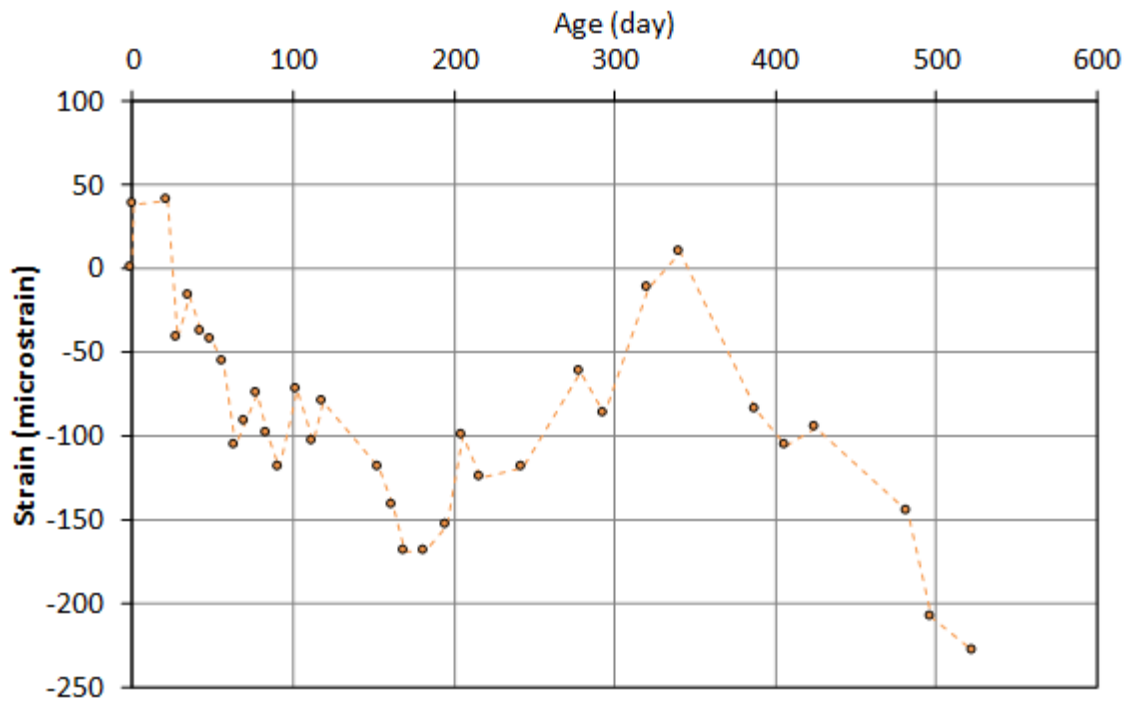


Figure A-78 Strain data for girder III-3, top gage ( $y = 43.5$  in.)

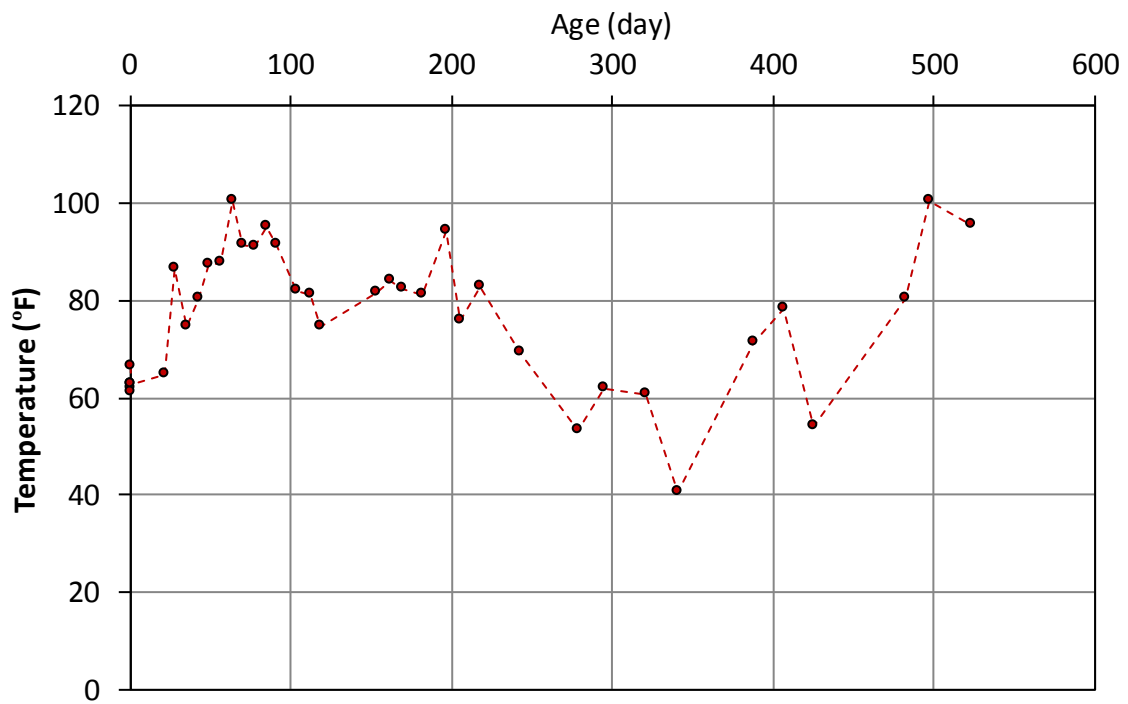


Figure A-79 Temperature data for girder III-3, top gage ( $y = 43.5$  in.)

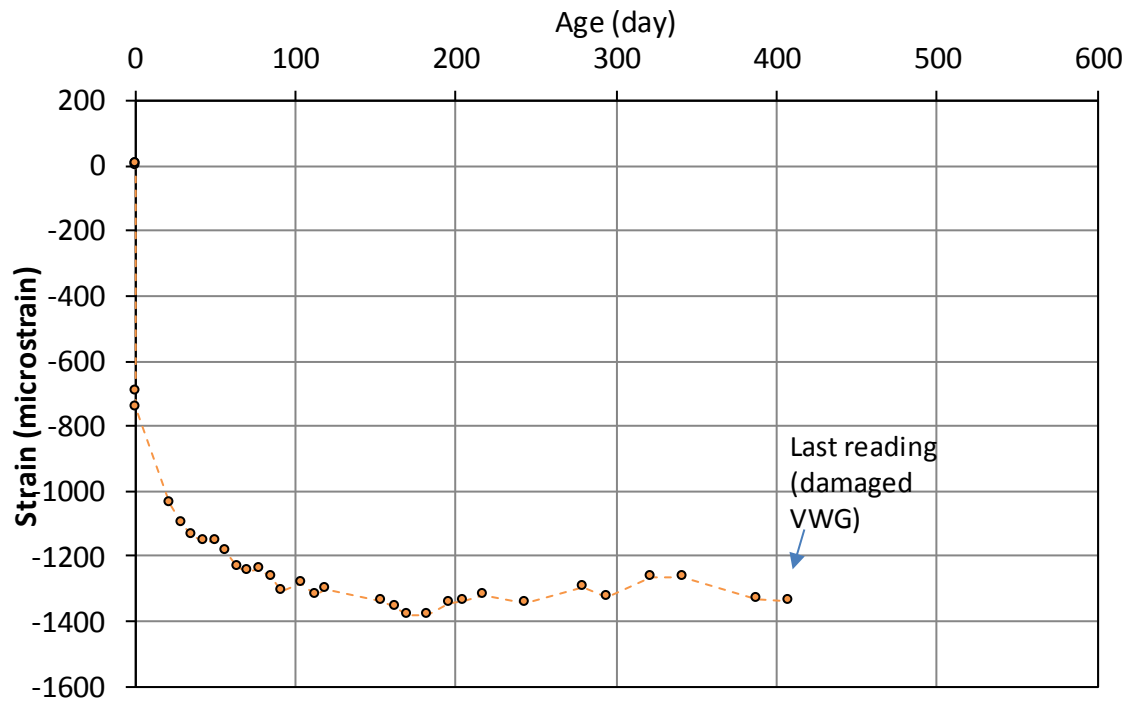


Figure A-80 Strain data for girder III-3, web gage ( $y = 16.5$  in.)

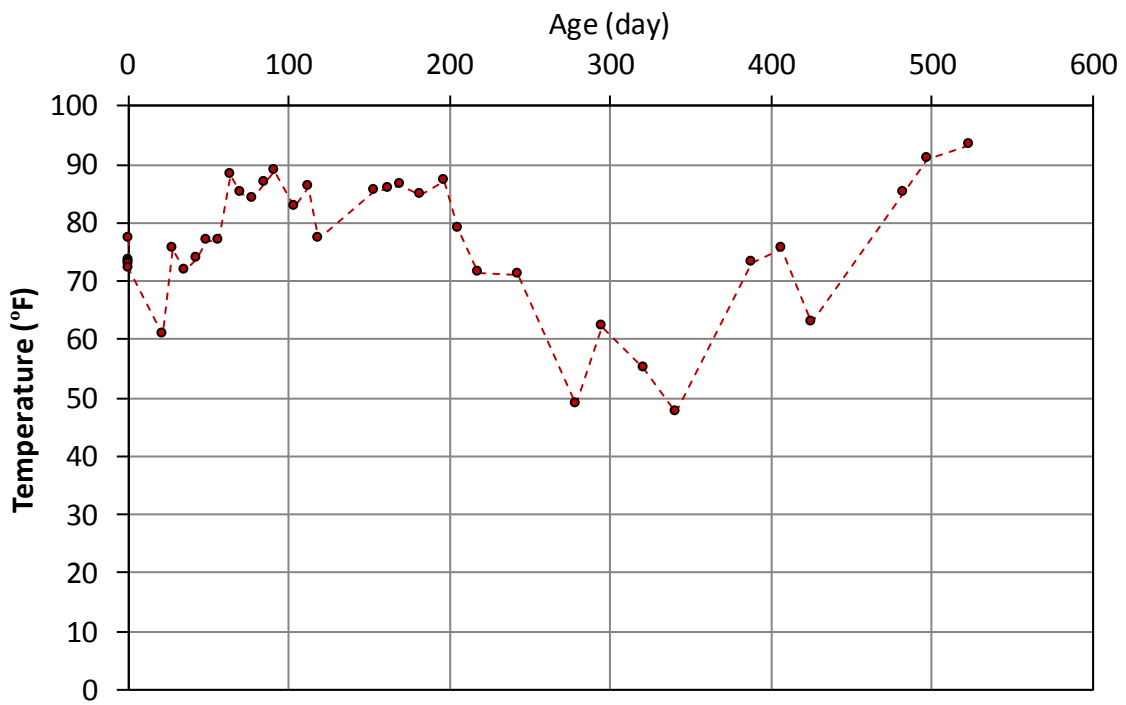


Figure A-81 Temperature data for girder III-3, web gage ( $y = 16.5$  in.)

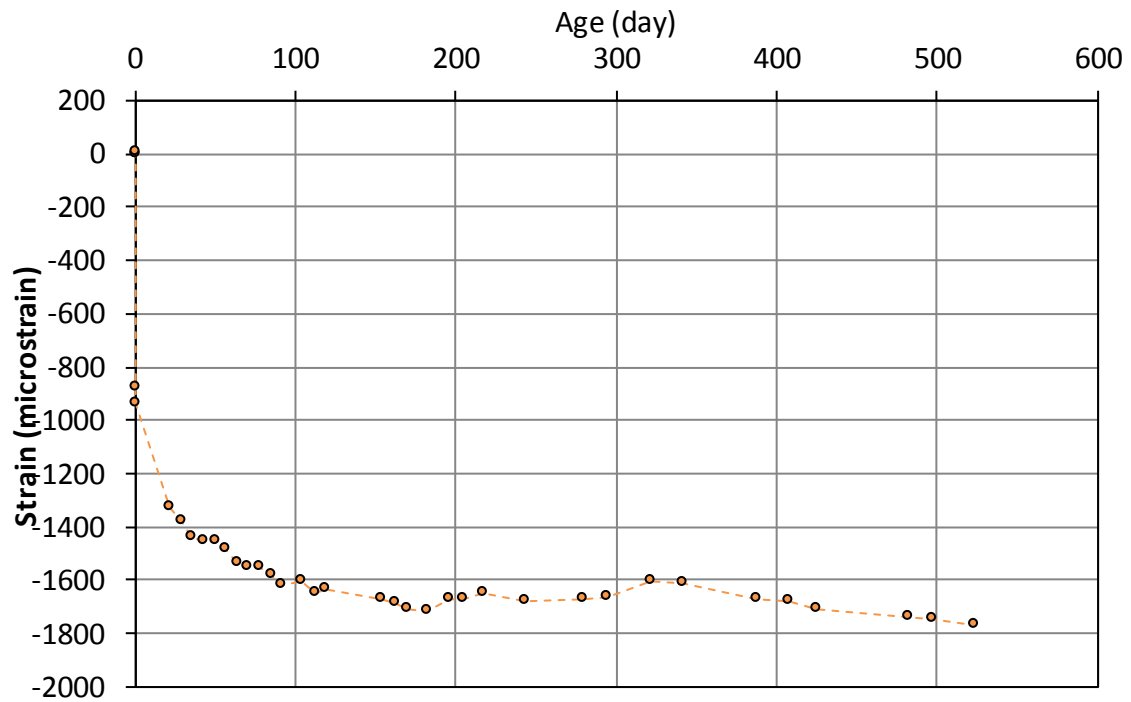


Figure A-82 Strain data for girder III-3, gage ( $y = 7.5$  in.)

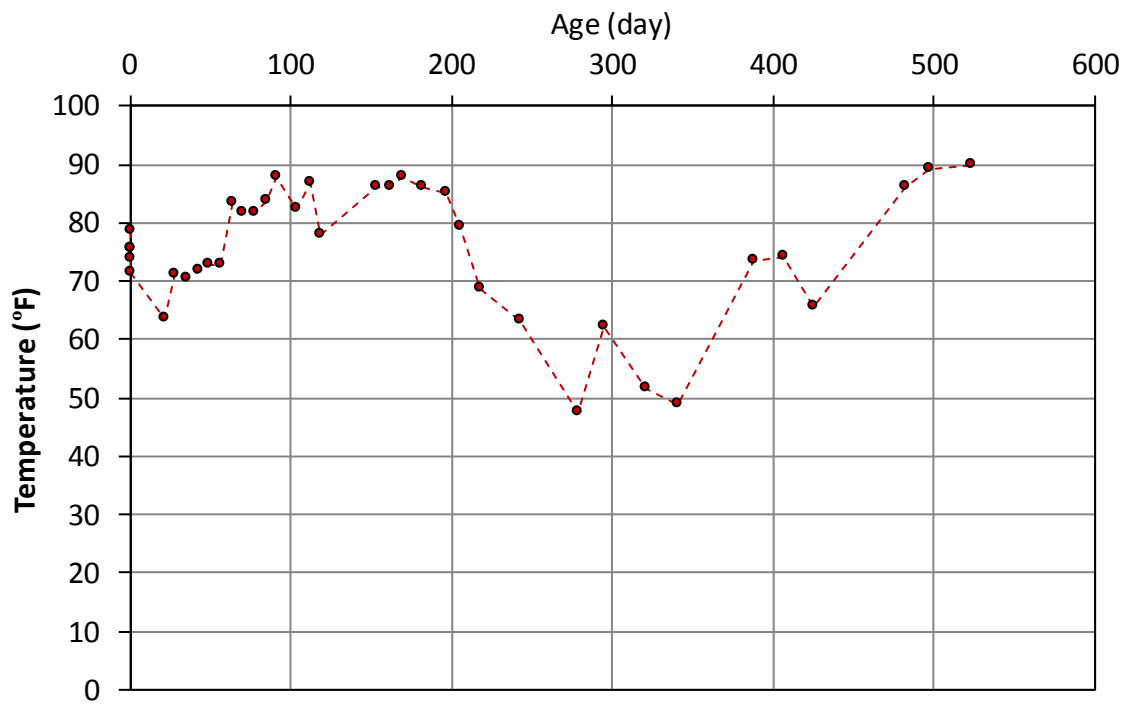


Figure A-83 Temperature data for girder III-3, gage ( $y = 7.5$  in.)



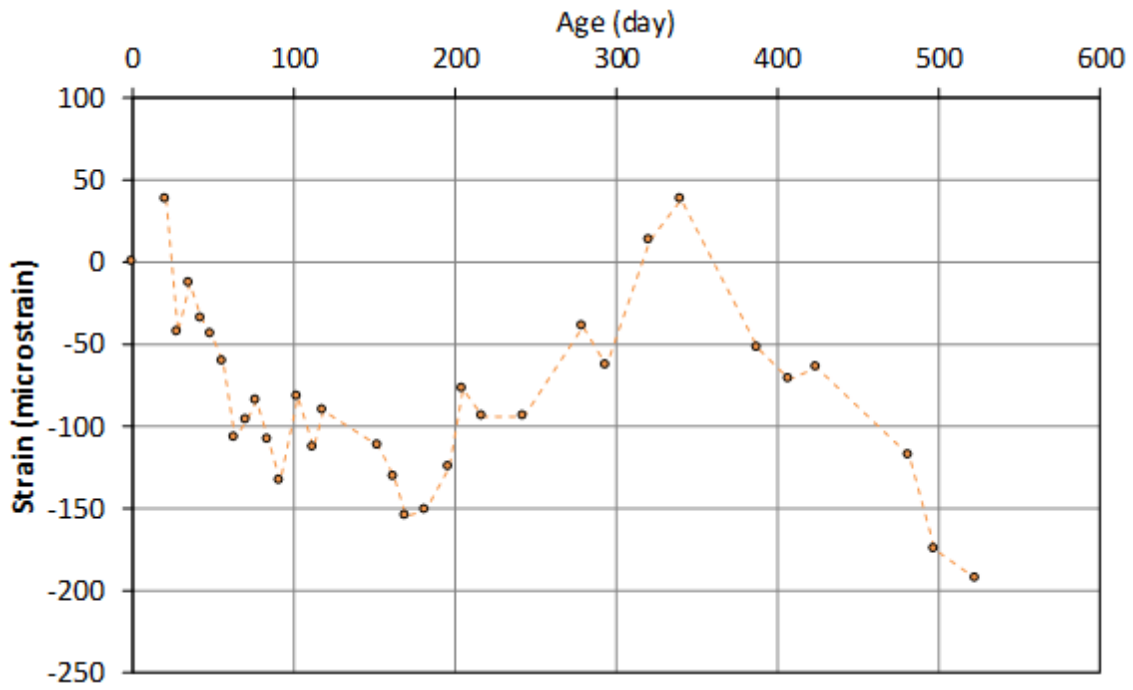


Figure A-84 Strain data for girder III-7, top gage ( $y = 43.5$  in.)

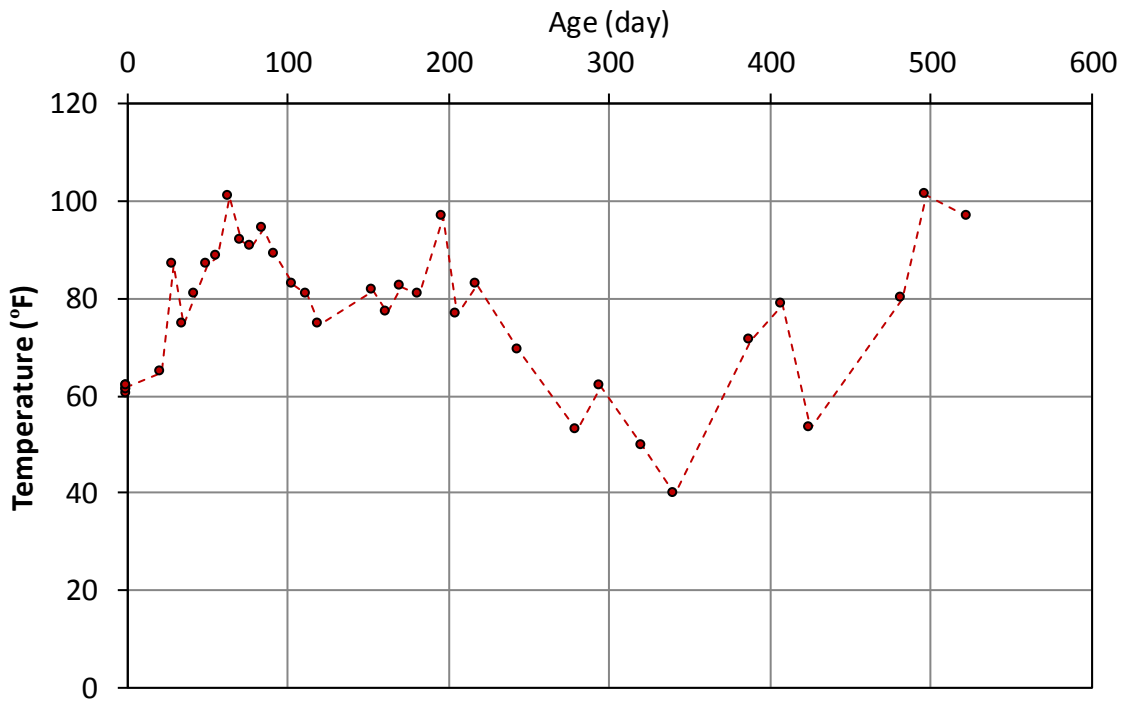


Figure A-85 Temperature data for girder III-7, top gage ( $y = 43.5$  in.)

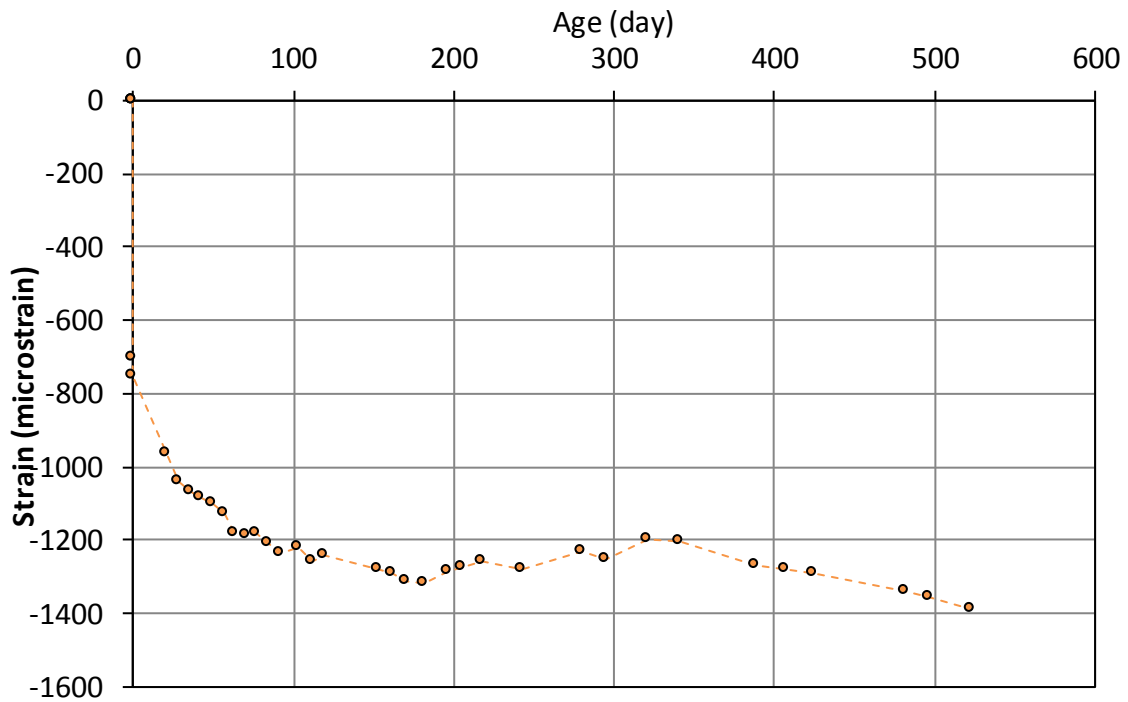


Figure A-86 Strain data for girder III-7, web gage ( $y = 16.5$  in.)

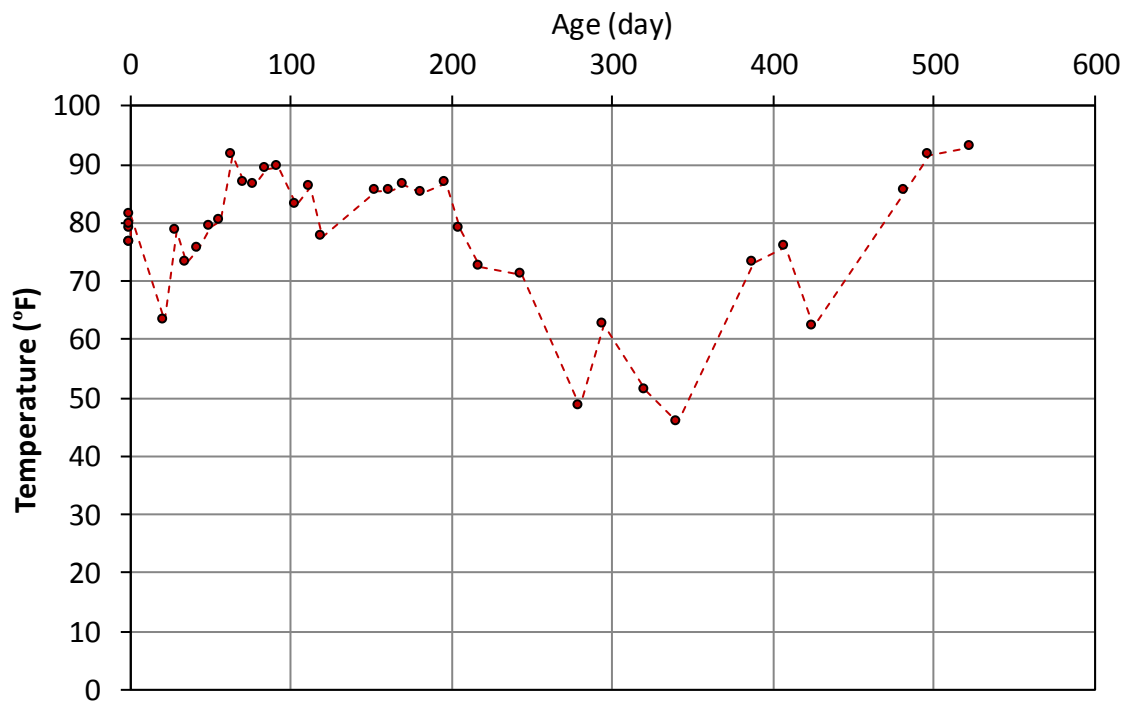


Figure A-87 Temperature data for girder III-7, web gage ( $y = 16.5$  in.)

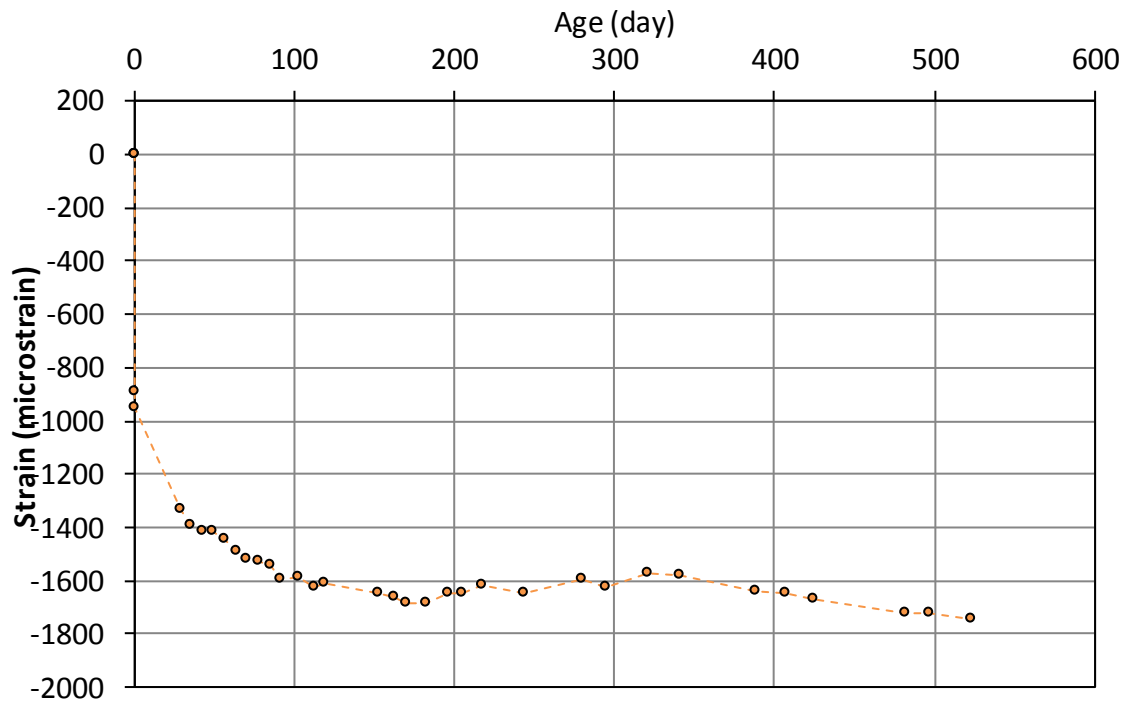


Figure A-88 Strain data for girder III-7, bottom gage ( $y = 7.5$  in.)

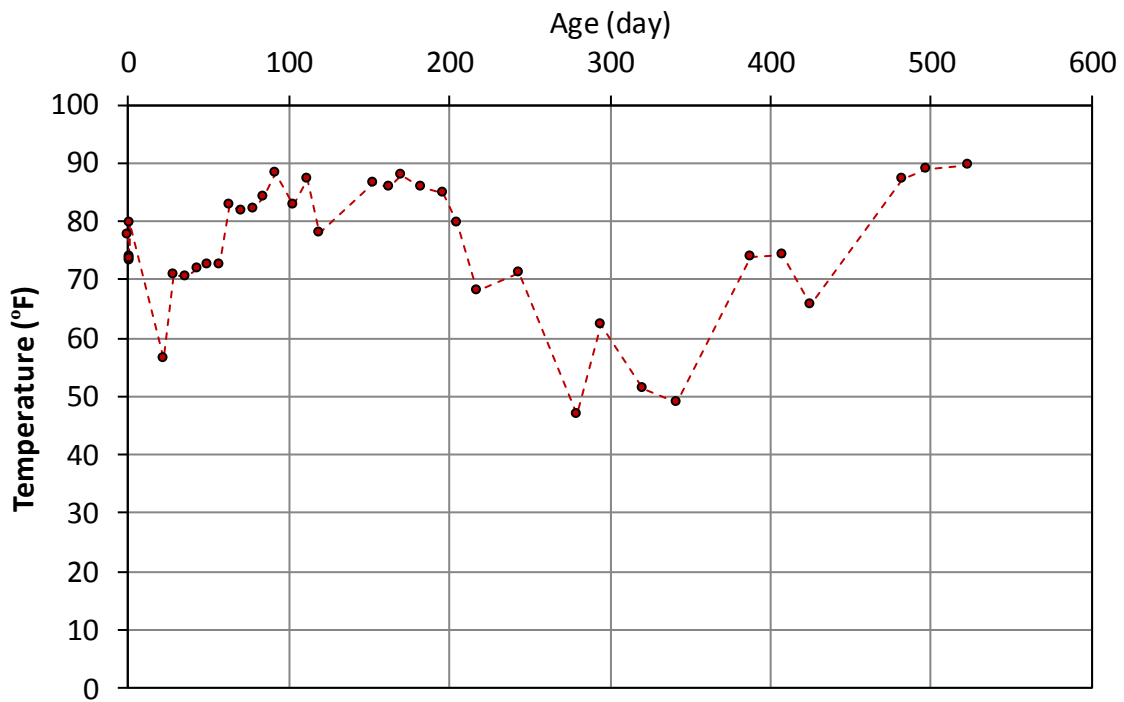


Figure A-89 Temperature data for girder III-7, bottom gage ( $y = 7.5$  in.)

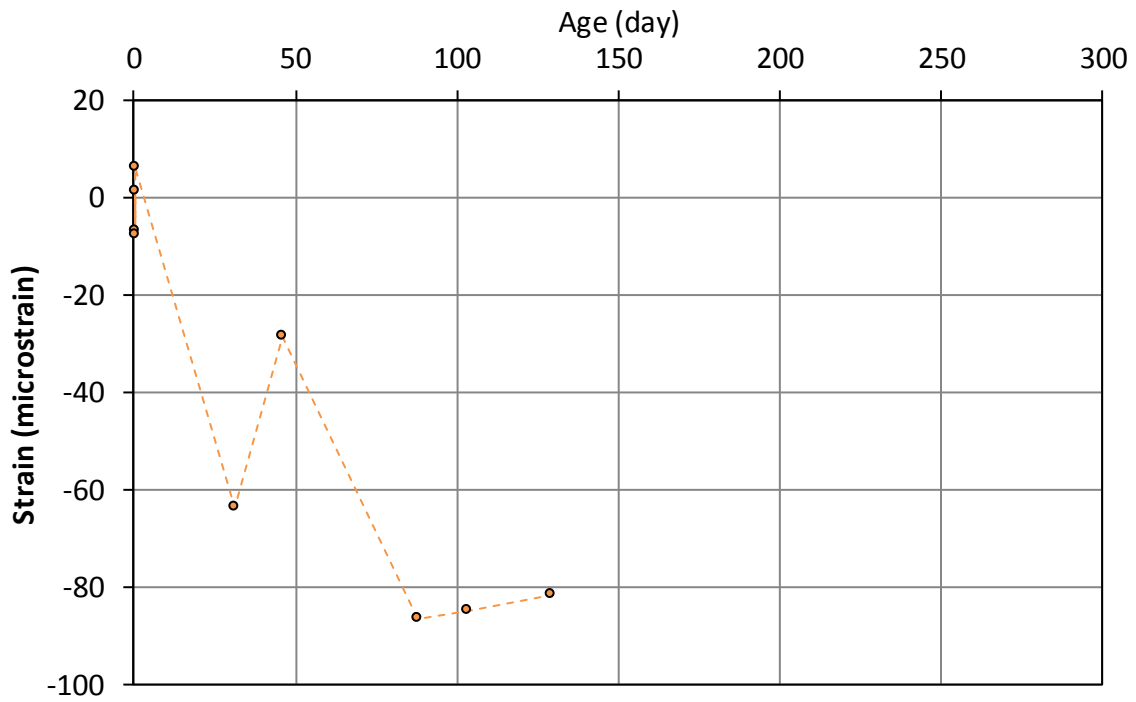


Figure A-90 Strain data for girder IV-SCC-1, top gage ( $y = 43$  in.)

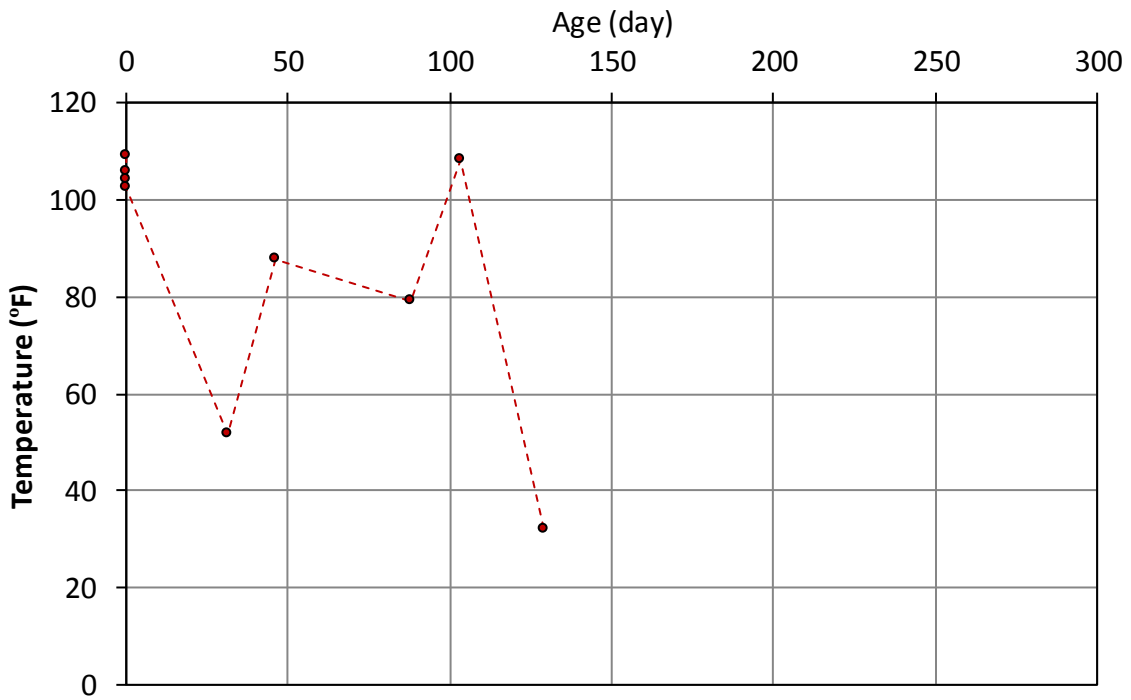
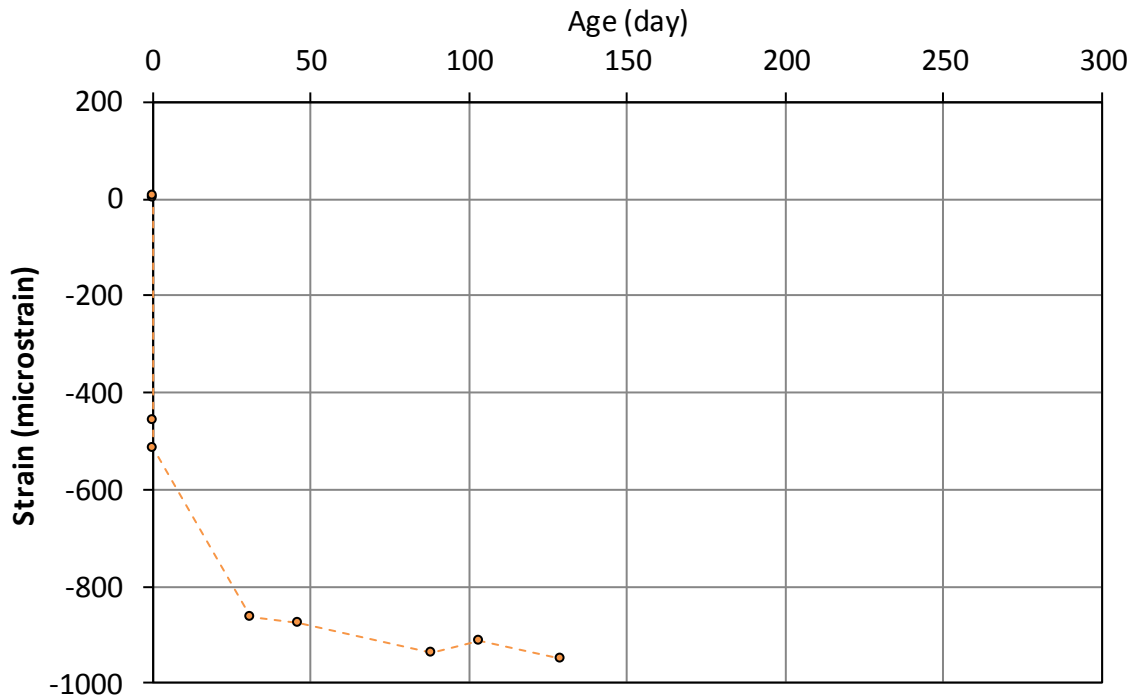
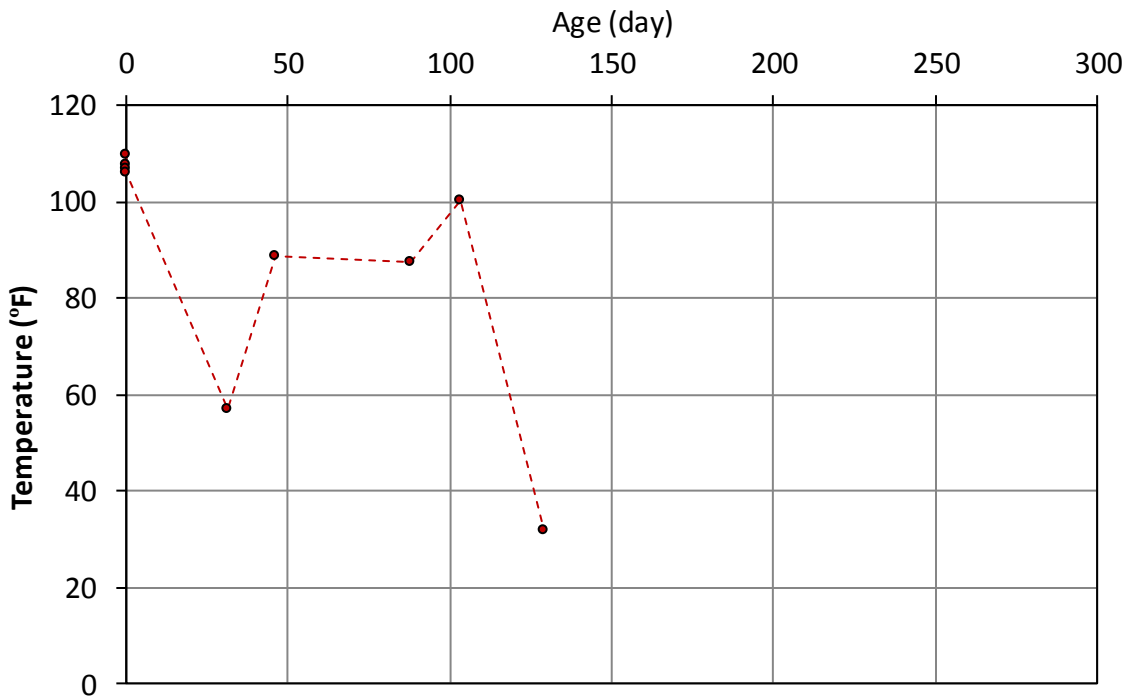


Figure A-91 Temperature data for girder IV-SCC-1, top gage ( $y = 43$  in.)



**Figure A-92 Strain data for girder IV-SCC-1, web gage ( $y = 18$  in.)**



**Figure A-93 Temperature data for girder IV-SCC-1, web gage ( $y = 18$  in.)**

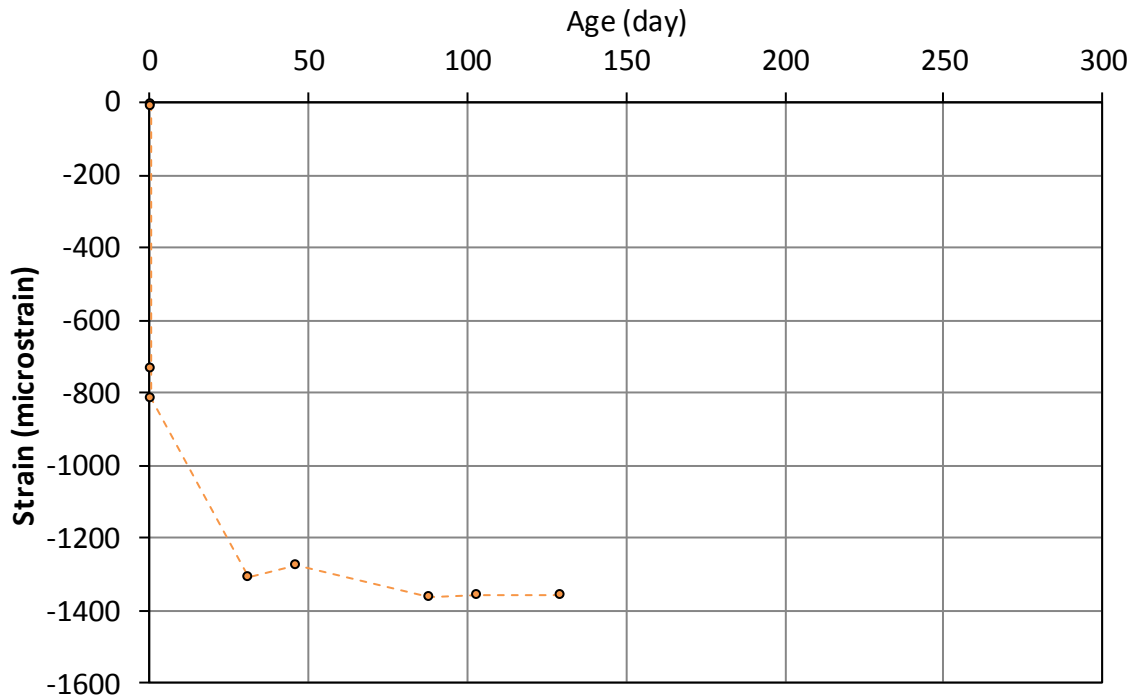


Figure A-94 Strain data for girder IV-SCC-1, bottom gage ( $y = 5.2$  in.)

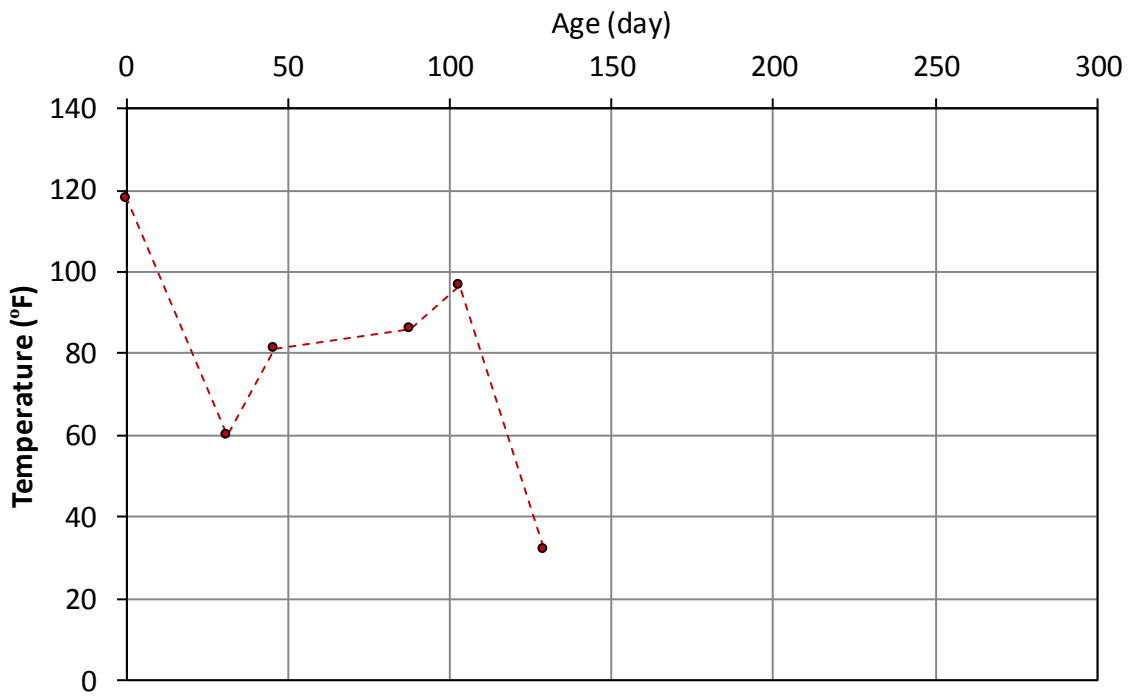


Figure A-95 Temperature data for girder IV-SCC-1, bottom gage ( $y = 5.2$  in.)

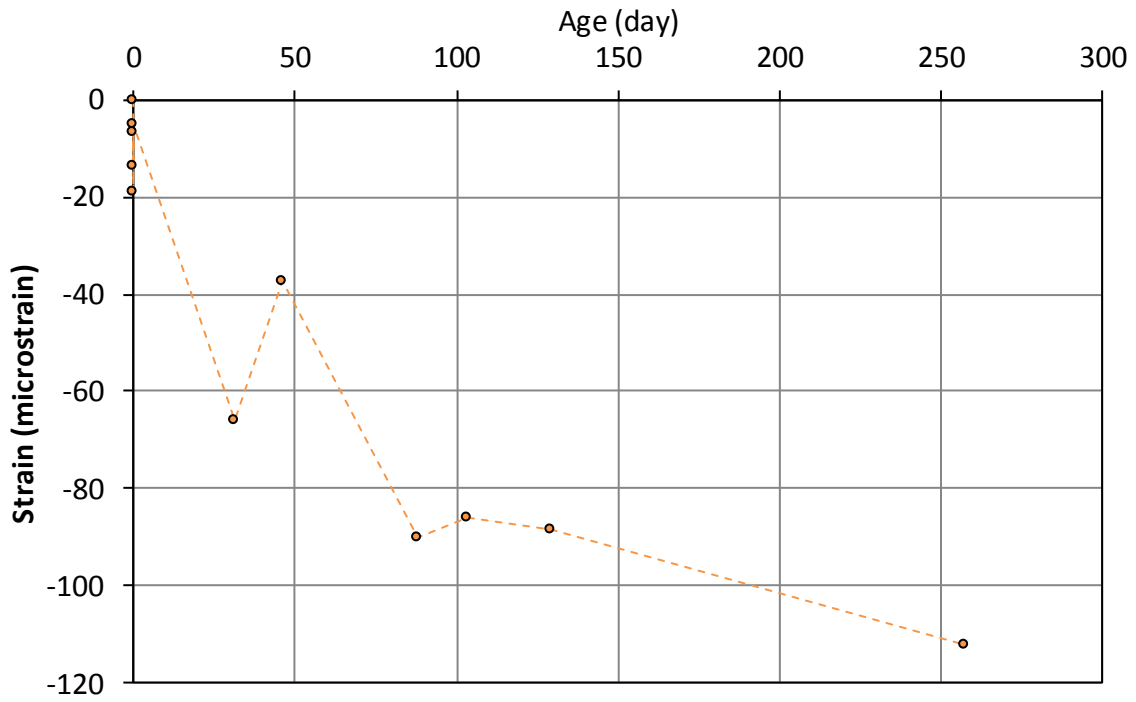


Figure A-96 Strain data for girder IV-SCC-2, top gage ( $y = 43$  in.)

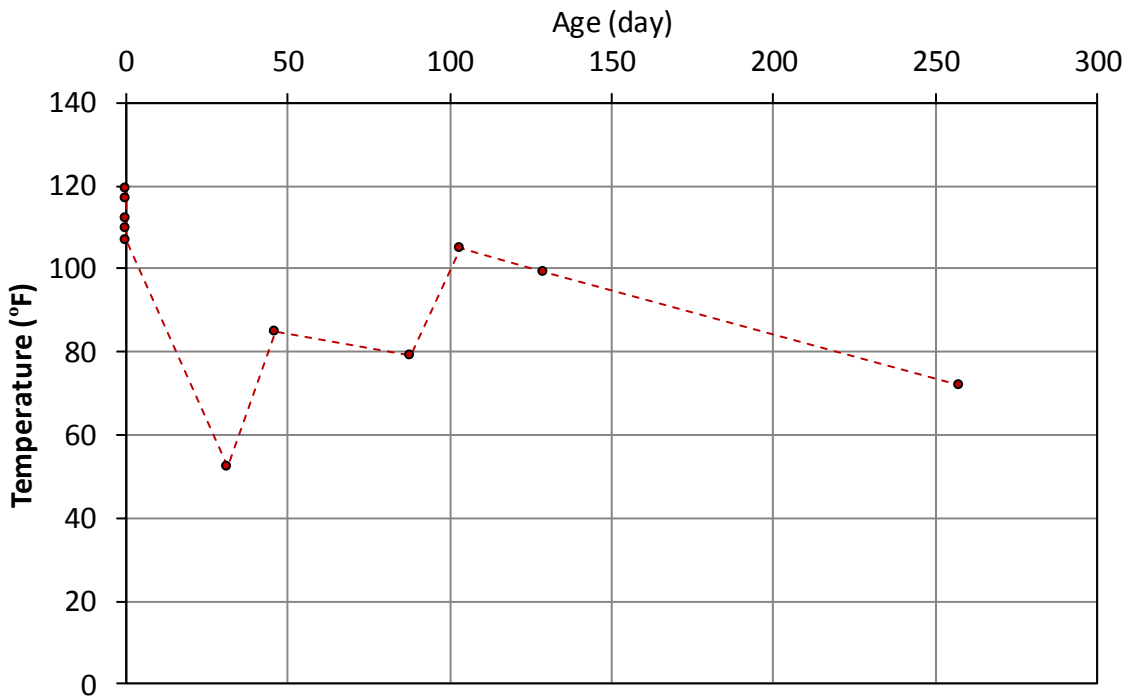
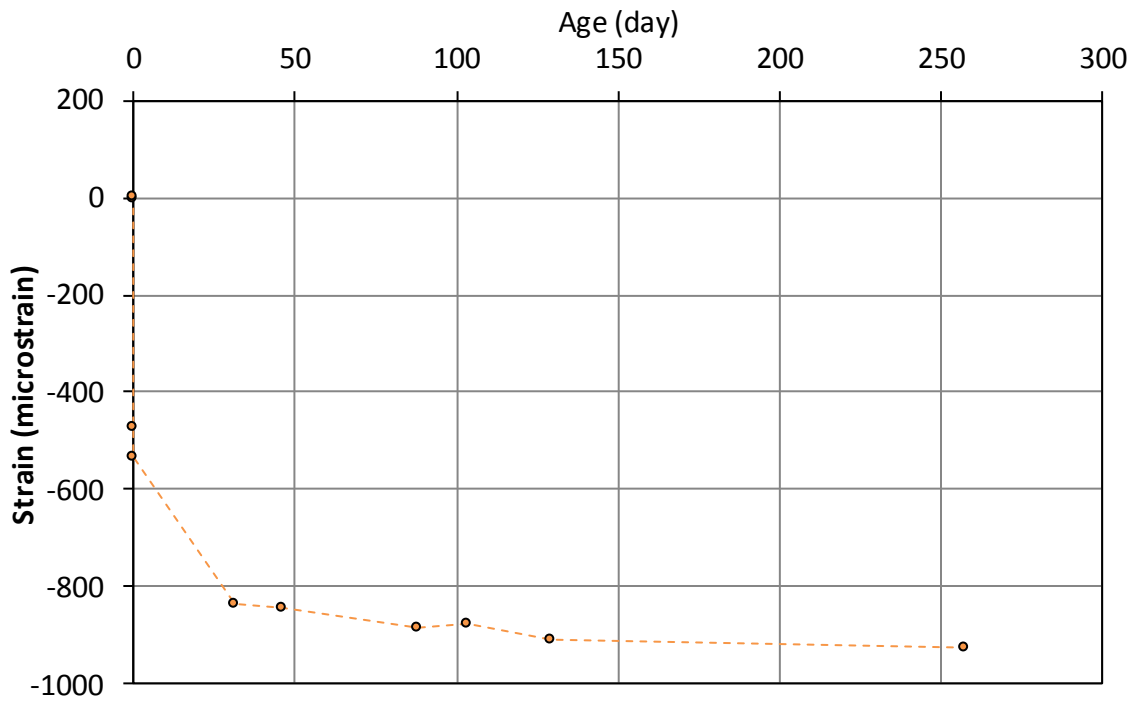
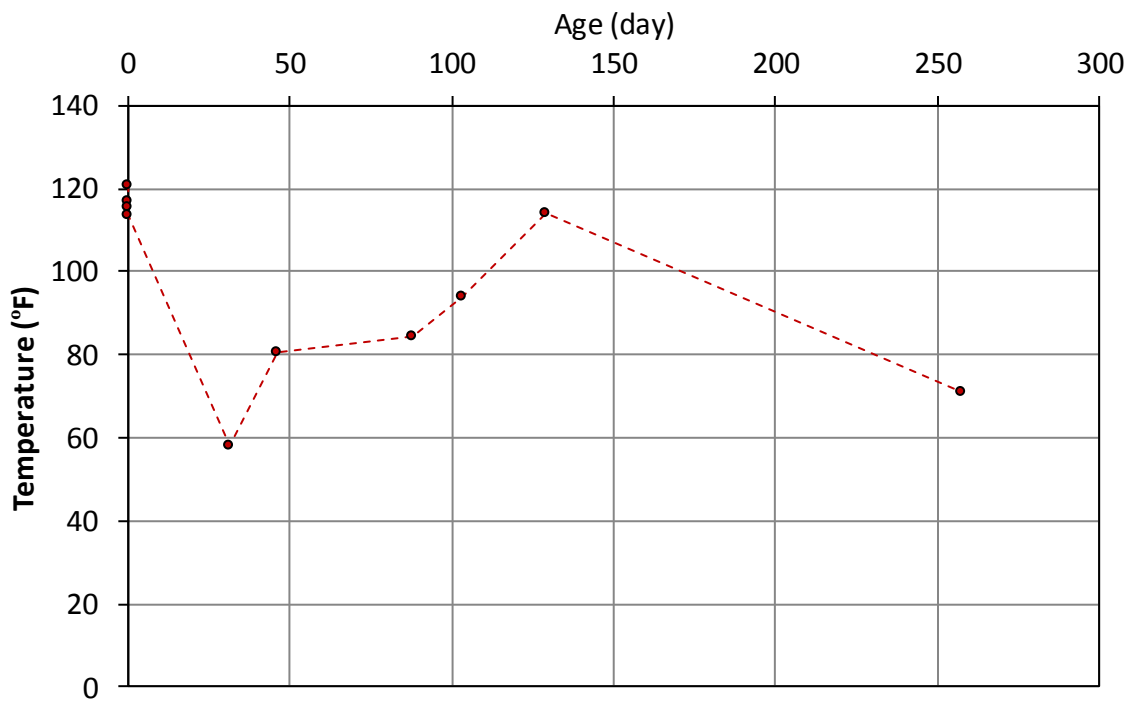


Figure A-97 Temperature data for girder IV-SCC-2, top gage ( $y = 43$  in.)



**Figure A-98 Strain data for girder IV-SCC-2, web gage ( $y = 18$  in.)**



**Figure A-99 Temperature data for girder IV-SCC-2, web gage ( $y = 18$  in.)**



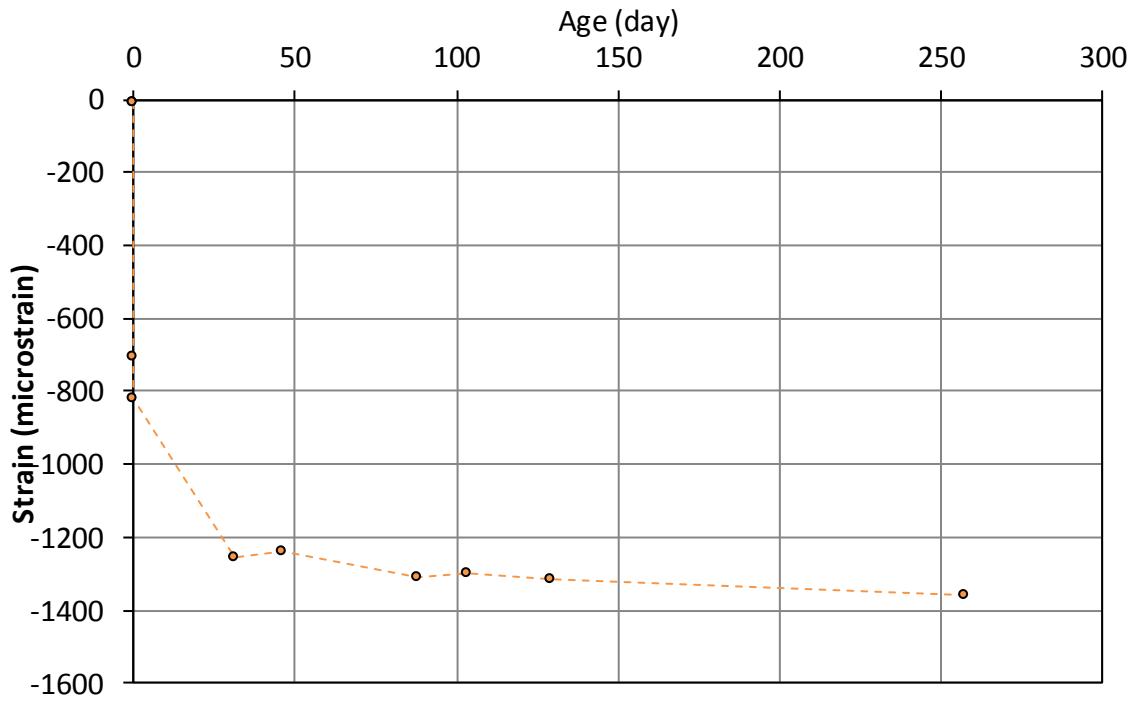


**Figure A-100 Strain data for girder IV-SCC-2, bottom gage ( $y = 5.2$  in.)**

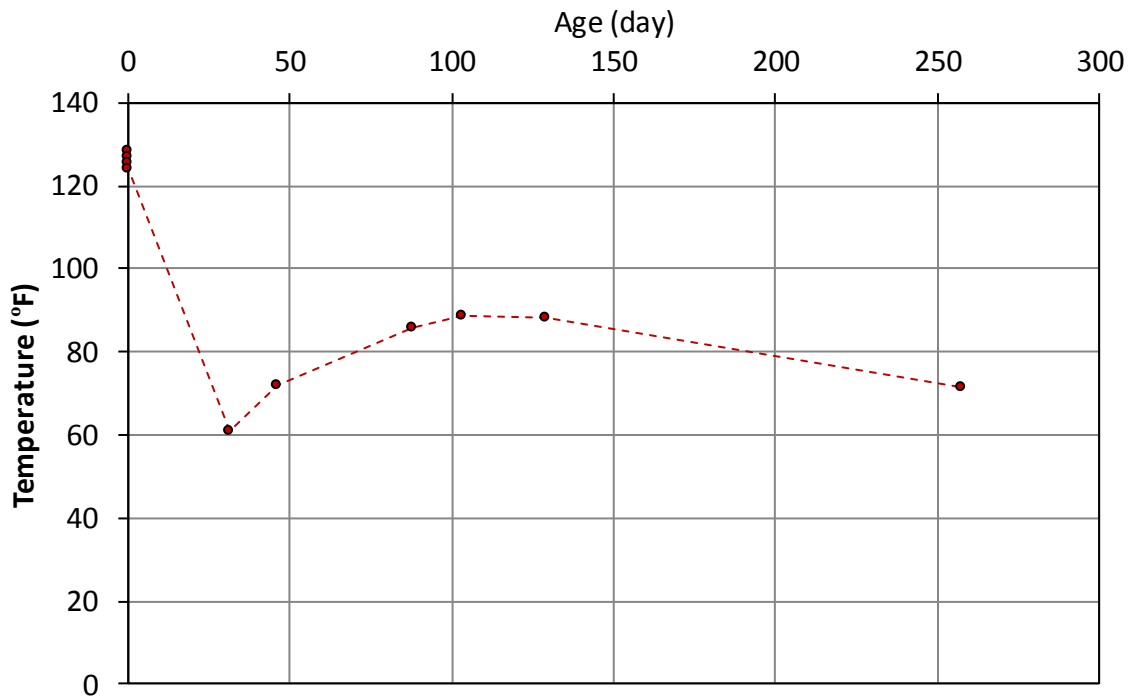


**Figure A-101 Temperature data for girder IV-SCC-2, bottom gage ( $y = 5.2$  in.)**

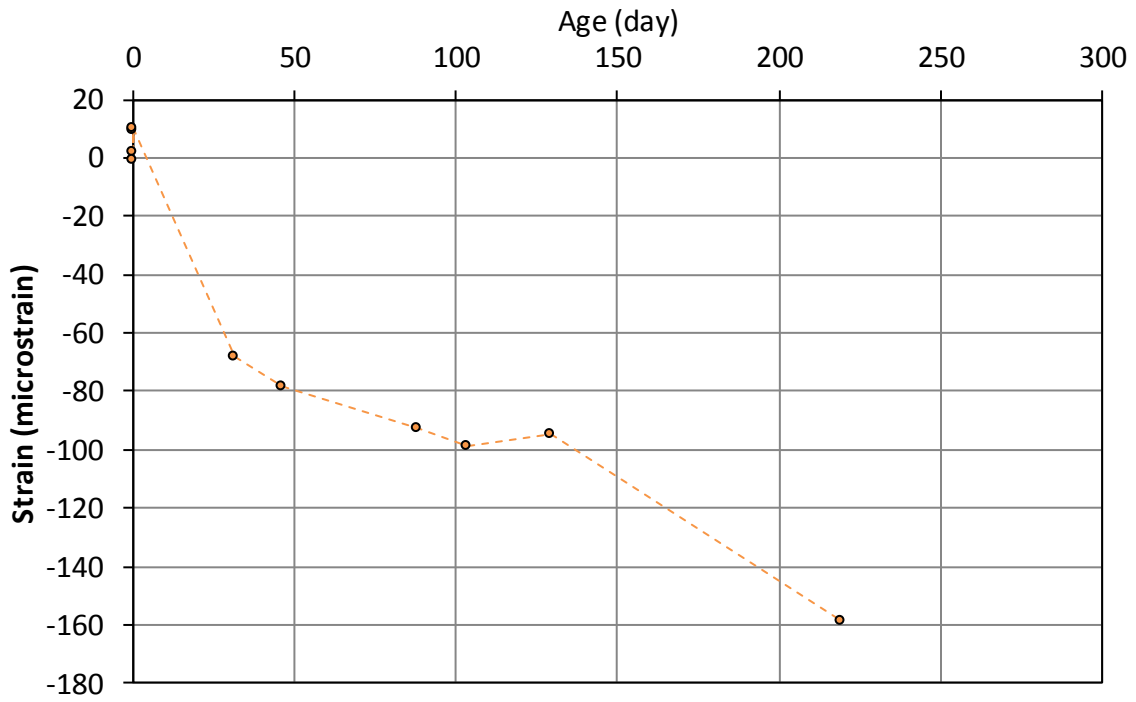


**Figure A-102 Strain data for girder IV-SCC-3, top gage ( $y = 43$  in.)**

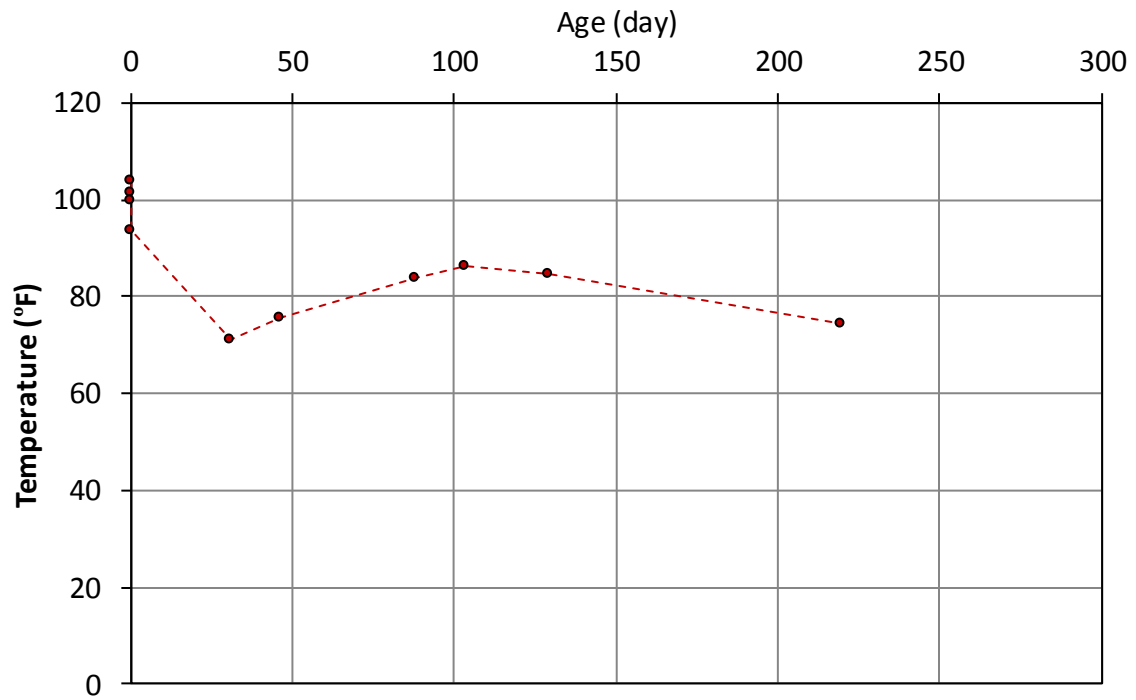


**Figure A-103 Temperature data for girder IV-SCC-3, top gage ( $y = 43$  in.)**

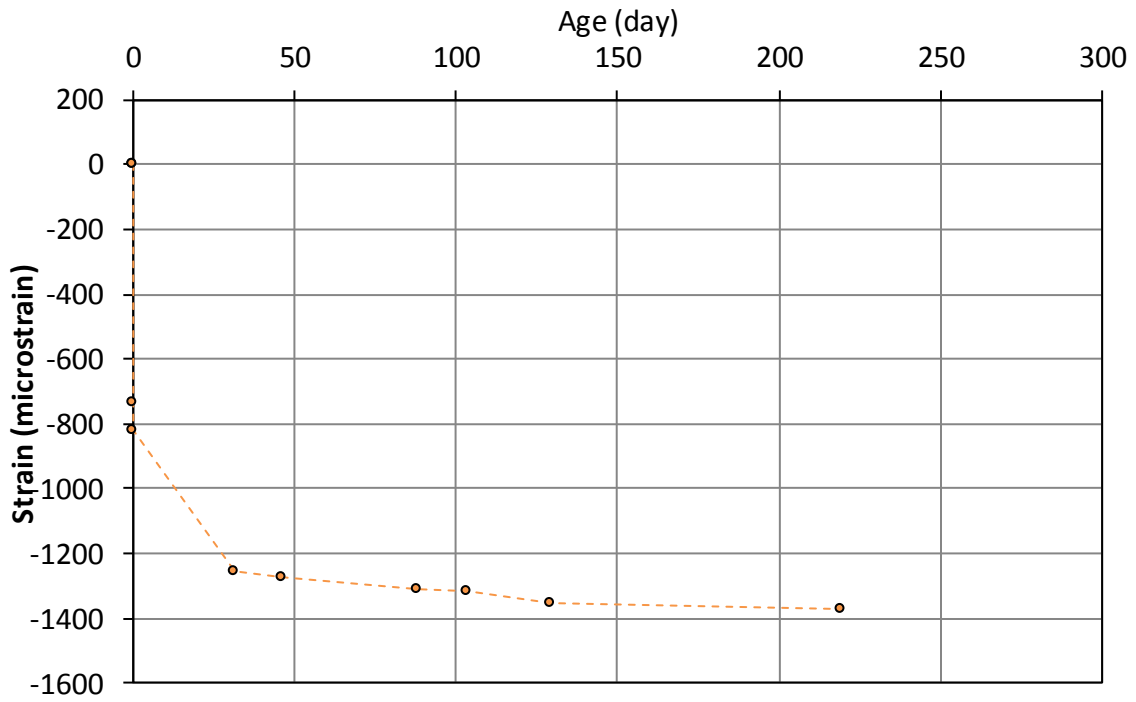


**Figure A-104 Strain data for girder IV-SCC-3, bottom gage ( $y = 5.2$  in.)**

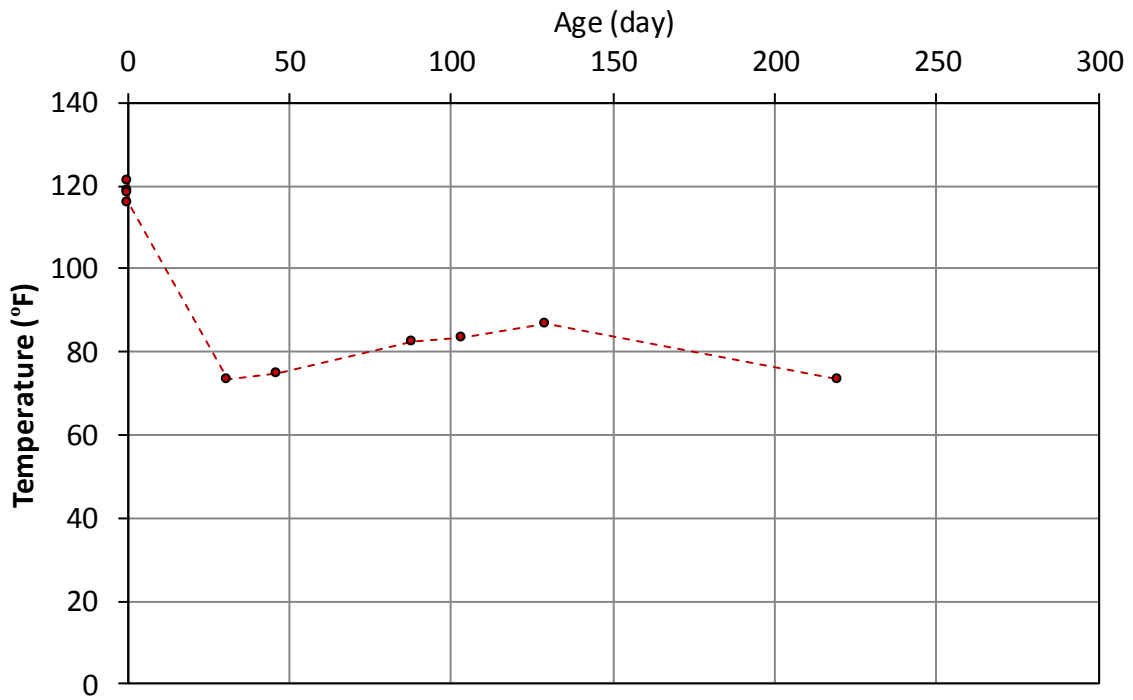


**Figure A-105 Temperature data for girder IV-SCC-3, bottom gage ( $y = 5.2$  in.)**

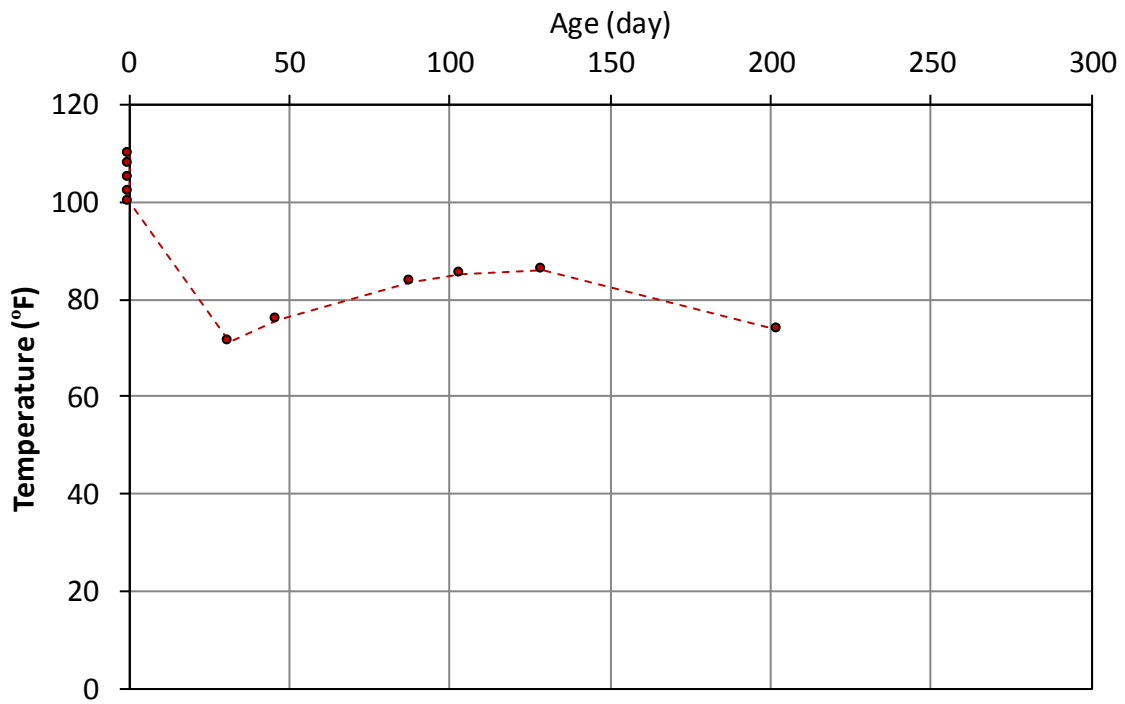


Figure A-106 Temperature data for girder IV-CC-1, top gage ( $y = 43$  in.)

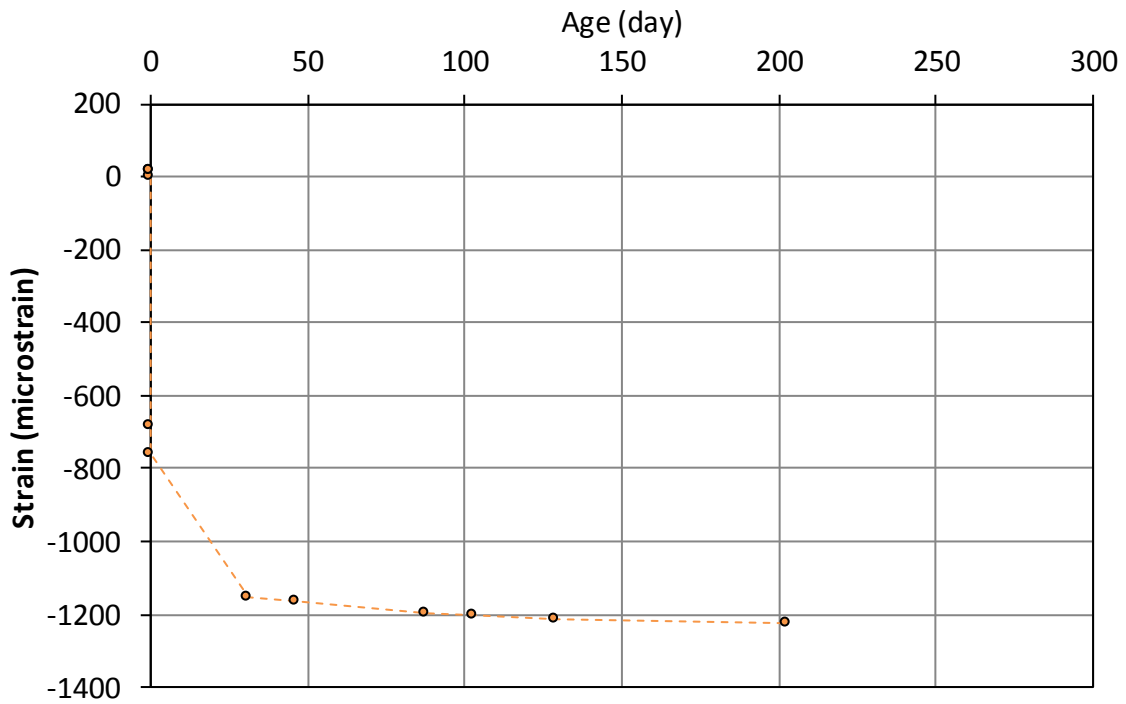


Figure A-107 Strain data for girder IV-CC-1, bottom gage ( $y = 5.2$  in.)

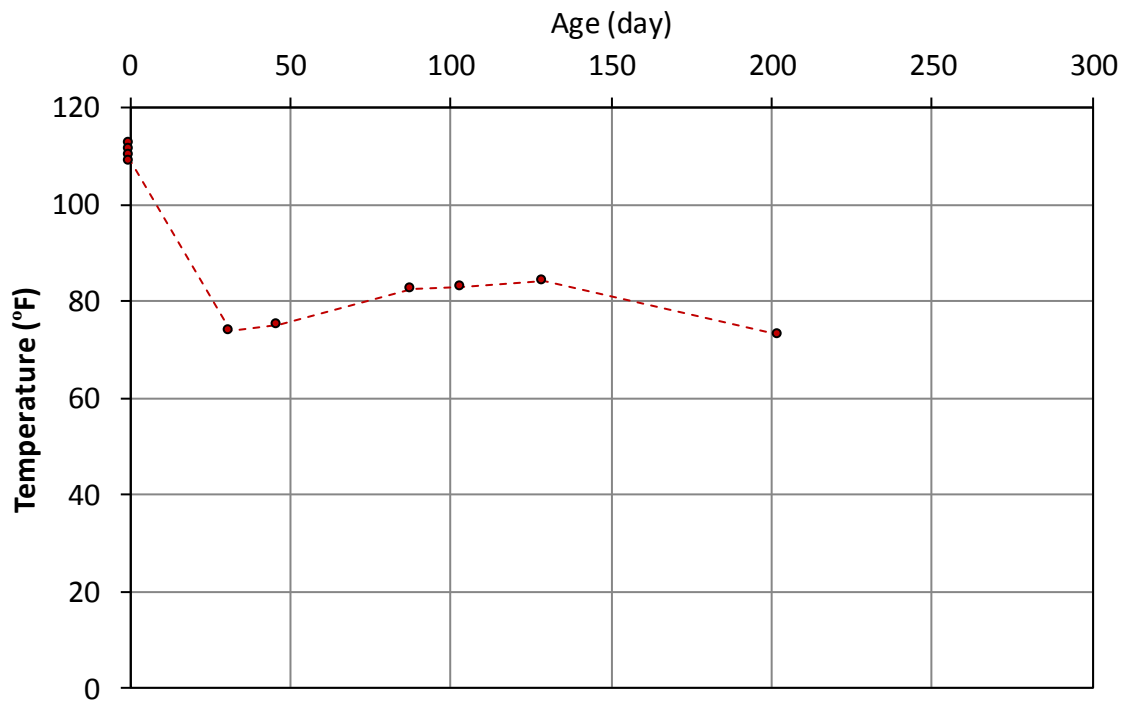


Figure A-108 Temperature data for girder IV-CC-1, bottom gage ( $y = 5.2$  in.)

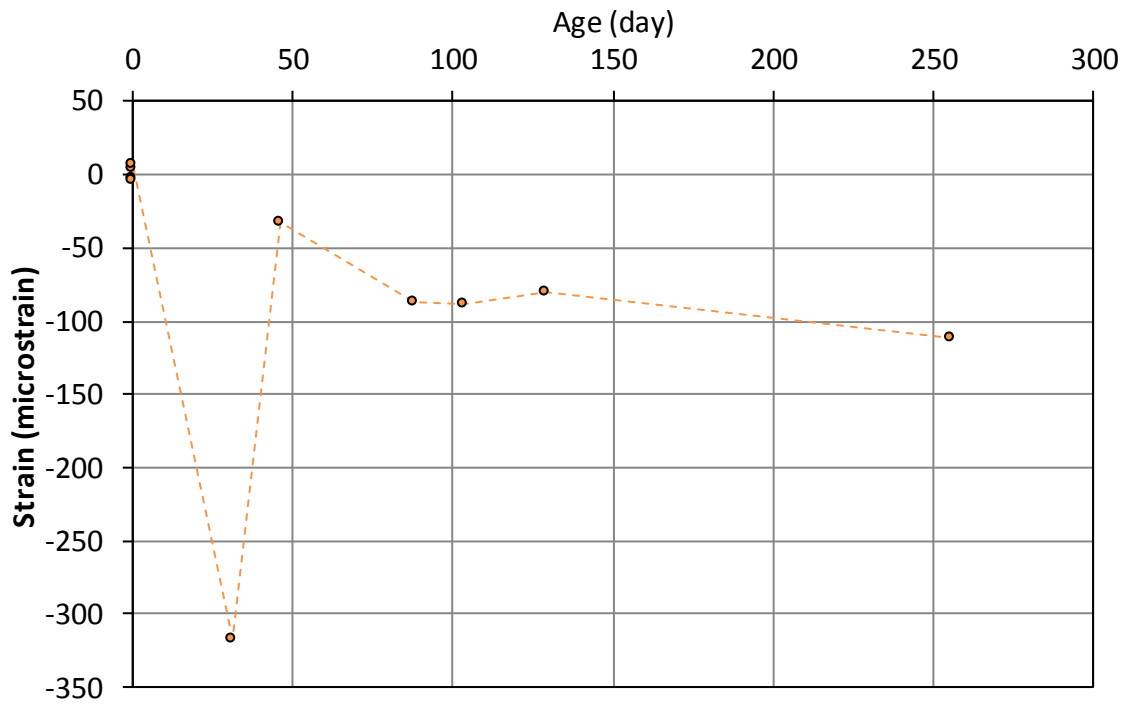


Figure A-109 Strain data for girder IV-CC-2, top gage ( $y = 43$  in.)

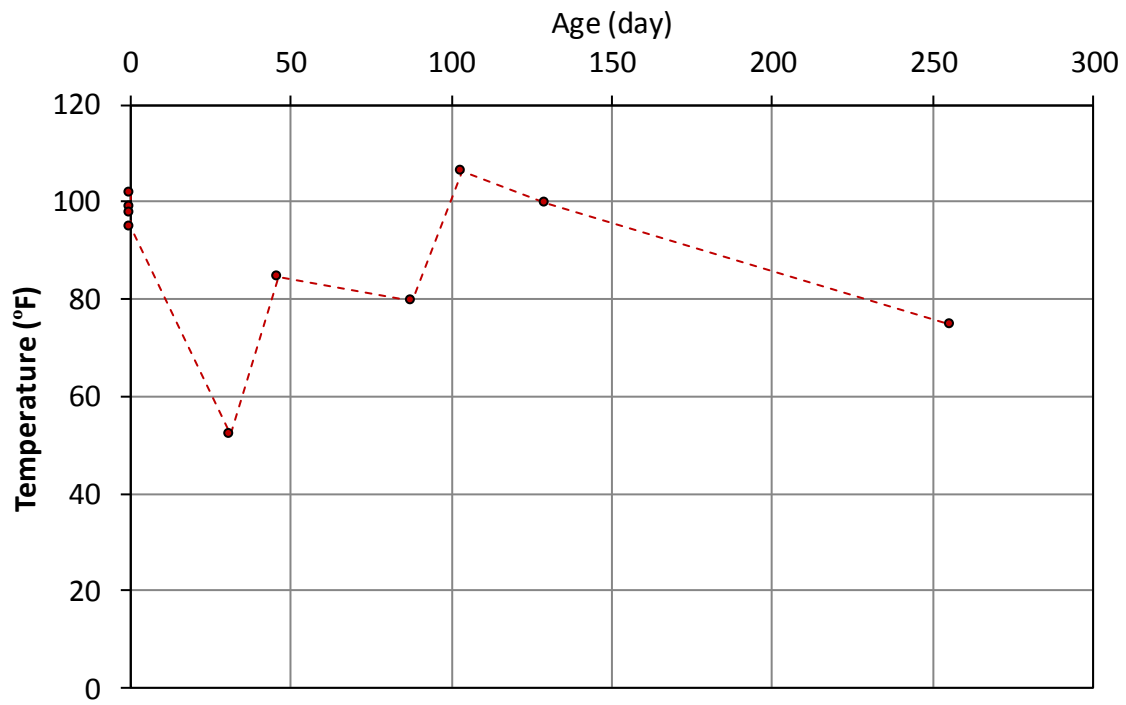


Figure A-110 Temperature data for girder IV-CC-2, top gage ( $y = 43$  in.)

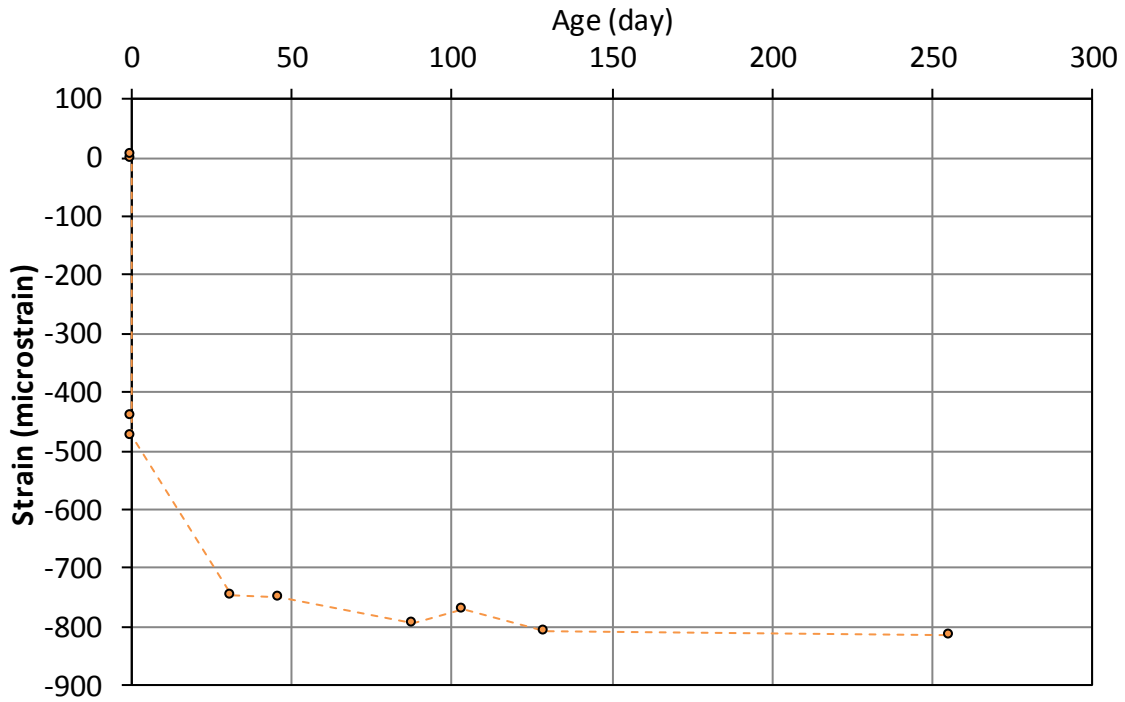


Figure A-111 Strain data for girder IV-CC-2, web gage ( $y = 18$  in.)

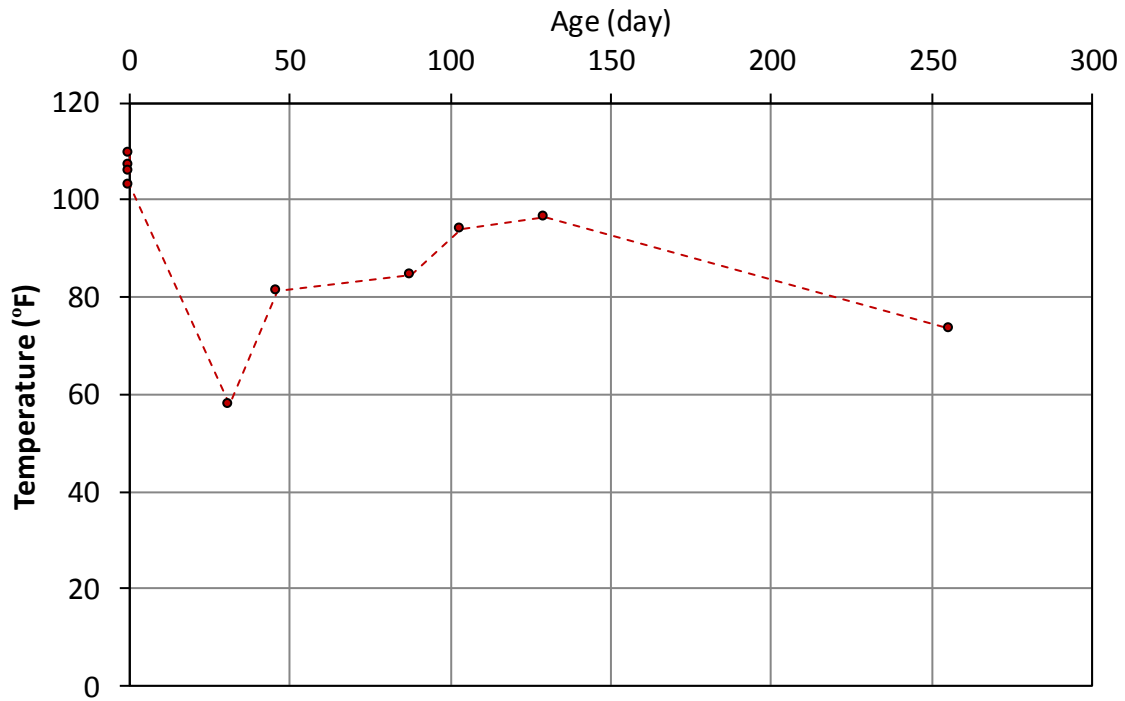


Figure A-112 Temperature data for girder IV-CC-2, web gage ( $y = 18$  in.)

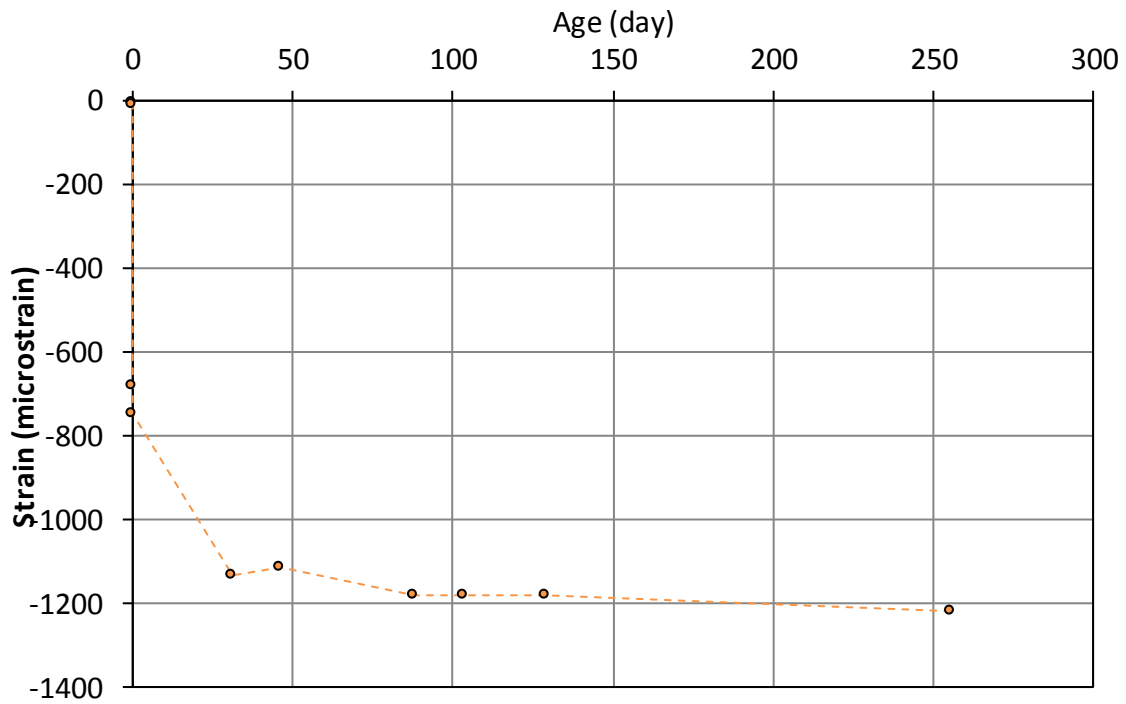


Figure A-113 Strain data for girder IV-CC-2, bottom gage ( $y = 5.2$  in.)

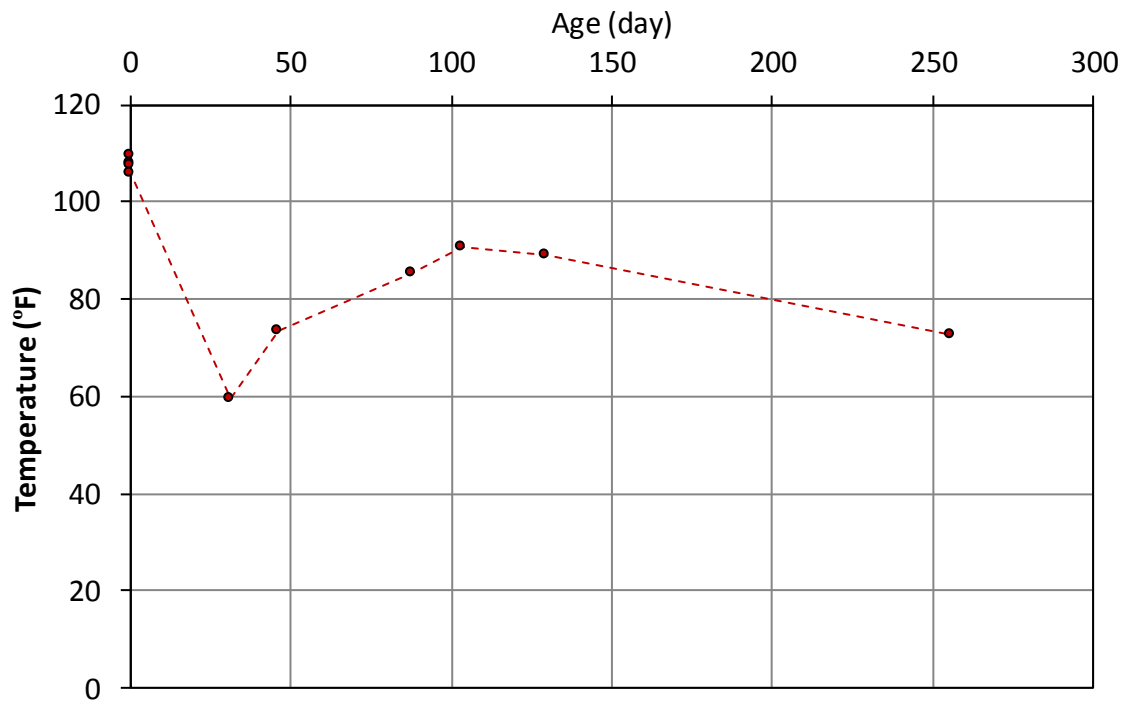


Figure A-114 Temperature data for girder IV-CC-2, bottom gage ( $y = 5.2$  in.)



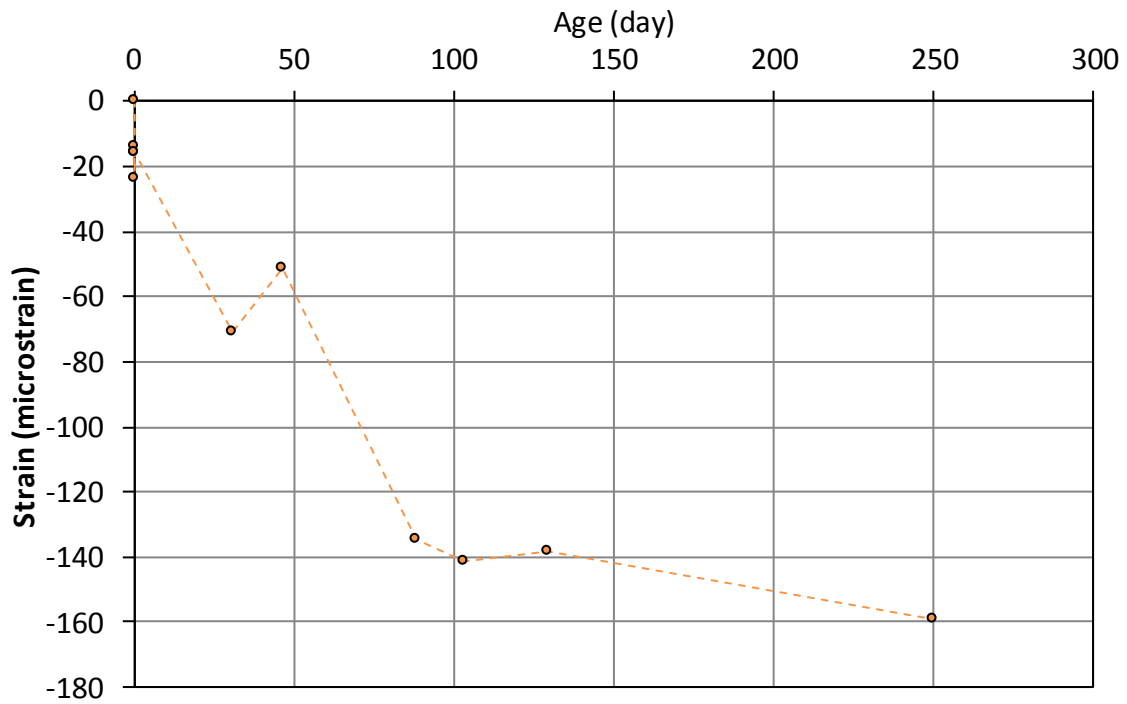


Figure A-115 Strain data for girder IV-SCC-3, top gage ( $y = 43$  in.)

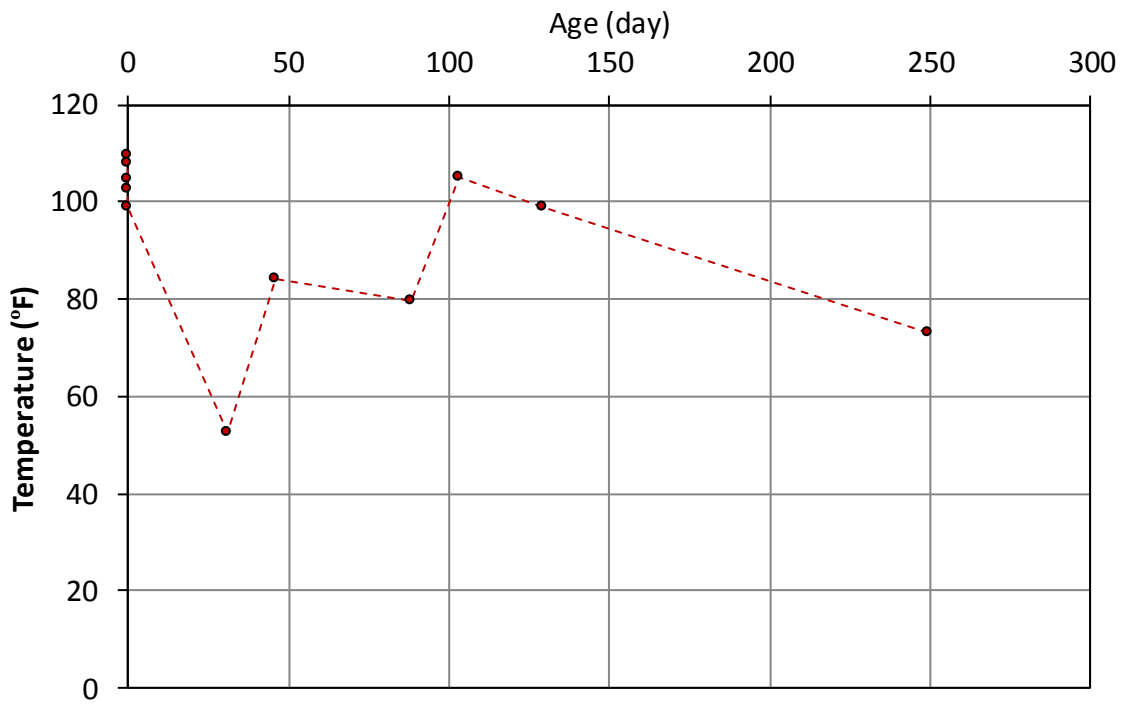


Figure A-116 Temperature data for girder IV-SCC-3, top gage ( $y = 43$  in.)

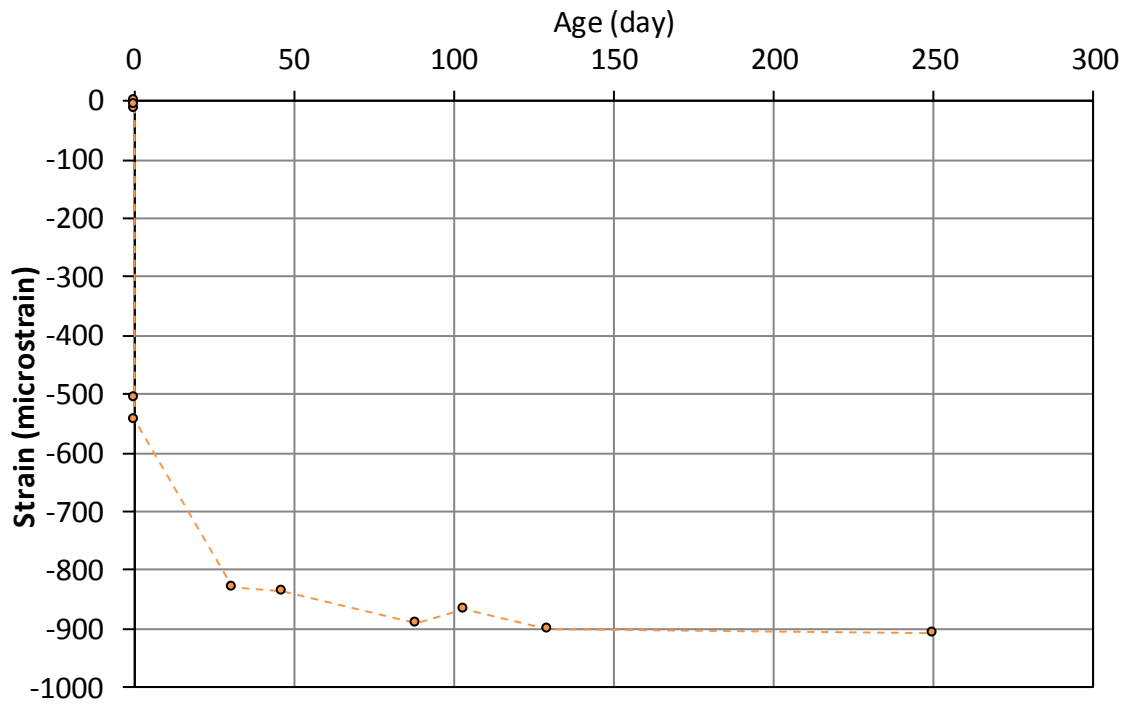


Figure A-117 Strain data for girder IV-CC-3, web gage ( $y = 18$  in.)

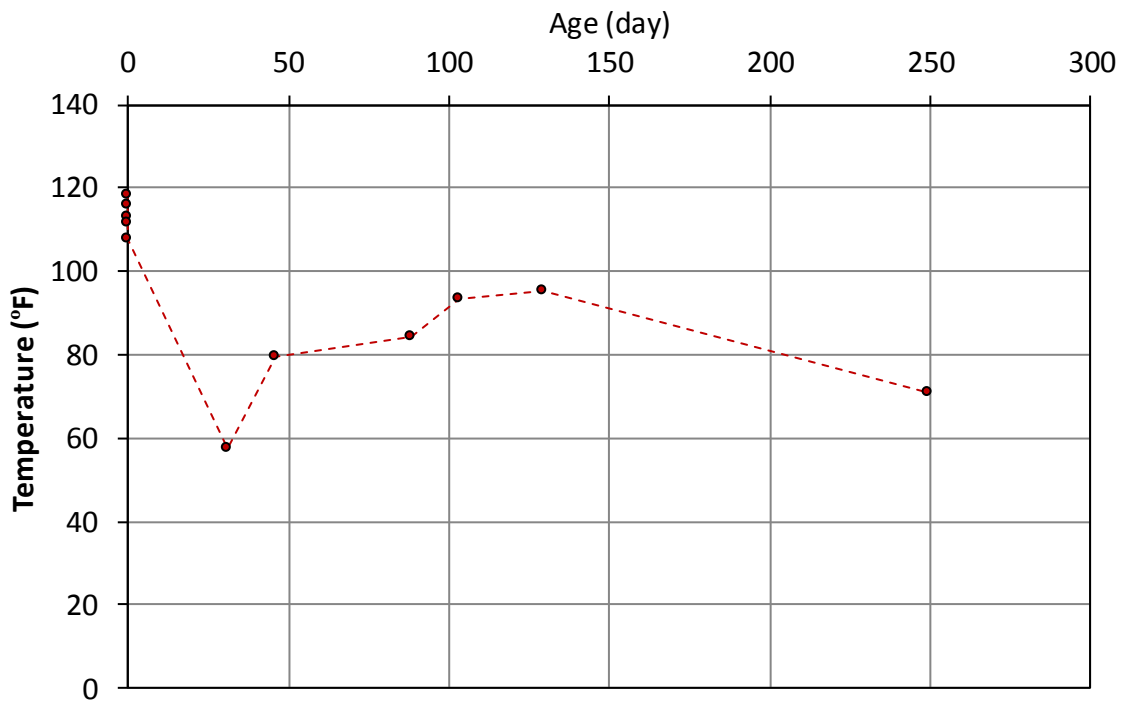


Figure A-118 Temperature data for girder IV-CC-3, web gage ( $y = 18$  in.)

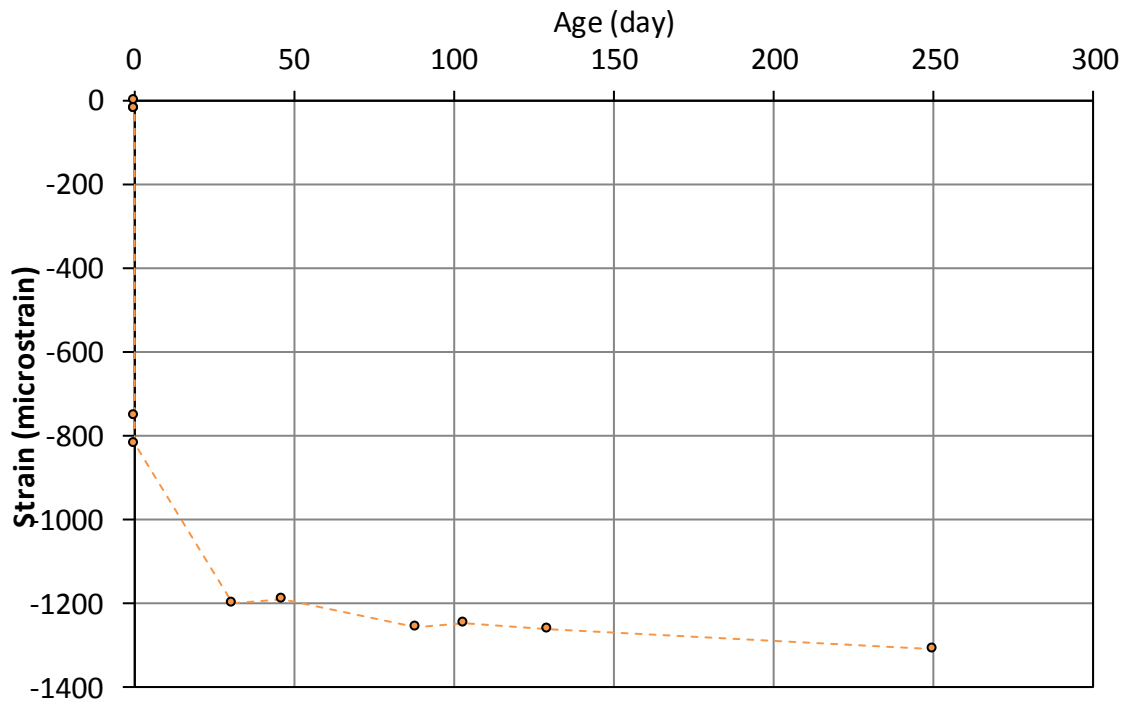


Figure A-119 Strain data for girder IV-CC-3, bottom gage ( $y = 5.2$  in.)

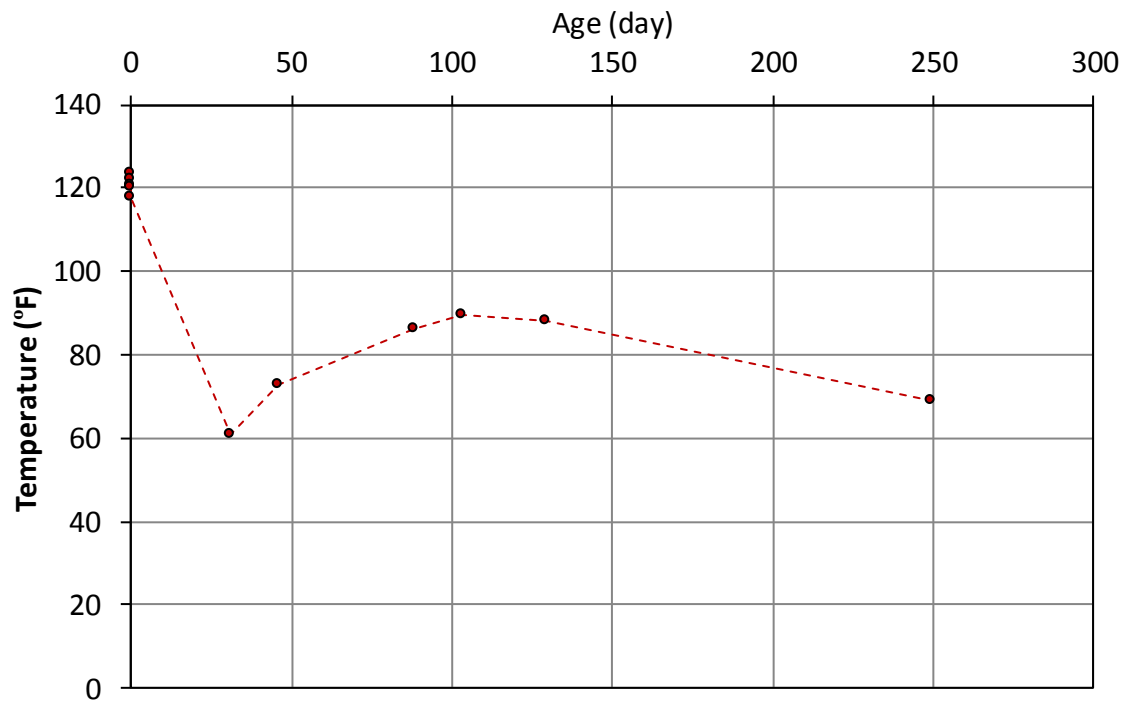
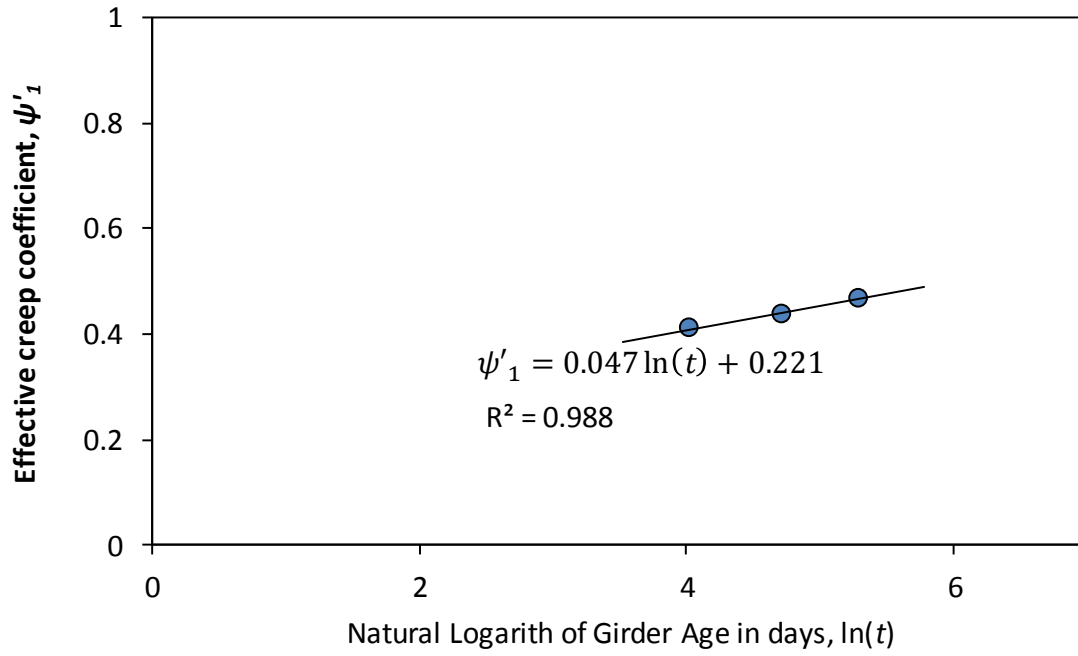


Figure A-120 Temperature data for girder IV-CC-3, bottom gage ( $y = 5.2$  in.)

## **APPENDIX B**

### **Time-Dependent Expressions for Sectional Creep Coefficients**

In this appendix the sectional creep coefficients obtained from the VWG data at three times are used to obtain expressions of sectional creep as function of time. The estimation of the sectional creep coefficient for each point in time is conducted as detailed in Section 6.3.3, and the development of the time-dependent expressions for sectional creep coefficients is detailed in Section 6.4.1.



**Figure B-1 Effective creep coefficient in terms of time for Girder UTPS#4 (2B)**

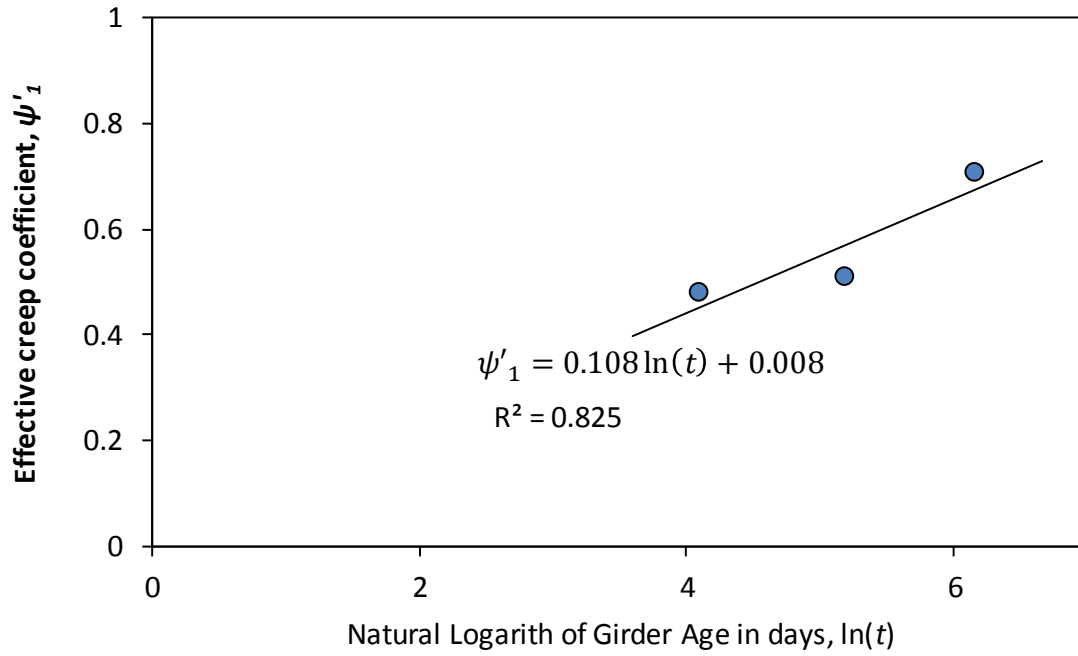


**Figure B-2 Effective creep coefficient in terms of time for Girder UTPS#59 (B-SCC1)**

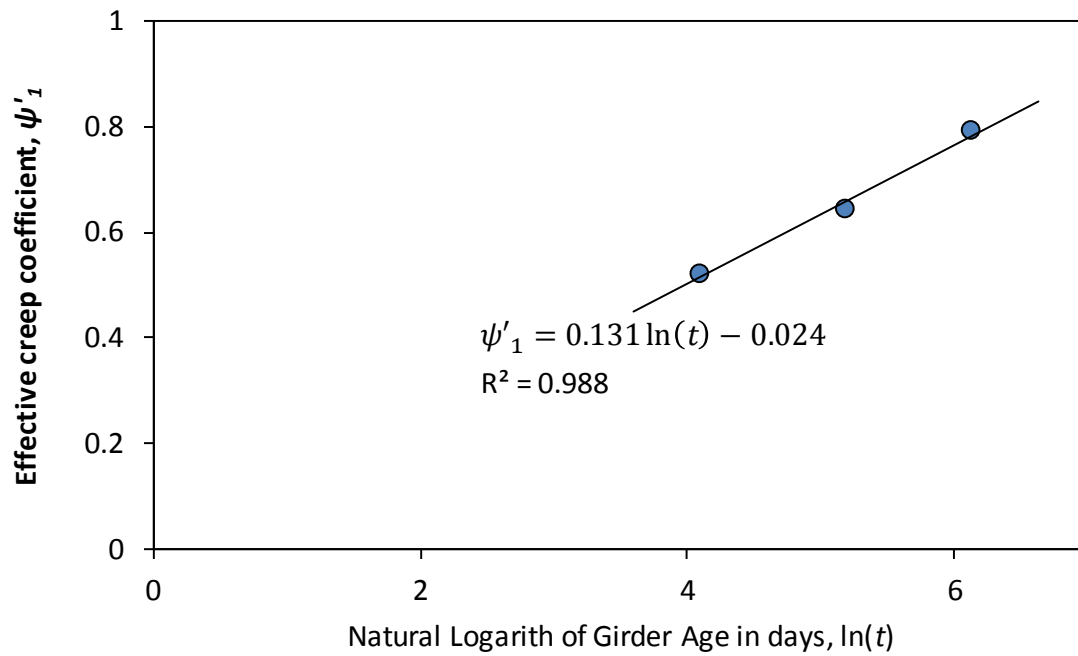


**Figure B-3 Effective creep coefficient in terms of time for Girder UTPS#60 (B-SCC2)**

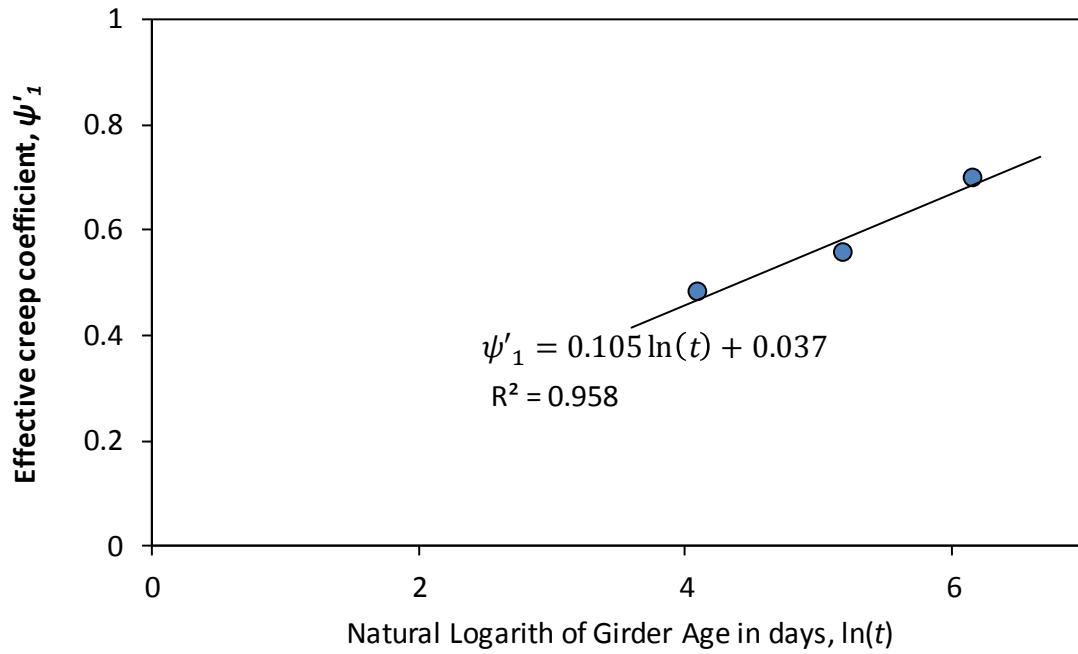


**Figure B-4 Effective creep coefficient in terms of time for Girder UTPS#61 (B-CM)**

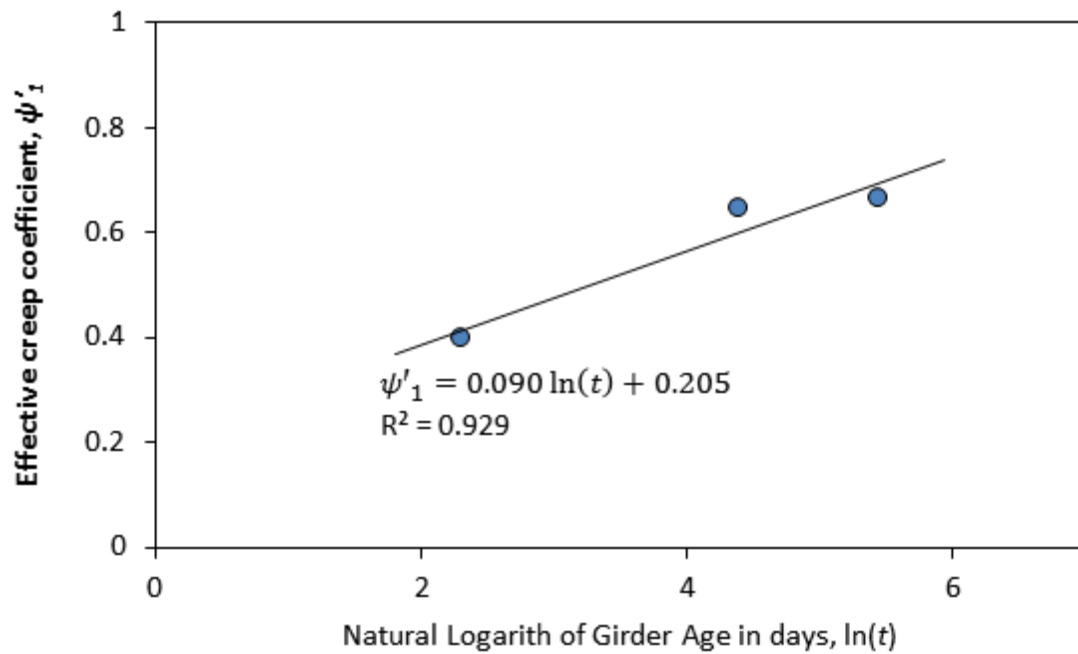


**Figure B-5 Effective creep coefficient in terms of time for Girder UTPS#62 (BX-1)**

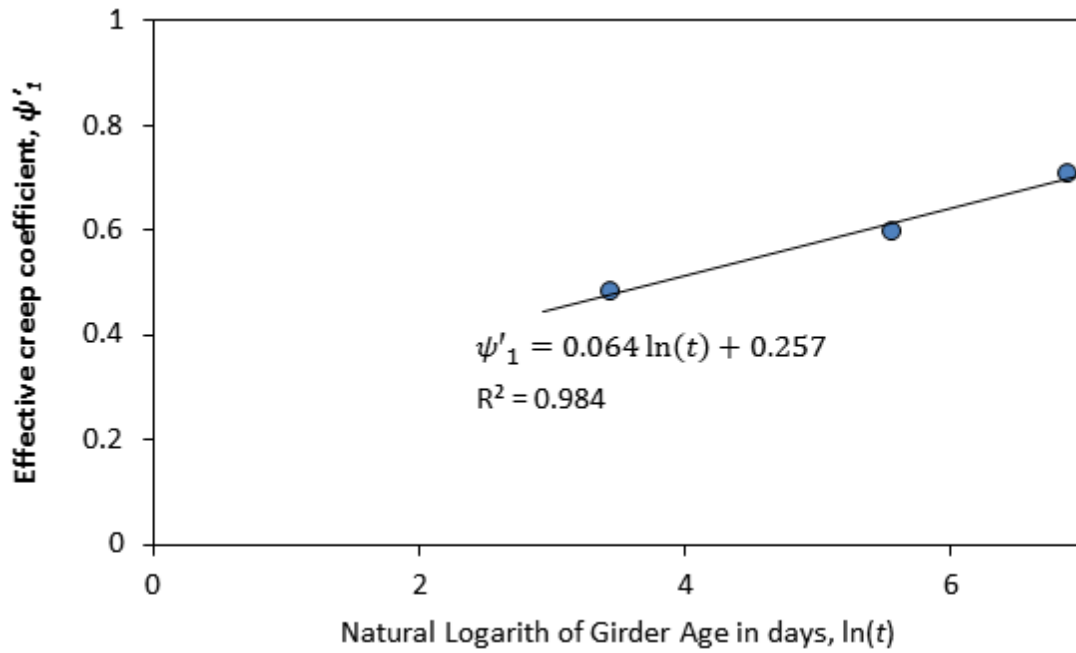


Figure B-6 Effective creep coefficient in terms of time for Girder UTPS#222 (I-1)

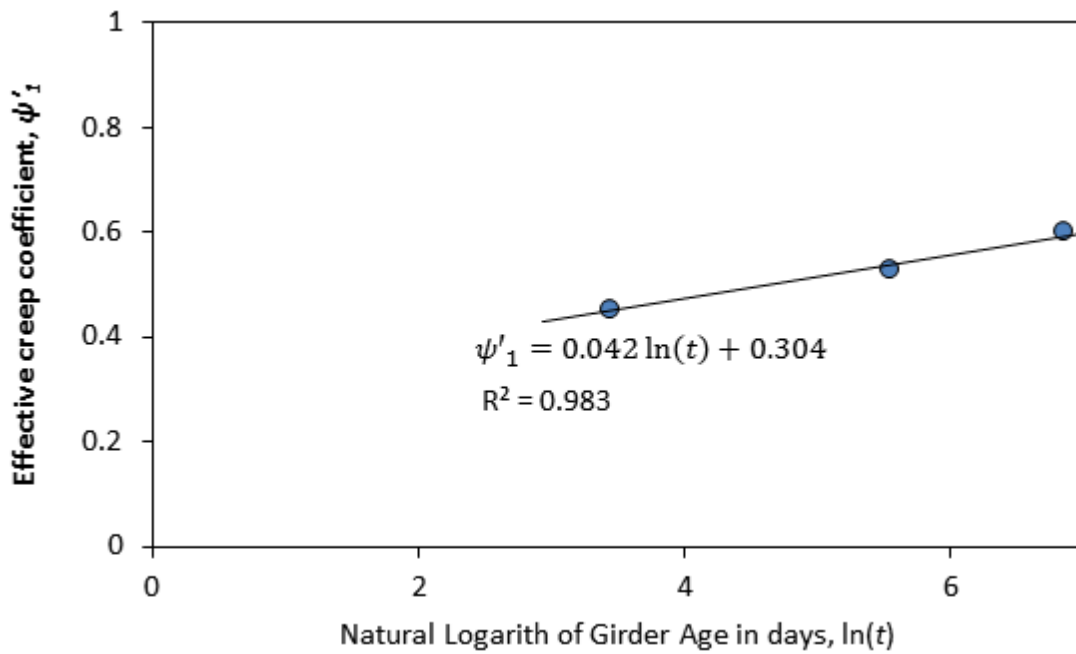


Figure B-7 Effective creep coefficient in terms of time for Girder UTPS#228 (I-7)



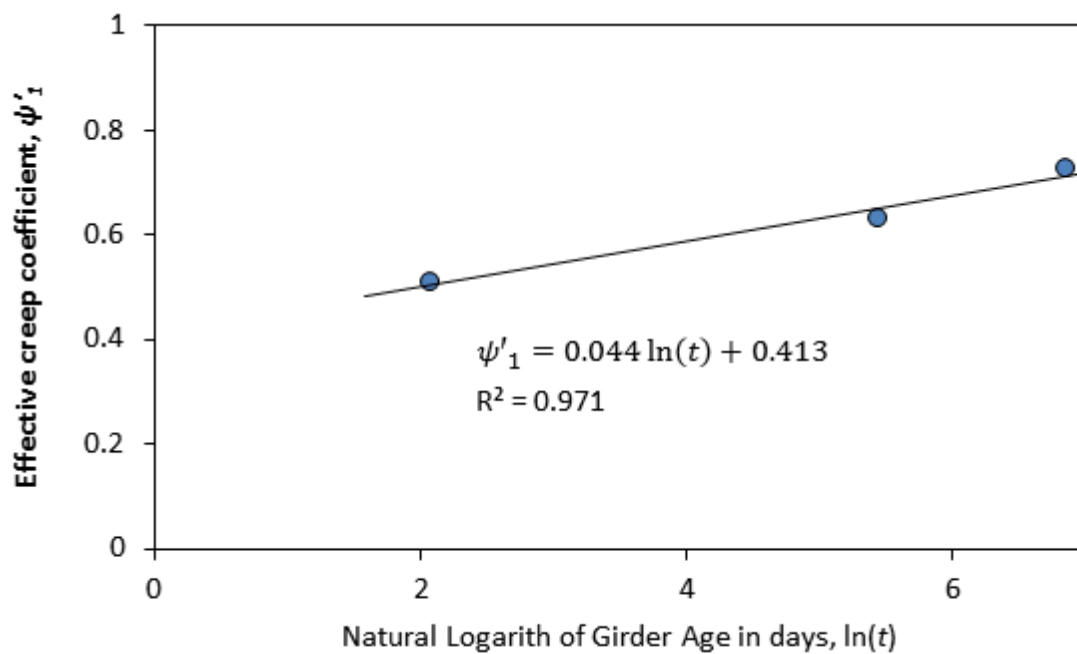


Figure B-8 Effective creep coefficient in terms of time for Girder UTPS#230 (II-1)

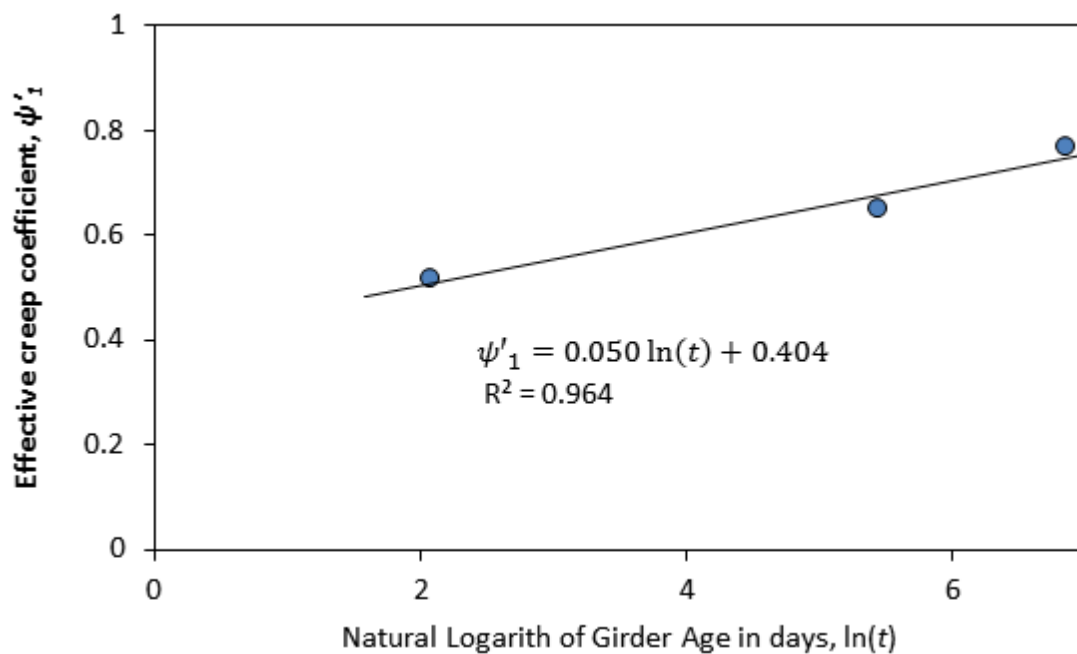


Figure B-9 Effective creep coefficient in terms of time for Girder UTPS#235 (II-6)



Figure B-10 Effective creep coefficient in terms of time for Girder UTPS#232 (II-3)

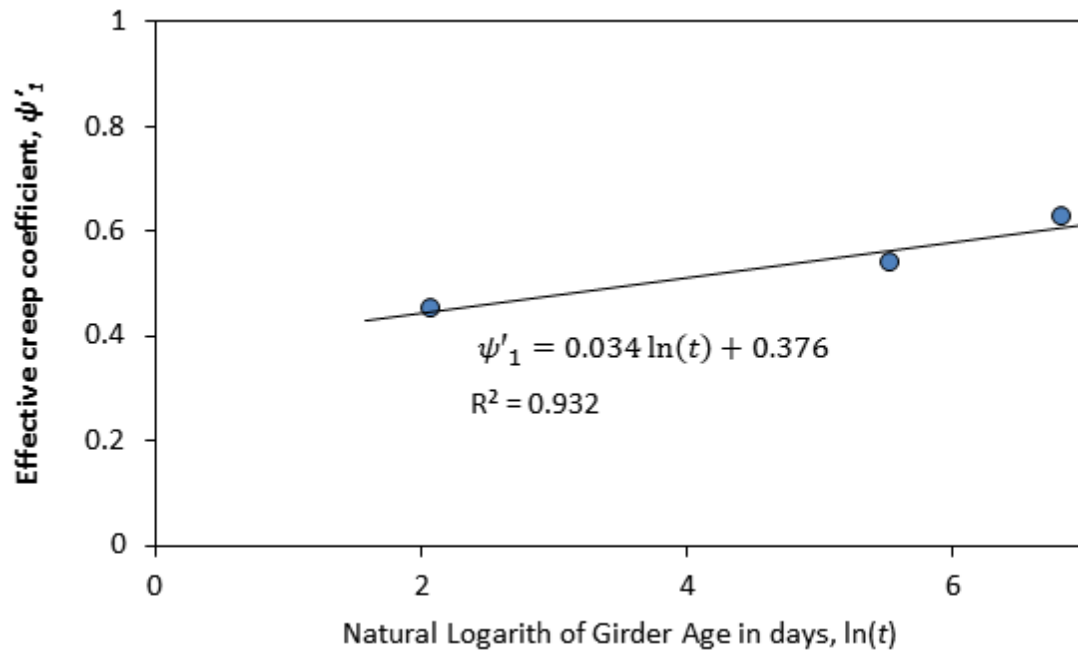


Figure B-11 Effective creep coefficient in terms of time for Girder UTPS#237 (II-8)

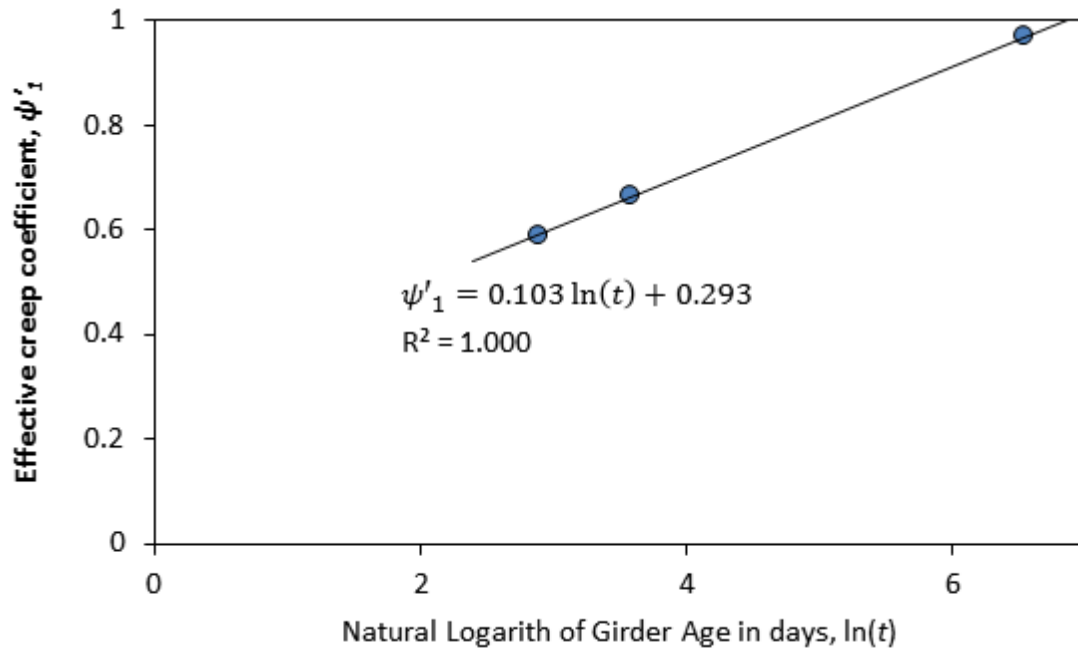


Figure B-12 Effective creep coefficient in terms of time for Girder UTPS#238 (III-1)

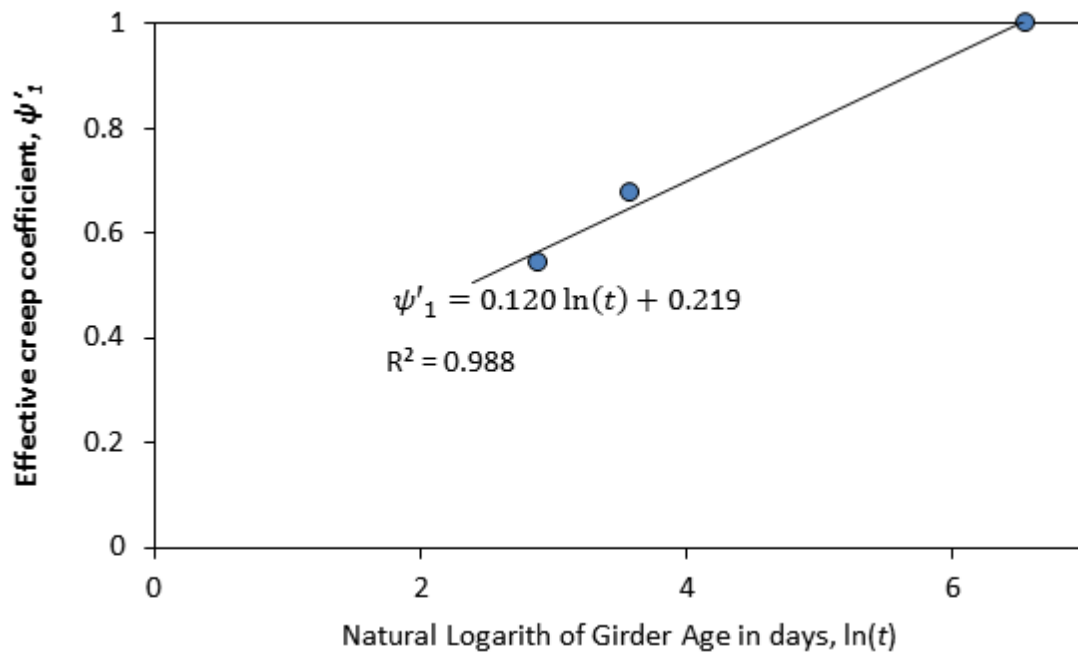


Figure B-13 Effective creep coefficient in terms of time for Girder UTPS#242 (III-5)

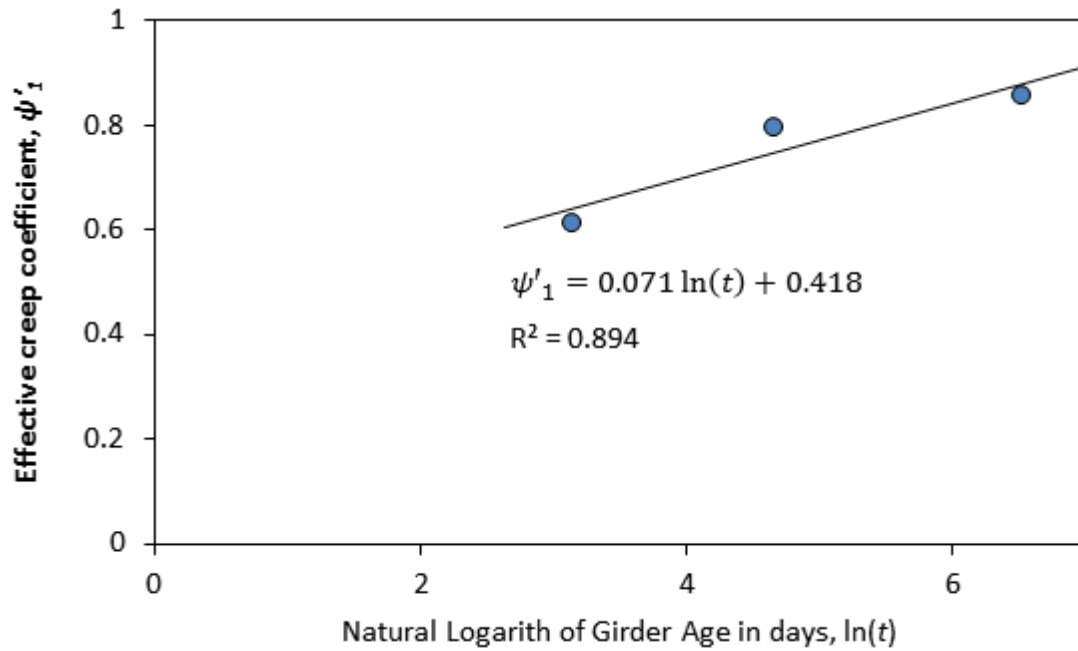


Figure B-14 Effective creep coefficient in terms of time for Girder UTPS#240 (III-3)

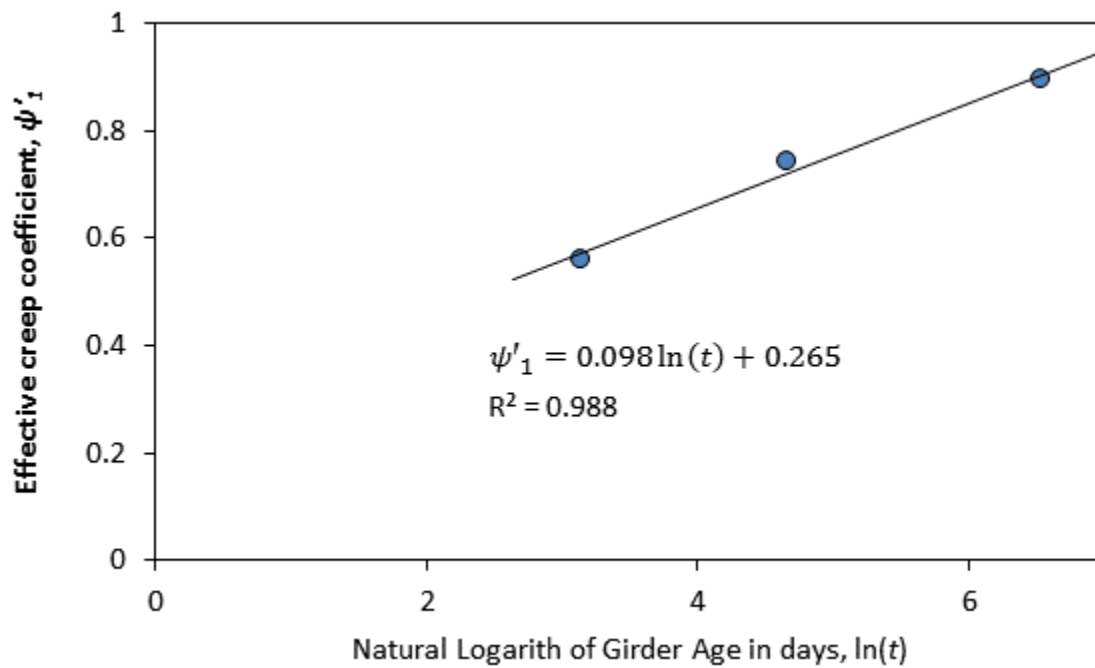


Figure B-15 Effective creep coefficient in terms of time for Girder UTPS#244 (III-7)

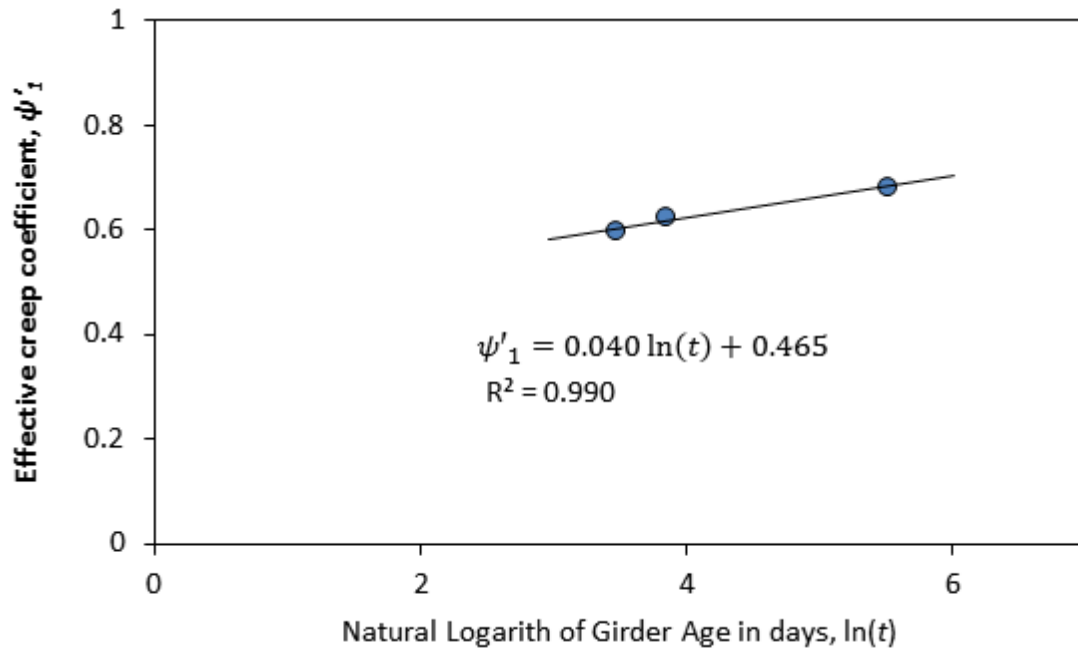


Figure B-16 Effective creep coefficient in terms of time for Girder UTPS#246 (SCC-1)

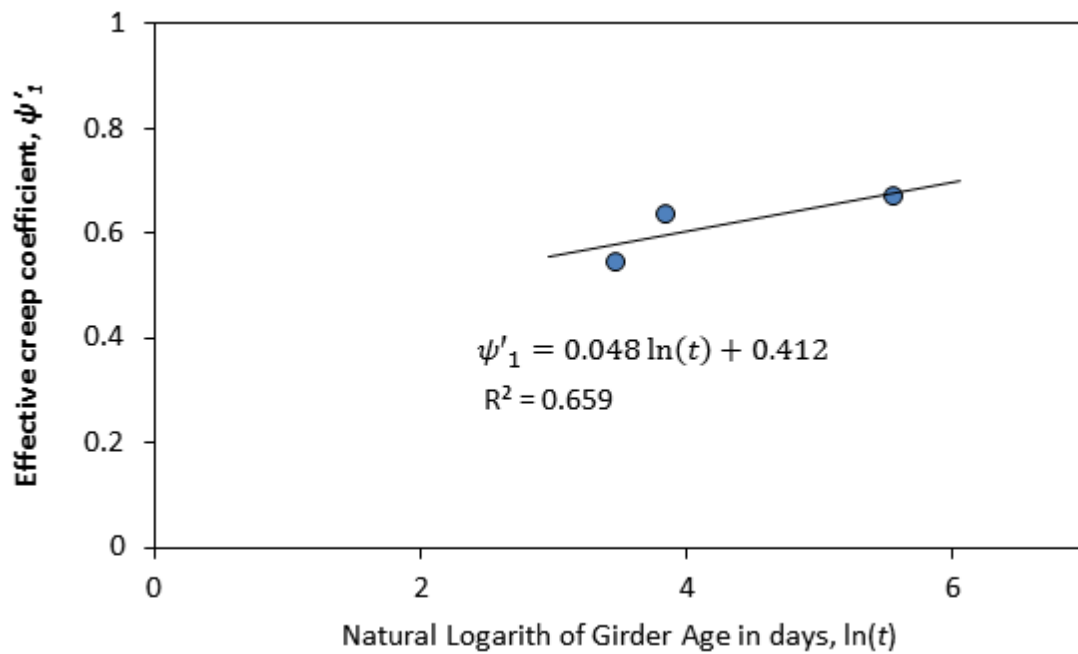


Figure B-17 Effective creep coefficient in terms of time for Girder UTPS#247 (SCC-2)

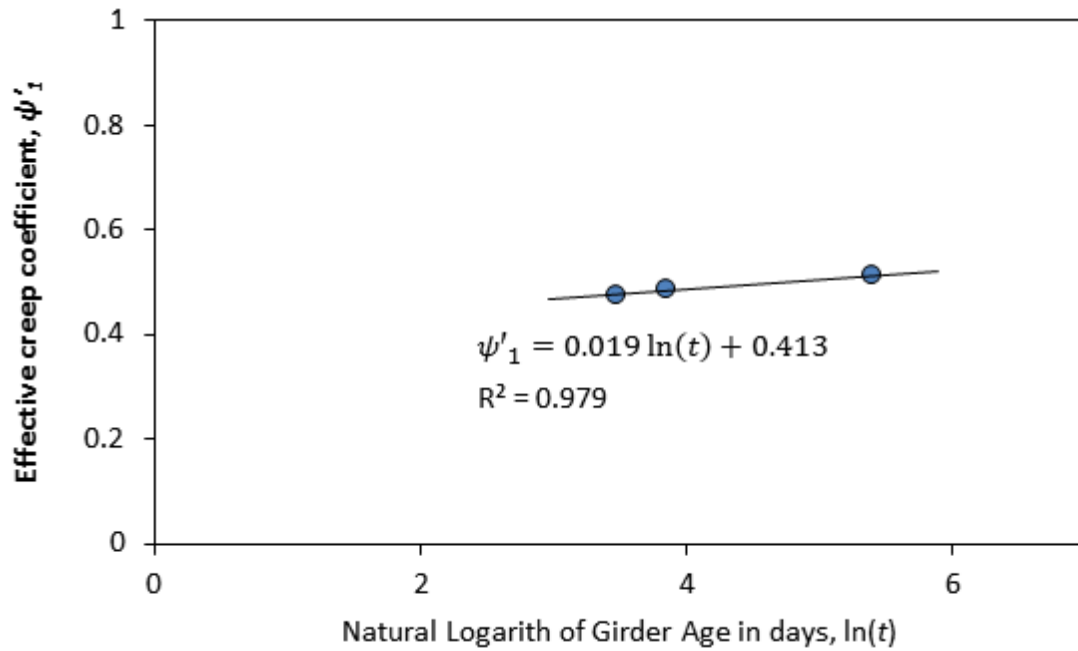


Figure B-18 Effective creep coefficient in terms of time for Girder UTPS#248 (SCC-3)

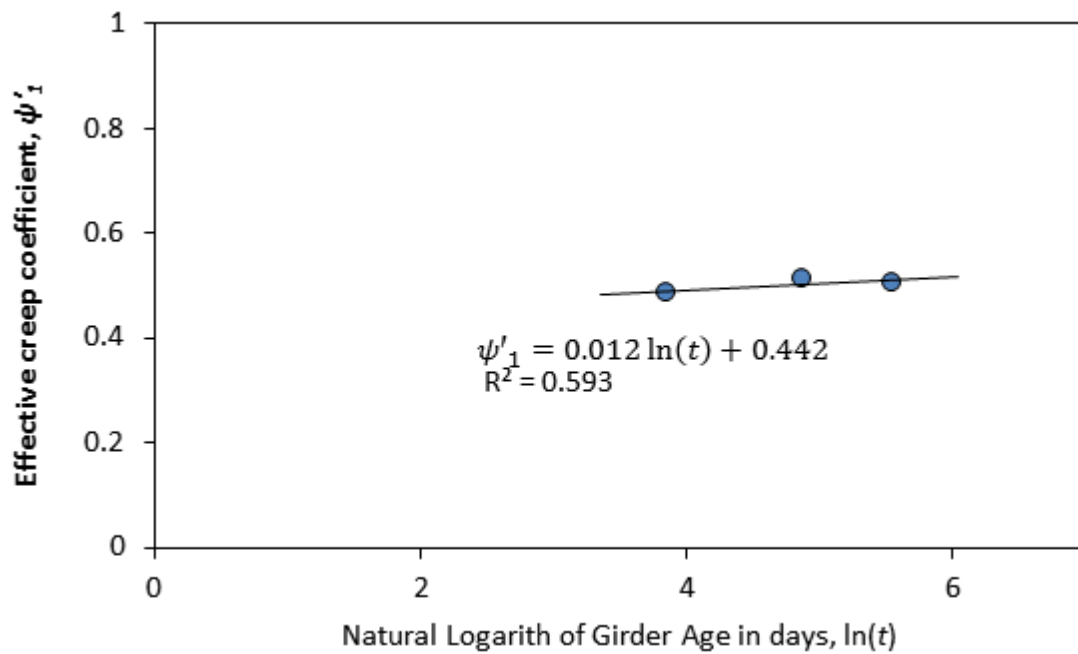
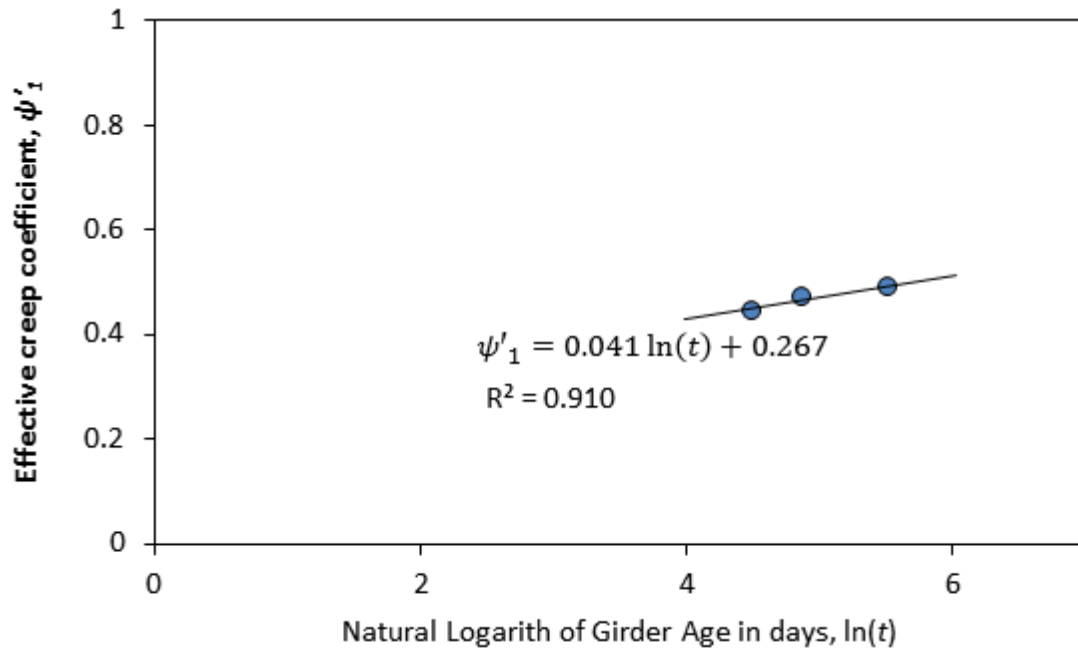


Figure B-19 Effective creep coefficient in terms of time for Girder UTPS#250 (CC-2)



**Figure B-20 Effective creep coefficient in terms of time for Girder UTPS#251 (CC-3)**

## APPENDIX C

### Alternative Procedures to Develop Simplified Expressions to Estimate Prestress Losses

In this section a series of simplistic expressions to estimate prestress losses in pretensioned simply supported bridge girders are developed using diverse approaches. Such expressions are oriented to an approximate and most simple estimation.

#### C.1 ESTIMATION BASED ON THE MEASURED PRESTRESS LOSSES VERSUS ELASTIC SHORTENING

The strain-related, prestress losses can be estimated as the summation of three types of strains: the elastic, creep, and shrinkage strains, as shown in Equation (C-1). Out of these three strain types, elastic deformation of concrete is a relatively well-known phenomenon, while creep and shrinkage are not. Moreover, creep is commonly expressed in terms of the elastic strains, shown in Equation (C-2). With the aim of a simplistic solution for the estimation of strain related prestress losses, Equation (C-2) can be further simplified. The creep due to applied loads (other than the pretensioning) is neglected, which allows for Equation (C-2) to be simplified to the form of Equation (C-3). Ignoring the creep recovery due to applied loads is conservative and introduces only a small error.

If the creep coefficients ( $\theta$ ) and the shrinkage loss ( $\Delta f_{p\_SH}$ ) are considered as fixed for a given set of conditions, then the level of simplicity of this equation is comparable to that of the early prestress losses estimation methods, such as ACI 323 (1958).



$$\Delta f_{p\_strain} = \Delta f_{p\_elastic} + \Delta f_{p\_CR} + \Delta f_{p\_SH} \quad (C-1)$$

$$\Delta f_{p\_strain} = \Delta f_{p\_ES} + \Delta f_{p\_load} + (\theta_{ES})\Delta f_{p\_ES} + (\theta_{load})\Delta f_{p\_load} + \Delta f_{p\_SH} \quad (C-2)$$

$$\Delta f_{p\_strain} = (1 + \theta_{ES})\Delta f_{p\_ES} + \Delta f_{p\_load} + \Delta f_{p\_SH} \quad (C-3)$$

While such simplistic expressions have proven to be imprecise when applied to a broad range of cases, these expressions could offer enough accuracy if calibrated correctly (i.e. using data obtained from experiments conducted in structures subjected to comparable conditions). Calibration using a set of structural elements having a small variation of some relevant parameters will lead to an expression with more consistent behavior, than calibration based on structural elements having large variation of parameters. In this sense, there are some relevant parameters that usually show small variation within prestressed pretensioned simple supported bridge girders, as presented in Chapter 6. The most relevant of this parameters are :

- *Time of Release*: Prestress forces are almost exclusively placed on a girder between 0.75 and 3 days.
- *Source of Elastic Strain*: Elastic strains caused by the prestressing force are much larger than all other elastic strains.
- *Initial Concrete Stress Ranges*: The compressive stress range in the concrete is typically within  $0.6f'_{ci}$  and  $0.7f'_{ci}$  and the tensile stress is always kept below prescribed stress limits.

The alternative approximate equation can be obtained directly from the experimental data by using measured values of  $\Delta f_{p\_ES}$ ,  $\Delta f_{p\_load}$ , and  $\Delta f_{p\_strain}$  to calibrate the values of  $\theta_{ES}$  and  $\Delta f_{p\_SH}$ , as shown in Equation (C-4). This procedure results in a constant value for the creep coefficient, and for the shrinkage induced losses; this means the effect of all parameters other than those involved in the calculation of elastic strains are neglected. While the use of a creep coefficient as a means to estimate creep in novel estimation methods has been discouraged in the literature, considering the

approximate nature of this procedure, and its resemblance with old estimation equations it is considered as the most convenient choice.

$$\Delta f_{p_{ES+CR+SH}} = \Delta f_{p_{strain}} - \Delta f_{p_{load}} = (1 + \theta_{ES})\Delta f_{p_{ES}} + \Delta f_{p_{SH}} \quad (C-4)$$

The parameters within Equation (C-4) were calibrated using the filtered database presented in Chapter 2. For calibration purposes, the value of  $\Delta f_{p_{strain}} - \Delta f_{p_{load}}$  was plotted versus  $\Delta f_{p_{ES}}$ , as shown in Figure C-1. It can be observed that the dispersion is large, but a conservative and approximate estimation of the losses can be obtained by using an equation defining the upper-bound of all the experimental data, Equation (C-5). This upper-bound expression implies  $\theta_{ES} = 1.3$  and  $\Delta f_{p_{SH}} = 8 \text{ksi}$ , values falling well within the range proposed in ACI 1958.

$$\Delta f_{p_{CR+SH}} = 2.3\Delta f_{p_{ES}} + 8 \text{ksi} \quad (C-5)$$

The conservative creep coefficient obtained here is low if compared to material testing results, which can be on the order of 2 to 3. This is a result of the different behavior of an element compared to cylinder testing.

Due to the use of experimental data, this equation should be limited in application to the ranges of variables that were well represented within the database (see Chapter 2).

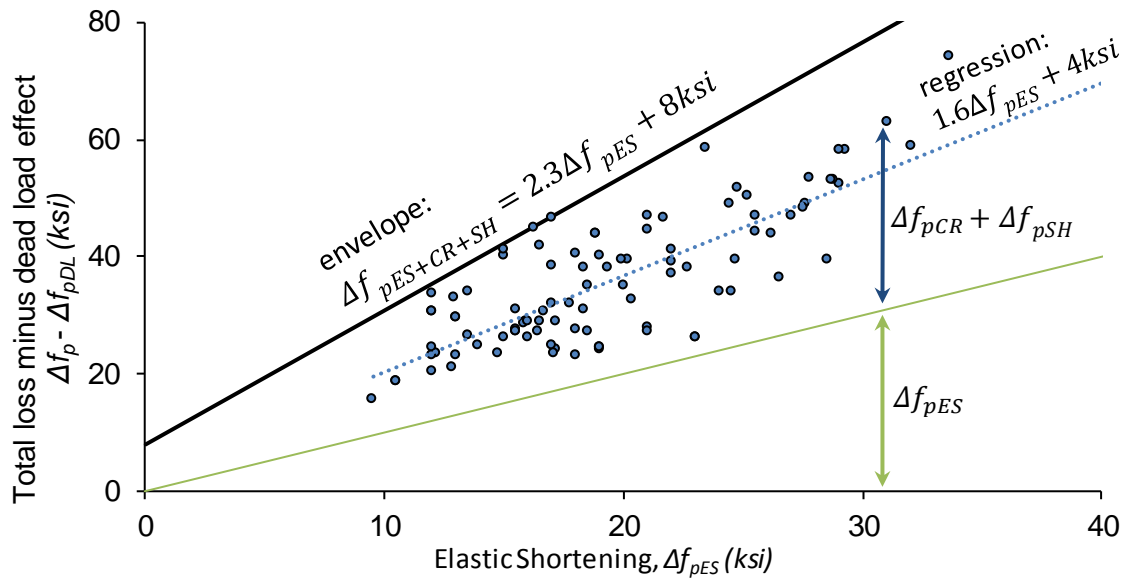


**Figure C-1 Calibration of equation based on experimental prestress losses and elastic shortening**

## C.2 ESTIMATION BASED ON SIMPLIFICATION OF EXISTING METHODS

Simplistic equations to estimate prestress losses can be obtained through the simplification of existing methods. Simplifications of the expressions contained in the PCI Design Handbook (PCI 2004), ACI 209 (ACI Committee 209 1992), and TxDOT 0-6374 (Garber, et al. 2013) are presented in this section. These methods are simple, and clearly present the basics of the elastic shortening and creep. These two phenomena are calculated in terms of (1) the stress applied to concrete and (2) the stress-strain proportionality constants for both: “elastic” and long-term strains.

For common bridge girders (pretensioned, simply-supported girders), conservative prestress loss estimations can be obtained through the use of a set of conservative, but realistic, parameter values (see Table C-1). These values were used to obtain a simplified version of code equations. Implicitly, the use of the resultant simplified equations should be limited to cases in which these set of values (as a whole) represent conservative assumptions. In the Table C-2 the nomenclature used for other parameters is presented.

**Table C-1 Set of values and categories used on prestress losses equation simplifications**

Parameter	Value used	Nomenclature used in each method		
		TxDOT 0-6374	PCI	ACI 209
Ambient Relative Humidity(%)	H= 60	H	R.H.	$\lambda$
Concrete Strength at Release	$f'_{ci} = 4 \text{ ksi}$	$f'_{ci}$	--	$f_{ci}$
Concrete Stiffness at Release	$E_{ci} = 3640 \text{ ksi}$	$E_{ci}$	$E_{ci}$	--
Modulus of Elasticity of Strand	$E_p = 28500 \text{ ksi}$	$E_p$	$E_{ps}$	$E_s$
Effect of permanent External Forces (e.g from deck weight and deck-girder interaction)	$\Delta f_{cd} = 0$	$\Delta f_{cd}$	$f_{cds}$	(Non composite behavior) <sup>1</sup>
Volume to Surface Ratio	V/S = 3 in.	--	V/S	$v/s$
Age of concrete at Release	$t_i = 1 \text{ day}$	--	--	$t_{ia}$
Curing method	Moist curing	--	--	Curing method
Curing period	$t_{curing} = 1 \text{ day}$	--	--	Moist curing duration
Coefficient Related to Restrain due to Reinforcement	$1 + n\rho\xi_s = 1.25$ (ACI-209 4.6.1)	--	--	$1 + n\rho\xi_s$

---

<sup>1</sup>Equations from Section 4.4 (ACI Committee 209, 1992) for noncomposite prestressed beams were simplified.

**Table C-2 Additional Nomenclature used on prestress losses equations for each method**

Parameter	Nomenclature used in this document	Nomenclature used in Codes		
		TxDOT 0-6374	PCI	ACI 209
Creep Coefficient at final age	$\psi$	--		$\nu_u$
Shrinkage strain at final age	$\epsilon_{SH}$			$(\epsilon_{SH})_u$
Total Prestress losses	$\Delta f_p$		TL	$\frac{\lambda_u}{100} \times f_{si}$
Initial or tensioning stress in prestressing steel	$f_{pi}$		$f_{pi}$	$f_{si}$
Initial stress in the concrete at the centroid of the strands	$f_{cgp_i}$		$f_{cir}$	$f_c$
Initial Force in strand	$P_i$	--	$P_i$	$F_i$
Ratio of Modulus of Elasticity of Strand to Modulus of Elasticity of Concrete at release	$n_i$			$n$

### C.2.1 Simplifications to TxDOT 0-6374

The main product of the project TxDOT 0-6374 was a procedure to estimate prestress losses, which include strain related losses that can be summarized using Equations (C-6), (C-7), and (C-9). These expressions are based on the AASHTO LRFD 2012 procedure, which was simplified through extensive parametric analysis and calibrated using experimental results from the comprehensive database presented in Chapter 2. The further simplification of this procedure is straight forward, and it is presented in Table C-3.

$$\Delta f_{pES} = \frac{E_p}{E_{ci}} \left[ 0.7 f_{pu} A_{ps} \left( \frac{1}{A_g} + \frac{e_p^2}{I_g} \right) - \frac{M_g e_p}{I_g} \right] \quad (C-6)$$

**Table C-3 Simplified creep induced losses for TxDOT 0-6374**

Conditions	Equation
	$\Delta f_{pCR} = 0.1 \left( \frac{195 - 60}{4.8 + 4} \right) \left( \Delta f_{pES} + 0.6 \Delta f_{cd} \frac{E_p}{E_{ci}} \right) \quad (C-7)$
H = 60, $f'_{ci} = 4 \text{ ksi}$ , $\Delta f_{cd} = 0$	$\Delta f_{pCR} = 1.5 \Delta f_{pES} \quad (C-8)$

**Table C-4 Simplified shrinkage induced losses for TxDOT 0-6374**

Conditions	Equation
	$\Delta f_{pSR} = E_p \left( \frac{140 - H}{4.8 + f'_{ci}} \right) (4.4 * 10^{-5}) \quad (C-9)$
H = 60, $E_p = 28500 \text{ ksi}$ , $f'_{ci} = 4 \text{ ksi}$	$\Delta f_{pSR} = 11 \text{ ksi} \quad (C-10)$

### C.2.2 Simplifications to ACI 209R-92 Method

The ACI report on “Prediction of Creep, Shrinkage, and Temperature Effects in Concrete Structures” (ACI Committee 209 1992) contains methods for the prestress loss. The elastic shortening losses ( $\Delta f_{pES-ACI}$ ) is calculated using Equation (C-11). Based on the values listed in Table C-1 a conservative creep coefficient and shrinkage strains (applicable to standard pretensioned bridge girders) are calculated in Table C-5 and

Table C-6, respectively, and Equations (C-12) to (C-21). The derivation of conservative expressions to estimate creep- and shrinkage-related prestress losses are presented in Table C-7 and Table C-8 respectively.

$$\Delta f_{pES-ACI} = n_i \left[ f_{pi} A_{pi} (1 - n\rho) \left( \frac{1}{A_g} + \frac{e^2}{I_g} \right) - \frac{M_D e}{I_g} \right] \quad (C-11)$$

**Table C-5 Conservative creep coefficient (ACI),  $\psi_{ACI}$**

Conditions	Equation
--	$\psi_{ACI} = v_u = 2.35 \times \gamma_{la} \times \gamma_{\lambda} \times \gamma_{vs}$ (C-12)
moist cured	$\gamma_{la} = 1.25(t_{la})^{-0.118} = 1.25$ , (C-13)
$\lambda = 60\%$	$\gamma_{\lambda} = 1.27 - 0.0067 \times \lambda = 0.868$ (C-14)
$v/s = 3 \text{ in.}$	$\gamma_{vs} = \frac{2}{3} [1 + 1.13e^{-0.54v/s}] = 0.816$ (C-15)
$\psi_{ACI} = v_u \approx 2.1$ (C-16)	

**Table C-6 Conservative shrinkage strain (ACI),  $\epsilon_{SH-ACI}$**

Conditions	Equation
--	$\epsilon_{SH-ACI} = (\epsilon_{SH})_u = 780 \times 10^{-6} \gamma_{cp} \gamma_{\lambda} \gamma_{vs}$ (C-17)
curing period=1day	$\gamma_{cp} = 1.2$ (C-18)
$\lambda = 60\%$	$\gamma_{\lambda} = 1.40 - 0.0102 \times \lambda = 0.788$ (C-19)
$v/s = 3 \text{ in.}$	$\gamma_{vs} = 1.2e^{-0.12 \times v/s} = 0.837$ (C-20)
$\epsilon_{SH-ACI} = (\epsilon_{SH})_u \approx 620 \times 10^{-6}$ (C-21)	

**Table C-7 Simplified creep-related losses for ACI-209**

Conditions	Equation
--	$\Delta f_{pCR-ACI} = \Delta f_{pES-ACI} \cdot v_u \left(1 - \frac{F_u}{2F_0}\right)$ (C-22)
$v_u = 2.1$ (Eq. (C-16)) $\frac{F_u}{F_0} = 0.18$ (ACI-209 table 4.4.1.2)	$\Delta f_{pCR-ACI} = 1.9 \Delta f_{pES-ACI}$ (C-23)

**Table C-8 Simplified shrinkage-related losses for ACI-209**

Conditions	Equation
--	$\Delta f_{pSH-ACI} = (\varepsilon_{sh})_u \frac{E_s}{1 + n\rho\xi_s} \quad (C-24)$
$(\varepsilon_{sh})_u = 620 \times 10^{-6}$ (Eq. (C-21)) $1 + n\rho\xi_s = 1.25$ (design simplification ACI 209 4.6- Example)	$\Delta f_{pSH-ACI} = 14ksi \quad (C-25)$

### C.2.3 Simplifications to PCI Method

The PCI Design Handbook (PCI 2004) contains a method to estimate prestress losses based on a document sponsored by ACI-ASCE committee 423 (Zia, et al. 1979). The equations to calculate the strain-related prestress losses for pretensioned member based on the PCI Design Handbook are discussed in this section.

The equation to calculate elastic shortening losses ( $\Delta f_{pES-PCI}$ ) is presented in Equation (C-26). The derivation of a conservative expression to estimate total creep- and shrinkage-related prestress losses are presented in Table C-9 and Table C-10 (Equations (C-27) to (C-30)).

$$\Delta f_{pES} = \frac{E_{ps}}{E_{ci}} \left[ 0.9A_p f_{pi} \left( \frac{1}{A_g} + \frac{e^2}{I_g} \right) - \frac{M_g e}{I_g} \right] \quad (C-26)$$

**Table C-9 Simplified creep induced loss for PCI Design Handbook**

Conditions	Equation
Pretensioned girder	$\Delta f_{pCR} = 2 \frac{E_{ps}}{E_{c_28}} (f_{cir} - f_{cds}) \quad (C-27)$
$f_{cds} = 0, E_{c_28} = 1.25E_{ci}$	$\Delta f_{pCR-PCI} = 1.6\Delta f_{pES} \quad (C-28)$



**Table C-10 Simplified shrinkage induced loss for PCI Design Handbook**

Conditions	Equation
Pretensioned girder	$\Delta f_{p_{SH}} = 8.2 \times 10^{-6} E_{ps} (1 - 0.06 v/s) (100 - RH)$ <span style="float: right;">(C-29)</span>
$v/s = 3 \text{ in.}, E_{ps} = 28500 \text{ ksi}, RH = 60$	$\Delta f_{p_{SH-PCI}} = 8 \text{ ksi}$ <span style="float: right;">(C-30)</span>

**C.3 RECOMMENDED APPROXIMATE METHOD TO ESTIMATE PRESTRESS LOSSES.**

The various methods presented above lead to the equations shown in Table C-11. It is important to mention that the direct comparison of the coefficients multiplying the elastic shortening to obtain the creep loss is not an exact method of comparison, because the elastic shortening is calculated different for each method. Considering that the differences in calculated elastic shortening are rather small, the ratio of creep losses to elastic shortening is considered a good comparison parameter. Moreover, expressing the creep in terms of elastic shortening is necessary to allow the comparison with the results from experimental methods. These coefficients are presented in Figure C-2 and Figure C-3. The estimation of the elastic shortening is conducted here using the equation proposed during TxDOT 6374 as listed in Table C-11. The format presented here is different from that presented in (Garber, et al. 2013), but it is the same equation if  $f_{pi}/f_{pu} = 0.75$ .

**Table C-11 Summary of equations for simplified method to estimate losses**

Method	Elastic Shortening, $\Delta f_{pES}$	Creep, $\Delta f_{pCR}$	Shrinkage, $\Delta f_{pSH}$
Experimental Prestress Losses vs. Elastic Shortening	--	$1.3 \Delta f_{pES}$	8 ksi
6374_s	$n_i \left[ 0.93 A_p f_{pi} \left( \frac{1}{A_g} + \frac{e^2}{I_g} \right) - \frac{M_g e}{I_g} \right]$	$1.5 \Delta f_{pES}$	11 ksi
ACI 209_s	$n_i \left[ (1 - n\rho) A_p f_{pi} \left( \frac{1}{A_g} + \frac{e^2}{I_g} \right) - \frac{M_g e}{I_g} \right]$	$1.9 \Delta f_{pES}$	14 ksi
PCI_s	$n_i \left[ 0.9 A_p f_{pi} \left( \frac{1}{A_g} + \frac{e^2}{I_g} \right) - \frac{M_g e}{I_g} \right]$	$1.6 \Delta f_{pES}$	8 ksi

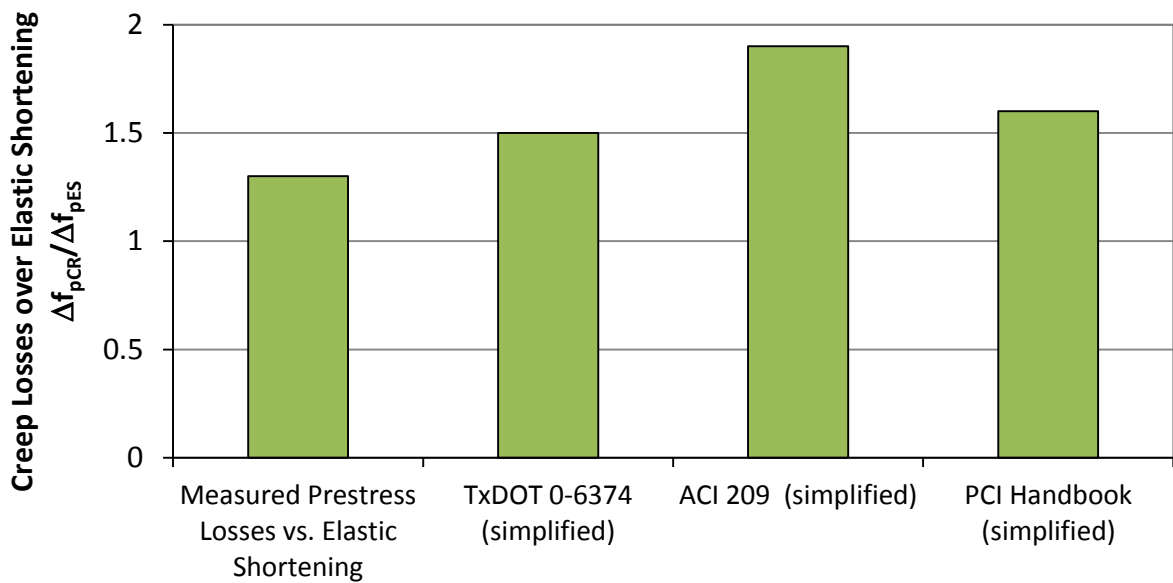


**Figure C-2 Ratio of Creep Losses to Elastic Shortening for Proposed Simplistic Methods**

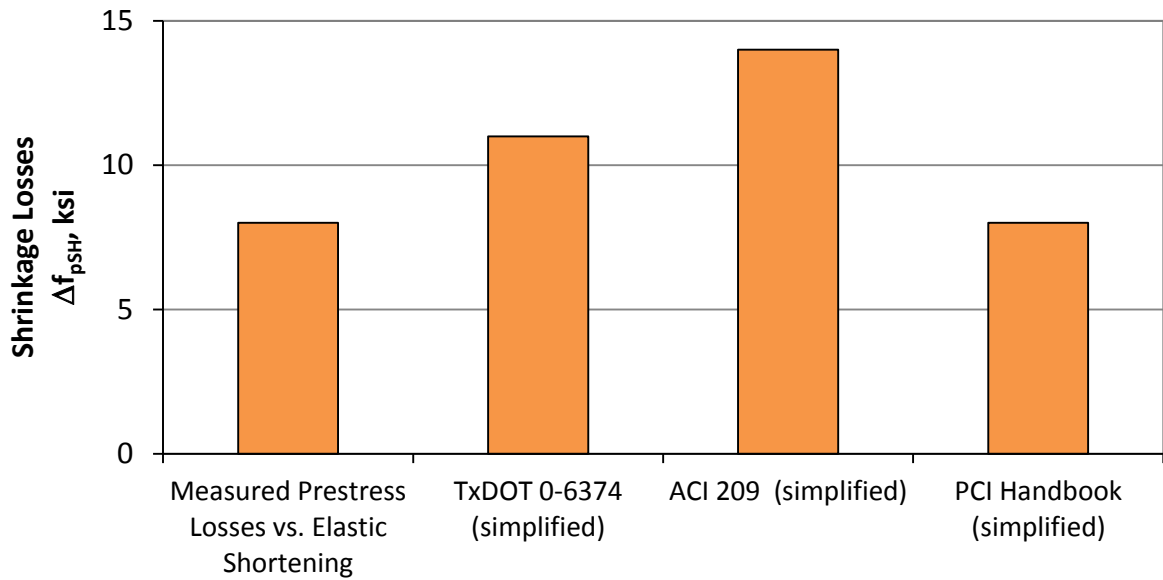


**Figure C-3 Shrinkage losses for Proposed Simplistic Methods**

The difference in coefficients between the methods is not significant when considering the variability in the material behavior. The coefficient of variation of creep strain estimations presented in the literature are in the range of 20% to 30% ( (Keitel and Dimmig-Osburg 2010), (Bazant and Baweja, Creep and shrinkage prediction model for analysis and design of concrete structures: Model B3 2000)), making the limiting values for 95% confidence roughly  $\pm 50\%$ . In view of the above, it is considered reasonable to round the proposed creep coefficient to the nearest 0.5. Since most of the methods fall near 1.5, the creep coefficient of  $\psi' = 1.5$  seems to be adequate. Using the same logic, a shrinkage-related loss of  $\Delta f_{pSH} = 10 \text{ ksi}$  is proposed. With these coefficients, the proposed method to estimate strain related prestress losses is presented in (C-31). Other type of losses (e.g. relaxation) should be added to this loss during design.

$$\Delta f_{p-s} = 2.5 \Delta f_{pES} + 10 \text{ ksi} \quad (\text{C-31})$$

The proposed method is evaluated based on its performance on estimating the measured losses for the specimens from the evaluation database (96 specimens), using

the measured elastic shortening as input. It can be observed in Figure C-4 that the expression results in conservative estimation, with low variability (COV =20%).

An evaluation of the performance of the expression based on measured material properties would indicate the performance of the complete method. The calculation of the elastic shortening is based on TxDOT 6374 method. The results of these estimations are presented in Figure C-5, further statistics related to the performance of the method are presented. Based on the statistics of the results, it is considered that the method can satisfactorily estimate prestress losses of pretensioned, simple-supported girders with precision comparable to currently used methods.

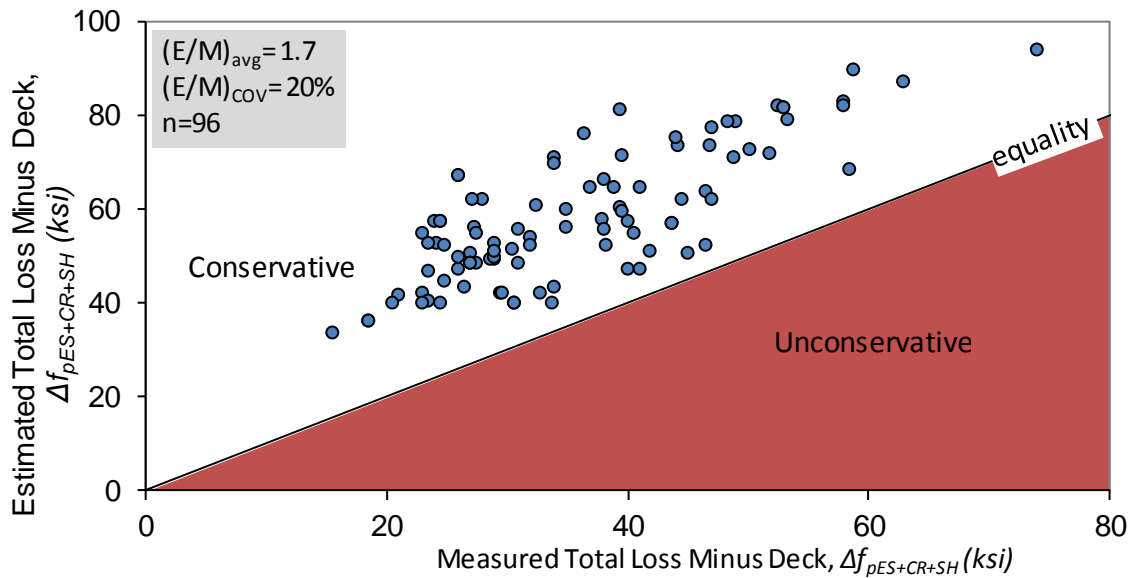


**Figure C-4 Estimated vs. Measured Total Prestress losses (deck weight effect not included). Estimation using proposed simplified equation & measured elastic shortening.**

**Table C-12 Statistics for the ratio of estimated to measured strain related losses for the proposed Simplified method**

Estimated/Measured Ratio	Proposed Simplified
Max	2.3
Average	1.6
Min	0.84
unconservative cases	2%
COV	21%

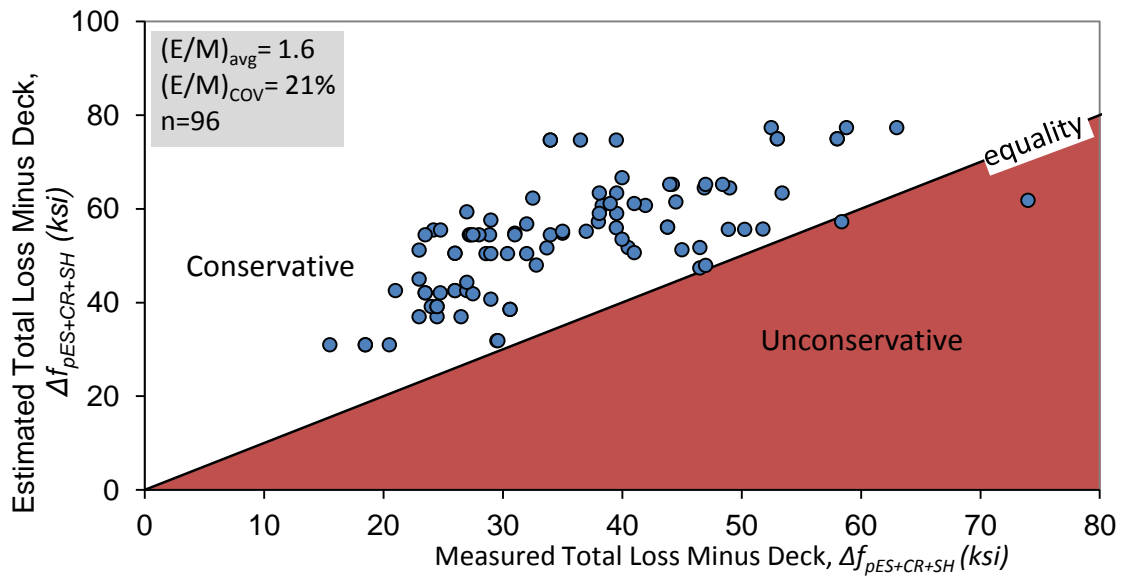


**Figure C-5 Estimated vs Measured Total Prestress losses (deck weight effect not included). The estimations are based on measured concrete strength and modulus of elasticity when reported.**

## APPENDIX D

### Database Specimen Information

#### D.1 OVERVIEW

In this appendix the bibliographies for all of the references contained in the collection database are first presented. Also, a select number of important variables were chosen to be reported for all of the specimens contained in the evaluation database.

#### D.2 COLLECTION DATABASE REFERENCES

- Barr, P., Eberhard, M., Stanton, J., Khaleghi, B., & Hsieh, J. C. (2000). *High Performance Concrete in Washington State SR18/SR516 Overcrossing: Final Report on Girder Monitoring*. Seattle: Washington Stat Transportation Center.
- Birrcer, D. B. (2006). *Effects of Increasing the Allowable Compressive Stress at Release of Prestressed Concrete Girders*. Austin: The University of Texas at Austin.
- Brewe, J. E., & Myers, J. J. (2009). Shear Behavior of Reduced Modulus Prestressed High-Strength Self-Consolidating Concrete (HS-SCC) Members Subjected to Elevated Concrete Fiber Stresses. *PCI/NBC*, 1-17.
- Brewe, J. E., & Myers, J. J. (2011). High-strength self-consolidating concrete girders subjected to elevated compressive fiber stresses, part 2: Structural behavior. *PCI Journal*, 92-109.
- Canfield, S. R. (2005). *Full Scale Testing of Prestressed, High Performance Concrete, Composite Bridge Girders*. Atlanta: Georgia Institute of Technology.
- Erkman, B., Shield, C. K., & French, C. E. (2007). Time-Dependent Behavior of Full-Scale Self-Consolidating Concrete Precast Prestressed Girders. *ACI SP-247-12*, 139-153.
- Gamble, W. L. (1970). *Field Investigation of a Continuous Composite Prestressed I-Beam Highway Bridge Located in Jefferson County, Illinois*. Urbana: University of Illinois.
- Gamble, W. L. (1979). *Long-Term Behavior of a Prestressed I-Girder Highway Bridge in Champaign County, Illinois*. Urbana-Champaign: University of Illinois.
- Gross, S. P., & Burns, N. H. (2000). *Field Performance of Prestressed High Performance Concrete Highway Bridges in Texas*. Austin: Texas Department of Transportation.

- Gross, S. P., Yost, J. R., & Gaynor, E. (2007). Experimental Study of Prestress Land and Camber in High-Strength SCC Beams. *ACI SP-247-7*, 77-91.
- Hale, W. M., & Russell, B. W. (2006). Effect of Allowable Compressive Stress at Release on Prestress Losses and on the Performance of Precast, Prestressed Concrete Bridge Girders. *PCI Journal*, 14-25.
- Hodges, H. T. (2006). *Top Strand Effect and Evaluation of Effective Prestress in Prestressed Concrete Beams*. Blacksburg: Virginia Polytechnic Institute and State University.
- Houdeshell, D. M., Anderson, T. C., & Gamble, W. L. (1972). *Field Investigation of a Prestressed Concrete Highway Bridge Located in Douglas County, Illinois*. Urbana: University of Illinois.
- Idriss, R. L., & Solano, A. (2002). Effects of Steam Curing Temperature on Early Prestress Losses in High-Performance Concrete Beams. *Transportation Research Record*, 218-228.
- Labia, Y., Saiidi, M. S., & Douglas, B. (1997). Full-Scale Testing and Analysis of 20-Year-Old Pretensioned Concrete Box Girders. *ACI Structural Journal*, 471-492.
- Larson, K. H. (2006). *Evaluating the Time-Dependent Deformations and Bond Characteristics of a Self-Consolidating Concrete Mix and the Implication for Pretensioned Bridge Applications*. Manhattan, Kansas: Kansas State University.
- Naito, C., Sause, R., & Thompson, B. (2008). Investigation of Damaged 12-Year Old Prestressed Concrete Box Beams. *Journal of Bridge Engineering*, 139-148.
- Nassar, A. J. (2002). *Investigation of Transfer Length, Development Length, Flexural Strength and Prestress Loss Trend in Fully Bonded High Strength Lightweight Prestressed Girders*. Blacksburg: Virginia Polytechnic Institute and State University.
- Ozyildirim, C. (2008). *Bulb-T Beams with Self Consolidating Concrete on the Route 33 Bridge Over the Pamunkey River in Virginia*. Charlottesville: Virginia Transportation Research Council.
- Pessiki, S., Kaczinski, M., & Wescott, H. H. (1996). Evaluation of Effective Prestress Force in 28-Year-Old Prestressed Concrete Bridge Beams. *PCI Journal*, 78-89.
- Roller, J. J., Russell, H. G., Bruce, R. N., & Alaywan, W. R. (Winter 2011). Evaluation of prestress losses in high-strength concrete bulb-tee girders for the Rigolets Pass Bridge. *PCI Journal*, 110 - 134.
- Roller, J. J., Russell, H. G., Bruce, R. N., & Martin, B. T. (1995). Long-Term Performance of Prestressed, Pretensioned High Strength Concrete Bridge Girders. *PCI Journal*, 48-59.
- Ruiz, E. D., Staton, B. W., Do, N. H., & Hale, W. M. (2007). Prestress Losses in Beams Cast with Self-Consolidating Concrete. *ACI SP-247-8*, 93-104.

- Schnittker, B. A. (2008). *Allowable Compressive Stress at Prestress Transfer*. Austin: The University of Texas at Austin.
- Shenoy, C. V., & Frantz, G. C. (1991). Structural Tests of 27-Year-Old Prestressed Bridge Beams. *PCI Journal*, 80-90.
- Smith, M., Shield, C., Eriksson, W., & French, C. (2007). Field and Laboratory Study of the Mn/DOT Precast Slab Span System. *Mid-Continent Transportation Research Symposium*, 1-13.
- Tadros, M. K., Al-Omaishi, N., Seguirant, S. J., & Galt, J. G. (2003). *Prestress Losses in High-Strength Concrete Bridge Girders*. Washington, D.C.: National Cooperative Highway Research Program.
- Yang, Y., & Myers, J. J. (2005). Prestress Loss Measurements in Missouri's First Fully Instrumented High-Performance Concrete Bridge. *Transportation Research Record: Journal of the Transportation Research Board*, 118-125.



### D.3 EVALUATION DATABASE

The following details are presented in Table D-1 for the specimens in the Evaluation Database:

$h$	= beam height (in.)
$A_g$	= area of gross section (in. <sup>2</sup> )
$I_g$	= moment of inertia of gross section (in. <sup>4</sup> )
$f'_{ci}$	= compressive strength of concrete at release (ksi)
$f'_c$	= compressive strength of concrete at 28 days (ksi)
$A_{ps}$	= total prestressing strand area (in. <sup>2</sup> )
$y_p$	= distance from extreme compression fiber to centroid of prestressing strands (in.)
$E_p$	= modulus of prestressing tendons (ksi)
$f_{pi}$	= stress in prestressing steel immediately prior to transfer (ksi)
$RH$	= average relative humidity (%)
$t_f$	= age of concrete at time of final loss measurement (days)
$\Delta f_{pT}$	= total measured prestress loss (ksi)

**Table D-1 – Evaluation Database (1 of 9)**

Beam ID	Section Type	h (in.)	A <sub>g</sub> (in. <sup>2</sup> )	I <sub>g</sub> (in. <sup>4</sup> )	f' <sub>ci</sub> (ksi)	f' <sub>c</sub> (ksi)	A <sub>ps</sub> (in. <sup>2</sup> )	Y <sub>p</sub> (in.)	E <sub>p</sub> (ksi)	f <sub>pi</sub> (ksi)	Deck?	RH (%)	t <sub>f</sub> (days)	Δf <sub>pT</sub> (ksi)
Garber, et al. (2013)														
I-1	Type C	40.0	494.4	82602	7.0	10.8	5.8	6.63	28800	202.9	No	49	979	46
I-2	Type C	40.0	494.4	82602	7.0	10.8	5.8	6.63	28800	202.9	No	65	939	49
I-3	Type C	40.0	494.4	82602	7.0	10.8	5.8	6.63	28800	202.9	No	65	948	46
I-4	Type C	40.0	494.4	82602	7.0	10.8	5.8	6.63	28800	202.9	No	65	962	41
I-5	Type C	40.0	494.4	82602	7.0	10.8	5.8	6.63	28800	202.9	No	49	976	51
I-6	Type C	40.0	494.4	82602	7.0	10.8	5.8	6.63	28800	202.9	No	49	975	56
I-7	Type C	40.0	494.4	82602	7.0	10.8	5.8	6.63	28800	202.9	No	65	946	49
I-8	Type C	40.0	494.4	82602	7.0	10.8	5.8	6.63	28800	202.9	No	65	966	50
II-1	Type C	40.0	494.4	82602	6.6	11.6	5.8	6.63	29400	203.0	No	49	954	32
II-2	Type C	40.0	494.4	82602	6.6	11.6	5.8	6.63	29400	203.0	No	65	922	39
II-3	Type C	40.0	494.4	82602	6.6	11.6	5.8	6.63	29400	203.0	No	65	932	34
II-4	Type C	40.0	494.4	82602	6.6	11.6	5.8	6.63	29400	203.0	No	65	936	32
II-5	Type C	40.0	494.4	82602	6.6	11.6	5.8	6.63	29400	203.0	No	49	953	24
II-6	Type C	40.0	494.4	82602	6.6	11.6	5.8	6.63	29400	203.0	No	49	951	36
II-7	Type C	40.0	494.4	82602	6.6	11.6	5.8	6.63	29400	203.0	No	65	937	24
II-8	Type C	40.0	494.4	82602	6.6	11.6	5.8	6.63	29400	203.0	No	65	923	33
III-1	Tx46	46.0	761.0	198089	6.6	9.6	8.9	6.43	28800	209.0	No	45	693	58
III-2	Tx46	46.0	761.0	198089	6.6	9.6	8.9	6.43	28800	209.0	No	65	988	54

**Table D-1 – Evaluation Database (2 of 9)**

Beam ID	Section Type	h (in.)	A <sub>g</sub> (in. <sup>2</sup> )	I <sub>g</sub> (in. <sup>4</sup> )	f' <sub>ci</sub> (ksi)	f' <sub>c</sub> (ksi)	A <sub>ps</sub> (in. <sup>2</sup> )	Y <sub>p</sub> (in.)	E <sub>p</sub> (ksi)	f <sub>pi</sub> (ksi)	Deck?	RH (%)	t <sub>f</sub> (days)	Δf <sub>pT</sub> (ksi)
<i>Garber, et al. (2013)</i>														
III-3	Tx46	46.0	761.0	198089	6.6	9.6	8.9	6.43	28800	209.0	No	65	676	54
III-4	Tx46	46.0	761.0	198089	6.6	9.6	8.9	6.43	28800	209.0	No	65	674	54
III-5	Tx46	46.0	761.0	198089	6.6	9.6	8.9	6.43	28800	209.0	No	45	699	58
III-6	Tx46	46.0	761.0	198089	6.6	9.6	8.9	6.43	28800	209.0	No	65	686	56
III-7	Tx46	46.0	761.0	198089	6.6	9.6	8.9	6.43	28800	209.0	No	65	680	53
III-8	Tx46	46.0	761.0	198089	6.6	9.6	8.9	6.43	28800	209.0	No	45	699	54
IV-SCC-1	Tx46	46.0	761.0	198089	6.3	11.5	8.6	6.64	28800	202.5	No	65	130	43
IV-SCC-2	Tx46	46.0	761.0	198089	6.3	11.5	8.6	6.64	28800	202.5	No	65	258	42
IV-SCC-3	Tx46	46.0	761.0	198089	6.3	11.5	8.6	6.64	28800	202.5	No	65	220	43
IV-CC-1	Tx46	46.0	761.0	198089	6.9	11.6	8.6	6.64	28800	202.5	No	65	203	39
IV-CC-2	Tx46	46.0	761.0	198089	6.9	11.6	8.6	6.64	28800	202.5	No	65	256	38
IV-CC-3	Tx46	46.0	761.0	198089	6.9	11.6	8.6	6.64	28800	202.5	No	65	250	40
<i>Barr, Eberhard, Stanton, Khalegh and Hsieh (2000)</i>														
1A	Bulb-T	73.5	752.2	546571	7.8	10.0	3.0	3.00	28500	202.5	Yes	80	1095	29
1C	Bulb-T	73.5	752.2	546571	7.8	10.0	3.0	3.00	28500	202.5	Yes	80	1095	31
2A	Bulb-T	73.5	752.2	546571	8.0	11.4	8.7	3.37	28500	202.5	Yes	80	1095	58
2B	Bulb-T	73.5	752.2	546571	7.6	11.4	8.7	3.37	28500	202.5	Yes	80	1095	49
2C	Bulb-T	73.5	752.2	546571	7.6	11.4	8.7	3.37	28500	202.5	Yes	80	1095	61

**Table D-1 – Evaluation Database (3 of 9)**

Beam ID	Section Type	h (in.)	Ag (in.2)	Ig (in.4)	f'ci (ksi)	f'c (ksi)	Aps (in.2)	yp (in.)	Ep (ksi)	fpi (ksi)	Deck?	RH (%)	tf (days)	ΔfpT (ksi)
Birrcher (2006)														
A55-T25	I-Beam	28.0	275.4	22658	5.5	8.3	2.1	4.00	28500	202.5	No	70	28	34
A60-T26	I-Beam	28.0	275.4	22658	5.0	7.8	2.1	4.00	28500	202.5	No	70	29	31
A63-T27	I-Beam	28.0	275.4	22658	4.8	8.5	2.1	4.00	28500	202.5	No	70	28	32
A66-T28	I-Beam	28.0	275.4	22658	4.6	9.6	2.1	4.00	28500	202.5	No	70	28	33
A67-T29	I-Beam	28.0	275.4	22658	4.5	7.1	2.1	4.00	28500	202.5	No	70	28	38
A66-T30	I-Beam	28.0	275.4	22658	4.5	8.1	2.1	4.00	28500	202.5	No	70	28	43
A69-T31	I-Beam	28.0	275.4	22658	4.3	7.7	2.1	4.00	28500	202.5	No	70	28	39
A68-T32	I-Beam	28.0	275.4	22658	4.4	7.8	2.1	4.00	28500	202.5	No	70	28	46
A67-T33	I-Beam	28.0	275.4	22658	4.5	8.4	2.1	4.00	28500	202.5	No	70	29	32
Canfield (2005)														
BT-56	Bulb-T	56.3	717.5	312529	10.4	14.3	9.5	9.05	29682	205.4	Yes	70	182	40
TYPE IV	I-Beam	54.6	795.1	271606	11.7	14.6	11.3	7.37	29682	205.4	Yes	70	161	35
Erkman, Shield, French (2007)														
A-SCC1	Bulb-T	36.0	570.0	93528	8.2	8.7	6.1	6.90	28600	202.5	No	70	325	40
A-CM	Bulb-T	36.0	570.0	93528	11.1	11.6	6.1	6.90	28600	202.5	No	70	325	31
B-SCC1	Bulb-T	36.0	570.0	93528	7.8	10.9	6.1	6.90	29000	202.5	No	70	80	33
B-SCC2	Bulb-T	36.0	570.0	93528	7.7	11.0	6.1	6.90	29000	202.5	No	70	82	35
B-CM	Bulb-T	36.0	570.0	93528	9.4	13.7	6.1	6.90	29000	202.5	No	70	82	31

**Table D-1 – Evaluation Database (4 of 9)**

Beam ID	Section Type	h (in.)	A <sub>g</sub> (in. <sup>2</sup> )	I <sub>g</sub> (in. <sup>4</sup> )	f' <sub>ci</sub> (ksi)	f' <sub>c</sub> (ksi)	A <sub>ps</sub> (in. <sup>2</sup> )	Y <sub>p</sub> (in.)	E <sub>p</sub> (ksi)	f <sub>pi</sub> (ksi)	Deck?	RH (%)	t <sub>f</sub> (days)	Δf <sub>pT</sub> (ksi)
<i>Gamble (1970)</i>														
BX-1	I-Beam	48.0	524.0	147800	4.2	5.5	4.3	3.74	27000	170.0	Yes	70	1220	28
<i>Gamble (1979)</i>														
BX-5	I-Beam	42.0	464.5	90956	5.6	6.6	2.6	9.0	27750	158.1	Yes	70	367	19
BX-6	I-Beam	42.0	464.5	90956	5.6	6.6	2.6	9.0	27750	158.1	Yes	70	367	19
<i>Gross and Burns (2000)</i>														
N32	U-Beam	54.0	1025	380420	10.5	13.6	13.9	3.82	28500	202.5	Yes	75	761	43
S15	U-Beam	54.0	1025	380420	11.0	14.3	13.9	3.82	28500	202.5	Yes	75	748	38
S16	U-Beam	54.0	1121	404230	8.7	13.3	14.8	4.46	28500	202.5	Yes	75	1262	40
S25	U-Beam	54.0	1121	404230	10.3	13.4	14.8	4.46	28500	202.5	Yes	75	1221	34
E13	I-Beam	54.0	789.0	260400	10.8	13.7	18.2	11.1	28500	202.5	Yes	57	422	51
E14	I-Beam	54.0	789.0	260400	10.8	13.7	18.2	11.1	28500	202.5	Yes	57	422	28
E24	I-Beam	54.0	789.0	260400	13.1	14.2	14.3	7.0	28500	202.5	Yes	57	404	51
E25	I-Beam	54.0	789.0	260400	9.8	14.8	14.3	7.0	28500	202.5	Yes	57	746	52
E34	I-Beam	54.0	789.0	260400	12.4	13.8	18.2	11.1	28500	202.5	Yes	57	316	57
E35	I-Beam	54.0	789.0	260400	11.3	14.5	18.2	11.1	28500	202.5	Yes	57	309	58
E44	I-Beam	54.0	789.0	260400	9.4	14.6	17.4	10.0	28500	202.5	Yes	57	305	56
W14	I-Beam	54.0	789.0	260400	8.6	10.1	8.0	5.62	28500	202.5	Yes	57	771	35
W15	I-Beam	54.0	789.0	260400	8.6	10.1	8.0	5.62	28500	202.5	Yes	57	771	34

**Table D-1 – Evaluation Database (5 of 9)**

Beam ID	Section Type	h (in.)	A <sub>g</sub> (in. <sup>2</sup> )	I <sub>g</sub> (in. <sup>4</sup> )	f' <sub>ci</sub> (ksi)	f' <sub>c</sub> (ksi)	A <sub>ps</sub> (in. <sup>2</sup> )	Y <sub>p</sub> (in.)	E <sub>p</sub> (ksi)	f <sub>pi</sub> (ksi)	Deck?	RH (%)	t <sub>f</sub> (days)	Δf <sub>pT</sub> (ksi)
<i>Gross and Burns (2000), continued</i>														
W16	I-Beam	54.0	789.0	260400	8.6	10.1	8.0	5.62	28500	202.5	Yes	57	771	33
W17	I-Beam	54.0	789.0	260400	8.1	10.3	8.0	5.62	28500	202.5	Yes	57	766	30
<i>Hale and Russell (2006)</i>														
Girder 1	Bulb-T	24.0	163.3	12400	8.7	11.1	2.2	6.45	28500	204.3	No	60	360	53
Girder 3	Bulb-T	24.0	163.3	12400	6.1	8.4	1.7	7.06	28500	200.8	No	60	360	58
Girder 4	Bulb-T	24.0	163.3	12400	8.7	11.1	1.7	5.81	28500	204.5	No	60	360	52
<i>Houdeshell, Anderson, Gamble (1972)</i>														
BX-3	I-Beam	48.0	569.8	144117	4.9	5.1	4.1	5.95	27700	169.3	Yes	70	784	32
BX-4	I-Beam	48.0	569.8	144117	4.9	5.1	4.1	5.95	27700	169.3	Yes	70	784	29
<i>Idriss and Solano (2008)</i>														
AC	Bulb-T	63.0	713.0	392638	8.0	9.1	6.4	6.00	27000	215.7	Yes	50	374	34
AW	Bulb-T	63.0	713.0	392638	8.0	9.1	6.4	6.00	27000	215.7	Yes	50	374	29
BC	Bulb-T	63.0	713.0	392638	8.0	9.1	6.4	6.00	27000	215.7	Yes	50	374	29
BW	Bulb-T	63.0	713.0	392638	8.0	9.1	6.4	6.00	27000	215.7	Yes	50	374	30
<i>Larson (2006)</i>														
A3	I-Beam	45.0	525.0	127490	5.6	5.9	2.4	7.75	28500	202.5	Yes	65	330	20
B3	I-Beam	45.0	525.0	127490	5.6	5.9	2.4	7.75	28500	202.5	Yes	65	330	18
B1	I-Beam	45.0	525.0	127490	5.6	5.9	2.4	7.75	28500	202.5	Yes	65	330	15

**Table D-1 – Evaluation Database (6 of 9)**

Beam ID	Section Type	h (in.)	A <sub>g</sub> (in. <sup>2</sup> )	I <sub>g</sub> (in. <sup>4</sup> )	f' <sub>ci</sub> (ksi)	f' <sub>c</sub> (ksi)	A <sub>ps</sub> (in. <sup>2</sup> )	Y <sub>p</sub> (in.)	E <sub>p</sub> (ksi)	f <sub>pi</sub> (ksi)	Deck?	RH (%)	t <sub>f</sub> (days)	Δf <sub>pT</sub> (ksi)
<i>Larson (2006), continued</i>														
C3	I-Beam	45.0	525.0	127490	5.6	5.9	2.4	7.75	28500	202.5	Yes	65	330	18
E3	I-Beam	45.0	525.0	127490	5.0	5.6	2.4	7.75	28500	202.5	Yes	65	330	23
D3	I-Beam	45.0	525.0	127490	5.0	5.6	2.4	7.75	28500	202.5	Yes	65	330	23
E3	I-Beam	45.0	525.0	127490	5.0	5.6	2.4	7.75	28500	202.5	Yes	65	330	26
<i>Nassar (2002)</i>														
LW-4	I-Beam	54.0	789.0	260730	4.8	6.4	6.1	7.20	28500	205.0	No	70	266	46
<i>Pessiki, Kacqinski, Wescott (1996)</i>														
3-J	I-Beam	60.0	848.0	355800	5.1	8.8	5.4	5.60	28500	200.9	No	70	10227	39
4-J	I-Beam	60.0	848.0	355800	5.1	8.2	5.4	5.60	28500	200.9	No	70	10227	34
<i>Roller, Russell, Bruce, Martin (1995)</i>														
Girder 3	Bulb-T	54.0	659.0	268077	8.9	9.9	4.6	3.60	30000	202.5	Yes	75	529	23
<i>Roller, Russell, Bruce, Alaywan (2011)</i>														
43 A	Bulb-T	78.0	1105	935586	9.3	10.9	12.2	7.46	27950	202.5	Yes	75	800	23
43 B	Bulb-T	78.0	1105	935586	9.3	10.9	12.2	7.46	27950	202.5	Yes	75	800	23
43 C	Bulb-T	78.0	1105	935586	9.3	10.9	12.2	7.46	27950	202.5	Yes	75	800	23
43 D	Bulb-T	78.0	1105	935586	9.3	10.9	12.2	7.46	27950	202.5	Yes	75	800	24
<i>Schnittker (2008)</i>														
CA-60-1	I-Beam	40.0	494.9	82602	4.5	10.5	4.0	5.23	29000	202.5	No	70	57	35

**Table D-1 – Evaluation Database (7 of 9)**

Beam ID	Section Type	h (in.)	A <sub>g</sub> (in. <sup>2</sup> )	I <sub>g</sub> (in. <sup>4</sup> )	f' <sub>ci</sub> (ksi)	f' <sub>c</sub> (ksi)	A <sub>ps</sub> (in. <sup>2</sup> )	Y <sub>p</sub> (in.)	E <sub>p</sub> (ksi)	f <sub>pi</sub> (ksi)	Deck?	RH (%)	t <sub>f</sub> (days)	Δf <sub>pT</sub> (ksi)
<i>Schnittker (2008), continued</i>														
CA-60-2	I-Beam	40.0	494.9	82602	4.5	10.7	4.0	5.23	29000	202.5	No	70	62	33
CA-60-3	I-Beam	40.0	494.9	82602	4.5	11.1	4.0	5.23	29000	202.5	No	70	70	36
CA-65-1	I-Beam	40.0	494.9	82602	4.4	10.2	4.0	5.23	29000	202.5	No	70	70	36
CA-65-2	I-Beam	40.0	494.9	82602	4.4	11.2	4.0	5.23	29000	202.5	No	70	87	42
CA-65-3	I-Beam	40.0	494.9	82602	4.3	11.4	4.0	5.23	29000	202.5	No	70	49	33
CA-65-4	I-Beam	40.0	494.9	82602	4.3	11.5	4.0	5.23	29000	202.5	No	70	93	38
CA-65-5	I-Beam	40.0	494.9	82602	4.3	11.8	4.0	5.23	29000	202.5	No	70	98	37
CA-65-6	I-Beam	40.0	494.9	82602	4.3	11.9	4.0	5.23	29000	202.5	No	70	100	40
CD-70-1	I-Beam	40.0	494.9	82602	5.6	11.0	5.5	6.00	29000	202.5	No	70	29	42
CD-70-2	I-Beam	40.0	494.9	82602	5.5	11.6	5.5	6.00	29000	202.5	No	70	34	41
CD-65-1	I-Beam	40.0	494.9	82602	5.7	9.6	5.5	6.00	29000	202.5	No	70	38	39
CD-65-2	I-Beam	40.0	494.9	82602	5.7	9.6	5.5	6.00	29000	202.5	No	70	42	49
CD-65-3	I-Beam	40.0	494.9	82602	5.7	9.6	5.5	6.00	29000	202.5	No	70	45	47
CD-65-4	I-Beam	40.0	494.9	82602	5.9	10.7	5.5	6.00	29000	202.5	No	70	41	49
CD-65-5	I-Beam	40.0	494.9	82602	5.9	11.2	5.5	6.00	29000	202.5	No	70	46	35
CD-65-6	I-Beam	40.0	494.9	82602	5.9	11.4	5.5	6.00	29000	202.5	No	70	48	41
CD-60-1	I-Beam	40.0	494.9	82602	6.3	11.7	5.5	6.00	29000	202.5	No	70	54	41
CD-60-2	I-Beam	40.0	494.9	82602	6.3	12.0	5.5	6.00	29000	202.5	No	70	61	38



**Table D-1 – Evaluation Database (8 of 9)**

Beam ID	Section Type	h (in.)	A <sub>g</sub> (in. <sup>2</sup> )	I <sub>g</sub> (in. <sup>4</sup> )	f' <sub>ci</sub> (ksi)	f' <sub>c</sub> (ksi)	A <sub>ps</sub> (in. <sup>2</sup> )	Y <sub>p</sub> (in.)	E <sub>p</sub> (ksi)	f <sub>pi</sub> (ksi)	Deck?	RH (%)	t <sub>f</sub> (days)	Δf <sub>pT</sub> (ksi)
<i>Schnittker (2008), continued</i>														
CD-60-3	I-Beam	40.0	494.9	82602	6.3	12.4	5.5	6.00	29000	202.5	No	70	69	43
CC-65-1	I-Beam	40.0	494.9	82602	6.0	11.1	5.5	6.00	29000	202.5	No	70	64	49
CC-65-2	I-Beam	40.0	494.9	82602	6.0	11.2	5.5	6.00	29000	202.5	No	70	68	43
CC-65-3	I-Beam	40.0	494.9	82602	6.1	11.2	5.5	6.00	29000	202.5	No	70	69	51
CC-65-4	I-Beam	40.0	494.9	82602	6.1	11.5	5.5	6.00	29000	202.5	No	70	76	52
CC-65-5	I-Beam	40.0	494.9	82602	6.4	11.5	5.5	6.00	29000	202.5	No	70	77	44
CC-65-6	I-Beam	40.0	494.9	82602	6.3	11.5	5.5	6.00	29000	202.5	No	70	78	42
CC-60-1	I-Beam	40.0	494.9	82602	6.4	10.8	5.5	6.00	29000	202.5	No	70	72	56
CC-60-2	I-Beam	40.0	494.9	82602	6.4	10.8	5.5	6.00	29000	202.5	No	70	77	56
CC-60-3	I-Beam	40.0	494.9	82602	6.4	10.8	5.5	6.00	29000	202.5	No	70	78	47
BB-01	Box-Beam	28.0	678.8	68745	4.1	11.3	4.6	3.17	29000	202.5	No	70	28	46
BB-02	Box-Beam	28.0	678.8	68745	4.1	11.3	4.6	3.17	29000	202.5	No	70	28	43
BB-06	Box-Beam	28.0	678.8	68745	4.1	9.5	4.6	3.17	29000	202.5	No	70	38	57
BB-07	Box-Beam	28.0	678.8	68745	4.1	9.6	4.6	3.17	29000	202.5	No	70	43	65
BB-08	Box-Beam	28.0	678.8	68745	4.0	8.7	4.6	3.17	29000	202.5	No	70	29	57
BB-09	Box-Beam	28.0	678.8	68745	4.0	8.9	4.6	3.17	29000	202.5	No	70	30	56
BB-10	Box-Beam	28.0	678.8	68745	4.0	9.7	4.6	3.17	29000	202.5	No	70	35	57

**Table D-1 – Evaluation Database (9 of 9)**

Beam ID	Section Type	h (in.)	A <sub>g</sub> (in. <sup>2</sup> )	I <sub>g</sub> (in. <sup>4</sup> )	f' <sub>ci</sub> (ksi)	f' <sub>c</sub> (ksi)	A <sub>ps</sub> (in. <sup>2</sup> )	Y <sub>p</sub> (in.)	E <sub>p</sub> (ksi)	f <sub>pi</sub> (ksi)	Deck?	RH (%)	t <sub>f</sub> (days)	Δf <sub>pT</sub> (ksi)
<i>Tadros, Al-Omaishi, Seguirant, Gallt (2003)</i>														
IW2-1	Bulb-T	78.7	903.8	790592	6.3	9.0	8.6	4.50	28800	202.5	Yes	65	470	30
IW2-2	Bulb-T	78.7	903.8	790592	6.3	9.0	8.6	4.50	28800	202.5	Yes	65	469	34
G3	Bulb-T	55.1	857.2	351968	5.8	10.1	8.7	5.56	28800	202.8	Yes	70	490	42
G4	Bulb-T	55.1	857.2	351968	5.8	10.1	8.7	5.56	28800	202.8	Yes	70	490	41
G7	U-Beam	54.0	1121	404230	7.2	10.7	13.9	3.47	28800	202.3	Yes	70	400	24
G18	Bulb-T	82.6	972.0	956329	7.5	10.3	13.0	5.00	28800	202.5	Yes	80	380	40
G18	Bulb-T	82.6	972.0	956329	7.5	10.3	13.0	5.00	28800	202.5	Yes	80	380	38
<i>Yang and Myers (2005)</i>														
B13	I-Beam	32.0	311.0	33255	10.5	11.7	3.9	4.22	28000	202.5	Yes	70	275	38
B14	I-Beam	32.0	311.0	33255	10.5	11.7	3.9	4.22	28000	202.5	Yes	70	275	39
B14	I-Beam	32.0	311.0	33255	9.8	12.8	4.3	4.00	28000	202.5	Yes	70	275	39
B14	I-Beam	32.0	311.0	33255	9.8	12.8	4.3	4.00	28000	202.5	Yes	70	275	38

## APPENDIX E

### Sectional Creep and Shrinkage Coefficients

In this appendix the plots used for the determination of sectional creep and shrinkage coefficients (sectional CR&SH coefficients) are presented. The estimation of the sectional creep and shrinkage coefficient is conducted for the time before deck casting, as detailed in Section 6.3.3.

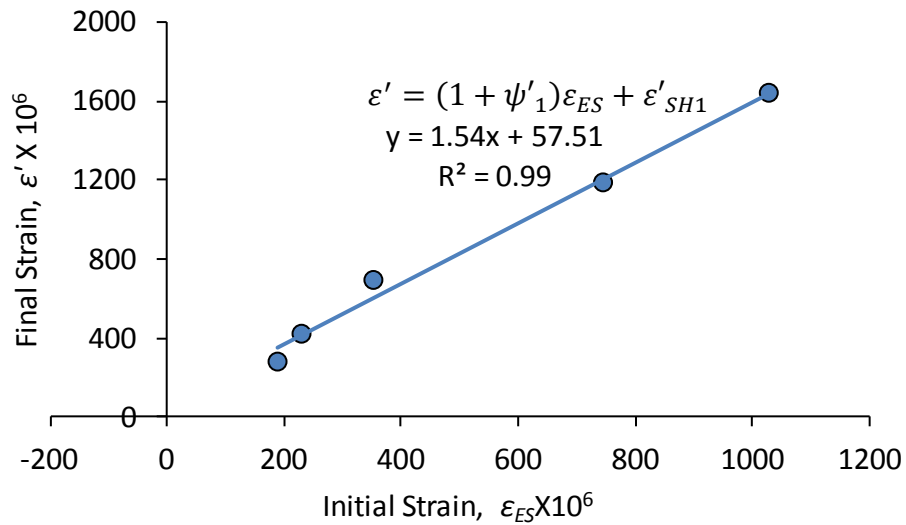
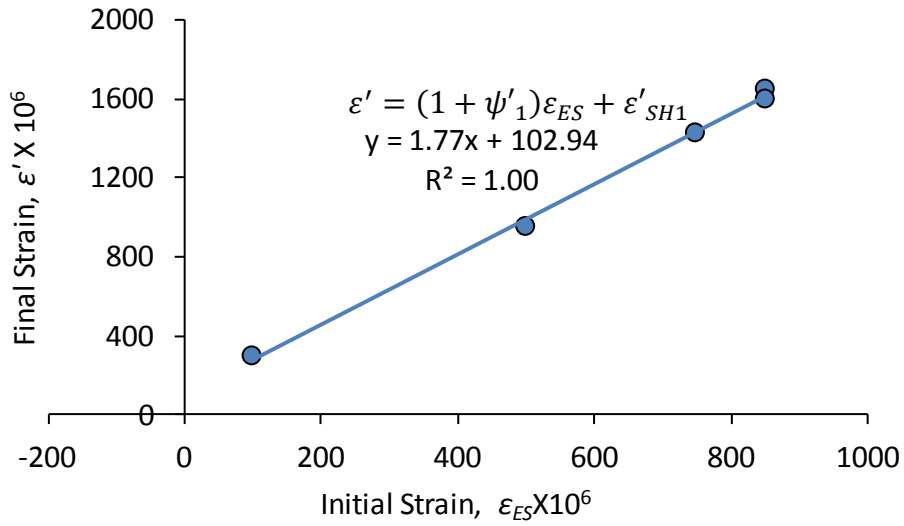
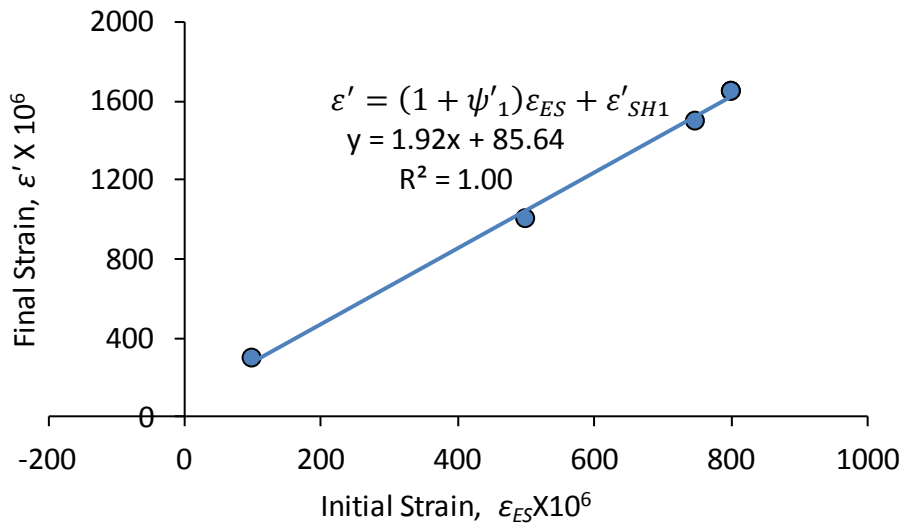


Figure E-1 Sectional CR&SH Coefficients Set 1: Girder UTPS#4 (2B)



**Figure E-2 Sectional CR&SH Coefficients Set 1: Girder UTPS#56 (A-SCC1)**



**Figure E-3 Sectional CR&SH Coefficients Set 1: Girder UTPS#57 (A-SCC2)**

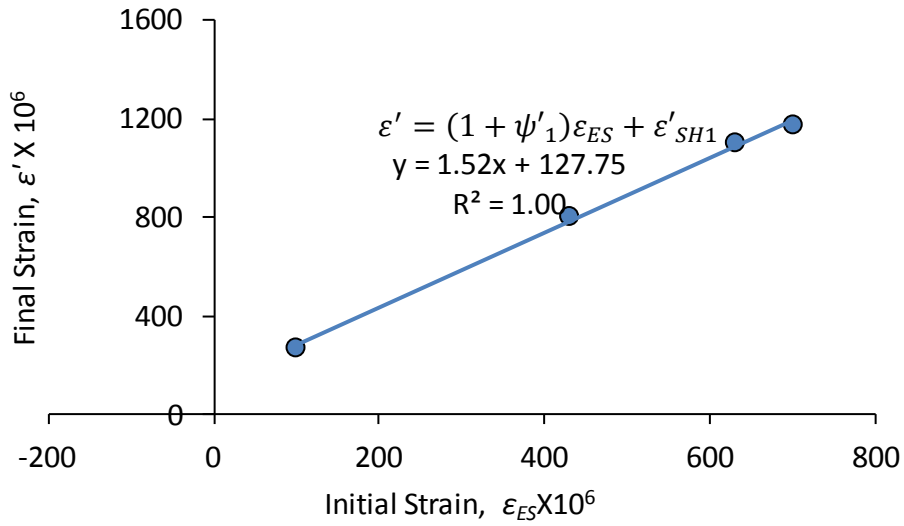


**Figure E-4 Sectional CR&SH Coefficients Set 1: Girder UTPS#58 (A-CM)**

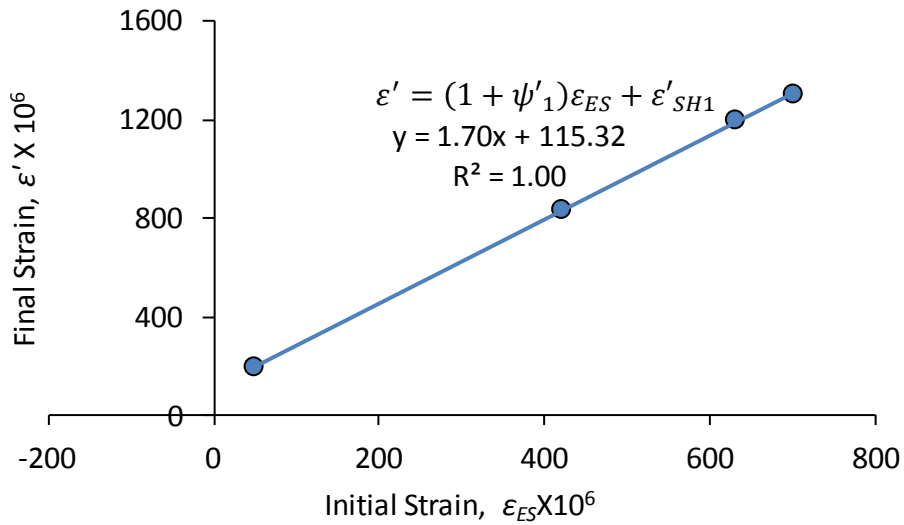


**Figure E-5 Sectional CR&SH Coefficients Set 1: Girder UTPS#59 (B-SCC1)**

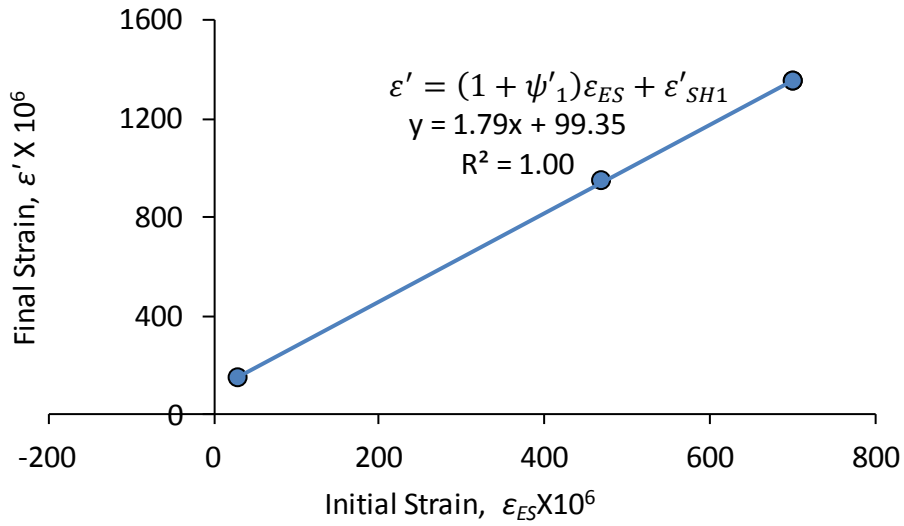


**Figure E-6 Sectional CR&SH Coefficients Set 1: Girder UTPS#60 (B-SCC2)**

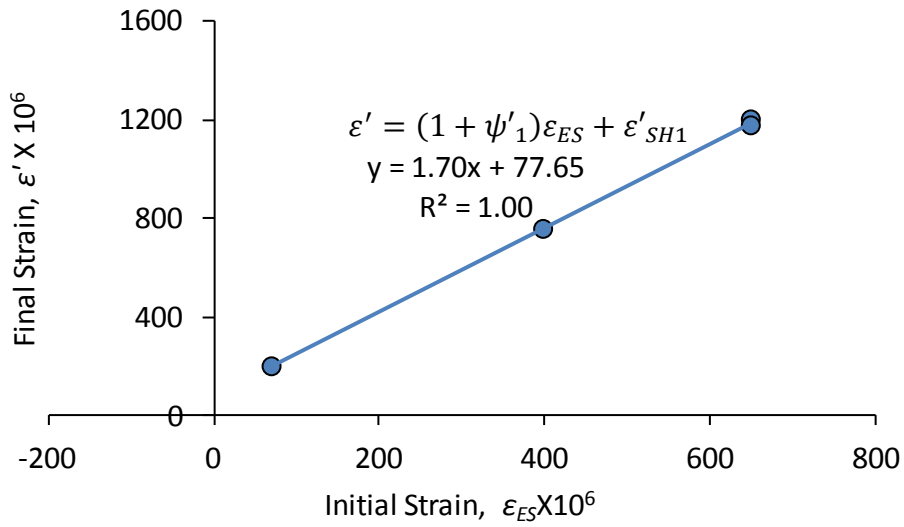


**Figure E-7 Sectional CR&SH Coefficients Set 1: Girder UTPS#61 (B-CM)**

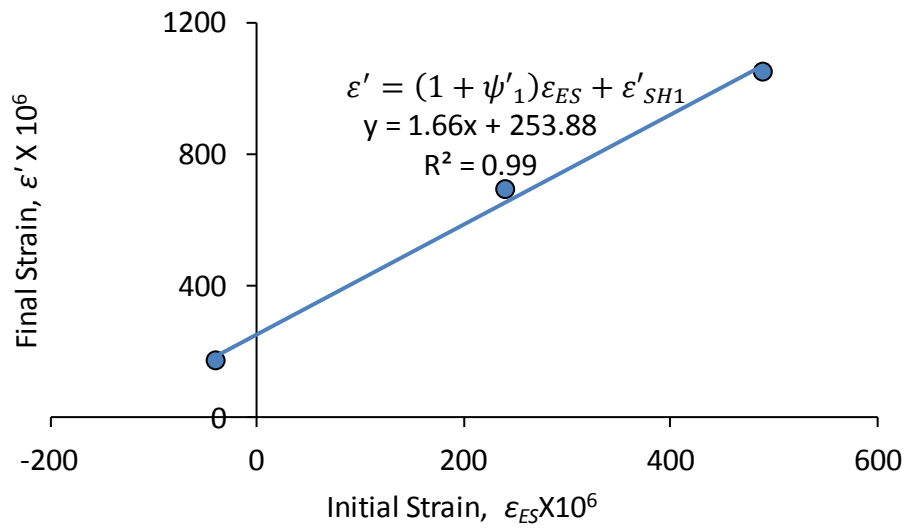


**Figure E-8 Sectional CR&SH Coefficients Set 1: Girder UTPS#62 (BX-1)**

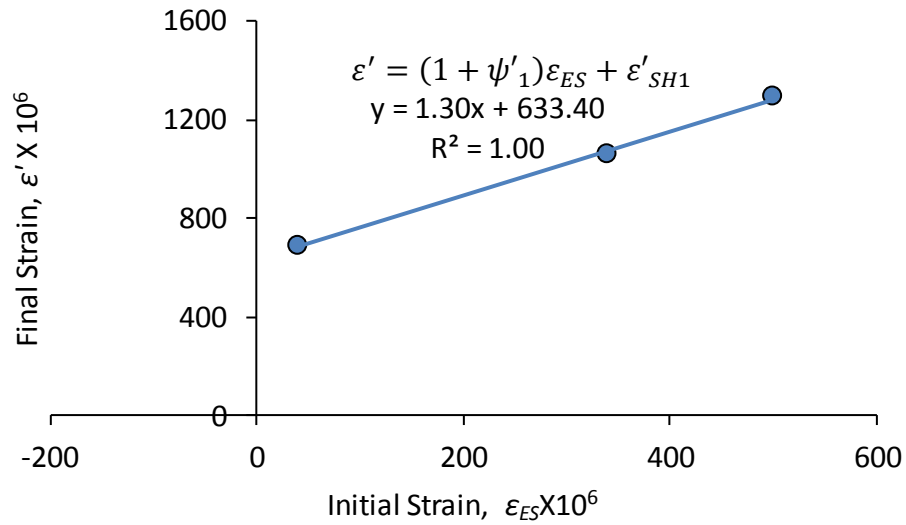


**Figure E-9 Sectional CR&SH Coefficients Set 1: Girder UTPS#105 (BX-3)**

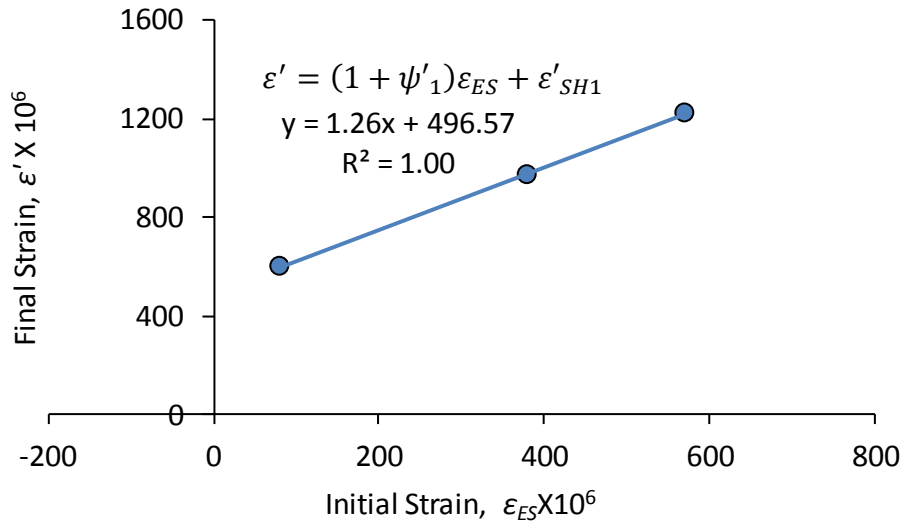


**Figure E-10 Sectional CR&SH Coefficients Set 1: Girder UTPS#106 (BX-4)**

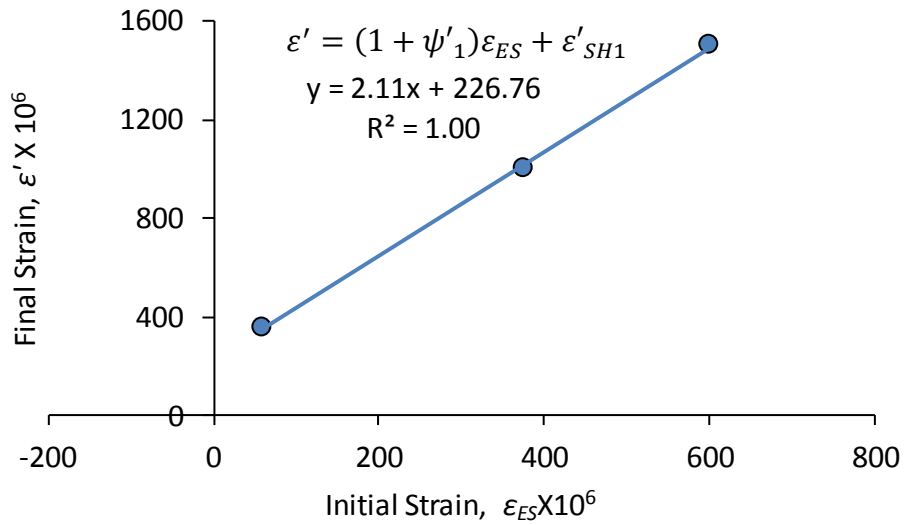


**Figure E-11 Sectional CR&SH Coefficients Set 1: Girder UTPS#119 (FT#1)**



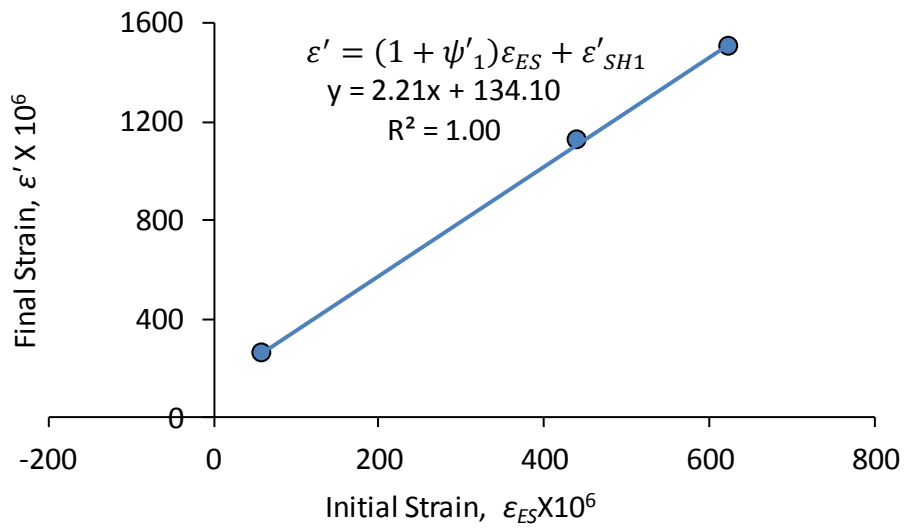


**Figure E-12 Sectional CR&SH Coefficients Set 1: Girder UTPS#120 (FT#2)**

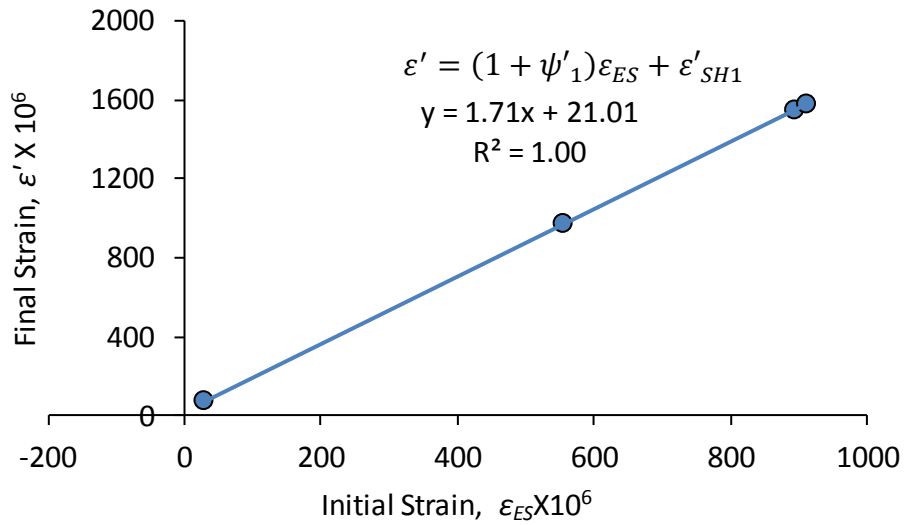


**Figure E-13 Sectional CR&SH Coefficients Set 1: Girder UTPS#222 (A1)**

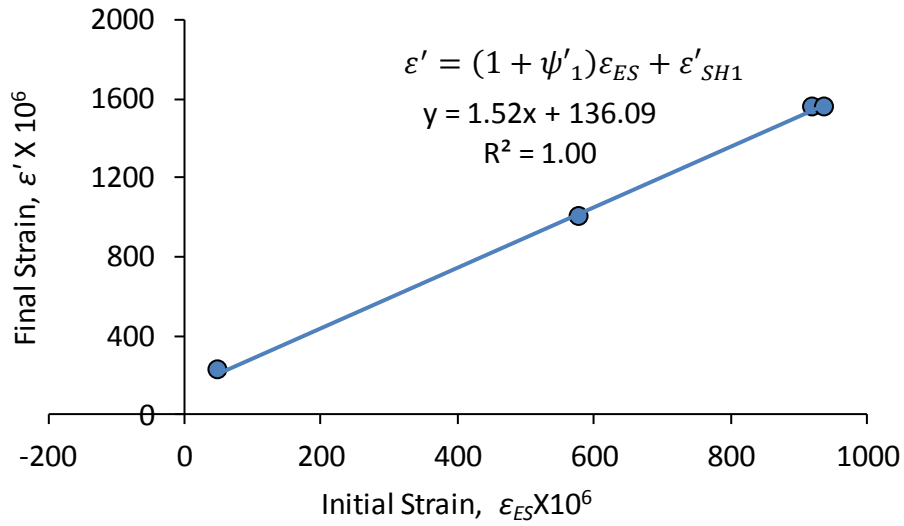


**Figure E-14 Sectional CR&SH Coefficients Set 1: Girder UTPS#224 (A3)**

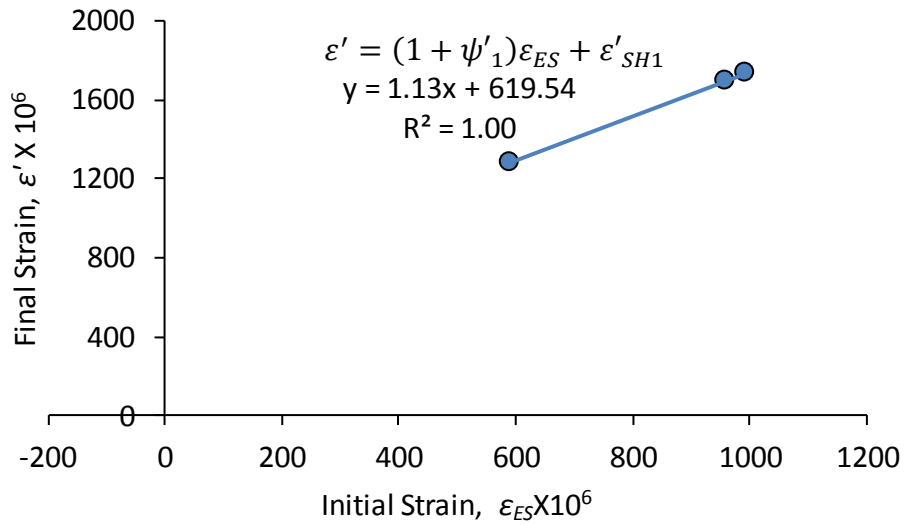


**Figure E-15 Sectional CR&SH Coefficients Set 1: Girder UTPS#226 (A5)**

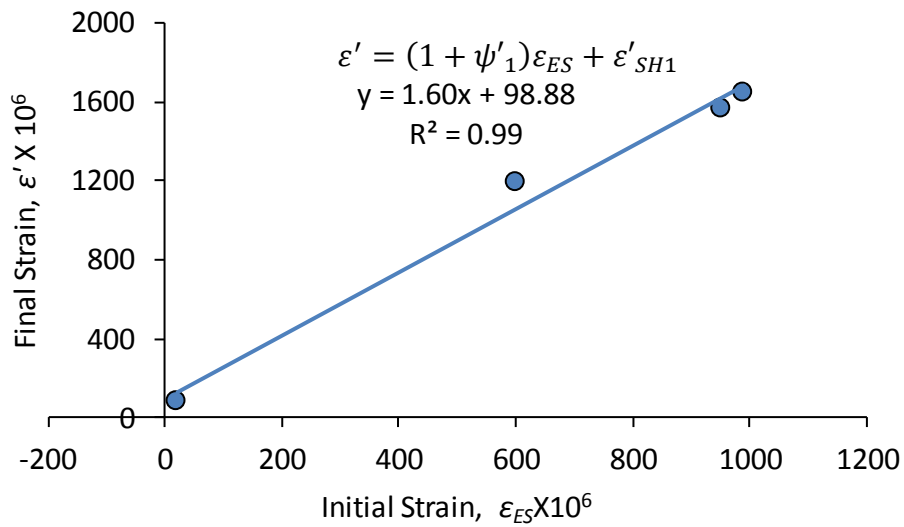


**Figure E-16 Sectional CR&SH Coefficients Set 1: Girder UTPS#228 (A7)**

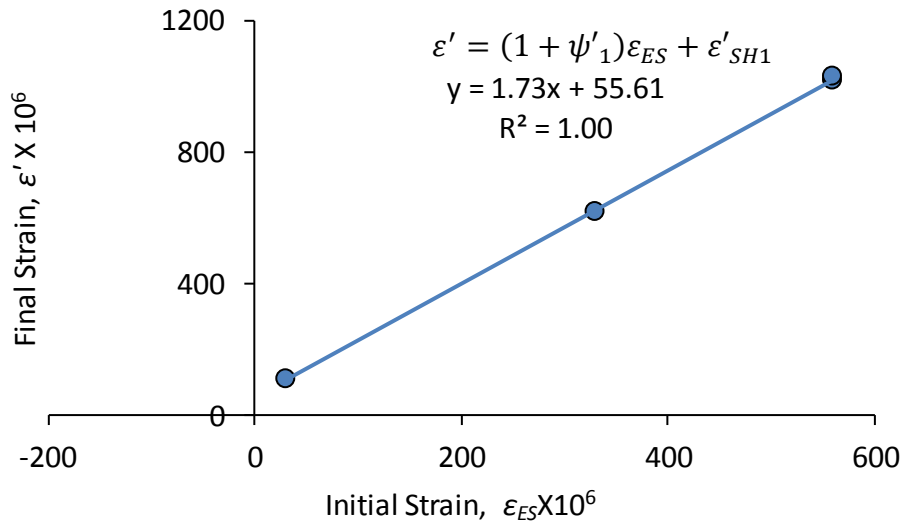


**Figure E-17 Sectional CR&SH Coefficients Set 1: Girder UTPS#230 (E1)**

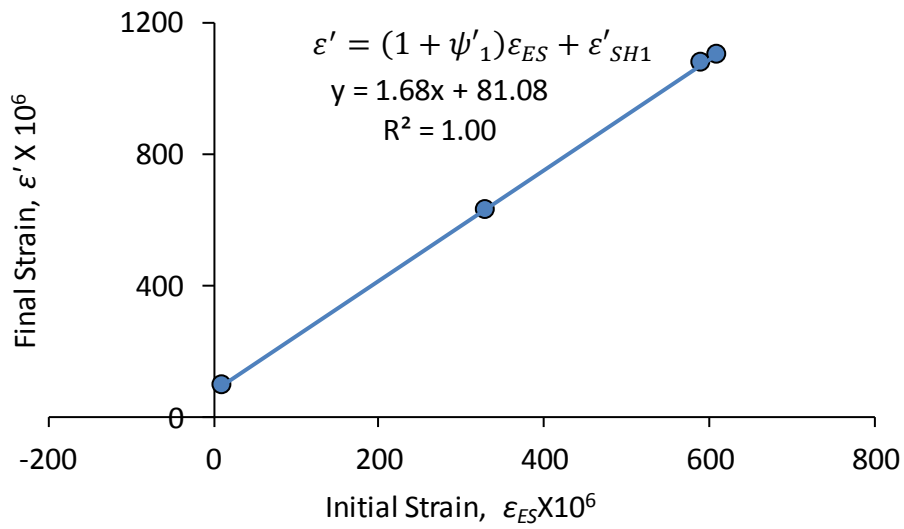


**Figure E-18 Sectional CR&SH Coefficients Set 1: Girder UTPS#232 (E3)**

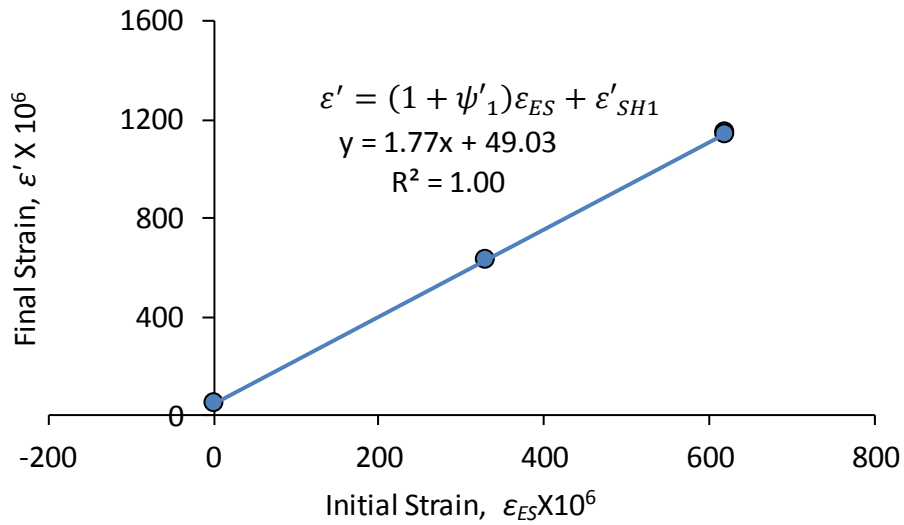


**Figure E-19 Sectional CR&SH Coefficients Set 1: Girder UTPS#235 (E6)**

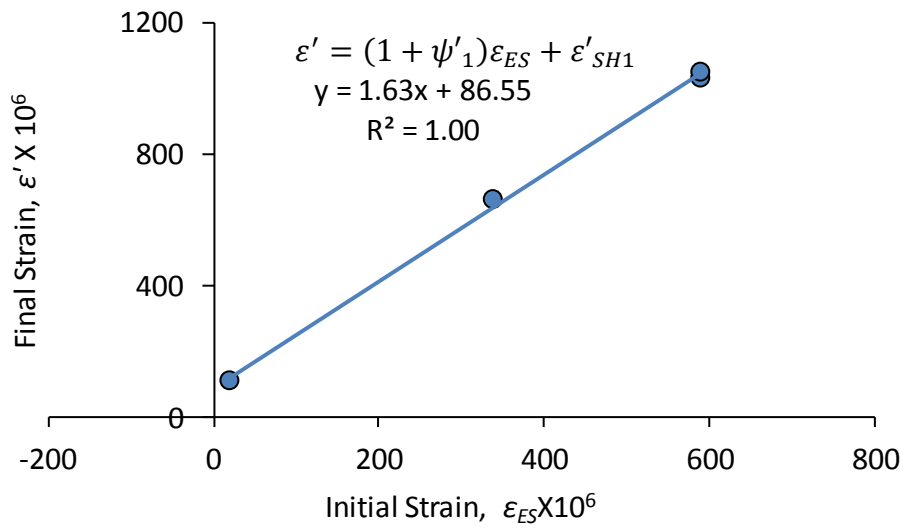


**Figure E-20 Sectional CR&SH Coefficients Set 1: Girder UTPS#237 (E8)**

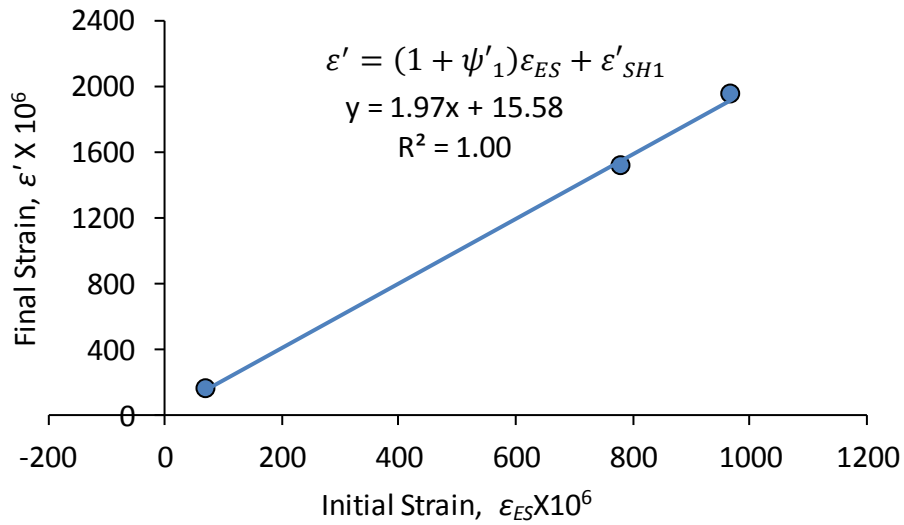


**Figure E-21 Sectional CR&SH Coefficients Set 1: Girder UTPS#238 (Q1)**

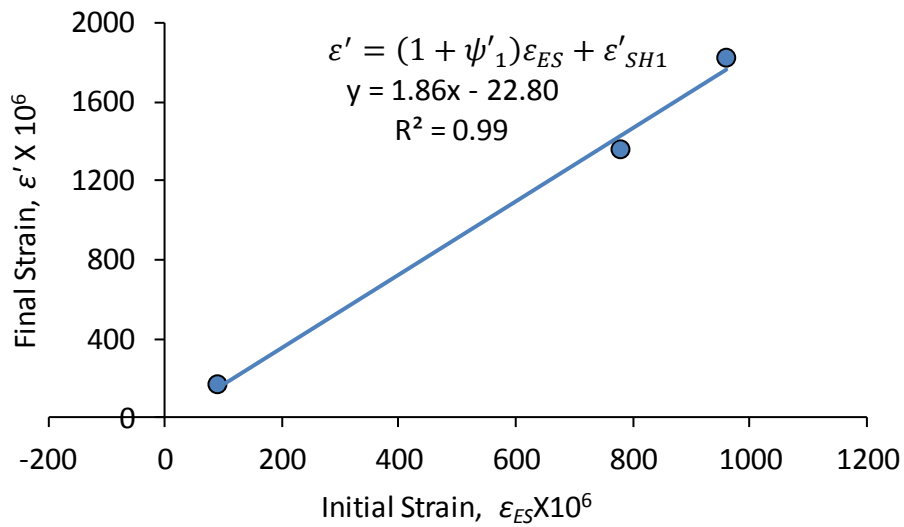


**Figure E-22 Sectional CR&SH Coefficients Set 1: Girder UTPS#240 (Q3)**

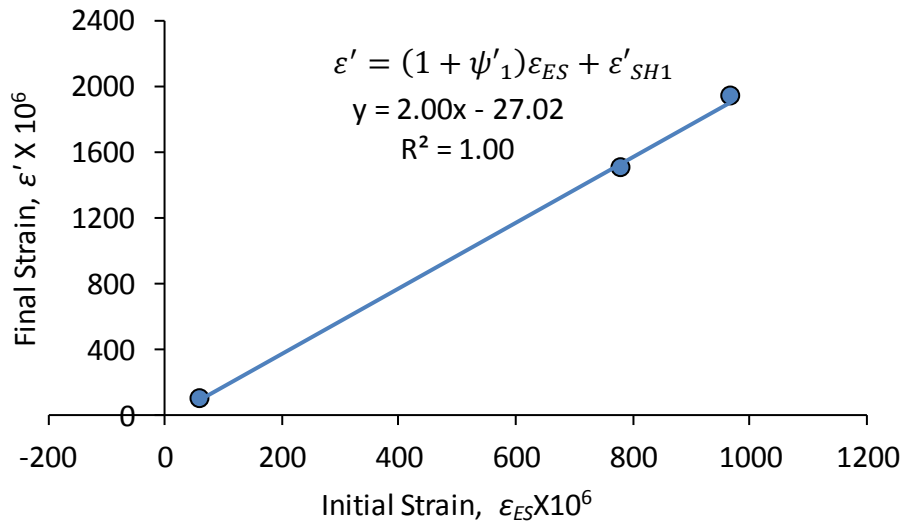


**Figure E-23 Sectional CR&SH Coefficients Set 1: Girder UTPS#242 (Q5)**

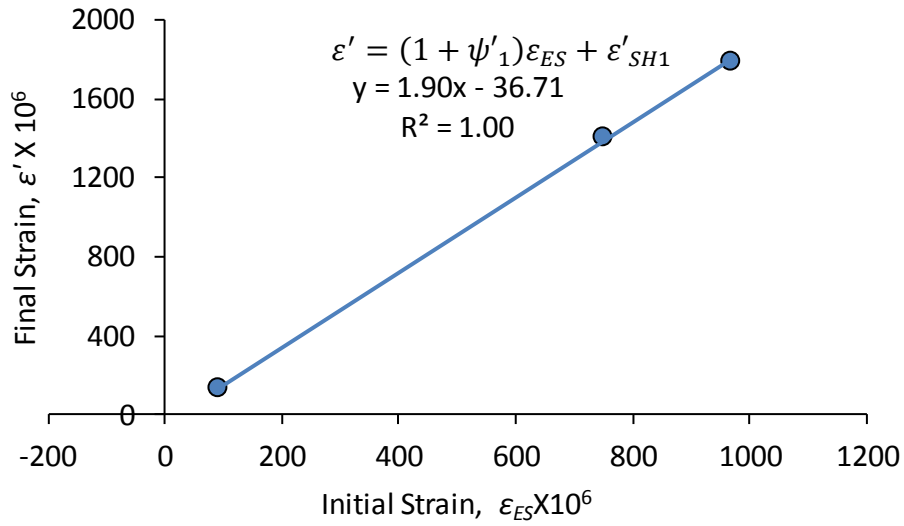


**Figure E-24 Sectional CR&SH Coefficients Set 1: Girder UTPS#244 (Q7)**

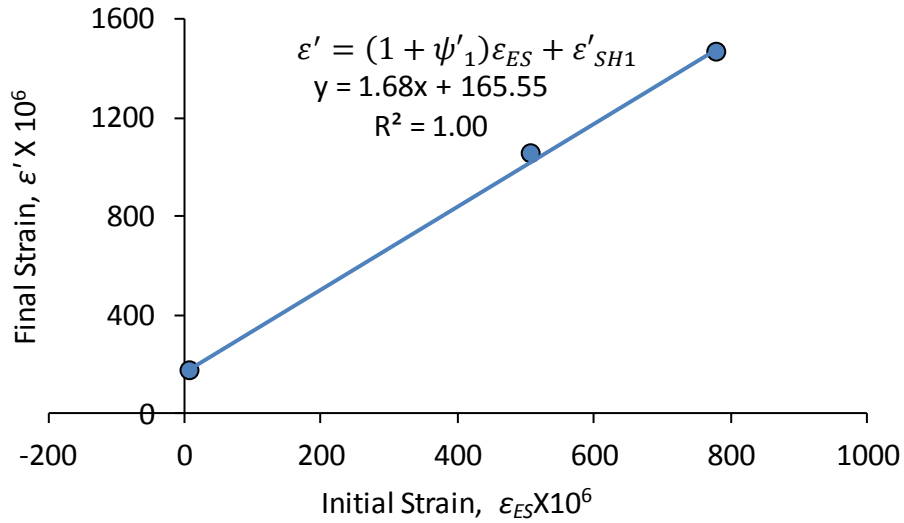


**Figure E-25 Sectional CR&SH Coefficients Set 1: Girder UTPS#246 (SCC-1)**

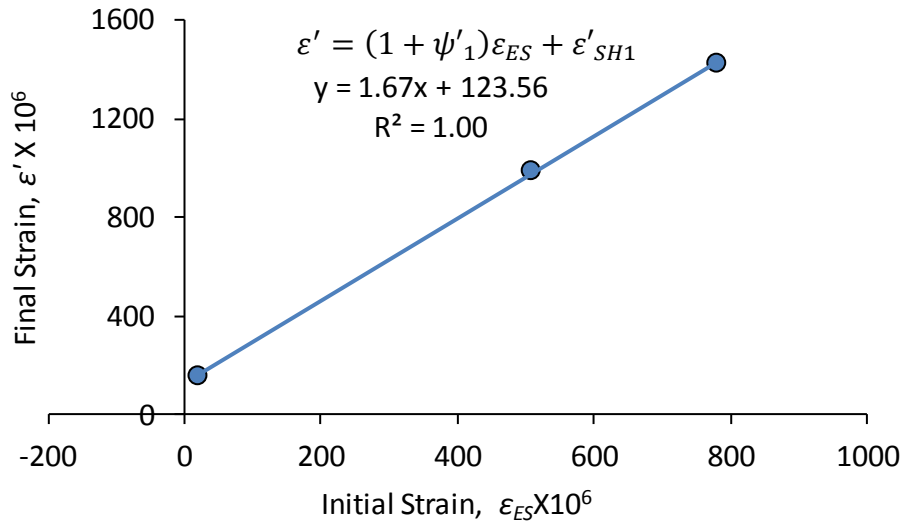


**Figure E-26 Sectional CR&SH Coefficients Set 1: Girder UTPS#247 (SCC-2)**

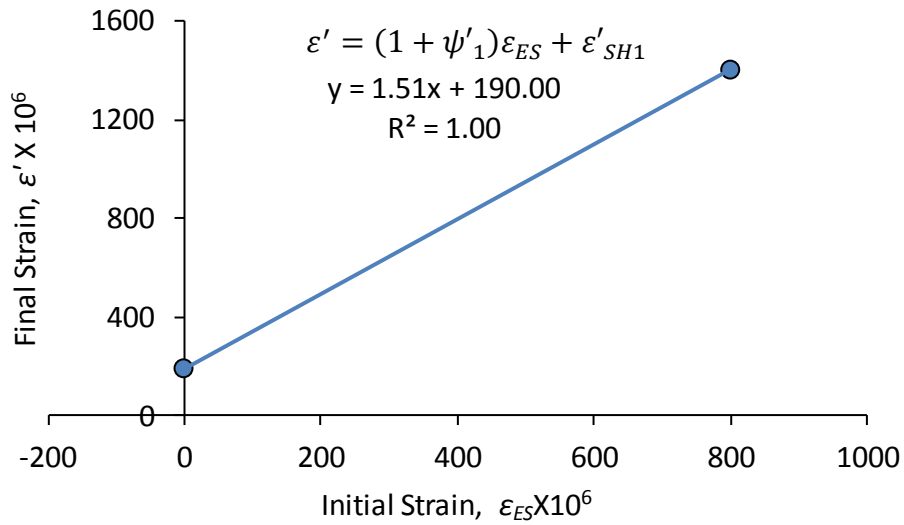


**Figure E-27 Sectional CR&SH Coefficients Set 1: Girder UTPS#248 (SCC-3)**



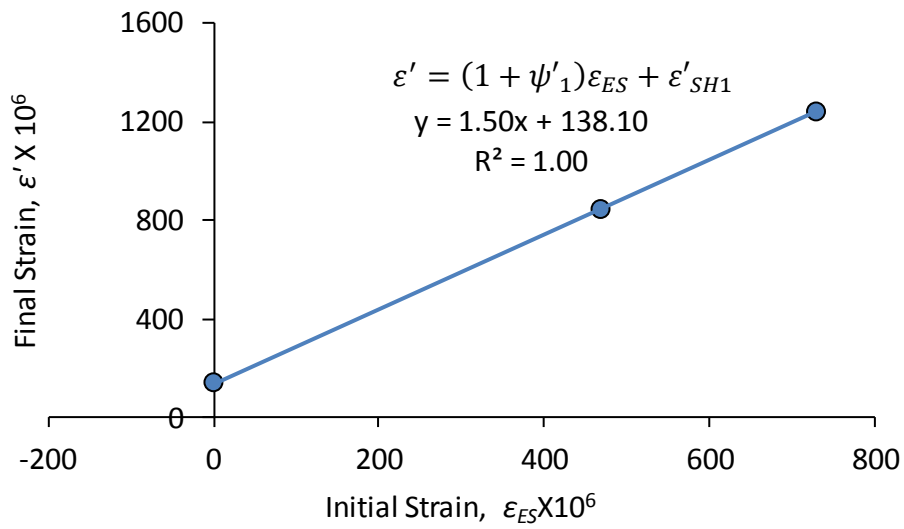


**Figure E-28 Sectional CR&SH Coefficients Set 1: Girder UTPS#250 (CC-2)**

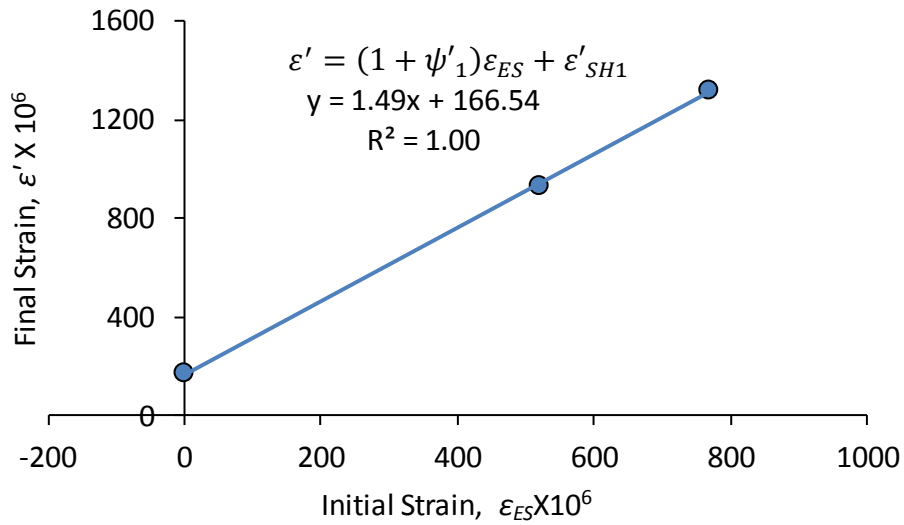


**Figure E-29 Sectional CR&SH Coefficients Set 1: Girder UTPS#251 (CC-3)**

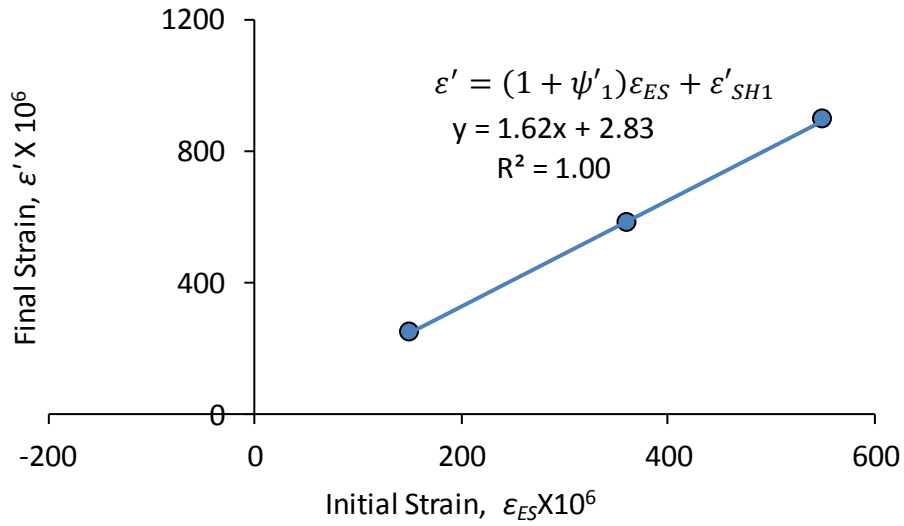


**Figure E-30 Sectional CR&SH Coefficients Set 1: Girder UTPS#262-624 (average of girders A, B & C)**

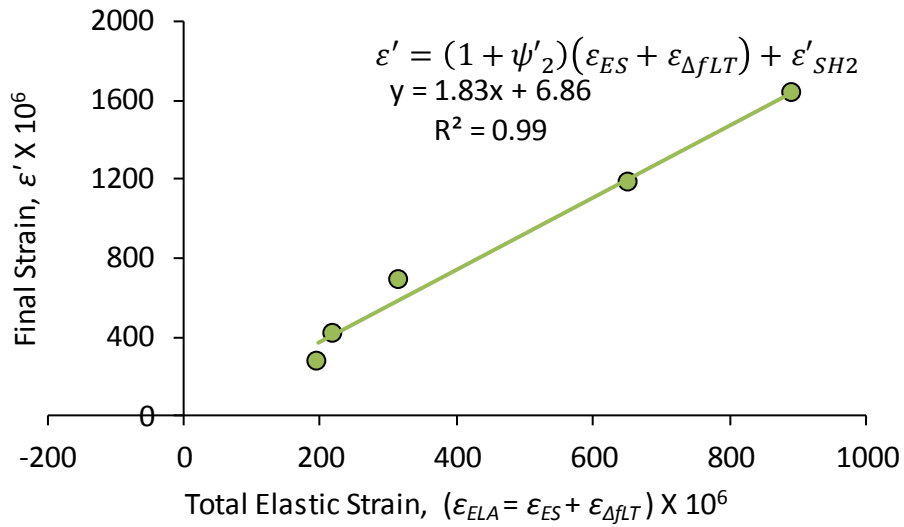


**Figure E-31 Sectional CR&SH Coefficients Set 2: Girder UTPS#4 (2B)**

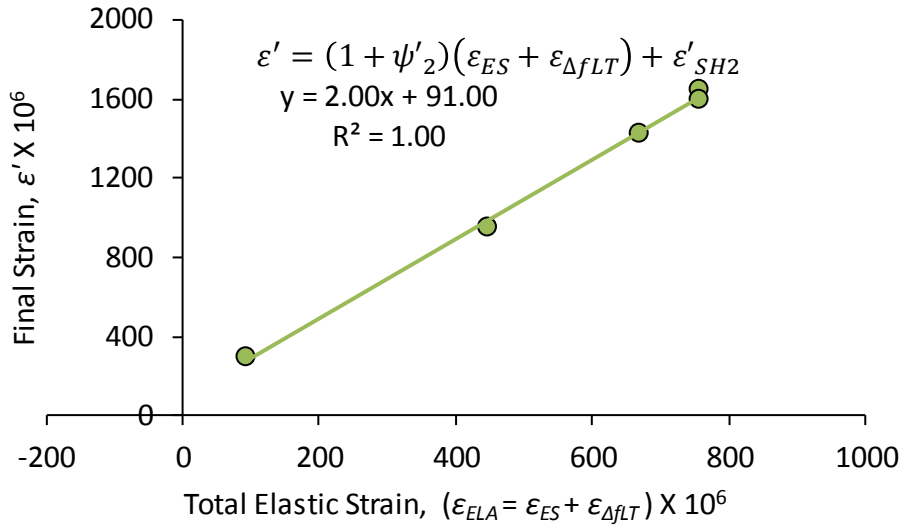


**Figure E-32 Sectional CR&SH Coefficients Set 2: Girder UTPS#56 (A-SCC1)**

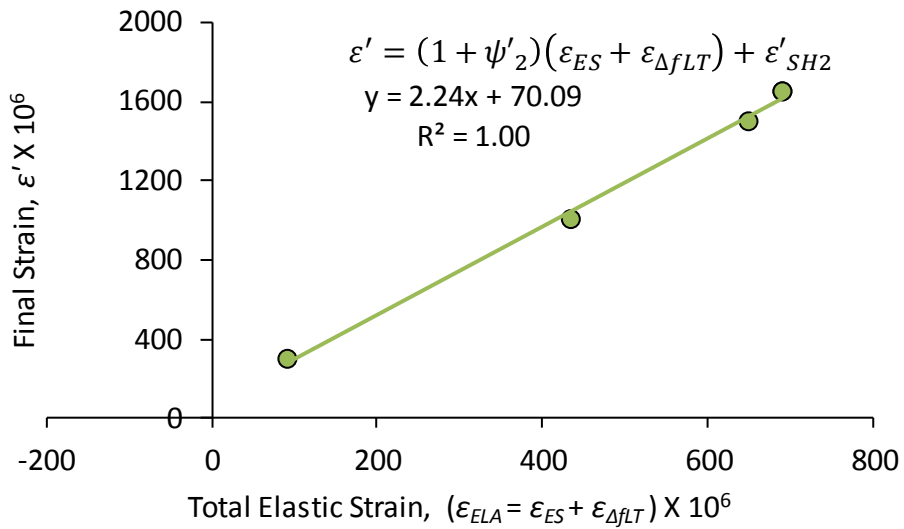


**Figure E-33 Sectional CR&SH Coefficients Set 2: Girder UTPS#57 (A-SCC2)**

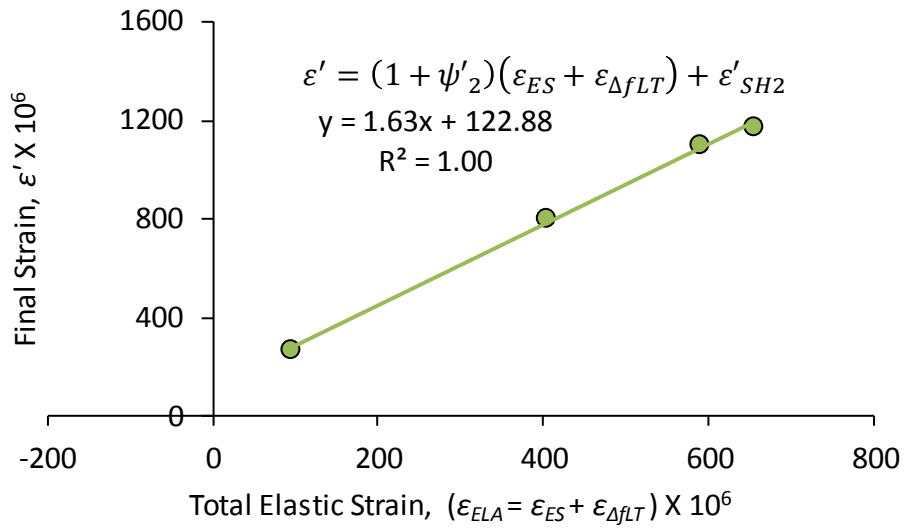


**Figure E-34 Sectional CR&SH Coefficients Set 2: Girder UTPS#58 (A-CM)**

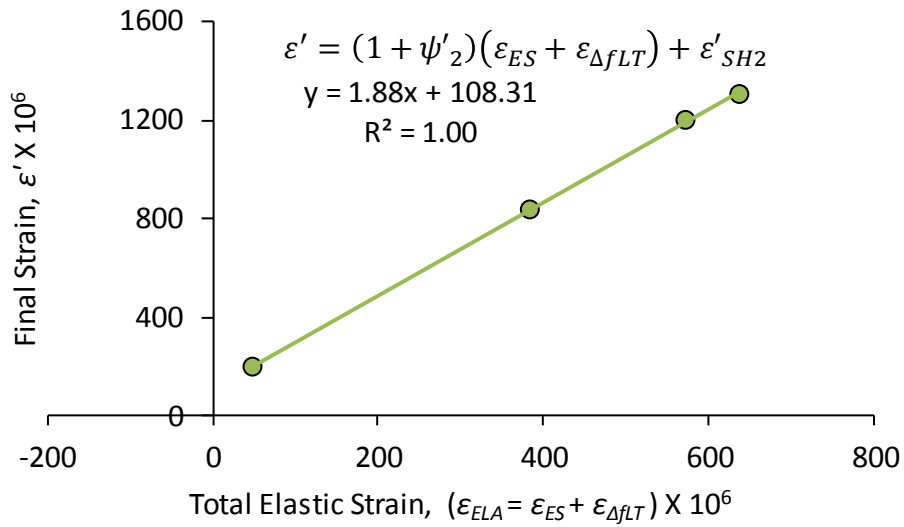


**Figure E-35 Sectional CR&SH Coefficients Set 2: Girder UTPS#59 (B-SCC1)**

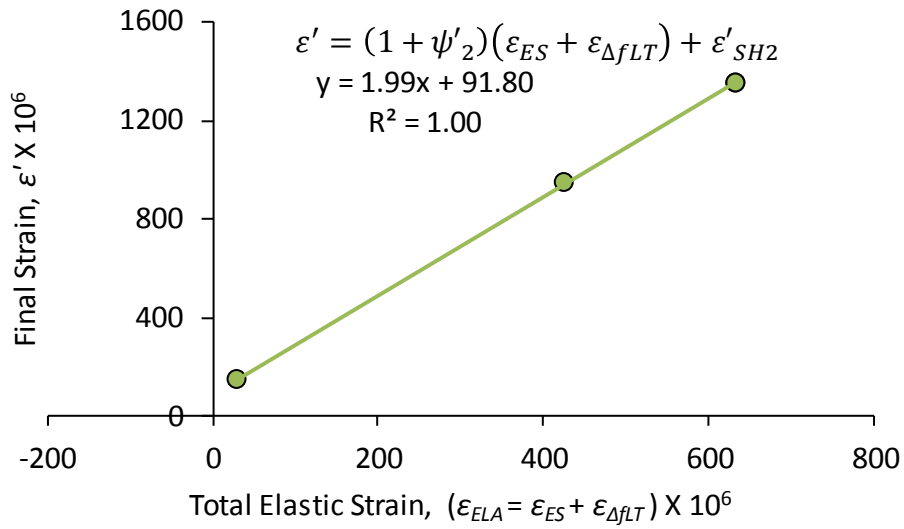


**Figure E-36 Sectional CR&SH Coefficients Set 2: Girder UTPS#60 (B-SCC2)**

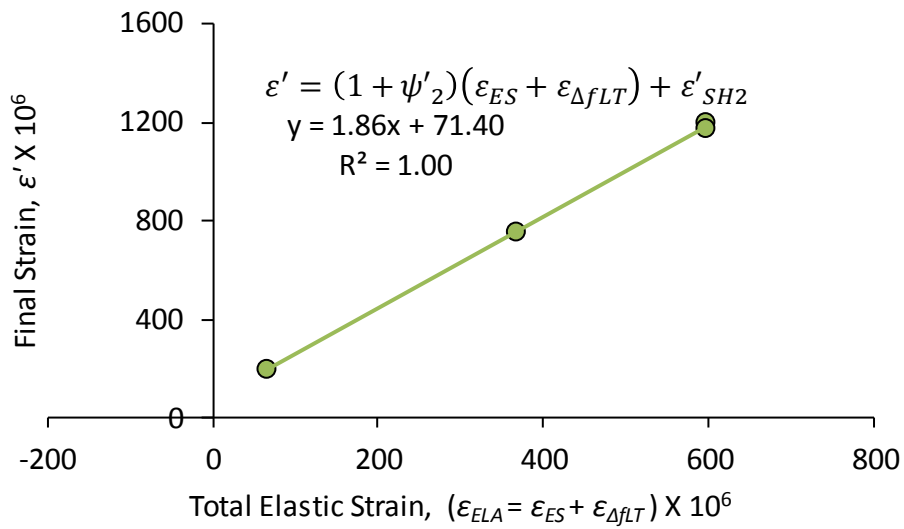


**Figure E-37 Sectional CR&SH Coefficients Set 2: Girder UTPS#61 (B-CM)**

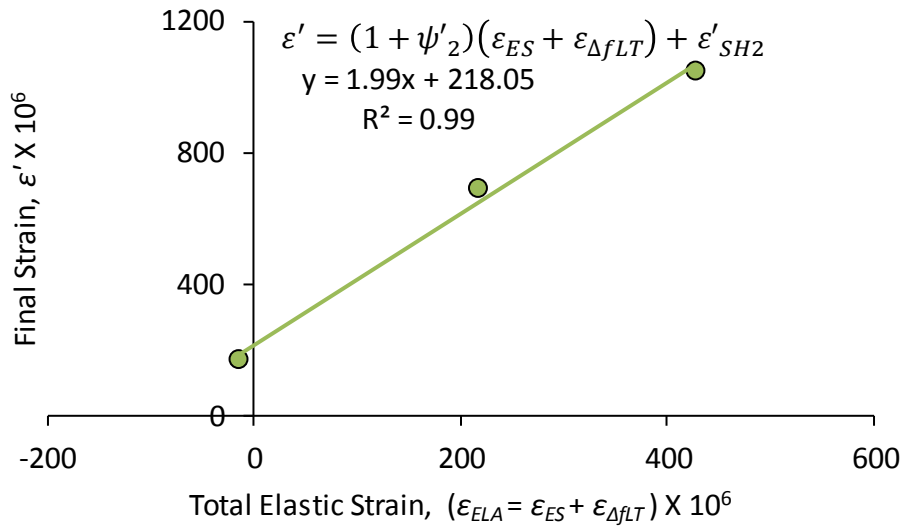


**Figure E-38 Sectional CR&SH Coefficients Set 2: Girder UTPS#62 (BX-1)**

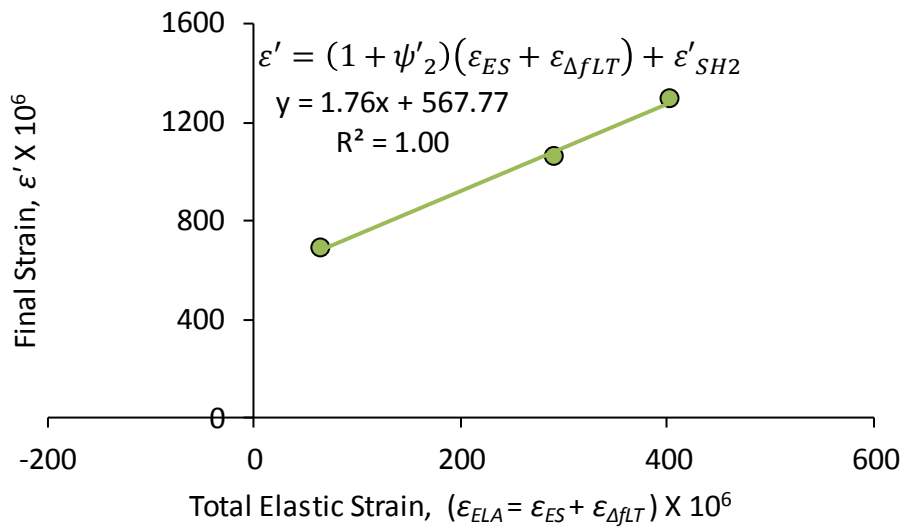


**Figure E-39 Sectional CR&SH Coefficients Set 2: Girder UTPS#105 (BX-3)**

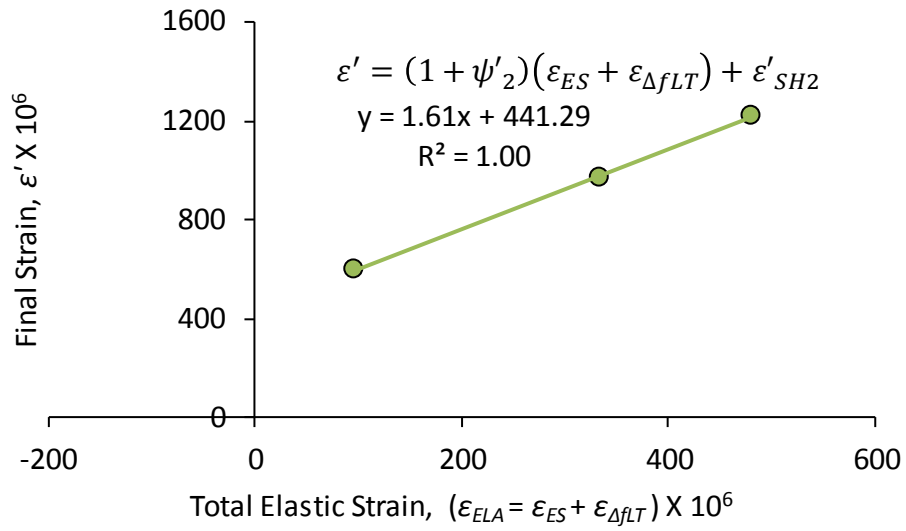


**Figure E-40 Sectional CR&SH Coefficients Set 2: Girder UTPS#106 (BX-4)**

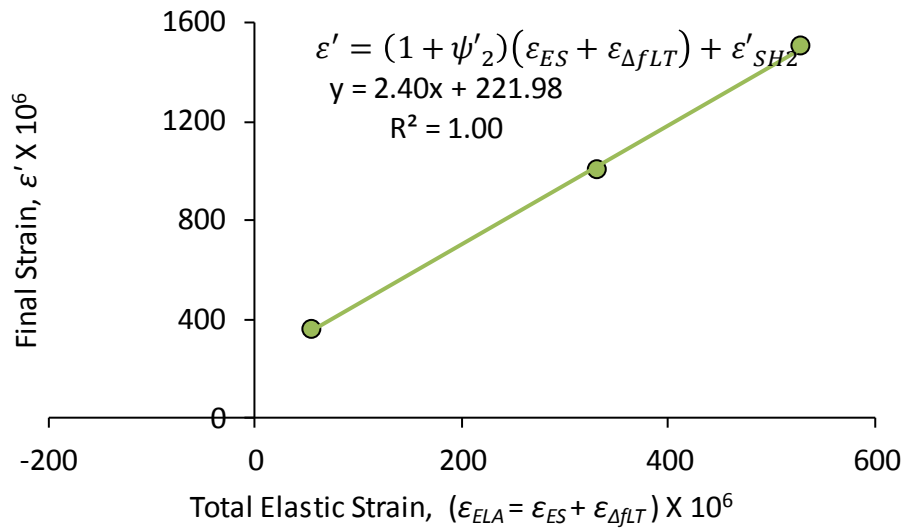


**Figure E-41 Sectional CR&SH Coefficients Set 2: Girder UTPS#119 (FT#1)**

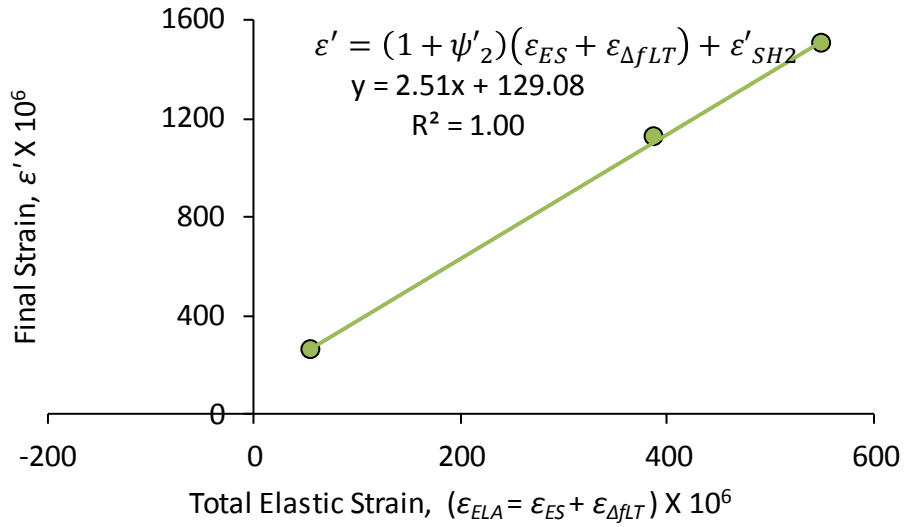


**Figure E-42 Sectional CR&SH Coefficients Set 2: Girder UTPS#120 (FT#2)**

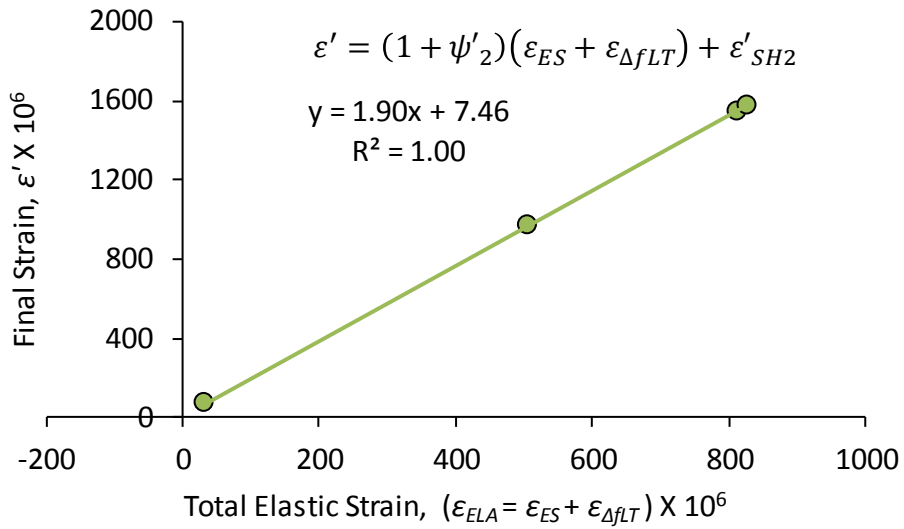


**Figure E-43 Sectional CR&SH Coefficients Set 2: Girder UTPS#222 (A1)**



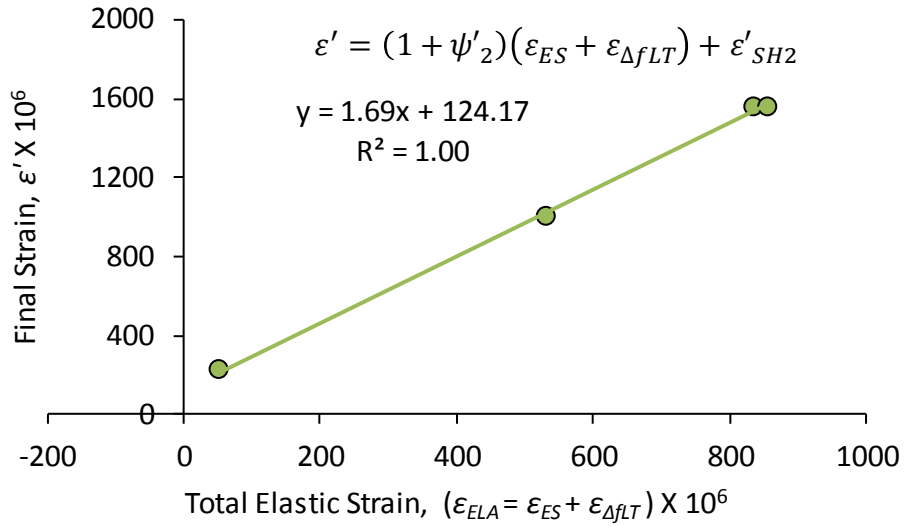


**Figure E-44 Sectional CR&SH Coefficients Set 2: Girder UTPS#224 (A3)**

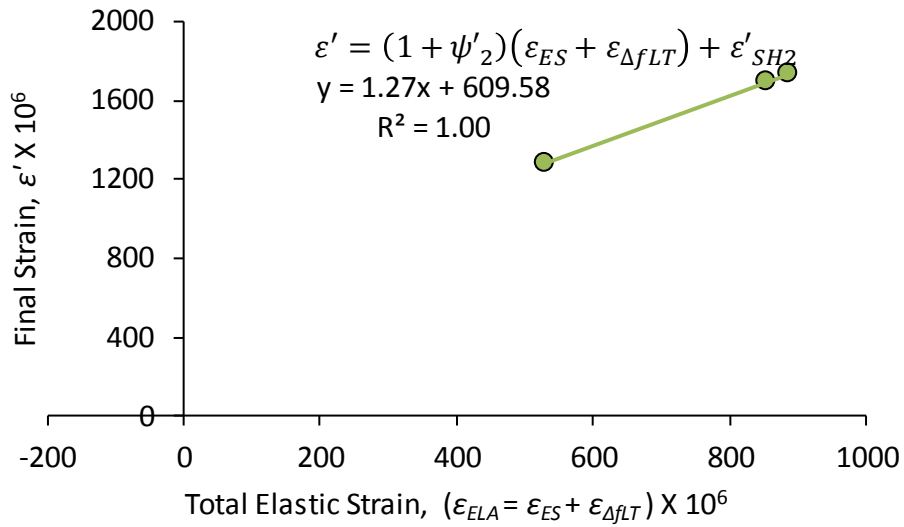


**Figure E-45 Sectional CR&SH Coefficients Set 2: Girder UTPS#226 (A5)**

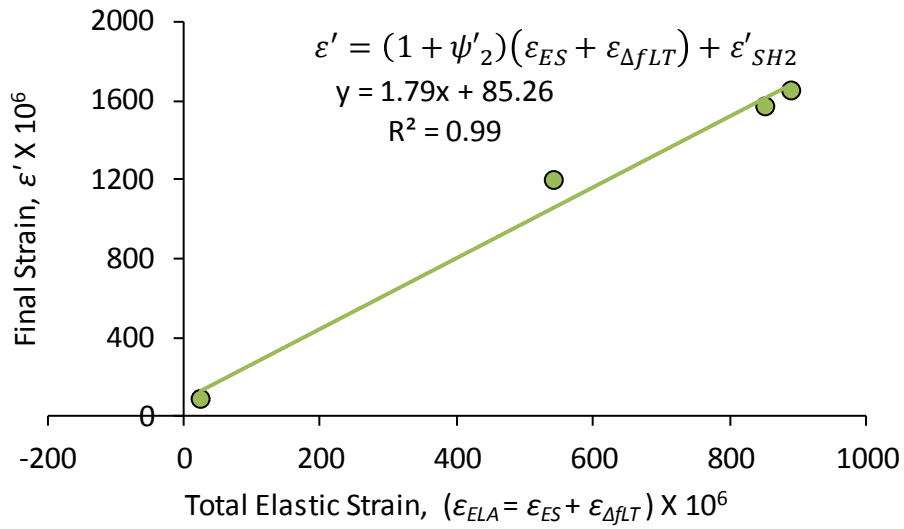


**Figure E-46 Sectional CR&SH Coefficients Set 2: Girder UTPS#228 (A7)**

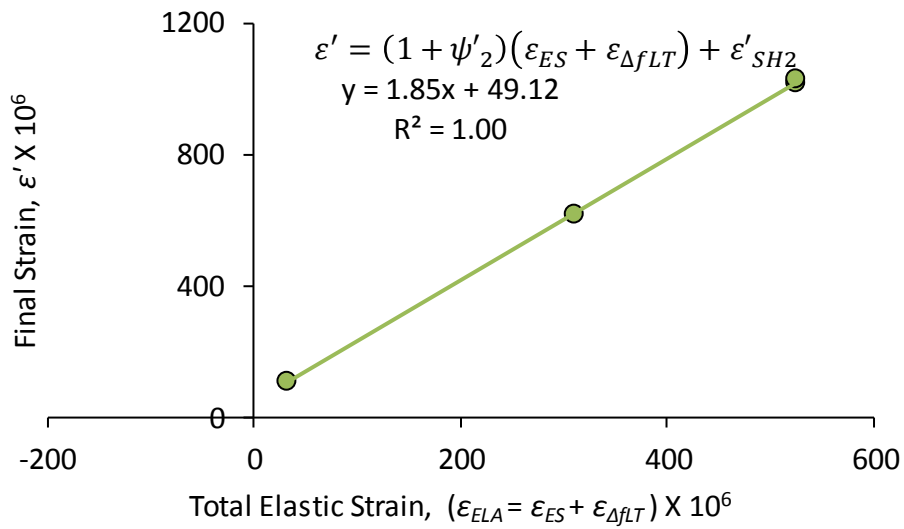


**Figure E-47 Sectional CR&SH Coefficients Set 2: Girder UTPS#230 (E1)**

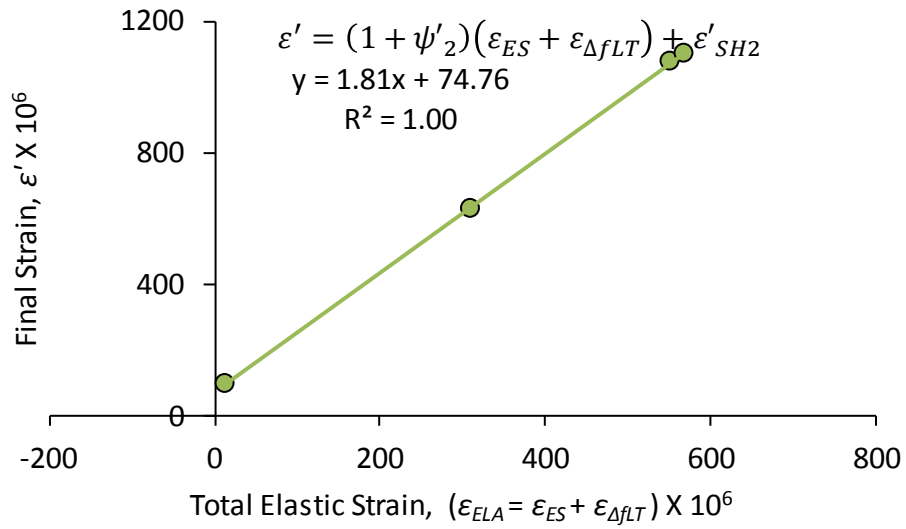


**Figure E-48 Sectional CR&SH Coefficients Set 2: Girder UTPS#232 (E3)**

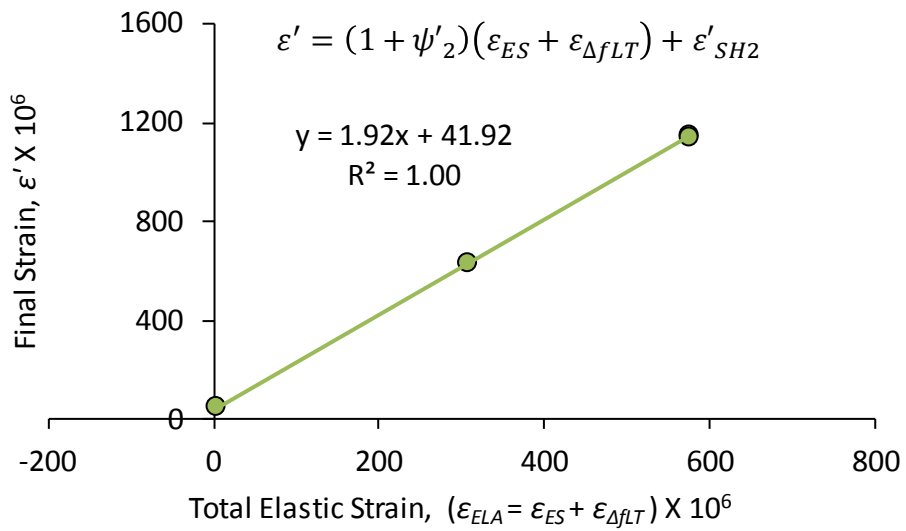


**Figure E-49 Sectional CR&SH Coefficients Set 2: Girder UTPS#235 (E6)**

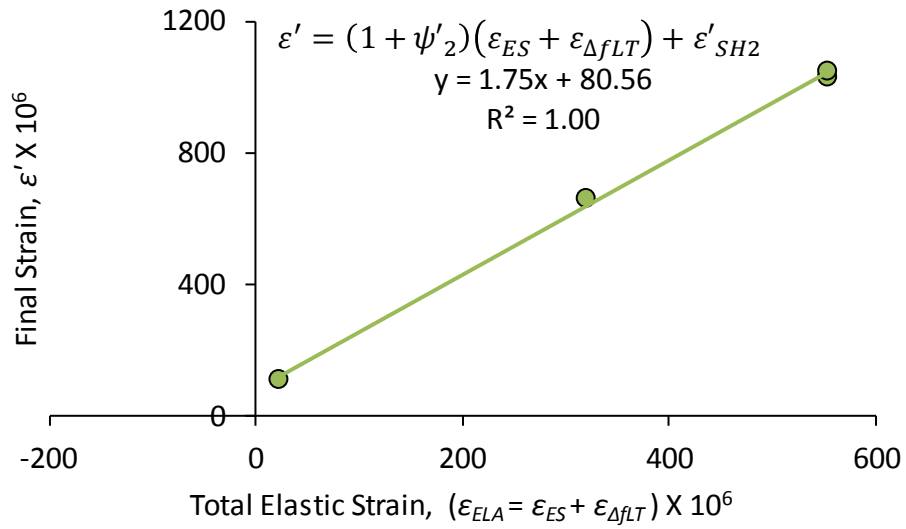


Figure E-50 Sectional CR&SH Coefficients Set 2: Girder UTPS#237 (E8)

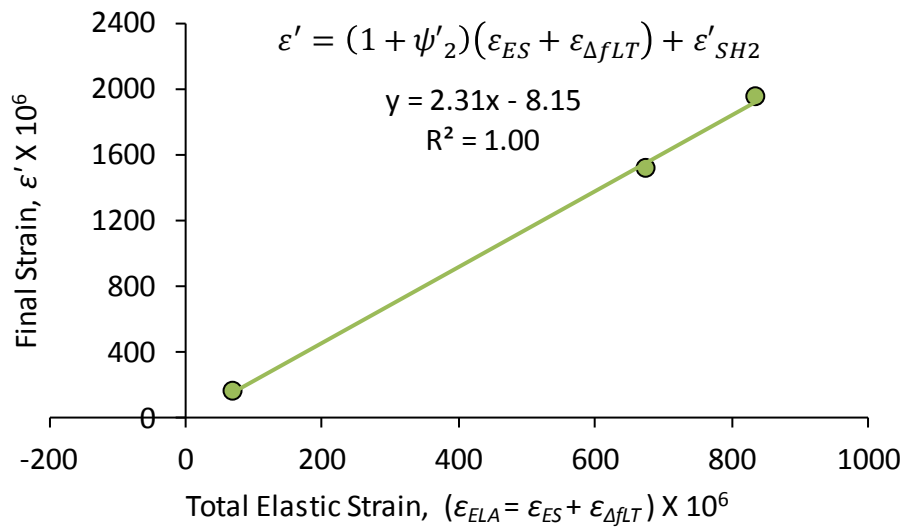
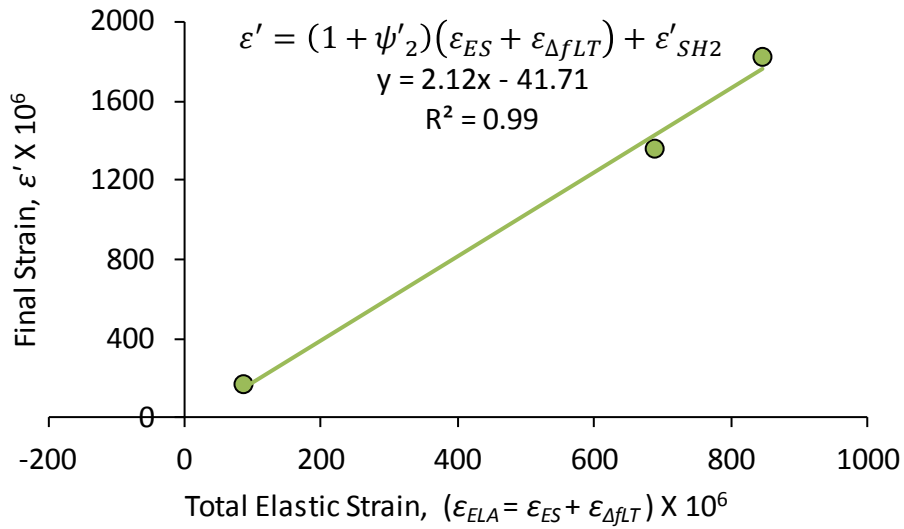
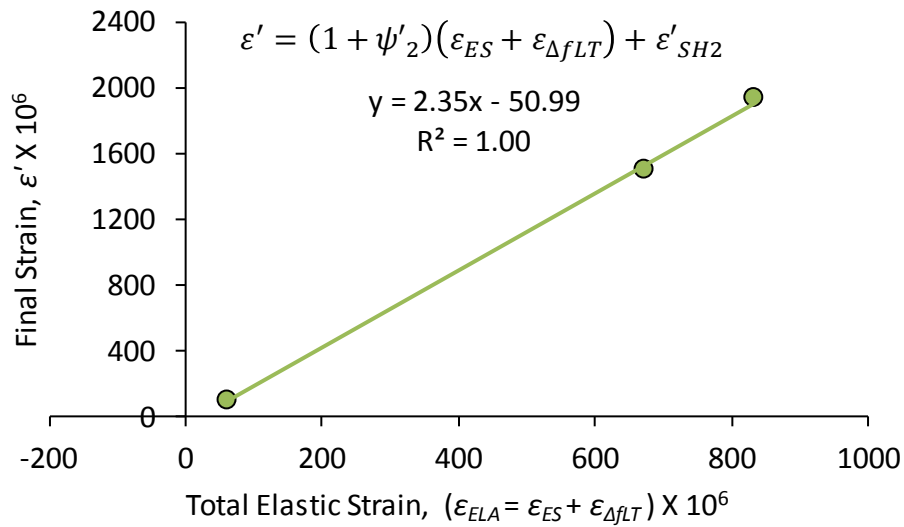


Figure E-51 Sectional CR&SH Coefficients Set 2: Girder UTPS#238 (Q1)



**Figure E-52 Sectional CR&SH Coefficients Set 2: Girder UTPS#240 (Q3)**



**Figure E-53 Sectional CR&SH Coefficients Set 2: Girder UTPS#242 (Q5)**

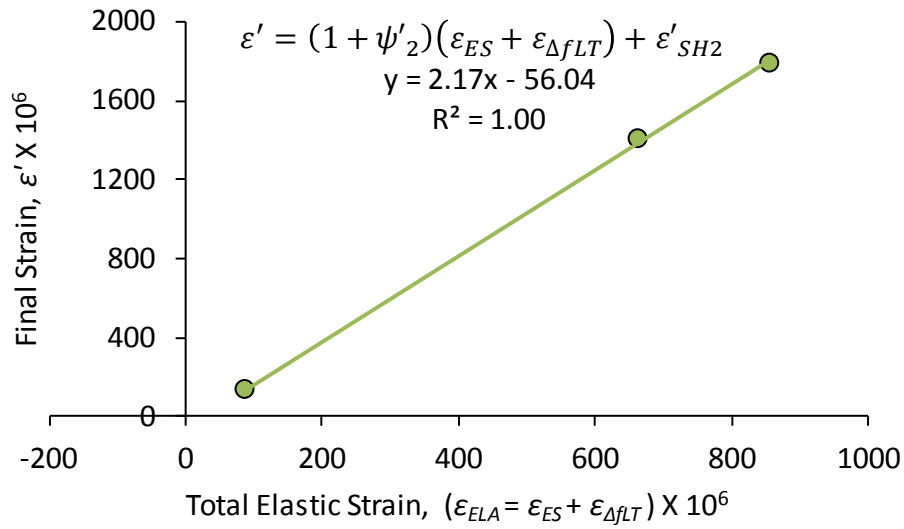


**Figure E-54 Sectional CR&SH Coefficients Set 2: Girder UTPS#244 (Q7)**

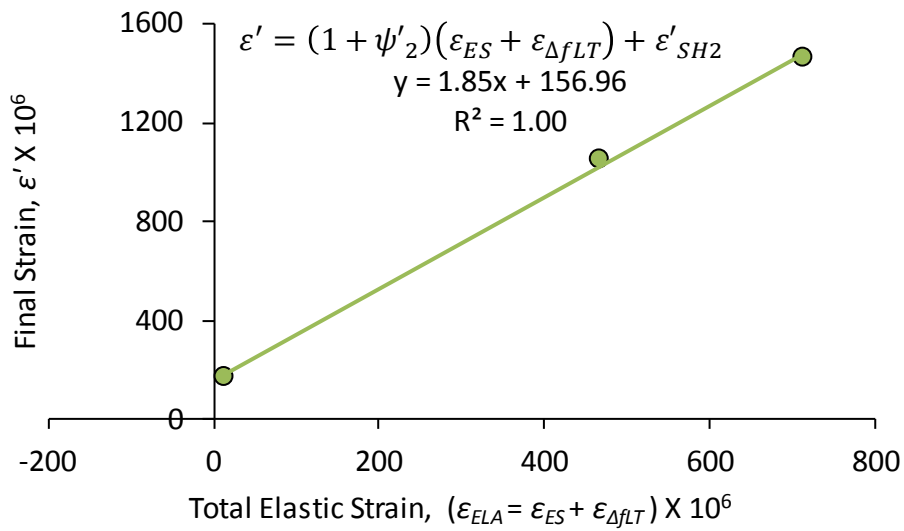


**Figure E-55 Sectional CR&SH Coefficients Set 2: Girder UTPS#246 (SCC-1)**

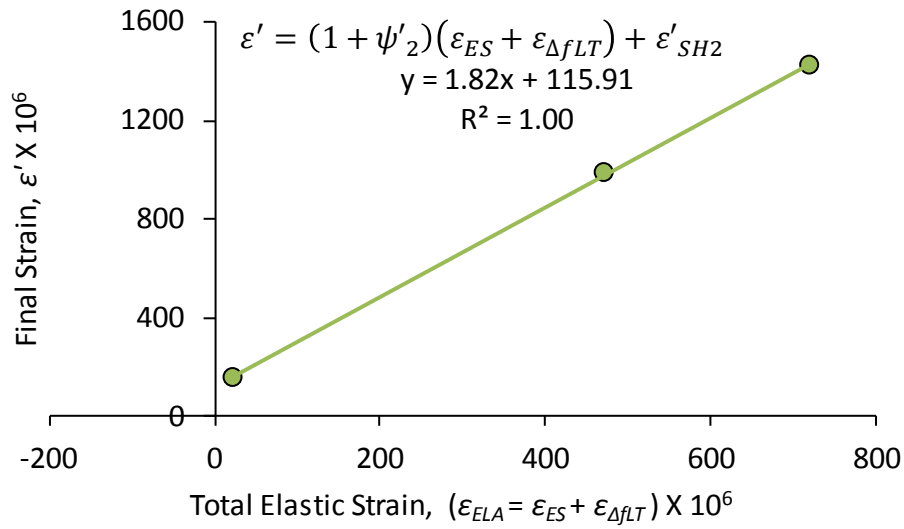


**Figure E-56 Sectional CR&SH Coefficients Set 2: Girder UTPS#247 (SCC-2)**

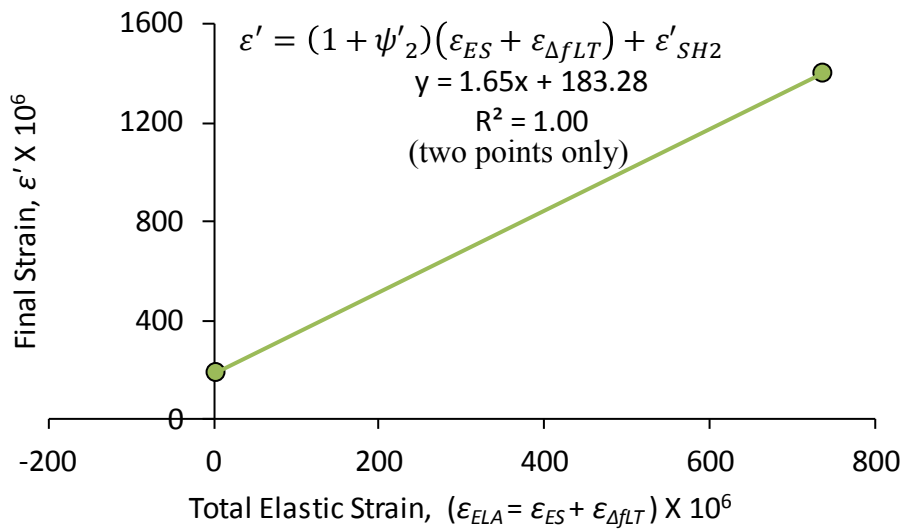


**Figure E-57 Sectional CR&SH Coefficients Set 2: Girder UTPS#248 (SCC-3)**

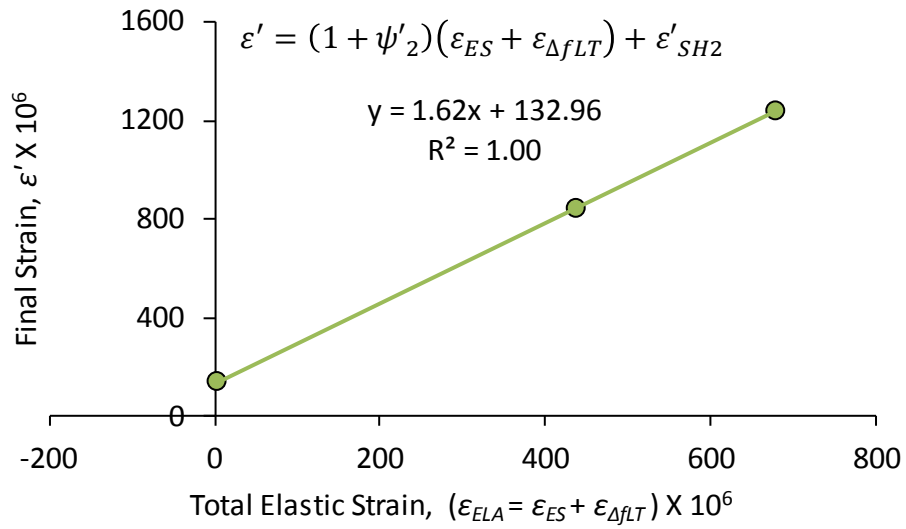


**Figure E-58 Sectional CR&SH Coefficients Set 2: Girder UTPS#250 (CC-2)**

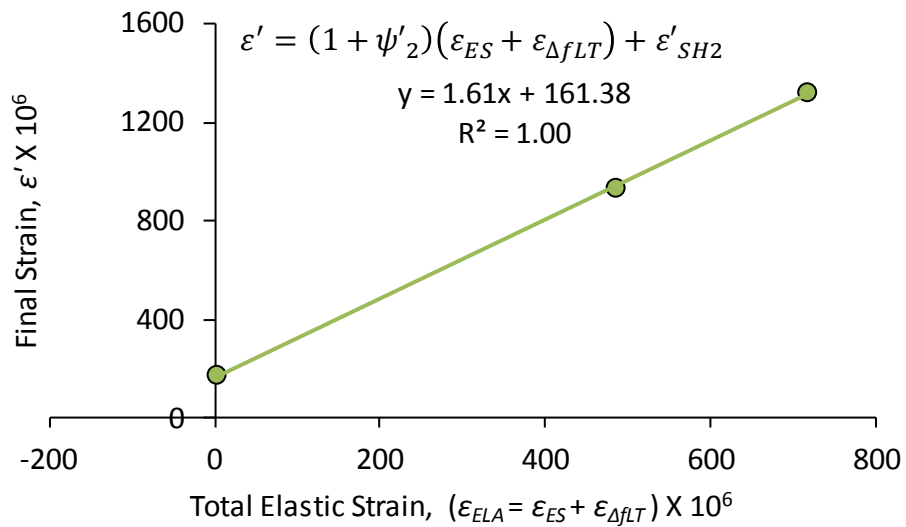


**Figure E-59 Sectional CR&SH Coefficients Set 2: Girder UTPS#251 (CC-3)**



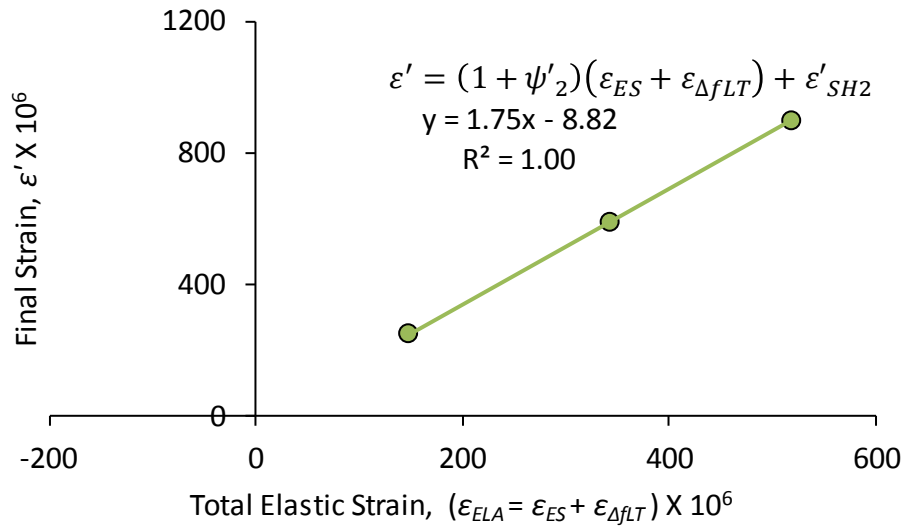


**Figure E-60 Sectional CR&SH Coefficients Set 2: Girder UTPS#262-624 (average of girders A, B & C)**

## References

- AASHTO, American Association of State Highway and Transportation Officials. *AASHTO LRFD Bridge Design Specification, Customary U.S. Units, 6th Edition*. Washington, DC., 2012.
- ACI committee 209. *ACI-209R-92: Prediction of Creep, Shrinkage and Temperature Effects in Concrete Structures*. ACI committee 209, 2005.
- ACI-ASCE Committee 323. "Tentative Recommendations for Prestressed Concrete." (ACI) 54, no. 1 (1958).
- Bažant, Zdeněk P. "Criteria for rational prediction of creep and shrinkage of concrete." *ACI SPECIAL PUBLICATIONS 194*, 2000: 237-260.
- Bažant, Zdeněk P., and Folker H. Wittmann. *Creep and shrinkage in concrete structures*. Chichester: Wiley, 1982.
- Bažant, Zdeněk P., and Guang-Hua Li. "Comprehensive database on concrete creep and shrinkage." *ACI Materials Journal* 105, no. 6 (2008): 635-637.
- Bažant, Zdeněk P., and Joong-Koo Kim. "Consequences of diffusion theory for shrinkage of concrete." *Materials and structures* 24, no. 5 (1991): 323-326.
- Bažant, Zdeněk P., and Sandeep Baweja. "Creep and shrinkage prediction model for analysis and design of concrete structures: Model B3." *ACI SPECIAL PUBLICATIONS 194* (2000): 1-73.
- Bažant, Zdeněk P., Anders Boe Hauggaard, Sandeep Baweja, and Franz-Josef Ulm. "Microprestress-solidification theory for concrete creep. I: Aging and drying effects." *Journal of Engineering Mechanics* 123, no. 11 (1997): 1188-1194.
- Brooks, J. J. "30-year creep and shrinkage of concrete." *Magazine of concrete research* 57, no. 9 (2005): 545-556.
- De Schutter, Geert. "Degree of hydration based Kelvin model for the basic creep of early age concrete." *Materials and Structures* 32, no. 4 (1999): 260-265.
- Feldman, Rolf F. "Mechanism of creep of hydrated Portland cement paste." *Cement and Concrete Research* 2, no. 5 (1972): 521-540.

- Gamble, William Leo. *Field Investigation of a Continuous Composite Prestressed I-Beam Highway Bridge Located in Jefferson County, Illinois*. Urbana: University of Illinois, 1970.
- Garber, David, Jose Gallardo, Dean Deschenes, David Dunkman, and Oguzhan Bayrak. *Effect of New Prestress Loss Estimates on Pretensioned Concrete Bridge Girder Design*. Austin, 2013.
- Geokon, Inc. . "Instruction Manual Model 4200 Series Vibrating Wire Strain Gage." Lebanon, NH: Geokon, Ing., 2012.
- Gilbert, Raymond Ian, and Gianluca Ranzi. *Time-dependent behaviour of concrete structures*. Taylor & Francis, 2011.
- Hansen, Torben C., Fariborz Radjy, and Erik J. Sellevold. "Cement paste and concrete." *Annual Review of Materials Science* 3, no. 1, 1973: 233-268.
- Hatt, W. K. "Notes on the effect of time element in loading reinforced concrete beams." *ASTM proceedings*. ASTM, 1907. 421-433.
- Hilaire, A., et al. "Analysis of concrete creep in compression, tension and bending: Numerical modeling." *Mechanics and Physics of Creep, Shrinkage, and Durability of Concrete. A Tribute to Zdenk P. Bazant*. Boston: ASCE, 2013. 348-355.
- Jennings, H. M., J. J. Thomas, and I. Vlahinic. "Can nano-models lead to improved concrete? Materials science as the intersection of chemistry and mechanics." *Creep, Shrinkage and Durability Mechanics of Concrete and Concrete Structures*. Ise-Shima, Japan: CRC Press, 2009. 11-23.
- Jennings, Hamlin M. "Colloid model of C– S– H and implications to the problem of creep and shrinkage." *Materials and Structures* 37, no. 1 (2004): 59-70.
- Juenger, Maria C. Garci, and Hamlin M. Jennings. "Examining the relationship between the microstructure of calcium silicate hydrate and drying shrinkage of cement pastes." *Cement and concrete research* 32, no. 2 (2002): 289-296.

- Keitel, Holger, and Andrea Dimmig-Osburg. "Uncertainty and sensitivity analysis of creep models for uncorrelated and correlated input parameters." *Engineering Structures* 32, no. 11 (2010): 3758-3767.
- Kovler, Konstantin, and Semion Zhutovsky. "Overview and future trends of shrinkage research." *Materials and structures* 39, no. 9 (2006): 827-847.
- Lee, Yun, Seong-Tae Yi, Min-Su Kim, and Jin-Keun Kim. "Evaluation of a basic creep model with respect to autogenous shrinkage." *Cement and concrete research* 36, no. 7 (2006): 1268-1278.
- Lin, T. Y. *DESIGN OF PRESTRESSED CONCRETE STRUCTURES*. New York: John Wiley and Sons, 1955.
- Mindess, Sidney, J. Francis Young, and David Darwin. *Concrete*. Upper Saddle River: Prentice Hall, 2003.
- Mossiossian, Varoujan. "Time-dependent behavior of noncomposite and composite prestressed concrete structures under field and laboratory conditions." Urbana, Illinois: University of Illinois at Urbana-Champaign, 1972.
- Neville, Adam M., Walter H. Dilger, and Jeffery J. Brooks. *Creep of plain and structural concrete*. London and New York: Construction Press, 1983.
- PCI, Industry Handbook Committee. *PCI Design Handbook: Precast and Prestressed Concrete*. 2004.
- Powers, T. "The thermodynamics of volume change and creep." *Matériaux et Construction* 1, no. 6 (1968).
- Tazawa, Ei-ichi, Ryoichi Sato, Etsuo Sakai, and Shingo Miyazawa. "Work of JCI committee on autogenous shrinkage." *Shrinkage 2000—Int. RILEM Workshop on Shrinkage of Concrete*. 2000. 21-40.
- Torrenti, J. M., and F. Benboudjema. "Desiccation shrinkage of large structures: is there a size effect?" *Mechanics and Physics of Creep, Shrinkage, and Durability of Concrete. A Tribute to Zdenk P. Bazant*. Boston: ASCE, 2013. 404-411.
- Ulm, F., F. Le Maou, and C. Boulay. "Creep and Shrinkage of Concrete - Kinetics Approach." *ACI SP-194*, 2000: 135-153.

- Vandamme, M., et al. "Creep Properties of Cementitious Materials from Indentation Testing: Significance, Influence of Relative Humidity, and Analogy Between CSH and Soils." *Mechanics and Physics of Creep, Shrinkage, and Durability of Concrete. A Tribute to Zdenk P. Bazant*. Boston: ASCE, 2013. 48-61.
- Vandamme, Matthieu, and Franz-Josef Ulm. "Nanogranular origin of concrete creep." *Proceedings of the National Academy of Sciences (PNAS)*, 2009: 10552-10557.
- White, A. H. "Destruction of cement mortars and concrete through expansion and contraction." *ASTM Proceedings*. ASTM, 1911. 531-555.

## **Vita**

José Manuel Gallardo Méndez was born from and raised by Xiomara del Socorro Méndez Moreira de Gallardo y José Manuel Gallardo Araúz since 1979 in David, Chiriquí, Panamá. He received his Bachelor's of Science in Civil Engineering in 2003 and the Master in Structural Engineering in 2006, both from Universidad Tecnológica de Panamá. His thesis were about soil amplification of earthquake waves and about earthquake induced damage in concrete frames. From 2003 to 2006 he worked in the Universidad Tecnológica de Panamá in various research projects. From 2006 to 2009 he worked in the construction industry; as part of such works he was in charge of the design and construction of two small-span bridges. In 2010 he started his studies in Doctor of Philosophy in Civil Engineering in The University of Texas at Austin. He conducted his research for this dissertation at the Phil M. Ferguson Structural Engineering Laboratory. After graduation, he plan to work in Chiriquí, Panamá in: a quarry and precast concrete plant, and as lecturer in the Universidad Tecnológica de Panamá and the Universidad Santa María La Antigua.

Permanent email address: -jose@hotmail.com

This dissertation was typed by the author.